

AIR QUALITY MODELING

Theories, Methodologies,
Computational Techniques, and
Available Databases and Software

Volume I - Fundamentals

[Table of Contents](#)
(click here)

Editor

Paolo Zannetti

Chapter Authors

Domenico Anfossi
Peter J.H. Builtjes
Daewon W. Byun
Elisa Canepa
Joseph L. Eastman
Cecil S. Keen
Avraham Laeser
Russell Lee

Walter A. Lyons
Dennis A. Moon
Nicolas Moussiopoulos
Thomas E. Nelson
Dietmar Oettl
Steven D. Reynolds
Philip M. Roth
Roberto San Jose

Zbigniew Sorbjan
Jesse Thé
Paraskevi-Maria Turlou
Han van Dop
Akula Venkatram
Robert J. Yamartino
Paolo Zannetti

AIR QUALITY MODELING

Theories, Methodologies, Computational Techniques,
and Available Databases and Software

Volume I – Fundamentals

Blank Page

Dedicated to SAZ

Blank Page

AIR QUALITY MODELING
Theories, Methodologies, Computational Techniques,
and Available Databases and Software

Volume I – Fundamentals

Editor

Paolo Zannetti

Chapter Authors

Domenico Anfossi, Peter J.H. Bultjes, Daewon W. Byun, Elisa Canepa,
Joseph L. Eastman, Cecil S. Keen, Avraham Lacser, Russell Lee, Walter A. Lyons,
Dennis A. Moon, Nicolas Moussiopoulos, Thomas E. Nelson, Dietmar Oettl,
Steven D. Reynolds, Philip M. Roth, Roberto San Jose, Zbigniew Sorbjan, Jesse Thé,
Paraskevi-Maria Turlou, Han van Dop, Akula Venkatram, Robert J. Yamartino, Paolo Zannetti

Published by



AIR & WASTE MANAGEMENT
A S S O C I A T I O N

◆
SINCE 1907

Copyright © 2003 EnviroComp Institute and Air & Waste Management Association. All rights reserved.

Notice regarding copyrights: Chapter authors retain copyrights to their original materials. All requests for permission to reproduce chapter material should be directed to the appropriate author(s); all other requests should be directed to the Air & Waste Management Association, One Gateway Center, 3rd Floor, 420 Ft. Duquesne Blvd., Pittsburgh, PA 15222 USA.

ISBN 0-923204-56-3

Printed in the United States of America.

Copies of this book may be purchased by visiting the Air & Waste Management Association's online bookstore at www.awma.org/pubs/bookstore, or by contacting A&WMA directly at 1-800-270-3444 or 1-412-232-3444. Please reference A&WMA Order Code OTHP-24. This book is also available in CD-ROM format.

For updates, additional information, and online discussion regarding this book series, please visit www.envirocomp.org/aqm

Table of Contents¹

	<u>Preface</u>	<u>xi</u>
	<u>About the Editor</u>	<u>xiii</u>
	<u>About the Publishers</u>	<u>xv</u>
	<u>About the Chapter Authors</u>	<u>xvii</u>
<u>1</u>	<u>The Problem – Air Pollution</u>	<u>1</u>
	1 <u>Our Natural Environment</u>	<u>1</u>
	2 <u>Air Pollution, Some Definitions</u>	<u>3</u>
	3 <u>Primary and Secondary Pollutants</u>	<u>4</u>
	4 <u>A Short History of Air Pollution Modeling</u>	<u>5</u>
	5 <u>Air Pollution Regulations</u>	<u>8</u>
<u>2</u>	<u>The Tool – Mathematical Modeling</u>	<u>13</u>
	1 <u>Why Air Quality Modeling</u>	<u>13</u>
	2 <u>Modeling Categorized</u>	<u>14</u>
	3 <u>Modeling the Atmosphere</u>	<u>19</u>
	4 <u>Modeling Alternatives</u>	<u>20</u>
	5 <u>Spatial and Temporal Scales</u>	<u>22</u>
	6 <u>Spatial and Temporal Resolution</u>	<u>23</u>
	7 <u>Uncertainty: Bias, Imprecision, and Variability</u>	<u>24</u>
	8 <u>Evaluation of Model Performance</u>	<u>25</u>
	9 <u>Data Needs</u>	<u>27</u>
	10 <u>Uses of Models</u>	<u>29</u>
<u>3</u>	<i><u>Emission Modeling</u></i>	<u>33</u>
<u>4</u>	<u>Air Pollution Meteorology</u>	<u>37</u>
	1 <u>Synoptic Meteorology</u>	<u>38</u>
	2 <u>Boundary-Layer Meteorology</u>	<u>61</u>
<u>5</u>	<i><u>Meteorological Modeling</u></i>	<u>101</u>
<u>6</u>	<u>Plume Rise</u>	<u>103</u>
	1 <u>Introduction</u>	<u>108</u>
	2 <u>Semi-Empirical Formulations</u>	<u>112</u>
	3 <u>Advanced Plume Rise Models</u>	<u>131</u>
	4 <u>Particle Models for Plume Rise</u>	<u>137</u>
	5 <u>Special Cases</u>	<u>157</u>
<u>7</u>	<i><u>Gaussian Plume Models</u></i>	<u>183</u>

¹ Chapters in italics will be provided in subsequent volumes.

<u>7A</u>	<u>Introduction to Gaussian Plume Models</u>	<u>185</u>
1	<u>Introduction</u>	<u>186</u>
2	<u>The Point Source in the Atmospheric Boundary Layer</u>	<u>186</u>
3	<u>The Atmospheric Boundary Layer</u>	<u>190</u>
4	<u>Dispersion in the Atmospheric Boundary Layer</u>	<u>193</u>
5	<u>Building Downwash</u>	<u>197</u>
6	<u>Terrain Treatment</u>	<u>199</u>
7	<u>Modifications to the Gaussian Framework</u>	<u>202</u>
8	<u>Concluding Remarks</u>	<u>206</u>
<u>8</u>	<u>Gaussian Puff Models</u>	<u>209</u>
<u>9</u>	<u>Special Applications of Gaussian Models</u>	<u>211</u>
<u>10</u>	<u>Eulerian Dispersion Models</u>	<u>213</u>
1	<u>Air Quality Modeling Methods</u>	<u>214</u>
2	<u>Eulerian Formulations</u>	<u>218</u>
3	<u>Analytical Solutions for Ideal Atmospheric Conditions</u>	<u>232</u>
4	<u>Numerical Solution Methods</u>	<u>237</u>
5	<u>Numerical Algorithms for Advection</u>	<u>244</u>
6	<u>Horizontal Diffusion Algorithm</u>	<u>251</u>
7	<u>Vertical Diffusion Algorithm</u>	<u>258</u>
8	<u>Simplified Eulerian Models</u>	<u>268</u>
	<u>Appendix A</u>	<u>272</u>
	<u>Appendix B</u>	<u>276</u>
	<u>Appendix C</u>	<u>279</u>
<u>11</u>	<u>Lagrangian Particle Models</u>	<u>293</u>
<u>12</u>	<u>Atmospheric Transformations</u>	<u>297</u>
<u>13</u>	<u>Deposition Phenomena</u>	<u>301</u>
<u>14</u>	<u>Indoor Air Pollution Modeling</u>	<u>303</u>
<u>15</u>	<u>Modeling of Adverse Effects</u>	<u>305</u>
<u>16</u>	<u>Statistical Modeling</u>	<u>307</u>
<u>17</u>	<u>Evaluation of Air Pollution Models</u>	<u>309</u>
<u>18</u>	<u>Regulatory Air Quality Models</u>	<u>311</u>
<u>19</u>	<u>Case Studies – Air Pollution Modeling at Local, Regional, Continental, and Global Scales</u>	<u>313</u>
1	<u>List of Case Studies</u>	<u>314</u>
2	<u>Additional Information on Case Studies Relevant to Air Pollution Modeling/Simulation</u>	<u>323</u>

<u>20</u>	<u>The Future of Air Pollution Modeling</u>	<u>325</u>
	<u>1 Processor Technology and Air Pollution Modeling</u>	<u>325</u>
	<u>2 Comprehensive Modeling Systems (CMS)</u>	<u>330</u>
<u>21</u>	<u>Active Groups in Air Pollution Modeling</u>	<u>355</u>
	<u>1 List of Active Groups</u>	<u>356</u>
	<u>2 Additional Information on Groups Working on Air Pollution Modeling Issues</u>	<u>360</u>
<u>22</u>	<u>Available Software</u>	<u>363</u>
	<u>1 Short-Range Models</u>	<u>366</u>
	<u>2 Urban and Regional Photochemical Models</u>	<u>380</u>
	<u>3 Long-Range Transport Models for Acid Deposition, Visibility Impairment and Complex Terrain</u>	<u>387</u>
	<u>4 Emergency Release and Dense Gas Models</u>	<u>394</u>
	<u>5 Meteorological Models</u>	<u>406</u>
<u>23</u>	<u>Available Databases</u>	<u>409</u>
	<u>1 Overview</u>	<u>409</u>
	<u>2 The Challenges</u>	<u>411</u>
	<u>3 Characteristics of Weather Data Sets</u>	<u>413</u>
	<u>4 NCEP Gridded Data Products</u>	<u>414</u>
	<u>5 Data Archival</u>	<u>416</u>
	<u>6 Reanalysis Techniques</u>	<u>418</u>
	<u>7 Mesoscale Prognostic Models</u>	<u>421</u>
	<u>8 Future Developments</u>	<u>423</u>
	<u>Authors' Index</u>	<u>427</u>
	<u>Subject Index</u>	<u>429</u>

Preface

“Never again!”

That was my reaction when my original book on air pollution modeling was finally published in 1990 (<http://www.witpress.com/acatalog/1002.html>). Although I was proud of the book and my efforts in putting it together, it was a great relief to have such a large project behind me.

Time, however, has a way of softening one’s memory. So, about ten years later, I found myself thinking that the time had come to revisit the entire project. No comprehensive new books on air pollution modeling had been printed since 1990, and my book was starting to show its age. Something needed to be done.

I decided to launch a new book series on air quality modeling. This time, however, I would enlist the help of leading scientists to author different chapters. By serving primarily as the editor, I assumed, my workload would be reduced and things would proceed more smoothly than with the previous book.

Of course, as scientists tend to do, I underestimated the effort required. Nevertheless, the first volume of the new book series—now called, more appropriately, “Air Quality Modeling: Theories, Methodologies, Computational Techniques, and Available Databases and Software”—is complete, and that is all that counts. I am extremely proud of this first volume and pleased to co-publish it with the Air & Waste Management Association, of which I have been a member for more than 20 years.

Subsequent volumes in this series will provide additional chapters on new and related topics, and also revise and expand upon previous chapters. Each new volume, then, will expand the latitude of our effort, ensuring that the reader is provided a growing and fully updated body of information.

The EnviroComp Institute has pioneered the production of electronic books in environmental sciences, so the books in this series will be in both CD-ROM format and as traditional, bound textbooks. Although the CD-ROM version has additional features that the printed book does not—such as text search capabilities, internet pointers, color pictures and animations—it is also less expensive to produce. As a result, we are charging less for the CD-ROM in hopes of encouraging more readers to try electronic books.

Another new, and hopefully useful, feature of this book series is that it has its own Web page on the EnviroComp site. We encourage readers and potential readers to visit <http://www.envirocomp.org/aqm> for information on forthcoming volumes, purchasing options, errata/corrige, and other relevant issues. In addition, there is a unique forum in which readers and chapter authors can publicly discuss the important issues raised in the books.

Allow me to conclude by offering my heartfelt thanks to the chapter authors, referees, and friends and colleagues who have helped me with encouragement and constructive criticism. The quality, extensiveness, and completeness of the work provided by the chapter authors have exceeded even my most optimistic expectations. Sincere appreciation is extended to Scott Cragin, who provided valuable help by patiently reviewing, formatting, and finalizing the chapters.

It is my sincere hope that a new generation of air quality scientists will use this book series as a tool to learn in two years what it took us twenty years to try to master. That would be a most satisfying accomplishment.

*Paolo Zannetti
Fremont, California*

About the Editor

Dr. Paolo Zannetti is the President of the EnviroComp Institute and EnviroComp Consulting, Inc. in Fremont, California. He received a Doctoral Degree in Physics from the University of Padova (Italy) and has managed a range of environmental projects throughout his professional career. With a specialization in air pollution and environmental modeling and software, Dr. Zannetti's experience has covered research and development studies, teaching, consulting, modeling software development, project management, editorial activities, and expert testimony. In addition to authoring in 1990 the first comprehensive textbook on this topic (*Air Pollution Modeling — Theories, Computational Methods and Available Software*), Dr. Zannetti has authored more than 200 publications, primarily for peer-reviewed journals and conference proceedings. For more information, visit <http://www.envirocomp.org/html/meetus/zannetti.htm>.

**BRITISH
LIBRARY**

About the Publishers

The EnviroComp Institute

The International Institute of Environmental Sciences and Environmental Computing (EnviroComp) is a nonprofit, Internet-based institute and software laboratory dedicated to the study of environmental sciences and pollution phenomena. Founded in 1996, the EnviroComp Institute also promotes the publication of a unique, new-generation series of environmental books in electronic format. For more information, visit the institute's Web site at <http://www.envirocomp.org>.

The Air & Waste Management Association

The Air & Waste Management Association (AWMA) is a nonprofit, nonpartisan professional organization that provides information, training, and networking opportunities to thousands of environmental professionals around the world. AWMA was founded in 1907 and is headquartered in Pittsburgh, Pennsylvania. For more information, visit the association's Web site at <http://www.awma.org>.

BRITISH
PAPER

About the Chapter Authors

([Additional information](#) is provided in the CD-ROM version)

Anfossi

Dr. Domenico Anfossi
CNR-ISAC Sezione di Torino
Corso Fiume 4
10133 Torino
ITALY

Phone: +39 011 6606376
Phone direct: +39 011 3839826
Fax: +39 011 6600364
Email: anfossi@to.infn.it and d.anfossi@isac.cnr.it
Work site: <http://www.isac.cnr.it>

Builtjes

Dr. Peter J.H. Builtjes
Professor
TNO Environment, Energy and Process Innovation
Department of Environmental Quality
Laan van Westenenk 501
P.O. Box 342
7300 AH Apeldoorn
THE NETHERLANDS

Phone: +31 555493038
Fax: +31 555493252
Email: p.j.h.builtjes@mep.tno.nl

Byun

Dr. Daewon W. Byun
Professor
312 Science & Research Bldg. 1
Geoscience Department
University of Houston
Houston, Texas 77204-5007
USA

Email: dwbyun@math.uh.edu

Canepa

Elisa Canepa, Ph.D.
Atmospheric and Oceanic Physics Group
INFN - Department of Physics
University of Genova
Via Dodecaneso 33
I-16146 Genova
ITALY

Phone: +39 010 353 6354
Email: elisa.canepa@fisica.unige.it
Work site: <http://www.fisica.unige.it/~atmosfe/>
Personal site: <http://www.fisica.unige.it/~canepae/>

Eastman

Joseph L. Eastman, Ph.D.
Research Faculty
UMBC/GEST
Hydrological Sciences Branch
NASA/GSFC Code 974
Building 33, Room A322
Greenbelt, MD 20771
USA

Phone: (410) 279-9702
Fax: (301) 614-5808
Email: eastman@hsb.gsfc.nasa.gov or
jleastman@comcast.net
Work site: <http://gest.umbc.edu/directory.html>

Keen

Professor Cecil S. Keen
Atmospheric Sciences / Geography (c/o Box 2)
Minnesota State University
Mankato, MN 56002-8400
USA

Phone: (507) 389-5169
Fax: (507) 345-1283
Email: cecil.keen@mnsu.edu
Work site: <http://www.mnsu.edu/weather>

Lacser

Avraham Lacser, Ph.D.
Israel Institute for Biological Research (IIBR)
POB 19
NESS ZIONA 74100
ISRAEL

Phone: +972 8 9381488
Fax: +972 8 9401404
Email: lacser@iibr.gov.il
Work site: <http://www.iibr.gov.il>

Lee

Russell Lee
Meteorologist
5806 Prosperity Church Road
Suite A2-128
Charlotte, NC 28269
USA

Phone: (704) 947-8024
Fax: (704) 947-8024
Email: Russell.Lee@RFLee.com
Work site: <http://www.RFLee.com>

Lyons

Walter A. Lyons, Ph.D., CCM
FORENSIC METEOROLOGY ASSOCIATES, Inc. (FMA)
46050 Weld County Road 13
Fort Collins, CO 80524
USA

Phone: (800) 854-7219
Fax: (970) 482-8627
Email: walyons@frie.com
Work site: <http://www.forensic-weather.com>

Moon

Dennis A. Moon, Ph.D.
Chief Scientist
SSESCO
Itasca Technology Exchange
201 NW 4th St.
Grand Rapids, MN 55744
USA

Phone: (218) 327-8844
Email: dmoon@ssesco.com
Work site: <http://www.ssesco.com>

- Moussiopoulos** Dr.-Ing. Nicolas Moussiopoulos
Professor and Laboratory Director
Laboratory of Heat Transfer and Environmental Engineering
Box 483, Aristotle University
GR-54124 Thessaloniki
GREECE
- Phone: +30 2310 996011
Fax: +30 2310 996012
Email: moussio@vergina.eng.auth.gr
Work site: <http://aix.meng.auth.gr/lhtee/>
Personal site: <http://www.envirocomp.org/html/meetus/moussio.htm>
- Nelson** Thomas E. Nelson
FMA Research, Inc.
Yucca Ridge Field Station
46050 Weld County Road
Fort Collins, CO 80524
USA
- Email: tnelson@frii.com
- Oettl** Dietmar Oettl
Institute for Internal Combustion Engines and
Thermodynamics
Graz University of Technology
Inffeldgasse 25
A-8010 Graz
AUSTRIA
- Phone: +43 316 873 8081
Email: oettl@vkmb.tu-graz.ac.at
Work site: <http://fvkma.tu-graz.ac.at>
- Reynolds** Steven D. Reynolds
Envair
12 Palm Avenue
San Rafael, CA 94901
USA
- Email: steve@sreynolds.com
Personal site: <http://www.sreynolds.com>

Roth

Philip M. Roth, Ph.D.
836 Fawn Drive
San Anselmo, CA 94960
USA

Phone: (415) 456-0333
Fax: (415) 456-3405
Email: pmr39@comcast.net

San Jose

Prof. Roberto San Jose
Director
Environmental Software and Modelling Group
Computer Science School - Technical University of Madrid
Campus de Montegancedo - Boadilla del Monte
28660 Madrid
SPAIN

Phone: +34 91 336 7465
Fax: +34 91 336 7412
Email: roberto@fi.upm.es
Work site: <http://artico.lma.fi.upm.es>

Sorbjan

Prof. Zbigniew Sorbjan
Department of Physics
Marquette University
Milwaukee, WI 53201
USA

Phone: (414) 288-7458
Fax: (414) 288-3989
Email: sorbjanz@mu.edu
Work site: <http://www.mu.edu/~sorbjanz>

Thé

Jesse Thé, Ph.D., P.Eng.
Lakes Environmental Software Inc.
306 Milla Court
Waterloo - Ontario - N2L 6N4
CANADA

Phone: (519) 746-5995
Fax: (519) 746-0793
Email: Jesse@WEBLAKES.com
Work site: <http://www.WEBLAKES.com>

Tourlou

Dr. –Eng. Paraskevi-Maria Tourlou
Hellenic Ministry of Transport and Communications
Land Transport Safety Directorate
Anastaseos 2 & Tsigante str.
GR-10191 Papagos, Athens
GREECE

Phone: +30 210 6508468 and 2310 996011
Fax: +30 210 6508493 and 2310 996012
Email: evelina@aix.meng.auth.gr
Work site: <http://aix.meng.auth.gr/lhtee/>

van Dop

Han van Dop, Ph.D.
Institute for Marine and Atmospheric Research Utrecht
(IMAU)
Princetonplein 5
P.O. Box 80005
NL-3508 TA Utrecht
THE NETHERLANDS

Phone: +31/0 030 253 3154
Fax: +31/0 030 254 3163
Email: h.vandop@phys.uu.nl
Personal site: <http://www.phys.uu.nl/~dop/>

Venkatram

Akula Venkatram, Ph.D.
Professor of Mechanical Engineering
A343 Bourns Hall
Riverside, CA 92521
USA

Phone: (909) 787-2195
Fax: (909) 787-2899
Email: venky@engr.ucr.edu
Personal Sites: <http://www.engr.ucr.edu/mechanical/people/venkatram.html>
<http://www.engr.ucr.edu/~venky/>

Yamartino

Dr. Robert J. Yamartino
191 East Grand Ave. #206
Old Orchard Beach, ME
USA

Email: rjy@maine.rr.com

Zannetti

Dr. Paolo Zannetti, QEP
President, EnviroComp Consulting, Inc. and The EnviroComp
Institute
2298 Ocaso Camino
Fremont, CA 94539
USA

Phone: (510) 490-3438

Fax: (510) 490-3357

Email: zannetti@envirocomp.com

Work site: <http://www.envirocomp.com> and

<http://www.envirocomp.org>

Personal site: <http://www.envirocomp.org/html/meetus/zannetti.htm>

БІЛГІЛІК
Тарау

Builtjes, P. (2003) *The Problem – Air Pollution*. Chapter 1 of *AIR QUALITY MODELING - Theories, Methodologies, Computational Techniques, and Available Databases and Software. Vol. I - Fundamentals* (P. Zannetti, Editor). Published by The EnviroComp Institute (<http://www.envirocomp.org>) and the Air & Waste Management Association (<http://www.awma.org>).

Chapter 1

The Problem – Air Pollution

Peter Builtjes

*TNO-MEP, Department of Environmental Quality, Apeldoorn, The Netherlands
and Free University Berlin, Department of Meteorology, Germany
p.j.h.builtjes@mep.tno.nl*

Abstract: An introduction is given about general aspects of air pollution. In addition, an overview is presented about the history of air pollution modeling.

Key words: Air pollution, Air pollution regulations, Air pollution modeling.

1 Our Natural Environment

Air pollution can be seen as the result of emissions of man-made, anthropogenic trace gases and particles into our environment.

The chemical composition of the current atmosphere differs considerably from the chemical composition of the natural atmosphere, as it existed in pre-industrial times. This means that, at the moment, nowhere on earth is there natural air, which could also be considered clean air. Our atmosphere is polluted everywhere, which means that the chemical composition differs from the pre-industrial situation.

The chemical composition of the natural atmosphere has shown gradual changes as long as the earth has existed. Life started on earth, in the oceans in fact, in an atmosphere that hardly contained any oxygen, only about 0.015% against the current level of about 21%. The atmosphere at that moment contained nearly 99% CO₂, some N₂, and only traces of H₂O and O₂. Because of the low oxygen level, no stratospheric ozone layer could have been formed. So, the surface of the earth received all the UV-B radiation that is captured these days by the ozone layer. This

also explains why life had to start in the oceans, at about 10 m below sea level - a depth where the UV-B radiation was substantially lower.

At first, life on earth, which started about 3 billion years ago, was plant-like and with the aid of photosynthesis-produced oxygen. This way, the oxygen level slowly increased in the atmosphere. This increase in oxygen contributed to the development of a stratospheric ozone layer, making life on the surface of the earth possible, about 400 million years ago. Although fluctuations may have occurred, for example in the oxygen level, with possible maximum values up to 23%, the overall chemical composition of the natural atmosphere, as far as we know, has been relatively stable over the last 10 million years.

The chemical composition of the pre-industrial/natural global averaged atmosphere is shown in table 1:

Table 1. The chemical composition of the natural atmosphere.

	Gas	% by volume	ppm	ppm by the year 2000
Nitrogen	N ₂	78.1		
Oxygen	O ₂	20.9		
Argon	Ar	0.92		
Neon	Ne		18.2	
Helium	He		5.2	
Krypton	Kr		1.14	
Xenon	Xe		0.09	
Carbon dioxide	CO ₂		280.0	360.0
Methane	CH ₄		0.750	1.75
Nitrous oxide	N ₂ O		0.270	0.310

The composition given in table 1 is that of the dry atmosphere. H₂O-vapour has a concentration fluctuating between 40 ppm and 40,000 ppm (4%).

The ecosystem “life” created the chemical composition of the atmosphere in which this ecosystem can exist, i.e., a chemical composition in which life can sustain. The chemical composition with its high oxygen level is not in chemical equilibrium, but this non-equilibrium state can be maintained by life itself.

Based on this fact, James Lovelock developed the Gaia-theory (Gaia, the Greek goddess of the earth), [Lovelock (1972, 1979)]. In short, his theory states that the earth, including the atmosphere, is a 'living', homeostatic organism. In contrast, the surrounding planets where there is no life, Venus and Mars, have a completely different chemical composition, which is in chemical equilibrium (their atmosphere contains about 99% CO₂, some N₂, and nearly no O₂ and H₂O).

In other words, our atmosphere is a very special one, and we should handle it with care.

2 Air Pollution, Some Definitions

There are several conceivable approaches to define air pollution. For example, the change in the global, chemical composition of the pre-industrial atmosphere, as given in Table 1, and which is due to human influence, can be called air pollution; all man-made, anthropogenic emissions into the air can be considered air pollution. So air pollution - but at a very local scale, not detectable at a global scale - did not start until mankind started 'to play with fire'.

The global increase in the concentrations of CO₂, CH₄ and N₂O (shown in Table 1), all greenhouse gases, could, and should be called 'air pollution' in the broad sense, even though these species are not toxic for human beings and the ecosystem.

Another approach is to distinguish between the emissions of safe, non-toxic, and harmful compounds, and only consider the last as air pollution. This distinction, however, has two clear drawbacks. About 1940 and even much later, manmade emissions of CFCs were considered safe because they are inert in the troposphere. However, the decrease of the stratospheric ozone layer has taught us differently. In the same way, CO₂ emissions are safe in the sense that they are not toxic, but their increase leads – most likely – to a climate change, which in turn will be harmful to large parts of the ecosystem.

The second drawback is that natural emissions can also be harmful, such as emissions of dioxine caused by a forest fire as a result of lightning.

Next to anthropogenic emissions, it is possible to distinguish between natural emissions and biogenic emissions.

Natural emissions should be defined as emissions caused by the non-living world, such as volcanic emissions, sea-salt emissions, and natural fires.

Biogenic emissions are emissions resulting from the ecosystem, like VOC-emissions from forests, and CH₄-emissions from swamps. In principle, natural and biogenic emissions lead to the chemical composition of the pre-industrial, natural atmosphere.

The philosophical question [whether manmade emissions should also be considered as biogenic, because man is part of the ecosystem] can be retorted by the distinction that mankind, by making fires, creates anthropogenic emissions.

Although the distinction in these three categories: anthropogenic, natural, and biogenic could be useful, quite a number of intermediate emissions exist. Examples are the NO-emissions by soil bacteria, which is a function of the earlier deposited

nitrogen on the soil due to anthropogenic emissions of N-compounds or earlier deposited manure containing nitrogen. There is the question of whether or not VOC-emissions are due to planting or not planting of trees, and whether or not dust-emissions are the consequence of paving or not paving sandy roads. These are such intermediate emissions, biogenic or natural, but with a clear human influence.

Although anthropogenic emissions started when man learned to make fire, and the air quality, especially the concentrations of fine particles, surpassed air quality guidelines in and around the cave dwellings of the Neanderthal man, the impact of air pollution has been of a local character for a long time.

In Europe, elevation of concentration levels occurred for the first time in the middle ages, resulting in the first laws on air pollution that were often focused on odor nuisance around local factories. Also, burning coal for heating and cooking led to air pollution, until well into the last century. London for example, was 'famous' for its fog. Subsequently, the industrial revolution involved a tremendous increase in the use of fossil fuel. Consequently, as from about 1850, a number of gases started to increase in concentration, like the gases mentioned in Table 1 - CO₂, CH₄ and N₂O – and in addition, for example, sulfate aerosols.

It should be emphasized here that air pollution in the strict sense ('toxic') and global (climate) change are interrelated phenomena. Directly, because they often have the same emission sources, and more indirectly because species like tropospheric ozone and aerosols play a role both in local and regional air quality, as well as in climate change.

3 Primary and Secondary Pollutants

The main, primary – i.e., directly emitted – gaseous pollutants are the following:

- Carbon compounds, e.g. CO₂, CO, CH₄, the VOC's (volatile organic compounds)
- Nitrogen compounds, e.g. N₂O, NO, NH₃
- Sulfur compounds, e.g. SO₂, H₂S
- Halogen compounds, e.g. chlorides, fluorides, bromides

The main, primary particle pollutants are the following:

- Particles smaller than 2.5 μm in diameter. Included are the Aitken nuclei, particles smaller than 0.1 μm in diameter, which grow rather fast by coagulation to larger particles. The chemical composition of these primary particles is, to a large extent, carbon but also heavy metals as iron, zinc, copper, etc will also be contained in these particles.
- Particles with a diameter from 2.5 to 10 μm. These larger particles are often composed of sea salt and dust.

Most air pollutants, except the halogen compounds, will be chemically transformed in the troposphere by the OH-radical. The OH-radical is formed in the troposphere by photo-dissociation of O_3 , and subsequent reaction of oxygen with H_2O -vapour to OH (Levy, 1971). The OH-radical reacts not with N_2 , O_2 , H_2O , CO_2 , but with other compounds as CO , CH_4 , H_2 , NO , NO_2 , SO_2 , NH_3 . The OH-radical can be seen as the cleansing agent of the atmosphere, since it transforms primary air pollutants into secondary pollutants, which are subsequently removed from the atmosphere by dry and wet deposition. In this way the OH-radical determines the atmospheric residence time of most compounds in the atmosphere.

The main, secondary (i.e., formed in the atmosphere) gaseous pollutants are:

- NO_2 and HNO_3 formed from NO
- O_3 formed through photochemical reactions

The main, secondary particles are:

- Sulfate aerosols formed from SO_2 , and Nitrate aerosols formed from NO_2 followed by the reaction with NH_3 to form ammonium (bi) sulfate and ammonium nitrate.
- Organic aerosols formed from gaseous organic compounds.

These secondary particles consist mainly of small particles with a diameter less than $2.5 \mu m$.

4 A Short History of Air Pollution Modeling

Because the focus of Volume I is on air pollution modeling, we now give a short history of air pollution modeling up to about 1980.

Air pollution modeling is an attempt to describe the causal relation between emissions, atmospheric concentrations, and deposition. Air pollution measurements give quantitative information about concentrations and deposition, but they can only give the levels at specific locations. In principle, air pollution modeling can give a more complete and consistent description, including an analysis of the causes - emissions sources, meteorological processes, physical and chemical transformations - that have led to these concentrations/deposition.

Air pollution models play an important role in science, because of their capability to assess the importance of the relevant processes. Air pollution models are the only method that quantifies the relationship between emissions and concentrations/depositions, including the consequences of future scenarios and the determination of the effectiveness of abatement strategies.

The concentrations of species in the atmosphere are determined by transport and diffusion. This means that in considering the history of air pollution modeling,

some remarks should be made concerning transport and diffusion. Transport phenomena, characterized by the mean velocity of the fluid, have been measured and studied for centuries. For example, the average wind was studied for sailing purposes. The study of diffusion (turbulent motion) is more recent. Although turbulent motions have been observed from the moment people looked at rivers and streams, one could mention Reynolds' paper in 1895 as the scientific starting point for the formulation of the famous criterion for laminar-to-turbulent flow transition in pipes.

One of the first articles in which turbulence in the atmosphere is mentioned was published by Taylor (1915). In later years, he developed the 'Taylor-theory of turbulent diffusion', Taylor (1921). In this theory, it is shown that the diffusion from a point source can only be described with a constant eddy diffusivity, K , for travel times, which are much larger than the turbulent integral time scale, the so-called diffusion limit. For smaller time-scales the effective turbulent diffusivity is proportional to the travel time.

Until about 1950, a number of studies were performed on the subject of diffusion in the atmosphere (Richardson et al., 1925; Sutton, 1932; Bosanquet, 1936; Church, 1949; Thomas et al., 1949; Inoue, 1950; Batchelor, 1950). Already, the paper by Richardson considered long-range aspects; up to over 80 km. Bosanquet is one of the first who published about the impact of chimney plumes. A paper by Chamberlain (1953) already considered the deposition of aerosols.

4.1 Modeling of Point Sources

The study of the dispersion from low and high level point sources, especially experimental, was a major topic shortly after 1955. Papers on this subject appeared by Smith (1957), Gifford (1957 a, b), Hay and Pasquill (1957), Record (1958) and Haugen (1959) both devoted to the Prairie grass experiment, Stewart (1958), Monin (1959), Ogura (1959). Perhaps the first paper on this subject was by Roberts (1923).

The publication by Pasquill 'Atmospheric Diffusion', which appeared in 1962, was a major milestone in summarizing the work performed until that moment. It illustrates that air pollution modeling around the beginning of the sixties was focused on local dispersion phenomena, mainly from point sources with SO_2 as major component in the application studies.

The Gaussian plume model was formulated, in which the horizontal and vertical spread of the plume was determined experimentally. Tables appeared with the famous Pasquill-Gifford sigma-values in the horizontal and vertical direction, and as a function of the atmospheric stability ranging from very stable, class F, up to very unstable, class A. The experimental sigma values are in their functions with distance from the source in reasonable agreement with the Taylor-theory. The

differences are caused by the fact that the Taylor-theory holds for homogeneous turbulence, which is not the case in the atmosphere.

In the sixties, the studies concerning dispersion from a point source continued and were broadening in scope. Major studies were performed by Högstrom (1964), Turner (1964), Briggs (1965) - the famous plume-rise formulas -, Moore (1967), Klug (1968). The use and application of the Gaussian plume model spread over the whole globe, and became a standard technique in every industrial country to calculate the stack height required for permits, see for example Beryland (1974) who published a standard work in Russian. The Gaussian plume model concept was soon applied also to line and area-sources. Gradually, the importance of the mixing height was realized (Holzworth, 1967, Deardorff, 1974) and its major influence on the magnitude of ground level concentrations.

In reviewing the air pollution modeling papers published in the sixties and seventies, these papers appear to be mainly written by meteorologists, specialized in boundary layer meteorology and atmospheric turbulence. These studies focused often on the effect of atmospheric stability on plume spread. During the next decade, besides research on local dispersion (for a good overview, see Nieuwstadt and van Dop, 1982), the spatial scale of air pollution modeling increased substantially.

4.2 Air Pollution Modeling at Urban and Larger Scales

Shortly after 1970, scientists began to realize that air pollution was not only a local phenomenon. It became clear - firstly in Europe - that the SO_2 and NO_x emissions from tall stacks could lead to acidification at large distances from the sources. It also became clear - firstly in the US - that ozone was a problem in urbanized and industrialized areas. And so it was obvious that these situations could not be tackled by simple Gaussian-plume type modeling.

Two different modeling approaches were followed, Lagrangian modeling and Eulerian modeling. In Lagrangian modeling, an air parcel is followed along a trajectory, and is assumed to keep its identity during its path. In Eulerian modeling, the area under investigation is divided into grid cells, both in vertical and horizontal directions.

Lagrangian modeling, directed at the description of long-range transport of sulfur, began with studies by Rohde (1972, 1974), Eliassen (1975) and Fisher (1975). The work by Eliassen was the start for the well-known EMEP-trajectory model which has been used over the years to calculate trans-boundary air pollution of acidifying species and later, photo-oxidants. Lagrangian modeling is often used to cover longer periods of time, up to years.

Eulerian modeling began with studies by Reynolds (1973) for ozone in urbanized areas, with Shir and Shieh (1974) for SO_2 in urban areas, and Egan (1976) and

Carmichael (1979) for regional scale sulfur. From the modeling studies by Reynolds on the Los Angeles basin, the well-known Urban Airshed Model-UAM originated. Eulerian modeling, in these years, was used only for specific episodes of a few days.

So in general, Lagrangian modeling was mostly performed in Europe, over large distances and longer time-periods, and focused primarily on SO₂. Eulerian grid modeling was predominantly applied in the US, over urban areas and restricted to episodic conditions, and focused primarily on O₃. Also hybrid approaches were studied, as well as particle-in-cell methods (Sklarew et al., 1971). Early papers on both Eulerian and Lagrangian modeling are by Friedlander and Seinfeld (1969), Eschenroeder and Martinez (1970) and Liu and Seinfeld (1974).

A comprehensive overview of long-range transport modeling in the seventies was presented by Johnson (1980).

The next, obvious step in scale is global modeling of earth's troposphere. The first global models were 2-D models, in which the global troposphere was averaged in the longitudinal direction (see Isaksen, 1978). The first, 3-D global models were developed by Peters (1979) (see also Zimmermann, 1988).

It can be stated that, since approximately 1980, the basic modeling concepts and tools were available to the scientific community. Developments after 1980 concerned the fine-tuning of these basic concepts.

5 Air Pollution Regulations

In Europe, the European commission has developed a general “Mother” directive to consider ambient air pollution. Derived from it, “Daughter” directives have been formulated for SO₂, NO₂, particulate matter-PM, lead, and tropospheric ozone. These directives give limit values and also define the reporting requirements for the countries, and the monitoring methods and number of observations.

Air pollution modeling can be used as an integral part of the description of the air quality situation in the member countries. More information can be found on <http://europe.eu.int/comm/environment/air/ambient.htm>.

Under the UN-ECE, protocols have been defined to reduce trans-boundary air pollution. Air pollution modeling is an essential part for these long-range transport calculations, which include “blame-matrices” and the calculation of cost-effective abatement strategies. More information can be found at <http://www.emep.int>.

The new developments in air pollution research and modeling that are used to formulate air pollution regulations in Europe can be found in the EUROTRAC-project.¹

References

- Batchelor, G.K., 1950, The application of the similarity theory of turbulence to atmospheric diffusion *Quart. J.R.Met.Soc.* 76:133.
- Beryland, M.Y., 1975, Contemporary problems of atmospheric diffusion and pollution of the atmosphere. Gidrometezdat, Leningrad, translated into English by NERC, US EPA.
- Bosanquet, C.H., and Pearson, J.L., 1936, The spread of smoke and gases from chimneys *Trans. Faraday Soc.* 32:1249.
- Briggs, G.A., 1965, A plume rise model compared with observations *J.Air Poll. Control Association* 15:433.
- Carmichael, G.R., and Peters, L.K., 1979, Numerical simulation of the regional transport of SO₂ and sulfate in the eastern United States, Proc. 4 th *Symp. on turbulence, diffusion and air pollution*, AMS 337.
- Chamberlain, A.C., 1953, Aspects of travel and deposition of aerosol and vapour clouds A.E.R.E., HP/R 1261, H.M.S.O.
- Church, P.E., 1949, Dilution of waste stack gases in the atmosphere *Ind.Eng. Chem.* 41:2753.
- Deardorff, J.W., and Willis, G.E., 1975, A parameterization of diffusion into the mixed layer *J. Appl. Met* 14:1451.
- Deardorff, J.W., 1970, Convective velocity and temperature scales for the unstable planetary boundary layer and for Rayleigh convection. *J. Atm. Sci.* 27, 1211-1213.
- Dyun, D.W. and J.K.S. Ching, 1999, Science algorithm of the EPA Models-3 Community Multiscale Air Quality (CMAQ) Modeling System., EPA-Dep./600/R-99/030.
- Egan, B.A., Rao, K.S., and Bass, A., 1976, A three dimensional advective-diffusive model for long-range sulfate transport and transformation 7 th *ITM*, 697, Airlie House.
- Eliassen, A., and Saltbones, J., 1975, Decay and transformation rates of SO₂ as estimated from emission data, trajectories and measured air concentrations *Atm. Env.* 9:425.
- Eschenroeder, A.Q. and J.R. Martinez, 1970, "Mathematical Modeling of Photochemical Smog", American Institute Aeronautics and Astronautics (Proceedings), Eight Aerospace Sciences Meeting, New York, Jan 19-21.
- Fisher, B.E.A., 1975, The long-range transport of sulfur dioxide, *Atm.Env.* 9,: 1063.
- Friedlander, S.K. and J.H. Seinfeld, 1969, A Dynamic Model of Photochemical Smog, *Environ., Science Technol.*, 3, 1175 (1969).

¹ <http://www.gsf.de/eurotrac>

- Gifford, F.A., 1957a, Relative atmospheric diffusion of smoke plumes *J. Met.* 14:410.
- Gifford, F.A., 1957b, Further data on relative atmospheric diffusion *J. Met.* 14:475.
- Haugen, D.A., 1959, Project Prairie grass, a field programme in diffusion *Geographical research paper* 59, vol III, G.R.D.A.F.C., Bedford, Mass.
- Hay, J.S., and Pasquill, F., 1957, Diffusion from a fixed source at a height of a few hundred feet in the atmosphere *J. Fluid Mech.* 2:299.
- Högstrom, U., 1964, An experimental study on atmospheric diffusion *Tellus*, 16:205.
- Holzworth, G.C., 1967, Mixing depth, wind speed and air pollution potential for selected locations in the U.S.A., *J.Appl.Met.* 6:1039.
- Inoue, E., 1950, On the turbulent diffusion in the atmosphere *J.Met.Soc.* Japan, 28:13.
- Isaksen, I.S.A., and Rohde, H., 1978, A two-dimensional model for the global distribution of gases and aerosol particles in the troposphere *Rep. AC-47*, Dep. of Meteor. Univ Stockholm, Sweden.
- Junge, C.E., 1963, Air chemistry and radioactivity, *academic press*, New York, London.
- Johnson, W.B., 1980, Interregional exchange of air pollution: model types and applications *10 th ITM*, 3, Amsterdam.
- Klug, W., 1968, Diffusion in the atmospheric surface layer: comparison of similarity theory with observations *Quart. J.R. Met.Soc.* 94:555.
- Kolmogorov, A.N., 1941, The local structure of turbulence in incompressible viscous fluid for very large Reynolds numbers, *C.R. Acad. Sci. U.R.S.S.*, 30, 301.
- Lamb, R.G. and J.H. Seinfeld, 1973. Mathematical modeling of urban air pollution - General theory. *Envir. Sci. Technol.* 7, 253-261.
- Levy, H., 1971, Normal atmosphere: large radical and formaldehyde concentrations predicted *Science* 173:141.
- Liu, M.K. and J.H. Seinfeld, 1974, On the Validity of Grid and Trajectory Models of Urban Air Pollution, *Atmos. Environ.*, Vol. 9, pp. 555-574.
- Lovelock, J.E. Gaia as seen through the atmosphere *Atm. Env.* 6,579, 1972
- Lovelock, J.E. Gaia, a new look at life on earth' Oxford Univ. Press, 1979
- Monin, A.S., 1959, Smoke propagation in the surface layer of the atmosphere Atmospheric diffusion and air pollution, ed. Frenkiel and Sheppard, advances in *Geophysics*, 6:331, Academic Press.
- Monin, A.S., 1955, The equation of turbulent diffusion, *Dokl. Akad. Naak.*, 105, 256.
- Moore, D.J., 1967, Physical aspects of plume models *Atm.Env.* 1:411.
- Nieuwstadt, F.T.M., and Dop, H. van, 1982, Atmospheric turbulence and air pollution modeling, D.Reidel Publish. Comp.

Ogura, Y., 1959, Diffusion from a continuous source in relation to a finite observation interval' Atmospheric diffusion and air pollution, ed. Frenkiel and Sheppard, advances in Geophysics 6,149, Academic Press.

Pasquill, F., 1962, Atmospheric diffusion *Van Nostrand*, New York.

Peters, L.K., and Jouvanis, A.A., 1979, Numerical simulation of the transport and chemistry of CH₄ and CO in the troposphere, *Atm.Env.* 13:1443.

Record, F.A., and Cramer, H.E., 1958, Preliminary analysis of Project Prairie grass diffusion measurements *J.Air Poll.Cont.Ass* 8:240.

Reynolds, S., Roth, P., and Seinfeld, J., 1973, Mathematical modeling of photochemical air pollution *Atm.Env* 7.

Reynolds, O., 1895, On the dynamical theory of incompressible viscous fluids and the determination of the criterion Phil. *Transactions of the Royal Soc. of London.* series A, 186:123.

Richardson, L.F., and Proctor, D., 1925, Diffusion over distances ranging from 3 to 86 km. *Memoirs of the R.Met. Soc.*, vol 1:1.

Roberts, O.F.T., 1923, The theoretical scattering of smoke in a turbulent atmosphere Proc. Roy. Soc. A, 104, 640.

Rohde, H., 1972, A study of the sulfur budget for the atmosphere over northern Europe *Tellus*, 24:128.

Rohde, H., 1974, Some aspects of the use of air trajectories for the computation of large scale dispersion and fallout patterns Adv. in *Geophysics* 18B: 95, academic press.

Roth, P.M., P.J.W. Roberts, J.K. Liu, S.D. Reynolds and J.H. Seinfeld, 1974, Mathematical Modeling of Photochemical Air Pollution - Part II. A Model and Inventory of Pollutant Emissions, *Atmos. Environ.*, Vol. 8, pp. 97-130.

Seinfeld, J.H., 1986, Atmospheric chemistry and physics of air pollution, *John Wiley & Sons*.

Shir, C.C. and L.J. Shieh, 1974, A generalized urban air pollution model and its application to the study of SO₂-distribution in the St. Louis Metropolitan area, *J. Appl. Met.* 19, 185-204.

Sklarew, R.C. et al., 1971, A particle-in-cell method for numerical solution of the atmospheric diffusion equation and application to air pollution problems; *Systems, Science and Software*, Ca-Reg 35R-844, Vol I.

Smith, F.B., 1957, The diffusion of smoke from a continuous elevated point source into a turbulent atmosphere *J.Fluid Mech.* 2:49.

Stewart, N.G. et al., 1958, The atmospheric diffusion of gases discharged from the chimney of the Harwell Pile *Int J.Air Poll.* 1:87.

Sutton, O.G., 1932, A theory of eddy diffusion in the atmosphere *Proc. Roy. soc. A*, 135:143.

Taylor, G.I., 1915, Eddy motion in the atmosphere Phil. *Transactions of the Royal Soc. of London.* Series A, 215:1.

Taylor, G.I., 1921, Diffusion by continuous movements *proc. London Math. soc.* 20:196.

Thomas, M.D., et al., 1949, Dispersion of gases from tall stacks *Ind. and En. Chemistry*, 41:2409.

Turner, D.B., 1964, A diffusion model for an urban area *J.Appl. Met.* 3:83.

Warneck, P., 1988, Chemistry of the natural atmosphere, *Int.Geoph.Series* 41, Academic Press.

Willis and Deardorff, 1978, A laboratory study of dispersion from elevated source within a modeled convection mixed layer, *Atm. Env.* 12, 1305-1311.

Zimmermann, P.H., 1988, Moguntia: a handy global tracer model *17 th ITM.* 593, Cambridge.

Roth, P. M. and S. D. Reynolds (2003) *The Tool – Mathematical Modeling*. Chapter 2 of *AIR QUALITY MODELING - Theories, Methodologies, Computational Techniques, and Available Databases and Software. Vol. I - Fundamentals* (P. Zannetti, Editor). Published by The EnviroComp Institute (<http://www.envirocomp.org/>) and the Air & Waste Management Association (<http://www.awma.org/>).

Chapter 2

The Tool – Mathematical Modeling

Philip M. Roth and Steven D. Reynolds

Envair

Marin County, California, USA

pmr39@comcast.net and steve@sreynolds.com

Abstract: This chapter addresses modeling background – needs and concepts - and definitions in a brief survey. Topics include uses of models (regulatory compliance and resolution of litigation), categorization of model by general type (Gaussian and grid-based), general governing equations, categories of model inputs, types of solutions of equations, alternative model formulations, spatial and temporal scales addressed and resolutions adopted, types of uncertainty of concern, experience and current and proposed approaches to evaluation of model performance, and data needs.

Key Words: Gaussian model, photochemical models, grid-based models, air quality modeling, simulation models, emissions modeling, dispersion modeling, chemical transformation, regulatory application, resolution, uncertainty, model performance evaluation, data needs.

1 Why Air Quality Modeling

Understanding the relationship between primary pollutant emissions and air quality, represented by the ambient concentrations of atmospheric pollutants, is essential to developing emissions control strategies. The better this understanding is achieved, the more effective will be the strategies and the greater the opportunity for minimizing control costs while maintaining an acceptably low risk of exceeding a NAAQS. Federal ambient standards exist for 8 pollutants and pollutant groups: CO, SO₂, NO₂, ozone, fine particles, particles less than 10 microns in diameter (PM₁₀), total suspended particles (TSP) and lead. In some cases the emissions-ambient concentration (e/ac) relationship is reasonably straightforward: linear, proportional, scalable. In others it is extremely complex: nonlinear, controlled either by a number of key chemical reactions or by mixing

rates, and necessitating an understanding of a range of dynamic phenomena, such as deposition rates and emissions of biogenic species.

Air quality simulation models (AQSMs) provide a means for relating emissions and air quality. They range in form from quite simple to extremely complex. Many types have been developed during the past three decades. However, two have emerged as the main types in use: (a) the Gaussian model, for use in simulating dynamic plumes, and (b) the grid-based photochemical AQSM, for use originally in simulating ambient ozone concentrations, and more recently for aerosols, SO₂ and its reaction products, and other reactive pollutants. The framework of the grid-based model, omitting chemistry, is also being used to simulate CO concentration fields.

The main premises in adopting models for use are that:

- they will serve as accurate estimators of air quality for any selected combinations of emissions
- the time, cost, and staffing requirements that attend their use will be commensurate with the need, and
- if the accuracy of estimates falls short, the model deficiencies will be correctable within the availability of the resources

Presuming that a suitable model is available, it may see a number of uses:

- Regulatory planning and analysis, such as the preparation of federal and state implementation plans (FIPs and SIPs)
- Estimation of uncertainties through sensitivity analysis
- Planning for the conduct of field studies, and
- Identification of research and development needs

The most common and most critical use is modeling to support FIP and SIP preparation. Generally, planners attempt to ensure that recommendations for emissions controls are consistent with emissions control requirements formulated through modeling. Consequently, participants in the planning process have an interest in models being as accurate as possible. Oftentimes, then, focus is on improving simulation accuracy, evaluating model performance, conducting sensitivity studies and uncertainty analyses, and simulating alternative emissions control scenarios. If these steps can be conducted with satisfaction, the planner's job is greatly facilitated.

2 Modeling Categorized

2.1 Applications of Models

Air quality simulation models are employed in a wide variety of applications, most of which are associated with local, state or federal regulatory requirements.

2.1.1 Dispersion Modeling

The primary focus of dispersion modeling is estimation of ambient concentrations of primary pollutants that have been dispersed in the atmosphere through turbulent diffusion. Strictly speaking, this modeling category applies to pollutants that do not undergo atmospheric chemical transformation. However, it also applies for pollutants for which simple assumptions are incorporated to mirror chemical transformation, such as linear decay terms.

Models in use include:

- The Gaussian formula in one of its many manifestations. This formula represents the first of the commonly used models, and is applied primarily to plumes, both individual and multiple. If circumstances permit, it may also be applied to groups or aggregations of sources. Also, the Gaussian formula can be written in a form to simulate the dispersion of individual puffs, instead of plumes.
- The approximate solution of the governing equation of mass conservation, which includes a simplifying assumption that relates turbulent fluxes, $\langle u'c' \rangle$, to concentration gradients, $\partial c / \partial x_i$, through the adoption of an eddy diffusivity, K_i ,

$$\langle u'c' \rangle = -K_i \left(\partial c / \partial x_i \right) \quad (1)$$

This equation is commonly applied for more widely or uniformly distributed pollutants such as carbon monoxide (CO), where large individual plumes are not dominant.

- An approximate solution of the governing equations of mass conservation in a coordinate system that moves with the average wind velocity – the so-called “trajectory model”. The solutions in the fixed and moving coordinate systems are related. They differ in that certain assumptions are made for the trajectory model that do not apply for the “gridded model”, notably neglect of horizontal wind shear, horizontal turbulent diffusion, and vertical advective transport (Liu and Seinfeld, 1974). Also, acceptance of the trajectory model implies that parcel integrity is reasonably maintained for the length of time of the model simulation.
- The solution of the governing equation of mass – usually in parallel with the governing equation of momentum – using more rigorous and complex procedures, and thus avoiding the application of K-theory. Such models tend to be research models, in development, computing-intensive, and one-of-a-kind. They are not in common use.

2.1.2 Modeling of Chemical Transformations

By far the most common approach is through use of coupled mass balance equations incorporating K-theory, one for each pollutant that is being modeled. Virtually all models now in use for estimating tropospheric ozone concentrations and the concentrations of secondary fine particles are based on these equations, with differences among models being in the submodels or modules for one or more dynamic processes, such as transport, chemistry, and deposition, and in the numerical integration procedure. These models are used for SIP and FIP preparation, regional planning, and other regulatory applications.

Trajectory models are also used in special applications. However, each assumption noted earlier still must be considered; in most situations encountered they will not all apply.

2.1.3 Modeling of Pollutant Deposition

Generally, the same family of models, based on the governing equation of mass conservation, is used to estimate deposition fluxes as a function of location, and integrated over time, the accumulation of deposited material. Use of the “non-reactive” form of the model, incorporating simplifying assumptions, allows for calculation over longer simulated times at reasonable computational times. Deposition calculations, less common than the calculation of ambient concentrations, are of interest for estimation of:

- acidic deposition and acid loadings over a seasonal period
- ecosystem impacts of air pollutants, such as deposition of nitrogen compounds onto sensitive watersheds, and
- contributions to accumulation of pollutants in lakes and subsequent eutrophication

The sub-models or modules that address deposition can vary greatly in formulation, rigor, and level of detail. In the past, several of the simulation models in use incorporated rather primitive treatments of deposition. More recently, improved algorithms have been developed and included in models. Nevertheless, considerable uncertainty attends deposition estimates.

2.1.4 Modeling of Adverse Impacts

The objective of modeling “impacts”, in contrast to ambient concentrations, is to examine more directly certain selected effects. An example mentioned earlier is the estimation of acidic fluxes. Health effects of pollution are, of course, a major issue as far as adverse impacts are concerned.

Visibility degradation also falls under the heading of “impacts”, as does ecosystem loading. Again, the same category of models – solution of one or more of the governing equations of mass conservation – serves as the most common

approach for such analyses, incorporating those modifications or additions needed to address the specific effect. For example, in the case of visibility degradation (an adverse effect of pollution, in the sense that visibility impairment does not allow a full enjoyment of vistas, especially in high sensitive areas, such as National Parks), a post-calculation algorithm is included to convert estimated concentrations into a measure of visibility impairment. This general category of modeling is experiencing increasing use because the range of issues now being examined in the regulatory arena is broadening.

Note that for all modeling applications, spatial extent is a key attribute. Early applications tended to be limited to urban or metropolitan scale. Today regional scale is of primary concern because of the recognition that pollutant problems are not confined to a local area, but can extend for many hundreds of miles and include a number of emissions centers. Modeling outlined here applies in principle at local to regional – and in some cases – subcontinental scales.

2.2 Estimating Inputs to Air Quality Simulation Models

Three major categories of information are required to formulate inputs to models: air quality, emissions, and meteorology. Consequently, it is appropriate to think in terms of *a modeling system*, as depicted in Figure 1 and not only an air quality model. Emissions and meteorological information, as well as boundary and initial conditions must be supplied to the air quality model, as shown by the flows in the figure.

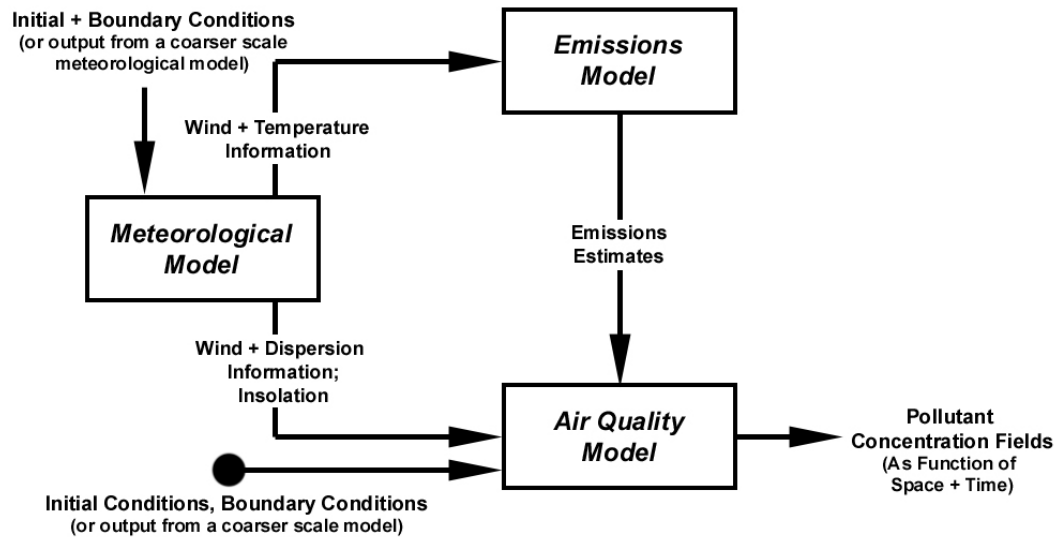


Figure 1. The Air Quality Modeling System.

Boundary and initial conditions are needed to drive models based on conservation of mass. Boundary conditions are generally difficult to estimate, data are sparse, and often no independent means of estimation exists. The two primary approaches to estimation include acquisition of data at the inflow boundaries, both

upwind and overhead, and estimation using a model of much broader spatial scale but coarser spatial resolution.

Emissions are estimated using a wide array of options, from hand-counts and bookkeeping to sophisticated modeling. Where possible, computer-based emissions models and management of emissions data are used – to insure uniformity of procedure, reduce error rates, greatly enhance data handling, and increase the rate at which estimation is conducted. Even for a given geographical application, a wide range of approaches to emissions estimation – for the different emissions categories – might be adopted.

In the early stages of air quality modeling, simple approaches to estimation of meteorological variables were prevalent – from hand-prepared wind maps to the use of straightforward diagnostic models, the latter including parameterized treatments of key variables. More recently, prognostic models have been widely accepted for use. These models are based on solving the equations of conservation of mass, energy, and momentum. They have proven to be quite helpful and an excellent complement to the use of air quality models based on the equations of mass conservation.

2.3 Categories of Air Quality Models Primarily in Use

The primary models (and modeling systems) in use today are those based on the numerical integration of the equations of conservation of mass and those based on the Gaussian formula, the latter for a range of source configurations and extensions of the basic equation.

2.3.1 Numerical Solution of the Equations of Conservation of Mass

The governing equations of conservation of mass are given by:

$$\begin{aligned} \frac{\partial c_i}{\partial t} + u_x \frac{\partial c_i}{\partial x} + u_y \frac{\partial c_i}{\partial y} + u_z \frac{\partial c_i}{\partial z} = \frac{\partial}{\partial x} \left(K_x \frac{\partial c_i}{\partial x} \right) + \frac{\partial}{\partial y} \left(K_y \frac{\partial c_i}{\partial y} \right) + \frac{\partial}{\partial z} \left(K_z \frac{\partial c_i}{\partial z} \right) \\ + R_i(c_1, c_2, \dots, c_n) + E_i(x, y, z, t) - S_i(x, y, z, t) \end{aligned} \quad (2)$$

where: u_x, u_y, u_z = velocity
 c_i = concentration of i^{th} species
 R_i = chemical generation rate of species i
 E_i = emissions flux
 S_i = removal flux

Emissions, meteorological, and air quality fields are provided as inputs, and the equations are integrated forward numerically in time to produce pollutant concentration fields.

Note that in special circumstances the simpler trajectory solution may apply. However, the trajectory model is not currently accepted for general use for regulatory applications in the US.

2.3.2 Gaussian Models

The basic Gaussian equation,

$$c(x, y, z) = \frac{q}{2\pi \bar{u} \sigma_y \sigma_z} \exp\left(-\frac{y^2}{2\sigma_y^2}\right) \cdot \left[\exp\left(-\frac{(z-h)^2}{2\sigma_z^2}\right) + \exp\left(-\frac{(z+h)^2}{2\sigma_z^2}\right) \right] \quad (3)$$

where: q = source strength
 h = stack height
 σ_y, σ_z = lateral and vertical dispersion coefficients

is a solution to the equation of mass conservation where conditions are steady state ($\partial c / \partial t = 0$), velocity \bar{u} is constant, and diffusion in the x-direction can be neglected. [See Seinfeld and Pandis, 1998, section 18-1 to 18-2, for a full derivation.] Many variants of the Gaussian plume and puff formulas exist; formulas for individual sources are summarized in Seinfeld and Pandis, section 18-3.

These two approaches to modeling dominate applications today and have done so for the past two decades. Consequently, these formulations and supporting emissions and meteorological modeling will receive the preponderance of attention in this book.

3 Modeling the Atmosphere

3.1 Deterministic Modeling and Stochastic Processes

The atmosphere is stochastic; transport and dispersion exhibit random behavior. Thus, for a given set of parameters – temperature profiles, average wind velocity, solar radiation, surface roughness – different manifestations might occur in the atmosphere, purely dependent on random events. Consequently, model outputs should in principle be expressed as distributions that display the random character of the variables of interest. In fact, all models in use are deterministic; they display the average behavior of the spectrum of random outcomes that might occur. Those using models or their results should be aware of this aspect of their formulation.

3.2 Modeling Representative Conditions vs. A Long-Term Time Record

Typically, modeling is conducted for average conditions or for a limited period of time, sometimes termed “an episode”. A great deal can be learned from such an exercise, and the results themselves are generally useful. However, atmospheric and man-made conditions, such as wind fields and traffic intensity, vary, and can vary in many ways and combinations.

Modeling longer periods of time provides a means for examining a range of outcomes, but does so at additional cost, use of staff time, and level of detail. In the past modeling was largely confined to shorter intervals – from one day to a few days. More recently, investigators have demonstrated the use of models – even the more complex models - for longer periods, up to a season or a year (Winner and Cass, 1999). With attention being given to longer averaging periods in the formulation of new ambient air quality standards, the application of models for longer periods is becoming more attractive. The increasing memory and speed of the computer is facilitating this change. Nevertheless, the modeler must think carefully about the length of the time period to be studied, and be aware of the commitment being made when one opts for the longer periods.

4 Modeling Alternatives

While grid models and Gaussian models provide a means for simulating a broad range of atmospheric processes, alternative modeling approaches may prove as or more useful in supporting particular avenues of research and analysis. For example, box models play a central role in air chemistry research studies. Receptor models provide direct *emissions-air quality* relationships using basic source information and measured ambient pollutant concentrations. In recognition of the stochastic character of the atmosphere, limited efforts have been devoted to developing suitable statistical models. Although each of these approaches has a limited range of applicability, they provide insight into certain aspects of air pollution phenomena and in some cases may serve to corroborate or place in question the results obtained from comprehensive simulation models.

4.1 Box Models

A box model is a mathematical representation of pollutant dynamics that take place in a well-mixed volume of air. In general, these models provide very limited representations of atmospheric transport phenomena. However, they are well suited to supporting atmospheric chemistry research studies. For example, a smog chamber is a stirred vessel that employs natural light or ultraviolet lamps to study the chemical transformations of precursors in forming ozone and other photochemical reaction products under controlled laboratory conditions. Fresh precursors may be added to the chamber to simulate basic characteristics of actual diurnal emissions patterns that occur in urban or rural areas. Since chamber-

specific wall effects may be important, they need to be characterized and simulated in the box model. Typically, the governing equations of a box model are a set of coupled, nonlinear, stiff ordinary differential equations derived from a chemical kinetics mechanism that are solved using suitable numerical solution procedures.

4.2 Receptor Models

Receptor models are based on statistical analyses of ambient pollutant measurements and pertinent emissions information. They are of particular value in situations where detailed knowledge of actual emissions rates is subject to significant uncertainties. For example, receptor models provide an important means for apportioning measured values of certain types of primary particulates. Establishing such relationships using a source-oriented model is much more problematic given the large uncertainties in emissions estimates for fugitive sources of particulates.

Receptor models can be grouped into three major categories (Seigneur et al., 2001): (1) models that apportion primary PM using source information, (2) models that apportion primary PM without using source information, and (3) models that apportion primary and secondary PM. In each of these categories, there exist some well-established techniques as well as some recent emerging techniques. For example, the chemical mass balance approach has been applied to PM₁₀ problems throughout the western U.S. with generally good success (PM₁₀ is defined as particulate matter – PM – made of particles less than 10 µm in diameter). New methods of factor analysis can also be employed in areas where source profiles are not available. The reliability of receptor models for PM_{2.5} is quite different since the majority of the fine particle mass is due to secondary particle formation (PM_{2.5} is defined as particulate matter – PM – made of particles less than 2.5 µm in diameter). The ability of these models to provide quantitative apportionment of the measured aerosol mass to the pertinent sources is more uncertain. In regulatory applications, a key issue is the ability of these models to adequately represent source-receptor relationships associated with nonlinear chemical reaction phenomena that lead to secondary fine particle formation.

4.3 Statistical Models

Statistical models provide estimates of concentration levels as a function of some combination of space, time, meteorological, emissions and other pertinent variables. These relationships are derived using various regressions, statistical and analysis techniques. Since these relationships are derived from available measurements, their range of applicability is limited to the conditions under which the data were collected. Nonlinear relationships between reactive precursors and secondary pollutants are particularly difficult to accurately represent in such models. To date, limited effort is being devoted to the development of statistical

models largely because of their constrained range of applicability, the lack of physical characterizations in the model, and, often, a limited database.

4.4 Lagrangian Particle Models

Lagrangian particle models – often referred to as Monte Carlo models – simulate atmospheric diffusion by tracking the movement of thousands of fictitious particles representing air pollution. Particles move according to average wind and turbulence parameters and include semi-random pseudo-velocities calculated using a computer-based random-number generator. These models apply well for unreactive pollutants, but revert to a gridded formulation for reactive systems, with various imposed limitations. Their use is becoming more common, particularly for unreactive species, though regulatory applications are still rare.

5 Spatial and Temporal Scales

Models are typically applied to study impacts of individual sources, multiple-source industrial facilities, metropolitan areas, or larger regional areas up to subcontinental scale. The spatial scales of concern can range from up to a few tens of kilometers for large industrial point sources, to a few hundred kilometers for individual urban areas, to a few thousand kilometers for larger regional areas comprised of several metropolitan areas. When applying models to regional-scale domains, consideration must be given to the spatial scale of important atmospheric phenomena that ultimately contributes to regional air quality problems. Nested grid capabilities, an important feature of contemporary regional models, allow them to resolve important phenomena and concentration gradients in areas of the domain where significant sources are present.

The time scales of concern are related to ambient air quality standards, which have averaging times ranging from one hour to one year. In Gaussian model regulatory applications in the US, simulations using up to five years of meteorological data may be carried out to develop estimates of peak concentrations with averaging times ranging from one hour to one year. In photochemical model regulatory applications in the US, simulations may be carried out for time periods of from a few days to a few weeks to develop estimates of peak 1- to 24-hour average concentrations. Only recently have photochemical models been used to simulate entire annual time periods.

Models are formulated to represent key phenomena on the spatial and temporal scales of interest. For example, urban models typically do not provide sufficient treatment of upper air dynamics and, therefore, are generally not applicable to regions of the order of several hundreds of kilometers where vertical transport in the free troposphere, up to several kilometers above ground, may be important. Air quality models that include a detailed treatment of chemistry tend to be limited in their applications to a few days of simulation because of the

computational costs associated with the numerical integration of the chemical kinetic equations. Models that use a simplified treatment of atmospheric chemistry can be applied to longer time periods (e.g., one year or more) without prohibitive computational costs. The ability to simulate long time periods is generally obtained at the expense of some accuracy (since the treatment of chemistry is less accurate in long-term models). Another approach for estimating annual-average concentrations is to apply an episodic model for several typical meteorological scenarios and to reconstruct a full year by combining these scenarios with appropriate weighting factors. This approach involves making approximations with the representativeness of the meteorology, whereas the use of a long-term model involves making approximations with the chemistry. To date, no comprehensive evaluation of these two methods has been carried out.

6 Spatial and Temporal Resolution

Short-term Gaussian plume models are typically applied using hourly meteorological data spanning a period of up to five years. Such models provide hourly concentration estimates at any user-specified point downwind of the source. However, because these models are based on steady-state assumptions, they cannot truly resolve concentration fluctuations.

Grid-based models provide concentration estimates that are spatially averaged over the volume of a grid cell, whose size may range from 1 to 40 km or more in the horizontal directions and from ten meters to several hundred meters in the vertical direction. Contemporary grid models employ nested grids with relatively fine spatial resolution in dense and/or heterogeneous source areas (such as cities where significant spatial gradients may exist in the concentration field) and relatively coarse resolution in rural areas (where spatial gradients are much smaller). Use of nested grids is largely motivated by a desire to optimize the computational time required to perform a simulation.

The ability to provide variable vertical resolution can also be important. In general, relatively fine vertical resolution is used near the ground where large vertical gradients in the concentration field are likely to occur because of the near proximity of most sources. Concentration gradients aloft are often much smaller, allowing the use of coarser vertical grid resolution. In establishing the vertical grid structure, careful consideration must be given to the spatial features of elevated stable layers aloft and the possible need to adequately resolve elevated plumes from large point sources. If such plumes are not adequately resolved, they may be subject to significant averaging errors. In addition, the timing and location of plume fumigation to the ground may be in error. For nitrogen oxides (NO_x) plumes, this can have a significant effect on VOC/ NO_x in the areas where plume fumigation is predicted to occur (or not occur) and can also have a profound influence on the relative effectiveness of VOC versus NO_x controls on

ozone formation in such areas. (VOC stands for volatile organic compounds, for example, reactive, non-methane hydrocarbons)

7 **Uncertainty: Bias, Imprecision, and Variability**

Uncertainty attends all elements of the modeling enterprise: accuracy and precision of the supporting and test data bases, the model-generated emissions and meteorological fields, initial and boundary conditions, and at the end of the sequence, air quality modeling and the results of interest. Variability also accompanies meteorological and biogenic emissions variables (natural variability) and activities that derive from human behavior, such as traffic loading (man-derived variability). As should be apparent, the contributions of uncertainty to modeling results are broadly-based, and the results of modeling are quite susceptible to errors. Modelers, of course, attempt to reduce error levels as effectively as possible, but uncertainties will persist, as many sources of uncertainty are outside the modeler's range of influence. Notable among these are errors in inputs, particularly emissions-related, and variability of all types. Model outputs may range widely in their sensitivity to uncertainties. Where they are insensitive, errors or variability may be of only casual concern; where sensitivity is high, errors particularly may be a major issue.

Typically, little attempt is made to estimate quantitatively the bias or error in model output. While it may be important to know and of particular interest to the decision-maker, it may be quite difficult or impossible to calculate. In these circumstances, modelers sometimes use "best judgment" to estimate errors; however, this cannot be expected to be reliable.

Sensitivities are often estimated. They generally provide information on the response of the output to uncertainties in inputs, under the assumption that the model is basically correctly formulated and the inputs are sound. If there is error in the model or inputs, the results of sensitivity analyses may be derivatively tainted.

Efforts are being made to introduce more sophisticated approaches to uncertainty analysis into modeling. For example, Yang, Wilkinson, and Russell (1997) have developed techniques for facilitating the conduct of sensitivity analysis through use of the direct decoupled method. However, if there is an unknown error in the model or inputs, no sensitivity analysis will properly address its presence. Rather, an attempt must be made to detect its presence, determine the cause or causes and the importance of the error (if feasible) and, as appropriate, correct, mitigate, or eliminate the problem and repeat the modeling and sensitivity analysis.

See Morgan and Henrion (1990) for a detailed introduction to and treatment of uncertainty.

8 Evaluation of Model Performance

Model performance evaluation (MPE) is the process of testing a model's ability to estimate accurately observed measures of air quality over a range of meteorological, emissions, and air quality conditions. When conducted thoughtfully and thoroughly, the process focuses and directs the continuing cycle of model development, data collection, model testing, diagnostic analysis, refinement, and retesting. Far too often in the past this process has been foreshortened in order to "validate" the model with readily available data so that its use in regulatory decision-making could be justified. Obviously, serious inquiry into the model's adequacy or reliability is difficult if not impossible in such a situation.

The performance of Gaussian models has been the subject of numerous studies. Typically, an inert tracer gas is released from a source and measured at various downwind locations. Assessments of model performance rely on comparisons of calculated and measured concentration levels. Routine application of these models in a regulatory setting generally does not involve any performance evaluation. At best, the models are applied using site-specific meteorological data.

In contrast, there is a long history of MPE for photochemical models involving the comparison of observed and estimated concentrations of ozone and, to a lesser extent, other pollutant species. The principal comparisons included temporal comparisons of differences between observation and estimation for individual monitoring sites, spatial comparisons of differences, as shown through deficit-enhancement maps, and a range of statistics, including regional and subregional average bias, gross error, and differences in area-wide maximum ozone concentrations, independent of time and location. The focus of all these types of comparisons has been on ozone. Although NO_x and VOC comparisons have been carried out for some time, no requirement or informal rule was ever developed stipulating that NO_x or VOC estimates correspond at any prescribed level. Furthermore, no standard practice for judging model performance has evolved. Traditionally, the EPA guideline model (Urban Airshed Model) (EPA, 1990) was accepted for use in control strategy assessment when average discrepancies (e.g., gross errors) for ozone were of the order of 35% or less, and inaccuracy or bias is "not large." (i.e., ± 5 -15% according to EPA's definition) (EPA, 1991). Often, however, it was determined that models passing these arbitrary performance criteria contained significant flaws, commonly in the form of internal, compensating errors that compromised the overall reliability of the entire modeling demonstration.

While in many scientific disciplines "hands-off" testing of models is required, a different tradition evolved in the evaluation of grid-based photochemical models. The improvement of model performance is an integral part of MPE. In cases in which differences between observations and estimates are unacceptably large, the

modeler is expected (allowed) to carry out a diagnostic analysis, identify the potential causes of the discrepancies, suggest and make changes in model formulation or processing of input data, and repeat model testing. Thus, evaluation and improvement make up an iterative sequence and, in fact, they are inextricably coupled. Evolving from this philosophy is the common practice of undertaking model performance improvement activities with each modeling episode separately; lack of “hands-off” testing of the second and subsequent episodes has led in many cases to inadvertent, but nonetheless inappropriate “tuning” of the model inputs to provide acceptable UAM output ozone predictions.

A key limitation in MPE to date has been the generally inadequate level of stressfulness to which models have been subjected in testing. Three main outcomes of testing are possible: A model performs inadequately and is so judged, a model performs well and is so judged, or a model appears to perform adequately but is, in fact, significantly flawed. To ensure during testing that a model reveals its flaw(s), it must be adequately "stressed," that is, subjected to testing that is designed to reveal and even highlight or amplify inherent inadequacies.

Because testing has not been properly implemented, flawed models containing compensatory errors internally have been widely accepted for use. The most notable instance is the long-standing use of underestimates of VOC emissions as input to the UAM. Modelers have either directly or inadvertently compensated for these underestimates by introducing offsetting bias into the model. In one instance modelers compensated for suspected underestimation of the emissions inventory by artificially elevating the boundary conditions (on the top and sides). In another study, a "lid" was placed on the vertical velocity in the UAM to prevent or reduce the loss of surface ozone to layers aloft and thus improve model performance. In a third case, meteorological inputs were "beneficially altered" to advect the high ozone cloud directly toward the peak ozone monitoring station. These types of input modifications no doubt changed the source-receptor emissions characteristics of the air basins and had unknown effects on the reliability of the emissions control strategies. In these and other situations, the changes were asserted to be "within the range of experimental or scientific uncertainty."

Recommendations for improvements to the MPE process have been proffered by several scientists, motivated by a number of objectives. They include improving the process, adequately stressing models, improving the quality of available databases, standardizing the practice, and demystifying the practice through clearer communication. Indeed, guidelines have been developed (Roth et al., 1996) for providing a sound context for performance evaluation, establishing a common understanding of the process, and ensuring that evaluation efforts are properly formulated and reasonably complete. Elements of such a comprehensive and satisfactory model evaluation process include:

- (a) evaluating the scientific formulation of the model through a thorough review process
- (b) assessing the fidelity of the computer code to the scientific formulation, governing equations, and numerical solution process
- (c) evaluating the predictive performance of individual process modules and preprocessor models (e.g., emissions and meteorological)
- (d) evaluating the predictive performance of the full model
- (e) conducting sensitivity analyses
- (f) carrying out corroborative analyses
- (g) carrying out comparative modeling, and
- (h) implementing a quality assurance activity

All of these activities should be carried out in accordance with the procedures prescribed in an application-specific MPE protocol.

Obviously, the effort suggested above is considerably greater than that customarily devoted to MPE. However, air quality models are being viewed as essential tools in the development of emissions control plans. The costs of controls are sufficiently high that society will wish assurance that imposed controls will be effective in reducing air pollution levels. It is thus vital that the overall planning process includes sufficient time and resources for conducting thorough evaluations of model performance. In addition, there is likely to be a significantly increased demand for the collection of suitable emissions, meteorological, and air quality data to support MPE. The comprehensive evaluation of model performance should be considered essential to the overall air quality management program for an area.

9 Data Needs

AQSMs require various types of emissions, meteorological, air quality, and geophysical data. Model inputs may be assembled directly from suitable data sources or may be generated through use of other preprocessor models (e.g., emissions or prognostic meteorological modeling systems). The availability of appropriate data to derive model inputs, to evaluate model performance, and to diagnose and rectify model performance problems is crucial to the successful application of an air quality model.

9.1 Gaussian Models

Gaussian models are typically applied using one to five years of on-site surface meteorological data, including wind speed and direction, temperature, relative humidity, standard deviation of the horizontal wind direction, and rainfall. Upper air meteorological data are employed to estimate hourly mixing height estimates. Some models require estimates of other boundary layer parameters. Geophysical data include estimates of terrain height at source and receptor locations as well as

land use. Tracer release experiments with suitable downwind measurements might be carried out to provide a database for evaluating model performance, although this is typically not carried out in routine applications of Gaussian models.

9.2 Photochemical Grid Models

Photochemical grid models are mostly used for ozone simulations and require several data sets for input preparation and model evaluation: air quality, meteorological, emissions, and geophysical. Such models require a complete specification of the spatial and temporal variations of key atmospheric phenomena. Unfortunately, the available data needed to derive such estimates fall far short of what is desired.

A typical air quality data set with which to evaluate model performance consists of hourly surface measurements of ozone and oxides of nitrogen (NO_x) derived from monitoring stations operated by air regulatory agencies, usually located in or immediately downwind of urban areas. Those monitoring sites located in rural areas are often in the general proximity of commercial or industrial sources. Very little routine NO/NO_x monitoring is conducted at true rural sites, nor is there routine collection of total or speciated volatile organic compounds (VOC) data. No routine monitoring of ozone or precursors aloft is conducted. Data are rarely available for direct specification of pollutant concentrations on upwind boundaries of the modeling domain.

Photochemical grid models require a complete specification of the temporal and spatial variations of key meteorological variables, such as wind velocity, temperature, and cloud cover. The National Weather Service collects surface weather data supplemented by twice-daily radiosonde soundings at various locations throughout the country. These data supplemented with the surface meteorological data gathered at the air monitoring stations constitute the typical meteorological database available for developing meteorological inputs to photochemical grid models.

Photochemical grid models also require a complete specification of gridded, temporally resolved emissions estimates for all chemical species. Emissions data are normally assembled by air regulatory agencies with varying quality, representativeness, and reliability, often influenced by the ozone National Ambient Air Quality standards - NAAQS - attainment status of the particular area. (A region in the US is defined as an attainment region if air pollution measurements indicate the NAAQS are not exceeded). An emission modeling system may be needed to provide an effective means to organize, manipulate, and process emissions data for a large modeling domain.

Geophysical data are needed for specifying gridded terrain and land use inputs. Various federal agencies maintain geophysical data bases for topography, land

use/land cover, population, employment, and so on that are used in various ways to develop the inputs needed by photochemical modeling systems.

In a few nonattainment areas, such as the northeast US, special field measurement studies have been performed to provide a better characterization and understanding of meteorological and air quality conditions than is otherwise provided by routine surface monitoring. Typically, these programs are carried out over a limited time period and consist of intensive monitoring of aloft meteorological and air quality conditions via instrument aircraft and remote sounding devices, enhanced surface monitoring of ozone and precursor species (sometimes including VOCs) in urban and rural sites, tracer-diffusion studies for model evaluation, and intensive, focused collection of emissions data from key source categories such as power plants, on-road motor vehicles, and targeted area sources. Though useful, these studies are very costly, capture a fraction of aerometric conditions associated with ozone exceedances, and have decreasing utility to support modeling as time passes.

Occasionally, major field studies are designed and implemented in parallel with integrated model development, testing and refinement activities. The SARMAP (Demassa, 1996) study in central California is a noteworthy example. Here, models were used to assist in the design of an intensive emissions, air quality, and meteorological data collection activity, supplemented with many research-grade investigations into specific processes: dry deposition and turbulence, biogenic emissions from various plant species, on-road motor vehicle driving patterns, boundary layer transport dynamics, and so on. Though very costly, these programs provide a solid basis for further model development as well as the opportunity for testing of individual process modules in the overall modeling system.

10 Uses of Models

Several uses of models have been listed earlier, ranging from the practical to the research-oriented. In this section we discuss two practical arenas of application: regulatory compliance and resolution of litigation.

10.1 Regulatory Compliance

Today models are commonly used in planning to estimate if a geographical area:

- that now exceeds a specified standard will attain the standard if certain prescribed emissions reductions are implemented
- now in attainment will remain so due to the favorable offsetting effects of growth and emissions controls, and
- now in attainment is likely to exceed a standard due to the effects of growth and insufficient emissions control

As noted, these modeling activities are often included under the general umbrella of SIP and FIP preparation. A comprehensive process might include:

- detailed planning and protocol preparation
- conduct of a field program to obtain data needed for many purposes, including the preparation of model inputs and the evaluation of model performance
- independent programs for quality assurance and control
- archiving and error-checking for the complete data base, including emissions
- adaptation and testing of a model system selected for use, including air quality, emissions, and meteorological models
- iterative improvement of model performance consistent with good scientific practice until a specified standard of performance is met
- conduct of sensitivity studies, to better understand the system being modeled
- control strategy analysis, and
- estimation and analysis of uncertainties and risks

Funding needed for such efforts may range from a \$2-5M to \$25M or more. If a comprehensive field program is included, that component alone may cost from \$3M to \$15M or more. The total elapsed time required ranges from 4 to 6 years or more. Clearly, such commitments are substantial.

While grid-based photochemical modeling offers the best opportunity for long range planning for the attainment and maintenance of secondary air pollutant standards, its potential may be limited in one or more of the following ways:

- Components of an ambient air quality and meteorological data base may be sparse, inaccurate, or lacking
- Funding to conduct a comprehensive study may be inadequate
- Staff to conduct the work may be available for only a portion of the time needed, or may be unacceptably inexperienced in modeling
- The calendar time available may be inadequate, and/or
- Model performance may be inadequate and not easily correctable

See Roth, Tesche and Reynolds (1998), for an evaluation of regulatory modeling efforts conducted during the 1990-95 period.

10.2 Resolution of Litigation¹

Environmental litigation has been steadily increasing over the last two decades. This phenomenon is particularly noticeable in the United States (US). However, this trend is also affecting European countries and courts that deal with

¹Section written by P. Zannetti

EnviroComp Consulting, Inc. Fremont, California, USA. (<http://www.envirocomp.com>).

international issues. The parties and their attorneys involved in litigation need expert witnesses such as scientists, engineers, medical doctors, in order to comprehend various cases and to help define litigation strategy, producing accurate and convincing written reports as well as providing expert testimony to judges and juries.

In the past, experts hired for litigation cases were required to provide opinions and subsequently support them with published citations, professional experience, and simple “pen-and-paper” calculations. Today computer simulations are used in virtually all technical fields. For example, in air pollution, computer simulation models have been used in the US since the early 1970s as “regulatory tools”, i.e., official tools recommended by regulatory agencies to simulate the concentration impact of emissions of chemicals into the atmosphere. But the same “regulatory” models, or similar tools, can also be used to simulate the past, e.g., to simulate an accidental release from an industrial facility. Accidental releases in the US are often litigated in court, whereas experts are hired in order to perform a reconstruction of the incidents. Today, these experts commonly use simulation models to estimate the concentration impact in the neighboring areas downwind from the release. The use of computer simulation models is clearly necessary in accidental release cases (as well as in many other environmental litigation cases, e.g., groundwater contamination). The formidable task for attorneys on both sides is to understand as much as possible about modeling techniques and to be able to present or criticize the results of those models in court.

If modeling is to be used in a litigation case the expert witness must make several important choices. First of all, does the case warrant the use of a complex computer model? Should perhaps a simple model be chosen? Which model will be easier to explain to a jury? In one case, for example, the expert may use a computer model developed and recommended by the US Environmental Protection Agency (EPA). In another scenario, the expert might use a “research prototype” code developed at a university or a national laboratory. In yet another case, the expert might utilize a model recently developed, or even a model (or a set of calculations) expressly developed for the case at hand. The expert should bear in mind that each choice has advantages and disadvantages. Clearly, models that are widely used by other scientists and recommended by regulatory agencies can be perceived as more reliable than others. However, in litigation, an expert witness has ample latitude in selecting the tools that are most appropriate for the case. Whatever tool is chosen, the expert witness must be able to persuasively present it as reliable, peer-reviewed science whose results can be trusted. In all cases, the expert witness must feel comfortable in the ability to justify results and opinions to a non-technical audience under cross-examination. For additional information on the subject of the use of air pollution models in litigation cases, see Zannetti (2001).

References

DeMassa, J. et al. Performance Evaluation of SAQM in Central California and Attainment Demonstration for the 3-6 August 1990 Ozone Episode. California Air Resources Board, Sacramento, CA, 1996.

EPA. User's Guide for the Urban Airshed Model-Volume I: User's Manual for UAM (CBIV). U.S. Environmental Protection Agency, EPA-450/4-90-007a, Research Triangle Park, NC, 1990.

EPA. Guideline for Regulatory Application of the Urban Airshed Model, EPA-450/4-91-013, Office of Air Quality Planning and Standards, Research Triangle Park, NC, 1991.

Liu, M. K., and Seinfeld, J. H., On the Validity of Grid and Trajectory Models of Urban Air Pollution. Atmos. Environ., 9, pp. 555-574, 1974.

Morgan, M. G., and Henrion, M., Uncertainty: A Guide to Dealing with Uncertainty in Quantitative Risk and Policy Analysis. Cambridge Univ. Press, 1990.

Roth, P. M., Tesche, T. W. and Reynolds, S. D., A Critical Review of Regulatory Air Quality Modeling for Tropospheric Ozone. North American Research Strategy for Tropospheric Ozone (NARSTO), Research Triangle Park, NC, September 1998.

Seigneur, C. Current Status of Air Quality Models for Particulate Matter. Journal of the Air & Waste Management Association, 51, pp. 1508-1521. 2001.

Seinfeld, J. H., and Pandis, S. N., Atmospheric Chemistry and Physics. Wiley-Interscience, 1998.

Winner, D.A., and Cass G.R. Modeling the Long-Term Frequency Distribution of Regional Ozone Concentrations. Atmos. Environ. 33, pp. 431-451, 1999.

Yang, Y.J., Wilkinson, J.G., and Russell, A.G., Fast Direct Sensitivity Analysis of Multidimensional Photochemical Models. Environ. Sci. Technol., 31, pp. 2859-2868, 1997.

Zannetti, P., Environmental Litigation – Air Pollution Models and Modelers in Court (Invited Paper), Air Pollution 2001, Ninth International Conference on Modeling, Monitoring, and Management of Air Pollution, 12-14 Sept 2001, Ancona, Italy, Wessex Institute of Technology, Ashurst, Southampton, U.K.

Chapter 3

Emission Modeling

Future volumes in the book series will address the issues related to the modeling of air pollution emissions. A brief introduction to this subject is presented below, courtesy of James G. Wilkinson

jwilkins@themis.ce.gatech.edu

In the context of air quality modeling, emission modeling is the process by which emissions estimates are prepared for use in an air quality model. In general terms, the emissions model is the suite of tools that are used to estimate and spatially and temporally allocate emissions for use in deterministic and statistical air quality models. The field of emissions modeling is rapidly being transformed from a discipline that has typically been viewed as more of an art to a field that is more scientifically rigorous. Though, even today, the methods that are used to estimate emissions for air quality modeling purposes are many times poorly documented and receive little if any peer review (NRC, 1991). Yet the emissions estimates that result from the emissions modeling process are the critical link in the air quality modeling process, as shown in Figure 1 below. In comparison to the other input components to the air quality modeling process, the emissions estimates tend to receive the greatest degree of scrutiny.

However, with each successive deployment of a new emissions modeling tool, whether that tool is a model meant to estimate only biogenic emissions or an entire emissions modeling system meant to estimate emissions for all sources, there has been a growing movement away from much of the ad-hoc nature of the development of emissions estimates, for use in air quality modeling, towards emissions estimates whose lineage, as well as the methods used to develop them, is documented and more open to scientific debate. Most notably, the Emissions Inventory Improvement Program¹ (EIIP) has resulted in numerous, quasi-official

¹ <http://www.epa.gov/ttn/chief/eiip/>

standards documents for the development, storage, transfer, and use of emissions estimates.

In future chapters, we will explore how emissions are estimated for the myriad of sources that exist. We will also examine the impact that emissions control strategies have on emissions estimates. However, the focus will be on the tools and techniques that are employed to estimate emissions, or to manipulate existing emissions estimates, for use in an air quality model.

Within the context of this book series, emissions estimation tools are viewed from two perspectives:

- The emissions estimates model; and
- The emissions modeling system.

The emissions estimates model is a computerized system that utilizes data to estimate emissions from a specific source. For example, the US EPA Biogenic Emissions Inventory System² (BEIS2) is a good example of an emissions estimates model. BEIS2 uses land cover, species-specific emissions factors, temperature, and solar radiation to estimate the emissions of volatile organic compounds from plants.

The emissions modeling system is a computerized framework under which emissions estimates models operate. Further, the emissions modeling system functions to house all the tools necessary to prepare a comprehensive set of emissions estimates for use in an air quality model. The Emissions Modeling Systems³ (EMS-95) and the Sparse Matrix Operator Kernel Emissions⁴ (SMOKE) modeling system are good examples of emissions modeling systems. Each system has the ability to estimate emissions from major stationary sources, area sources, on-road mobile sources, and biogenic sources and to prepare the emissions estimates for use by a number of air quality models including the Comprehensive Air Quality Model with extensions⁵ (CAMx), the Community Multiscale Air Quality⁶ (CMAQ) model, the Urban Airshed Model⁷ (UAM-V), and the Multiscale Air Quality Simulation Platform⁸ (MAQSIP).

² <ftp://ftp.epa.gov/amd/asmd/beis2/>

³ <http://www.ladco.org/emis/guide/ems95.html>

⁴ <http://www.emc.mcnc.org/products/smoke/>

⁵ <http://www.camx.com/>

⁶ <http://www.epa.gov/asmdnerl/models3/index.html>

⁷ <http://uamv.saintl.com/>

⁸ <http://www.emc.mcnc.org/products/maqsip/>

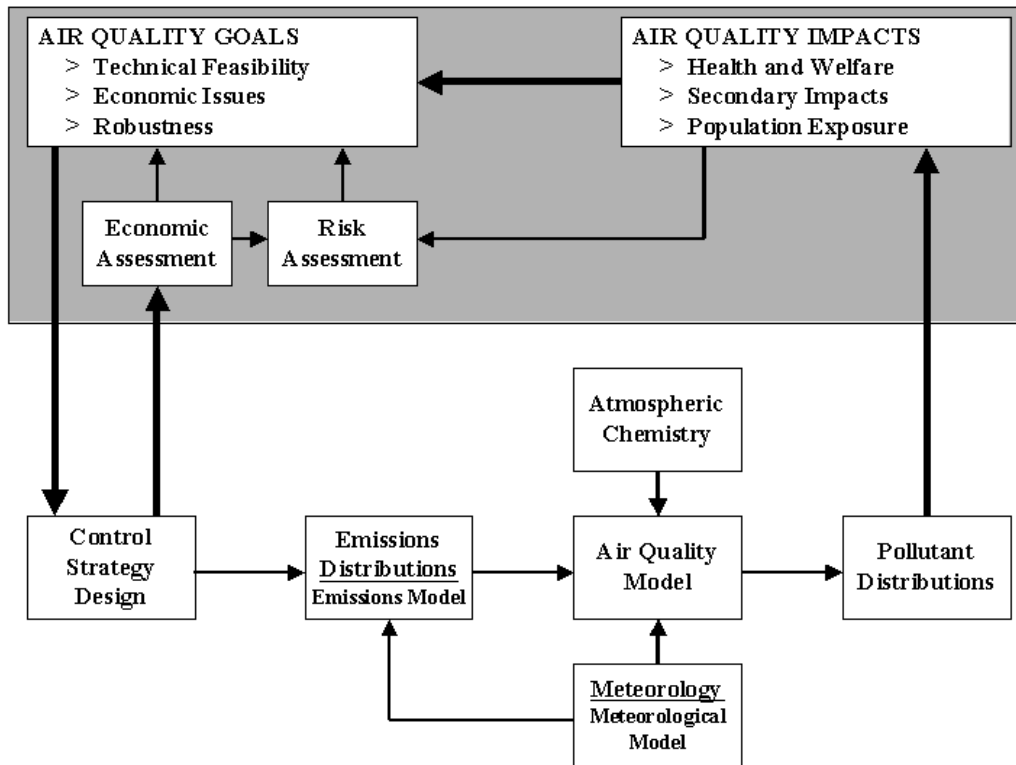


Figure 1. Overview of the air quality modeling process (adapted from Russell and Odman, 1993).

References

- NRC, 1991. Rethinking the Ozone Problem in Urban and Regional Air Pollution. National Research Council, National Academy Press, Washington, D.C.
- Russell, A. G. and M. T. Odman, 1993. Future directions in air quality modeling, *Water Air Soil Pollution*, 67:181-193.
- USEPA, 2000. AP-42: Compilation of Air Pollutant Emission Factors Mobile Sources, United States Environmental Protection Agency, Office of Transportation and Air Quality, Ann Arbor, MI. <http://www.epa.gov/otaq/ap42.htm>
- USEPA, 1999. Handbook for Criteria Pollutant Inventory Development: A Beginner's Guide for Point and Area Sources, United States Environmental Protection Agency, Office of Air Quality Planning and Standards, Research Triangle Park, NC. EPA-454/R-99-037. September. <http://www.epa.gov/ttn/chief/eidocs/beginner.pdf>
- USEPA, 1995. Compilation of Air Pollutant Emission Factors AP-42, Fifth Edition, Volume I: Stationary Point and Area Sources, United States Environmental Protection Agency, Office of Air Quality Planning and Standards, Research Triangle Park, NC. <http://www.epa.gov/ttn/chief/ap42/>
- USEPA, 1991. Procedures for the Preparation of Emissions Inventories for Carbon Monoxide and Precursors of Ozone, Volume I: General Guidance for Stationary Sources, United States Environmental Protection Agency, Office of Air Quality Planning and Standards, Technical Support Division, Research Triangle Park, NC. EPA-450/4-91-016.

USEPA, 1989. Procedures for Estimating and Applying Rule Effectiveness In Post-1987 Base Year Emissions Inventories for Ozone and Carbon Monoxide State Implementation Plans, United States Environmental Protection Agency, Office of Air Quality Planning and Standards, Technical Support Division, Research Triangle Park, NC. EPA-452/4-92-010.

Sorbjan, Z. (2003) *Air-Pollution Meteorology*. Chapter 4 of *AIR QUALITY MODELING - Theories, Methodologies, Computational Techniques, and Available Databases and Software. Vol. I - Fundamentals* (P. Zannetti, Editor). Published by The EnviroComp Institute (<http://www.envirocomp.org/>) and the Air & Waste Management Association (<http://www.awma.org/>).

Chapter 4

Air Pollution Meteorology

Zbigniew Sorbjan

Department of Physics, Marquette University, Milwaukee, WI 53201, USA
sorbjanz@mu.edu

Abstract: The primary object of this chapter is to introduce meteorological fundamentals related to the transport of air pollutants in the atmosphere. The material contained in the chapter is divided into two sections. Section 1 is very basic and mostly related to atmospheric flows in larger scales. It discusses forms of atmospheric motions, weather systems, forces, and clouds. The material contained in Section 2 is more detailed and focused on processes in the atmospheric boundary layer. Turbulence, mixing and diffusion in this layer are examined and explained. Various regimes, such as stable flows, free and forced convection, in cloud-less and cloud-topped mixed layers are discussed. Their mathematical and physical description is also reviewed, including similarity theories and mixed layer models.

Key words: atmospheric motions, weather systems, atmospheric boundary layer, turbulence, mixing, diffusion, convection, mixed layers, similarity theories.

Meteorology has an important, practical application in the area of control and management of air quality. Its significance was first realized when the increasingly heavy use of coal for home heating and industrial power led to episodes of extreme sulfur pollution during certain weather conditions. The most famous case occurred in London during foggy December in 1952, when approximately 4000 people died as the direct result of air pollution. Four years later, in January 1956, under similar conditions, 1000 deaths were blamed on an extended fog in London. Since that time, the problem has grown as a result of industrialization. High air pollution concentrations are no longer local and restricted to urban areas, but can be transported for long distances by large-scale weather patterns.

The primary object of this chapter is to introduce meteorological fundamentals related to the transport of air pollutants in the atmosphere. The material contained in Section 1 is very basic and mostly related to atmospheric flows in larger scales. More extensive coverage of topics included in this Section can be found in such text-books as Aguada and Burt (2001), Moran and Morgan (1995) or Lutgens and Tarbuck (1995). Readers who are familiar with general meteorology could simply skip it and begin with Section 2.

The material contained in Section 2 is more detailed and describes meteorological processes in the atmospheric boundary layer, where most human and biological activities take place. For further information on boundary layer processes, the reader is referenced to text-books on the subject, including monographs of Kaimal and Finnigan (1994), Garratt (1992), Plate et al. (1998), Sorbjan (1989), or Stull (1988). Air pollution diffusion is investigated in detail by Arya (1999), Venkatram and Wyngaard (1988), or Pasquill (1974).

1 Synoptic Meteorology

1.1 Atmospheric Air

Photographs taken from outer space show that the Earth's atmosphere forms a very thin layer surrounding the globe. Its height can be estimated to be about 80 km, which is 1.25% of the Earth's radius. The composition of the atmosphere is almost uniform with height. Table 1 shows the abundance of the various gases in the atmosphere. The gases listed in the left column of the table are permanent, i.e., their concentrations do not change in time and space. The gases in the other column can vary.

Table 1. Abundance of the atmospheric gases

Permanent Gas	Symbol	% by Variable	Gas	Symbol	% by Volume
Nitrogen	N ₂	78.08	Water vapor	H ₂ O	0.0 – 4.0
Oxygen	O ₂	20.95	Carbon dioxide	CO ₂	0.0351
Argon	Ar	0.93	Methane	CH ₄	0.00017
Neon	Ne	0.0018	Carbon monoxide	CO	0.00002
Helium	He	0.00052	Ozone	O ₃	0.000004
Hydrogen	H ₂	0.00005	Sulfur dioxide	SO ₂	0.000001
Xenon	Xe	0.000009	Nitrogen dioxide	NO ₂	0.000001

Nitrogen and oxygen are the most abundant atmospheric gases. Their total amount is about 99.03%. The abundance of the remaining permanent gases is only about 0.9324%. The concentration of water vapor, which is also one of the variable atmospheric gases, changes as a part of the natural hydrologic cycle. The concentration of the carbon dioxide (CO₂) and methane (CH₄) show cyclic

oscillations associated with the annual vegetation cycle (see website¹). The amount of sulfur dioxide (SO₂) may vary due to volcanic eruptions into the upper atmosphere and also due to anthropogenic activities.

Most of the ozone is found in the higher atmosphere, about 30 km above the Earth's surface. At this height, ozone is produced naturally and forms the so-called ozone layer. The ozone layer absorbs most of the ultraviolet radiation from the sun. Ultraviolet radiation is harmful to life. Therefore, the presence of the ozone layer in the atmosphere protects life on Earth against radiation.

In 1974, M.Molina, F.S.Rowland and P.Crutzen, determined that certain man-made substances have been destroying the ozone layer. Among these substances were chloro-fluoro-carbons (CFCs) from spray cans and air-conditioning systems. When released into the atmosphere, CFCs slowly move upwards. In the upper atmosphere they are transported to remote regions including the Arctic and Antarctic. During this transport CFCs break up as a result of solar radiation. Chlorine molecules are produced which react with ozone and reduce its amount. Evidence of massive ozone layer destruction, called the ozone hole (see website²), has been observed over Antarctica. As a consequence, an increase in skin cancer in humans may be expected, as well as various adverse effects on plants and animals. To solve the ozone reduction problem, over forty industrialized countries in the world have pledged to eliminate completely the use of ozone-depleting chemicals in the 21st century.

Some of the variable atmospheric gases in the atmosphere change their amounts as a result of anthropogenic industrial activities. For example, ozone (O₃), nitrogen dioxide (NO₂), and carbon monoxide (CO) are emitted into the lower atmosphere by motor vehicles, due to the high-temperature combustion of fuel. Ozone is also formed as a result of photochemical reactions. Carbon dioxide (CO₂) and sulfur dioxide (SO₂) are produced by burning wood and coal. Sulfur dioxide readily oxidizes to sulfur trioxide (SO₃). In moist air, sulfur trioxide reacts with water and produces sulfuric acid (H₂SO₄). Sulfuric acid can be transported within clouds for hundreds of kilometers. When it is removed from the clouds, it can result in acid rain.

1.2 Atmospheric Energy

The Earth's atmosphere acts as a giant heat engine transforming available energy into the movement of huge masses of air. Practically all "fuel" for this engine is supplied by the sun. The contribution of all other sources (e.g. the Earth's interior) is smaller than 0.02%. Since the Earth's atmosphere is semi-transparent to incoming solar radiation, it obtains roughly 20% of its energy strictly by

¹ <http://www.oism.org/pproject/s33p36.htm>

² <http://www.epa.gov/ozone/science/hole/>

absorption. About 30% of solar radiation is reflected or scattered into space. The rest passes through the atmosphere and is absorbed by the Earth's surface.

The surface of the Earth has a considerable influence on air temperature. Differences in temperature near the ground are caused by the variation of thermal properties of the underlying surface. Because water has an enormous specific heat, it takes far more heat to raise the temperature of water than it does to raise the temperature of rocks or soil. Besides, the heating energy is deposited only in a few decimeters of soil, while in the oceans it is mixed through the top few meters of water. Consequently, since water covers 61% of the Northern Hemisphere and 81% of the Southern Hemisphere, there are considerably smaller annual temperature variations in the water-dominated Southern Hemisphere, as compared to the Northern one.

Temperature in the atmosphere changes with height. In the troposphere, which is the lowest layer of the atmosphere -- extending up to about 10 km above the ground, the temperature in average decreases with height at the rate of about 0.6°C per 100 m (Figure 1). Above, in the stratosphere, temperature generally increases with height, due to an absorption of solar radiation in the ozone layer. In the mesosphere, temperature decreases with height. In the thermosphere, the temperature of air molecules again increases with height. Departures from the plot in the figure can occur because of seasonal and latitudinal variations.

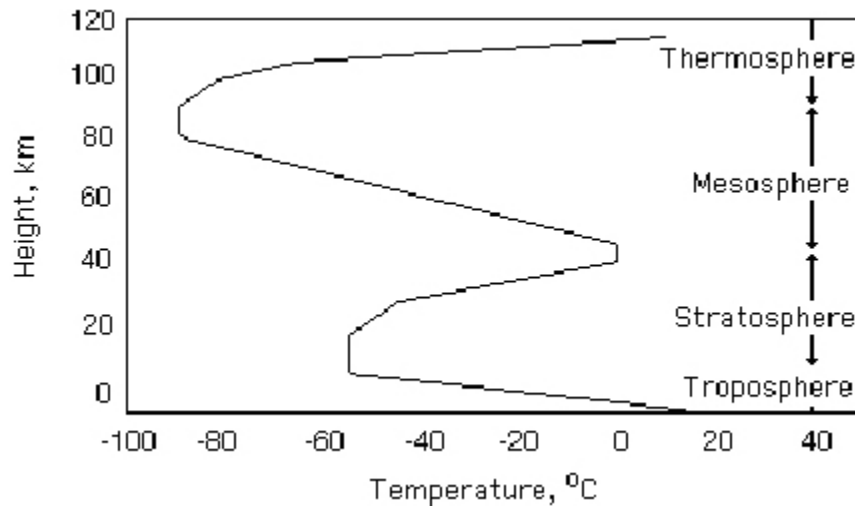


Figure 1. The vertical distribution of temperature in the standard atmosphere.

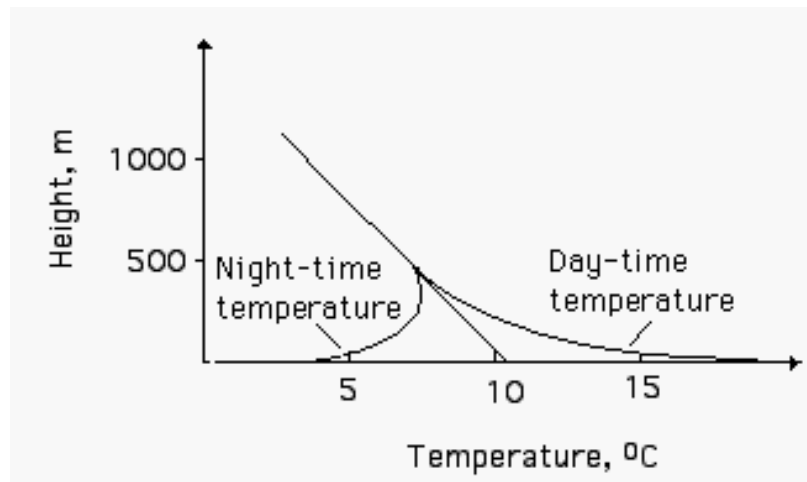


Figure 2. Typical temporal changes of temperature within the first few hundred meters above the Earth's surface.

Within the first few hundred meters, temperature significantly changes diurnally (Figure 2). At night, the Earth's surface cools radiatively and causes a decrease in air temperature near the surface. As a result, the so-called temperature inversion layer is formed near the Earth's surface. In the inversion layer, the temperature increases with height. On the other hand, during the day, the Earth's surface is heated by the sun. The warm surface causes an increase of the air temperature in a thin layer above the ground. As a result, the daytime air temperature near the ground readily decreases with height.

Temporal variations of the air temperature in the atmosphere can also be related to various natural, and anthropogenic factors, such as volcanic eruptions and increased levels of air pollutants. During volcanic eruptions, tons of dust and ash are spewed into the atmosphere. Some of this material reaches the levels above the troposphere and is redistributed around the Earth. The temporary presence of volcanic debris causes some of the sun's energy to be reflected back into outer space before it reaches the Earth's surface. Volcanic particles also intensify cloud formation. More clouds reflect more solar energy back into outer space. Even though the volcanic dust and clouds also prevent some of the Earth's heat from escaping, the resulting effect is a cooling of the Earth.

There has been concern that further industrial emissions of pollutants into the atmosphere will cause global warming, commonly referred to as the greenhouse effect. The greenhouse effect is triggered by such pollutants as carbon dioxide, methane, nitrous oxide, and chloro-fluoro-carbons. Greenhouse gases prevent part of the Earth's radiation from escaping into space, and keep the Earth warmer. A globally averaged surface temperature increase of 0.5°C has already been observed since 1880 (see web site³). As a result of the warming effects, glacier and continental ice could melt, resulting in rising sea levels. More water vapor

³ http://wfn.cdc.noaa.gov/img/climate/research/1998/anomalies/triad_pg.gif

could be released into the air causing greater precipitation. A weakening of the Gulf Stream current might also occur. The warming trend could shift climate zones around the world and make floods, droughts, storms, cold and heat waves to be more extreme and more frequent.

There is some skepticism in the scientific community about such an "apocalyptic" vision of the future. The observed 0.5°C temperature increase could merely be a natural climate fluctuation. Global warming caused by the greenhouse effect could be canceled due to radiative cooling by the increased presence of anthropogenic aerosols and clouds. Reduction of the ozone content, and consequently in the amount of the absorbed solar energy, is expected to cool the stratosphere.

Nonetheless, the recent model simulations imply that only about 3.3% of the greenhouse energy is used to warm the atmosphere. Most of this energy (92%) is stored in the oceans. In addition, about 4.1% of the greenhouse energy causes the melting of the ice cover in Antarctica and Greenland, and about 0.5% melts the world glaciers.

1.3 Atmospheric Forces

Atmospheric motion results from the action of atmospheric forces. Such forces may be classified into two categories -- body forces and surface forces. Body forces, such as gravity, act at a distance on the bulk of the air parcel (hence the word "body"). Surface forces, or stresses (forces per unit area), act through direct contact and are exerted directly on the surface of the air parcel. The surface forces can be divided into normal stresses and tangential (shear) stresses.

Surface forces reflect an interaction among air molecules or air parcels. If two layers of air flow with slightly different velocities, the random sidewise intrusions of some slower molecules into the faster stream tend to slow down the faster stream. The intrusion of faster molecules into the slower stream tend to speed up the slower stream. The wandering of individual molecules introduces internal friction in the fluid which is called viscosity.

The atmospheric pressure can be regarded as the weight of the atmosphere per unit area. Pressure differences in space generate the pressure gradient force which acts from higher to lower pressure regions of the atmosphere. As the atmospheric pressure decreases with height, one might expect that the vertical component of the pressure force should be able to move the atmospheric air out into space. But this does not occur because the vertical pressure gradient force is approximately balanced by the gravity force. This balance is expressed by the hydrostatic equation, which can be written in the following form:

$$-\frac{1}{\rho} \frac{dp}{dz} = g \quad (1)$$

where z is height, ρ is the air density, p is the air pressure, g is the gravity acceleration. The hydrostatic balance may be disturbed by the buoyancy force, due to density differences between parcels of moving air and their vicinity, as well as by varying motions in time and space.

Buoyancy forces act on individual parcels of air only when there are differences in density between the parcels and the ambient atmospheric air. For instance, the buoyancy force appears when a number of water vapor molecules is added to a fixed volume of air. In this case the same number of air molecules must leave this volume to keep the total number of molecules (Avogadro's law), as well as temperature and pressure constant. Assume that 10 moles (1 mole is a fixed number of molecules) of water vapor replace 10 moles of air, i.e., 8 moles of nitrogen and 2 moles of oxygen. The molecular weights of water vapor, nitrogen, and oxygen are: 18 g, 28 g, and 32 g, respectively. Therefore, the atomic weight budget is: $(10 \times 18 \text{ g}) - (8 \times 28 \text{ g} + 2 \times 32) = -108 \text{ g}$ (*lost*). This indicates that humid air is lighter than dry air of the same temperature and pressure. Other effects of the buoyancy force will be discussed in the next section.

The rotation of the Earth introduces the Coriolis force. The Coriolis force is perpendicular to the object's relative velocity, and is oriented to the right of the velocity vector in the northern hemisphere, and to the left in the southern one. Its magnitude is proportional to the product of an object's mass, its velocity, Earth's angular velocity (7.29×10^{-5} radians/s), and $\sin \phi$, where ϕ is the latitude at which wind occurs.

The Coriolis effect combines two factors, one that exerts its strongest force on objects traveling on a north-south axis, and another which affects objects moving on an east-west axis. The first factor results from the rotational velocity of the Earth's surface, which varies with latitude. A point residing on the Equator moves at a speed of $2\pi R/24h = 463.2 \text{ m/s}$, while the poles spin but do not move. Hence, air moving north from the Equator begins with a greater rotational speed and outruns slower moving portions of the globe. As a result, it relatively curves eastward and ahead of the Earth's rotation. Similarly, air traveling southward, toward the Equator, begins with a low initial velocity and curves west, as the faster-moving Earth exceeds it.

The east-west component of the Coriolis force is a consequence of the tendency of any orbiting object to fly off in a straight line. This tendency, together with the rotation of the Earth, produces a force which lies on the plane perpendicular to the Earth's axis, and thus has a sideways component in relation to the Earth's surface. Consequently, an object moving east will curve toward the Equator, while an object moving westward will curve toward the pole.

1.4 Static Stability

The buoyancy force can also appear when air parcels travel vertically in the atmosphere. A dry parcel of air moving upward expands adiabatically due to a decrease in the atmospheric pressure with height (the word adiabatic is derived from the Greek word *adiabatos*, meaning "impassible", i.e., occurring without loss or gain of heat). The process of expansion decreases the internal energy of parcel molecules, and causes the parcel to cool. When a dry parcel of air moves downwards, it contracts adiabatically due to an increase in the atmospheric pressure with height. The process of contraction increases the internal energy of parcel molecules, and causes the parcel to warm. Changes of the temperature in a dry adiabatic process are described by the Poisson equation:

$$\frac{T(z)}{T_o} = \left\{ \frac{p(z)}{p_o} \right\}^k \quad (2)$$

where T is the absolute temperature in Kelvins, p is pressure, $k = R/c_p = 0.286$, R is the gas constant of dry air ($R = 287 \text{ m}^2\text{s}^{-2}\text{K}^{-1}$), c_p is the specific heat of dry air ($c_p = 1007 \text{ m}^2\text{s}^{-2}\text{K}^{-1}$), z is the actual height and "o" indicates the initial level of the moving parcel.

Differentiating the above equation, with respect to height, with the help of the hydrostatic equation (1), and the equation of state:

$$p = \rho RT \quad (3)$$

which relates the pressure, temperature and density, one finds that the temperature of a vertically moving parcel changes in the atmosphere at the constant lapse rate $\gamma_a = -dT/dz = g/c_p \approx 1^\circ\text{C per } 100 \text{ m}$. This value is called the dry adiabatic lapse rate (the lapse rate is defined as a negative vertical gradient).

If the atmosphere were well mixed by vertical motions of air parcels, its temperature would not be constant but would decrease with height at the dry adiabatic lapse rate. In the well mixed atmosphere the so-called potential temperature would be constant. The potential temperature is defined as:

$$\Theta = T(z) \left\{ \frac{1000}{p(z)} \right\}^k \quad (4)$$

i.e., it is the temperature of a parcel which is brought adiabatically to the reference level of 1000 hPa. Note that the pressure p in (4) is expressed in hPa. By differentiating (4) with respect to height, with the help of (1), one can obtain $d\Theta/dz = dT/dz + \gamma_a$. This indicates that the potential temperature is indeed conserved (constant) during vertical adiabatic motions.

Condensation of water vapor has an important impact on the state of the atmosphere. When the rising parcel of air reaches saturation, vapor condenses and releases the latent heat of condensation. The released heat increases the air parcel's temperature. As a result, the adiabatic lapse rate decreases from the dry rate of $\gamma_a = 1^\circ\text{C}/100\text{ m}$ to the rate $\gamma_m = \gamma_a - L/c_p dq/dz$, where L is the latent heat of evaporation ($L = 2.5 \times 10^6\text{ J/kg at } 0^\circ\text{C}$), q is the specific humidity (mass of water vapor in a kilogram of humid air). The new rate is called the pseudo-adiabatic lapse rate or the moist adiabatic lapse rate. The moist adiabatic lapse rate for the standard atmosphere varies from $0.4^\circ\text{C}/100\text{ m}$ (in warm saturated air) to $0.9^\circ\text{C}/100\text{ m}$ (in cold saturated air). The release of latent heat causes the rising parcel to intensify its vertical motion. This mechanism provides additional "fuel" for the formation of thunderstorms.

The actual temperature lapse rate in the atmosphere varies in time and space and usually differs from the dry adiabatic rate. Therefore, in some situations, the rising parcel of air might be cooler, and thus heavier, than the surrounding air. Such a parcel is decelerated in its upward motion, and then forced to sink. Such a case is considered in Figure 3.

The ambient temperature in the figure increases with height from $T_1 = 300\text{ K}$ to $T_2 = 301\text{ K}$. A parcel, which initially has a temperature of $T_{p1} = 300\text{ K}$, is forced upwards. As a result, it expands and cools adiabatically to $T_{p2} = 299\text{ K}$. Being cooler and heavier than the ambient air, the parcel would tend to return to the initial level. When this occurs, the conditions are called statically stable.

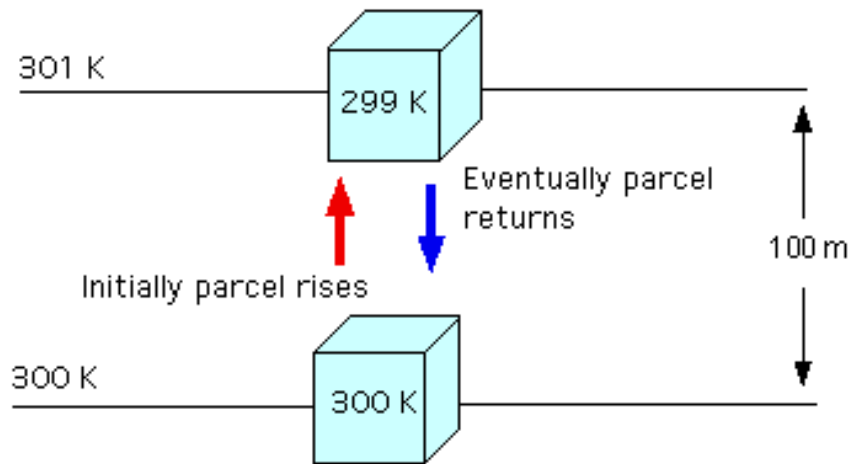


Figure 3. Static stability within thermal inversion (i.e., when the temperature of the atmosphere increases with height). The temperature is expressed in Kelvins.

If the temperature of the ambient air in the figure decreased with height from $T_1 = 300\text{ K}$ to $T_2 = 298\text{ K}$, the rising air at the upper level would be warmer ($T_{p2} = 299\text{ K}$), and therefore lighter, than the surrounding air ($T_2 = 298\text{ K}$). As a result, the parcel would continue rising. Consequently, this state would be called statically

unstable. In the statically neutral case, the rising particle has the same temperature along its path as the surrounding air ($T_1 = T_{p1}$, $T_2 = T_{p2}$).

To further understand the effects of thermal stability, consider the balance of the gravity and the pressure gradient forces given by Equation (1). It can be assumed that one parcel of air changes its density from the value ρ to a new value $\tilde{\rho}$. As a result of this change, the parcel starts moving vertically with the acceleration a :

$$-\frac{1}{\tilde{\rho}} \frac{dp}{dz} = g + a \quad (5)$$

Substituting (1) into(5) and employing the equation of state (3) yields:

$$a = -g \left(\frac{\tilde{\rho} - \rho}{\tilde{\rho}} \right) = -g \left(\frac{T - \tilde{T}}{T} \right) = -\frac{g}{T} \left(\frac{dT}{dz} - \frac{d\tilde{T}}{dz} \right) z = -\frac{g}{T} \frac{d\Theta}{dz} z \quad (6)$$

where T and \tilde{T} are the temperatures of the atmosphere and the parcel respectively, $-d\tilde{T}/dz = \gamma_a$, Θ is the potential temperature, and z is the height above the Earth's surface.

When $d\Theta/dz > 0$ then $a < 0$. In this case the vertical motion is decelerated. When $d\Theta/dz < 0$ then $a > 0$. In this case the vertical motion is intensified. Based on the above analysis we may conclude that the static stability of the atmosphere can be characterized as follows:

- unstable (superadiabatic): $d\Theta/dz < 0$, $-dT/dz > \gamma_a$
- neutral (adiabatic): $d\Theta/dz = 0$, $-dT/dz = \gamma_a$
- stable (subadiabatic): $d\Theta/dz > 0$, $-dT/dz < \gamma_a$

and in addition:

- isothermal: $dT/dz = 0$, $d\Theta/dz = \gamma_a$
- inversion: $dT/dz > 0$, $d\Theta/dz > \gamma_a$

Equation (6) can be transformed into the form:

$$\frac{d^2 z}{dt^2} = -N^2 z \quad (8)$$

where N is the Brunt-Väisälä frequency defined as:

$$N^2 = \frac{g}{T_o} \frac{d\Theta}{dz} \quad (9)$$

The general solution of the differential equation (7) is:

$$z = A e^{iNt} + B e^{-iNt} \quad (10)$$

If $N^2 > 0$, the stratification is stable and equation (10) describes a vertical oscillation with angular frequency N . The period $2\pi/N$ is typically a few minutes long. These oscillations can be interpreted as gravity waves, since their nature is strongly affected by the action of gravity.

1.5 Scales of Atmospheric Motions

In 1926, L.F. Richardson (1881-1953) noted that atmospheric motion occurs over a broad range of horizontal length scales -- from thousands of kilometers to millimeters. The largest scale motion is caused by thermal and pressure contrasts over the globe, modified by the rotation of the Earth. Land and oceans introduce additional modifications to this primary flow and help to initiate secondary circulations. Local topography introduces tertiary circulations. A cascade process, in which eddies of the largest (global) size trigger smaller and smaller (local) ones, continues down to molecular motions, which finally cease due to viscosity. Richardson's poetic version depicts the changes quite accurately:

Big whirls have little whirls,
That feed on their velocity;
And little whirls have lesser whirls,
And so on to viscosity.

The range of scales of atmospheric motions can be adequately defined by considering fundamental frequencies of the atmospheric motions (e.g., Atkinson, 1995):

- the Brunt-Väisälä frequency: $N = (g/T_o d\Theta/dz)^{1/2} \sim 10^{-2} s^{-1}$
- the inertial frequency: $f = 2\Omega \sin \phi \sim 10^{-4} s^{-1}$
- the planetary frequency: $P = (U b)^{1/2} \sim 10^{-6} s^{-1}$

where f is the Coriolis parameter, the Ω angular velocity of the Earth, ϕ is the latitude, U is the horizontal velocity of air, b is the rate at which the Coriolis parameter changes with the latitude. The Brunt-Väisälä frequency N defines gravity oscillations in the stratified atmosphere. The inertial frequency f results from the rotation of the Earth. The planetary frequency P is related to oscillations in the westerlies flow in the middle and upper troposphere.

Based on these fundamental frequencies N , f , and P listed above, the following scales of atmospheric motions can be defined:

- planetary scale: $F < P$, or $F < 10^{-6} s$
- large scale: $P < F < f$, or $10^{-6} s < F < 10^{-4} s$
- meso-scale: $f < F < N$, or $10^{-4} s < F < 10^{-2} s$
- small scale: $F > N$, or $F > 10^{-2} s$

where F is the frequency of the atmospheric circulation under consideration. The corresponding length scale L can be obtained by assuming $L = 2\pi U/F$, where U is the velocity of the air ($U \sim 10$ km/h). Consequently:

- planetary scale: $L > 2\pi U/P$, or $L > 1500$ km, but limited by the circumference of the Earth
- large scale: $2\pi U/f < L < 2\pi U/P$, or 200 km $< L < 1500$ km
- meso-scale: $2\pi U/N < L < 2\pi U/f$, or 2 km $< L < 200$ km
- small scale: $L < 2\pi U/N$, or $L < 2$ km.

Atmospheric transport and diffusion closely follow this classification. Pollutants from local/urban sources (isolated factories, power plants, waste disposals, e.t.c) are quickly dispersed by small-scale motions near the Earth. Pollutants emitted from major industrial areas or forest fires retain high concentrations for greater distances and are dispersed on small and meso-scales. In cases of powerful sources (e.g., nuclear plant explosions or the burning of oil wells), high concentrations of air pollution can remain in the atmosphere for a very long time.

The planetary scale circulations transport material injected into higher levels of the atmosphere. Such injections can occur during volcanic eruptions, when tons of dust and ash are spewed into the atmosphere. Some of this material reaches to the levels of the stratosphere and can be slowly redistributed around the Earth by planetary-scale circulations. Pollutants which do not reach above the troposphere are dispersed much faster by large, meso- and small-scales motions. A more detailed discussion of atmospheric motions of various scales is introduced in the following sections.

1.6 Planetary-Scale Circulations

The planetary-scale circulation of the atmosphere is schematically illustrated in Figure 4. An understanding of planetary-scale circulations is necessary to an appropriate description of tropospheric and stratospheric transport and transformations of carbon dioxide, methane, ozone, water vapor, nitrous oxide, chloro-fluoro-carbons, and aerosols. For this reason the analysis of planetary-scale circulations is often performed in conjunction with atmospheric chemistry. This approach was used, for example, to explain the ozone-hole effect.

As depicted in Figure 4, at the equator (latitude 0°) air is thermally forced upward and begins its high-level flow to the north and to the south. At the same time, the air over the north pole begins its low-level journey southward. This simple convective transfer between the equator and the poles is disrupted by the Earth's rotation, and three separate circulation cells are established. The subtropical cell is called the Hadley cell, the middle one is called the Ferrel cell, and the third one is called the Polar cell.

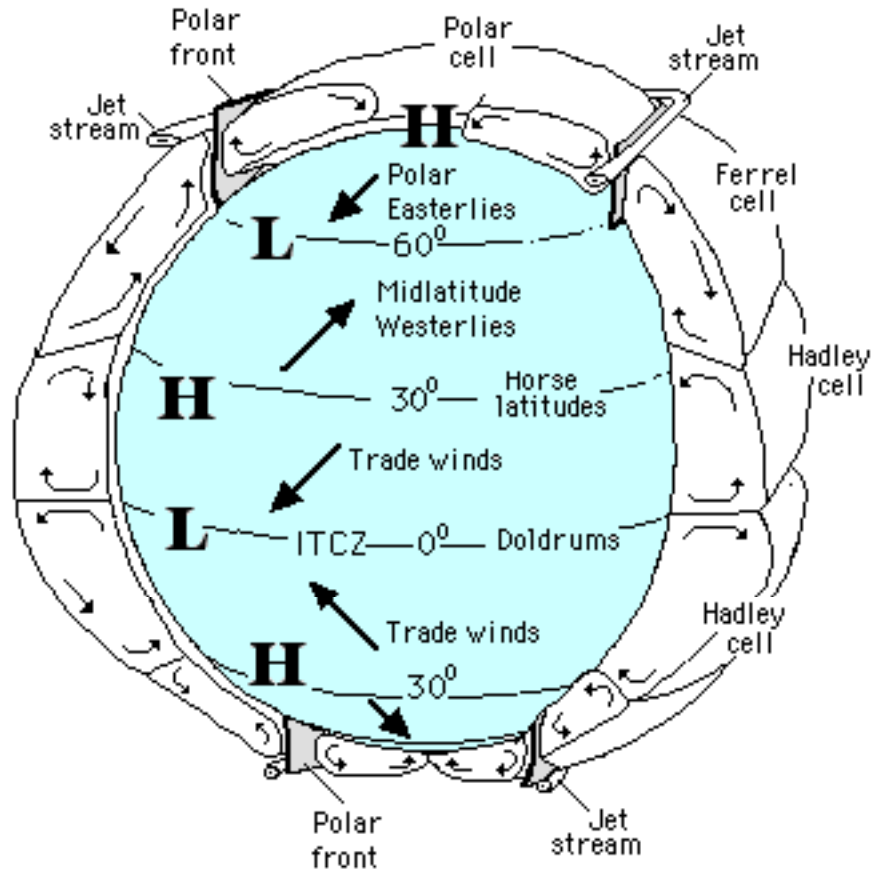


Figure 4. The general circulation of the atmosphere. Idealized zonal belts of high and low pressure systems are marked by letters H and L.

In the northern hemisphere, the Coriolis force turns the air to the right. As a result, below the 30° latitude, lower winds become easterly and upper winds westerly. At the same time, the air over the north pole is deflected to the right, and becomes easterly above 60° latitude. A similar picture occurs in the southern hemisphere.

A semi-permanent high pressure belt (marked by a letter H) is formed near the 30° latitude, in both the northern and southern hemispheres. Air ascends around 60° latitude in subpolar low pressure zones (marked by a letter L), which are created in both hemispheres. Subpolar lows are accompanied by a distinct boundary, which separates cold air moving south, and mild air traveling poleward. This boundary between the Polar and Ferrel cells is called the "polar front". In the tropopause, above the Polar front, there is a meandering globe-circling current of westerly winds. The current, called a "jet-stream", moves air with a typical speed of about 150 km/h. It is hundreds of kilometers wide and only a few kilometers deep (see its photo at web site⁴).

⁴ http://www.lpi.usra.edu/images/sclo/sclo_S02.gif

A zone near the equator is called the "intertropical convergence zone" (ITCZ, see web site⁵). This region of very monotonous weather and weak winds is referred to as the "doldrums". Steady east winds in the zone 0° to 30° are called the "trade winds". Trade winds provided sailing ships with a route from Europe to America. From the 16th to the 19th centuries, the northeast trades were used to transport goods to Africa, where they were exchanged for slaves. From Africa, sailing boats filled with human cargo voyaged to America, employing southeast trades. From America, with the help of prevailing westerlies, they returned to Europe loaded with sugar, rum and cotton.

Latitudes of about 30° are called the "horse latitudes". In this specific region, sailing was frequently very slow and when food dwindled, horses were eaten by the sailors.

1.7 Large-Scale Circulations

Large-scale circulations are characterized by horizontal length scales varying from few hundreds to few thousands kilometers. Such circulations affect mostly horizontal dispersion of pollutants in the troposphere on time scales of days to several weeks. Large-scale circulations in the atmosphere are dependent on distribution of pressure patterns. Five distinct pressure systems can be defined surface weather charts (see Figure 5):

1. Lows (marked by a letter L), also called cyclones, pressure systems surrounded on all sides by higher pressure;
2. Highs (marked by a letter H), also called anticyclones, pressure systems surrounded on all sides by lower pressure;
3. Troughs, elongated areas of low pressure with the lowest pressure along a line marking the maximum curvature of isobars;
4. Ridges, elongated areas of high pressure with the highest pressure along a line marking the maximum curvature; and
5. Cols, neutral areas between two lows and two highs.

Large-scale circulations transport various air masses. Atmospheric air masses are bodies of air with nearly uniform temperature and moisture. Air masses can be classified depending upon their source regions as polar (P), arctic (A), or tropical (T). Each of those masses can also be specified as continental (c), or marine (m). Moreover, a small letter (w) or (k) was used to indicate that an air mass was warmer or cooler than the underlying surface. Therefore, "mTw" would indicate hot and humid tropical air initiated over the ocean and warmer than the underlying surface.

⁵ http://www.cyf-kr.edu.pl/IMGW/sat/index_pl.html

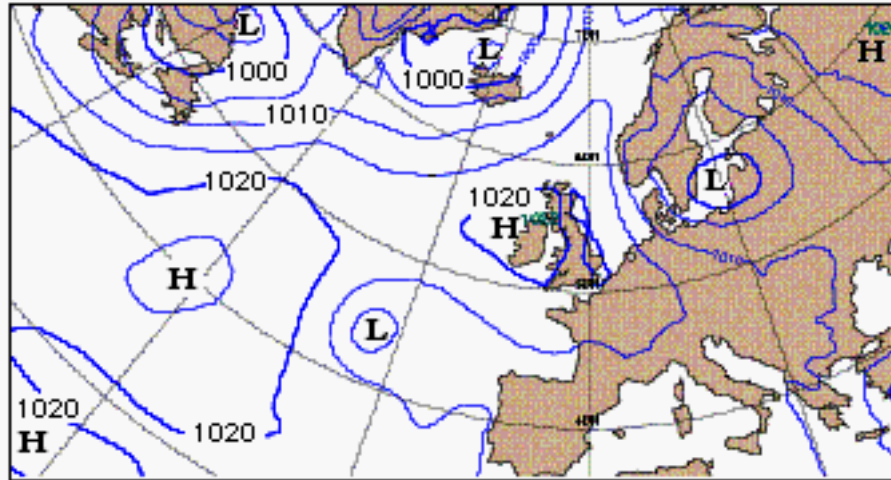


Figure 5. A typical surface weather chart.

A transition zone between two different air masses is called a front (see the photo on the web site⁶). Fronts form at outer boundaries of high-pressure systems and extend all the way to the center of the low-pressure system (Figure 6). Across the frontal zone, temperature, humidity and wind often change rapidly over short distances. Fronts can be classified into four groups: cold, warm, occluded and stationary. The cold front is the leading edge of an advancing cold air mass. Analogously, the leading edge of an advancing warm air mass is called the warm front. When the cold front catches up with the warm front, the two occlude (close together). The result is an occluded front. When neither the cold nor warm air masses are advancing, the front is called stationary.

At the cold front, colder and denser air wedges under the warmer air and forces it upward. The frontal edge has an average slope of 1:50 (1 unit of height: 50 units of length), which is due to friction which slows the flow near the ground. As the moist, unstable air rises, its water vapor condenses into a series of cumulus clouds, cumulonimbus (Cb), and altocumulus (Ac). Strong, upper level winds blow the cirrostratus (Cs) and cirrus (Ci) clouds, far in advance of the approaching front, as shown in the Figure 7.

⁶ <http://www.photolib.noaa.gov/historic/nws/wea00025.htm>

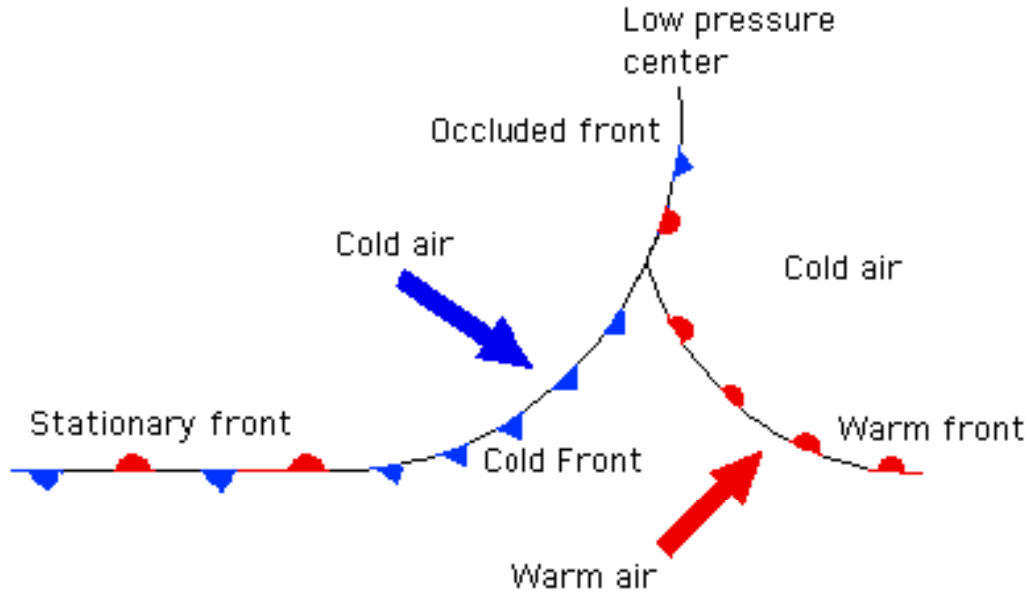


Figure 6. Atmospheric fronts on a surface weather chart.

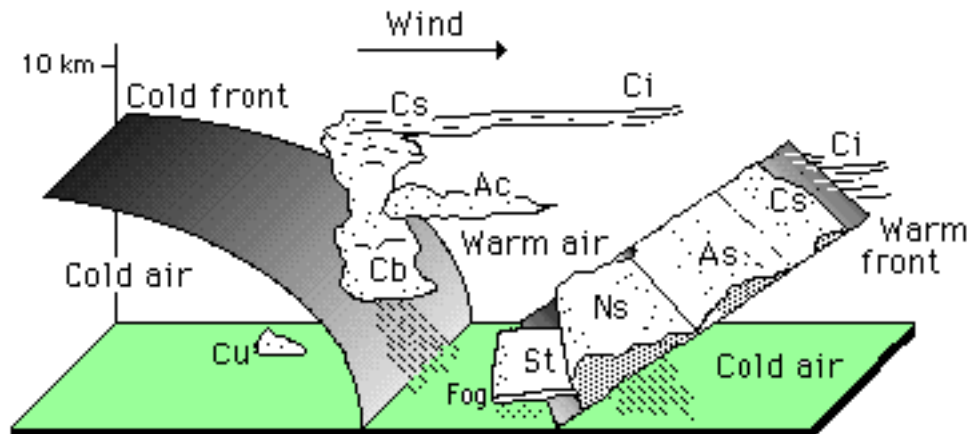


Figure 7. Frontal cloud systems.

The frontal surface of the warm front is less steep (about 1:100). Behind a warm front the stratus clouds (St) and fog are observed near the Earth's surface. Stratus clouds can produce drizzle. As air moves upward along the warm front, nimbostratus clouds (Ns) form, producing a broad area of rain or snow. Farther along the front, clouds gradually transform into altostratus (As), and then into a thin, white veil of cirrostratus (Cs). On top of the frontal surface, there are usually cirrus (Ci) clouds.

There is a simple empirical rule, known as the Buys-Ballot law, which relates the direction of the wind near the Earth's surface to the pressure field. The rule is strictly valid above the near-surface layer of frictional influence. According to the

Buys-Ballot law, if you stand in the Northern Hemisphere, with the wind blowing at your back, the low pressure center will be located to the left. In the southern hemisphere, with the wind blowing at your back, the low pressure will be located to the right. The explanation of the rule is shown in Figure 8.

When the air mass is pushed by the horizontal pressure gradient force, it initially moves towards the low pressure area (vector V_1 in the figure). The moving parcel is simultaneously under the influence of the Coriolis force (outlined arrows indicated as C_1 and C_2), which changes its direction (vectors V_2 and V_3). The air changes its direction until an equilibrium between the pressure and the Coriolis forces is reached. The wind resulting from this equilibrium blows along isobars (lines in the figure marked 1000 mb, 1004 mb), and is called geostrophic. The term was coined from the Greek words: ge, "the Earth", and strophein, "to turn".

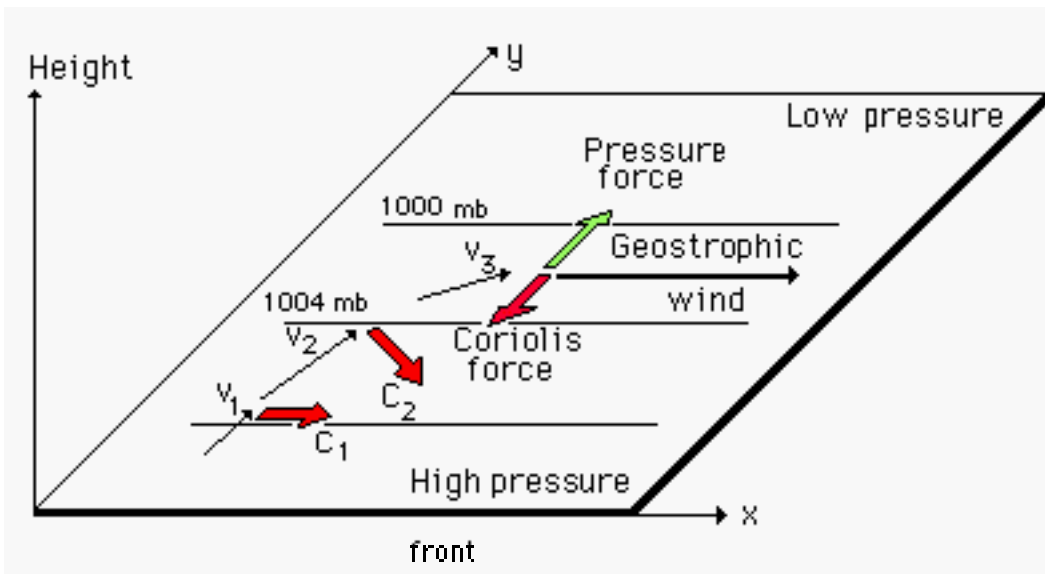


Figure 8. The geostrophic wind on the surface weather chart.

The isobars in Figure 8 are straight lines. In cases with strongly curved isobars, there is a balance of the pressure gradient, Coriolis, and the centrifugal forces (centri: center, fugio: to flee). In the Northern Hemisphere this balance is associated with a clockwise circulation in anticyclonic (high) pressure systems, and counterclockwise circulation in cyclonic (low pressure) ones (Figure 9a).

Near the Earth's surface, in the presence of friction, the pressure force is no longer balanced by the Coriolis and centrifugal forces, and the wind is directed from high pressure to low pressure, crossing isobars at an angle of about 30° (Figure 9b). The resulting inward motion toward a low pressure center is called horizontal convergence. In just the opposite, outflow in a high pressure center is called horizontal divergence. Horizontal convergence near the ground in the low-pressure system causes the accumulation of air in the center. To remove inward-flowing air, a very slow (a few cm/s) but persistent vertical upward motion is

generated. On the other hand, there is a descending flow of air to compensate for the high-pressure divergence near the ground.

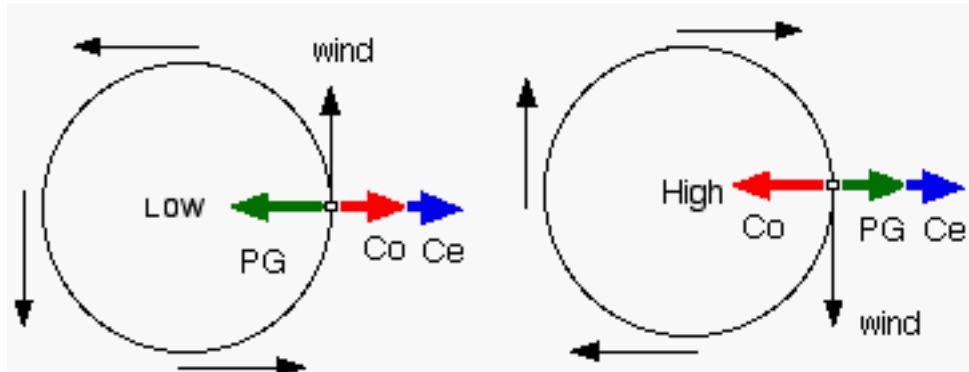


Figure 9a. Flow in the pressure systems without friction (upper row) near the Earth's surface. PG-the pressure gradient force, Co-the Coriolis force, Ce-the centripetal force

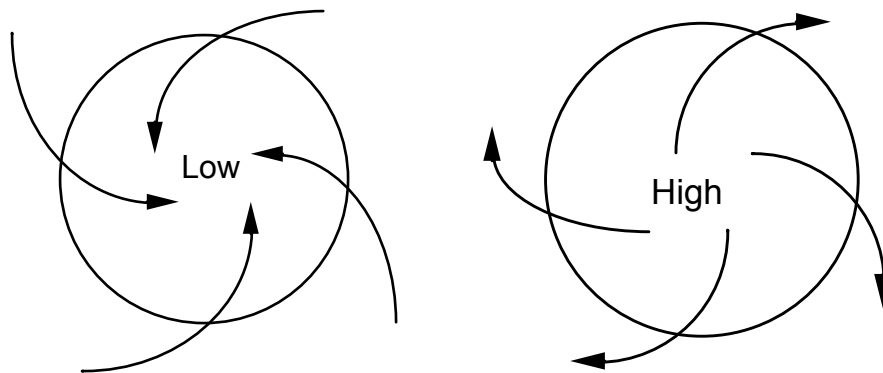


Figure 9b. Flow in the pressure systems with friction near the Earth's surface. PG-the pressure gradient force, Co-the Coriolis force, Ce-the centripetal force.

Because most fluid phenomena on the Earth involve rotation, the concept of vorticity is useful to explain complex atmospheric motions. Vorticity occurs as a result of different portions of fluid being moved by different amounts. To define vorticity, a cross-like element "+" between two mutually perpendicular infinitesimal fluid lines can be considered. The sum of their angular velocities (around an axis which is perpendicular to the plane of the cross "+") is called vorticity (around this axis). In laboratory conditions, vorticity (around an axis) can be measured by a simple vorticity-meter, which consists of four vanes rigidly attached at right angles to a vertical axis.

Vorticity is a vector quantity, since it depends on the orientation of the axis of rotation. In meteorology, rotation about a vertical axis is often considered. Vorticity is defined to be positive (cyclonic) when the fluid spins counter-

clockwise, and negative (anticyclonic) when the fluid spins clockwise (when viewed from above). Because the Earth spins, it also has vorticity. In the northern hemisphere, the Earth's vorticity is always positive, because the Earth spins counter-clockwise about its vertical axis.

The amount of the Earth's vorticity depends on latitude. If the vorticity-meter is placed on the north pole, it will spin about its vertical axis, with the speed of one revolution per day. Thus, according to our definition, the Earth's vorticity equals the doubled angular velocity of the Earth. When the vorticity-meter is placed on the equator, it will not spin about its vertical axis. Its vorticity is nil. The absolute vorticity is defined as a sum of the Earth's vorticity and the vorticity of the air relative to the Earth.

The concept of vorticity is useful for explaining many phenomena in the atmosphere. For instance, it can be used to explain the development of Rossby waves in westerlies flow (Figure 10), in the middle and upper troposphere. Rossby waves are wavelike patterns, usually three to five in number, which extend completely around the Earth. The wave flow of the westerlies provides an important mechanism for heat and contaminant transfer across mid-latitudes.

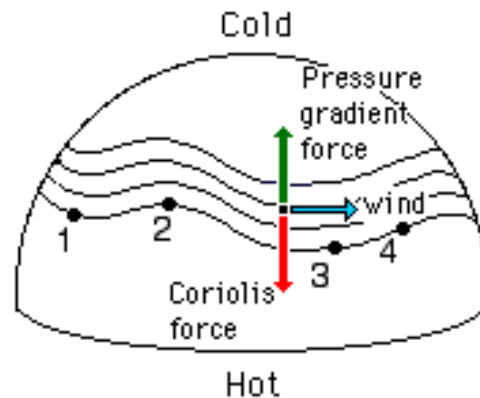


Figure 10. Rossby waves: wave-like patterns in westerlies flow.

Westerlies depicted in Figure 10 exist as a result of a balance between the horizontal pressure gradient and Coriolis forces. To explain Rossby waves consider a parcel of air in the middle troposphere (about 5 km above the Earth) at position "1". It has been proven that such a parcel conserves its absolute vorticity. Imagine that the parcel is heading toward the pole, to the region of increasing Earth's vorticity. To keep the absolute vorticity constant, there must be a corresponding decrease in the relative vorticity of the parcel. Consequently, at position "2", the parcel turns clockwise toward the southeast. Now the air is moving into a region where the Earth's vorticity is smaller. As a result, the parcel's relative vorticity must increase. At position "3", the air turns counterclockwise, and at position "4" begins to head toward the Pole again.

1.8 Meso-Scale Circulations

Meso-scale circulations can be characterized by horizontal length scales on the order of a few tens to several hundred kilometers. Meso-scale flows can be mechanically or thermally forced and generated near the Earth's surface due to the effects of the Earth's topography, or in the free-atmosphere. For example, up-slope or down-slope winds are circulations which are mechanically forced by topography. Examples of circulations, which are thermally forced in the free atmosphere, include hurricanes, (see photo at web site⁷), severe convective storms. (see web site⁸), and frontal circulations. Gravity waves are circulations which are dynamically or thermally forced by topography (see the web site⁹).

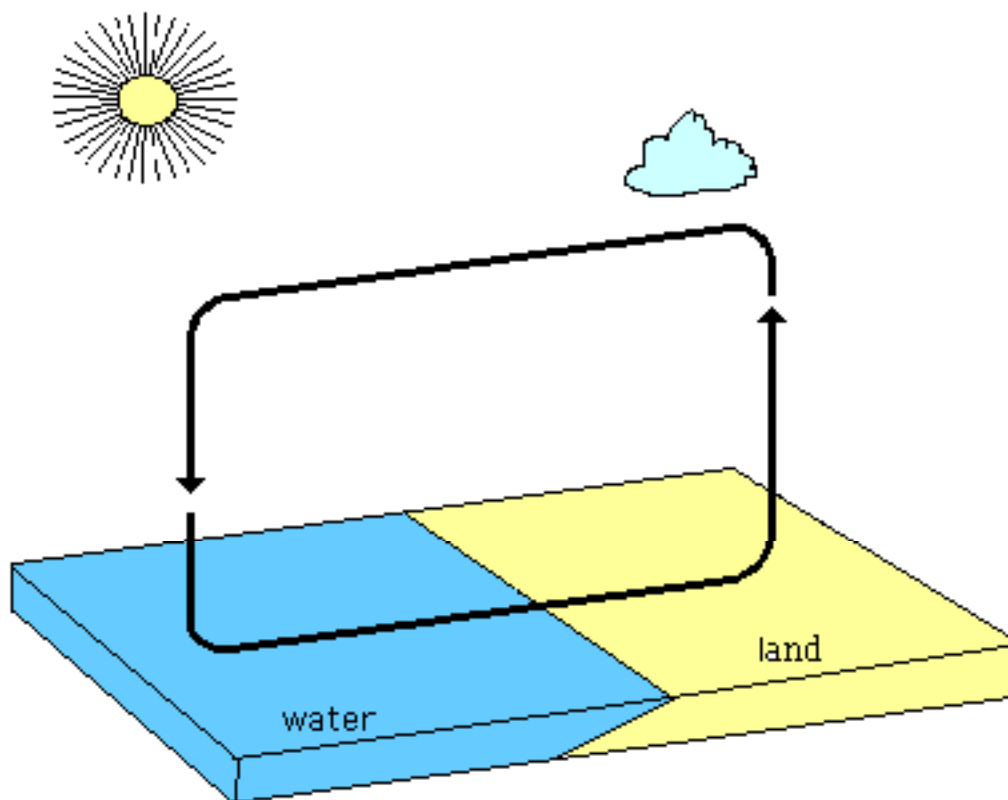


Figure 11. A schematic structure of the sea breeze.

Meso-scale convection is often induced by the temperature contrasts at the Earth's surface. Resulting circulations include sea/land breezes, lake breezes, urban heat islands, mountain and valley winds, and monsoons. They are best developed when large-scale winds are weak. One example is the sea/land breeze generated by the diurnal differences of temperature between the sea and the land. During the daytime, the coast heats more rapidly than the sea, which causes convection

⁷ http://www.lpi.usra.edu/images/sclo/sclo_S30.gif

⁸ http://www.lpi.usra.edu/images/sclo/sclo_S05.gif

⁹ http://www.lpi.usra.edu/images/sclo/sclo_S20.gif

over hot land. Conversely, at night, land cools more quickly than the sea, which causes subsidence of air (Figure 11). As a result, the compensating flow during the day (sea breeze) is directed toward the land, and in the opposite direction at night (land breeze).

Traces of meso-scale flows, such as hexagonal cells and horizontal rolls, can often be seen from high flying aircraft or from a satellite perspective, if clouds are present. The photo in Figure 12 depicts characteristic cloud bands which indicate the presence of rolls in the atmosphere. The presence of horizontal roll vortices is marked by cloud streets which form in the regions of upward-moving air.

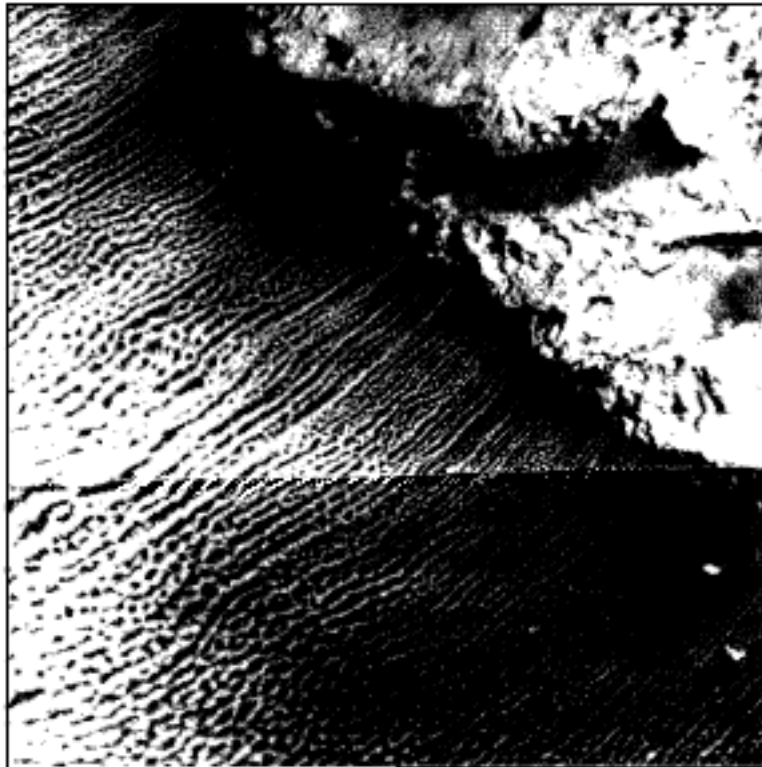


Figure 12. Cold air flowing off an ice pack over the Bering Sea. February 22 1983. (NOAA Satellite photo)

Studies of Brown (1980) that show the angle between the roll direction and the free stream vary from about 30° in the stable case to about 5° for the convective case. Kuettner (1959, 1971) found the following typical properties of rolls: length: 20 - 500 km, spacing: 2 - 8 km, height: 0.8 - 2 km, width/height ratio: 2 - 4 : 1. The structure of such rolls is very difficult to determine from tower measurements since their axes are parallel to the wind, their crosswind propagation velocity is small, and also because the spacing between rolls is several kilometers.

1.9 Small-Scale Circulations, Turbulence

Small-scale motions are characterized by a horizontal length scales from millimeters to a few kilometers. Consequently, they are considered local with respect to air pollutant sources. Small-scale motions can be generated by temperature contrasts at the Earth's surface, wind shear, effects of the Earth's topography. They can also occur above the Earth's surface in statically stable flows or on a density discontinuity interfaces, when the destabilizing influence of the wind shear overcomes the stabilizing effect of the buoyancy force.

The last effect is called Kelvin-Helmholtz instability. If the static stability of the flow is not sufficient to dampen perturbations excited by the wind shear, they may amplify. Eventually the waves may break and dissipate into smaller scale complex and chaotic motion called turbulence. Turbulence is an essential part of the mechanism which disperses air pollutants and is crucial for the efficiency of many natural processes, such as the evaporation of water, dissipation of fog, and dispersion of plant seeds.

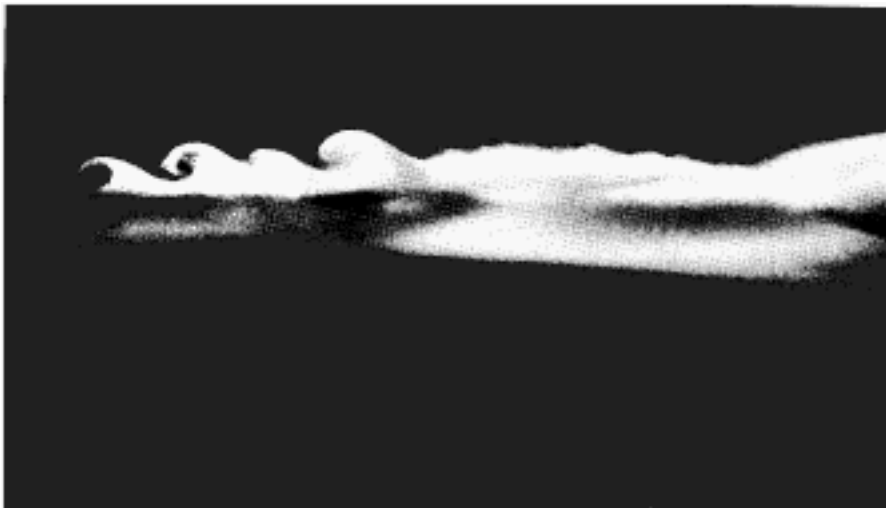


Figure 13. Kelvin-Helmholtz instability, revealed by the cloud patterns in the atmosphere (NCAR.NSF Photo Archive)

Kelvin-Helmholtz instabilities have been observed by radar [Gossard and Richter (1970), Gossard, et al. (1971), Gossard, et al. (1973), and Richter, et al. (1973)]. The internal waves, originated through Kelvin-Helmholtz instability, are typically several hundred meters in length. Their velocity of propagation was found to be about the same as the mean velocity of the layer in which they are embedded (Hooke, et al. 1973). With the passage of internal gravity waves, very thin shear layers of small-scale turbulence are observed moving up and down. Sometimes this type of instability is revealed by the cloud patterns on top of the boundary layer (Figure 13).

To further analyze small-scale motions let us assume that a horizontally homogeneous flow is affected by a small-scale disturbance characterized by length scale λ , velocity scale v_λ , and temperature scale θ_λ . The rate at which the kinetic energy of the motion is produced by the disturbance in the unit of time is:

$$R_{1\lambda} \sim v_\lambda^3 / \lambda \quad (11)$$

The kinetic energy of the disturbance is later employed as work against viscosity force:

$$R_{2\lambda} \sim \nu v_\lambda^2 / \lambda^2 \quad (12)$$

and also against the buoyancy force:

$$R_{3\lambda} \sim \beta \theta_\lambda v_\lambda \quad (13)$$

where $\beta = g/T$ is the buoyancy parameter. The disturbance persists only, if $R_{1\lambda} > R_{2\lambda} + R_{3\lambda}$. When the role of the buoyancy force is small then $R_{2\lambda} \gg R_{3\lambda}$ and $R_{1\lambda} > R_{2\lambda}$, which is equivalent to:

$$\lambda v_\lambda / \nu = Re_\lambda > 1 \quad (14)$$

where Re_λ is the Reynolds number for the disturbance.

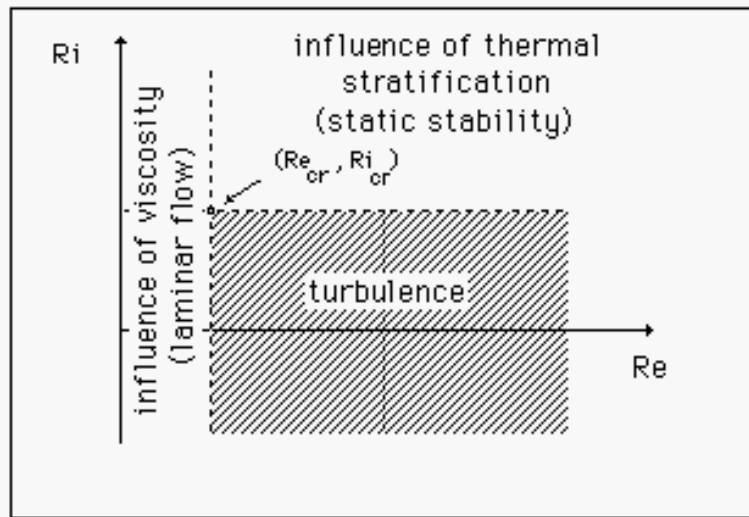


Figure 14. Regions of turbulent flows.

In contrast, if the role of the buoyancy force is large and $R_{3\lambda} \gg R_{2\lambda}$ then $R_{3\lambda} < R_{1\lambda}$, which is equivalent to:

$$\beta \theta_\lambda \lambda / \omega_\lambda^2 = Ri_\lambda < 1 \quad (15)$$

where Ri_λ is the Richardson number for the disturbance.

In conclusion, turbulence is maintained if the Reynolds number Re is larger or, more precisely, if it is greater than its critical value Re_{cr} and, similarly, if the Richardson number R_i is smaller than its critical value Ri_{cr} . This is illustrated in Figure 14.

To describe turbulence, it is convenient to adopt the approach of O.Reynolds (1842-1912) who in 1895 proposed decomposing any flow variable into a mean quantity (marked by overbars) and a fluctuation about the average (letters with primes). For example, for wind components and the potential temperature we have:

$$u_i = \bar{u}_i + u'_i \quad (16)$$

$$\Theta = \bar{\Theta} + \theta'$$

The averaging procedure can be defined in different ways, as time average, space average or ensemble average. In a conventional theoretical procedure the mean quantities are ensemble averages. It is assumed that atmospheric flows are members of an ensemble whose individual realizations obey the Navier-Stokes equations. Ensemble averages have the following properties:

$$u_i(t) = \lim_{N \rightarrow \infty} \frac{u_i(t;1) + \dots + u_i(t;N)}{N} \quad (17)$$

where $u_i(t; j)$ is the j -member of an ensemble of i -components of the wind velocity ($i = 1, 2, 3$) and the overbar denotes the ensemble averaging operator. From (17) it follows that an ensemble average of a primed quantity is zero, and doubled averaging produces the same average. The average of the nonlinear term $u_i u_j$ has the form:

$$\overline{u_i u_j} = \bar{u}_i \bar{u}_j + \overline{u'_i u'_j} \quad (18)$$

Thus, ensemble averaging of the product $u_i u_j$ introduces additional terms $\overline{u'_i u'_j}$ called the Reynolds stress terms. Since $i, j = 1, 2, 3$, there are 9 Reynolds terms. Because of symmetry, 3 terms are equal and only 6 terms are different.

Similarly, the average of the nonlinear temperature term has the form:

$$\overline{u_j \Theta} = \bar{u}_j \bar{\Theta} + \overline{u'_j \Theta'} \quad (19)$$

The ensemble averaging of the products $u_j \Theta$ introduces 3 additional terms.

In order to explain the meaning of the additional terms which appear in (18)-(19), consider two horizontal layers of air flow with slightly different horizontal velocities and temperatures. The random vertical intrusions of some slower

parcels of air into the faster stream tend to slow down the faster stream. The intrusion of faster parcels into the slower stream tend to speed up the slower stream. Similarly intrusions of cooler parcels of air will cool while intrusions of warmer parcels will warm the stream. Therefore, the wandering of individual parcels introduces the vertical momentum (stress) and the heat flux in the turbulent flow. The resulting horizontal turbulent stress vector is usually denoted as $\tau = (-\rho\overline{u'w'}, -\rho\overline{v'w'})$ where ρ is the air density. The vertical heat flux can be expressed as $H = c_p \rho\overline{w'\Theta'}$, where conventional meteorological notation was applied: $u_1 = u$, $u_2 = v$, $u_3 = w$, and c_p is the specific heat of dry air.

2 Boundary-Layer Meteorology

2.1 General Description

The planetary boundary layer (PBL) is the lowest portion of the atmosphere, about 1 - 2 km deep, which intensively exchanges heat as well as mass (water, gases) with the Earth's surface. Although the PBL contains only about 2% of the total kinetic energy of the atmosphere, it contributes as much as 25% to its total generation and 35% to its total dissipation. The atmospheric boundary layer is of great practical and scientific importance. Essentially, all human and biological activities take place in this layer. Practically all air pollutants from natural and anthropogenic sources are emitted within the PBL.

Flow in the boundary layer is controlled by the diurnal cycle of the surface energy budget. The energy balance at the surface is expressed as $R_n + G + H + E = 0$, where R_n is the flux of net radiation (global solar radiation received by the surface plus atmospheric radiation minus terrestrial radiation), G is the vertical heat flux into the soil, H and E are the sensible (conduction) and latent (resulting from water phase changes) heat fluxes to the atmosphere. The diurnal changes of the energy balance are shown in Figure 15.

In Figure 15, a quantity has a positive value, when energy is transferred away from the interface, and a negative value in the case of transfer towards the interface. Net radiation flux R_n is negative (down) during the day, reaching minimum values at local solar noon. At night, R_n is positive, illustrating the loss of energy by terrestrial radiation. R_n is zero just before sunset, and just after sunrise. At night, the term E can become negative, if dew forms.

During the day, energy gained at the surface is transferred to the atmosphere, to the soil, and also is used in the evaporation processes. This transfer of heat, from the ground surface to the air directly above it, can generate vertical motions, called convection. Convection redistributes heat throughout the atmospheric boundary layer. The influence of the surface sensible heat flux decreases with height. As a result, the diurnal temperature amplitude also decreases with height.

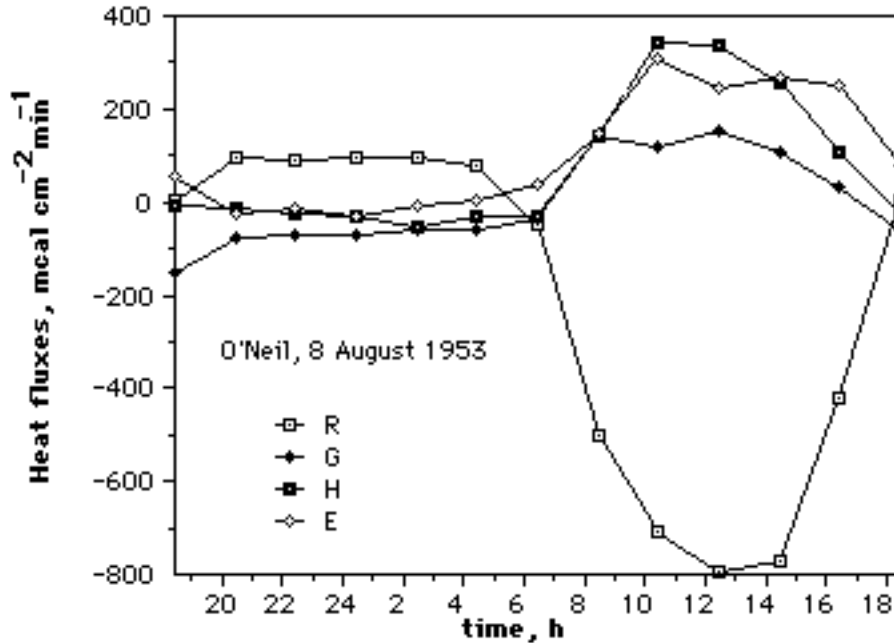


Figure 15. Diurnal distribution of heat fluxes at the Earth's surface, during the 1953 O'Neil experiment. R is the flux of net radiation on the surface, G is the heat flux to the ground, H is the sensible heat flux and E is the latent heat flux from the surface to the atmosphere (after Sorbjan, 1989).

It is generally assumed that over a flat and homogeneous surface, the planetary boundary layer is horizontally homogeneous, but organized vertically into several layers (Figure 16). Within a few millimeters of the surface, there is a viscous sublayer, where the flow is mostly laminar. Above this layer, there is a surface layer, 1-100 m deep, where the turbulent fluxes of momentum, heat, and moisture are approximately constant with height (i.e., they change in magnitude no more than 10% from their surface values).

The wind direction in the surface layer is approximately constant with height. In the first few meters of the surface layer the wind velocity, humidity, and temperature are nearly logarithmic in neutral, and also in stable and convective conditions. Above the logarithmic sublayer the profiles of various meteorological parameters differ depending on thermal stratification. The portion of the boundary layer beyond the surface layer is called the outer layer.

In day-time conditions the potential temperature, humidity and wind velocity in the outer layer are approximately constant with height, and the layer is often called the "mixed layer". At night, the temperature inversion is usually formed near the surface. In the upper portion of the outer layer, called the residual layer, the potential temperature remains constant with height. At the level of few hundred meters above the surface, the wind velocity reaches a maximum, and exceeds the value of the geostrophic wind. This maximum is often called the "low-level nocturnal jet".

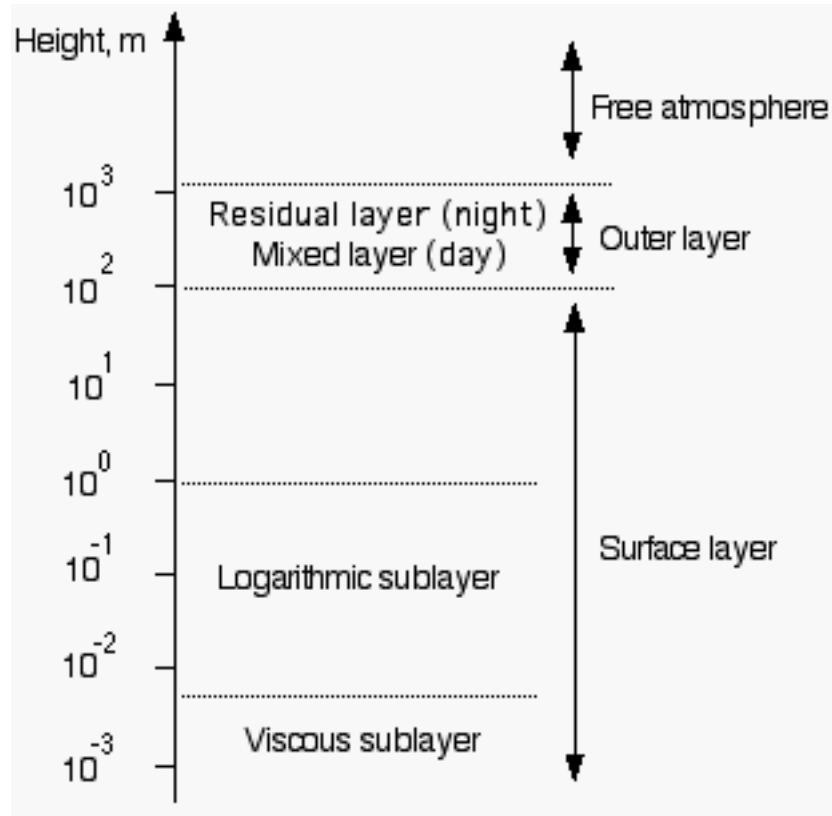


Figure 16. A schematic structure of the planetary boundary layer.

The diurnal changes of temperature are accompanied by changes of wind velocity and wind direction. Above the surface layer the winds are observed to reach maximum speeds at night and minimum speeds during the day. But near the surface, the opposite behavior of wind velocity is observed. The surface wind speed increases after sunrise, peaks in the early afternoon and decreases near sunset. Above the surface layer, the diurnal wave is nearly 12 hours out of phase.

Friction causes the wind velocity in the boundary layer to cease to zero at the surface. The wind direction varies with height because of the influence of the Coriolis force. The latter fact was first discovered in the ocean by F.Nansen (1861-1930), and later explained by V.V.Ekman (1874-1954) in 1905. By examining data from the 1893-1896 Norwegian North Polar Expedition, Nansen noted that sea ice did not drift in the direction of the wind, but at an angle of about 40° to the right of the wind direction (Figure 17). Based on this observation Ekman concluded that each layer of the sea was set in motion by the layer just above it, and successively more deflected by the balance of the Coriolis and friction forces. In honor of his work, the spiraling of the currents in the ocean is named the Ekman spiral.

It was realized later that the Ekman spiral can be observed not only in the ocean but also in the atmospheric boundary layer, where winds in average spiral with height from about 5° (during the daytime) to about 50° at night, clockwise in the

northern hemisphere, but counter-clockwise on the southern hemisphere. The spiraling effect in the atmosphere is caused by the balance of the Coriolis, pressure gradient, and friction forces, and strongly depends on thermal stability. Note that thermal advection of cold or warm (baroclinicity) air can strongly modify this picture.

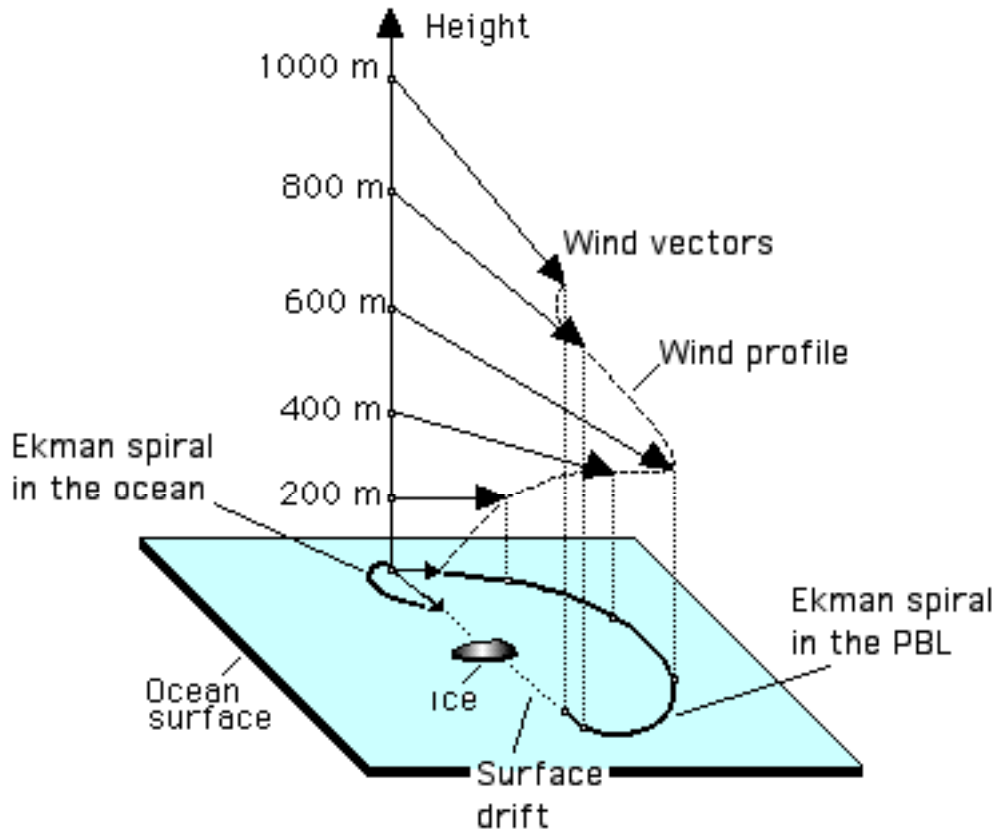


Figure 17. The Ekman spirals in the atmosphere and in the ocean.

During the last several decades, the structure of the atmospheric boundary layer has been intensively studied, not only because of the striking beauty of its coherent structures (e.g., Agee, 1987), but mostly because understanding its flows and clouds is essential in environmental studies, numerical weather prediction, and climate analyses. As a result, since the 1950s, the fundamental knowledge of boundary layer turbulence has been achieved as a result of extensive experimental effort, and also due to numerical modeling. Especially, large-eddy simulations (LES) contributed to our present knowledge of turbulence and diffusion in the ABL (e.g., Deardorff (e.g., 1970, 1972, 1974 a, b, 1976; Mason, 1989; Moeng, 1984, 1998, Moeng and Sullivan, 1994; Nieuwstadt et al., 1992, Schem and Lipps, 1976; Schmidt, H., and U. Schumann, 1989, Sommeria, G., 1976, Sorbjan, 1996 a, b, 1997).

2.2 Viscous and Logarithmic Sublayers

A simple analytical formulation of idealized conditions in the atmospheric boundary layer can be obtained based on similarity and dimensional analysis (Buckingham, 1914). During the last four decades the elegant similarity framework has allowed classification of knowledge on atmospheric turbulence obtained through extensive experimental effort.

The idea of similarity lies in dimensional analysis. The method is based on the assumption that some physical quantities which are necessary and sufficient to describe a certain physical phenomenon are dimensionally dependent on others. One can then form dimensionless groups of these variables which are independent of the system of units chosen: $\pi_o = f(\pi_1, \pi_2, \dots, \pi_{n-r})$, where n is the number of physically relevant variables, such as velocity, density, stress, and r is the number of independent physical units, such as length, time, mass, and the π_i are the nondimensional products. A group of variables which is applied in order to nondimensionalize another variable is often called a scale (e.g., Sorbjan, 1989).

To describe the mean flow in the viscous layer we will seek an expression for the mean wind shear using the π -theorem. We first assume that $dU/dz = f(u_*, \nu, z)$, where $u_* = (\tau_o/\rho)^{1/2}$ is the friction velocity -- representing the surface stress, ν is the molecular viscosity and z is the height. Based on this assumption, the following two nondimensional groups may be formed: $\pi_o = z/u_* dU/dz$, and $\pi_1 = zu_*/\nu$. The first group is the nondimensional wind shear, and the second one may be recognized as the local Reynolds number. In the viscous sublayer, both parameters can be assumed to be of the same order of magnitude, i.e., $z/u_* dU/dz \sim zu_*/\nu$. We may integrate this expression to determine:

$$U \sim u_*^2 z / \nu \quad (20)$$

for the velocity in the viscous sublayer.

Above the viscous layer, the two parameters π_o and π_1 are not of the same order of magnitude. For $z = 10$ m, $u_* = 0.1$ m/s, and $\nu = 10^{-5}$ m²/s, one can easily verify that the wind shear is $O(1)$, and the Reynolds number is $Re \sim u_* z / \nu \sim 10^5$. This difference in magnitude reflects the empirical fact that the viscous stress is negligible compared to the turbulent stress in the surface layer. Thus, for a similarity solution $\pi_o = F(\pi_1)$ to exist in the surface layer (where π_1 is large), F must be asymptotically constant when π_1 is large i.e., for $\pi_1 \rightarrow \infty$, $F(\pi_1) \rightarrow const$. This yields: $z/u_* dU/dz = const = \kappa^{-1}$, where κ is the von Karman constant, empirically estimated to be 0.4. The obtained result may be integrated to yield the logarithmic profile:

$$U(z) = \frac{u_*}{\kappa} \ln\left(\frac{z}{z_o}\right) \quad (21)$$

where the roughness parameter z_o is an integration constant that represents the aerodynamic roughness of the underlying surface. Note that at $z = z_o$, the wind velocity vanishes.

The similarity approach may also be employed to characterize the roughness parameter, z_o , of a homogeneous surface with physical roughness elements of characteristic height, h_o . Applying the π -theorem we obtain: $z_o/h_o = F(u_*h_o/\nu)$, where the product u_*h_o/ν is the roughness Reynolds number Re_r . The thickness of the viscous sublayer is characterized by the parameter $\delta \sim \nu/u_*$.

When the $Re_r \ll 1$, then $h_o \ll \delta$, and the roughness elements are completely submerged in the viscous sublayer. In this hydrodynamically smooth case, we must drop h_o from the list of the governing parameters. Consequently, $z_o/h_o \sim Re_r^{-1}$ or $z_o \sim \nu/u_*$. If $Re_r \gg 1$, then $h_o \gg \delta$, and the roughness elements protrude beyond the viscous sublayer, i.e., the flow is called hydrodynamically rough. We may claim that for $Re_r \rightarrow \infty$, $F(Re_r)$ becomes a constant. The conclusion is $z_o \sim h_o$.

2.3 Surface Layer

Turbulence in the thermally stratified surface layer can be elegantly characterized in terms of the surface layer similarity theory. The theory was formulated about five decades ago by A.S.Monin and A.M.Obukhov (1954). Since then a simple and effective framework of this approach has found many practical applications in experimental analysis of surface layer turbulence, as well as in the parametrization of mass and energy exchange across the Earth's surface.

According to the Monin and Obukhov (M-O) theory, similarity scales in the surface layer can be formulated based on constant values of the kinematic turbulent fluxes $H_o = \overline{w'\theta'}$, $Q_o = \overline{w'q'}$, and $\tau_o / \rho = \overline{w'u'}$:

$$u_*^2 = \tau_o / \rho, \quad T_* = -H_o / u_*, \quad q_* = -Q_o / u_*, \quad L = u_*^2 / (\beta \kappa T_*) \quad (22)$$

where u_* , T_* , q_* , L are the velocity, temperature, humidity (or other scalars, such as ozone or carbon dioxide concentration), and height scales respectively, $\beta = g/T_o$ is the buoyancy parameter, and L is called the Monin-Obukhov length. The sign convention is chosen so that L is negative in unstable and positive in stable stratification. Note that the potential temperature flux H_o in the definition of T_* and L should be replaced by the virtual potential temperature flux H_{ov} when moisture stratification is included. The virtual potential temperature flux is defined as $H_{ov} = H_o + 0.61 T Q_o$, where Q_o is the surface humidity flux. The virtual temperature Θ_v is defined as $\Theta_v = \Theta (1 + 0.61 q)$, where q is the specific humidity.

The Monin-Obukhov length L is roughly the height at which the shear production of turbulent kinetic energy ($= u_*^3/L$) is equal to the buoyant production ($= \beta H_o$). In

the stable boundary layer $H_o < 0$, $T_* > 0$ and $L > 0$. In the unstable boundary layer $H_o > 0$, $T_* < 0$ and $L < 0$. In this case, the turbulent energy production is mainly mechanical (produced by shear) for $z < -L$ (closer to the surface) and buoyant (produced by the heat flux) when $z > -L$.

The similarity theory predicts that any turbulent characteristics of the flow, non-dimensionalized with surface layer scales, will be a universal function of the stability parameter $\zeta = z/L$, e.g.,

$$\begin{aligned} \frac{\overline{w'^2}}{u_*^2} &= \Psi_w(z/L), & \frac{\overline{\theta'^2}}{T_*^2} &= \Psi_\theta(z/L), & \frac{\overline{q'^2}}{q_*^2} &= \Psi_q(z/L), \\ \frac{L}{u_*} \frac{dU}{dz} &= \Psi_m(z/L), & \frac{L}{T_*} \frac{d\Theta}{dz} &= \Psi_h(z/L), & \frac{L}{q_*} \frac{dq}{dz} &= \Psi_q(z/L) \end{aligned} \quad (23)$$

where U , Θ , and q are the mean wind velocity, potential temperature and specific humidity. Usually, the nondimensional gradients are divided by $\zeta = z/L$ and substituted by new similarity functions ϕ , defined as: $\phi_m = \zeta \Psi_m$, $\phi_h = \zeta \Psi_h$, $\phi_q = \zeta \Psi_q$. Consequently:

$$\frac{z}{u_*} \frac{dU}{dz} = \Phi_m(z/L), \quad \frac{z}{T_*} \frac{d\Theta}{dz} = \Phi_h(z/L), \quad \frac{z}{q_*} \frac{dq}{dz} = \Phi_q(z/L) \quad (24)$$

where ϕ_m , ϕ_h and ϕ_q are new similarity functions.

Monin and Obukhov pointed out that the limiting forms of the similarity functions can be determined for three extreme stratification regimes -- neutral, very stable, and very unstable (free-convection).

In neutral stratification, the heat flux is zero, and $z/L = 0$. Thus, all similarity functions ψ must be constant. Consequently $\phi_m, \phi_h, \phi_q \sim \zeta^{-1}$ (and L cancels). This leads directly to logarithmic profiles for wind velocity, temperature and humidity (or other passive scalar). Note that logarithmic profiles are obtained for $0 < |z/L| \ll 1$ (neutral stratification), and also for $0 < z \ll |L|$ (any stratification very close to the surface).

In the very stable layer, when $z/L \rightarrow \infty$, z is no longer a governing variable. Physically, this means that the turbulence is local and suppressed by stratification effects. In this case, $\phi_m \sim \zeta$, $\phi_h \sim \zeta$ and $\phi_q \sim \zeta$, so “ z ” crosses out on both sides of (24). This leads to linear velocity, temperature, and humidity profiles.

In the free-convection case ($z/L \rightarrow \infty$), the mean wind is negligible, so $u_* \rightarrow 0$ (no surface stress), As a result, u_* must be dropped from the list of governing

variables. This leads to a new set of scales: $u_f = (\beta z H_o)^{1/3}$ for velocity, $T_f = H_o/u_f$ for temperature, $q_f = Q_o/u_f$ for humidity (Wyngaard et al., 1971). Note that there is no specific height scale in this case. If we form new nondimensional quantities using these scales, we expect them to be constant, because there is no dimensionless height parameter in this case, which would be equivalent to z/L .

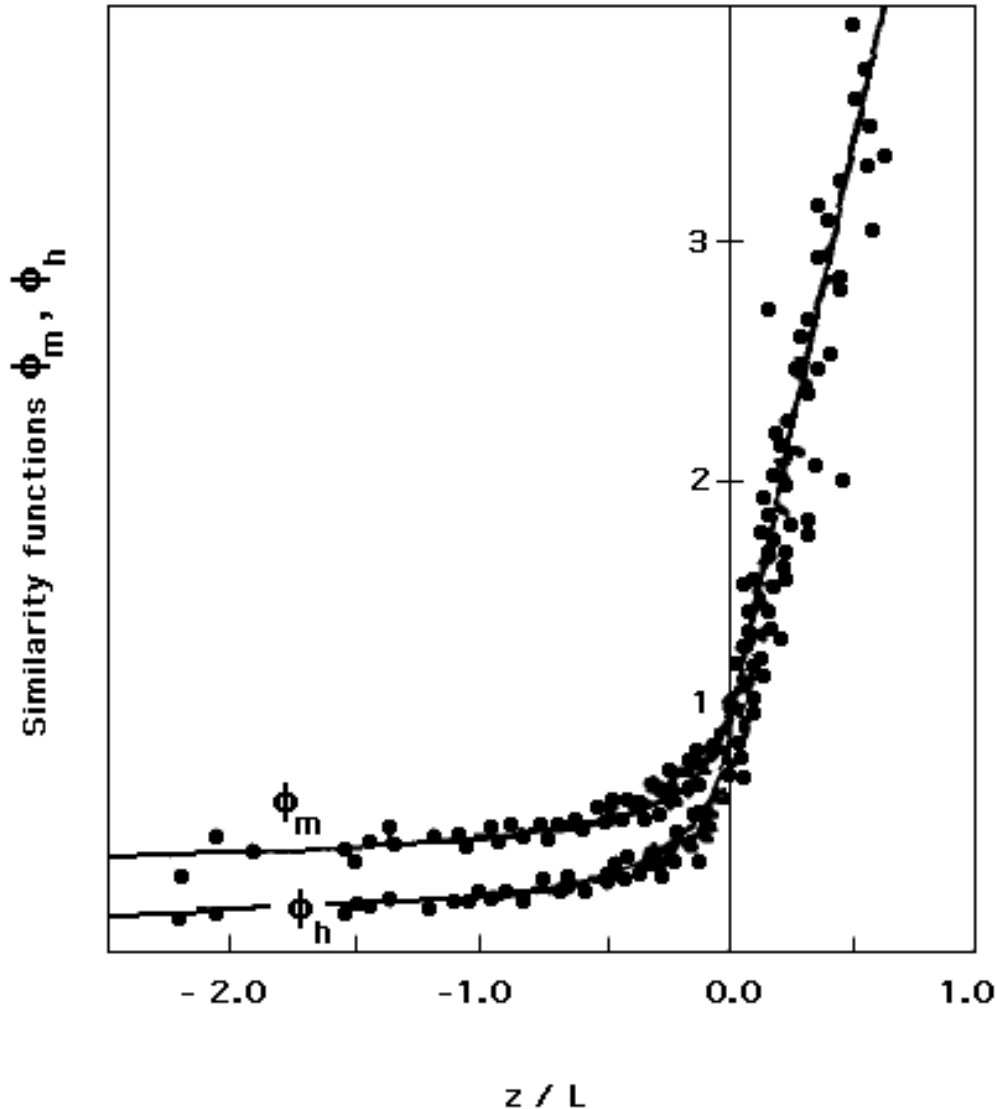


Figure 18. M-O similarity function for wind velocity ψ_m , and temperature ψ_h from the Kansas experiment. The data have been fit with formulas $\phi_m = (1 - 15 \zeta)^{-1/4}$ and $\phi_h = 0.74 (1 - 9 \zeta)^{-1/2}$ for $\zeta < 0$, and $\phi_m = (1 + 4.7 \zeta)$ and $\phi_h = 0.74 + 4.7\zeta$ for $\zeta > 0$ (after Businger et al, 1971).

The direct application of the free-convection scales yields to a prediction for the potential temperature, obtained earlier by Monin and Obukhov: $z/T_f d\Theta/dz = const$. Taking into consideration that $T^*/T_f = \kappa^{-1/3} (-z/L)^{1/3}$, this implies that the dimensionless temperature gradient ϕ_h is proportional to $(-z/L)^{-4/3}$. Consequently,

the mean temperature varies with height as $z^{-1/3}$. In forced convection (convection with wind shear), we could assume that the ratio of momentum and heat fluxes can be evaluated as: $(\tau_o/\rho) / H_o = u_*^2 / (u_* T_*) = (K_m dU/dz) / (K_h d\Theta/dz)$, where K_m and K_h are the eddy viscosity and diffusivity. Assuming that in this case, the Prandtl number $Pr = K_m / K_h = \text{constant}$, we will obtain $\phi_m \sim \phi_h$. This indicates that the mean wind in forced convection should also be proportional to $z^{-1/3}$.

Validity of the Monin and Obukhov surface layer similarity theory has been extensively tested during the last few decades. The measurements of Zilitinkevich and Chalikov (1968) confirmed the convective prediction $\zeta^{-1/3}$ for ψ_m and ψ_h , where $\zeta = z/L$. On the other hand, in the famous "Kansas" field experiment, e.g., Businger et al. (1971), the dependence of the nondimensional temperature gradient and shear profiles (Figure 18) were found to be: $\psi_m \sim \zeta^{-1/4}$ and $\psi_h \sim \zeta^{-1/2}$ for $\zeta > -2$. A later experiment using the BAO tower in Colorado (Kaimal et al., 1982) verified the free-convection limit predictions for standard deviations (Figure 19).

In the stable surface layer, observations confirm similarity predictions, however, the scatter increases as ζ increases. Measurements in this case are very difficult to make due to low levels of turbulence intensity. The increased scatter is most likely due to the increased importance of gravity wave effects.

At this point, words of caution should be expressed that making automatic assumptions regarding dimensional analysis can lead to conclusions that do not reflect reality (e.g., Sorbjan, 1993). For example, refer to Figure 20. In Figure 20a, dimensionless vertical velocity standard deviation follows the M-O theory prediction $\sigma_w/u_* \sim (-\zeta)^{1/3}$ in the convective limit. A similar prediction may be made for the horizontal velocity standard deviations σ_u or σ_v , and Figure 20b appears at first glance to confirm this prediction. However, on closer examination, if the data are grouped either by constant L value, or by constant height, z , (Figure 20 c and d), we see that the data are independent of z . Thus, σ_u is independent of ζ and does not follow the M-O similarity theory. It was later determined that σ_u depends on the non-dimensional parameter $-z_i/L$ because of the influence of large (PBL-scale) eddies on the surface layer turbulence statistics (Panofsky et al., 1977).

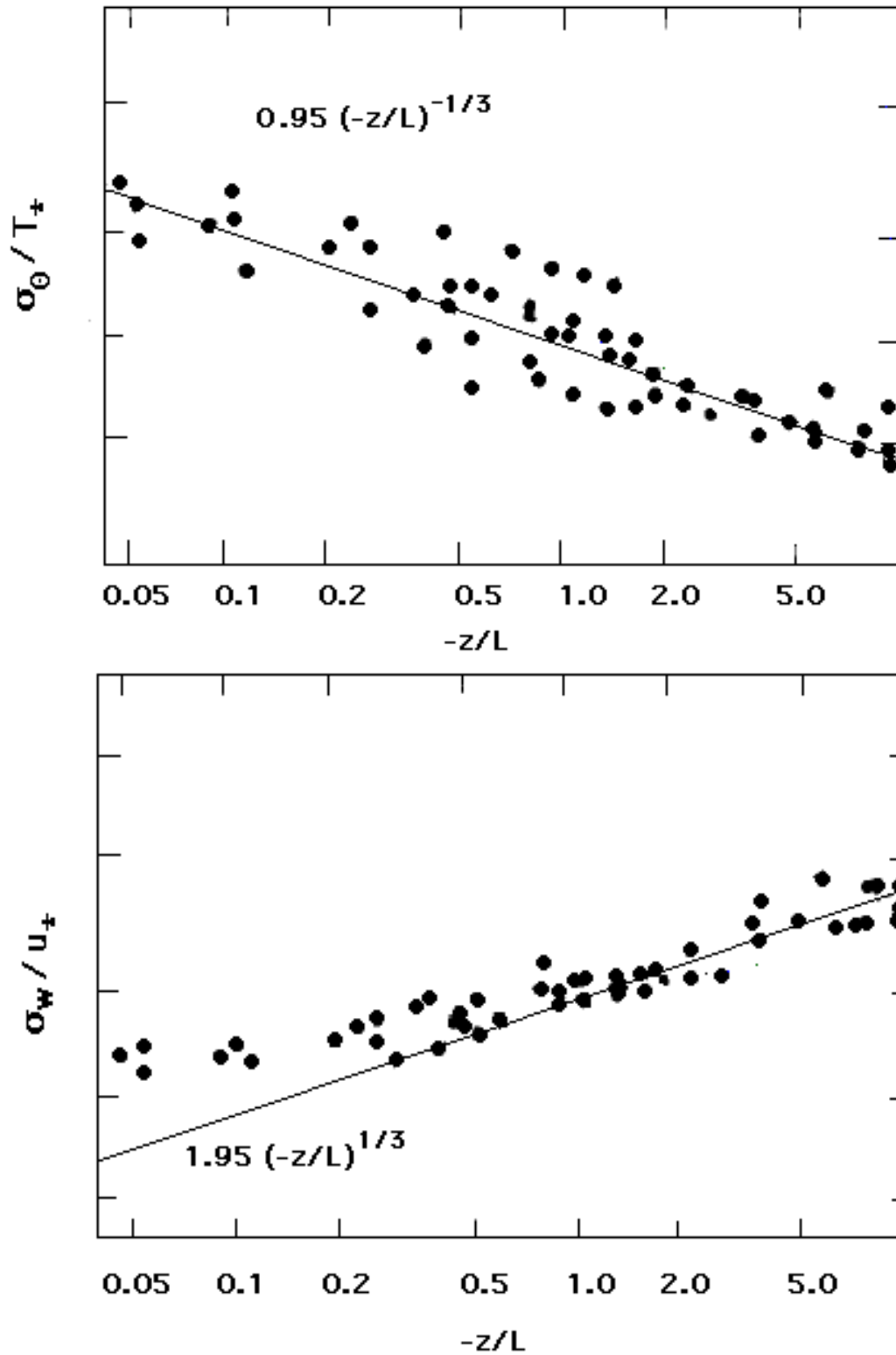


Figure 19. Non-dimensional profiles of the standard deviations σ for (a) temperature, and (b) vertical velocity, as functions of z/L in unstable stratification (after Kaimal et al., 1982).

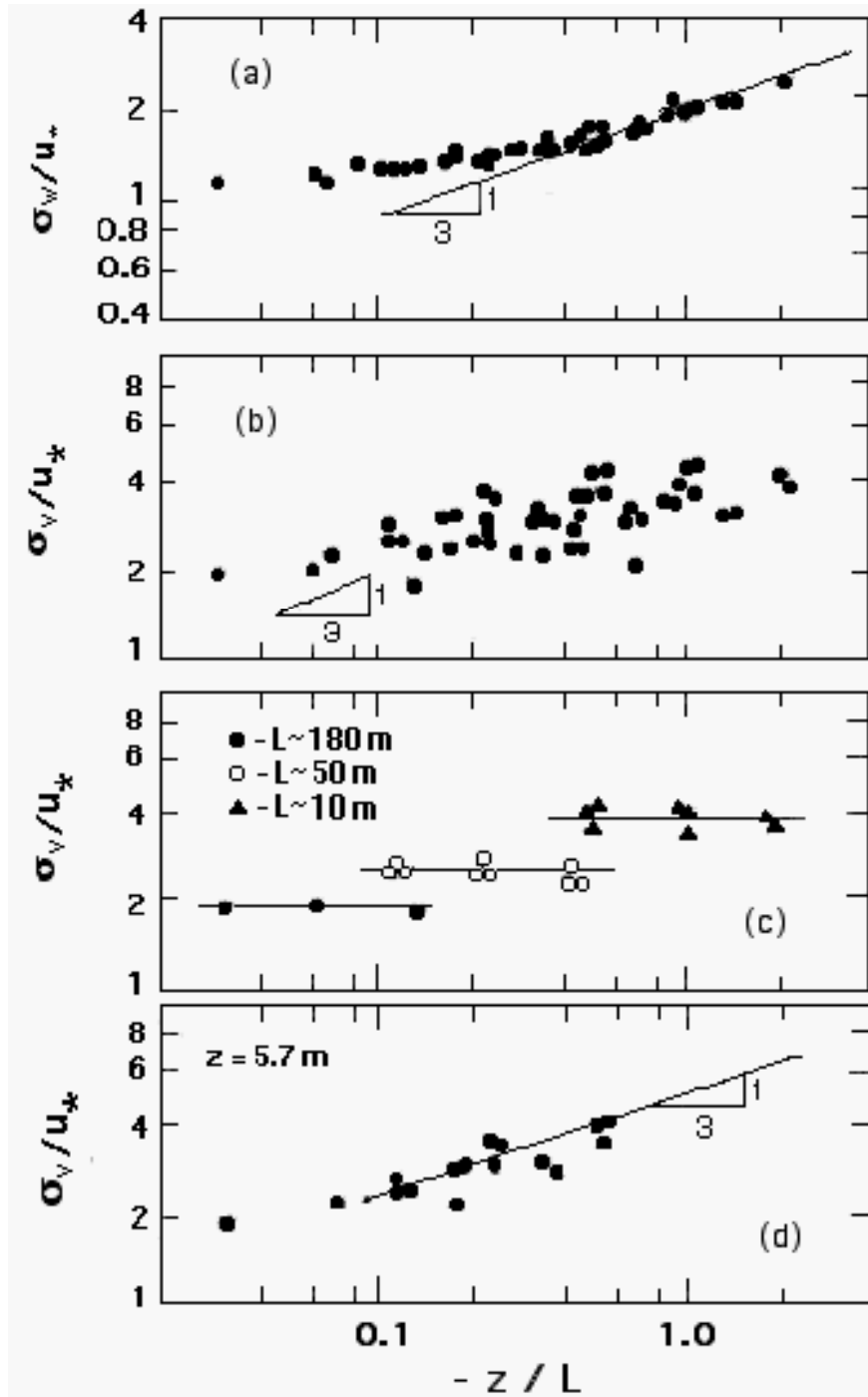


Fig. 20. (a) The standard deviation of the vertical velocity in unstable stratification. Note that the data follow the "1/3" law as the stratification becomes more unstable. (b) The standard deviation of the horizontal velocity in unstable stratification. Note that the data appear to follow the "1/3" law as well, although there is more scatter than for the vertical velocity. (c) The same data as in (b) except only those data with $L=180$, -50 , and -10 m are plotted. (d) The same data as in (b) except only those data for $z=5.7$ m are plotted (after Wyngaard, 1988).

2.4 Stable Outer Layer

The success of the Monin-Obukhov theory in the surface layer has raised natural questions, such as whether the upper portion of the boundary layer also has a self-similar structure, and whether this structure can be expressed in terms of an equally simple and elegant approach. The positive answer to these questions in the case of the moderately stable boundary layer was found by Nieuwstadt (1984), who introduced the local (height dependent) similarity scales. Based on these local scales, the M-O similarity functions for various statistical moments, spectra, and cospectra, could be simply extended for the entire stably stratified boundary layer (Sorbjan, 1986, Sorbjan, 1988 a, b, Sorbjan, 1989, Sorbjan, 1995).

Let us introduce the following height-dependent, local similarity scales for velocity, temperature, humidity, and length:

$$\begin{aligned}
 U^*(z) &= \left[\overline{w'^2} + \overline{u'w'}^2 \right]^{1/4} \\
 \Xi^*(z) &= -\frac{\overline{w'\theta'(z)}}{U^*(z)} \\
 Q^*(z) &= -\frac{\overline{w'q'(z)}}{U^*(z)} \\
 \Lambda^*(z) &= -\frac{U_*^2(z)}{\kappa\beta\Xi^*(z)}
 \end{aligned} \tag{25}$$

Note that the fluxes in the above definitions are functions of height. In the surface layer, where all fluxes are approximately constant, the above scales coincide with the surface layer scales u_* , T_* , q_* , and L , which were previously introduced.

One can argue that in stable stratification, turbulence is suppressed by buoyancy, and its characteristics should be local. Consequently, similarity functions obtained by non-dimensionalization with the local scales (12) should be constant (Sorbjan, 1986), e.g.:

$$\begin{aligned}
 \frac{\overline{w'^2}}{U_*^2} &= const, & \frac{\overline{\theta'^2}}{\Xi_*^2} &= const, & \frac{\overline{q'^2}}{Q_*^2} &= const, \\
 \frac{\Lambda_*}{U_*} \frac{dW}{dz} &= const, & \frac{\Lambda_*}{\Xi_*} \frac{d\Theta}{dz} &= const, & \frac{\Lambda_*}{Q_*} \frac{dq}{dz} &= const
 \end{aligned} \tag{26}$$

where W is the wind vector modulus. It can be noted that the above local similarity predictions coincide with the M-O functions, defined in the previous

section. For example, the surface layer prediction for the wind velocity is: $dU/dz = u_*/\kappa z (1 + 4.7 z/L)$ (Businger et al., 1971). Its "outer layer" analog can be written as $dW/dz = U_*/\kappa z (1 + 4.7 z/\Lambda)$. Note that the local similarity theory does not predict how the wind direction varies with height.

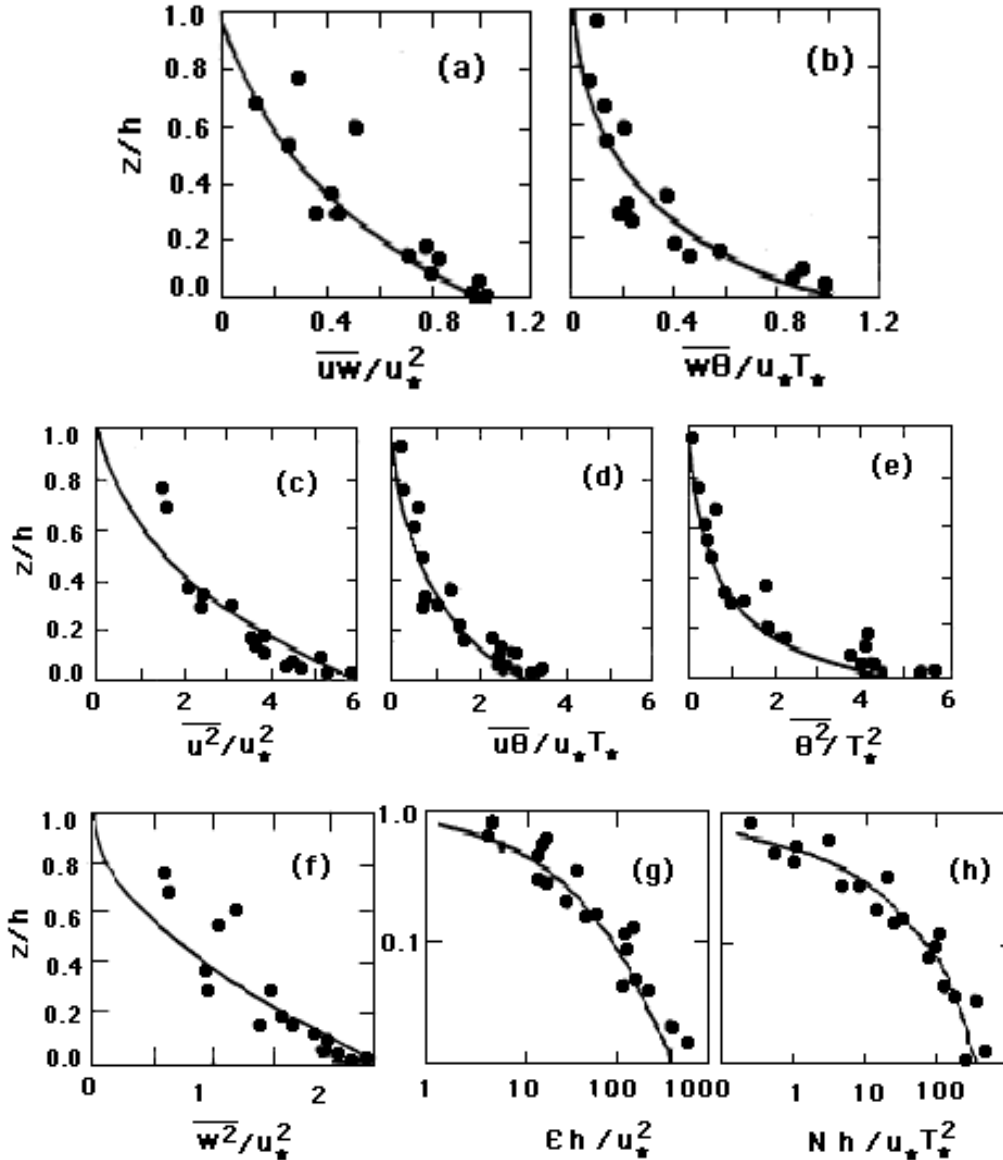


Figure 21. Comparison of the local similarity predictions (curves) in the stable boundary layer with the 1973-Minnesota data (dots):

a. the momentum flux, b. the vertical heat flux, c. the horizontal velocity variance, d. the horizontal heat flux, e. the temperature variance, f. the vertical velocity variance, g. the dissipation of the turbulent kinetic energy, h. the destruction of the temperature variance. In the figure, the presented moments are scaled by the friction velocity u_* , temperature scale T_* and depth of the stable boundary layer h .

We may assume now that the distributions of stress and heat flux with height can be expressed as follows:

$$U_*^2(z) = u_*^2 (1 - z/h)^{\alpha_1} \quad (27)$$

$$H(z) = H_o (1 - z/h)^{\alpha_2}$$

where h is the depth of the stable layer, defined as the level of the nocturnal jet, u_* is the friction velocity, H_o is the surface value of the heat flux, and α_1 , α_2 are parameters.

The values of α_1 and α_2 must be found empirically, and are case dependent. Once they are determined, all turbulent statistics of the flow may be predicted. For example, based on (13) and (16), we can obtain the following prediction for the temperature lapse rate:

$$L / T_* d\Theta/dz = C (1 - z/h)^{2(\alpha_2 - \alpha_1)} \quad (28)$$

where C is an empirical constant, which can be evaluated from surface layer measurements. To avoid singularity at $z = h$, we must require, $\alpha_1 \leq \alpha_2$.

To illustrate how local similarity predictions agree with atmospheric observations, we will present results from the 1973 Minnesota experiments. Based on data collected during the 1973 Minnesota experiment (Figures 21a and 21b), we found that $\alpha_1 = 2$ and $\alpha_2 = 3$ (Sorbjan, 1986). From this, the local scales (25) and local predictions (26) were evaluated and are shown in Figures 21c - 21h.

2.5 Convective Outer Layer

After sunrise on a clear day, the Earth's surface becomes warmer than the air above it. The sensible heat is transferred from the ground to the air, causing intense convective mixing within the boundary layer. Depending on the time which has elapsed since the sunrise, the convective boundary layer over land usually exists in one of the following four regimes: morning convection, morning free-encroachment, early afternoon convection, and late afternoon decaying convection.

During the early morning convection, the surface heat flux increases with time (see Figure 16). Convective thermals erode the temperature inversion and the "mixed layer" is formed (Figure 22). Free-encroachment takes place when the mixed layer starts growing into a residual of the well-mixed layer from the previous day. During early afternoon convection, the surface heat flux is nearly constant with time. In the late afternoon, the surface heat flux begins to weaken and convection decays.

2.5.1 Morning Convection

Despite of a fast growth in time of the surface heat flux and the height of the mixed layer, early morning convection is usually in a quasi-steady state. As a result, the heat flux is linear with height. The value of the heat flux at the top of the mixed layer is negative and approximately equal to 20% of the surface value. In the developing mixed layer, potential temperature, specific humidity, wind velocity, and wind direction are nearly uniform with height (not in time).

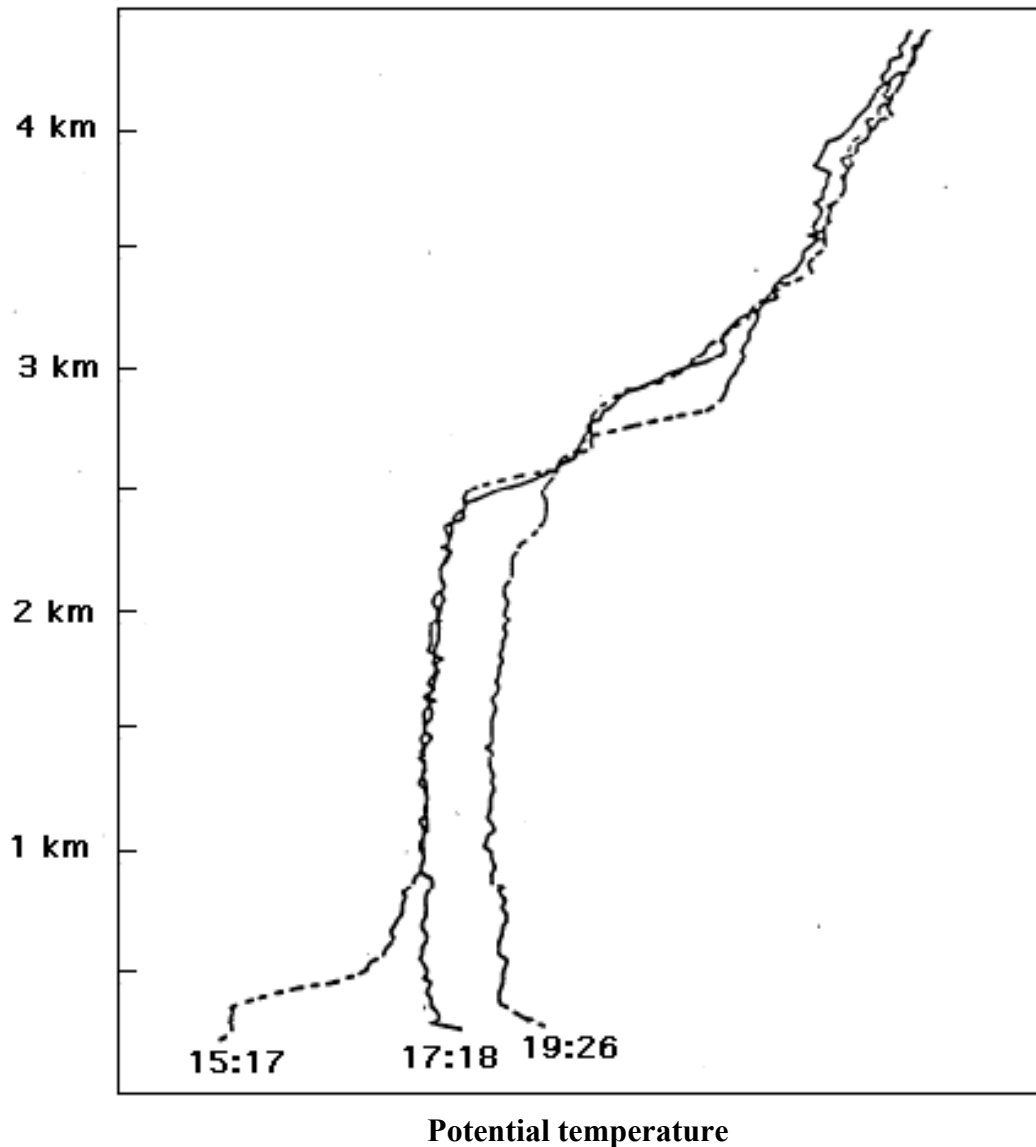


Figure 22. Sounding of the potential temperature measured on 10.07.1994 during Boreas experiment at 15:17, 17:18 and 19:26 GMT (9:17, 11:18, 12:16 LT). In the figure, the free-encroachment occurs around 17 GMT (11 LT) (after McPherson and Betts, 1995).

When an elevated residual mixed layer, left over from the previous day, becomes part of the newly growing mixed layer, free encroachment takes place (Figure 23). It lasts typically from a few minutes to about an hour. During this regime, updrafts penetrate the residual layer, nevertheless, the entrained air does not differ thermally from the air in the mixed layer. This causes the heat flux at the top of the mixed layer to vanish (Sorbjan, 1996b). Convection during encroachment is not in a steady-state. The heat flux is non-linear due to the intense growth of the mixed layer into the neutrally stratified layer, with a zero gradient Γ . This fact explains the role of the temperature gradient Γ , as the factor controlling a growth of the mixed layer. When Γ is near zero, a non-steady (growing) mixed layer is developed. When Γ is large enough, the resulting mixed layer is in a quasi-steady state with a linear heat flux profile.

2.5.2 Early Afternoon Convection

Early afternoon convection is in a quasi-steady state, due to the fact that the surface heat flux is nearly constant with time (Figure 15). In this state, the time rate changes of turbulent quantities can be ignored as small with respect to the dominant production and dissipation terms. In the mixed layer, meteorological parameters (potential temperature, humidity, wind) are nearly uniform with height. At the same time, profiles of the heat flux, humidity flux, and scalar fluxes are approximately linear.

The mixed layer reaches a depth ranging from a few hundred to a few thousand meters by late afternoon. Its top is marked by a sharp increase in temperature within the interfacial layer, where warmer and dryer air from the free atmosphere is entrained into the mixed layer. Entrainment (see its numerical simulation at¹⁰) is caused by updrafts which impinge the stably stratified free-atmosphere and originate local inflows of air into the mixed layer (e.g., Sullivan et al, 1998). Due to the entrainment, the mixed layer can deepen at a rate of a few tens of centimeters per second. This deepening can be limited by a large scale subsidence or thermal advection.

Convection in the shearless mixed layer (no wind) is organized in a characteristic cell pattern, depicted in Figure 23. In the figure, areas of faster updrafts (shaded areas) are surrounded by areas of slowly sinking air. Downdrafts cover more than half the area of the horizontal plane over the bulk of the mixed layer depth. The presence of wind breaks the cells and replaces them with horizontal rolls, often marked by cloud patterns at the top (as depicted in Figure 12).

The structure of the convective boundary layer has been extensively investigated during the last four decades (e.g., Ball, 1960; Lilly, 1968; Betts, 1973; Tennekes, 1973; Deardorff, 1974 b; 1976; 1979; Zeman and Tennekes, 1977; Mahrt, 1979).

¹⁰ <http://www.mmm.ucar.edu/asr96/sullivan1.html>

As a result, simple mixed-layer models have been developed. To explain this approach, we will refer to Figure 24.

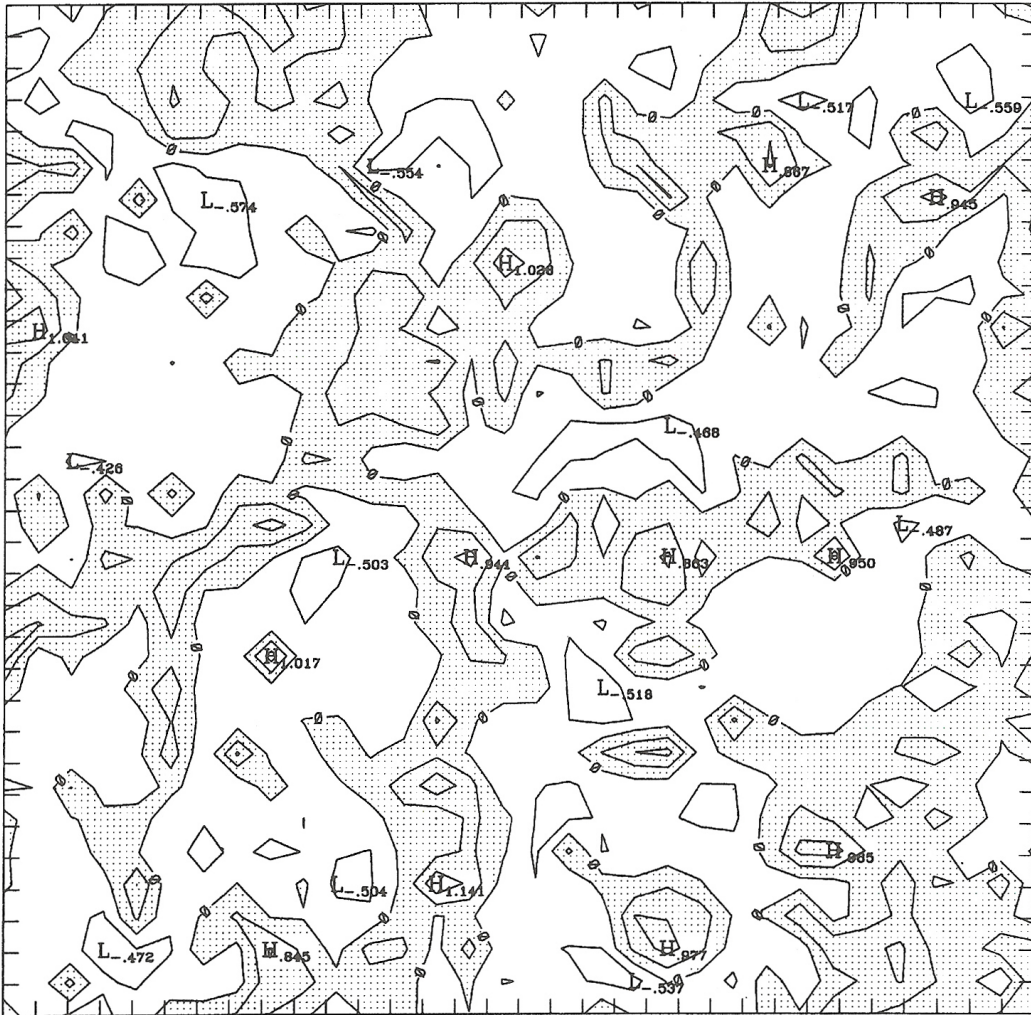


Figure 23. Horizontal cross-section of the vertical velocity field at $z/z_i = 0.3$ based on a large-eddy simulation. Contours plotted from -0.4 m s^{-1} to 0.8 m s^{-1} by 0.4 m s^{-1} . The shaded areas indicate updrafts (after Sorbjan, 1997).

In Figure 24, two profiles of the potential temperature in the mixed layer are depicted in Figure 24. Subscripts "1" and "2" in the figure refer to time instants $t = t_1$ and $t = t_2$. The mixed layer height z_i is defined as a level of the minimum heat flux H . The potential temperature in the mixed layer (above the surface layer) is constant with height. There is a rapid increase in the virtual potential temperature $\Delta\theta$ in the interfacial layer, which is assumed to be very thin (usually, it is about 100-200 m deep). In the free atmosphere, the potential temperature gradient Γ is assumed to be constant. Note that there is a rapid increase in the wind speed at the top of the mixed layer.

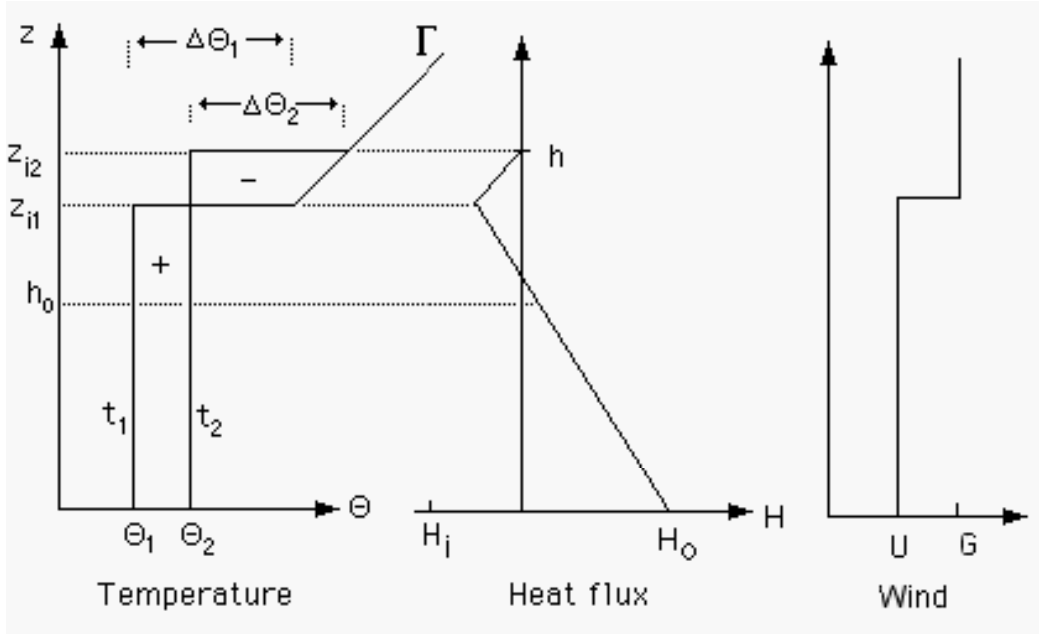


Figure 24. Schematic profiles of the virtual potential temperature, its flux and the wind velocity in the cloud-free mixed layer (G is the geostrophic wind).

The temperature changes in the mixed layer can be expressed by the following, horizontally-averaged equation (e.g., Sorbjan 1995):

$$\frac{\partial \Theta}{\partial t} = - \frac{\partial H}{\partial z} \quad (29)$$

where Θ is the potential temperature and H is the horizontally averaged turbulent heat flux.

Averaging this equation within an interval from t_1 to t_2 yields:

$$\frac{\delta \Theta}{\delta t} = - \frac{\delta H}{\delta z} \quad (30)$$

where $\delta \Theta = \Theta_2 - \Theta_1$, $\delta \tau = \tau_2 - \tau_1$, and H is the temporal and horizontal average of the turbulent heat flux. Integrating (30) with respect to z , we obtain:

$$H(z) = H_0 - \int_0^z \frac{\delta \Theta}{\delta t} dz \quad (31)$$

Since $\delta \Theta / \delta t$ is positive and constant with height in the mixed layer, we see that the heat flux has to linearly decrease with height from H_0 to the most negative value $H_i = H_0 - z_i \delta \Theta / \delta t$, at $z = z_i$.

From (31) it follows that the area between the temperature profiles $\Theta(t_1)$ and $\Theta(t_2)$, but below $z = h_o$, equals to $H_o \delta t$. Therefore, it represents the heating of the mixed layer by the positive heat flux at the Earth's surface.

The area between the same profiles in the layer between $z = h_o$ and $z = z_{i1}$ (marked as "+" in Figure 23) is equal to H_i . Thus, it indicates the heating of the mixed layer by entrainment at the top of the mixed layer. The area between the temperature profiles in the layer between $z = z_{i1}$ and $z = h$ (marked as "-" in Figure 23) represents the cooling of the inversion layer by thermals:

$$H_i = - \int_{h_o}^{z_{i1}} \delta\Theta/\delta t \, dz = \int_{z_{i1}}^h \delta\Theta/\delta t \, dz \quad (32)$$

From Figure 24, and from (32), we can also obtain that:

$$H_i = \int_{z_{i1}}^h \delta\Theta/\delta t \, dz = - (z_{i2} - z_{i1})/\delta t [\Delta\Theta_2 - \Gamma(z_{i2} - z_{i1})/2] \approx - dz_i/dt [\Delta\Theta - \Gamma dz_i/dt \delta t/2] \quad (33)$$

where we assumed that $(z_{i2} - z_{i1})/\delta t \approx dz_i/dt$. When $\Gamma dz_i/dt \delta t/2$ is small, the result coincides with the result derived analytically by Lilly (1968) by using Leibnitz's rule, $H_i = - dz_i/dt \Delta\Theta$. When subsidence w_s is present, its value has to be subtracted from the entrainment rate dz_i/dt . The typical value of H_i/H_o is -0.2 for Γ about 3K/km. Wind shear increases this value to $-(0.2 + u^{*3}/w^{*3})$ (e.g., Moeng and Sullivan 1994, Sullivan et al., 1998).

From Figure 24, we will also obtain that $\Delta\Theta_2 = \Delta\Theta_1 - (\Theta_2 - \Theta_1) + \Gamma (z_{i2} - z_{i1})$, which yields in the limit of $\delta t \rightarrow 0$:

$$d(\Delta\Theta)/dt = \Gamma dz_i/dt - d\Theta/dt \quad (34)$$

The obtained expression indicates that (in absence of subsidence) $\Delta\Theta$ increases in time as z_i grows and decreases as the temperature in the mixed layer increases. The above formula was first obtained by Betts (1973).

2.5.3 Self-Similar Structure of the Mixed Layer

Deardorff (1970 a, b) noted that in the core portion of a quasi-steady mixed layer, turbulence has a self-similar structure, described by the following convective scales:

$$\begin{aligned}
z_i & \text{ for height,} \\
w^* & = (z_i \beta H_o)^{1/3} \text{ for velocity,} \\
\Theta^* & = H_o/w^* \text{ for temperature,} \\
q^* & = Q_o/w^* \text{ for humidity,}
\end{aligned} \tag{35}$$

where z_i is the mixed layer height, H_o and Q_o are the surface temperature and humidity fluxes, and $\beta = g/T_o$ is the buoyancy parameter. Consequently, the statistical moments of turbulence (i.e., variances, covariances, etc) were implied by him to be functions of only z/z_i , when non-dimensionalized by these scales. The general form of such functions, however, has not yet been found.

Measurements showed, however, that in the upper portion of the mixed layer, a substantial scatter of dimensionless quantities exists. This scatter indicated that the list of scales provided by Deardorff was incomplete in this region. Large-eddy simulation performed by Sorbjan (1996 a, b) demonstrated that the statistical moments involving temperature are strongly sensitive to changes of the potential temperature gradient in the free-atmosphere Γ . On the other hand, the moments involving only the vertical velocity were found practically independent of Γ . The ratio $R = -H_i/H_o$ of the heat fluxes at the top and bottom of the mixed layer was found to increase when Γ increased. For the values of Γ from 1 K/km to 10 K/km, typically observed in the atmosphere, the heat flux ratio R varied in the range 0.2 to 0.3. When Γ decreased to zero, the heat flux H_i at the top of the mixed layer also decreased to zero.

Further investigations revealed that the appropriate scales at the top of the shear-free convective atmospheric boundary layer (no mean wind) are (Sorbjan, 2003):

$$\begin{aligned}
w^*N/\beta & \quad \text{for temperature,} \\
w^* & \quad \text{for velocity,} \\
N^{-1} & \quad \text{for time,} \\
w^*/N & \quad \text{for height,}
\end{aligned} \tag{36}$$

where N is the Brunt-Våisälå frequency in the interfacial layer, $N = [\beta \gamma_i]^{1/2}$, γ_i is the potential temperature gradient in the interfacial layer, and β is the buoyancy parameter.

The presence of two different regimes, in the core of the mixed layer and at its top, with two different sets of scales, makes formulating the similarity functions very difficult. One might suspect, however, that such functions should be expressed in terms of two components F_1 and F_2 :

$$m_s = F_1(z/z_i) + F_2(z/z_i, \dots) \tag{37}$$

where m_s is the dimensionless moment, scaled in terms of (35), F_1 is the universal function dependent only on the dimensionless height z/z_i , and F_2 is the correction due to entrainment, expressed in terms of z/z_i , as well as the scales (35) and (36).

In the shearless case, the function F_2 is expected to be non-zero only for moments involving temperature. For example for the heat flux $H(z)$ and for the temperature variance σ_θ^2 , one might propose:

$$H/H_o = (1 - z/z_i) + c w_* N / (\beta\Theta^*) z/z_i \quad (38)$$

$$\sigma_\theta^2 / \Theta^{*2} = c_1 (1 - z/z_i)^{4/3} / z/z_i^{2/3} + c_2 (w_* N)^2 / (\beta\Theta^*)^2 z/z_i^{4/3} / (1 - z/z_i + c_3)^{4/3}$$

where H_o is the surface heat flux ($H_o = w_*\Theta^*$), and c, c_1, c_2, c_3 are empirical constants.

The presence of wind shear introduces further complications. In this case, characteristics of turbulence at the top of the mixed layer seem to be dependent not only on the temperature gradient, but also on velocity gradients. As a result, function F_2 in (37) will be dependent on an additional variable Ri^{-1} , where Ri is the Richardson number, defined as:

$$Ri = \beta d\Theta/dz / [(du/dz)^2 + (dv/dz)^2] \quad (39)$$

and β is the buoyancy parameter. In this case, the function F_2 is expected to be non-zero for all moments. Note, that when $Ri \rightarrow \infty$ (the shearless case), $Ri^{-1} \rightarrow 0$, and the dependence of F_2 on Ri vanishes (Sorbjan, 2001, 2003).

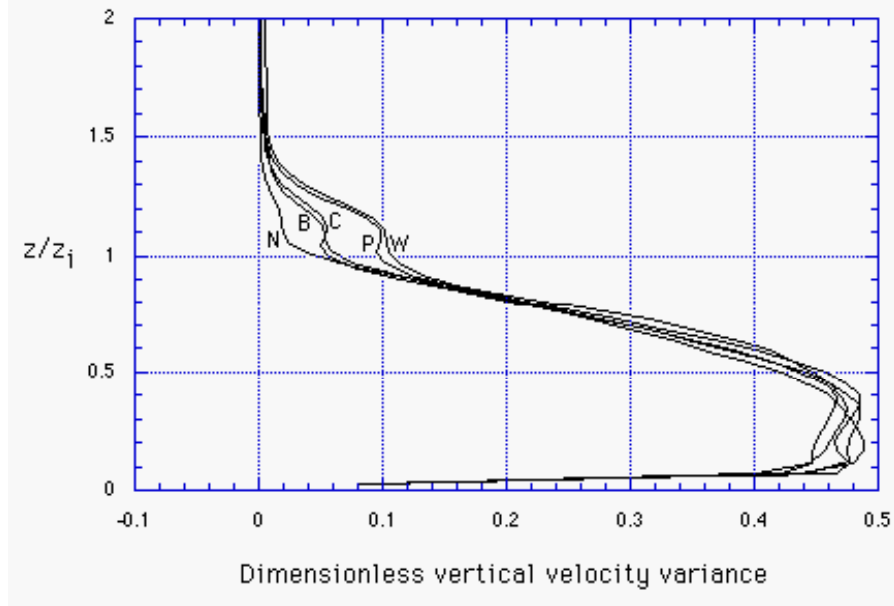


Figure 25. The vertical velocity variances scaled by w_*^2 , for five LES runs: B - barotropic case ($s_x = 0, s_y = 0$), W-warm advection ($s_x = 0, s_y = -5$), C-cold advection ($s_x = 0, s_y = 5$), P-positive shear ($s_x = 5, s_y = 0$), N - negative shear ($s_x = -5, s_y = 0$), where $s_x = du_g/dz, s_y = dv_g/dz$ are the components of the geostrophic shear, expressed in m/s per km (after Sorbjan, 2003)

Figure 25 shows profiles of the vertical velocity variance, scaled by w_*^2 , in the boundary layer with wind shear. The profiles were obtained based on a numerical model (LES), for the surface geostrophic wind $G_o = 15$ m/s, and for five different values of a geostrophic shear in the atmosphere (Sorbjan, 2003).

2.5.4 Decaying Mixed Layer

Eventually in the late afternoon, the surface heat flux H_o begins to weaken in response to the decreasing sun's elevation. As a result, the turbulent time scale $t^* = z_i / w_*$ increases (because w_* decreases and z_i stays nearly constant), and becomes comparable with the forcing time scale (a few hours). From this moment, quasi-stationarity and convective similarity disappear.

A numerical study of the decaying atmospheric convective mixed layer, caused by a gradual shut-off of the upward surface heat flux, was performed by Sorbjan (1997). It indicated that during decay, turbulent eddies persist even when the heat flux at the surface becomes negative, and the surface inversion develops near the Earth's surface. Large-scale updrafts are able to penetrate the stable layer aloft and cause entrainment from the capping stable layer. The resulting profiles of the heat flux are depicted in Figure 26. The x-y cross-section of the vertical velocity in the decaying mixed layer is shown in Figure 27.

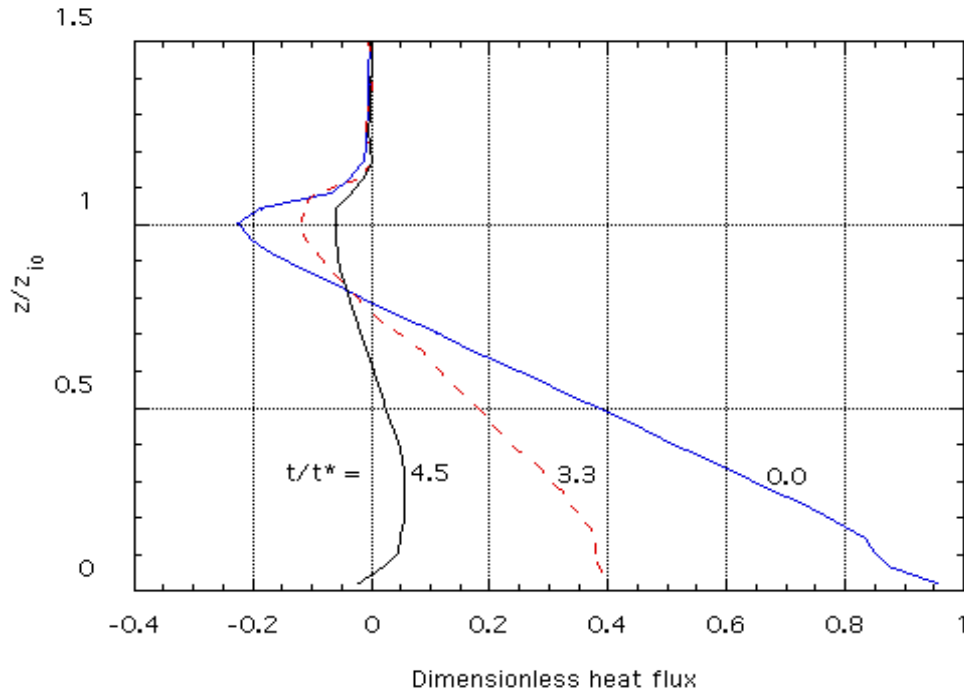


Figure 26. Profiles of the dimensionless heat fluxes in the decaying mixed layer, scaled by the surface heat flux at $t/t^* = 0.0$ (a large-eddy simulation of Sorbjan, 1997).

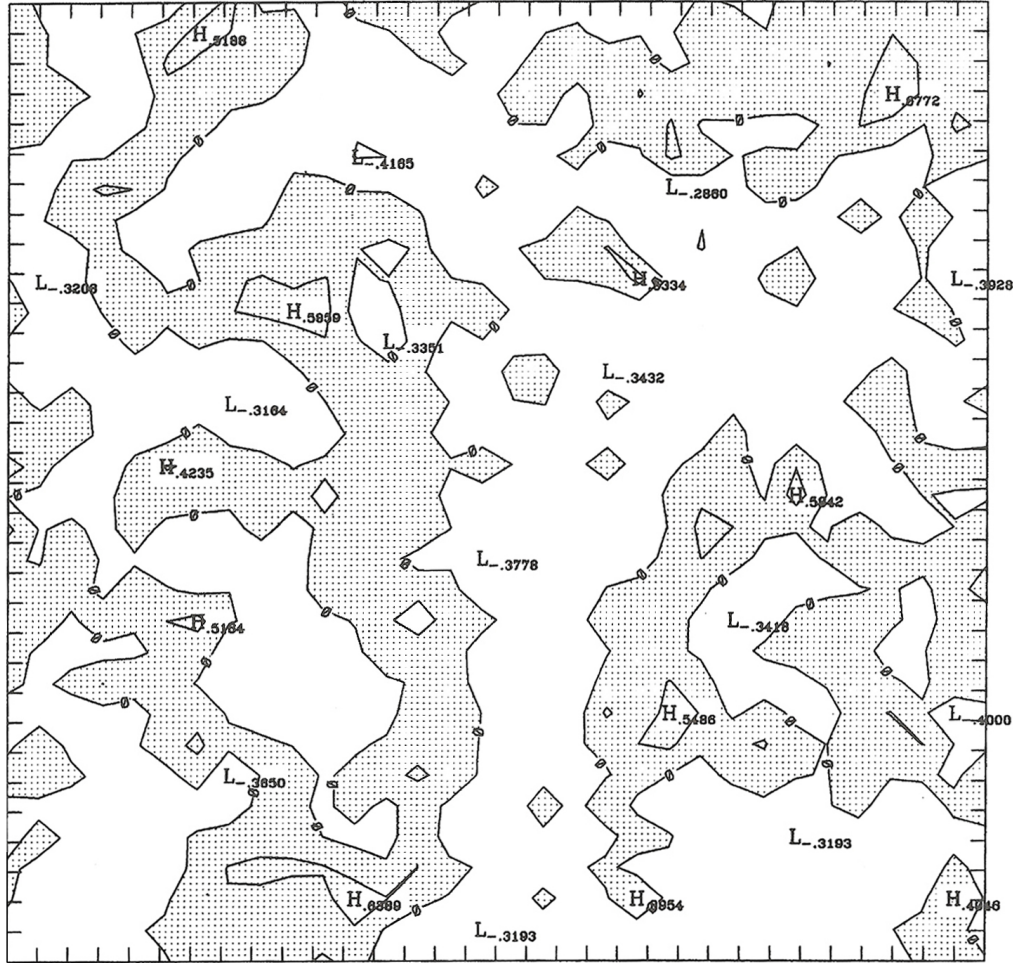


Figure 27. Horizontal cross-section of the vertical velocity field at $z/z_i = 0.3$ during decaying convection, $t/t_* = 4.5$, based on a large-eddy simulation. Contours plotted from -0.4 m s^{-1} to 0.8 m s^{-1} by 0.4 m s^{-1} . The shaded areas indicate updrafts (after Sorbjan, 1997).

Figure 26 was plotted for $z/z_i = 0.3$, and at $t/t_* = 4.5$. At $t/t_* = 4.5$, the heat flux at the surface is already negative. Nevertheless, convective cells are still present in Figure 27. Even though the vertical motions are weakened, the structure of the largest eddies seem almost unchanged with respect to the initial state in Figure 23.

2.5.4 Diffusion in the Mixed Layer

The understanding of diffusion associated with point sources located within the mixed layer was significantly advanced by the numerical simulations of Deardorff (1972) and Lamb (1982), as well as the laboratory experiments of Willis and Deardorff (1976, 1978, 1981). Their investigations indicated that for elevated sources the average plume center-line, defined as the mean maximum concentration, descended within a short distance from the source until it reached the ground. In contrast, the average centerline from near surface releases ascended after a short downwind distance (see Figure 28).

Figure 28 shows averaged and cross-wind integrated concentrations released from two sources. The first source is located near the surface while the second one is elevated. The figure indicates that the locus of the maximum concentrations ascends with a distance from the source for the case of the first source. In the second case, the locus of the maximum concentrations first descends, reaches the Earth's surface and then ascends. The presented results indicate that the obtained patterns differ from those produced by the Gaussian plume models.

This rather surprising plume behavior has been the subject of many subsequent studies. The main objective was not only to offer a physical explanation, but also to improve simpler diffusion models which had failed in this particular case. The first support for Willis and Deardorff's laboratory observations was obtained from the numerical experiments of Lamb (1982). Lamb used the results from the LES model of Deardorff (1972) to trace the motions of thousands of particles released into a numerical field. Later, other types of particle models were successfully employed in simulating convective plume behavior (e.g., Misra, 1982; Baerentsen and Berkowicz, 1984; Sawford and Guest, 1987). The laboratory observations also agreed with the atmospheric diffusion data (e.g., Moninger et al., 1982; Eberhart et al., 1988).

It soon became clear that the position of maximum concentrations could be explained by the probability distributions of the vertical velocity. Distributions of the vertical velocity in the clear-sky convective boundary layer were found to be positively skewed with a negative mode (e.g., LeMone, 1990). A positive vertical velocity skewness indicates strong narrow updrafts surrounded by larger areas of weaker downdrafts, as depicted in Figure 23. It also implies that downdrafts cover more than half the area of the horizontal plane over the bulk of the mixed layer depth. As a result, the majority of material released by an elevated source starts descending and continues to descend for a significant amount of time. On the other hand, material released at the surface can only ascend or move horizontally. Contaminants released into the base of an updraft begin to rise immediately, while those emitted into a downdraft move approximately horizontally until they encounter updrafts, and are transferred upward. After a sufficiently long travel time, in which a majority of pollutants enter the updrafts, the location of the maximum concentration lifts off the ground and rises toward the top of the mixed layer.

We shall now discuss the diffusion of passive species (such as humidity, ozone, radon, and carbon dioxide) which are associated with area sources (or sinks) located at the Earth's surface, and at the top of the mixed layer. Dispersion of such species in the mixed layer can be described by the following equation:

$$\partial c / \partial t = - \partial Q / \partial z \quad (40)$$

where c is the concentration, and Q is the concentration flux.

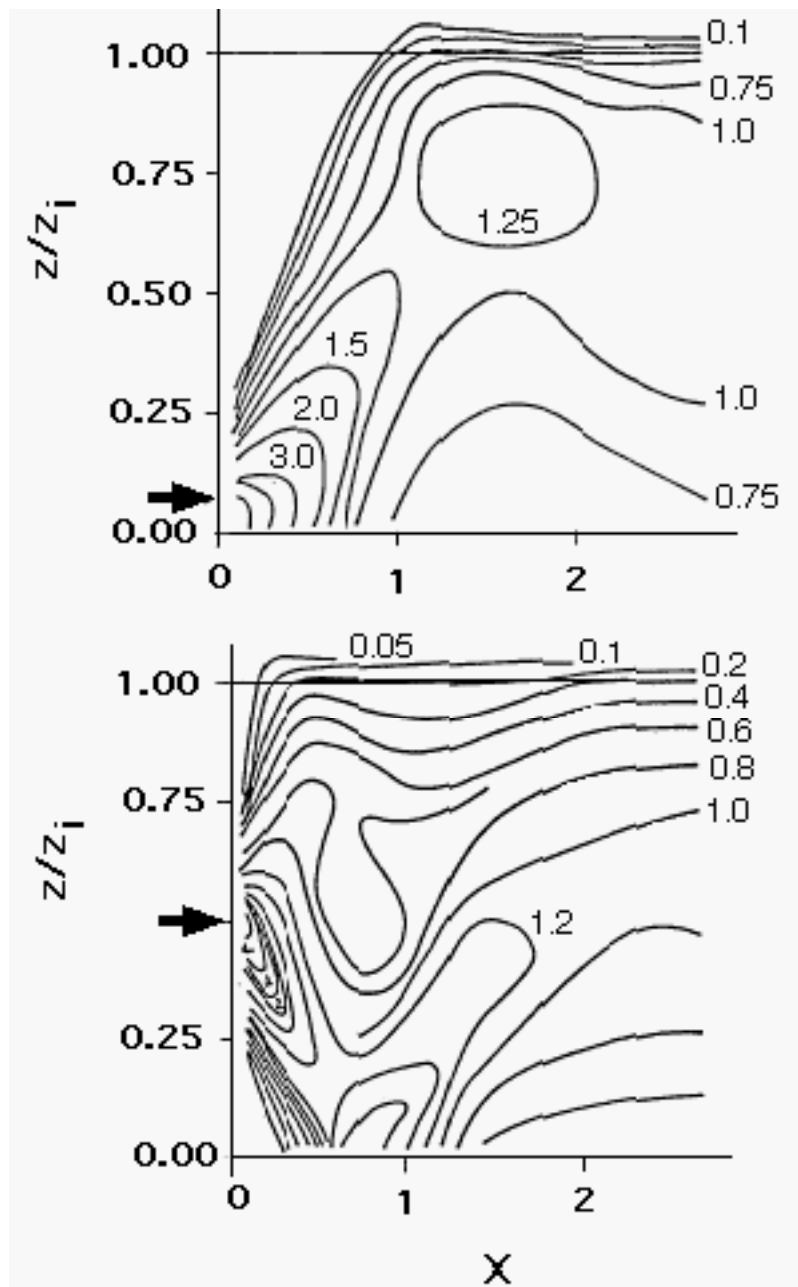


Figure 28. Vertical concentration distributions as a function of non-dimensional dispersion distance $X = w_*x/(Uz_i)$ for a low and high-level sources (after Willis and Deardorff, 1976 and 1982).

When the scalar is "well mixed", the concentration flux Q is a linear function of height: $Q(z) = Q_0 (1-z/z_i) + Q_i z/z_i$ where Q_0 is the turbulent flux at the surface, Q_i is the turbulent flux at $z = z_i$. Due to linearity of (40) with respect to c and Q , the mixing of a passive scalar in the mixed layer is additive, i.e., it can be expressed as a superposition of two processes, "bottom-up" and "top-down" (e.g., Wyngaard, 1984).

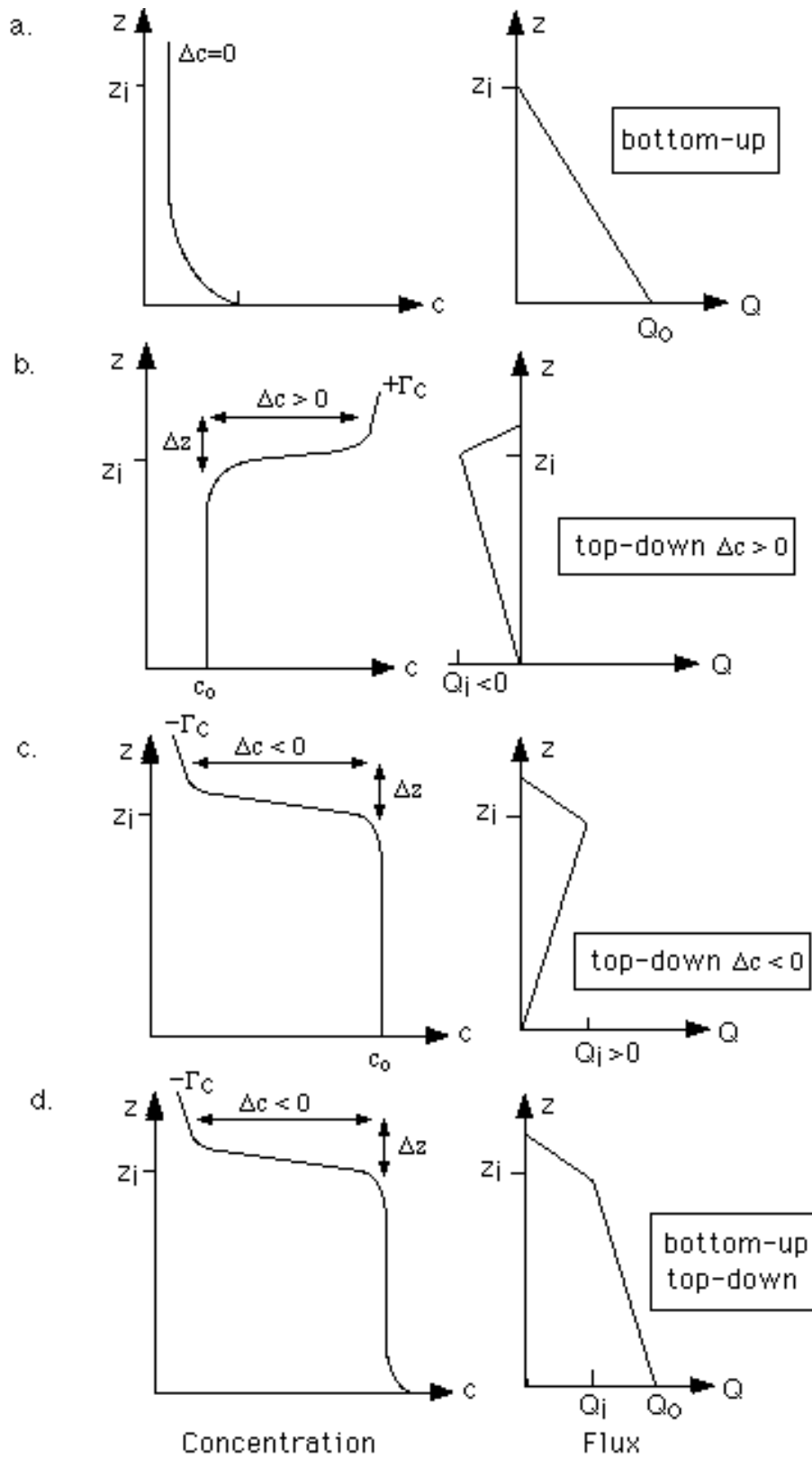


Figure 29. Bottom-up and top-down diffusion in the mixed layer for a passive scalar emitted from a surface source (after Sorbjan 1999a).

The first process (hereafter denoted by subscript "b") is associated with a transfer (emission or absorption) of a scalar across the Earth's surface. The second process (hereafter denoted by subscript "t") is due to entrainment of a scalar at the top of the mixed layer. Consequently, the mean concentration of the passive scalar and its flux can be decomposed as: $c = c_b + c_t$, $Q = Q_b + Q_t$.

The considered diffusion processes are schematically shown in Figure 29. In the pure "bottom-up" case (Figure 29a), the concentration quickly decreases with height and reaches a constant value in the mixed layer. At the same time, the "bottom-up" concentration flux decreases linearly from $Q_o > 0$ at the Earth's surface to zero at the top of the mixed layer. In the pure "top-down ($\Delta c > 0$)" case (Figure 29b), the concentration in the free atmosphere exceeds the concentration in the mixed layer. The scalar flux decreases linearly with height, from zero at the surface to $Q_i < 0$ at the top of the mixed layer.

On the other hand, during a pure "top-down ($\Delta c < 0$)" case (Figure 29c), the concentration in the mixed layer is larger than the concentration in the free atmosphere, and the flux increases linearly with height, from zero at the surface to $Q_i > 0$ at the top of the mixed layer.

Diffusion of a passive scalar in Figure 29d ($\Delta c < 0$, $Q_o > Q_i > 0$) can be represented by a sum of two processes: pure "bottom-up" ($\Delta c = 0$, $Q_o > 0$) as in Figure 29a, and pure "top-down" ($\Delta c < 0$, $Q_o = 0$, $Q_i > 0$) as in Figure 29c. A superposition of processes in Figures 29b and 29c yields a constant concentration (equal to $2c_o$), and a zero concentration flux in the mixed layer, and also above.

2.6 Cloud-Topped Mixed Layers

Even though stratocumuli clouds have a strong impact on the dynamics of the PBL (e.g., Lenschow et al. 1980, Betts 1990, Betts and Boers 1990, Siems et al. 1990, Nichols and Leighton 1986, Turton and Nicholls 1987, Chai and Telfort 1983, Telfort and Chai 1984, Agee and Hart 1990, Moeng and Schumann, 1991, Paluch and Lenschow 1991), their effects are usually neglected in air pollution studies.

The structure of the cloud-topped boundary layer (CTBL) depends on radiative cooling and heating in clouds, phase changes, subsidence, sensible and latent fluxes, and wind shear. Surface fluxes generate convection and provide the water substance. Radiative cooling contributes to the generation of a positive heat flux, convection, and entrainment at the top of the mixed layer. Wind shear increases entrainment. Entrainment brings warmer and drier air down into the ABL and promotes evaporative cooling. The evaporative cooling may lead to an instability process in which parcels cool even more and then sink. This can generate greater entrainment, resulting in the breaking up of a solid cloud deck.

Mixed layer convection requires a source of energy. In the cloud-free mixed layer, the energy is provided by the heated Earth's surface. The presence of stratocumuli clouds introduces additional buoyancy sources and sinks through radiative cooling and heating and evaporative cooling. The shortwave heating is smaller than the longwave cooling, and is distributed over a thicker layer within a cloud. Due to radiative and evaporative cooling the depth of the interfacial layer is very thin and the temperature jump quite large. Numerical simulations (e.g., Lock and MacVean, 1999, Krueger et al, 1995) show that thermals hindering on the inversion interface are flattened and only slightly deform the interface. They spread out horizontally, generating enhanced shears at the interface and small-scale Kelvin-Helmholtz type mixing.

The day-time CTBL has two distinct layers, cloud and subcloud layer, decoupled by the formation of a slightly stable layer near the cloud base. The decoupling is primarily a consequence of the shortwave heating in the cloud layer. The decoupling prevents the moisture from being transported upward. This leads to a rapid thinning of the cloud layer during the daytime, and also has an important influence on the radiative balance at the Earth's surface. In addition, cooling introduced by the evaporation of drizzle can cool the sub-cloud layer relative to the cloud layer, and consequently can further stabilize the interface between the cloud and sub-cloud layers.

A physical description of the cloud-topped boundary layer is more complex than in the dry case considered above. In a cloud-topped mixed layer, the virtual potential temperature is no longer a conservative variable (Figure 30). Instead, the liquid water potential temperature:

$$\Theta_L = \Theta - L/c_p q_L \quad (41)$$

can be considered as an invariant in moist adiabatic processes, where L is the latent heat of evaporation, c_p is the specific heat of air at constant pressure, q_L is the liquid water mixing ratio (e.g., Moeng, 1998).

To illustrate the impact of clouds in this section we will modify the analysis presented in section 2.5.2 by assuming that stratocumuli clouds are present on the top of the PBL. We will consider only a nocturnal (no solar radiation), horizontally homogeneous, cloud-topped mixed layer, schematically depicted in Figure 31.

In a cloud-topped mixed layer, the liquid water potential temperature Θ_L is approximately constant with height. At the top of the mixed layer, there is a sudden jump in the liquid water potential temperature $\Delta\Theta_L$ ($\Delta\Theta_1$ at $t = t_1$ and $\Delta\Theta_2$ at $t = t_2$). The temperature jump takes place in the transition layer of very small depth, which could be in the order of 10 m thick or even less. Consequently, we will assume here that the transition layer is infinitesimal in Figure 31. Above the

mixed layer the liquid water potential temperature gradient Γ is assumed to be constant. The value of the surface heat flux is assumed to be near zero.

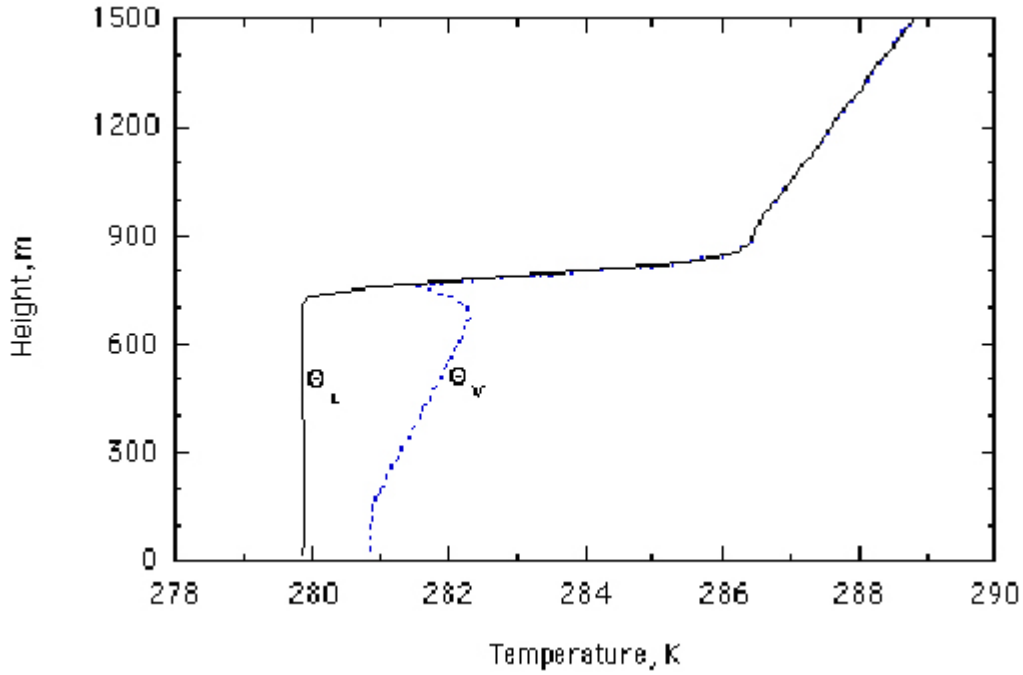


Figure 30. Typical vertical profiles of the liquid water potential temperature Θ_L , and the virtual temperature Θ_v in the cloud-topped boundary layer (a large-eddy simulation of Sorbjan and Uliasz, 1999b).

The liquid water potential temperature changes in the mixed layer can be expressed by the following time-averaged equation:

$$\delta\Theta_L/\delta t = -\partial F/\partial z \quad (42)$$

where, $\delta\Theta_L = \Theta_2 - \Theta_1$, F is the time and horizontally-averaged total flux, which consists of the liquid water potential temperature heat flux H_L , and the net radiative flux R , i.e., $F = H_L + R$. Integrating (42), we obtain:

$$F(z) = F_o - \int_0^z \delta\Theta_L/\delta t \, dz \quad (45)$$

Referring to Figure 31, we can note that since $\delta\Theta_L/\delta t$ is negative and constant with height in the mixed layer, the total heat flux linearly increases with height, from F_o at the Earth's surface to $F_i = F_o - z_i\delta\Theta_L/\delta t$, at $z = z_{i1}$. Above $z = z_{i1}$, the total heat flux is non-linear.

We will assume that the mean radiative flux R increases with height from zero at $z \leq h_r$ to R_a at $z = h = z_{i2}$. The turbulent temperature flux can be obtained as the

difference between the total and radiative fluxes, $H_L = F - R$. Below $z = h_r$, $R = 0$, and consequently H_L is linear, $H_L = H_o - \delta\Theta_L/\delta t z$. H_L is non-linear for $z > h_r$. At $z = h_o$, where the radiative flux R and the total flux F are equal, and H_L is nil. At $z = z_m$, where the difference between R and F is the greatest, and H_L is the most negative. At $z = h$, H_L is zero again. The area between curves $\Theta_L(t_1)$ and $\Theta_L(t_2)$, below $z = h_r$ (where $R = 0$), represents the cooling of the mixed layer by the positive heat flux H_L . The area between profiles $\Theta_L(t_1)$ and $\Theta_L(t_2)$ above $z = h_r$ (where $R \neq 0$) represents the direct radiative cooling of the mixed layer.

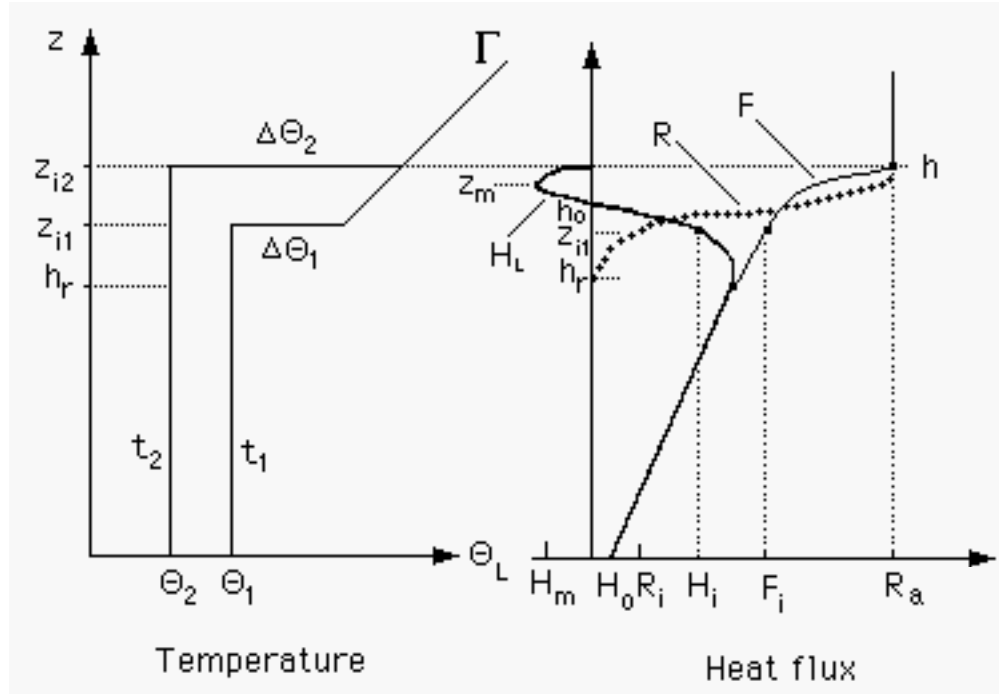


Figure 31. Schematic profiles of the liquid water potential temperature and its flux in the cloud-topped nocturnal mixed layer

The above analysis indicates that the presence of stratocumuli clouds above the boundary layer generates a positive heat flux, convection and mixing in nocturnal conditions. The numerical diffusion simulations performed by Sorbjan and Uliasz (1998) demonstrated that vertical mixing in the nocturnal cloud-topped boundary layer is non-Gaussian, resulting from the negatively skewed vertical velocity field in most of the layer.

2.7 Stability Categories

The structure of the atmospheric boundary layer is quite complex to non-meteorologists. Therefore, a simplifying alternative proposed over 40 years ago by Pasquill (1961) has been very popular since then among engineers dealing with air-pollution problems.

Pasquill's classification of weather conditions in the boundary layer is based on five stability categories. The key to these categories are described in the following table:

Table 2. Pasquill's Stability Categories

Surface Wind Speed (m/s)	Daytime Insolation			Nighttime cloud cover	
	Strong	Moderate	Slight	Thinly overcast or $\geq 4/8$ low cloud	$\leq 3/8$
< 2	A	A - B	B	-	-
2 - 3	A - B	B	C	E	F
3 - 5	B	B - C	C	D	E
5 - 6	C	C - D	D	D	D
> 6	C	D	D	D	D

According to Pasquill, strong insolation is equivalent to a sunny midday in summer in England and slight insolation to conditions in midwinter. The neutral category *D* corresponds to overcast conditions during day or night, and sky conditions during the hour preceding or following night (Pasquill's night begins 1 hour before sunset and lasts to 1 hour after dawn), regardless of wind speed. The categories *A* and *F* have traditionally been associated with very unstable and very stable conditions.

Our understanding of the boundary layer has progressed since the 1960's, when Pasquill's classification was proposed. Therefore, today his stability categories could be refined as follows:

- A. free-convection with or without cumulus clouds,
- B. forced-convection with or without cumulus clouds,
- C. weaker day-time convection,
- D. very weak or no convection during daytime, nighttime, or day-night transitions,
- E. weak stable nocturnal regime with thin low clouds or with medium clouds,
- F. strong stable conditions under clear skies.

As correctly indicated by Pasquill (1961) dispersion of pollutants in the atmosphere strongly depends on meteorological conditions. The vertical appearance of an instantaneous plume offers considerable information as to how the thermal and dynamic state of the lower atmosphere influences the transport of atmospheric pollutants. Some idealized patterns of vertical smoke spreading can be identified as looping, fumigation, lofting, coning, and fanning,. The listed cases are briefly discussed below.

"Looping" is frequently evident by midday in the mixed layer (Figure 32). It can be identified as category *A*, *B* or *C*. In this case convection generates large eddies which bring the plume to the ground and also lift it upward. This causes the

looping behavior and intense turbulent mixing. The average ground-level concentration increases very rapidly with distance from the stack, attains its peak value and then decreases farther downwind

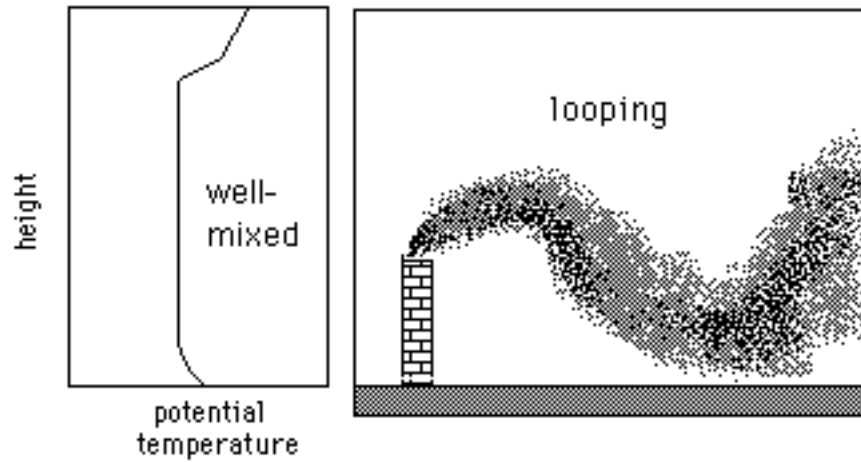


Figure 32. The looping conditions in the well-mixed layer.

The second case is called "fumigation" (Figure 33). Shortly after the sun rises on a clear morning, the existing nocturnal inversion begins dissipating and is slowly replaced by the mixed layer. The inversion layer is present just above the top of the stack and acts as a lid. The newly developed convective eddies spread the pollutants within the mixed layer. It causes a sudden rise in ground-level concentrations. Depending upon the stack height and the deepening-rate of the inversion layer, the fumigation condition may be very transitory or could persist for several hours. The case should be identified as category *A*, *B*, or *C*.

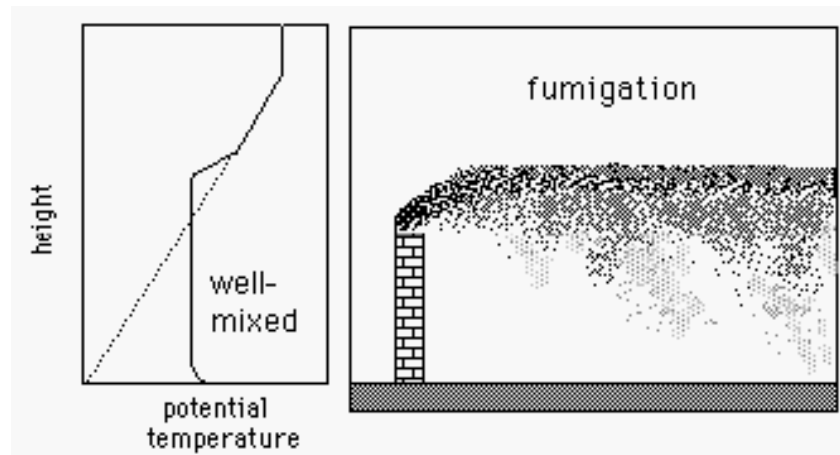


Figure 33. The fumigation conditions in the evolving morning mixed layer.

"Coning" usually accompanies cloudy conditions, with moderate winds and with very weak convection (Figure 34). It can occur either during the day or night. Therefore it should be identified as category *D*. In this case the plume is shaped

like a cone with a horizontal axis. The distance from the stack at which the smoke first comes to the ground is greater than it would be in looping conditions because the thermally induced turbulence is lower in this case.

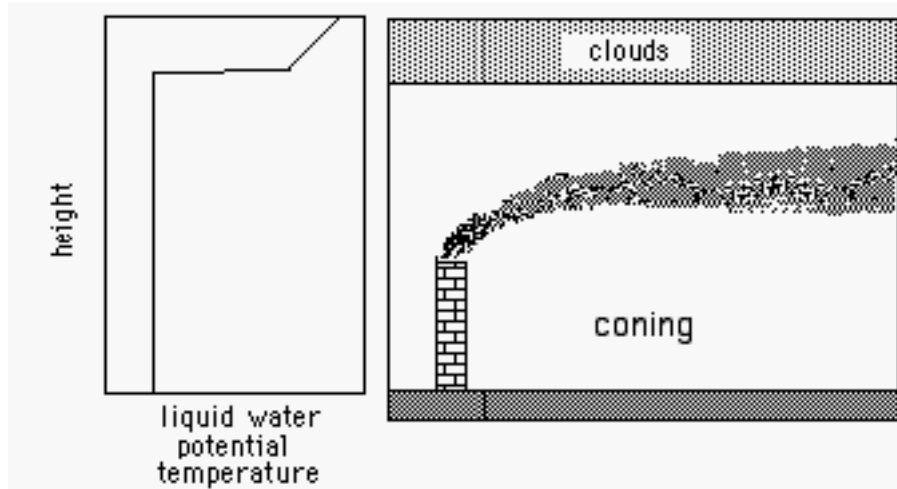


Figure 34. The coning conditions in the cloud-topped boundary layer.

"Lofting" is most often observed near sunset (Figure 35). It should be identified as categories *E* or *F*. When the surface inversion is developed just below the top of the stack, it reduces diffusion downward. At the same time, eddies in the residual mixed layer can still be active and cause intensive diffusion above the surface inversion. Depending upon the stack height and the deepening-rate of the inversion layer, the lofting condition may be very transitory or could persist for several hours. When the source is above the surface inversion, lofting may be the most favorable condition.

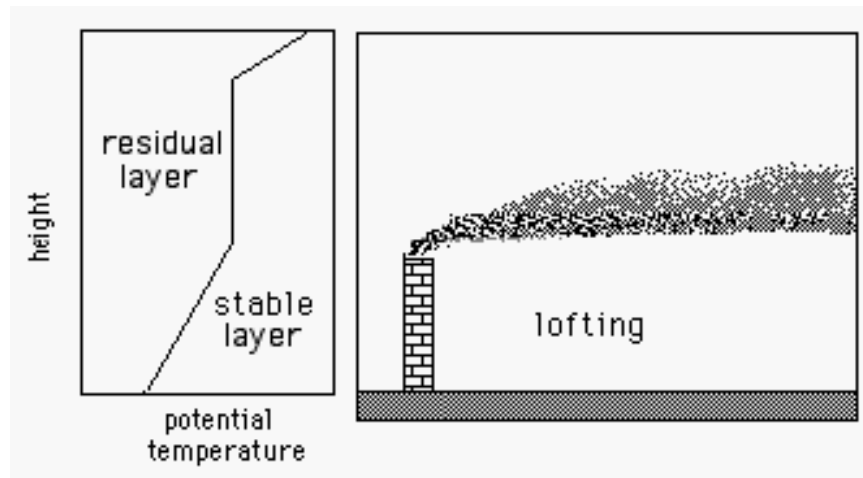


Figure 35. The lofting conditions during evening or nocturnal conditions.

The so called "fanning" occurs at night in the stable PBL (Figure 36). Therefore, it can be associated with category F . Since vertical mixing is suppressed, the plume expands very little in depth over long distances. Lateral diffusion may proceed quite differently. The slow meandering of the wind results in a similar meandering of the plume. Therefore, the time-averaged plume may appear quite broad. When the horizontal spreading is small, the plume can be observed for long distances. Fanning behavior of plumes is not considered an unfavorable condition for tall stacks. This situation might be unfavorable, however, when the stack is short.

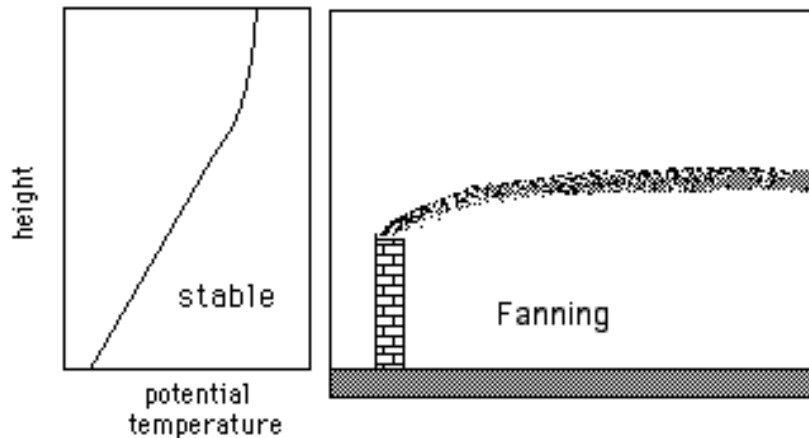


Figure 36. The fanning conditions in the stable boundary layer.

References

- Agee, E.M., 1987: Mesoscale cellular convection over the oceans. *Dynamics of Atmospheres and Oceans*, 10, 317-341.
- Agee, E.M., and M.L. Hart, 1990: Boundary layer and mesoscale structure over lake Michigan during winter time cold outbreak. *J. Atmos. Sci.*, 47, 2293-2316.
- Arya, S.P., 1999, *Air Pollution Meteorology and Dispersion*. Oxford University Press
- Atkinson, B.W. 1995: Introduction to the fluid mechanics of meso-scale flow field. In: *Diffusion and Transport of Pollutants in Atmospheric Mesoscale Flow Fields*. Kluwer Academic Publishers, Eds. Albert Gyr and Franz-S. Rys, 216 pp.
- Baerentsen, J.H. and R. Berkowicz, 1984: Monte Carlo simulation of plume dispersion in the convective boundary layer. *Atmos. Envir.*, 18, 701-712.
- Ball, F.K., 1960: Control of the inversion height by surface heating. *Quart. J. Roy. Meteor. Soc.*, 86, 483-494.
- Betts, A.K., 1973: Non-precipitating cumulus convection and its parameterization. *Quart. J. Roy. Meteor. Soc.*, 99, 178-196.

- Betts, A. 1990: Diurnal variation of California coastal stratocumulus from two days of boundary layer soundings, *Tellus*, 42A, 302-304.
- Betts A.K., and R. Boers, 1990: A cloudiness transition in a marine boundary layer. *J. Atmos. Sci.*, 47, 1480-1497.
- Brown, R.A., 1980: Longitudinal instabilities and secondary flows in the planetary boundary layer: A review. *Reviews of Geophysics and Space Physics*, 18, 3, 683-697.
- Buckingham, E., 1914: On physically similar systems. Illustration of the use of dimensional equations. *Phys. Rev.* 4, 345-376.
- Businger, J.A., J.C. Wyngaard, Y. Izumi, and E.F. Bradley, 1971: Flux profile relationships in the atmospheric surface layer. *J. Atmos. Sci.*, 28, 181-189.
- Chai S.K., and J.W. Telfort, 1983: Convection model for stratus cloud over a warmwater surface. *Bound.-Layer Meteor.*, 26, 25-49.
- Deardorff, J.W., 1970 a: Convective velocity and temperature scales for unstable planetary boundary layer and for Rayleigh convection. *J. Atmos. Sci.*, 29, 1211-1212
- Deardorff, J.W., 1970 b: Preliminary results from numerical integration of the unstable planetary boundary layers. *J. Atmos. Sci.*, 27, 1209-1211.
- Deardorff, J. W., 1972. Numerical investigation of neutral and unstable planetary boundary layer. *J. Atmos. Sci.*, 29, 91-115.
- Deardorff, J.W., 1974 a: Three-dimensional numerical study of the height and mean structure of a heated planetary boundary layer. *Bound.-Layer Meteor.*, 7, 81-106.
- Deardorff, J.W., 1974b: Three-dimensional numerical study of turbulence in an entraining mixed layer. *Bound.-Layer Meteor.*, 7, 199-226.
- Deardorff, J.W., 1976: On the entrainment rate of a stratocumulus-topped mixed layer. *Quart. J. Roy. Meteor Soc.*, 102, 563-582.
- Deardorff, J.W., 1979: Prediction of convective mixed-layer entrainment for realistic capping inversion structure. *J. Atmos. Sci.*, 36, 424-436.
- Eberhart, W.L., W.R. Moninger, and G.A. Briggs, 1988: Plume dispersion in the convective boundary layer. Part I: CONDORS field experiment and example measurements. *J. Appl. Meteor.*, 27, 5, 600-616
- Garratt, J.R., 1992: *The Atmospheric Boundary Layer*. Cambridge University Press, 316 pp.
- Gossard, E. E. and J. H. Richter, 1970. The shape of internal waves of finite amplitude from high-resolution radar sounding of the lower atmosphere *J. Atmos. Sci.*, 27, 971-973.
- Gossard, E. E., D. R. Jensen and J. H. Richter, 1971. Analytical study of tropospheric structure as seen by high-resolution radar. *J. Atmos. Sci.*, 28, 794-807.
- Gossard, E. E., J. H. Richter and D. R. Jensen, 1973. Effect of wind shear on atmospheric wave instabilities revealed by FM/CW radar observations. *Boundary-Layer Meteorol.* 4, 113-130.

Hooke, W. H., F. F. Hall and E. E. Gossard, 1973. Observed generation of an atmospheric gravity wave by shear instability in the mean flow of the planetary boundary layer. *Boundary-Layer Meteorol.*, 5, 29-41.

Kaimal, J.C., J.C. Wyngaard, D.A. Haugen, O.R. Coté, Y. Izumi, S.F. Caughey, and C.J. Readings, 1976: Turbulence structure in the convective boundary layer. *J. Atmos. Sci.*, 33, 2152-2169.

Kaimal, J.D., R.A. Eversole, D.H. Lenschow, B.B. Stankov, P.H. Khan, and J.A. Businger, 1982: Spectral characteristics of the convective boundary layer over uneven terrain. *J. Atmos. Sci.* 39, 1098-1114.

Kaimal J.C. and J.J. Finnigan, 1994: Atmospheric Boundary Layer Flows. Oxford University Press, 287 pp.

Krueger, S. K., G. T. McLean and Q. Fu, 1995: Numerical simulation of the stratus to cumulus transition in the subtropical marine boundary layer. Part I: Boundary-Layer Structure. *J. Atmos. Sci.*, 52, 2839-2868.

Kuettner, J. , 1959. The band structure of the atmosphere . *Tellus*, 11, 267-296.

Kuettner, J. P. , 1971. Cloud bands in the Earth's atmosphere. *Tellus*, 23, 4040-426.

Lamb, R. G., 1982. Diffusion in the convective boundary layer. In : Atmospheric Turbulence and Air Pollution Modelling. F.T.M. Nieuwstadt and H. van Dop, Eds. Reidel, Dordrecht, Holland. Landau, L. D. and E. M. Lifshitz, 1944. Fluid Mechanics. English edn. Pergamon Press, London, 1959, 536 pp.

LeMone, M.A., 1990: Some observations of vertical velocity skewness in the planetary boundary layer. *J. Atmos. Sci.*, 47, 1163-1169.

Lenschow, D.H., J.C. Wyngaard, W.T. Pennell, 1980: Mean-field and second-moment budgets in a baroclinic, convective boundary layer. *J. Atmos. Sci.*, 37, 1313-1326.

Lock, A. P., and M. K. McVean, 1999: Parameterization of entrainment driven by surface heating and cloud-top cooling. *Quart. J. Roy. Meteorol. Soc.*, 120,

Lilly, D.K., 1968: Models of cloud-capped mixed layers under a strong inversion. *Quart. J. Roy. Meteor. Soc.*, 94, 292-309.

Lutgens, F.K. and E.J. Tarbuck. 1995: The Atmosphere. Prentice-Hall, 462 pp.

McPherson, J.I., and A.K. Betts, 1995: Aircraft encounters with strong coherent vortices Over boreal forest. The Symposium on Boundary Layers and Turbulence. Charlotte, N.C., AMS, 424-427.

Mahrt, L., 1979: Penetrative convection at the top of a growing boundary layer. *Quart. J. Roy. Meteor. Soc.*, 105, 969-985.

Mason, P.J., 1989: Large-eddy simulation of the convective atmospheric boundary layer. *J. Atmos. Sci.*, 46, 1492-1516.

Misra, P.K., 1982: Dispersion of nonbuoyant particles inside a convective boundary layer. *Atmos. Envir.*, 16, 239-243.

Moeng, C.-H., 1984: A large-eddy simulation model for the study of planetary boundary-layer turbulence. *J. Atmos. Sci.*, 41, 2052-3169.

- Moeng C.-H. and U. Schumann, 1991: Composite structure of plumes in stratus-topped boundary layers. *J. Atmos. Sci.*, 48, 2280-2291.
- Moeng, C.-H., P.P.Sullivan, 1994: A comparison of shear- and buoyancy driven planetary boundary layer flows. *J. Atmos. Sci.*, 51, 999-1022.
- Moeng, C.-H., 1998: Stratocumulus-topped atmospheric planetary boundary layer. In: *Buoyant Convection in Geophysical Flows*, NATO ASCI Series, vol 513, 421-440. Eds E.J. Plate, E.E.Fedorovich, D.X.Viegas and J.C. Wyngaard.
- Moeng, C.-H., 1998: Stratocumulus-topped atmospheric planetary boundary layer. In: *Buoyant Convection in Geophysical Flows*, NATO ASCI Series, vol 513, 421-440. Eds E.J. Plate,
- Monin, A.S., and A.M. Obukhov, 1954: Basic laws of turbulent mixing in the atmosphere near the ground. *Trans. Geof. Inst. Akad. Nauk USSR*, 151, 163-187.
- Moninger, W.R., and R.A. Kropfli, 1982: Radar observations of a plume from an elevated continuous point source *J. Appl. Meteor.*, 21, 11, 1685-1697
- Moran, J.M. and M.D.Morgan, 1995: *Essentials of Weather*. Prentice-Hall, 351 pp.
- Nichols S., and J. Leighton, 1986: An observational study of the structure of stratiform cloud sheets: Part I: Structure. *Q.J.R.Meteor. Soc.* 112, 431-460.
- Nieuwstadt, F.T.M., 1984: The turbulent structure of the stable, nocturnal boundary layer. *J. Atmos. Sci.*, 41, 2202-2216.
- Nieuwstadt, F. T. M., P.J. Mason, C. H. Moeng, and U. Schumann, 1992: Large-eddy simulation of convective boundary-layer: A comparison of four computer codes. *Turbulent Shear Flows 8* (Eds. F. Durst, R. Friedrich, B.E.Lauder, F.W. Schmidt, U. Schumann, and J.H.Whitelaw), Springer-Verlag, pp. 343-367.
- Paluch I.R., and D.H. Lenschow, 1991: Stratiform cloud formation in the marine boundary layer. *J. Atmos. Sci.*, 48, 2141-2158.
- Panofsky, H.A., H. Tennekes, D.H. Lenschow, and J.C.Wyngaard, 1977: The characteristics of turbulent components in the surface layer under convective conditions. *Bound.-Layer Met.* 11, 355-361.
- Pasquill, F. , 1961: The estimation of dispersion of windborne material. *Meteor.Mag.*, 90, 33.
- Pasquill, F. , 1974: *Atmospheric Diffusion*, J.Willey @ Sons.439 pp.
- Plate, E.J. E.E. Fedorovich, D.X. Viegas, and J.C. Wyngaard , 1998: *Buoyancy Convection in Geophysical Flows*. NATO ASI Series, 491 pp.
- Sawford, B.L., and F.M. Guest, 1987: Lagrangian stochastic analysis of flux-gradient relationships in the convective boundary layer. . *J. Atmos. Sci.*, 44, 1152-1165.
- Schemm, C. E., and F. B. Lipps, 1976: Some results from a simplified three-dimensional numerical model of atmospheric turbulence. *J. Atmos. Sci.*, 33, 1021-1041.
- Schmidt, H., and U. Schumann, 1989: Coherent structure of the convective boundary layer derived from large-eddy simulation. *J. Fluid Mech.*, 200, 511-562.

- Siems S.T, C.S.Bretherton, M.B.Baker, S.S.Shy, and R.E.Breidenthal, 1990: Buoyancy reversal and cloud-top entrainment instability. *Q.J.R.Meteor.Soc.*, 116, 705-739.
- Sommeria, G., 1976, Three-dimensional simulation of turbulent processes in an undisturbed trade wind boundary layer. *J. Atmos. Sci.*, 33, 216-241.
- Sorbjan, Z., 1986: On similarity in the atmospheric boundary layer. *Bound.-Layer Met.* 34,377-397.
- Sorbjan, Z., 1988a: Structure of the stably-stratified boundary layer during the SESAME-1979 experiment. *Bound.-Layer Met.* 44, 255-266.
- Sorbjan, Z., 1988 b: Local similarity of spectral and cospectral characteristics in the stable-continuous boundary layer. *Bound.-Layer Meteor.*, 35, 257-275.
- Sorbjan, Z., 1989: Structure of the Atmospheric Boundary Layer. Prentice Hall, 317pp..
- Sorbjan, Z., 1993: Monin-Obukhov similarity for refractive index revisited. *J. Atmos. Sci.*, 50, 3677-3679.
- Sorbjan, Z., 1995: Toward evaluation of heat fluxes in the convective boundary layer. *J. Appl. Meteor.*, 34, 1092-1098
- Sorbjan, Z., 1995: Self-similar structure of the planetary boundary layer. In: The Planetary Boundary Layer and its Parameterizations. 1995 Summer Colloquium. NCAR. Boulder, Colorado, USA.
- Sorbjan, Z., 1996a: Numerical study of penetrative and “solid lid” nonpenetrative convective boundary layers. *J. Atmos. Sci.*, 53, 101-112.
- Sorbjan, Z., 1996b: Effects caused by varying the strength of the capping inversion based on a large-eddy simulation model of the shear-free convective boundary layer. *J. Atmos. Sci.*, 53, 2015-2024.
- Sorbjan, Z., 1997: Decay of convective turbulence revisited. *Bound.-Layer Meteor.*, 82, 501-515.
- Sorbjan, Z., 1999a: Similarity of scalar fields in the convective boundary layer. *J. Atmos. Sci.*, 56, 2212-2221
- Sorbjan, Z. and M.Uljasz, 1999b: Large-eddy simulation of air pollution dispersion in the nocturnal cloud-topped atmospheric boundary layer. *Bound.-Layer Meteor.*, 91, 145-157.
- Sorbjan, Z., 2001: An evaluation of local similarity on the top of the mixed layer based on large-eddy simulations. *Bound.-Layer Meteor.*, 101, 183-207.
- Sorbjan, Z., 2003: Large-eddy simulation of the baroclinic mixed layer. *Bound.-Layer Meteor.* (accepted).
- Stull, R.B.,1973: Inversion rise model based on penetrative convection. *J.Atmos. Sci.*, 30, 1092-1099.
- Stull, R., 1976: The energetic of entrainment across a density interface. *J. Atmos. Sci.*, 33, 1260-1267.
- Stull, R.B., 1988: An Introduction to Boundary Layer Meteorology. Kluwer Academic Publishers, 666 pp.

Sullivan, P.P., C.-H.Moeng, B, Stevens, D.H.Lenschow, and S.D.Mayor, 1998: Structure of the entrainment zone capping the convective boundary layer. *J.Atmos. Sci.*, 55, 3042-3064.

Sun W.-Y., and Y. Ogura, 1980, Modeling the evolution of the convective planetary boundary layer. *J. Atmos. Sci.*, 37, 1558-1572.

Sun W.-Y., 1993. Numerical simulation of a planetary boundary layer: Part i: Cloud-free case. *Beitr.Phys. Atmosph.*, 66, 3-16.

Telfort, J.W., and S.K. Chai, 1984: Inversion and fog, stratus and cumulus formation in warm air over cooler water. *Bound.-Layer Meteor.*, 29, 109-137.

Tennekes, H., 1973: A model for the dynamics of the inversion above a convective boundary layer. *J. Atmos. Sci.*, 30, 558-567.

Turton J., and S. Nicholls, 1987: A study of the diurnal variation of stratocumulus using a multiple mixed-layer model. *Q.J.R.Meteor. Soc.* 113, 969-1011.

Yamada, T., and G. Mellor, 1975: A simulation of the Wangara atmospheric boundary layer data. *J. Atmos. Sci.*, 32, 2309-2338.

Venkatram A. and J.C.Wyngaard (Eds), 1988. Lectures on Air Pollution Modelling. American Meteorological Society.,

Willis, G. E. and J. W. Deardorff, 1976. A laboratory study of dispersion from an elevated source in a convective mixed layer. *Atmos. Environ.*, 12, 1305-1313.

Willis, G. E. and J. W. Deardorff, 1978. A laboratory study of diffusion into a convective planetary boundary layer. *Quart.J. R. Meteorol. Soc.*, 105, 109-117.

Willis, G. E. and J. W. Deardorff, 1981. A laboratory study of dispersion from a source in the middle of the convective mixed layer. *Atmos. Environ.*, 12, 1305-1313.

Wyngaard, J.C., O.R. Cote, and Y. Izumi, 1971: Local free convection, similarity, and the budgets of shear stress and heat flux. *J. Atmos. Sci.* 28, 1171-1182.

Wyngaard J. C., module. *J. Atmos. Sci.*, 41, 1959-1969.

Wyngaard J.C., and R. A.Brost, 1984: Top-down and bottom-up diffusion in the convective boundary layer. *J. Atmos. Sci.*, 41, 102-112.

Wyngaard, 1988: Advances and applications. In Flow and Transport in the Natural Environment. W.L. Steffen and O.T. Denmead (Eds.). Springer-Verlag, 384 pp.

Wyngaard, J. C. and O. R. Coté, K. S. Rao, 1974. Modelling the atmospheric boundary layer. *Adv. Geophys.*, 18A, 193-211.

Zeman O., and J.L. Lumley, 1976: Modeling buoyancy driven mixed layers. *J. Atmos. Sci.*, 33, 1974-1988.

Zeman, O., and H. Tennekes, 1977: Parameterization of the turbulent energy budget at the top of the daytime atmospheric boundary layer. *J. Atmos. Sci.*, 34, 111-123.

Zilitinkievich, S.S., and D.V. Chalikov, 1968: On the computation of the vertical turbulent fluxes in the surface layer of the atmosphere from data of profile observations. *Izv. AN USSR, ser. Fiz. Atmosph. i Okeana*, 4, 915-929 (in Russian).

BRANK
Page

Chapter 5

Meteorological Modeling

Meteorological models are developed and used for two main purposes: 1) to understand and forecast local, regional, or global meteorological phenomena; and 2) to provide the meteorological input required to run air pollution models. Future volumes in the book series will address meteorological modeling issues.

Numerical meteorological models can be divided in two groups: 1) diagnostic models, i.e., models that are based on interpolation/extrapolation of available measurements and contain no time-tendency terms; and 2) prognostic models, i.e., models that perform space-time integration of the conservation equations of mass, heat, motion, water, and if necessary other substances, such as gases and aerosols.

For information, the reader can examine:

- <http://www.mmm.ucar.edu/mm5/mm5-home.html> (MM5 - prognostic)
- <http://rams.atmos.colostate.edu/> (RAMS - prognostic)
- <http://www.src.com/calpuff/calpuff1.htm> (CALMET - diagnostic)
- http://www.caps.ou.edu/ARPS/index_flash.html (ARPS - prognostic)

BRANK
Page

Anfossi, D. et al. (2003) *Plume Rise*. Chapter 6 of *AIR QUALITY MODELING - Theories, Methodologies, Computational Techniques, and Available Databases and Software. Vol. I - Fundamentals* (P. Zannetti, Editor). Published by The EnviroComp Institute (<http://www.envirocomp.org/>) and the Air & Waste Management Association (<http://www.awma.org/>).

Chapter 6

Plume Rise

Domenico Anfossi ⁽¹⁾, Elisa Canepa ⁽²⁾ and Han van Dop ⁽³⁾

⁽¹⁾ *CNR Istituto di Scienze dell'Atmosfera e del Clima, Corso Fiume 4, I-10133 Torino, Italy*

anfossi@to.infn.it

⁽²⁾ *INFN (National Institute for the Physics of Matter), Department of Physics - University of Genova, Via Dodecaneso 33, I-16146 Genova, Italy*

canepae@fisica.unige.it

⁽³⁾ *Institute for Marine and Atmospheric Research Utrecht, P.O. box 80.005, 3508 TA Utrecht, The Netherlands*

dop@phys.uu.nl

Abstract: Plume rise determination is one of the main processes encountered in air pollution modeling. Therefore, the most commonly used methods for introducing plume rise in dispersion models are presented. They encompass simple but robust and documented semi empirical formulations, easy to be implemented in operative models, and advanced plume rise models. Then, the problem of how to account for plume rise in Lagrangian dispersion particle models is addressed. Finally, special situations of plume rise, like the occurrence of an elevated inversion, or the presence of building and/or stacks features interacting with the plume, are investigated.

Key Words: buoyant plumes, jet plumes, ambient turbulence, self-induced turbulence, dispersion modeling, effective plume heights, stability conditions.

List of Symbols

A	dimensional constant in Equation (57) [$L^{3/4} M^{-1/4} T^{-1/4}$]
A_i	drift coefficient for velocity in Equations (97) [$L T^{-2}$]
A_p	dimensionless constant in Equation (87)
A_s	stack outlet area [L^2]
A_1	dimensional constant in Equation (36) [$T^{6/5} L^{-6/5}$]
A_2	dimensional constant in Equation (36) [$T^{6/5} L^{-3/5}$]
A_3	dimensional constant in Equation (37) [$T^{15/8} L^{-3/2}$]
A_4	dimensional constant in Equation (37) [$T^{6/5} L^{-3/5}$]
A^g	drift coefficient for potential temperature in Equations (97) [$K T^{-1}$]
a	drift coefficient in Equation (77) [$L T^{-2}$]
B	plume particle buoyancy [$L T^{-2}$]
B_0	initial plume buoyancy [$L T^{-2}$]
b_i	acceleration of air displaced through an inversion [$L T^2$]
b_{ij}	diffusion coefficient for velocity in Equations (97) [$L T^{-3/2}$]
b_p	lower edge of the plume [L]
b^g	diffusion coefficient for potential temperature in Equations (97) [$K T^{-1/2}$]
C	parameter in Equation (138) [$L^{-1/3} T$]
C_0	dimensionless constant in Equation (77)
c_B	dimensional constant in Equations (92) [$L^2 T^{-5}$]
c_p	specific heat at constant pressure [$L^2 T^{-2} K^{-1}$]
c_w	dimensional constant in Equations (92) [$L^2 T^{-3}$]
c_1	dimensionless constant in Equations (91)
c_2	dimensionless constant in Equations (91)
D	dimensionless parameter in Equation (139)
D_0	dimensional constant in Equation (57) [L]
D_1	dimensionless constant in Equation (57)
D_2	dimensional constant in Equation (57) [$T K$]
d	spacing between adjacent stacks [L]
d_s	internal diameter of the stack outlet [L]
d_1	dimensionless constant in Equation (70)
d_2	dimensionless constant in Equation (70)
d_3	dimensionless constant in Equation (71)
d_4	dimensionless constant in Equation (72)
dW	random increment in Equation (77)
$d\omega_B$	random increments for buoyancy in Equations (84) [$T^{1/2}$]
$d\omega_j$	random increments for velocity in Equations (97) [$T^{1/2}$]
$d\omega_w$	random increments for velocity in Equations (84) [$T^{1/2}$]
$d\omega^g$	random increments for potential temperature in Equations (84) [$T^{1/2}$]

E	turbulent kinetic energy [$L^2 T^{-2}$]
E_n	dimensionless enhancement factor
f	dimensionless stack tip downwash correction factor
f'	dimensionless fraction of the plume trapped below inversion
f_b	atmospheric turbulence buffet frequency [T^{-1}]
F_b	buoyancy flux parameter [$L^4 T^{-3}$]
F_b^i	buoyancy flux of i-th particle [$L^4 T^{-3}$]
F_e	plume buoyancy flux at the end of bending-over phase [$L^4 T^{-3}$]
F_j	buoyancy of the j-th stack [$L^4 T^{-3}$]
F_m	momentum flux parameter [$L^4 T^{-2}$]
F_{m^*}	dimensionless momentum flux
F_m^i	momentum flux of i-th particle [$L^4 T^{-3}$]
F_r	dimensionless Froude number
F_*	dimensionless buoyancy flux
G	plume volume in Equations (79) [$L^3 T^{-1}$]
G_s	G value at stack outlet [$L^3 T^{-1}$]
g	acceleration due to gravity [$L T^{-2}$]
k_v	dimensionless added mass
H	upward surface sensible heat flux times $g/(c_p \rho_a \theta)$ [$L^2 T^{-3}$]
H^*	dimensional parameter in Equation (57) [L]
H_b	building height [L]
H_i	merging point height in Equation (138) [L]
H_j	height of the j-th stack in Equation (138) [L]
H_{\max}	highest stack in Equation (139) [L]
H_{\min}	lowest stack in Equation (139) [L]
h	mixing height [L]
h'	inversion height with respect to stack top [L]
h_e	effective stack height [L]
h_t	height of the base of atmospheric thermal discontinuity [L]
L_b	buoyancy length scale [L]
L_e	effective length [L]
L_m	momentum length scale [L]
M_e	plume momentum flux at the end of bending-over phase [$L^4 T^{-2}$]
N	Brunt-Väisälä frequency [T^{-1}]
N'	modified Brunt-Väisälä frequency [T^{-1}]
n	dimensionless number of stacks
P_b	dimensionless buoyancy flux in Equation (127)
P_s	dimensionless buoyancy flux in Equation (136)
Q_f	total heat release rate of a flare [$M L^2 T^{-3}$]
Q_h	stack effluent heat emission rate [$M L^2 T^{-3}$]
Q_m	stack effluent mass emission rate [$M T^{-1}$]
R	plume radius [L]

R_e	plume radius at end of bending-over phase [L]
R_s	dimensionless initial plume radius
R_0	dilution radius [L]
r_a	radius of air eddies [L]
r_s	internal radius (or equivalent radius) of the stack outlet [L]
S_{wa}^3	third moment of ambient Eulerian PDF [$L^3 T^{-3}$]
S	dimensionless parameter in Equation (137)
s	stability parameter [T^{-2}]
s_c	distance along the centerline [L]
T_a	ambient temperature [K]
T_{a0}	ambient temperature at stack outlet height [K]
T_e	Eulerian time scale [T]
T_m	Lagrangian time scale in Equation (90) [T]
T_{s0}	temperature of stack effluent at stack outlet [K]
T_p	Lagrangian time scale of the plume [T]
t	travel time [T]
t_p	upper edge of the plume [L]
t_0	initial turbulent timescale of the plume particle [T]
U_a	wind speed that can vary with height [$L T^{-1}$]
U_i	particle velocity component ($i = 1, 2, 3$) [$L T^{-1}$]
U_{sc}	velocity along the centerline [$L T^{-1}$]
$U_z(t)$	mean vertical wind component [$L T^{-1}$]
u	mean uniform horizontal wind speed in Equation (59) [$L T^{-1}$]
u_p	horizontal particle velocity [$L T^{-1}$]
$u'(t)$	turbulent velocity fluctuation in Equation (77) [$L T^{-1}$]
u_*	friction velocity [$L T^{-1}$]
u_0	mean wind speed at the stack outlet height [$L T^{-1}$]
u_5	wind speed at the $1.5 z_s$ [$L T^{-1}$]
v'_a	r.m.s. velocity of an air eddy with respect to the plume [$L T^{-1}$]
v_{s0}	effluent emission speed at stack outlet [$L T^{-1}$]
v_a	relative velocity of two particles [$L T^{-1}$]
v_e	entrainment velocity [$L T^{-1}$]
W	vertical velocity of the plume [$L T^{-1}$]
w_b	buoyancy contribution to the vertical velocity [$L T^{-1}$]
w_m	momentum contribution to the vertical velocity [$L T^{-1}$]
w_p	vertical velocity of the particle [$L T^{-1}$]
$w'(t)$	turbulent velocity fluctuation in Equation (66) [$L T^{-1}$]
w_*	convective velocity scale [$L T^{-1}$]
X_i	particle position component ($i = 1, 2, 3$) [L]
X_*	dimensionless downwind distance
X_z	plume particle's vertical position [L]
x	downwind distance from stack [L]
x^*	function of downwind distance from Equation (56) [L]

x_c^*	critical distance defined by Equation (36) [L]
x_f	downwind distance of maximum plume rise [L]
x_T	length defined by Equation (56) [L]
y	lateral space coordinate or radial distance from axis [L]
z	elevation a.g.l. [L]
z'_{eq}	equilibrium height with respect to the stack top [L]
z_s	stack height [L]
α	dimensionless constant in Equations (79)
α_B	dimensionless constant in Equations (92)
α_v	dimensionless constant in Section (4.3.3)
α_w	dimensionless constant in Equations (92)
β	dimensionless classic entrainment parameter
β_1	dimensionless neutral entrainment parameter in Equation (116)
β_2	dimensionless stable entrainment parameter in Equation (117)
β_j	dimensionless jet entrainment parameter in Equation (116)
γ	dimensionless constant in Equations (79)
γ_1	dimensionless constant in Equation (80)
γ_2	dimensionless constant in Equation (82)
ΔH_{\min}	maximum single plume rise from lowest stack in Equation (139) [L]
ΔH^N	final rise for merged plumes [L]
Δh	final plume rise [L]
$\Delta h(t)$	plume rise as a function of travel time [L]
$\Delta h(x)$	plume rise as a function of distance downwind of stack [L]
$\Delta h'$	final plume rise corrected for the stack tip downwash [L]
$\Delta h''$	actual plume rise in Equation (123) [L]
Δh_d	plume rise of a building downwashed plume [L]
Δh_i	thickness of the inversion layer [L]
Δh_1	plume rise from a single stack in multiple sources [L]
Δh_{\max}	maximum plume rise [L]
ΔT_c	critical temperature difference [K]
ΔT_0	temperature difference between air and plume at the stack outlet [K]
Δt	time step [T]
Δu	difference in the horizontal velocity between the plume and the ambient environment [L T ⁻¹]
Δz	vertical increment [L]
$\Delta \mathcal{G}^*$	dimensional parameter in Equation (57) [K]
$\Delta \mathcal{G}_i$	potential temperature jump of the inversion [K]
$\Delta \mathcal{G}_m$	maximum excess temperature [K]
$\Delta \mathcal{G}_{100}$	potential temperature variation over 100 m in Section 2.7.1 [K]
δ	dimensionless parameter in Equation (133)

$\partial \mathcal{G} / \partial z$	vertical gradient of absolute potential temperature [K L^{-1}]
ε_a	ambient rate of dissipation of turbulent kinetic energy [$\text{L}^2 \text{T}^{-3}$]
ε_B	dissipation rate of buoyancy of the plume particle [$\text{L}^2 \text{T}^{-5}$]
ε_m	dissipation rate in Equation (96) [$\text{L}^2 \text{T}^{-3}$]
ε_p	rate of dissipation of turbulent kinetic energy in the plume [$\text{L}^2 \text{T}^{-3}$]
ε_w	dissipation rate of velocity of the plume particle [$\text{L}^2 \text{T}^{-3}$]
λ	dimensionless parameter in Equation (132)
η_{eq}	dimensionless parameter in Equation (133)
ϕ	angle between the horizontal and the centerline [deg]
μ_a	air molecular weight [M mol^{-1}]
μ_s	emission molecular weight [M mol^{-1}]
ρ_a	density of ambient atmosphere [M L^{-3}]
ρ_{a0}	ambient density at stack outlet height [M L^{-3}]
ρ_s	density of effluent [M L^{-3}]
ρ_{s0}	density of effluent at stack outlet [M L^{-3}]
σ_{y0}	enhanced horizontal dispersion coefficient [L]
σ_z	plume width [L]
σ_{z0}	enhanced vertical dispersion coefficient [L]
σ_{up}^2	longitudinal velocity variance due to the plume rise [$\text{L}^2 \text{T}^{-2}$]
σ_{vp}^2	crosswind velocity variance due to the plume rise [$\text{L}^2 \text{T}^{-2}$]
σ_{wa}^2	second moment of ambient Eulerian PDF [$\text{L}^2 \text{T}^{-2}$]
σ_w^2	vertical wind velocity variance [$\text{L}^2 \text{T}^{-2}$]
σ_{wp}^2	vertical velocity variance due to the plume rise [$\text{L}^2 \text{T}^{-2}$]
\mathcal{G}_a	ambient potential temperature [K]
\mathcal{G}_p	potential temperature of the plume particle [K]
τ	dimensionless travel time

1 Introduction

The behavior of a chimney plume in the atmosphere is a rather complex process, which is influenced by the emission characteristics, the nearby terrain features, the actual wind profiles, stratification (vertical gradient of potential temperature) and turbulence. Basically, plumes emitted into the atmosphere rise under the action of their initial momentum and buoyancy (if they possess a temperature which is greater than the ambient temperature). For power plants and other moderate-to-large industrial sources, the major contribution to the rise is from the heat flux. For example, a modern power plant typically discharges ≈ 100 MW of heat from its stack. These are called buoyant plumes. In such conditions plumes can rise for hundreds of meters. Initial momentum can be important for smaller

sources, with little or no buoyancy, such as those typically found in light manufacturing. Plumes from these sources are referred to as jet plumes.

A jet plume, moving through the ambient atmosphere, experiences a shear force at its perimeter, where momentum is transferred from the jet to the surrounding air. This causes an increase of the plume diameter and a decrease of its velocity. This phenomenon is known as entrainment. In a buoyant plume, air is entrained in the same way as in a jet and the buoyancy forces help maintain the motion of the plume as it transfers momentum to the surrounding air. For this reason, buoyant plumes generally rise higher than jet plumes. The entrained ambient air mixes with the plume air, thus diluting the plume components before they reach ground level and, in the case of buoyant plumes, decreasing the average temperature difference between air and plume. In a calm atmosphere, plumes rise almost vertically, whereas in windy situations they bend over. In this case, the velocity of any plume parcel is the vector composition of horizontal wind velocity and vertical plume velocity in the first stage and then approaches the horizontal wind velocity.

The motion of bent over plumes can be schematically divided into three phases (Slawson and Csanady, 1967; 1971): an initial phase, in which the self-generated turbulence, due to the action of their mechanical and thermal energy, prevails; an intermediate phase, where the ambient turbulence in the inertial sub-range is important; a final phase, in which the main mechanism is the mixing due to the large atmospheric energy containing eddies (see Figure 1).

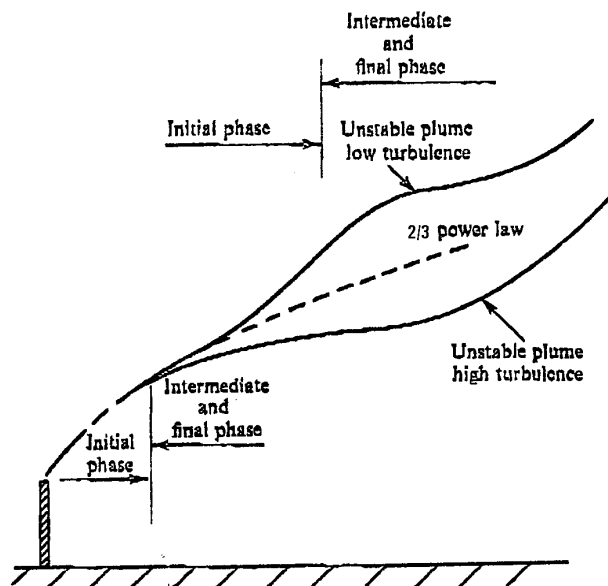


Figure 1. Two possibilities of unstable plume behavior (adapted from Slawson and Csanady, 1971). [Reprinted with permission from Cambridge University Press]

Effective plume height h_e (elevation of plume centerline relative to ground level) results from the sum of stack height z_s and plume rise Δh (Figure 2)

$$h_e = z_s + \Delta h \quad (1)$$

Thus, a correct estimation of buoyant plume rise is one of the basic requirements for the determination of ground level concentrations of airborne pollutant emitted by industrial stacks. In fact maximum ground level concentration is roughly inversely proportional to the square of the final height h_e . For this reason, in many

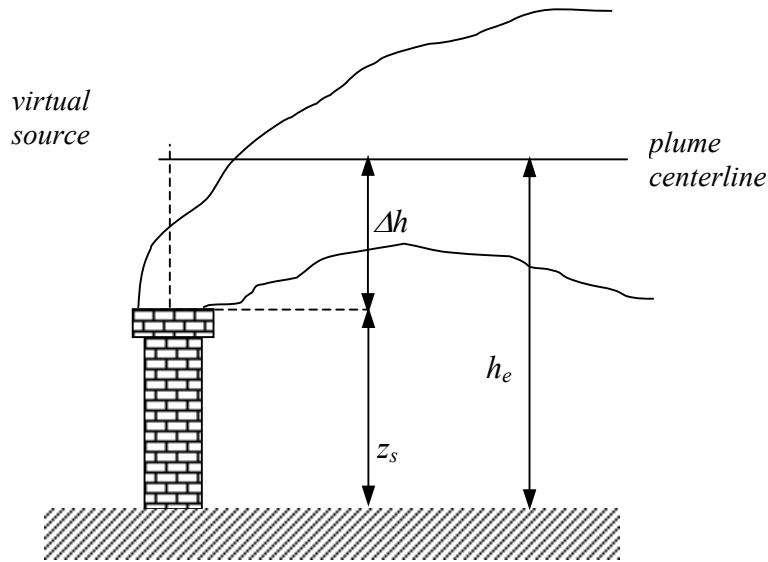


Figure 2. The plume rise: schematic representation.

simple dispersion models, stack gases are assumed to be emitted from a virtual source located at a height h_e (see Figure 2) along the vertical above the stack.

The description of plume rise is based on the fluid dynamic equations, namely on the mass, momentum and energy conservation equations. A complete, exhaustive theory is not yet available. Therefore some simplifying assumptions need to be made. These will give rise to simplified models that can just take into account the main variables of the examined case.

Plume rise formulae can be ranked either empirical or theoretical, but the distinction is not so clear:

- the empirical formulae are based almost exclusively on experimental data both for their numerical parameters and for their functional form
- the theoretical formulae, in spite of including some parameters with an experimental origin, have a functional form based on the solution of equations expressing laws of mass, momentum and energy conservation

Some formulae provide the plume rise as a function of the distance, but most of them provide a constant value (final plume rise) that the plume reaches at a large downwind distance. These formulae contain height depending atmospheric variables normally specified at the stack outlet height.

Several studies and review works have provided semi-empirical formulae for evaluating Δh (e.g., Holland, 1953; Brummage, 1966; Bringfelt, 1969; Fay et al., 1970; Carpenter et al., 1971; Briggs, 1975; Strom, 1976; Hanna et al., 1982; and many others); others have provided more complex and comprehensive descriptions of several physical interactions between the plume and the ambient air (e.g., Golay, 1982; Netterville, 1990). Relevant and exhaustive review papers on the plume rise subject can be found in the literature, such as, for instance, Briggs (1975) and Weil (1988). In this chapter, we will utilize a great deal of material from these reviews.

For many specific applications, literature supplies functional forms and empirically determined parameters, but such models may provide wildly inaccurate results, if they are used beyond the context where they have been obtained. In uncertain cases, Briggs (1975) recommends to use, in the application, the formula that provides the minimum plume rise; this result is “the most conservative”, since it gives rise to the maximum values of concentration expected at the ground, thus limiting the risk of a possible underestimation. It is hard to specify clearly the accuracy of plume rise formulae: some discordance up to 25% between the observed and the expected value are not unusual.

This chapter, which is concerned with plume rise from continuous releases, focuses on:

- semi-empirical formulations
- advanced plume rise models
- particle models for plume rise
- special cases (like building downwash, penetration of elevated inversion, multiple source, flare stacks, fires and so on)

The semi-empirical formulations, expressed as analytical relationships, have a functional form obtained from the solution of mass, momentum and energy conservation equations in simplified conditions (such as steady conditions, uniform wind and stability) and their numerical parameters are generally deduced from experimental data. These are the plume rise estimations mostly used in regulatory model applications.

In the advanced plume rise models the conservation equations are numerically integrated, thus giving practical solutions for varying winds and thermal structure. Due to present days computer capabilities, these models may also be used for regulatory applications. However it cannot be automatically accepted that these fully 3D models always yield results better than simpler models due to the

difficulty, in some applications to real cases, of getting the needed input data with the necessary time and space resolution.

The particle models for plume rise are relatively new methods, not yet widely used for regulatory purposes. We think that it is important to present and discuss them in some detail since the Lagrangian approach is a more natural way of describing the dispersion process (Sawford, 1985). Furthermore these are probably the methods of the future and allow a high resolution, particularly the small time behavior of plume dispersion (Nguyen et al., 1997)

The section on special cases covers many aspects of the plume rise phenomenon that are of practical importance in many applications.

Our discussion of plume rise addresses fundamental aspects and major problems, but it is not exhaustive. We intend neither to make any ranking of the models presented in the next sections, nor to recommend which model is the best for a specific application, because we want to avoid any subjective judgment which may be also influenced by the particular national regulatory laws. We wish to present a review of updated and validated existing techniques that can be used by modelers according to their specific needs. Even if no guidance is given whether a reader should use one of the models out of those suggested for a specific problem, the general rule might be to preferably use those formulas, if any, that are validated, recommended or suggested by National Environmental Protection Agencies. Being used and tested by hundreds of users, these models will, at least, guarantee that the major bugs and/or uncertainties were identified and amended and unrealistic results avoided.

2 Semi-Empirical Formulations

2.1 Governing Equations

As above anticipated, the differential equations expressing the conservation of the total fluxes of mass, momentum, and energy through a plume cross section (e.g., Morton et al., 1956; Briggs 1975; Weil, 1988) are the basis of all the analytical plume rise models. These equations are closed using the entrainment assumption (Morton et al., 1956), which prescribes that the entrainment velocity, i.e. the rate at which ambient air is entrained into the plume, is proportional to the mean local rise velocity. It may be worth mentioning that Priestley (1956) provided an alternative entrainment assumption, based on energy arguments, that gives the same basic plume rise results as Morton et al. (1956).

The following simplifications are made: the plume rises in a steady, horizontal wind of constant direction and variable with height speed $U_a(z)$; stratification, if present, is constant with the height; plume cross section is circular with radius R ; plume properties (mass, velocity, temperature) have a “top hat” distribution (that

is to say in each section the cited quantities are constant inside the plume and null outside); the plume pressure is the same as in the local environment; the density differences are sufficiently small to allow making the Boussinesq approximation; since the efflux volume quickly mixes with a large volume of ambient air, the effluent has the same molecular weight and specific heat as air.

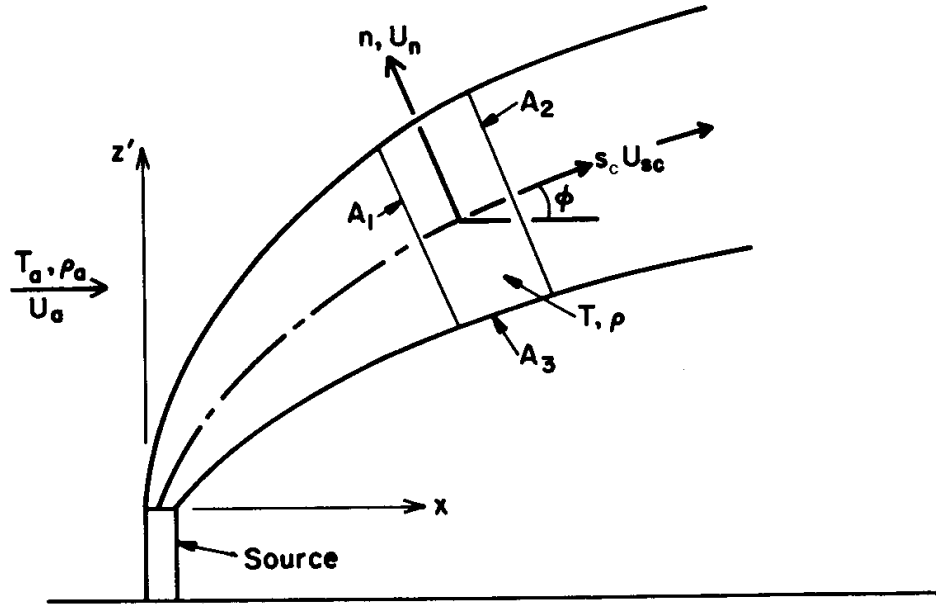


Figure 3. Schematic and nomenclature for plume in a crosswind (adapted from Weil, 1988). [Reprinted with permission from American Meteorological Society].

In the case of a crosswind, conservation of mass, horizontal momentum, vertical momentum and energy are given respectively by (Weil, 1988)

$$\frac{d}{ds_c}(U_{sc}R^2) = 2R\beta W \quad (2)$$

$$\frac{d}{ds_c}(U_{sc}R^2\Delta u) = -R^2W \frac{dU_a}{dz} \quad (3)$$

$$\frac{d}{ds_c}(U_{sc}R^2W) = gR^2 \frac{(\rho_a - \rho_s)}{\rho_s} \quad (4)$$

$$\frac{dF_b}{ds_c} = sWR^2 \quad (5)$$

where (see also Figure 3): s_c and U_{sc} are the distance and velocity along the centerline, β is the dimensionless entrainment parameter, W is the plume vertical velocity, Δu is the difference in the horizontal velocity between the plume and the ambient environment, g is the acceleration due to gravity, ρ_a and ρ_s are the air and plume density, respectively, F_b is the buoyancy flux defined by

$$F_b = U_{sc} R^2 g \frac{(\rho_a - \rho_s)}{\rho_a} \quad (6)$$

and s is the stability parameter defined by

$$s = \frac{g}{g_a} \frac{\partial g_a}{\partial z} \quad (7)$$

g_a being the potential temperature of the air and $\partial g_a / \partial z$ its vertical gradient. The plume trajectory, $\Delta h(x)$, can be obtained from the above equations and from the following relationships (kinematic conditions)

$$\frac{d\Delta h}{ds_c} = \frac{W}{U_{sc}}, \quad \frac{dx}{ds_c} = \frac{U_a + \Delta u}{U_{sc}} \quad (8)$$

For sake of completeness, and for reference to previous and/or related work on the plume rise, the following remarks may be important.

F_b is related to the heat emission rate Q_h by the following relationship

$$F_b = g Q_h / \pi c_p \rho_a T_a \quad (9)$$

where T_a = temperature of the air;
 c_p = specific heat of air at constant pressure.

Q_h is given by the following equation

$$Q_h = Q_m c_p (T_{s0} - T_{a0}) \quad (10)$$

where Q_m = effluent mass emission rate;
 T_{s0} = absolute temperature of effluent at stack outlet;
 T_{a0} = absolute temperature of ambient atmosphere at stack outlet height.

Q_m may be expressed in terms of other variables as follows

$$Q_m = \rho_{s0} A_s v_{s0} \quad (11)$$

where ρ_{s0} = mass density of effluent at stack outlet;

A_s = stack outlet area;

v_{s0} = effluent emission speed at stack outlet.

Using Equation (11) and the following equality

$$\rho_{s0}(T_{s0} - T_{a0}) = T_{a0}(\rho_{a0} - \rho_{s0}) \quad (12)$$

Q_h can be expressed in terms of the mass density of ambient air at stack outlet height, ρ_{a0} , and of the pollutants, ρ_{s0} , as follows

$$Q_h = A_s v_{s0} T_{a0} c_p (\rho_{a0} - \rho_{s0}) \quad (13)$$

In the plume rise formulae for jet plumes, where the initial momentum plays the major role in the rising process, F_b is substituted by the momentum flux F_m , given by the following equation

$$F_m = v_{s0}^2 \frac{A_s \rho_{s0}}{\pi \rho_{a0}} \quad (14)$$

Notice that the buoyancy and momentum fluxes - Equations (6) and (14) - by convention are divided by π . This convention derives (Briggs, 1984) from the assumption of round top hat profile of all the plume quantities in the early plume rise studies. This assumption leads to the presence of π on both sides of the flux conservation equations.

In some plume rise formulations (e.g., Hewett et al., 1971), the buoyancy flux is defined by $F_b = U_{sc} R^2 g (\rho_a - \rho_s) / \rho_s$. According to Briggs (1972), this definition is equivalent to assuming that the buoyant force acts on a fluid of density ρ_s . However, the density of the fluid driven by the buoyant force is better approximated by ρ_a , since a turbulent plume is made up mostly of entrained fluid (Briggs, 1984).

In some formulae, the Brunt-Väisälä frequency, N , defined as

$$N = +\sqrt{s} \quad (15)$$

is used instead of the stability parameter s - see Equation (7). In stable conditions, the Brunt-Väisälä frequency is the natural frequency of oscillation of a fluid particle if perturbed from its equilibrium position; for plumes, N^{-1} is the time

scale for the depletion of the buoyancy flux and for the maximum rise in a stable environment (in the atmosphere a typical value of N^{-1} is 1 min).

The formulae that are going to be presented in the following sections are mostly, but not exclusively, derived from Briggs (1969, 1972, 1975, 1984). Briggs formulae, together with some new result recently appeared in the literature due to other authors, have been incorporated into most of the U.S. EPA models (<http://www.epa.gov/scram001/t22.htm>). These formulae represent a reasonable compromise between accuracy and simplicity, even though, according to many (e.g., Henderson-Sellers and Allen, 1985), they may tend to overestimate the plume rise at large downwind distances. Note that some authors (Strom, 1976; Hanna, 1994) suggest, in the absence of particular expressions derived for specific problems, using Briggs formulae.

It is worthwhile pointing out that Manins (1985) summarized evidence (from large fires, volcanic eruptions and clouds from thermonuclear explosions) showing that the vertical plume rise equation derived in the next section - Equation (45) - holds for over four orders of magnitude variation in rise height.

2.2 Plume Rise in the Transitional Phase

By solving the system of equations presented in Section 2.1, simple analytical expressions, easy to use in dispersion models, can be achieved.

2.2.1 Neutral and Unstable Case

Let us firstly consider the rise of a bent over plume in neutral conditions ($s = 0$) and uniform wind (no shear) and neglect ambient turbulence. At some distance from the source, plume can be considered as nearly horizontal and the following approximations can be made: $U_{sc} \cong U_a = \text{const}$ and $W \ll U_a$. From Equation (2) it follows that the plume radius grows linearly with height. In these stability conditions, Equation (5) implies that the buoyancy flux F_b is conserved. Thus, F_b is expressed by means of its value at the stack outlet, in terms of, respectively, temperatures and densities

$$F_b = g v_{s0} \frac{A_s (T_{s0} - T_{a0})}{\pi T_{s0}} \quad (16)$$

$$F_b = g v_{s0} \frac{A_s (\rho_{a0} - \rho_{s0})}{\pi \rho_{a0}} \quad (17)$$

Similarly, F_m is expressed by

$$F_m = v_{s0}^2 r_s^2 \frac{T_{a0}}{T_{s0}} \quad (18)$$

$$F_m = v_{s0}^2 r_s^2 \frac{\rho_{s0}}{\rho_{a0}} \quad (19)$$

where r_s is the internal radius of the stack outlet.

Note that, usually, in Equations (16) and (17), instead of A_s , we find r_s (or, for a non-circular stack having an area A_s , the equivalent radius given by $r_s = \sqrt{A_s/\pi}$). It may be worth pointing out that for the emissions whose molecular weight, μ_s , differs considerably from the air molecular weight, μ_a , Hanna et al. (1982) suggests, in relation to Equation (16), replacing T_{s0} with T_{s0}/μ_s and T_{a0} with T_{a0}/μ_a .

The resulting equation of the plume centerline trajectory $\Delta h(t)$ is (Briggs, 1975)

$$\Delta h(t) = \left(\frac{3}{\beta^2} \frac{F_m}{u_0} t + \frac{3}{2\beta^2} \frac{F_b}{u_0} t^2 \right)^{1/3} \quad (20)$$

Equation (20) takes into account both the buoyancy and initial vertical momentum contributions. In the very initial stage, the momentum dominates and the plume rise is described by

$$\Delta h(t) = \left(\frac{3}{\beta^2} \frac{F_m}{u_0} t \right)^{1/3} \quad (21)$$

whereas, when t is larger than $2F_m/F_b$ (about 10 s for many sources, Briggs 1975) the buoyancy dominates and Equation (20) reduces to

$$\Delta h(t) = \left(\frac{3}{2\beta^2} \frac{F_b}{u_0} \right)^{1/3} t^{2/3} \quad (22)$$

Expressed as a function of downwind distance, Equations (20), (21) and (22) become

$$\Delta h(x) = \left(\frac{3}{\beta^2} \frac{F_m x}{u_0^2} + \frac{3}{2\beta^2} \frac{F_b x^2}{u_0^3} \right)^{1/3} \quad (23)$$

$$\Delta h(x) = \left(\frac{3}{\beta^2} \right)^{1/3} F_m^{1/3} x^{1/3} u_0^{-2/3} \quad (24)$$

and

$$\Delta h(x) = \left(\frac{3}{2\beta^2} \right)^{1/3} F_b^{1/3} x^{2/3} u_0^{-1} \quad (25)$$

In order to use the above equations in practical models, the value of β , the dimensionless entrainment parameter, must be empirically established. In the bent over buoyant plumes ($\phi \rightarrow 0$, where ϕ is the angle between the horizontal and the centerline) $\beta = 0.6$, whereas for vertical buoyant plumes ($\phi \rightarrow 90^\circ$) $\beta = 0.11$ (Briggs, 1975; Hoult and Weil, 1972). For jet plumes (Briggs, 1975, 1984)

$$\beta = 0.4 + 1.2 \frac{u_0}{v_{s0}} \quad (26)$$

In particular, Equation (25) becomes

$$\Delta h(x) = 1.6 F_b^{1/3} x^{2/3} u_0^{-1} \quad (27)$$

This equation is widely known as the “two-thirds” law. It was confirmed by a large amount of experimental work (see Briggs, 1975 for a comprehensive summary). Figure 4 is an example of the quality of the agreement found in the literature. Consequently, most practical models use the “two-thirds” law to describe the plume rise in the transitional phase under neutral and unstable conditions. However some models - see, for instance, AERMOD (U.S. EPA, 1998) or Weil et al. (1997) - use the complete Equation (20). In this case they use the value $\beta = 0.6$ for the momentum term too.

By defining the momentum length scale L_m and the buoyancy length scale L_b as

$$L_m = \frac{\sqrt{F_m}}{u_0} \quad \text{and} \quad L_b = \frac{F_b}{u_0^3} \quad (28)$$

Equations (23 - 25) become

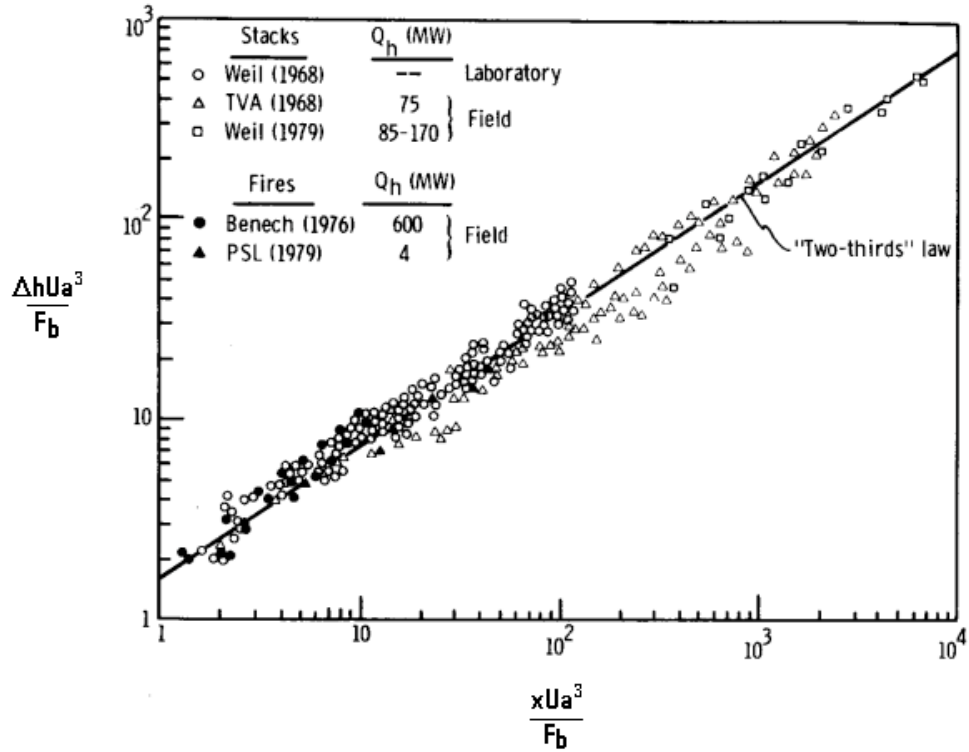


Figure 4. Observed trajectories of buoyancy-dominated plumes compared with the “two-thirds” law (from Weil, 1988). [Reprinted with permission from American Meteorological Society].

$$\frac{\Delta h(x)}{L_b} = \left[\frac{3}{\beta^2} \left(\frac{L_m}{L_b} \right)^2 \frac{x}{L_b} + \frac{3}{2\beta^2} \left(\frac{x}{L_b} \right)^2 \right]^{1/3} \quad (29)$$

$$\frac{\Delta h(x)}{L_m} = \left(\frac{3}{\beta^2} \frac{x}{L_m} \right)^{1/3} \quad (30)$$

$$\frac{\Delta h(x)}{L_b} = \left(\frac{3}{2\beta^2} \frac{x^2}{L_b^2} \right)^{1/3} \quad (31)$$

L_m and L_b allow an alternative criterion to establish in which range of downwind distances the buoyancy or the momentum dominates the plume rise: momentum dominates for $x \ll L_m^2/L_b$ whereas buoyancy dominates for $x \gg L_m^2/L_b$.

2.2.2 Stable Case

In case of a stable atmosphere ($s = \text{const}$, $s \neq 0$), again neglecting ambient turbulence, and considering uniform wind and the bent-over phase, integration of the conservation equations leads to the following expression (Briggs, 1975)

$$\Delta h(x) = \left(\frac{3(I + k_v)}{\beta^2 u_0 s} \right)^{1/3} \left\{ N' F_m \sin \left(N' \frac{x}{u_0} \right) + F_b \left[1 - \cos \left(N' \frac{x}{u_0} \right) \right] \right\}^{1/3} \quad (32)$$

for $x \leq \pi u_0 / N'$, where $N' = s^{1/2} / (I + k_v)^{1/2}$. The term, $I + k_v$, accounts for the so-called “added mass” (Briggs, 1972, 1975, 1984; Weil, 1988, 1994). This added mass takes into account the momentum of the ambient air displaced by the rising plume. Consequently, the effective plume radius is larger than the visible plume radius. Many models did not consider this aspect that can explain the difference found in the value of the entrainment parameter from the measurements of plume rise in different stability conditions. Concerning the numerical value of the added mass, Briggs (1975) and Weil (1994) suggest $I + k_v = 2.25$.

When the atmosphere is stable, ambient turbulence is very low and a plume levels off where its density difference with respect to ambient air approaches zero. For distances greater than $\pi u_0 / N'$ a plume, in principle, overshoots its equilibrium height and displays a quickly damped oscillation. This was experimentally verified in some occasions (Briggs, 1975). However, often plumes approach an asymptotic height with no overshoot at all (Briggs, 1984). In this range of distances a plume drifts downwind with a very small increase in thickness, due to its mixing with stable, almost non turbulent, air.

In the two asymptotic cases in which the momentum dominates ($F_b \ll N' F_m$) or the buoyancy dominates ($F_b \gg N' F_m$), the above equation reduces to, respectively

$$\Delta h(x) = \left[\frac{3(I + k_v)^{1/2} F_m \sin \left(N' \frac{x}{u_0} \right)}{\beta^2 u_0 s^{1/2}} \right]^{1/3} \quad (33)$$

$$\Delta h(x) = \left\{ \frac{3(1+k_v)F_b \left[1 - \cos\left(N' \frac{x}{u_0} \right) \right] \right\}^{1/3} \beta^2 u_0 s \quad (34)$$

Notice that, by approximating $\cos\left(N' \frac{x}{u_0}\right)$ as $1 - \left(N' \frac{x}{u_0}\right)^2$ for $\frac{x}{u_0} \ll \frac{1}{N'}$ in Equation (32), the “two third law” - Equation (27) - is recovered.

2.3 Formulae for the Final Height of Buoyant Plumes

Stable stratification is the only condition in which a plume levels off and, consequently, the definition of a final height is correct. Since in neutral and unstable conditions the buoyancy flux F_b is conserved, plumes cannot, in principle, level off. However, ambient turbulence significantly affects the buoyant plume growth. Another limitation to the continuous rise of the plume is the presence, above the mixing height, of a capping inversion (see Section 5.2).

The importance of assessing correct ways to determine the plume “final height” derives from the wide use of Gaussian models in dispersion calculations. These dispersion models disregard the transitional phase and assume that a plume is emitted by a virtual height (see Figure 2) located at a final effective height h_e , given by the sum of stack height z_s and plume final rise Δh - see Equation (1).

2.3.1 Neutral and Unstable Case

For neutral or unstable conditions, Briggs (1969) suggested using Equation (27) up to $x = x_c^*$, and the following equation

$$\Delta h(x) = 1.6 F_b^{1/3} u_0^{-1} (x_c^*)^{2/3} \left[\frac{2}{5} + \frac{16x}{25x_c^*} + \frac{11}{5} \left(\frac{x}{x_c^*} \right)^2 \right] \left(1 + \frac{4x}{5x_c^*} \right)^{-2} \quad (35)$$

for $x > x_c^*$. x_c^* is a critical distance representing the downwind distance at which ambient turbulence begins to dominate the entrainment process, which can be expressed either by

$$\begin{aligned} x_c^* &= A_1 F_b^{2/5} z_s^{3/5} & z_s < 305m \\ x_c^* &= A_2 F_b^{2/5} & z_s > 305m \end{aligned} \quad (36)$$

or

$$\begin{aligned}
 x_c^* &= A_3 F_b^{5/8} & F_b < 55 \text{ m}^4/\text{s}^{-3} \\
 x_c^* &= A_4 F_b^{2/5} & F_b > 55 \text{ m}^4/\text{s}^{-3}
 \end{aligned} \tag{37}$$

in which the values of the four dimensional constants are the following: $A_1 = 2.16 \text{ s}^{6/5} \text{ m}^{-6/5}$, $A_2 = 67.0 \text{ s}^{6/5} \text{ m}^{-3/5}$, $A_3 = 49.0 \text{ s}^{15/8} \text{ m}^{-3/2}$, and $A_4 = 119.0 \text{ s}^{6/5} \text{ m}^{-3/5}$.

In the case of fossil fuel plants with Q_h of 20 MW or more, x_c^* can be satisfactory approximated by the following equation

$$x_c^* = 10z_s \tag{38}$$

Subsequently, Briggs (1975) made a distinction between neutral and unstable conditions accounting for the effects of ambient turbulence on the plume rise. While self-generated turbulence affects the entrainment process near the source, ambient turbulence (with both small and large scale eddies) becomes important further downwind. Small scale eddies (with typical length scale $\leq R$), are responsible for the increase of the plume growth rate beyond that given by self-induced turbulence. The breakup model (Briggs, 1984; Weil, 1988), assumes that plume rise finishes when ambient turbulence “breaks up” the self-generated structure of the plume, causing a vigorous mixing and, consequently, plume gradually loses buoyancy and momentum and eventually level off. Thus, this process leads to an asymptotic rise. According to Briggs, the plume breakup occurs when the ambient rate of dissipation of turbulent kinetic energy, ε_a , exceeds the one of the plume ε_p . Large scale eddies (updrafts and downdrafts in the CBL) may transport plume segments up and down, thereby dispersing the plume by vertical meandering and pushing some of them to the surface. When this happens, the time averaged ground level concentration is more dependent on how many times, during the averaging period, the plume touches the ground than on the height of the asymptotic rise. As a consequence, in the CBL case the surface sensible heat flux, which plays the major role in the development of updrafts and downdrafts is assumed to be the leading parameter.

Therefore, for neutral conditions, in which the rise is limited by the mechanical ambient turbulence, Briggs proposed the iterative formula

$$\Delta h = 1.2 \left(\frac{F_b}{u_0 u_*^2} \right)^{3/5} (z_s + \Delta h)^{2/5} \tag{39}$$

where u_* is the friction velocity. For unstable conditions, in which the termination of the rise is due to the breakup by plume-scale, Briggs (1975, 1984) proposed

$$\Delta h = 3.0 \left(\frac{F_b}{u_0} \right)^{3/5} H^{-2/5} \quad (40)$$

where H is the upward surface sensible heat flux times $g/(c_p \rho_a \vartheta)$. This equation may be also written as

$$\Delta h = 3.0 F_*^{3/5} h \quad (41)$$

where

$$F_* = F_b / (u_0 w_*^2 h) \quad (42)$$

is the dimensionless buoyancy flux, w_* is the convective velocity scale and h is the mixing height. Notice that Hurley and Physick (1993) derived an expression similar to (41), but with the constant equal to 2 instead of 3. Examining the Willis and Deardorff (1983) CBL water tank experiment, they also found that a value of 2 gave better agreement than the value 3. Best et al. (1990, reference from Hurley and Physick, 1993), found 2.3 by fitting field ground level concentration (g.l.c.) data. It is difficult to decide which constant value is to be preferred due to the lack of direct measurements of the final height in this conditions and to the large scatter in the indirect methods (g.l.c.).

2.3.2 Stable Case

Let us consider Equation (32). This equation has its maximum, Δh_{\max} , for $x_f = \pi u_0 / N'$. Considering that for most hot plumes the effect of the initial momentum can be neglected, and that the leveling off or equilibrium height is observed to occur at about $5/6 \Delta h_{\max}$, the following expression for the final height in stable and windy conditions ($u_0 > 1 \text{ ms}^{-1}$) is obtained

$$\Delta h = 2.8 (F_b / u_0 s)^{1/3} \quad (43)$$

However, Briggs (1975; 1984) on the analysis of many field and laboratory observations, found that a slightly different numerical coefficient, 2.6, yielded the best fit to the observation. Consequently, Briggs recommended that the most accurate estimate of the plume final height in stable conditions is given by

$$\Delta h = 2.6 (F_b / u_0 s)^{1/3} \quad (44)$$

For stable and calm conditions ($u_0 < 1 \text{ ms}^{-1}$), in which a plume rises nearly vertically, Briggs (1969), on the basis of previous work of Morton et al. (1956) and the examination of many field observations, proposed

$$\Delta h = 5.0 F_b^{1/4} s^{-3/8} \quad (45)$$

Subsequently, Briggs (1984) proposed for the same conditions

$$\Delta h = 5.3 F_b^{1/4} s^{-3/8} - 6r_s \quad (46)$$

2.4 Formulae for Jet Plumes in the Transitional Phase

Also these formulae, as the ones for buoyant plumes, have a semi-empirical origin.

The formulae for the transitional phase of jet rise, in neutral/unstable or stable conditions, were already introduced, namely Equations (24) and (33), in which the entrainment parameter β was defined by Equation (26).

2.5 Formulae for the Final height of Jet Plumes

For neutral conditions Briggs (1969) previously suggested

$$\Delta h = \frac{3v_s d_s}{u_0} \quad (47)$$

where d_s is the internal diameter of the stack outlet, and later (1975, 1984) suggested

$$\Delta h = \frac{0.9}{\beta} \left(\frac{F_m}{u_0 u_*} \right)^{1/2} \quad (48)$$

For unstable conditions Briggs (1975) suggested

$$\Delta h = 2.3 \left(\frac{F_m}{u_0} \right)^{3/7} H^{-1/7} \quad (49)$$

and, subsequently, Briggs (1984) suggested for the same conditions

$$\Delta h = \frac{1.3}{\beta^{6/7}} \left(\frac{F_m}{u_0 w_*} \right)^{3/7} h^{1/7} \quad (50)$$

Also in Equations (48) and (50) β is defined by Equation (26).

Briggs (1969, 1975) suggested for stable and windy conditions ($u_0 > 1 \text{ ms}^{-1}$)

$$\Delta h = 1.5 (F_m u_0^{-1} s^{-1/2})^{1/3} \quad (51)$$

This is obtained from considering that Equation (33) attains its maximum Δh_{\max} for $x_f = \pi u_0 / (2N')$ and that the equilibrium height occurs at about $2/3 \Delta h_{\max}$.

For stable and calm conditions ($u_0 < 1 \text{ ms}^{-1}$), Briggs (1969, 1975) suggested, on the basis of a few observations, the following relationship

$$\Delta h = 4.0 (F_m s^{-1})^{1/4} \quad (52)$$

Taking into account that observations on the rise of jet plumes in stable conditions are very sparse, Briggs suggests considering the above formulae as tentative.

2.6 Buoyant Plumes or Jet Plumes

While for jets plumes or for highly buoyant plumes it is clear which type of plume rise formulae is to be used in practical dispersion applications, for cases in which $\Delta T_0 = T_{s0} - T_{a0}$ (where ΔT_0 is the temperature difference between emission and ambient air at the stack mouth) is greater than zero but not very high, whether the plume rise is dominated by momentum or by buoyancy must be determined. Two methods able to solve this problems are presented. The first one - see, for instance, AERMOD (U.S. EPA, 1998) - consists in using Equation (23) or (32) for the transitional phase in neutral/unstable or stable case, respectively. These cited equations include both contributions. The final plume height is calculated according to the methods resumed in Section 2.3.

The second one is based on the U.S. EPA models PTPLU (Pierce et al., 1982), SCREEN3 (U.S. EPA, 1995a), and ISC3 model (U.S. EPA, 1995b). In this method a critical temperature difference ΔT_c is defined. If $\Delta T_0 > \Delta T_c$ the plume has to be treated as buoyant; otherwise the plume has to be treated as a jet. ΔT_c is defined as:

- in stable atmosphere

$$\Delta T_c = 0.19 v_{s0} T_{a0} s^{1/2} g^{-1} \quad (53)$$

- in neutral or unstable atmosphere

$$\Delta T_c = \begin{cases} 0.29 v_{s0}^{1/3} T_{s0} d_s^{-2/3} g^{-1} & \text{if } F_b < 55 m^4 s^{-3} \\ 0.056 v_{s0}^{2/3} T_{s0} d_s^{-1/3} g^{-1} & \text{if } F_b \geq 55 m^4 s^{-3} \end{cases} \quad (54)$$

The units of the two dimensional coefficients in Equation (54) are $m^{4/3} s^{-5/3}$ and $m^{2/3} s^{-4/3}$ respectively. Equation (53) is obtained by equating Equations (44) and (51) and solving for ΔT_o . Similarly, Equations (54) are obtained by inserting Equations (37) into (27) and then equating Equation (47).

2.7 Moore's and Netteterville's Models for the Plume Rise of Buoyant Plumes

The formulae for the buoyant plume rise presented in the previous part of this Section form a complete and validated set of equations, widely used by the modeler community. However we briefly introduce also the Moore and Netteterville models because we think that these two models are important for scientific and/or historical reason. As such, they may be of interest for the reader. Moreover, Netteterville's parameterization of ambient turbulence is used later in the chapter (see Sections 3.2 and 4.4).

2.7.1 The Moore Model

Briggs models are, as we have seen above, derived by assuming that a plume is continuous, accounts for the crosswind and vertical spread and disregards the along wind spread and its diameter increases as it rises and travels downwind. For this reason this kind of approach is called “two-dimensional”. Instead Moore, (1974) points out that the dilution of an hot smoke plume is a three-dimensional phenomenon, because the plume, rather than rising as a continuous cone, breaks up into a discrete series of puffs which tend to recombine and merge into each other as the plume travels downwind, so that the number of puffs per unit length of plume decreases with downwind distance. The problem becomes three-dimensional because the along wind spread must be considered as well. One of the main interest in the Moore's model is in the recognition that observations of stack plumes sometimes reveal some three-dimensional features (Ooms, 1972) either due to its dynamic (formation of two counter-rotating vortices as it leaves the stack which may cause the plume bifurcation, split of the plume in lumps) or to terrain characteristics in case of low emissions.

Moore model is a generalized one that can be applied in a large variety of meteorological situations both during the transitional and final stage of rise without switching to various different expressions.

The basic difference between the two-dimensional and the three-dimensional approach is that in the former the plume rise is proportional to $F_b^{1/3}$, that is to $Q_h^{1/3}$, see Equations (9) and (27), whereas in the latter it results proportional to $Q_h^{1/4}$, namely

$$\Delta h(x) = A Q_h^{1/4} x_*^{3/4} u_{1.5}^{-1} \quad (55)$$

where: $u_{1.5}$ is the wind speed at the height $1.5 z_s$; $x_* = x$ for short distances and $x_* = x_T$ for large distances. These two asymptotic values are connected by a smooth curve possessing the correct asymptotic and near field limiting forms:

$$x_* = \frac{x_T x}{\sqrt{x_T^2 + x^2}} \quad (56)$$

and x_T is given by the following expression

$$x_T = \frac{(D_0 + D_1 H^*) u_{1.5}}{\sqrt{(D_0 + D_1 H^*)^2 \frac{\Delta \mathcal{G}^*}{D_2^2} + u_{1.5}^2}} \quad (57)$$

A , D_0 and D_2 are dimensional constant, whereas D_1 is dimensionless. Their values were estimated by Moore to be: $A = 2.4 MW^{-1/4} m^{5/4} s^{-1}$ for $z_s > 120$ m while, for $z_s < 120$ m, $A = 2.4$ for very stable conditions (i.e. for $\frac{\partial \mathcal{G} / \partial z}{u_{1.5}^2} > 2.5 K s^2 m^{-3}$), otherwise $A = 2.4(0.16 + 0.007 z_s)$; $D_0 = 1920$ m, $D_1 = 19.2$, and $D_2 = 120$ ms. H^* and $\Delta \mathcal{G}^*$ are parameters related, respectively, to the following two assumptions: 1) the atmospheric turbulence effects on the first steps of the plume rise evolution are dependent on the height for low sources ($z_s < 120$ m), but independent of the height for high sources ($z_s > 120$ m); this assumption is parameterized setting: $H^* = z_s$ if $z_s < 120$ m, $H^* = 120$ m if $z_s > 120$ m; 2) the atmosphere is assumed to be stably stratified, even in convective conditions; since $\Delta \mathcal{G}_{100}$ is the variation in potential temperature per each 100 m of height increase, this assumption is parameterized setting: $\Delta \mathcal{G}^* = 0.08$ K if $\Delta \mathcal{G}_{100} < 0.08$ K, $\Delta \mathcal{G}^* = \Delta \mathcal{G}_{100}$ if $\Delta \mathcal{G}_{100} > 0.08$ K.

Moore claimed that his model is applicable when the difference in temperature between effluent and air ranges between 80 and 150 K, the effluent emission velocity v_{s0} does not considerably overtake the value of $30 m s^{-1}$ and in the following conditions: $x > 400$ m; $30m < z_s < 230m$; $10 MW < Q_h < 150 MW$.

An explicit expression of the final height is obtained by inserting $x_* = x_T / \sqrt{2}$ in Equation (55).

2.7.2 The Netterville Model

Netterville (1990) gave a detailed description of the entrainment process, which he called the “two-way model”. This is based on an understanding of several quantitative aspects of turbulent mixing within free shear layers and on the availability of more detailed ambient turbulence data from remote sensors, like SODARS and RASS.

The two-way entrainment model predicts that the turbulent atmosphere must entrain plume material just as the plume must entrain the atmosphere. Figure 5 (from Netterville, 1990) illustrates what is meant with two-way entrainment. It shows a turbulent plume of radius R that rises at relative speed W through an atmosphere containing turbulent eddies of length scale r_a and relative root-mean-square velocity v'_a . The plume cross-section is assumed to have a ‘spongy’ internal structure caused by atmospheric turbulence eddies, in transit through the plume, that form transient holes in the surrounding matrix of turbulent plume material. Similarly, also the ambient air eddies become spongy due to penetration by the plume’s internal turbulent eddies.

The entrainment process is split into three processes: direct entrainment (a process by which plume eddies, due the self-generated turbulence, capture ambient air masses), indirect entrainment (ambient air eddies in the plume that are in turn penetrated by eddies of the internal plume) and extrainment (transfer of plume mass from the plume itself to ambient air due to the turbulent eddies that enter the plume and carry off plume mass).

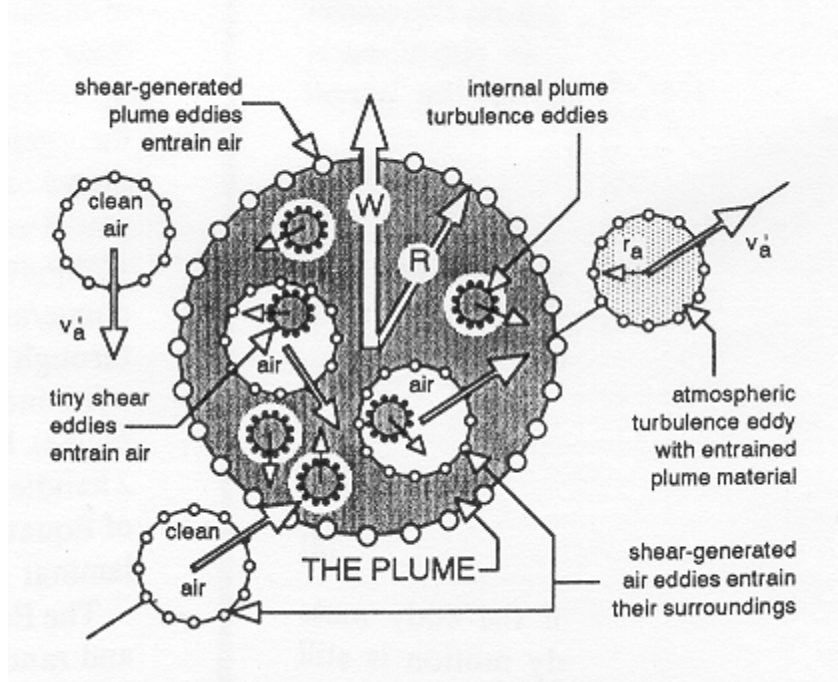


Figure 5. Schematic of plume/atmospheric interaction (from Nettetville, 1990). [Reprinted with permission from Elsevier Science]

Netterville plume rise model is based on this description of entrainment process, and on the solution of the mass, momentum and energy conservation equations. The same simplifying assumptions on the plume shape and atmospheric conditions as in the Briggs models are made, thus obtaining the following scheme.

In stable atmosphere ($N^2 > 0$)

$$\Delta h(\tau) = \left\{ \frac{3}{\beta^2 u (f_b^2 + s)} \left[F_e + f_b M_e + \left\{ N M_e \left[\sin\left(\frac{N}{f_b} \tau\right) - \frac{f_b}{N} \cos\left(\frac{N}{f_b} \tau\right) \right] + \right. \right. \right. \right. \quad (58)$$

$$\left. \left. \left. - F_e \left[\cos\left(\frac{N}{f_b} \tau\right) + \frac{f_b}{N} \sin\left(\frac{N}{f_b} \tau\right) \right] \right\} \exp(-\tau) + \left(\frac{R_e}{\beta}\right)^3 \right\}^{1/3} - \frac{R_e}{\beta}$$

where $\tau = t f_b$ is the dimensionless plume travel time given by the product of the plume travel time, t , and the atmospheric turbulence buffet frequency, f_b . This last is defined as

$$f_b = 2\beta\sigma_u / (u\tau_E) \quad (59)$$

in which τ_E is the Eulerian integral time scale of atmospheric turbulence and σ_u is the standard deviation of longitudinal horizontal wind.

In neutral atmosphere ($N^2 = 0$)

$$\Delta h(\tau) = \left\{ \frac{3}{\beta^2 f_b^2 u} [F_e + f_b M_e - \{f_b M_e + F_e(\tau + 1)\} \exp(-\tau)] + \left(\frac{R_e}{\beta} \right)^3 \right\}^{1/3} - \frac{R_e}{\beta} \quad (60)$$

In unstable atmosphere ($N^2 < 0$, $N \equiv +\sqrt{|N^2|}$)

$$\Delta h(\tau) = \left\{ \frac{3}{\beta^2 u (f_b^2 + s)} \left[F_e + f_b M_e - \left\{ N F_m \left[\sinh\left(\frac{N}{f_b} \tau\right) - \frac{f_b}{N} \cosh\left(\frac{N}{f_b} \tau\right) \right] + F_e \left[\cosh\left(\frac{N}{f_b} \tau\right) + \frac{f_b}{N} \sinh\left(\frac{N}{f_b} \tau\right) \right] \right\} \exp(-\tau) \right] + \left(\frac{R_e}{\beta} \right)^3 \right\}^{1/3} - \frac{R_e}{\beta} \quad (61)$$

As $t \rightarrow \infty$, all three solutions asymptotically approach the same functional form for final rise

$$\Delta h = \left[\left(\frac{3}{\beta^2 u} \right) \frac{F_e + f_b M_e}{(f_b^2 + s)} + \left(\frac{R_e}{\beta} \right)^3 \right]^{1/3} - \frac{R_e}{\beta} \quad (62)$$

In the above equations, F_e , M_e , and R_e are initial values of plume buoyancy, momentum and radius at the end of bending-over phase. Djurfors (1983) has shown that they are given by

$$R_e \cong r_s \left(2 \frac{v_{s0}}{u} \frac{T_a}{T_{s0}} \right)^{1/2} \quad (63)$$

$$M_e = F_m \left(\frac{v_{s0}}{u} \frac{T_a}{T_{s0}} \right) \quad (64)$$

$$F_e = F_b \quad (65)$$

For stable conditions ($s > 0$) the final rise is always finite. For neutral conditions ($s = 0$) the final rise is finite only if the atmosphere is turbulent ($f_b > 0$). For unstable conditions ($s < 0$) the final rise is finite or infinite depending on the sign

of $(f_b^2 + s)$, i.e. on whether thermal instability or atmospheric turbulence dominates plume motion.

The Netterville plume rise model is consistent with the ‘decay constant’ approach of Djurfors (1977), which recognized that the mathematical form of leveling-off behavior was one in which the vertical distance between the plume centerline and its final height would decrease exponentially with time.

The validation of this model is based on one data set of LIDAR measurements.

3 Advanced Plume Rise Models

3.1 Introduction

The semi-empirical formulations presented in the previous section have shown, on several occasions, a great degree of uncertainty. This is partly due to the simplifications introduced in such formulations. Advanced methods, based on the numerical integration of a set of differential equations expressing the conservation equations and on revised entrainment assumptions, have been proposed. They account explicitly sufficient transport mechanisms to be of general use, particularly in the cases that are too complicated to be modeled by simple analytical models. They provide, at least in principle, a better physical representation of the two basic phenomena related to plume rise: the grow of the plume centerline and the entrainment of ambient air into the plume and its consequent horizontal and vertical spreading. They also allow dealing with complex atmospheric conditions. However, they require more computational resources and more detailed input data.

Among the advanced models we may distinguish: integral models (they use spatially integrated forms of the fluid motion equations), differential models (they integrate on Eulerian grids Reynolds-averaged flow conservation equations) and large eddy simulation (LES) models. In all these models, the system of equations must be closed by a proper number of assumptions and closure hypothesis. Essentially they are empirical, but are based on physical reasoning and/or observations.

The first two categories, that are not so computationally costly (particularly for nowadays computers) are not only of scientific interest, but may also be useful tools in air pollution modeling, since they are able to deal with any kind of stack plume (jet, dense or buoyant plume) and complex atmospheric structures.

We would like to stress the importance of initialization in numerically solving the plume rise equations. Stack geometries and plume exit temperatures and

velocities may vary over wide ranges. Consequently, large errors in the plume rise estimations can be made if the initial conditions are not correctly formulated.

Many advanced models have been developed. It is hopeless to review them all, therefore only some of them are briefly presented below. We would also mention that a number of the most recent advanced plume rise models are based on Lagrangian particle techniques. These last models for plume rise are discussed in Section 4.

3.2 Integral Models

The models developed by Schatzmann (1979), Ooms and Mahieu (1981), Glendening et al. (1984), Chiang and Sill (1985), Gangoiti et al. (1997) and Janicke and Janicke (2001) are considered here. They give an overview of these kind of models developed during the last 20 years. There are some characteristics common to all these models. Since the trajectory of a plume (jet, dense or buoyant) in windy conditions is not a straight line, they generally use the natural coordinate (or curvilinear) system that moves and rotates as it follows the plume centerline trajectory, rather than the Cartesian coordinate system. They do not use the common Boussinesq approximation thus allowing the treatment of plumes with greatly different density from that of ambient air. The plume is assumed to exhibit local similarity, i.e., the shapes of the radial profiles of excess velocity, temperature and concentration do not change downstream. The profiles of plume velocity, temperature, and density are assumed to be of Gaussian (Schatzmann, 1979; Ooms and Mahieu, 1981; Chiang and Sill, 1985), “top hat” (Glendening et al., 1984) or exponential (Gangoiti et al., 1997) shape for mathematical simplicity. Models do not use different parameterizations for each phase (buoyancy dominate, intermediate and turbulence dominated) of the plume trajectory. Additional assumptions are steady state conditions for both plume and environment, zero environmental vertical velocity and absence of stack downwash effects (see Section 5.1), which is appropriate for plumes with large buoyancy, and exit velocity. In most models it is assumed that the mean excess and turbulent quantities plume are axisymmetric and, consequently, that the three-dimensionality of the plume motion can be ignored. Although it is recognized that two counter rotating vortices are formed at the stack mouth exit and that the plume may break into distinct puffs (that may also merge downwind), these effects are neglected since they are assumed to be incorporated in some way in the entrainment formulations. All the models were tested against laboratory and field data.

Basically, the main difference among the various models lies in the modeling of entrainment, i.e. the rate of mixing of ambient air into the plume. Other characteristics that make different the models are the inclusion in some of them of pollutant dispersion besides the path and spread of the plume or the capability of some models to treat arbitrary atmospheric structures, whereas the others should divide the atmosphere in a certain number of layers with different constant

atmospheric properties. Only a few models accounts for the plume rise modifications due to the condensation of plume water vapor.

The plume rise model of Schatzmann (1979) assumes that the wind velocity is constant in value and direction and that the atmosphere is stratified with a constant density gradient. It includes seven equations for the following seven unknowns: centerline excess velocity, temperature and concentration, centerline density defect, jet radius, angle of inclination and local rate of entrainment. A rather complex entrainment function is used which is based on the local densimetric Froude number, the plume radius, the macroscale of the energy-containing eddies, angle of the plume trajectory, free-stream velocity, centerline excess velocity and five empirical constant. The tests of the model performances against many observations including jets, buoyant and dense plumes, gave reasonable agreement. This model, however, fails to account for the inertia of “effective mass” outside the plume, seems to contain an unrealistic drag term, and shows problems in the mass conservation equation (Briggs, personal communication to Zannetti, from Zannetti, 1990).

Ooms and Mahieu (1981) proposed a model able to calculate both the path of the plume in a windy atmosphere and the ground level concentration. Such model is a development of the method for the calculation of the plume path, therefore of the plume rise as well, presented in Ooms (1972) and Ooms et al. (1974). The model contains eight equations: two equations relate the Cartesian coordinate to the curvilinear coordinates; six equations describe the entrainment, conservation of mass (pollutant), momentum in the x -direction and in the z -direction and energy; the last equation expresses the assumed atmospheric linear stratification. The description of the entrainment and the drag force, is based on the theoretical work of Abraham (1970) and Loh-Nien Fan (1967). The rate of entrainment of air into the plume due to atmospheric turbulence depends on the eddy energy dissipation ε . For neutral conditions a relation for ε due to Briggs (1969) is used and for the other stability conditions data from Kaimal et al. (1976) are considered. Cross-sections of the plume are assumed to be ellipses. Moreover, this model takes into account the first part of the plume, known as the zone of flow establishment, and also the turbulence and stratification of the atmosphere so that the influence of the different stability on the plume path can, in principle, be studied. The simulated ground level concentrations were compared with those obtained by a classical Gaussian plume model (using Briggs formulae – see Section 2 – for plume rise and Singer-Smith, 1966, sigma curves). The agreement was good in neutral and unstable conditions, while large differences were found in stable conditions.

The Ooms and Mahieu model is used in the ADMS model (e.g., Carruthers et al., 1999).

The plume rise model proposed by Glendening et al. (1984) is able to treat arbitrary complex atmospheric structures also when there are large vertical variations in atmospheric stability or wind velocity (conditions particularly common for near shoreline power plants). The model consists of a set of eight

ordinary differential equations (conservation of mass, energy, horizontal x and y momentum, vertical momentum, plus three relationships between curvilinear and Cartesian coordinates) and three equations (gas equation and the definitions of virtual temperature and virtual potential temperature). Entrainment is parameterized according to Hewett et al. (1971). Profiles of temperature and wind are needed to run the model. The accuracy of the model prediction, verified against field observations, were found satisfactory and superior to those from a standard plume rise formula - Equation (44).

The Glendening et al. plume rise model, as modified by Hurley and Manins (1995), is used in the models LADM (e.g., Physick, 1996) and TAPM (e.g., Hurley et al., 2001; see also Section 4.3.2).

The model developed by Chiang and Sill (1985) is applicable to all stability conditions but only to simple atmospheric structures (that can be expressed by analytical relationships). The governing equations express the conservation of mass, momentum in the direction oriented along the plume path and to the normal to it, thermal energy and tracer concentration. Two relationships between natural and Cartesian coordinates are also used and the system is closed with an entrainment model. Basically, the authors' interest was to develop new entrainment models. Thus they proposed different entrainment models for different turbulent mixing mechanisms (such as shear, buoyancy, or ambient turbulence). Then, these authors proposed that, when the turbulent mixing is due to the contemporary action of different mechanisms, the total entrainment rate is the linear combination of the various rates derived individually from growth rate models, i.e. a superposition approach.

The agreement between predicted plume trajectories, velocities and dilution rates and the observed ones was satisfactory.

Gangoiti et al. (1997) presented a three-dimensional plume rise model for tall stacks capable of dealing with complex atmospheric profiles. Ambient turbulence is assumed to be homogeneous and isotropic, the plume is considered to exit from the stack as a mixture of dry combustion gas, water vapor and liquid water. Dry air and ambient water vapor, but not liquid water, are then entrained during the plume motion. Thus the model allows for condensation and/or re-evaporation within the plume. Condensation in a moist atmosphere increases buoyancy through release of latent heat while evaporation of droplets absorbs latent heat from the plume, which consequently loses buoyancy. The classical parameterization for entrainment of air into plume due to the self-generated turbulence has been completed with entrainment-extrainment processes in turbulent winds. This is based on the model of turbulent mass transfer between plume and environment proposed by Netterville (1990, see Section 2.7). A set of equations describing in great details the balance of mass, momentum and energy in the plume constitutes the model. This can be used also to predict plume penetration into elevated inversion layers but can provide only qualitative

estimates of the fraction of plume material that penetrates into them (see Section 5.2).

These authors compared the performance of their numerical model with a set of simpler models widely used in regulatory applications for plume rise calculation. Plume condensation has been found to be a major cause of underestimation in those simpler models, while wind shear causes systematic overestimation in stably stratified atmospheres. The assumed power law similarity profiles for the plume temperature and velocity gave better results in light winds ($< 1.5 \text{ ms}^{-1}$) than the "top hat" profiles.

Also the PLURIS model (Janicke and Janicke, 2001) can be applied to situations with arbitrary three-dimensional wind fields and to both dry and moist plumes. Arbitrary directions of the source exit can be considered. Unlike models based on a similarity profile description, it is not necessary to make assumptions about the structure or symmetry of the plume cross-section or about the zone of flow establishment near the source exit. The similarity profiles enter into the model only via the definition of the liquid water content and affect mainly the prediction of the visible plume boundary. In the absence of condensation, the model is independent of any similarity profile assumptions. The model consists of 8 differential equations for mass, x , y , z -momentum, enthalpy, velocity fluctuations, total water content, and concentration. In addition, there are three differential equations for the three Cartesian coordinates of the plume axis. In the special case of a bent-over plume the model can be solved analytically. The model was validated by a direct comparison with various plume rise measurements obtained by means of water tank, wind tunnel, and field experiments. The model is presently implemented and used in combination with the Lagrangian dispersion model LASAT (Janicke, 1983).

3.3 Differential Models

Golay (1982) proposed a differential entrainment model. It is able to simulate bent-over plumes in complex vertical atmospheric structures by numerically integrating the conservation equations of mass, momentum, heat, water vapor, liquid water, and the two equations for the turbulent kinetic energy and eddy viscosity in a form presented by Stuhmiller (1974). It uses a mixed Eulerian-Lagrangian reference system. A two-dimensional Eulerian computational mesh translates downwind at a plume mass averaged wind speed.

Data from field study of airborne SO_2 plume and for ground level SO_2 concentration were used to test the model performances. The model simulations resulted in better agreement with observations than those obtained by standard analytical formulations.

The major limitation of Golay's approach is the detailed meteorological information that is required; i.e., the vertical profiles of wind speed, virtual

potential temperature, relative humidity, turbulent kinetic energy, and turbulent viscosity.

3.4 LES Models

Probably the most promising technique for the simulation of buoyant plumes in unstable conditions, at least from a theoretical viewpoint, is the Large Eddy Simulation (LES). These model simulations allow studying in great details the contribution to the plume motion caused by convective turbulence and that caused by plume buoyancy. Nieuwstadt and de Valk (1987) applied such a model to a line source, in which buoyancy was added by increasing the temperature of the source with respect to the ambient temperature. Then they solved the equation for the concentration conservation simultaneously with the other LES equations. Further work in this direction was performed by van Haren and Nieuwstadt (1989), who obtained reasonable agreement between the output of their LES, which however considered only a modest plume buoyancy, and the field experiments of Carras and Williams (1984). It was found that the fraction of the plume motion caused by plume buoyancy does not seem to obey the “two-thirds” law. Plume buoyancy strongly affects the contribution of ambient turbulence to the mean plume height. Nieuwstadt (1992a) showed that the two contributions (internal buoyancy and ambient turbulence) cannot simply be calculated independently but that they interact. Thus ambient convection influences the plume rise (large eddies modify the entrainment) and vice versa (the interaction ambient turbulence – plume motion depends on plume rise which transports the plume to different PBL heights).

Zhang and Ghoniem (1993, 1994 a,b) developed a computational model based on the Lagrangian interpretation of the dynamics of buoyancy-driven flows that uses the vortex element and transport element methods to solve the governing equations. The solution they have constructed causes the model to be considered as a LES model, since the governing equations describe the effects on the plume motions of the large scales and the small scales are modeled phenomenologically (Zhang and Ghoniem, 1993). They faced problems of increasing complexity in three subsequent papers: firstly they considered a neutral atmosphere with small scale turbulence in a horizontal uniform wind (Zhang and Ghoniem, 1993), then considered a linearly stratified atmosphere (Zhang and Ghoniem, 1994 a) and, finally, a linearly stratified atmosphere capped by an inversion layer (Zhang and Ghoniem, 1994 b). The following results may be important not only from a theoretical point of view but also for their practical implications. In neutral atmosphere it was found that the plume cross-section is kidney-shaped and that the initial shape of the cross-section (that can be circular or elliptical) has some effects on the plume trajectory. In the case of a circular plume the “two-third” law is closely followed. The entrainment is dominated by large scale engulfment which is inhomogeneous and non-isotropic. In the second case, linearly stratified atmosphere, it was found that the entrainment constant β (estimated equal to 0.49) mainly affects the equilibrium height, whereas the added mass constant k_v

(see Section 2.2.2 – estimated equal to 0.7) influences the downwind distance where this equilibrium height is reached. In the third case, the interaction of the plume with an inversion layer (i.e.: partial or total or null plume penetration - see also Section 5.2) has been studied. In particular it was found that when the plume bumps against an inversion layer, internal gravity waves are generated along the layer, radiating the energy of the plume and reducing its penetration capacity.

4 Particle Models for Plume Rise

4.1 Introduction

In Eulerian and Gaussian models, the final plume height Δh is generally computed by means of simple analytical expressions (like those presented in Section 2 of this chapter) and inserted in the model as an input parameter. On the contrary the inclusion of plume rise in Lagrangian Stochastic Models (LSM, see also Chapter 11) can be done dynamically, i.e. each particle, at each time step, can be acted upon by local wind speed and direction, ambient stability and turbulence (both the self-generated and ambient ones). Therefore it is possible to obtain a degree of resolution and accuracy not obtainable with other simulation techniques. Furthermore, the interaction of a plume with a capping inversion layer can be simulated in a rather "natural" way. However the correct incorporation of plume rise in LSM is still an open problem, since it is needed to simulate the entrainment phenomenon, that is the exchange processes between the plume particles and the turbulent environment must be described. Since entrainment acts, primarily, at the edge of a plume, the position, velocity and buoyancy of the other particles should be also taken into account.

A completely satisfying approach, based on fundamental particle behavior, is not yet available. Nevertheless many formulations have been proposed in the literature to practically solve the problem, with a different degree of approximation, allowing the plume rise calculation in LSM. They try to achieve a good compromise among computational requirements, physical consistency and reliability of the numerical results. Indeed, most of them proved to give reliable results when compared to laboratory and/or field data. In the following these approaches will be presented. They include: empirical methods; semi-empirical methods, in which the plume rise is computed by numerically integrating, at each time step, the conservation equations - see Equations (2 - 5) - and the plume spread is calculated by the Langevin equation for the vertical velocity; theoretical models, in which an attempt is made of directly simulating the rise of buoyant plumes in a Lagrangian framework.

4.2 Empirical Methods

The first attempt to include plume rise into LSMs, taking into account the vertical variation of wind and stability, was done by Zannetti and Al-Madani (1984). Let

us recall (see Chapter 11) that in LSMs, the vertical particle positions X_z is generally computed, at each time step Δt , as follows

$$X_z(t + \Delta t) = X_z(t) + [U_z(t) + w'(t)]\Delta t \quad (66)$$

where $U_z(t)$ represents the mean vertical wind component (generally equal to zero in flat terrain) and $w'(t)$ refers to the ambient turbulent term (random forcing) which is computed from a stochastic equation for the velocity fluctuation. The idea, is to add an additional vertical velocity accounting for the buoyant rise, w_b , to Equation (66), thus obtaining

$$X_z(t + \Delta t) = X_z(t) + [U_z(t) + w'(t) + w_b]\Delta t \quad (67)$$

They expressed this extra-velocity by time differentiating an empirical analytical plume rise equation for the transitional phase (TVA formula – Strom, 1976). The same plume rise contribution is given to all the particles provided they are at the same height and have the same age. The plume spreads in the vertical as a consequence of the ambient turbulence only. This last appears in the stochastic equation for the vertical velocity. This method can correctly simulate the ensemble averaged plume mean height (provided the used analytical formula is correct), but the vertical spread, particularly in convective conditions, is likely to be underestimated. The authors presented some numerical examples showing how the method works and its ability to give qualitatively reasonable results. However they did not indicate how to compute the time at which the plume rise stops contributing to the vertical particle motion. They also suggested a possible alternative method that could better simulate the vertical spread, but without developing it. It consisted in tagging each particle with a random buoyancy of "suitable intensity".

Cogan (1985) was the first to try to model the entrainment process, even if on an empirical basis. The plume is divided into layers of constant thickness and, within each layer, it is separated into an inner region (containing the particles included within the center of mass \pm one standard deviation) and an outer region. In the inner region the temperature of each particle is computed as a function of its distance from the center of mass, whereas in the outer region the particle temperature is reduced by a preset amount. This last depends on the chosen value of the entrainment constant.

Shimanuki and Nomura (1991) tried to numerically simulate the instantaneous images of chimney plumes under convective conditions. Their technique is based on single Lagrangian particle trajectories, whose velocity fluctuations are spatially correlated. The spatial auto-correlation function is prescribed in a completely empiric way and all the trajectories within a single cell assume the same value of the spatial auto-correlation function. The buoyancy effect is roughly accounted for by assigning a given initial vertical velocity to each

particle. The air stability does not affect directly the particle motion but is taken into consideration in the computation of turbulence scales.

The Zannetti and Al-Madani (1984) suggestion was applied by Anfossi et al. (1993) for buoyant plumes and by Anfossi (2000) for jet plumes. To each *i*-th particle a normally distributed buoyancy flux F_b^i is assigned at the stack exit, fixing the mean value equal to the mean buoyancy flux $\overline{F_b}$ and the standard deviation equal to $\overline{F_b}/3$ (this value, 1/3, was empirically fixed requiring that the plume radius near the source was approximately equal to $0.6\Delta h(z)$). In the case of a jet plume, F_m^i , $\overline{F_m}$ and $\overline{F_m}/3$ are used. Instead of computing w_b by means of an empirical analytical plume rise equation for the transitional phase only, they assumed that the plume centerline grows according to a plume rise formula describing both the transitional and final phases and different stability conditions. Thus, a simple algebraic expression giving a smooth curve and possessing the correct asymptotic and near field limiting forms was used. This interpolation curve was built following the Moore's suggestion - see Equation (56). For buoyant plumes, the interpolation curve has the following expression (Anfossi, 1985)

$$\Delta h(t) = 2.6 \left(\overline{F_b} t^2 / U_a \right)^{1/3} (t^2 s + 4.3)^{-1/3} \quad (68)$$

and was obtained considering the “two-thirds” law - Equation (27) - for the transitional phase both in neutral/unstable and stable conditions (Arya, 1999) and Equations (44) for the final rise in stable conditions. For neutral/unstable conditions ($s = 0$) the plume final height is fixed according to Equation (38). The low wind speed conditions are dealt with inserting a minimum wind speed (0.3 ms^{-1}). w_b is computed as follows

$$w_b = \frac{\Delta z}{\Delta t} = \frac{[\Delta h(U_a, s, t + \Delta t) - \Delta h(U_a, s, t)]}{\Delta t} \quad (69)$$

The model simulations were validated against DIAL measurements of a Thermal Power Plant plume in complex terrain (Anfossi et al., 1993). Predicted plume centerline height and horizontal and vertical plume width satisfactorily compared to the observed ones.

This method is used in the 3-D Lagrangian Stochastic Model SPRAY (Tinarelli et al., 2000; Finardi et al., 2001), which is also used (in some complex terrain cases) for regulatory purposes in Italy.

Equation (68) was also used by Graziani et al. (1997) for their LSM simulation of the dispersion of the volcanic emission from Vulcano Island.

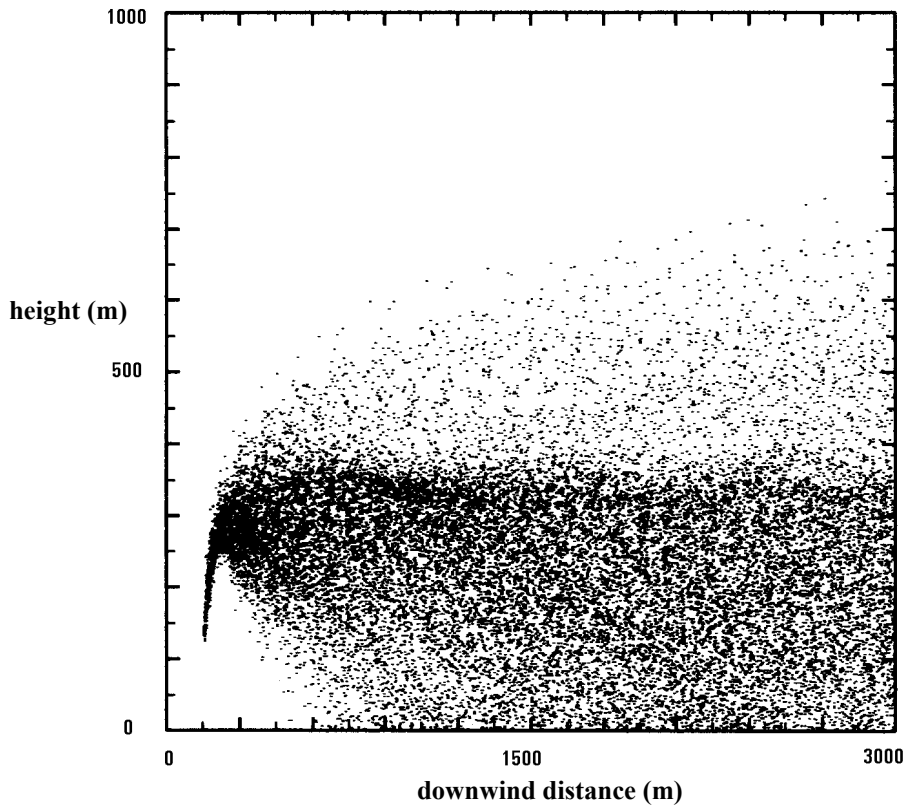


Figure 6. See the text (adapted from Anfossi et al., 1993). [Reprinted with permission from Elsevier Science].

Figure 6 shows a simulation result of this approach in non-homogeneous vertical meteorological conditions, in which simpler analytical approaches cannot be used. It refers to a typical fog situation in the Po Valley (Northern Italy): the fog layer extends from ground level to 250 m, an inversion layer with a large temperature increase ($8\text{ }^{\circ}\text{C}$) lies between 250 and 400 m and the superior layer is nearly isothermal. Nearly calm conditions prevail ($u_0 \cong 1\text{ m s}^{-1}$). Each point in Figure 6 represents a model particle position. One can see that the rise of the plume is stopped by the inversion layer, that the pollutant reaches the ground level very close to the stack (fumigation) and that a partial inversion penetration occurs.

The case of jet plume is similarly treated. The starting points are the Briggs' formulae for jet plumes, Equations (24), (48), (51), and (52). Equation (24) works in the transitional phase, where the other equations are valid for the final stage of rise both in neutral and stable windy or calm conditions. In this case, Equation (68) becomes:

- for neutral conditions

$$\Delta h(x) = d_1 F_m^{1/3} u_0^{-2/3} t^{1/3} \left[\left(\frac{d_1}{d_2} \right)^6 \frac{U_a^4 t^2}{F_m} + 1 \right]^{-1/6} \quad (70)$$

were: $d_1 = 2.3$ and $d_2 = \frac{0.9}{u_*^{1/2} \left(0.4 + 1.2 \frac{U_a}{v_s} \right)}$;

- for stable and windy conditions ($u > 1 \text{ m s}^{-1}$)

$$\Delta h(x) = d_1 F_m^{1/3} U_a^{-2/3} t^{1/3} \left[\left(\frac{d_1}{d_3} \right)^6 s^2 t^2 + 1 \right]^{-1/6} \quad (71)$$

were: $d_3 = 1.5$;

- for stable and calm conditions ($u < 1 \text{ m s}^{-1}$)

$$\Delta h(x) = d_1 F_m^{1/3} U_a^{-2/3} t^{1/3} \left[\left(\frac{d_1}{d_4} \right)^6 \frac{F_m^{1/2} s^{3/2} t^2}{U_a^2} + 1 \right]^{-1/6} \quad (72)$$

were: $d_4 = 4$.

The vertical velocity, w_m , is computed as in Equation (69) and the plume rise calculation is stopped when the difference between $\Delta h(x)$ and the corresponding asymptotic final value is less than a chosen small value.

Also Souto et al. (2001) estimated the rise of buoyant plumes according to Equation (67). The extra velocity due to the buoyancy effects, w_b , was estimated as follows

$$w_b = \frac{1.35 F^{1/3} x^{0.58}}{\Delta t u} \quad (73)$$

in unstable conditions and

$$w_b = \frac{2.04}{\Delta t} \left[\frac{0.86 F (1 - \cos(Nx/U_a))}{N^2 U_a} + r_s^3 \right]^{1/3} \quad (74)$$

in stable conditions. The numerical coefficients of these equations and the x exponent in Equation (73) were obtained by best fit of field observations. Equation (74) was proposed by Zhang and Ghoniem (1994a). This plume rise

calculation was inserted in two operational models, a LSM and an adaptive puff model.

4.3 Semi-Empirical Methods

Some interesting methods for incorporating buoyancy effects in LSM, were proposed by Luhar and Britter (1992), Hurley and Physick (1993), Hurley (1999, 2000) - these two methods are inserted and operative in the CSIRO models LADM and TAPM - and Weil (1994). Instead of assuming valid an analytical formula (or an interpolation formula), these methods compute the mean plume rise by directly solving the energy, mass and momentum conservation equations. This procedure is time consuming. However, also the Langevin equation, computing the velocity fluctuations, is already numerically solved. Therefore the increase in calculating time, with present days computer technology, is likely not to be a real problem. Different schemes are used to compute the plume spread and the interaction of ambient turbulence with the plume.

4.3.1 The Luhar and Britter (1992) Method

The LSM of Luhar and Britter (1992) accounts for the effects of source buoyancy on plume dispersion in the CBL by including the mean plume rise and the additional dispersion due to plume's self-generated turbulence. To incorporate the mean plume rise they added a new acceleration term in the Langevin equation for the vertical velocity component of their previously developed LSM (Luhar and Britter, 1992) for the dispersion of passive plumes in the CBL (consequently, the model is one-dimensional). The new acceleration term was based on the following expression

$$g \frac{(\rho_a - \rho(t))}{\rho_a} = -U_a \frac{dW}{dx} \quad (75)$$

where $\rho(t)$ is the plume density at travel time t ($= x/U_a$). In the model, it was assumed that in the CBL the effects of ambient stability and wind shear on plume dispersion and rise could be neglected since the potential temperature and horizontal wind do not change appreciably with the height. This assumption allowed using the conservation equations in a simplified form, valid in the neutral boundary layer. The solution obtained from these equations for the mean vertical velocity W for three phases of plume development was used in Equation (75). The three phases correspond to the three different entrainment relationships of Slawson and Csanady (1971). During the initial phase, the intermediate phase, and the final phase, plume's self-generated turbulence, inertial sub-range turbulence, and energy containing eddies, respectively, govern plume rise. The expression for W in the initial phase of the rise, for example, is

$$W = \left(\frac{4}{9\beta^2} \right)^{1/3} F_b^{1/3} x^{-1/3} \quad (76)$$

which corresponds to the well-known ‘two-thirds’ behavior of plume rise. Luhar and Britter (1992) emphasized the importance of including the ambient turbulence effects in calculating W through the use of the entrainment relationships of the last two phases. Effects of plume’s initial momentum on plume rise were also included.

To account for the additional dispersion due to the self-generated turbulence, the model assumed that the mass, and hence the computer particles and their velocity and acceleration, have a Gaussian distribution about the plume centerline. Thus the model uses two random numbers drawn from a Gaussian distribution: one for the random component of the acceleration due to the ambient turbulence and the other for the random acceleration due to buoyancy.

The model simulations of crosswind-integrated concentrations from a few laboratory and field studies reported in the literature appeared to be satisfactory.

4.3.2 The CSIRO Methods

Instead of accounting for the effects of buoyancy on plume dispersion simply by introducing an extra term into the random walk equation for displacement, Hurley and Physick (1993) compute the vertical velocity of each particle as the sum of the plume velocity due to the buoyancy and initial momentum effect and a stochastic perturbation due to the combined effects of the self generated and ambient turbulence. However, the problem of simulating the entrainment process is not solved since the classical entrainment assumption - the plume radius grows linearly with height - is imposed in both the deterministic and stochastic parts.

The deterministic vertical velocity is obtained by numerically integrating, at each time step, the basic conservation equations (see Section 2) in which the standard assumptions (Boussinesq approximation, top-hat profile and bent over plume) are made. The stochastic wind components are calculated by the Langevin equations for the velocity (Thomson, 1987; see also Chapter 11), namely

$$du'_i = a dt + \sqrt{C_0 \varepsilon_a} dW \quad (77)$$

where $i = 1, 2, 3$, u'_i are the Lagrangian velocity fluctuations, a depends on the Eulerian probability density function (PDF) of the turbulent velocity and is determined from the Fokker-Planck equation, C_0 is a numerical constant, dW is a random term, normally distributed (mean 0 and variance dt). For the simulation of plume rise in the CBL, the Gaussian form of the PDF is assumed for the two horizontal components, while a skewed distribution, obtained by a linear

combination of three Gaussian functions, is used for the vertical component. These three functions represent the contribution to the turbulence due to the updrafts, downdrafts and plume self-generation, respectively. In the LSM for passive tracers based on the Langevin equation, the coefficients of the Gaussian functions are obtained by equating the zeroth through third moments of the Eulerian ambient PDF $(0, \sigma_{wa}^2, S_{wa}^3)$. In this case, the first three moments of the resulting PDF are equated to $0, \sigma_{wa}^2 + \sigma_{wp}^2, S_{wa}^3$, where σ_{wp}^2 is the velocity variance due to the plume rise effects. The three plume velocity variances are defined, on the basis of the above mentioned classical entrainment assumption, as follows

$$\begin{aligned}\sigma_{up}^2 &= \sigma_{vp}^2 = (\beta w_p)^2 \\ \sigma_{wp}^2 &= (\beta w_p / 2)^2\end{aligned}\tag{78}$$

where w_p is the particle vertical velocity. The form of the PDF of the vertical velocity fluctuations for simulations in stable conditions is assumed to be Gaussian with the variance and the eddy dissipation rates being calculated as the sum of ambient plus plume rise induced components.

Plume rise computation is terminated either when $\varepsilon_p \leq \varepsilon_a$ (convective conditions) or when the buoyancy of a particle becomes less than or equal to zero (stable conditions). The plume penetration of the inversion layer capping the mixing height is simulated letting the plume particles to overcome the mixing height if they do not have yet satisfied the termination condition. When the plume rise calculation is stopped, particles are reflected at the mixing height.

The authors advise of some numerical problems in the first couple of time steps (1 s) after release due, very likely, to the height dependence of $\varepsilon_p (= 1.5 w_p^3 / \Delta h(x))$ on the rise height, which tends to diverge for $\Delta h \propto 0$. The problem was partially solved by imposing, near the stack mouth, $\varepsilon_p \leq \sigma_w^2 / (C_0 \Delta t)$.

Comparisons with CBL water tank dispersion experiments (Willis and Deardorff, 1987), characterized by different values of the dimensionless buoyancy flux F_* - see Equation (42) - were shown. Predicted final plume height Δh and plume entrapment above the CBL were found to be in reasonable agreement with the observed ones, even if a slight overestimation of Δh in three out of four experiments, causing peak entrainment values higher than observed, was found. This could be corrected by changing the value of the entrainment parameter β from 0.6 to 0.7. The overall distribution of concentration compared quite well.

An alternative approach to including plume-rise induced turbulence in a Lagrangian approach, which avoids some of the very-near-source numerical problems above mentioned is contained in the model TAPM (Hurley, 1999, 2000). The equations of conservation of plume volume, buoyancy and momentum flux, G , F_b and F_m , are written in this model - see, for comparison, Equations (2 - 5)

$$\begin{aligned}\frac{dG}{dt} &= 2R\left(\alpha W^2 + \beta U_a W + \gamma u_p E^{1/2}\right) \\ \frac{dF_b}{dt} &= -s \frac{F_m}{u_p} \left(\frac{1}{2.25} U_a + W\right) \\ \frac{dF_m}{dt} &= F_b\end{aligned}\quad (79)$$

where $G = \frac{T_a}{T_s} u_p R^2$, $F_m = GW$, F_b is defined as in Equation (6), $u_p = \sqrt{U_a^2 + W^2}$ is the plume velocity, E is the turbulent kinetic energy, $a = 0.1$, $\beta = 0.6$ and $\gamma = 0.1$ are the vertical plume, bent-over plume and ambient turbulence entrainment constants, respectively. The initial conditions for F_b and F_m are the same as in Equations (16) and (18),

$$G_s = F_m/v_{s0} \quad \text{and} \quad R_s = \sqrt{v_{s0}/\sqrt{u_0^2 + v_{s0}^2}}.$$

Equations (79) are based on the model proposed by Glendening et al. (1984), as simplified by Hurley and Manins (1995). Tests on these equations, performed by the authors, showed that they performed as good as the full original ones and collapsed to the Briggs form for a bent-over Boussinesq plume, and to the Briggs vertical plume model equations for calm conditions.

4.3.3 The Weil (1994) Method

This method was designed to deal with CBL dispersion of weakly to moderately buoyant plumes ($F_* \leq 0.1$). Also in this method, an extra acceleration term is added in the Langevin equation in order to account for plume rise. This is obtained by numerically solving the conservation Equations (2 - 5) in which the entrainment assumption appearing in Equation (2) is modified to account for the ambient and self-generated turbulence. Consequently, Equation (2) becomes

$$\frac{d}{dt}(U_{sc} R^2) = 2\beta R U_{sc} |w_p| + 2\gamma_l R U_{sc} v_e \quad (80)$$

where the identity ($d/dt = U_{sc} d/d_{sc}$) was used, v_e is the entrainment velocity and γ_1 an empirical parameter. The first term on the r.h.s of Equation (80) describes the entrainment due to the plume-generated turbulence, whereas the second term accounts for the ambient turbulence. For a jet plume $v_e = v_a$ where

$$v_a = (2\varepsilon_a R)^{1/3} \quad (81)$$

is the relative velocity of two particles separated by a distance R . Notice that in this approach the radius R is defined as “the region enclosing all of the buoyant fluid”. For a buoyant plume, having assumed $U_{sc} = U_a$, v_e is given by

$$v_e = \frac{v_a}{1 + \gamma_2 F_b / (U_a v_a^2 R)} \quad (82)$$

where γ_2 is another empirical parameter. Defining the dimensionless distance X_* and momentum flux F_{m^*} as

$$X_* = \frac{w_* x}{U_a h} \quad \text{and} \quad F_{m^*} = \frac{F_m}{U_a w_* h^2} \quad (83)$$

Weil (1994) obtained that ambient turbulence becomes effective at a non-dimensional distance $X_a = 1.6 \alpha_v^{3/5} F_{m^*}^{2/5}$ for a buoyant plume and $X_a = 0.6 \alpha_v^{9/7} F_{m^*}^{2/7}$ for a jet, having defined $\alpha_v = v_e / w_p$. Fitting his model to the Willis and Deardorff (1983) observations, this author determined the following values for the unknown parameters: $\gamma_1 = 0.4$, $\gamma_2 = 1$ and $\alpha = 0.49$ or 1.9 for buoyant and jet plumes, respectively. Notice that $\alpha = 0.49$ implies that ambient turbulence starts to dominate when the entrainment velocity is about half the plume velocity ($v_e \approx 0.5 w_p$).

When the plume reaches the temperature inversion height h (capping the CBL) and penetration occurs, the vertical plume velocity becomes zero (actually it oscillates about zero) but some plume segments may be brought into the CBL by negative ambient velocities. The buoyant acceleration, due to the fact that the potential temperature is greater than below h , provides a positive velocity tending to keep the plume aloft and the ambient velocity (calculated by the Langevin equation) varies randomly and therefore may be either positive or negative.

Weil (1994) also found that, despite the differences in the models, the mean fields computed with this model are very similar to those produced by the Luhar and Britter (1992) model.

4.4 Theoretical Models

4.4.1 The Van Dop (1992) Particle Model for Buoyant Plume Rise

A buoyant plume is defined as the volume, which contains a mixture of ambient and originally released, buoyant fluid. The envelope of the plume is the (imaginary) and in a way, arbitrary boundary of this volume. A fraction of the original buoyant fluid separates from the plume and becomes so remote that it is no longer considered to be part of it. On the other hand the volume of the plume expands due to turbulent intrusions of ambient air resulting in an increasing ambient fraction and consequently, a gradual loss of plume temperature and vertical acceleration.

A Lagrangian ‘plume particle’ can now be defined as a small entity, which possesses the mean characteristics (velocity, temperature) of the plume. Stochastic fluctuations, directly related to the turbulent intensity within the plume, determine the rate of growth of the plume width and are superimposed on the mean characteristics. Ultimately, due to the entrainment and extrainment processes, the plume (particle) dynamics must converge to the environmental dynamics. Hence, the equation of motion in the vertical dimension for a buoyant plume particle can be formulated as

$$dW = -\frac{W}{T_p} dt + B dt + \varepsilon_w^{1/2} d\omega_w(t)$$

$$dB = -\frac{B}{T_p} dt - NW^2 + \varepsilon_B^{1/2} d\omega_B(t) \quad (84)$$

$$dX_z = W dt$$

(see Van Dop, 1992). Here, W is the plume particle vertical velocity and B is the plume particle buoyancy, defined by

$$B = \frac{g}{T_a} (\vartheta_p - \vartheta_a) \quad (85)$$

The assumption that the buoyancy of each individual fluid particle is defined by the difference between the particle's temperature and the ambient temperature is a crude one, and in fact the proper buoyancy should be related to the full surrounding temperature field, which includes the temperatures of the other buoyant fluid particles. However, this inclusion would lead to a set of (coupled) Langevin equations for each individual fluid particle, and the attractiveness of the Lagrangian approach would be lost. The Lagrangian time scale of the plume is

assumed to be equal for velocity and buoyancy and is denoted by T_p . The dissipation of velocity and buoyancy is denoted by ε_w and ε_B , respectively. $d\omega_w(t)$ and $d\omega_B(t)$ are random increments in the Lagrangian equations for velocity and buoyancy respectively. The stratification of the environment is given by N - see Equation (15). X_z is the plume particle's vertical position.

The usual assumptions for the random terms are

$$\begin{aligned}\overline{d\omega_w(t)} &= 0 \\ \overline{d\omega_B(t)} &= 0 \\ \overline{d\omega_w(t')d\omega_w(t)} &= \delta_{tt'} dt \\ \overline{d\omega_B(t')d\omega_B(t)} &= \delta_{tt'} dt \\ \overline{d\omega_B(t')d\omega_w(t)} &= 0\end{aligned}\tag{86}$$

The last assumption implies that stochastic velocity and buoyancy changes are uncorrelated on the (small) Kolmogorov scales, which may be questionable, but is perhaps not very important for the present consideration. It should be noted that for the mean plume rise, $\overline{X_z}$, the Equations (84) reduce to a deterministic set - due to the properties listed in Equations (86), and thus $\overline{X_z}$ does not depend on the dissipation terms.

In order to simulate a power law behavior for plume rise, which, in the early stage in a calm neutral environment, is confirmed by experimental evidence (see for example Turner, 1973), the Lagrangian time scale must be proportional to t . Assuming $T_p = A_p (t + t_0)$, it is retrieved the similarity solution (Csanady, 1973), provided that

$$A_p = 3/4\tag{87}$$

and

$$t_0 = (2r_s / 3\beta B_0)^{1/2}\tag{88}$$

The relation with the 2/3 law is imposed by the choice of $A_p = 3/4$. The initial plume radius and buoyancy are denoted by r_s and B_0 , respectively, and β is the plume entrainment constant (~ 0.6). Through the definitions of the plume particle buoyancy, B , and the heat output of the source, Q_h , t_0 can be related to the buoyancy flux parameter F_b - see Equation (9) - by

$$\frac{9}{4} B_0^3 t_0^4 = \frac{1}{\beta^2} \frac{F_b}{u} \quad (89)$$

With this choice of parameters the Langevin formulation can be forced to correspond asymptotically ($t \rightarrow \infty$) to the classical plume rise formulae.

Plume rise in a turbulent environment was addressed in detail by Netterville (1990) (see Section 2.7.2), who introduced an additional turbulent exchange mechanism, ‘extrainment’, generated by the ambient turbulence. A logical consequence of his theory for the Lagrangian framework is that if the plume turbulence dominates, the turbulent time scale of the plume, T_p should be applied, whereas if the environmental turbulence dominates, the ambient time scale, T_e , should be used. This view is reflected in an modified expression for the time scale

$$\frac{1}{T_m} = \frac{1}{T_p} + \frac{1}{T_e} \quad (90)$$

The Lagrangian formulation using Equation (90) was compared with Netterville's expression for the mean plume rise and though the Lagrangian formulation results in somewhat lower values, it has the same leveling off behavior in the final stage.

The Lagrangian equations provide also for an independent evaluation of the plume variance or plume width. This requires, however, explicit expressions for the dissipation, ε_w and ε_B in Equations (84). Van Dop (1992) suggests to use the actual particle velocity and buoyancy to parameterize the dissipation and assumes

$$\varepsilon_w = c_1 W^2 / T_p \quad (91)$$

$$\varepsilon_B = c_2 B^2 / T_p$$

where c_1 and c_2 are constants $O(1)$. Numerical solutions for the plume width, σ_z , defined as $\left(\overline{X_z^2} - \overline{X_z}^2 \right)^{1/2}$, were obtained, but do not agree with the similarity prediction, $\sigma_z \propto t^{2/3}$.

Alternatively, the dissipation may be parameterized as

$$\varepsilon_w = c_w \left(\frac{t+t_0}{t_0} \right)^{-\alpha_w} \quad (92)$$

$$\varepsilon_B = c_B \left(\frac{t+t_0}{t_0} \right)^{-\alpha_B}$$

Choosing $\alpha_w > 5/3$ and $\alpha_B > 11/3$, and for example equal to 2 and 4, respectively, it can be proven numerically and (in the neutral case, $N = 0$) also analytically that the plume width converges to the similarity prediction

$$\sigma_z = \left(3c_B t_0^5\right)^{1/2} \left(\frac{t+t_0}{t_0}\right)^{2/3} \quad (93)$$

and the ratio $\sigma_z/\overline{X_z}$ is given by

$$\frac{\sigma_z}{\overline{X_z}} = \left(\frac{3c_B t_0}{B_0^2}\right)^{1/2} \quad (94)$$

Csanady (1973) suggests (pp. 176-195) that this ratio is approximately 1/3. From this a value for the coefficient c_B of

$$c_B = \frac{B_0^2}{27t_0} \quad (95)$$

is inferred. Finally, evaluating the plume width in a turbulent environment requires also that the ambient turbulent dissipation rate is considered. As in the case for the Lagrangian time scale - see Equation (90) - Van Dop (1992) suggests the parameterization

$$\varepsilon_m = \frac{\varepsilon_p + (T_p/T_e)^2 \varepsilon_a}{1 + (T_p/T_e)^2} \quad (96)$$

where ε_p is given by W^2/T_p .

The algorithm can without much difficulty be extended to an non-homogeneous and non-stationary ambient turbulence by including height dependent formulations for ambient time scales and dissipation rates and using the appropriate version of the Langevin equations in these conditions. Arbitrary stratification, including a CBL with a capping inversion can be accounted for by introducing a height dependent N .

Though the method contains a number of heuristic elements, the Lagrangian formulation is transparent and computationally straightforward. It is consistent with the classical formulations for plume rise in a calm environment (see Turner, 1973; Briggs, 1969; or Csanady, 1973), but also accommodates more recent Eulerian formulations in a turbulent environment (Netterville, 1990; Nieuwstadt, 1992a,b). This makes it attractive for various practical applications. Yamada (2000) included this algorithm in a modeling system (HOTMAC-RAPTAD) and

examined its performance. He concluded that the overall performance was ‘as least as good as those of the ‘better’ models reported by Hanna et al. (1993)’.

A drawback of the Lagrangian method is that in order to remove the statistical noise, a large number of flow realizations should be evaluated.

4.4.2 Buoyant Plume Rise Described by a Lagrangian Turbulence Model

The research interest in buoyant plume rise is driven by the theoretical aspects of the simulation of the turbulent mixing of fluids with different temperatures. Similarity theory provides parameterizations for the mean plume height and width (Csanady, 1973, Briggs, 1975) if the influence of the ambient turbulence can be neglected, i.e., if the turbulence is generated only by the plume. This applies to the initial stage of plume rise, and for emissions into neutrally stratified ambient flows with a negligible turbulence. However, for practical plume rise calculations, models are required that:

- are computationally not too expensive
- can be applied to both stages of the buoyant plume rise and different ambient conditions
- permit the assessment of fluctuations, i.e., provide also plume statistics

The attempt to derive directly such models leads within the Eulerian framework to Reynolds-averaged Navier-Stokes (RANS) equations, and within the Lagrangian framework to Lagrangian particle models. RANS equation methods (Weil, 1988, Nettekville, 1990, Gangoiti et al., 1997) apply parameterizations for terms that are related to the turbulent mixing of the plume and the ambient flow.

By means of Lagrangian methods both the mean plume behavior and the plume statistics can be described in accordance with constraints of the similarity theory and observations. This was demonstrated by van Dop (1992) (see Section 4.4.1) in a first systematic analysis of the description of buoyant plume rise by Lagrangian methods. Alternative methods are described by Anfossi et al. (1993) (see Section 4.2), where also a review can be found on earlier work (see Zannetti and Al-Madani, 1984, Cogan, 1985) to describe buoyant plume rise by means of Lagrangian methods. Lagrangian particle models simulate the plume dynamics, but they require knowledge about the flow field that has to be provided by Eulerian models, or has to be approximated.

Lagrangian turbulence models (LTM) give a full description of both the motion and properties of plume and of the ambient flow. In particular, these Lagrangian equations are constructed consistent with the Eulerian RANS equations. In analogy to direct numerical simulation (DNS) or large eddy simulation (LES) (Nieuwstadt and de Valk, 1987, Nieuwstadt, 1992a,b, Zhang and Ghoniem, 1993, 1994a,b; see Section 3.4), LTM resolves mixing for high-Reynolds number flows avoiding the high computational costs of DNS or LES. We shall derive a buoyant

plume rise model from an LTM, which can be used for regulatory applications and satisfies the constraints (i), (ii) and (iii) considered above.

The Lagrangian description of fluid motion (i.e., of plume- and ambient-air particles) requires Lagrangian equations that are consistent with the Navier-Stokes equations. Two methods are used to date which provide for this consistency: first, the derivation of stochastic Lagrangian equations that are consistent with RANS equations up to second-order (van Dop et al., 1985, Sawford, 1986, Pope, 1994, Heinz, 1997, 1998), and second, the derivation of these equations consistent with an Eulerian velocity PDF (Thomson, 1987). The first approach, which is applied here, requires closure assumptions for the pressure redistribution and dissipation terms in the RANS equations of second-order. Closure assumptions for the pressure redistribution and dissipation terms in the RANS equations are known and relatively well-investigated for buoyant flows (see, e.g., Craft et al., 1996).

Details about the derivation of stochastic Lagrangian equations for buoyant turbulence can be found elsewhere (Heinz, 1997, 1998; Heinz and Van Dop, 1999). Here we present a summary.

The change of particle position dX_i ($i = 1, 2, 3$), velocity dU_i and potential temperature $d\vartheta_p$ is described by a set of linear stochastic differential equations:

$$\begin{aligned} dX_i &= U_i dt \\ dU_i &= A_i dt + b_{ij} d\omega_j \\ d\vartheta_p &= A^\theta dt + b^\theta d\omega^\theta \end{aligned} \quad (97)$$

where

$$\begin{aligned} A_i &= a_i + G_{ij}(U_j - \bar{u}_j) + G_i(\vartheta_p - \bar{\theta}) \\ A^\theta &= a^\theta + G_j^\theta(U_j - \bar{u}_j) + G^\theta(\vartheta_p - \bar{\theta}) \end{aligned} \quad (98)$$

The (Eulerian) ensemble average is denoted by overbars and summation over repeated subscripts is assumed. Deterministic changes of the particle velocity are described through the first terms on the right-hand side of Equation (97) with the unknown coefficients $a_i, a^\theta, G_i, G_{ij}, G^\theta$ and G_j^θ . The second terms describe the stochastic force caused by the small-scale turbulence and contains the additional unknown coefficients b_{ij} and b^θ . The properties of $d\omega_j$ and $d\omega^\theta$, random increments for velocity and potential temperature (\sim buoyancy) - see Equation (84) - are defined in Section (4.4.1).

Equations (97) can be transformed into a Fokker-Planck equation for the one-point joint velocity-temperature PDF of the flow $P(\mathbf{u}, \theta, \mathbf{x}, t)$ (Gardiner, 1983; Risken, 1984)

$$\frac{\partial P}{\partial t} + \frac{\partial u_i P}{\partial x_i} = -\frac{\partial A_i P}{\partial u_i} - \frac{\partial A^\theta P}{\partial \theta} + \frac{\partial^2 B_{ij} P}{\partial u_i \partial u_j} + \frac{\partial^2 B^\theta P}{\partial \theta^2} \quad (99)$$

with

$$\begin{aligned} B_{ij} &= \frac{1}{2} b_{ik} b_{kj} \equiv \frac{1}{2} C_0 \varepsilon_q \delta_{ij} \\ B^\theta &= \frac{1}{2} (b^\theta)^2 \equiv \frac{1}{2} C_1 \varepsilon_\theta \end{aligned} \quad (100)$$

The viscous dissipation and potential temperature dissipation are denoted by ε_q and ε_θ , respectively. C_0 and C_1 are constants whose value will be determined later.

From Equation (99) arbitrary moments of velocity and potential temperature can be obtained. In this way we are able to derive a set of equations which are similar to the RANS equations. We can summarize the latter in a suitable approximation up to second order as

$$\begin{aligned} \frac{d\bar{u}_i}{dt} + \frac{\partial \bar{u}'_i \bar{u}'_k}{\partial x_k} &= -\frac{1}{\rho_a} \frac{\partial \bar{p}}{\partial x_i} + \frac{g}{T} (\bar{\theta} - \theta_a) \delta_{i3} + \nu \frac{\partial^2 \bar{u}_i}{\partial x_k \partial x_k} \\ \frac{d\bar{\theta}}{dt} + \frac{\partial \bar{u}'_k \bar{\theta}'}{\partial x_k} &= \kappa \frac{\partial^2 \bar{\theta}}{\partial x_k \partial x_k} \\ \frac{d\bar{u}'_i \bar{\theta}'}{dt} + \frac{\partial \bar{u}'_i \bar{u}'_k \bar{\theta}'}{\partial x_k} + \bar{u}'_k \bar{\theta}' \frac{\partial \bar{u}_i}{\partial x_k} + \bar{u}'_i \bar{u}'_k \frac{\partial \bar{\theta}}{\partial x_k} &= \frac{g}{T} \bar{\theta}'^2 \delta_{i3} + \frac{p'}{\rho_a} \frac{\partial \bar{\theta}'}{\partial x_i} \\ \frac{d\bar{\theta}'^2}{dt} + \frac{\partial \bar{u}'_k \bar{\theta}'^2}{\partial x_k} + 2\bar{u}'_k \bar{\theta}' \frac{\partial \bar{\theta}}{\partial x_k} &= -2\varepsilon_\theta \\ \frac{d\bar{u}'_i \bar{u}'_j}{dt} + \frac{\partial \bar{u}'_i \bar{u}'_j \bar{u}'_k}{\partial x_k} + \bar{u}'_j \bar{u}'_k \frac{\partial \bar{u}_i}{\partial x_k} + \bar{u}'_i \bar{u}'_k \frac{\partial \bar{u}_j}{\partial x_k} &= \\ = \frac{g}{T} (\bar{u}'_i \bar{\theta}' \delta_{j3} + \bar{u}'_j \bar{\theta}' \delta_{i3}) + \frac{p'}{\rho_a} \left(\frac{\partial \bar{u}'_i}{\partial x_j} + \frac{\partial \bar{u}'_j}{\partial x_i} \right) - 2\varepsilon_q \end{aligned} \quad (101)$$

Here, T is a boundary-layer reference temperature, and θ_a is the mean ambient potential temperature, ν is the molecular viscosity and κ the conductivity. In order to be able to solve Equations (101) we have to make a number of closure assumptions

$$2\nu \frac{\overline{\partial u'_p}}{\partial x_k} \frac{\overline{\partial u'_q}}{\partial x_k} = \frac{1}{3} \frac{\overline{u_i'^2}}{\tau} \delta_{pq} \quad (102)$$

where τ is a dissipation time scale, which obeys

$$\frac{d\tau}{dt} = C_{\varepsilon 2} - 1 - (C_{\varepsilon 1} - 1) \cdot \frac{2\tau}{q^2} \left\{ -\overline{u_k u_l} \frac{\partial \overline{u_l}}{\partial x_k} + \beta g \overline{u_3 \theta} \right\} \quad (103)$$

where $C_{\varepsilon 1}$ and $C_{\varepsilon 2}$ are constants equal to 1.56 and 1.9, respectively, and q is twice the turbulent kinetic energy.

$$\varepsilon_g = \frac{k_4}{2\tau} \overline{\theta'^2} \quad \varepsilon_q = \frac{q^2}{2\tau} \quad (104)$$

$$p' \left(\frac{\partial u'_i}{\partial x_j} + \frac{\partial u'_j}{\partial x_i} \right) = -\frac{k_1}{2\tau} \left(\overline{u'_i u'_j} - \frac{1}{3} q^2 \delta_{ij} \right) + k_2 q^2 \left(\frac{\partial \overline{u_i}}{\partial x_j} + \frac{\partial \overline{u_j}}{\partial x_i} \right) \quad (105)$$

$$p' \frac{\partial \theta'}{\partial x_j} = -\frac{k_3}{2\tau} \overline{u'_i \theta'} \quad (106)$$

In the closure assumptions appear a number of closure constants k_i ($i=1-4$), which will be determined later.

It can be shown (cf. Heinz, 1997; Heinz and van Dop, 1999) that first and second moment equations derived from Equation (99) can be written similar to Equations (101), provided that the Lagrangian constants appearing in Equations (97) obey the following relationships

$$\begin{aligned}
G_l^\theta &= 0 & G^\theta &= -\frac{2k_3 - k_1}{4\tau} \\
G_i &= \frac{g}{T} \delta_{i3} & G_{il} &= -\frac{k_1}{4\tau} \delta_{il} \\
C_0 &= \frac{k_1 - 2}{3} & C_1 &= 2k_3 - 2k_4 - k_1
\end{aligned} \tag{107}$$

An additional consistency requirement is that $k_2 = 0$. Hence we may reformulate the Lagrangian Equations (97) now as

$$\begin{aligned}
dX_z &= W dt \\
dW &= -\frac{k_1}{4\tau} W dt + B dt + \sqrt{\frac{C_0 g^2}{2\tau}} d\omega_w \\
dB &= -\frac{2k_3 - k_1}{4\tau} B dt - N^2 W dt + \sqrt{\frac{C_1 (g/T)^2 \overline{\theta^2}}{2\tau}} d\omega^\theta \\
\frac{d\tau}{dt} &= C_{\varepsilon 2} - 1 - (C_{\varepsilon 1} - 1) \cdot \frac{2\tau}{u_i'^2} \left\{ -\overline{u_k u_l} \frac{\partial \overline{u_l}}{\partial x_k} + \beta g \overline{u_3 \theta} \right\}
\end{aligned} \tag{108}$$

where N is the Brunt- Väisälä frequency and $B = (g/T)(\mathcal{G}_p - \overline{\theta})$. The constants $C_{\varepsilon 1}$ and $C_{\varepsilon 2}$ are related by $C_{\varepsilon 1} = 1 + (C_{\varepsilon 2} - 1)/1.6$ (Heinz, 1998). Note that for the evaluation of the Eulerian moments appearing in Equation (108) it is still required to solve Equation (101) numerically.

In order to determine the remaining constants in Equation (97) we have compared the Lagrangian predictions of plume rise with Eulerian approaches (Weil, 1988; Nettekville, 1990) in a still environment. This yields

$$C_{\varepsilon 2} = 1 + \frac{3k_1}{8} \cdot \left(\frac{k_3}{k_1} - \frac{1}{2} \right) \tag{109}$$

and

$$k_1 = 4 \left(\frac{3\pi\beta^2}{2} \right)^{1/4} \left(\frac{k_3}{k_1} - \frac{1}{2} \right)^{-1/4} \left[1 - \frac{1}{2} \left(\frac{k_3}{k_1} - \frac{1}{2} \right) \right]^{-3/4} \tag{110}$$

Similarity theory also provides algebraic scaling laws for the variances. Applying these we obtain

$$C_{\varepsilon 2} = 1 + \frac{3}{8} \cdot k_4 \quad (111)$$

Equations (109), (110), and (111) relate four unknown constants, $C_{\varepsilon 2}$, k_1 , k_3 and k_4 . A value for $C_{\varepsilon 2}$ was found from a comparison of our model results with the LES data of Zhang and Ghoniem (1994a) in stably stratified flow, yielding $C_{\varepsilon 2} = 1.286$. All constants in Equations (108) are now determined.

The full model was evaluated against experimental data collected by Erbrink (1994). The effects of ambient wind shear and stability were considered by solving the parameterized equations for q^2 , $\overline{\theta^2}$, $\overline{u_1 u_3}$ and $\overline{u_3 \theta}$, see Equations (101). Details are given in Heinz and Van Dop (1999).

Figure 7(a) shows a scatter plot of measured plume heights versus the corresponding modeled plume heights in neutral to slightly stable conditions. The figure shows that the agreement between the observed plume heights and our predictions is very good. This means in particular that the model predictions do not only agree with the two-thirds power law, but also estimate correctly the leveling-off of the plume due to ambient stability.

In Figure 7(b) the plume radii are compared. The agreement is still fair, though the scatter has increased. It gives some support for the observation that the 2/3 similarity prediction also holds for the spreading of the plume.

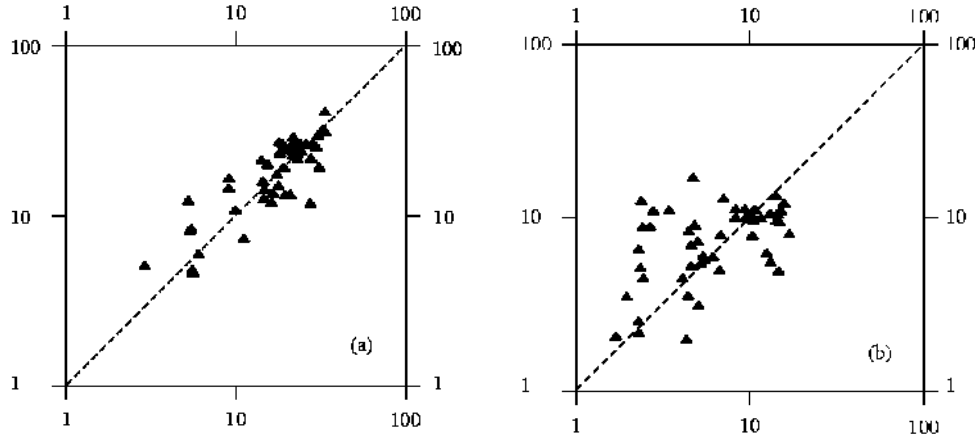


Figure 7. (a) Scatter plot of measured versus modeled normalized mean particle heights, $\overline{X_z} / B_0 \tau_0^2$. B_0 is the initial buoyancy and τ_0 is defined by $\tau_0 = (\pi^{1/2} r_s / B_0)^{1/2}$. (b) the same comparison but now for the plume widths defined as $\sqrt{X_z^2 - \overline{X_z}^2} / B_0 \tau_0^2$. Ambient stability conditions during the measurements varied from slightly stable to neutral.

5 Special Cases

All the plume rise estimates discussed in the previous four sections apply to effluents coming out from elevated and isolated sources, without accounting for possible effects of nearby buildings or stacks or of the presence of inversion layers. However, in practice, these situations (and others, like the case of ground level fires, of flares and of the presence of scrubber) need to be investigated since they may affect the plume rise and, consequently, modify the plume trajectory and the ground level concentration distribution. Generally these special topics are treated with “ad hoc” formulations. In this review we will briefly consider the following cases: downwash parameterization, penetration of elevated inversions, plume rise from multiple sources, plume rise from flare stacks, plume rise from fires, plume rise from stacks with scrubber. This review is not exhaustive and will give some examples of possible modeling solutions that are, in general, inserted in regulatory models.

5.1 Downwash Parameterization

In the plume rise computation, a special care must be paid to the possible occurrence of downwash effects. These can be classified as:

- stack tip downwash, a possible drag of the effluent in the wake downwind the stack due to the presence of the stack itself
- building downwash, effluent emitted from a stack near a building and brought downward by the flow of air over and around the building

- Stack tip and building downwash cause a decrease in the plume rise because of two concomitant phenomena
- the drag of the effluent in the stack and/or building wake; since this wake extends below the stack outlet, this drag causes the plume to decrease its height
- the increase of the entrainment with ambient air (causing a consequent decrease of buoyancy) due to the wake turbulence

In both cases, the reduced plume rise has the effects of increasing the ground level concentration. In particular, these last may be very high immediately downwind the stack or building if the plume is completely trapped in their wake.

Both stack tip downwash (e.g., Briggs, 1973; Bjorklund and Bowers, 1982; Overcamp, 2001) and building downwash (e.g., Briggs, 1973; Huber and Snyder, 1982; Schulman and Hanna, 1986) are to be considered when the ratio v_s/u is small. In the first case, the buoyancy amount has to be accounted for as well.

The procedures for the correction of the final plume rise, presented in the remainder of this section, do not provide any information about the plume trajectory near the stack outlet. They turn out useful in case one is interested in the prediction of pollutant concentrations in some areas that are at least a few hundreds of meters away from their source.

5.1.1 Stack Tip Downwash

The generally accepted practical rule (Briggs, 1969 and 1973) is that stack downwash will occur if the ratio of effluent speed, v_{s0} , to wind speed, u_0 , is less than about 1.5. However Briggs (1969) also suggested that this rule may be relaxed for highly buoyant plume (emitted by modern fossil-fuel power plants and larger industrial stacks). However, stack tip downwash is still an important problem for neutrally buoyant effluents or small industrial emissions. Furthermore, Overcamp (2001) stressed that it is a very important problem in simulating plumes in wind tunnels and towing tanks.

Bjorklund and Bowers (1982) proposed the following expression for the final plume rise corrected for the stack tip downwash, $\Delta h'$

$$\Delta h' = f \Delta h \quad (112)$$

where f is a dimensionless parameter calculated with the following procedure:

first, compute the Froude number of the effluent, F_r , defined as

$$F_r = \left(\frac{v_{s0}^2}{2g\sqrt{A_s/\pi}(T_{s0} - T_{a0})/T_{a0}} \right)^{1/2} \quad (113)$$

- if $F_r^2 < 3$ then $f = 1$ (no correction);
- if $F_r^2 \geq 3$:
 - if $v_s > 1.5 u_0$ then $f = 1$ (no correction);
 - if $u < v_s \leq 1.5 u_0$ then $f = 3(v_{s0} - u_0)/v_{s0}$;
 - if $v_s \leq u_0$ then $f = 0$ (no plume rise).

Snyder and Lawson (1991) modeled the downwash of neutrally buoyant effluent on the immediate lee side of a circular stack in a wind tunnel. They addressed the study to neutrally buoyant plumes solely because, as discussed in the paper, it appears not to be possible to perform the same study for buoyant plumes in a small-scale laboratory. They simulated both sub-critical (Reynolds numbers below the critical Reynolds number, $\cong 2 \times 10^5$) and supercritical (Reynolds numbers above the critical Reynolds number) turbulent flow. Sub-critical Reynolds numbers are typically attained by small-diameter stacks in relatively light winds; supercritical ones are attained by large-diameter stacks in strong winds (supercritical regimes are typical of the majority of full-scale stacks). The downwash characteristics differ markedly in the two regimes. For example, Snyder and Lawson (1991) found that downwash is much more serious in the sub-critical case than in the supercritical one. Furthermore, in the sub-critical regime, downwash begins when the ratio of effluent speed, v_{s0} , to wind speed, u_0 , is less than about 1.5; while in the supercritical regimes, downwash begins when such ratio is less than about 1.1. Empirical expressions are provided for vertical plume widths in the sub- and supercritical regimes, for lateral plume widths in the supercritical flow regime (not measured in sub-critical regime), and for plume centroids in the supercritical regime – the centroids in the sub-critical regime are too complex to be fitted by simple expressions.

Overcamp (2001) studied the range of conditions that may lead to downwash in designing simulation of buoyant plumes in wind tunnels and towing tanks. He made a comparison between data on the occurrence of downwash from ten sub-critical model studies and the theory proposed by Tatom (1986) - reference from Overcamp (2001). The Tatom's theory predicts that downwash does not occur if the following implicit relationship is satisfied

$$R' \geq \sqrt{\frac{(3C_D)^{2/3} - 1}{\pi A \left[\frac{1}{F_r^2} + \frac{4B}{(4 + B^2)^2} \right]}} \quad (114)$$

where:

$$R' = \left(\frac{\rho_{s0}}{\rho_{a0}} \right)^{1/2} \frac{v_{s0}}{u_0}; \quad A = 1 - \exp\left(-\frac{B^2}{2}\right); \quad B = \frac{R'}{\sqrt{\beta + \alpha R'}} \quad (115)$$

and C_D is the drag coefficient. All the ten independent experiments that Overcamp considered were characterized by $R' < 2$. He found that there was good agreement of Tatom's theory with the occurrence of downwash.

5.1.2 Building Downwash

We describe in some detail the method for taking into account the building downwash proposed by Schulman-Scire (Schulman and Scire, 1980; Scire and Schulman, 1980; Schulman and Hanna, 1986), because this method is implemented in both the ISC3 (U.S. EPA, 1995b) and AERMOD (U.S. EPA, 1998) models and is inserted in the CALPUFF code (Scire et al, 1999; <http://www.src.com/calpuff/calpuff1.htm>) as well. Then, more recently developed building downwash parameterizations will be also presented.

The Schulman-Scire method incorporates the effects of building downwash both on reducing plume rise and on enhancing dispersion parameters.

- $\sigma_{y0} \leq \sigma_{z0}$
neutral-unstable conditions

the plume rise, $\Delta h_d(x)$, of a downwashed plume is the real solution of the cubic equation

$$\Delta h_d^3 + \left(\frac{3R_0 \Delta h_d}{\beta_1} + \frac{3R_0^2}{\beta_1^2} \right) \Delta h_d = \frac{3F_m x}{\beta_j^2 u_0^2} + \frac{3F_b x^2}{2\beta_1^2 u_0^3} \quad (116)$$

where β_l is the neutral entrainment parameter (~ 0.6), β_j is the jet entrainment coefficient ($\beta_j = 1/3 + u_0/v_{s0}$), $R_0 = \sqrt{2} \sigma_{z0}$ is the dilution radius, and σ_{y0} , σ_{z0} are the horizontal and vertical dispersion coefficients, respectively, at a downwind distance of $3H_b$ (H_b = building height);

- final stable plume rise

$$\Delta h_d^3 + \left(\frac{3R_0 \Delta h_d}{\beta_2} + \frac{3R_0^2}{\beta_2^2} \right) \Delta h_d = \frac{3F_m}{\beta_j^2 u_0 s^{1/2}} + \frac{6F_b}{\beta_2^2 u_0 s} \quad (117)$$

where β_2 is the stable entrainment parameter (~ 0.36). Transitional plume rise during stable conditions is computed with Equation (116) until the final plume height predicted by Equation (117) is obtained.

- $\sigma_{y0} > \sigma_{z0}$

It is necessary to account for the elongated shape of the plume caused by horizontal mixing of the plume in the building wake; the plume can be represented as a finite line source:

- neutral-unstable conditions

the plume rise, $\Delta h_d(x)$, for a line source of length L_e is

$$\begin{aligned} \Delta h_d^3 + \left[\frac{3L_e}{\pi \beta_1} \right] \Delta h_d^2 + \left(\frac{3R_0 \Delta h_d}{\beta_1} + \frac{6R_0 L_e}{\pi \beta_1^2} + \frac{3R_0^2}{\beta_1^2} \right) \Delta h_d &= \\ = \frac{3F_m x}{\beta_j^2 u_0^2} + \frac{3F_b x^2}{2\beta_1^2 u_0^3} \end{aligned} \quad (118)$$

- final stable plume rise

$$\begin{aligned} \Delta h_d^3 + \left[\frac{3L_e}{\pi \beta_2} \right] \Delta h_d^2 + \left(\frac{3R_0 \Delta h_d}{\beta_2} + \frac{6R_0 L_e}{\pi \beta_2^2} + \frac{3R_0^2}{\beta_2^2} \right) \Delta h_d &= \\ = \frac{3F_m}{\beta_j^2 u_0 s^{1/2}} + \frac{6F_b}{\beta_2^2 u_0 s} \end{aligned} \quad (119)$$

The effective line length is $L_e = \sqrt{2\pi}(\sigma_{y0} - \sigma_{z0})$ if $\sigma_{y0} > \sigma_{z0}$; otherwise $L_e = 0$ and Equations (118) and (119) reduce to Equations (116) and (117).

The enhanced dispersion coefficients, σ_{y0} and σ_{z0} , vary with stack height, momentum rise, and building dimensions. As σ_{y0} and σ_{z0} approach zero (e.g., building downwash effects become negligible), Equations (116) to (119) approach the unmodified Briggs (1975) equations. The effect of R_0 and L_e is always to lower the plume height, thereby tending to increase the predicted ground-level concentration.

Hanna et al. (1998) developed a model to describe the lift-off of ground-based buoyant plumes using wind tunnel observations. Special emphasis was given to the development of simple empirical lift-off equations for buoyant plumes, which are trapped in building wakes. The model was developed using wind tunnel observations of plumes for which buoyancy was conserved, but the authors also proposed to use it for plumes whose buoyancy flux varies with distance (phenomenon that can occur due to the presence of aerosols, chemical reactions, and evaporation and condensation processes). Hanna et al. (1998) suggested that the effects of plume lift-off can be accounted for by multiplying the calculated ground-level concentration in the absence of lift-off by an exponential term depending on buoyancy flux. For buoyant plumes trapped in building wakes, the empirical formula that is proposed combines the exponential term with four additional terms related to the spread of plumes in building wakes. Such lift-off formula is incorporated in the HGSYSTEM/UF₆ hazardous gas dispersion code (Hanna and Chang, 1997).

The ADMS code (e.g., see Carruthers et al., 1999) includes a module for building effects based on the model of Hunt and Robins (1982). This module computes the dispersion of pollution from sources near isolated large buildings or closely spaced blocks. The model is able to deal with the influence on turbulent and mean velocity field of an extensive downstream wake. A simplified flow field is defined, based on a well mixed cavity (or recirculating flow region) and a downstream momentum wake. It takes into account the source position and allows for complete or partial entrainment into the recirculating flow region. Within the recirculating flow region concentrations are uniformly calculated. For partially entrained emissions, the entrained and non-entrained components form a two-plume structure downwind. Alternative spread parameters describe dispersion inside and outside the downstream wake.

Flowe and Kumar (2000) showed that a three-dimensional turbulent kinetic energy/dissipation (k - ε) numerical model, FLUENT, can be used as a tool for modeling air flow past a building and stack geometry, and the recirculation cavities associated with wide buildings, and to develop parameterizations useful to air quality modeling needs. These modeling capabilities were proved through the comparison with experimental wind tunnel data generated for several ratios of building width to building heights. Then, the flow field was examined to determine the length of the recirculation cavity as a function of the ratio of building width to building height both in front of and in the rear of the building. The height and length of the front recirculation cavity were parameterized as a function of the ratio of building width to building height. This is a novelty as far as regulatory models are concerned.

Schulman et al. (2000) proposed the Gaussian dispersion model PRIME for plume rise and building downwash. The plume trajectory within the modified fields downwind of the building is estimated using the Zhang and Ghoniem (1993 – see Section 3.4) numerical plume rise model. Such model is based on a numerical solution of the mass, energy and momentum conservation laws. It allows arbitrary

ambient temperature stratification, uni-directional wind shear, and initial plume size. A cavity module calculates the fraction of plume mass captured by and recirculated within the near wake. The captured mass is re-emitted to the far wake as a volume source and added to the uncaptured plume contribution to obtain the far wake concentrations. The PRIME model is implemented within the ISC3 code (Schulman et al., 1997), but it can be implemented in other refined or screening air quality models

5.2 Penetration of Elevated Inversions

Elevated inversions can be divided in thin and thick inversions according to their depth: when the plume cross section is greater than the inversion layer thickness, we have the case of the thin inversion, whereas when the entire plume cross section is contained in the inversion layer, we have the case of a thick inversion.

Plume buoyancy is often large enough to allow plumes to fully or partially penetrate an elevated temperature inversion layer (see Figure 8). Plume material will penetrate an inversion if the temperature excess of a part of the plume at a given height exceeds the temperature change through the layer at the same height. This typically happens during daytime, where the CBL is generally capped by stable air. In the case of a thin inversion, the potential temperature jump $\Delta\theta_i$ is the important parameter, whereas in the case of a deep inversion layer the potential temperature gradient, $\partial\theta_i/\partial z$ is the characteristic quantity. Consequently, the fate of the plume depends upon these parameters and on the inversion base height (Zannetti, 1990; Weil, 1988). A plume, which is able to completely penetrate the inversion, makes little or no ground level concentration contribution. On the contrary a plume trapped below the inversion can easily be diffused towards the ground bringing about consistent ground-level concentrations (fumigation).

Most of present applied dispersion models (Weil, 1988) only distinguish between complete penetration and no penetration. However many studies (see, for instance: Manins, 1979 or Thompson et al., 2000) have shown that the situation is not so simple and more detailed methods are needed. In particular, Manins (1979) and Zannetti (1990) concluded that a complete plume penetration is almost impossible since, upon reaching the inversion, there will be a part of the plume having insufficient buoyancy for further rise. This was also qualitatively shown by LSM simulations (Zannetti et Al Madani, 1983 and 1984). Thus, it is important to know the fraction of the plume that is trapped.

The simple method provided by Turner (1985) for discriminating between these two cases is presented in Section 5.2.1. Then, we review other penetration models for bent-over plume: first, for a thin inversion, the Briggs (1975), Manins (1979), and Weil (1988) models, see Section 5.2.2; then, for a thick one, the Briggs (1984), and Berkowicz et al. (1986) models, see Section 5.2.3.

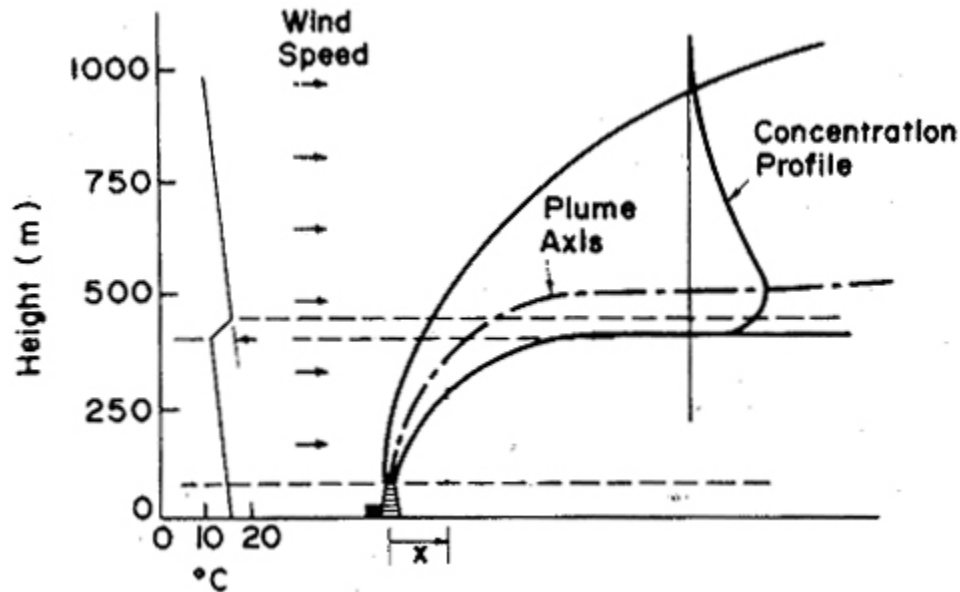


Figure 8. Schematic of the interaction of a buoyant plume and an elevated inversion layer (from Manins, 1979). [Reprinted with permission from Pergamon Press.]

5.2.1 The Turner Procedure

Turner (1985) worked out a pragmatic method using a modification to Briggs (1975, 1984) formulae for computing the final buoyant plume rise by layers and the possible (partial or total) penetration of the plume above the atmospheric thermal discontinuities (such as, typically, the mixing height).

Turner method considers that the plume, during its rise, may meet atmospheric layers of different wind speed and stability. To use this method, one must know or estimate the values of temperature and wind speed close to the stack, on at least two different levels. One at a height between ground level and the stack outlet height, the other at an elevation higher than that reached by the upper edge of the plume at the end of its rise (given by $h_e + 0.5\Delta h$). Obviously, to be able to make optimum use of Turner method, one ought to know the values of temperature and wind speed at numerous intermediate levels, as well as at the previous two levels. Furthermore it is also assumed that the mixing height and the rate of change of potential temperature with height above the mixing height are available.

This procedure for computing the final plume rise consists of the following steps.

- 1) Calculation of the stack tip downwash factor (f) through Bjorklund and Bowers' model (see Section 5.1.1);
 - if $f = 0$

Turner method provides a null final plume rise and an effective emission (see item 4 below) equal to the emission at the stack.

- if $f > 0$ we can go onto the following steps;

2) Calculation of the final plume rise keeping into account the plume transit through some atmospheric layers having different characteristics of temperature, wind speed and stability.

We start computing the final plume rise, by using a modification to Briggs (1975, 1984) formulae and the meteorological parameters of the atmospheric layer that includes the stack outlet. If either the obtained final plume rise (in neutral or unstable conditions) or the upper edge of the plume (in stable conditions) does not overtake the top of the layer containing the stack outlet, the calculated final plume rise is the results of the first part of Turner method. If neither of them does, we have to compute the residual buoyancy, and use it to repeat the computation procedure of the final plume rise of the next layer; the new plume rise has the same fate as the previous one. The process goes on from layer to layer till the result will be obtained.

3) The final plume rise computed through the procedure illustrated at point 2) is adjusted by the stack tip downwash factor (see Section 5.1.1).

4) To calculate the penetration of the plume above atmospheric thermal discontinuities, this procedure assumes that a fraction f' ($0 \leq f' \leq 1$) of the total emission, Q , remains trapped below the base of the thermal discontinuity, placed at the height h_t , and affects the concentration measured by receptors below this height. The product $f'Q$ is known as the “effective emission”.

As far as f' is concerned two options are possible:

a) $f' = 1$; this means that this option disregards the penetration of the plume above the thermal discontinuity, but takes only into account the modification made to the plume rise;

b) $f' \neq 1$ and the modified plume rise are calculated with the method discussed below.

Option b) can be chosen only if h_t is greater than the distance of receptors from ground level. With this method, three possibilities are considered, depending on the values taken by the parameters

$$t_p = h_e + 0.5\Delta h \quad (120)$$

and

$$b_p = h_e - 0.5\Delta h \quad (121)$$

assumed by Turner to represent the upper and the lower edge of the plume. These three possibilities are:

- if $t_p \leq h_t$, no penetration of the plume above the thermal discontinuity is assumed, i. e. $f' = 1$;
- if $b_p \geq h_t$, the entire plume is assumed to penetrate above the thermal discontinuity, i. e. $f' = 0$; no concentration is measured by receptors;
- in the intermediate case, i. e. $b_p < h_t < t_p$, Turner proposes

$$0 < f' = \frac{h_t - b_p}{\Delta h} < 1 \quad (122)$$

and

$$\Delta h'' = \frac{1 + f'}{2} \Delta h \quad (123)$$

as the actual plume rise, instead of Δh .

This plume rise/partial penetration technique provides a computationally simple solution for engineering calculations. However, the problem of correctly modeling partial penetration is still wide open.

One can observe that, since this method requires a detailed knowledge of the various atmospheric layers crossed by the plume (e.g., coming from vertical profile observations), it would be similarly simpler to solve directly the conservation equations as mentioned in Section 3. However, this method was recalled here since it is incorporated in some dispersion models, like, for instance, in the TUPOS model (Turner et al., 1986), in the PTSRCE preprocessor program of UAM-V (U.S. EPA¹²), and in the SAFE_AIR package (Canepa et al., 2000³) as a user option.

5.2.2 Thin Inversion

For a vertical plume, Briggs (1975) predicts that a thin inversion layer can be completely penetrated if the mean temperature excess of the plume at height h' ($h' = h_t - z_s$) exceeds the temperature jump $\Delta\theta_i$. Defining $b_i = (g/\theta)\Delta\theta_i$, complete penetration occurs if

¹<http://www.epa.gov/scram001>,

²<http://uamv.saintl.com/>

³http://155.207.20.121/mds/bin/show_long?SAFE_AIR

$$F_b > 0.019 b_i^{3/2} (h')^{5/2} \quad (124)$$

for a buoyant plume, and

$$F_m > 0.25 b_i (h')^3 \quad (125)$$

for a jet. This last equation is based upon experimental results by Vadot (1965).

For bent over buoyant plumes the finite depth of the plume cannot be neglected and, consequently, partial penetration is more likely than complete penetration. The Briggs (1975) model considers the plume buoyancy depletion during the inversion traverse. Defining an equilibrium height with respect to the top of the stack, z'_{eq} , where its buoyancy flux is equal to zero and assuming the plume cross-section to be rectangular with a depth equal to the rise Δh , and a width equal to $0.5 \Delta h$, z'_{eq} is found to be (Briggs, 1975; Weil, 1988):

$$\frac{z'_{eq}}{h'} = \frac{2}{3} (1 + 9\pi P_b)^{1/2} \quad (126)$$

where the dimensionless buoyancy flux P_b is given by

$$P_b = \frac{F_b}{U_a b_i h'^2} \quad (127)$$

The percentage of plume trapped by the inversion and thus diffused downwards is

$$f' = 1 - P_b = \frac{h'}{z'_{eq}} - 0.5 \quad (128)$$

From which the following simple criteria derive:

- $z'_{eq} < \frac{2}{3} h'$, no penetration ($f' = 1$);
- $\frac{2}{3} h' < z'_{eq} < 2 h'$, partial penetration - f' is given by Equation (128);
- $z'_{eq} > 2 h'$, complete penetration ($f' = 0$).

For bent over jets, substantial inversion penetration may be assumed (Briggs, 1975) when

$$F_m > 2.2 \beta^2 u_0 b_i^{1/2} (h')^{5/2} \quad (129)$$

The Manins (1979) model is based on the assumption that the density or temperature is normally distributed in a bent over buoyant plume when its centerline reaches the inversion. As in the previous Briggs (1975) model, the inversion is idealized as a jump of zero thickness. Defining $\Delta\mathcal{G}_m$ to be the maximum excess temperature, Manins also assumed that penetration starts when $\Delta\mathcal{G}_m = \Delta\mathcal{G}_i$, and found that this happens if

$$P_b = 0.08 \quad (130)$$

He suggested that partial penetration would occur, for the part of the plume with $\Delta\mathcal{G} > \Delta\mathcal{G}_i$, when $P_b > 0.08$. Accounting for the effects of the momentum overshoot of the plume and the re-entrainment back into the plume of material trapped within the inversion, the above condition leads to the following expression for the fraction of the plume trapped in the inversion layer

$$f' = \frac{0.08}{P_b} - (P_b - 0.08) \quad (131)$$

Weil (1988) compared laboratory observations (see Figure 9) of inversion penetration by Manins (1979) and Richards (1963) and noted that Manins model, Equation (131), fits reasonably well his data but overestimates most of Richards data while Briggs model, Equations (126) and (128), overestimates part of the observed f' . Weil argues that these differences between models and observations can possibly be due to some different configurations in the experimental conditions between the two experiments and, in particular, of the ratio $\Delta h_i/h'$, where Δh_i is the finite thickness of the inversion layer. As a consequence, Weil (1988) considers the effect of Δh_i on the plume penetration capacity and of a different temperature distribution. He found that the fraction of the plume below the inversion top, $h' + \Delta h_i$, is

$$f' = 1 - \frac{1}{\pi} \left[\cos^{-1} \lambda - \lambda(1 - \lambda^2)^{1/2} \right] \quad (132)$$

where

$$\lambda = \frac{1 + \delta - \eta_{eq}}{\beta' \eta_{eq}} \quad (133)$$

with $\eta_{eq} = \frac{z'_{eq}}{h'}$, and $\delta = \frac{\Delta h_i}{h'}$.

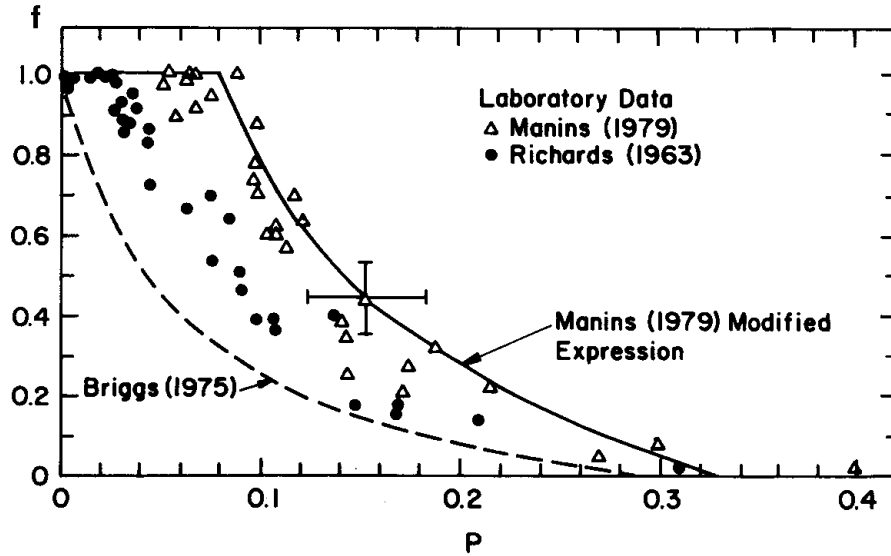


Figure 9. Models and laboratory measurements of the fraction of a plume trapped by an elevated inversion as a function of the dimensionless buoyancy flux P (adapted from Weil, 1988). [Reprinted with permission from American Meteorological Society]

5.2.3 Thick Inversion

In this case the reference inversion height h' , to calculate penetration and trapping probabilities of occurrence, is the height of the inversion base. Briggs (1975, 1984) considered the simple case in which s is constant with height. He also assumed that plume equilibrium height is given by Equation (44), namely

$$z'_{eq} = 2.6 \left(\frac{F_b}{su_0} \right)^{1/3} \quad (134)$$

in which s is computed from $d\varrho_i/dz$. To estimate the fraction of the plume trapped $f' = 1 - P_b$, he used Equation (128), obtaining

- $z'_{eq} < \frac{2}{3}h'$, no penetration ($f' = 1$);
- $\frac{2}{3}h' < z'_{eq} < 2h'$, partial penetration - f' is given by Equation (128);
- $z'_{eq} > 2h'$, complete penetration ($f' = 0$).

Briggs' (1984) model gives conservative estimates since the plume initially rises in an atmosphere with $s = 0$, in which it should not experience any buoyancy depletion.

Berkowicz et al. (1986) considered this aspect. By assuming that the process of buoyancy reduction initiates only when the upper boundary of the plume arrives at h' , they proposed the following equation for the ratio z'_{eq}/h'

$$\frac{z'_{eq}}{h'} = [2.6^3 P_s + (2/3)^3]^{1/3} \quad (135)$$

where

$$P_s = \frac{F_b}{U_a N_i^2 h'^3} \quad (136)$$

5.3 Plume Rise from Multiple Sources

When several stacks are located close to each other, the resulting plume rise is different from that of a single stack. Plumes coming from the various stacks generally merge during the rise stage thus causing enhanced rise due to reduced ambient air entrainment and increased buoyancy. Consequently, ground level concentration is reduced. This enhanced plume rise was observed both in laboratory experiments and in the field (Manins et al., 1992). In general the enhancement is greater in the case of flow parallel to the stacks than in the normal flow and, in both cases, the plume rise exceeds that of a single plume (Anfossi, 1985). Overcamp and Ku (1988) also confirmed that enhancement is a function of the angle between the direction of the wind and the line of stacks, finding that the rise is larger when the angle is small. In the same way, also plumes coming from cooling towers (Bornoff and Mokhtarzadeh-Dehghan, 2001) or from multiple fires (Trelles et al., 1999b) may merge and experience enhanced rise.

Briggs (1975) provided a semi empirical formulation for determining the plume rise in the case of stacks of equal height and buoyancy flux. He defined the enhancement factor, E_n , as the ratio of the plume rise from n stacks to that of one stack, whose expression is the following

$$E_n = \left(\frac{n+S}{1+S} \right)^{1/3}, \quad S = \left(\frac{n-1}{n^{1/3} \Delta h_1 / d} \right)^{3/2} \quad (137)$$

where d is the spacing between the stacks and Δh_1 is the plume rise from a single stack.

Anfossi et al. (1978) developed and tested (Anfossi et al. 1979; Anfossi, 1982, 1985; Sandroni et al., 1981) a virtual stack concept that allows two or more stacks of different buoyancy and heights to be merged. Their model for the plume rise from multiple sources is expressed by the following equation

$$\Delta H^N = H_i + C \sum_{j=1}^N \left\{ F_j^{1/3} - [(H_i - H_j)/C]^3 \right\}^{1/3} \quad (138)$$

in which

$$H_i = H_{\max} + \frac{\Delta H_{\min} - (H_{\max} - H_{\min})}{1 + [\Delta H_{\min} - (H_{\max} - H_{\min})]/D} \quad (139)$$

is the merging point height, ΔH_{\min} is the maximum single plume rise from lowest stack H_{\min} , $C = \Delta H_{\min} / F_{\min}^{1/3}$ and $D = (n-1)d$. In the case of stacks of equal height and buoyancy flux, Equations (138) and (139) reduce to

$$E_n = \frac{1 + n^{1/3}(\Delta h_1 / D)}{1 + (\Delta h_1 / D)} \quad (140)$$

Anfossi (1985) and Manins et al. (1992) demonstrated that Equations (137) and (140) give almost equal results.

5.4 Plume Rise from Flare Stacks

A flare stack is a vent gas stack with a small pilot flame at the stack exit. Combustible vent gases flowing from the stack exit are ignited by the pilot flame and burned in the open atmosphere just above the stack exit. The hot, combusted gas plume then rises and disperses in the atmosphere just as does any hot, buoyant plume. Flare stacks are widely used in industrial plants; in particular, flare stacks are an essential safety requirement in hydrocarbon processing facilities.

By means of direct observation, Leahey and Davies (1984) showed that the entrainment of ambient air into the flare plume is similar to what found in stack plumes and that the flare plumes rise according to the "two-third" law.

The SCREEN3 model (U.S. EPA, 1995a) deals with flare. Buoyancy flux for flare release is estimated from

$$F_b = 1.66 \cdot 10^{-5} Q_f \quad (141)$$

where Q_f is the total heat release rate of the flare (cal s^{-1}). This formula - see Equation (9) - was proposed by Briggs (1969). The value of the constant was derived fixing $T_a = 293 \text{ K}$, $\rho_a = 1205 \text{ g m}^{-3}$, $c_p = 0.24 \text{ cal g}^{-1} \text{ K}^{-1}$, and assuming the following relationship between Q_f and the sensible heat release rate Q_h : $Q_h = 0.45 Q_f$. The sensible heat rate is based on the assumption that 55 % of the total heat released is lost due to radiation (Leahey and Davies, 1984). The buoyancy flux

for flares is calculated in SCREEN by assuming effective stack parameters of $v_{s0} = 20 \text{ m s}^{-1}$, $T_{s0} = 1273\text{K}$, and solving for an effective stack diameter, $d_s = 9.88 \cdot 10^{-4} (Q_h)^{0.5}$.

5.5 Plume Rise from Fires

Environmental consequences of large fires are of interest since the rise and transport of combustion products can distribute potentially hazardous materials over a wide area (McGrattan et al., 1996). Plume rise simulation from fires is not straightforward. For example, the life cycles of a forest fire includes an initial developing stage with large increases in heat generation and pollutant emissions rates, followed by a stage of decreasing values. Therefore, the source parameters of a forest fire are usually not constant. The magnitude of the variation in heat generation and emission rates may be two orders of magnitude over the course of burn (Scire et al, 1999).

Various models dealing with plume rise from fires are available in the literature. For instance Manins (1985) considered plumes from fires from thermonuclear explosions (direct bomb fires, incineration of the immediate blast area and injection from fires which spread from the blast area). The prediction of fire plume-rise was based on the Boussinesq buoyant plume model of Morton et al. (1956) since this was shown by Turner (1973) and Briggs (1975) to give good results for small to large heat sources when the ambient wind is light (see also Section 2.1).

Recently McGrattan et al. (1996) presented a LES model of smoke plumes generated by large outdoor pool fires transported by a uniform ambient wind. This model was extended by Trelles et al. (1999a) to deal with the problem of large-scale fire plumes in the presence of winds, which vary, in the vertical direction. A further extension performed by Trelles et al. (1999b) investigated multiple fire plumes. In fact large scale fire scenarios commonly involve multiple combustion sources: the class of problems considered excludes fires large enough to alter the prevailing atmosphere, but it allows for fires sufficiently strong to interact with each other and to have local atmospheric influence.

Also some regulatory computer codes include the treatment of plume rise from fires. For example, the FIREPLUME code (Brown et al., 1999) and the CALPUFF code (Scire et al, 1999; <http://www.src.com/calpuff/calpuff1.htm>) that are briefly described below.

FIREPLUME (Brown et al., 1999) is able to simulate atmospheric dispersion and air quality impacts from fires. FIREPLUME deals with plume rise by means of the MCLDM Lagrangian particle model (Brown et al, 1996). The framework for treating source buoyancy closely follows from the “two-thirds” law, which is applicable in cases where the buoyant source has low initial momentum. Fires clearly fall into this category (Weil, 1982). Although the “two-thirds” law is

primarily used for stack emissions, its extension to fire buoyancy is straightforward. The plume rise relationships are incorporated into MCLDM to provide a mean vertical velocity for the individual particles. The vertical dispersion from a variety of buoyant release scenarios can be evaluated, from intensely buoyant sources typical in actively burning forest fires to very low buoyancy sources, such as, in the residual stages of smoldering biomass.

In CALPUFF (Scire et al, 1999; <http://www.src.com/calpuff/calpuff1.htm>) the area source plume rise model is formulated to calculate the rise of buoyant plumes resulting from forest fires, the burning of leaking oil, and other type of buoyant area sources. The model is designed to be applicable to the following conditions: 1) all types of ambient temperature stratifications; 2) all types of wind stratifications (wind shear is important because the forest fire plume starts at ground where there is a zone of large velocity gradients in the vertical); 3) any size of finite emission source; 4) include the effects of plume radiative heat loss; and 5) Boussinesq approximation is not assumed.

5.6 Plume Rise from Stacks with Scrubber

Desulfurization techniques have often been adopted for either the combustibles (e.g., coal cleaning) or the flue gas (scrubbers). The latter technique seems by far the most cost effective for SO_2 emission reduction. Most flue gas desulfurization devices employ a wet scrubbing technique in which a $Ca(OH)_2$ solution is used for partial removal of SO_2 .

Plumes from stacks with scrubbers are frequently modeled using the same techniques as the other plumes. Schatzmann and Policastro (1984) reviewed the problem of evaluating Δh for stacks with scrubbers, concluding that “the significant moisture content of the scrubbed plume upon exit leads to important thermodynamic effects during plume rise that are unaccounted for in the usual dry plume rise theories”.

Plume rise models for wet plumes (e.g., cooling tower plumes) have been developed by Hanna (1972), Weil (1974), and Wigley and Slawson (1975). Even these formulations, however, are inappropriate for scrubbed plumes, according to Schatzmann and Policastro (1984), because of the simplifications they adopt. Sutherland and Spangler (1980) compared observed plume rise heights for scrubbed and unscrubbed plumes and evaluated the performance of several plume rise formulations. They found that simple plume rise formulae are questionable even for dry plumes, while moisture effects in scrubbed plumes increase the plume buoyancy and almost compensate for the loss of plume rise due to the temperature decrease induced by the scrubbing system. Plume rise of moist plumes was reviewed by Briggs (1984).

Schatzmann and Policastro (1984) recommend integral-type models for scrubbed plumes, with the additional requirement of avoiding some common

simplifications such as the linearization of the equation of state, first-order approximations in the calculation of the local saturation deficit, and the Boussinesq approximation.

References

Abraham, G. (1970): Round buoyant jet in cross-flow. Paper presented at the 5th *International Conf. Water Pollut. Res.*, San Francisco, CA.

Anfossi, D., G. Bonino, F. Bossa, and R. Richiardone (1978): Plume rise from multiple sources: a new model. *Atmos. Environ.*, **12**:1821-1826.

Anfossi, D., G. Bonino, and R. Richiardone (1979): An application of plume rise model for multiple sources to the cooling tower plumes of John E. Amos Power Plant. *Il Nuovo Cimento*, **2C,N.4**:488-498.

Anfossi, D. (1982): Plume rise measurements at Turbigio. *Atmos. Environ.*, **16**:2565-2574.

Anfossi, D. (1985): Analysis of plume rise data from five TVA Steam Plants. *J. Clim. App. Met.*, **24**:1225-1236.

Anfossi, D., E. Ferrero, G. Brusasca, A. Marzorati, and G. Tinarelli (1993): A simple Way of Computing Buoyant Plume Rise in Lagrangian Stochastic Dispersion Models, *Atmos. Environ.*, **27A**:1443-1451.

Anfossi, D. (2000): Jet plume rise description in Lagrangian Stochastic Models. ICGF Rapp. Int. No 414/2000, 9 pp.

Arya, P. S., (1999) *Air pollution meteorology and dispersion*. Oxford University Press, New York. <http://www.oup-usa.org/>

Berkowicz, R., H.R. Olesen, and U. Torp (1986): The Danish Gaussian air pollution model (OML): description, test and sensitivity analysis in view of regulatory applications. *Air Pollution Modeling and Its Application V*. C. De Wispelaere, F.A. Schiermeier, and N.V. Gillani Editors., Plenum, New York, 453-481.

Bjorklund, J.R., and J.F. Bowers (1982): User's instruction for the SHORTZ and LONGZ computer programs, Volumes I and II. EPA Document EPA-903/9-82-004A and B, U.S. EPA, Middle Atlantic Region III, Philadelphia, Pennsylvania, USA.

Bornoff R.B. and Mokhtarzadeh-Dehghan M.R. (2001) A numerical study of interacting buoyant cooling-tower plumes. *Atmos. Environ.*, **35**, 589-598

Briggs, G.A. (1969): Plume rise. AEC Crit. Rev. Ser., TID-25075. Springfield (VA), pp. 80.

Briggs, G.A. (1972): Chimney plumes in neutral and stable surroundings. *Atmos. Environ.* **6**:507-510.

Briggs, G.A. (1973): Diffusion estimation for small emission. In Atmospheric Turbulence and Diffusion Laboratory 1973 Annual Report. (NOAA/ATDL, Oak Ridge, TN, publication no. ATDL-106, pp 739-747

- Briggs, G.A. (1975): Plume rise predictions. In: Lectures on air pollution and environmental impact analyses, D. Haugen (editor). Workshop proceedings, Boston, Massachusetts, September 29 – October 3, pp. 59-111, American Meteorological Society, Boston, Massachusetts, USA.
- Briggs, G.A. (1984): Plume rise and buoyancy effects. Technical Report Atmospheric Science and Power Production, DOE/TIC-27601, edited by D. Randerson, U.S. Department of Energy, Washington, D.C.
- Bringfelt, B. (1969): A study of buoyant chimney plumes in neutral and stable atmospheres. *Atmos. Environ.*, **3**:609-623.
- Brown, D.F., W. E. Dunn, A.J. Policastro, and D. Malony (1996): FIREPLUME model for plume dispersion from fires: applications to UF6 cylinder fires, ANL/EAD-PM69.
- Brown, D.F., W.E. Dunn, M.A. Lazaro, and A.J. Policastro (1999): The FIREPLUME model: tool for eventual application to prescribed burns and wildland fires. *The joint fire science conference and workshop*. Boise, Idaho, June 15-17, 1999.
- Brummage, K.G. (1966): The calculation of atmospheric dispersion from a stack. Stichting CONCAWE, The Hague, The Netherlands.
- Canepa, E., F. Modesti, and C.F. Ratto (2000): Evaluation of the SAFE_AIR code against air pollution field and laboratory experiments. *Atmos. Environ.*, **34(28)**:4805-4818.
- Carpenter, S.B., T.L. Montgomery, J.M. Leavitt, W.C. Colbaugh, and F.W. Thomas (1971): Principal plume dispersion models: TVA power plants. *J. Air Pollut. Control Ass.*, **21**:491-495.
- Carras, J.N., and D.J. Williams (1984): Experimental studies of plume dispersion in convective conditions – 1. *Atmos. Environ.*, **18**:135-144.
- Carruthers, D.J., A.M. Mckeown, D.J. Hall, and S. Porter (1999): Validation of ADMS against Wind Tunnel Data of Dispersion from Chemical Warehouse Fires. *Atmos. Environ.*, **33**:1937–1953.
- Chiang H.C. and Sill B.L. (1985): Entrainment models and their application to jets in a turbulent cross flow. *Atmos. Environ.*, **19**:1425-1438
- Cogan, J.L. (1985): Monte Carlo simulation of a buoyant dispersion. *Atmos. Environ.*, **19**:867-878.
- Craft, T.J., N.Z. Ince, and B.E. Launder (1996): Recent Developments in Second-Moment Closure for Buoyancy-Affected Flows. *Dynamics of Atmos. and Oceans*, **23**:99-114.
- Csanady, G.T. (1973): Turbulent Diffusion in the Environment. *Geophysics and Astrophysics Monographs, Vol. 3*. R. Reidel Publishing Company, Dordrecht-Holland, Boston-USA.
- Djurfors, S.G. (1977): On the rise of buoyant plumes in turbulent environments. Syncrude Canada Ltd. Professional Paper 1977-4.
- Djurfors, S.G. (1983): Discussion of effective source flux parameters for use in analytical plume rise models. *Atmos. Environ.*, **17**:197-198.
- Erbrink, H.J. (1994): Plume Rise in Different Atmospheres: A Practical Scheme and some Comparisons with LIDAR Measurements. *Atmos. Environ.*, **28**:3625-3636.

Fay, J.A., M.P. Escudier, and D.P. Hoult (1970): A correlation of field observations of plume rise. *J. Air Pollut. Control Assoc.*, **20**:391-397.

Finardi, S., G. Tinarelli, A. Nanni, D. Anfossi, E. Ferrero, S. Trini Castelli (2001): In situ diagnostic or nested prognostic meteorological models to drive dispersion simulations in complex area: a comparison in a real application. *Air Pollution Modelling and its Applications XIV*, S.E. Gryning and F.A. Schiermeier eds., Kluwer Academic / Plenum Press, New York.,641-649

Flowe, A.C., and A. Kumar (2000): Analysis of velocity fields and dispersive cavity parameters as a function of building width to building height ratio using a 3-D computer model for squat buildings. *Journal of Wind Engineering and Industrial Aerodynamics*, **86**:87-122.

Gangoiti, G., J. Sancho, G. Ibarra, L. Alonso, J.A. García, M. Navazo, N. Durana, and J.L. Ibarria (1997): Rise of Moist Plumes from Tall Stacks in Turbulent and Stratified Atmospheres. *Atmos. Environ.*, **31A**:253-269.

Gardiner, C.W. (1983): *Handbook of Statistical Methods*. Springer Verlag, Berlin, Heidelberg, New York, Tokyo.

Glendening, J.W., J.A. Businger, and R.J. Farber (1984): Improving plume rise prediction accuracy for stable atmospheres with complex vertical structure. *J. Air Pollut. Control Ass.*, **34**:1128-1133.

Golay, M.W. (1982): Numerical modeling of buoyant plumes in a turbulent stratified atmosphere. *Atmos. Environ.*, **16**:2373-2381.

Graziani G., Martilli A., Pareschi M.T. and Valenza M. (1997) Atmospheric dispersion of natural gases at Vulcano island. *Journal of Volcanology and Geothermal Research*, **75**, 283-308

Hanna, S.R. (1972): Rise and condensation of large cooling tower plumes. *J. Appl. Meteor.*, **11**:793-799.

Hanna, S.R., G.A. Briggs, and R.P. Jr. Hosker, (1982): Handbook on atmospheric diffusion. Prepared for the Office of Health and Environmental Research, Office of Energy Research, U.S. Department of Energy, DOE/TIC 11223, J.S. Smith, Publication Editor.

Hanna, S.R., Chang J.C. Strimaitis D.G. (1993): Hazardous gas model evaluation with field observations. *Atmos. Environ.*, **27A**:2265-2285.

Hanna, S.R. (1994): Lecture on Air quality modeling over short distances. College on atmospheric boundary layer and air pollution modelling. ICTP Trieste, 16 May-3 June 1994.

Hanna, S.R., and J.C. Chang (1997): HGSYSTEM/UF₆ model enhancements for plume rise and dispersion around buildings, lift-off of buoyant plumes, and robustness of numerical solver. K/SUB/93-XJ947/R, OSTI, P.O. Box 62, Oak Ridge, TN 37831.

Hanna, S.R., G.A. Briggs, and J.C. Chang (1998): Lift-off of ground-based buoyant plumes. *Journal of Hazardous Materials*, **59**:123-130.

Heinz, S. (1997): Nonlinear Lagrangian Equations for Turbulent Motion and Buoyancy in Inhomogeneous Flows. *Phys. Fluids*, **9**:703-716.

Heinz, S. (1998): Time Scales of Stratified Turbulent Flows and Relations between Second-Order Closure Parameters and Flow Numbers. *Phys. Fluids*, **10**:958-973.

- Heinz, S., and H. van Dop (1999): Buoyant plume rise described by a Lagrangian turbulence model. *Atmos. Environ.*, **33**:2031-2043.
- Henderson-Sellers, B., and S.E. Allen (1985): Verification of the plume rise/dispersion model USPR: plume rise for single stack emissions. *Ecological Modelling*, **30**:209-277.
- Hewett, T.A., J.A. Fay, and D.P. Hoult (1971) Laboratory experiments of smokestack plumes in a stable atmosphere. *Atmos., Environ.*, **5**:767-789.
- Holland, J.Z. (1953): Meteorology survey of the Oak Ridge area. ORO-99. U.S. At. Energy Comm., Oak Ridge, Tennessee.
- Hoult, D.P., and J.C. Weil (1972): A turbulent plume in a laminar crossflow. *Atmos. Environ.*, **6**:513-531.
- Huber, A.H., and W.H. Snyder (1982): Wind tunnel investigation of the effects of a rectangular-shaped building on the dispersion of effluents from short adjacent stacks. *Atmos. Environ.*, **17**:2837-2848.
- Hunt, J.C.R., and A.G. Robins (1982): A model for assessing dispersion of plumes from sources in the vicinity of cuboid shaped buildings. Proceedings of the EUROMECH Conference on Surface Mounted Bluff Bodies in Turbulent Boundary Layers, Lisbon.
- Hurley, P.J., and W. Physick (1993): Lagrangian particle modelling of buoyant point sources: plume rise and entrapment under convective conditions, *Atmos. Environ.*, **27A**: 1579-1584.
- Hurley, P.J., and P.C. Manins (1995): Plume rise and enhanced dispersion in LADM. ECRU Technical Note No.4, CSIRO Division of Atmospheric Research, Australia.
- Hurley, P.J. (1999): The Air Pollution Model (TAPM) Version 1: Technical Description and Examples. CSIRO Atmospheric Research Technical Paper No. 43.
- Hurley, P.J. (2000): TAPM Technical Report. TAPM web page <http://www.dar.csiro.au/res/eq/Tapm/default.htm>.
- Hurley, P.J., A. Blockley, and K. Rayner (2001): Verification of a prognostic meteorological and air pollution model for year-long predictions in the Kwinana industrial region of Western Australia. *Atmos. Environ.*, **35**:1871-1880.
- Janicke, L. (1983): Particle simulation of inhomogeneous turbulent diffusion. In: Weber, B. (Ed.), Air Pollution Modeling and its Application II. Plenum Press, New York, 527-535. <http://www.janicke.de>
- Janicke, U., and L. Janicke (2001): A three-dimensional plume rise model for dry and wet plumes. *Atmos. Environ.*, **35**:877-890.
- Kaimal, J.C., Wyngaard, J.C., Haugen, D.A., Cote', O.R., Izumi, Y., Caughey, S.J. and Readings, C.J. (1976). Turbulence structure in the convective boundary layer. *J. Atmos. Sci.*, **33**, 2152-2169.
- Leahey, D.M., and M.J.E. Davies (1984): Observations of plume rise from sour gas flares. *Atmos. Environ.*, **18**:917-922.
- Loh-Nien Fan (1967): Turbulent buoyant jets into stratified or flowing ambient fluids. Technical Report No. KH-R-15, California Institute of Technology, Pasadena, CA.

- Luhar, A.K., and R.E. Britter (1992): Random walk modelling of buoyant-plume dispersion in the convective boundary layer. *Atmos. Environ.*, **26A**:1283-1298.
- Manins, P.C. (1979): Partial penetration of an elevated inversion layer by chimney plumes. *Atmos. Environ.*, **13**:733-741.
- Manins, P.C. (1985): Cloud heights and stratospheric injections resulting from a thermonuclear war. *Atmos. Environ.*, **19**, 1245–1255
- Manins, P.C., Carras J.N. and Williams D.L. (1992): Plume rise from multiple stacks. *Clean Air*, **26**, 65-68.
- McGrattan K.B., Baum H.R. and Rehm R.G. (1996) Numerical simulation of smoke plumes from large oil fire. *Atmos. Environ.*, **30**:4125-4136
- Moore, D.J. (1974): A comparison of the trajectories of rising buoyant plumes with theoretical/empirical models. *Atmos. Environ.*, **8**:441-457.
- Morton, B.R., G.I. Taylor, and J.S. Turner (1956): Turbulent gravitational convection from maintained and instantaneous sources. *Proc. Roy. Soc. London*, **A234**:1-23.
- Netterville, D.D.J. (1990): Plume rise, entrainment and dispersion in turbulent winds. *Atmos. Environ.*, **24**:1061-1081.
- Nguyen K.C., Noonan J.A., Galbally I.E. and W.L. Physick (1997) Predictions of plume dispersion in complex terrain: Eulerian versus Lagrangian Models. *Atmos. Environ.*, **31**:947-958.
- Nieuwstadt, F.T., and J.P. de Valk (1987): A large-eddy simulation of buoyant and non-buoyant plume dispersion in the atmospheric boundary layer. *Atmos. Environ.*, **21**:2573-2587.
- Nieuwstadt, F.T.M. (1992a): A Large-Eddy Simulation of a Line Source in a Convective Atmospheric Boundary Layer - I. Dispersion Characteristics. *Atmos. Environ.*, **26A**:485-495.
- Nieuwstadt, F.T.M. (1992b): A Large-Eddy Simulation of a Line Source in a Convective Atmospheric Boundary Layer - II. Dynamics of a Buoyant Line Source. *Atmos. Environ.*, **26A**:497-503.
- Ooms, G. (1972): A new method for the calculation of the plume path of gases emitted by a stack. *Atmos. Environ.*, **6**: 899–909.
- Ooms, G., A.P. Mahieu, and F. Zelis (1974): The plume path of vent gases heavier than air. *First International Symposium on Loss Prevention and Safety Promotion in the Process Industries*, The Hague, The Netherlands.
- Ooms, G., and A.P. Mahieu (1981): A comparison between a plume path model and a virtual point source model for a stack plume. *Applied Scientific Research*, **36**: 339–356.
- Overcamp T.J and Ku T. (1988): Plume rise from two or more adjacent stacks. *Atmos. Environ.*, **22**: 625–637.
- Overcamp T.J (2001): A review of the conditions leading to downwash in physical modeling experiments. *Atmos. Environ.*, **35**: 3503–3508.

- Physick, W.L. (1996) Photochemical smog studies in Australian cities. In: *Urban air pollution, volume 2*. H. Power, and N. Moussiopoulos (editors). Southhampton: Computational Mechanics Publications. p. 141–184.
- Pierce, T.E., D.B. Turner, J.A. Catalano, and F.V. Hale (1982): PTPLU – A single source gaussian dispersion algorithm. User's Guide. Technical Report PB83-211235, U.S. Environmental Protection Agency, Environmental Sciences Research Laboratory, Research Triangle Park, NC.
- Pope, S.B. (1994): On the Relationship between Stochastic Lagrangian Models of Turbulence and Second-Moment Closures. *Phys. Fluids*, **6**:973-985.
- Priestley, C.H.B. (1956): A working theory of the bent-over plume of hot gas. *Quart. J. Roy. Met. Soc.*, **82**, 165–176
- Richards J.M. (1963): The penetration of interfaces by cylindrical thermals. *Quart. J. Roy. Met. Soc.*, **89**, 254-264
- Risken, H. (1984): *The Fokker-Planck Equation*. Springer Verlag, Berlin, Heidelberg, New York.
- Sandroni, S., P. Bacci, and D. Anfossi (1981): Aircraft observations of plume emitted from elevated sources. *Atmos. Environ.*, **15**:95-100
- Sawford, B.L. (1985): Lagrangian statistical simulation of concentration mean and fluctuating fields. *J. Climate Appl. Met.*, **24**, 1152-1166
- Sawford, B.L. (1986): Generalized Random Forcing in Random-Walk Turbulent Dispersion Models. *Phys. Fluids*, **29**:3582-3585.
- Schatzmann, M. (1979): An integral model of plume rise. *Atmos. Environ.*, **13**:721-731.
- Schatzmann, M., and A.J. Policastro (1984): An advanced integral model for cooling tower plume dispersion. *Atmos. Environ.*, **18**:663-674.
- Schulman, L.L., and J.S. Scire (1980): Buoyant line point source (BLP) dispersion model user's guide. Document P-7304-B, Environmental Research & Technology, Inc., Concord, MA.
- Schulman, L.L., and S.R. Hanna (1986): Evaluation of downwash modifications to the Industrial Source Complex Model. *J. Air Pollut. Control Assoc.*, **36**:258-264.
- Schulman, L.L., D.G. Strimaitis, and J.S. Scire (1997): Addendum to ISC3 user's guide. The PRIME plume rise and building downwash model. Electric Power Research Institute. <http://www.epa.gov/scram001/>
- Schulman, L.L., D.G. Strimaitis, and J.S. Scire (2000): Development and evaluation of the PRIME plume rise and building downwash model. *J. Air Waste Manag. Assoc.*, **50**:378-390.
- Scire, J.S., and L.L. Schulmann (1980): Modeling plume rise from low-level buoyant line and point sources. Proceedings Second Point Conference on Applications of Air Pollution Meteorology, 24-28 March 1980, New Orleans, LA, 133-139.
- Scire J.S., D.G. Strimaitis, and R.J. Yamartino (1999): A User's Guide for the CALPUFF Dispersion Model (Version 5.0). Technical Report. Earth Tech. Inc., 196 Baker Avenue, 01742 Concord, MA.

- Shimanuki, A., and Y. Nomura (1991): Numerical simulation on instantaneous images of the smoke released from a chimney. *J. Met. Soc. Japan*, **69**:187-196.
- Singer I.A. and Smith M.E. (1966): Atmospheric dispersion at Brookhaven National Laboratory. *Int. J. Air Water Poll.*, **10**, 125
- Slawson, P.R., and G.T. Csanady (1967): On the mean path of buoyant, bent-over chimney plumes. *J. Fluid Mech.*, **28**:311-322.
- Slawson, P.R., and G.T. Csanady (1971): The effect of atmospheric conditions on plume rise. *J. Fluid Mech.*, **47**:33-49.
- Snyder, W.H., and R.E. Lawson Jr. (1991): Fluid modeling simulation of stack-tip downwash for neutrally buoyant plumes. *Atmos. Environ.*, **12**:2837-2850.
- Souto M.J., J.A. Souto, V. Perez-Munuzuri, J.J. Casares, and J.L. Bermudez (2001): A comparison of operational Lagrangian particle and adaptive puff models for plume dispersion forecasting. *Atmos. Environ.*, **35**:2349-2360.
- Strom, G.H. (1976): *Transport and diffusion of stack effluents*. In: Stern, A.C. (editor) Air pollution, Vol.I. Academic Press, New York, USA.
- Stuhmiller, J. (1974): Development and validation of a two-variable turbulence model. Science Applications, Inc., Report SAI-74-509-LJ, La Jolla, California.
- Sutherland, V.C., and T.C. Spangler (1980): Comparison of calculated and observed plume rise heights for scrubbed and nonscrubbed buoyant plumes. Preprints, Second Joint Conference on Applications of Air Pollution Meteorology, New Orleans, American Meteorological Society, pp. 129-132.
- Thomson, D.J. (1987): Criteria for the Selection of Stochastic Models of Particle Trajectories in Turbulent Flows. *J. Fluid Mech.*, **180**:529-556.
- Thompson, R.S., Snyder W.H. and Weil J.C. (2000): Laboratory simulation of the rise of buoyant thermals created by open detonation. *J. Fluid. Mech.*, **417**: 127-156
- Tinarelli, G., D. Anfossi, M. Bider, E. Ferrero, S. Trini Castelli (2000): A new high performance version of the Lagrangian particle dispersion model SPRAY, some case studies. Air Pollution Modelling and its Applications XIII, S.E. Gryning and E. Batchvarova eds., Kluwer Academic / Plenum Press, New York, 499-507. http://www.aria-net.it/PDF/e_spray3.pdf
- Trelles J., K.B. McGrattan, H.R. Baum (1999a): Smoke transport by sheared winds. *Combust. Theory Modelling*, **3**:323-341.
- Trelles J., K.B., McGrattan, H.R. Baum (1999b): Smoke dispersion from multiple fire plumes. *AIAA Journal*, **37**:1588-1601.
- Turner, J.S. (1973): *Buoyancy effects in fluid*. Cambridge University Press, London.
- Turner, D.B. (1985): Proposed pragmatic methods for estimating plume rise and plume penetration through atmospheric layers. *Atmos. Environ.*, **7**:1215-1218.
- Turner D.B., T. Chico and J.A. Catalano (1986) TUPOS - A multiple source gaussian dispersion algorithm using on site turbulence data. EPA Publication No. EPA - 600/8 - 86/010 U.S. Environmental Protection Agency, Research Triangle Park, North Carolina

U.S. Environmental Protection Agency (1995a): *SCREEN3 Model User's Guide*. Technical Report EPA-454/B-95-004. Research Triangle Park, NC. <http://www.epa.gov/scram001/>

U.S. Environmental Protection Agency (1995b): *User's Guide for the Industrial Source Complex (ISC3) dispersion models. Volume II – description of model algorithms*. Technical Report A-454/B-95-003b. Research Triangle Park, NC. <http://www.epa.gov/scram001/>

U.S. Environmental Protection Agency (1998): *Revised draft user's guide for the AMS/EPA regulatory model – AERMOD*. Draft 11/10/98. <http://www.epa.gov/scram001/>

Vadot L. (1965): Study of diffusion of smoke plumes into the atmosphere (in French): Centre Interprofessionnel Technique d'Etudes de la Pollution Atmosphérique, Paris

van Dop, H., F.T.M. Nieuwstadt, and J.C.R. Hunt (1985): Random Walk Models for Particle Displacements in Inhomogeneous Unsteady Turbulent Flows. *Phys. Fluids*, **28**:1639-1653.

van Dop, H. (1992): Buoyant plume rise in a Lagrangian Framework. *Atmos. Environ.*, **26A**:1335-1346.

van Haren, L., and F.T. Nieuwstadt (1989): The behaviour of passive and buoyant plumes in a convective boundary layer, as simulated with a large-eddy model. *J. Appl. Meteor.*, **28**:818-832.

Yamada (2000) Numerical simulations of airflows and tracer transport in the southwestern United States. *J. Appl. Meteor.*, **39**: 399-411.

Weil, J.C. (1974): The rise of moist, buoyant plumes. *J. Appl. Meteor.*, **13**:435-443.

Weil, J.C. (1982): Source buoyancy effects in boundary layer diffusion. *Workshop on the parameterization of mixed layer diffusion*. R. Cionco (Ed.), Physical Science Laboratory, New Mexico State University, Las Cruces NM.

Weil, J.C. (1988): Plume Rise. In: *Lectures on Air Pollution Modeling*. A. Venkatram and J.C. Wyngaard, eds. American Meteorological Society, Boston, 119-166.

Weil J.C. (1994) A hybrid Lagrangian dispersion model for elevated sources in the convective boundary layer. *Atmos. Environ.*, **28**:3433-3448.

Weil J.C., L.A. Corio, and R.P. Brower (1997). APDF dispersion model for buoyant plumes in the convective boundary layer. *J. Appl. Meteor.*, **36**, 982-1003.

Wigley, T.M., and P.R. Slawson (1975): The effect of atmospheric conditions on the length of visible cooling tower plumes. *Atmos. Environ.*, **9**:437-445.

Willis G. and J. Deardorff (1983): On plume rise within a convective boundary layer. *Atmos. Environ.*, **17**:2435-2447.

Willis G. and J. Deardorff (1987). Buoyant plume dispersion and entrainment in and above a laboratory mixed layer, *Atmos. Environ.*, **21**:1725-1735.

Zannetti, P., and N. Al-Madani (1983): Numerical simulations of Lagrangian particle diffusion by Monte-Carlo techniques. VIth World Congress on Air Quality (IUAPPA), Paris, France, May 1983.

Zannetti, P., and N. Al-Madani (1984): Simulation of transformation, buoyancy and removal processes by Lagrangian particle methods. Proceedings of the 14th International Technical Meeting on Air Pollution Modelling and its Application (ed. Ch. de Wispelaere) Plenum Press, New York, 733-744.

Zannetti, P. (1990): *Air pollution modeling: theories, computational methods and available software*. Computational Mechanics Publications. Van Nostrand Reinhold, New York.

Zhang, X., and A.F.A. Ghoniem (1993): Computational Model for the Rise and Dispersion of Wind-Blown, Buoyancy Driven Plumes - I. Neutrally Stratified Atmosphere. *Atmos. Environ.*, **27A**:2295-2311.

Zhang, X., and A.F.A. Ghoniem (1994a): Computational Model for the Rise and Dispersion of Wind-Blown, Buoyancy Driven Plumes - II. Linearly Stratified Atmosphere. *Atmos. Environ.*, **28**:3005-3018.

Zhang, X., and A.F.A. Ghoniem (1994b): Computational Model for the Rise and Dispersion of Wind-Blown, Buoyancy Driven Plumes - III. Penetration of Atmospheric Inversion. *Atmos. Environ.*, **28**:3019-3032.

Chapter 7

Gaussian Plume Models

Gaussian plume models are the most frequently used air pollution models. In particular, the large majority of models used for regulatory applications throughout the world are based on the Gaussian plume model equation. An introduction to this topic is presented in Chapter 7A below. Future volumes in this book series will provide additional material.

The reader can examine additional information at:

- <http://www.rpi.edu/dept/chem-eng/Biotech-Environ/SYSTEMS/plume/gaussian.html> (general)
- <http://www.epa.gov/scram001/userg/regmod/isc3v2.pdf> (ISC3)
- http://www.epa.gov/scram001/7thconf/aermod/aermod_mfd.pdf (AERMOD)

BRANK
P
2000

Venkatram, A. and J. Thé (2003) *Introduction to Gaussian Plume Models*. Chapter 7A of *AIR QUALITY MODELING - Theories, Methodologies, Computational Techniques, and Available Databases and Software. Vol. I - Fundamentals* (P. Zannetti, Editor). Published by The EnviroComp Institute (<http://www.envirocomp.org/>) and the Air & Waste Management Association (<http://www.awma.org/>).

Chapter 7A

Introduction to Gaussian Plume Models

Akula Venkatram ⁽¹⁾ and Jesse Thé ⁽²⁾

⁽¹⁾ *College of Engineering, University of California, Riverside, CA 92521-0425, USA*

venky@engr.ucr.edu

⁽²⁾ *Lakes Environmental Software & University of Waterloo – Ontario, Canada*
Jesse@WebLakes.com

Abstract: This section describes the development of models used for regulatory applications at scales of the order of ten kilometers. These models are important because they are used extensively to permit industrial sources and assess risk associated with toxic releases in urban areas. AERMOD and ISC are examples of such models. The foundation of these models is the steady-state plume model that assumes that the concentration distributions normal to the direction of the mean flow are Gaussian.

We first discuss the structure of the Gaussian dispersion model as applied to a point source, and then show how this formulation can be used to estimate impact of other types of sources, such as line and area sources. The realism of models for plume spread determines the usefulness of the Gaussian dispersion model. Plume spread, in turn, depends on atmospheric turbulence. Thus, this section provides a brief description of the atmospheric boundary layer before describing models for plume spread.

We describe different approaches to modeling plume spread of surface and elevated releases in the boundary layer. We then show how the Gaussian dispersion model can be modified to incorporate the effects of buildings and complex terrain on dispersion. The section compares the Gaussian approach to other methods being used to model dispersion. We provide a brief description of one such method, the probability density function method that is currently being used in models of dispersion in the convective boundary layer. The section concludes by emphasizing the usefulness of the Gaussian framework in developing dispersion models for a variety of real world situations.

Keywords: Air pollution, air quality, air pollution model, AERMOD, ISC, dispersion, building effects. Gaussian dispersion model, regulatory model, atmospheric boundary layer, complex terrain dispersion, convective boundary layer, stable boundary layer.

1 Introduction

Air pollution models play an important role in the implementation of air pollution regulations. For example, before an industrial plant can be constructed, its impact on air quality is determined through an air pollution model to show that emissions from the plant do not lead to ambient concentrations that are above a regulated level. In the United States, the Industrial Source Complex (ISC) model is used to make such permitting decisions. U.S. regulations that govern air toxics recommend the use of the ISC model to quantify risk associated with emissions of toxic chemicals in urban areas. Air pollution models that include chemistry are used to make decisions to control emissions that are precursors of ozone and acidifying pollutants. Such decisions can have multimillion-dollar implications associated with installing equipment to reduce emissions, or delaying or even disallowing the construction of the industry responsible for the emissions.

This chapter examines air pollution models applicable to scales of the order of tens of kilometers. The effects of chemistry are assumed to be negligible at these scales, although this might not be always true. These models assume are commonly referred to as Gaussian models because they assume that the concentration distributions in the vertical and the horizontal are described by the Gaussian function.

The chapter also provides the background necessary to understand the approach used in the formulation of such models. This includes the essentials of the micrometeorology used to construct the inputs for the model.

2 The Point Source in the Atmospheric Boundary Layer

Most short-range dispersion models are based on the assumption that meteorological conditions are spatially homogeneous and vary little with time during the period of interest, which is typically one hour. This is equivalent to saying that the time scale governing the variation in meteorology is greater than the time of travel between source and receptor. If the meteorological time scale is one hour, and the wind speed is 5 m/s, the assumption of steady state is not likely to be valid for distances much greater than 10 km. At lower wind speeds, the “valid” distances become smaller. In spite of these limitations, steady state plume models are often applied beyond their range of applicability with the justification that the concentration at the receptor is representative of that when the plume eventually reaches the receptor. In principle, dispersion during unsteady and spatially varying conditions can be treated with puff or particle models, which

attempt to model the dispersion of puffs or particles as the unsteady wind field carries them along their trajectories. This paper will not discuss models based on puff dispersion.

Models such as ISC and AERMOD are based on the steady state Gaussian dispersion equation. If the release point is taken to be the origin ($z=0$), with the x -axis of the co-ordinate system aligned along the wind direction at the source, the time averaged (typically one hour) concentration field can be described in terms of the Gaussian distribution (See Figure 1):

$$C(x, y, z) = \frac{Q}{2\pi\sigma_y\sigma_zU} \exp\left[-\frac{z^2}{2\sigma_z^2} - \frac{y^2}{2\sigma_y^2}\right], \quad (1)$$

where y is the cross-wind co-ordinate, Q is the source strength (mass/time), U is the time-averaged wind speed at source height, and σ_y and σ_z are the plume spreads normal to the mean wind direction. Equation (1) can be “derived” from the mass conservation equation after making assumptions about turbulent transport. Because these assumptions cannot be readily justified, it is just as valid to simply postulate Equation (1) as an empirical description of observations.

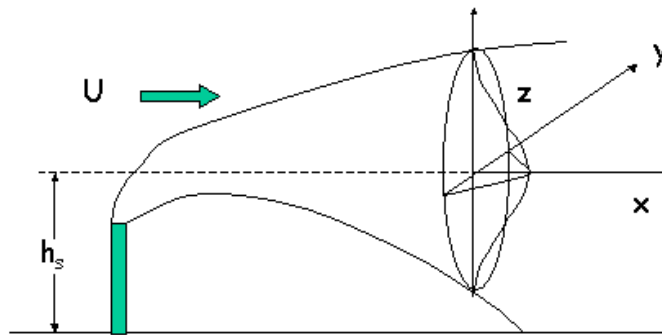


Figure 1. Gaussian distribution used to model plume from point source. For the time being, we have ignored the effects of the impermeable ground on the concentration field. Equation (1) assumes that along-wind dispersion is much smaller than transport by the mean wind. This assumption breaks down when the mean wind is comparable to the turbulent velocity along the wind, σ_u . The form of the dispersion model under such low wind speed conditions is discussed in a later section.

The effect of the ground on concentrations is accounted for by making sure that there is no flux of material through the ground, which we now take to be $z=0$. The mathematical trick to achieve this is to place an “image” source at a distance $z = -h_s$, where h_s is the height of the source above ground. The upward flux from this image source essentially cancels out the downward flux from the real source without affecting the mass balance. Then, the concentration becomes

$$C(x, y, z) = \frac{Q}{2\pi\sigma_y\sigma_z U} \exp\left[-\frac{y^2}{2\sigma_y^2}\right] \left\{ \exp\left[-\frac{(z-h_s)^2}{2\sigma_z^2}\right] + \exp\left[-\frac{(z+h_s)^2}{2\sigma_z^2}\right] \right\} \quad (2)$$

In the real atmosphere, dispersion in the upward direction is limited by the height of the atmospheric boundary layer. This limitation of vertical mixing is incorporated into the Gaussian formulation by “reflecting” material off the top of the mixed layer. Then, Equation (2) can be modified to account for the infinite set of “reflections” from the ground and the top of the mixed layer. When the pollutant is well mixed through the depth of the boundary layer, z_i , the expression for the concentration becomes:

$$C(x, y) = \frac{Q}{\sqrt{2\pi}\sigma_y z_i} \exp\left(-\frac{y^2}{2\sigma_y^2}\right) \quad (3)$$

The Gaussian formulation for a point source can be used to model both volume as well as point sources because each of these source types can be discretized into point sources; the associated concentrations are simply the sums of the contributions from these point sources.

In applying Equation (2) to model line or volume sources, it is important to make sure that the x co-ordinate system is aligned along the mean wind direction. Specifically, if (X_r, Y_r) and (X_s, Y_s) are the co-ordinates of the receptor and the source in an arbitrary co-ordinate system, and θ is the angle that the mean wind velocity vector makes with x -axis, then the co-ordinates used in the Gaussian equation are given by (See Figure 2)

$$\begin{aligned} x &= X \cos \theta + Y \sin \theta \\ y &= X \sin \theta - Y \cos \theta \end{aligned} \quad (4)$$

where

$$\begin{aligned} X &= X_r - X_s \\ Y &= Y_r - Y_s \end{aligned} \quad (5)$$

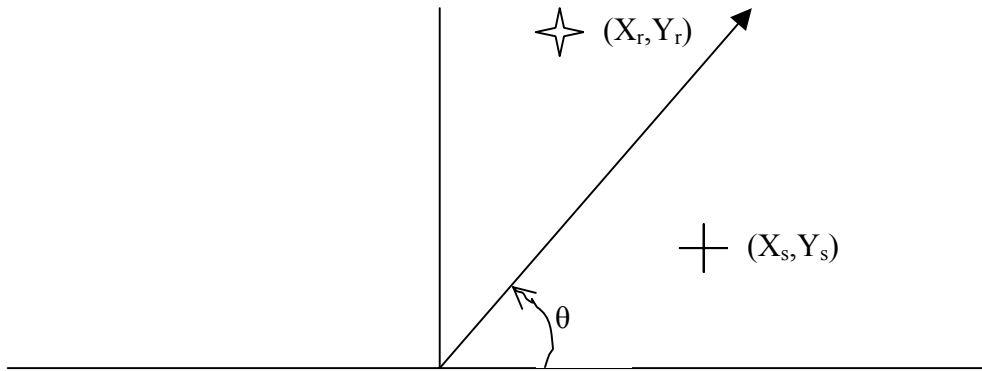


Figure 2. Co-ordinate system to derive Equations (4) and (5). θ is the angle that the mean wind velocity vector makes with x-axis.

Consider modeling dispersion from a ground-level line source such as freeway. If we align the line source along the Y axis, and the emission rate per unit length of the line source is q , the expression for the concentration associated with an elemental length dY_s becomes

$$dC(X_r, Y_r) = \frac{qdY_s}{\pi U \sigma_y \sigma_z} \exp\left(-\frac{y^2}{2\sigma_y^2}\right) \exp\left(-\frac{z^2}{2\sigma_z^2}\right), \quad (6)$$

where the lower case symbols refer to the co-ordinate system with the x-axis along the mean wind.

Then, the concentration associated with a line-source between Y_1 and Y_2 becomes

$$C(X_r, Y_r) = \int_{Y_1}^{Y_2} \frac{qdY_s}{\pi U \sigma_y \sigma_z} \exp\left(-\frac{y^2}{2\sigma_y^2}\right) \exp\left(-\frac{z^2}{2\sigma_z^2}\right) \quad (7)$$

The expression assumes a simple form if the mean wind is perpendicular to the road ($\theta=0^\circ$) and the line source is infinitely long (this is a good approximation if a receptor is close to the line source)

$$C(X_r, Y_r) = \sqrt{\frac{2}{\pi}} \frac{q}{U \sigma_z} \exp\left(-\frac{z^2}{2\sigma_z^2}\right) \quad (8)$$

where the plume spread, σ_z , is evaluated at $x=X_r$. If the wind blows at a “small” angle, θ , to the X axis, we can still use Equation (8) by replacing U by $U \cos \theta$, and evaluating vertical plume spread at $X_r / \cos \theta$. But this only an approximation that

breaks down when θ exceeds the smaller of the angles formed by joining the ends of the line source to the receptor in question.

Models for the plume spread parameters, σ_y , and σ_z determine the usefulness of the concentration estimates from the Gaussian model. Most of the currently used regulatory dispersion models, such as ISC, use expressions derived empirically from field experiments. The new generation of regulatory dispersion models, such as AERMOD (Cimorelli et al., 2002), estimate dispersion using information, measured or modeled, on the mean and turbulent structure of the atmospheric boundary layer. The next section on the atmospheric boundary provides the background necessary to understand the formulation of these dispersion curves, described in section 4.

3 The Atmospheric Boundary Layer

Turbulence in the atmospheric boundary layer is generated by wind shear and buoyancy associated with radiative heating at the ground. During the daytime, sensible heating at the surface results in parcels of air that are warmer, and hence less dense than their surroundings. These parcels are subject to buoyancy forces that accelerate them upwards. The mixing induced by these moving parcels gives rise to the boundary layer or mixed layer, whose growth is inhibited by a layer in which the rising parcels are denser than their surroundings. This layer, referred to as an inversion, is characterized by increasing temperature with height. This inversion usually develops when there is large-scale downward motion or subsidence of the air. It can be shown that at heights below about a tenth of the mixed layer height, z_i , buoyancy generates turbulent velocities given by:

$$\sigma_w = 1.3u_f; z \leq 0.1z_i \quad (9)$$

where the free convection velocity scale, u_f is defined by:

$$u_f = \left(\frac{g}{T_s} Q_o z \right)^{1/3} \quad (10)$$

In Equation (9), Q_o is the surface kinematic heat flux, which is the sensible heat flux (Watts/m^2) divided by the product of the density and the specific heat of air, and T_s is the surface temperature in degrees Kelvin. The heat flux, Q_o , is taken to be positive when it is directed away from ground and into the atmosphere as during the daytime, and is negative when it is into the ground as during most nights.

Between $0.1z_i$ and close to the top of the mixed layer, σ_w associated with buoyancy production of turbulence is proportional to the convective velocity scale given by

$$w_* = \left(\frac{g}{T_s} Q_o z_i \right)^{1/3} \quad (11)$$

where z_i is the mixed layer height. In this region, we find that

$$\sigma_w = \sigma_v = \sigma_u \cong 0.6w_* \quad (12)$$

It is found that σ_u and σ_v are also proportional to w_* , even below $0.1z_i$.

Where turbulence production is dominated by wind shear, σ_w close to the ground is roughly proportional to the surface friction velocity, u_*

$$\sigma_w = 1.3u_* \quad (13)$$

where u_* is related to the shear stress at the ground, τ_o , through

$$u_* = \sqrt{\frac{\tau_o}{\rho_a}} \quad (14)$$

where ρ_a is the density of air. The absolute value of the Monin-Obukhov length, L , is roughly the height at which the turbulent velocity generated by buoyancy is equal to that produced by shear,

$$L = -\frac{T_s u_*^3}{gkQ_o} \quad (15)$$

where the Von Karman constant $k=0.4$.

Thus, shear production of turbulence dominates that by buoyancy at heights below the Monin-Obukhov length. L is usually negative during the daytime when the heat flux is into the atmospheric boundary layer, and positive during nighttime when the heat flux is directed towards the ground.

In describing the structure of the atmospheric boundary layer, it is convenient to define a potential temperature at given height with temperature T , and pressure, p ,

$$\theta = T \left(\frac{p_0}{p} \right)^{\frac{R_a}{C_p}} \quad (16)$$

where $p_0=1000$ mb is a reference pressure, R_a is the gas constant, and C_p is the specific heat of air. The potential temperature, θ , represents the temperature that a parcel with temperature, T , would acquire if it is moved adiabatically from p to p_0 .

The potential temperature definition allows us to make statements about the stability of a parcel of air when it is displaced adiabatically without worrying about the effects of pressure changes in the atmosphere. It can be shown that a parcel resists vertical motion in an atmosphere in which the potential temperature increases with height; it is in stable equilibrium. A decreasing potential temperature denotes an unstable atmosphere, while a potential temperature that is constant with height characterizes an atmosphere that is neutral to parcel motion.

In the daytime boundary layer, the potential temperature decreases with height near the surface. Above a tenth of the mixed layer height, the potential temperature and the horizontal velocity are relatively uniform because of vigorous vertical mixing. The mixed layer is usually capped by a sharp temperature inversion, and the velocity can also change rapidly across the inversion.

When the sun sets, turbulence energy production by buoyancy ceases. Over a period of an hour, the turbulence in the mixed layer collapses, and shear becomes the primary mechanism for the production of turbulence. Because the ground is initially warmer than the atmosphere, the thermal radiation leaving the ground exceeds that being supplied by the atmosphere. This deficit leads to a cooling of the ground.

Initially, both the sensible heat flux and the ground heat flux are directed away from the earth's surface. The surface cools rapidly, and a point is reached at which the ground becomes colder than the layers above in the atmosphere. At this stage, the heat flux from the atmosphere is directed towards the earth's surface, and the surface boundary layer becomes stable with the potential temperature increasing with height.

The stable potential temperature gradient in the nighttime boundary layer suppresses the production of turbulence because it opposes vertical motion. Under these circumstances, shear production of turbulence is matched by the destruction associated with the stable temperature gradient and viscous dissipation. This balance between these processes of production and destruction leads to relatively small levels of turbulence in the nocturnal boundary layer. We know that turbulence levels in the stable boundary layer are of the order of the surface friction velocity. However, estimating the height of the stable boundary

layer or the variation of turbulence levels with height is an uncertain exercise. The horizontal turbulent velocities in the stable boundary layer do not appear to be related to micrometeorological variables. They are affected by mesoscale flows and local topography, which are difficult to characterize using models.

The next section describes how regulatory models use information on the turbulent and mean flow fields in the atmospheric boundary layer to estimate plume spreads.

4 Dispersion in the Atmospheric Boundary Layer

ISC uses plume spread formulations based on those derived empirically by Pasquill (1961) in the 1960s from observations made during the Prairie Grass dispersion experiment conducted in Nebraska in 1956 (Barad, 1958). These formulations were modified subsequently by Gifford and Turner, and are commonly referred to as the Pasquill-Gifford-Turner (PGT) curves. For dispersion in urban areas, ISC uses the McElroy-Pooler curves that are derived from experiments conducted in St. Louis, Missouri (McElroy and Pooler, 1968).

The dispersion curves are keyed to stability classes that are related to ranges in the wind speed and incoming solar radiation. The wind speed, measured at 10 m, is an indicator of turbulence produced by shear, while the incoming solar radiation is a surrogate for the sensible heat flux, which generates turbulence. Thus, the stability classes contain information on shear and buoyancy produced turbulence.

Classes A, B, and C correspond to unstable conditions when buoyancy production of turbulence adds to that due to shear. The sensible heat flux under these conditions is upward. Class A, the most unstable, is associated with the most rapid dispersion rates; the plume sigmas for a given distance decrease as we go from class A to C. Class D corresponds to neutral conditions when turbulence production is dominated by shear. Classes E and F are associated with stable conditions. Class F corresponds to the lowest dispersion rates. The dispersion curves are only functions of distance from the source, and can be cast into the form

$$\sigma_z = ax^b \quad (17)$$

where the coefficients “a” and “b” generally increase as the stability classes range from E to A. Thus, 6 dispersion curves are used to describe the entire range of possible dispersion conditions.

The major advantage of the PGT curves is that they are based on observations, and thus provide realistic concentration estimates under a variety of

meteorological conditions. Their shortcoming is that they are derived from dispersion of surface releases, and are thus not applicable to elevated releases. Furthermore, their formulation does not allow the use of on-site turbulence levels to describe dispersion more accurately than the “broad brush” PGT curves.

In the more recently formulated models (Weil, 1985), such as AERMOD, the expressions for plume spread are based on theoretical analysis first proposed by Taylor (1921). His equation describes the variance of particle positions as a function of travel time from a fixed point of release in a flow that is steady and the turbulence statistics do not depend on location. Rather than present all of his analysis, we will highlight the major results using the asymptotic behavior of the plume spread (Csanady, 1973),

$$\begin{aligned}\sigma_y &= \sigma_v \tau \quad \text{for } \tau \ll T_{Lv} \\ \sigma_y &= \sigma_v (2\tau T_{Lv})^{1/2} \quad \text{for } \tau \gg T_{Lv}\end{aligned}\tag{18}$$

where τ is the travel time from the source, given by

$$\tau = \frac{x}{U}\tag{19}$$

and σ_v is the standard deviation of the horizontal turbulent velocity fluctuations. A similar expression applies to the vertical spread of the plume.

In Equation (18), T_{Lv} is the Lagrangian time scale, which can be formally defined in terms of the statistics of the turbulent flow. For our purposes, it is sufficient to interpret the time scale as roughly the time over which a particle retains its initial velocity. For small travel times, a particle’s velocity remains essentially unchanged from its value at the release point, and the particle trajectory is a straight line. This explains the result that, for small travel times, the spread of particles is proportional to the travel time from the source (Equation (18)). On the other hand, when the travel time is large compared to the Lagrangian time scale, the plume spread is proportional to the product of the “average” step size, $\sigma_v T_{Lv}$, and the square root of the number of steps, τ/T_{Lv} , taken by the particle.

The new generation of dispersion models, such as AERMOD, relates dispersion to atmospheric turbulence using the theoretical framework described earlier. The problem in doing so is that the theory applies to a boundary layer in which the mean and turbulent properties are constant in space and time. To apply it to a real boundary layer in which the properties are highly inhomogeneous, we can use one of two approaches. The first is to average the turbulence and mean properties over the region of interest, and use the average properties in the (homogeneous) formulations discussed earlier. This is not as straightforward as it seems because the limits of the average requires an estimate of the plume dimensions, which in

turn depends on the average properties. Furthermore, the averaging procedure is necessarily arbitrary. The validity of the method needs to be established by comparing the results obtained from the formulations with observations or theory that accounts for inhomogeneity more explicitly. In general, empirical knowledge derived from observations plays a major role in the development of practical models of dispersion. As in most turbulence research, theory can suggest plausible forms for a dispersion model, but the model almost always contains parameters that have to be estimated from observations.

Even if we could treat the boundary layer as vertically homogeneous, the presence of boundaries, such as the ground and the top of the mixed layer, makes it difficult to estimate the Lagrangian time scale, T_{Lv} , from a priori considerations. Thus, the time-scale is often treated as an empirical parameter that is derived by fitting plume spread expressions to observations. Let us illustrate this by using an expression that is often used to describe plume spread

$$\sigma_y = \frac{\sigma_v \tau}{(1 + \tau/2T_{Lv})^{1/2}} \quad (20)$$

Note that Equation (20) satisfies the asymptotic limits given by Equation (18). We then postulate an expression for T_{Lv} in terms of a length scale l as follows

$$T_{Lv} = \frac{l}{\sigma_v} \quad (21)$$

The length scale is taken to be proportional to a length characterizing the eddies responsible for transport, and the constant of proportionality is obtained by fitting estimates of plume spread from Equation (20) to observations. In AERMOD, the vertical spread for elevated releases in the stable boundary layer is given by an expression similar to Equation (20).

The second approach to accounting for inhomogeneity in the boundary layer is based on the solution of the species conservation equation

$$\frac{\partial C}{\partial t} + \frac{\partial}{\partial x_i} (U_i C) = \frac{\partial}{\partial x_i} \left(K^i \frac{\partial C}{\partial x_i} \right) \quad (22)$$

where K^i is the so-called eddy diffusivity, and the superscript negates the summation convention. The eddy diffusivity is defined as the ratio of the turbulent mass flux to the local mean concentration gradient. The concept, which is based on an analogy with molecular transport, cannot be justified rigorously for turbulent transport. However, it has heuristic value, and is useful for developing semi-empirical models of turbulent transport.

It can be shown that the eddy diffusivity concept is most applicable when the scale of concentration variation, the plume spread, is larger than the scale of the eddies responsible for plume spreading. In the surface boundary layer, plume spread in the vertical direction is comparable to the length scale of the eddies responsible for vertical transport. It turns out that the eddy diffusivity concept is useful in the surface boundary layer, where semi-empirical theories, referred to as Monin-Obukhov similarity, provide useful relationships between velocity and temperature gradients and the corresponding heat and momentum fluxes. These relationships can be used to derive eddy diffusivities for heat and momentum, which can be used to describe dispersion by evaluating them at some fraction of the plume height.

Existing regulatory models for short-range dispersion do not use the eddy diffusivity based mass conservation equation to avoid the associated numerical effort and to make the most efficient use of observations of plume spread. However, the eddy diffusivity concept can be useful in deriving expressions for plume spread in the inhomogeneous surface layer. For example, AERMOD's expressions for plume spread are based on this approach (Venkatram, 1992):

$$\begin{aligned}
 \sigma_z &= \sqrt{\frac{2}{\pi}} \frac{u_* L}{U} \bar{x}; \text{ for } \bar{x} \leq 1.4 \\
 &= \sqrt{\frac{2}{\pi}} \frac{u_* L}{U} 1.12 \bar{x}^{2/3}; \text{ for } \bar{x} > 1.4, L > 0 \\
 &= \sqrt{\frac{2}{\pi}} \frac{u_* |L|}{U} \frac{\bar{x}}{(1 + 0.006 \bar{x}^2)^{-1/2}}; \text{ for } L < 0
 \end{aligned}
 \tag{23}$$

where $\bar{x} = x/|L|$, and the wind speed U corresponds to an average over the surface layer. In practice, the ground-level concentration is insensitive to the choice of U , because the dilution is determined by the combination $\sigma_z U$. These expressions provide a good description of the cross-wind integrated concentrations observed during the Prairie Grass experiment (see Van Ulden, 1978 for a listing of the data).

In AERMOD, the horizontal spread, σ_y , is based on an equation similar to Equation (20). The Lagrangian time scale was derived by fitting the equation to observations of plume spread from the Prairie Grass experiment.

In order to use the Gaussian dispersion model, we need estimates of plume rise, which is treated in Chapter 9. Dispersion and plume rise are also affected by the presence of buildings in the vicinity of the source. This is treated in the next section.

5 Building Downwash

Buildings and other structures near a relatively short stack can have a substantial effect on plume transport and dispersion, and on the resulting ground-level concentrations that are observed. The “rule of thumb” is that a stack should be at least 2.5 times the height of adjacent buildings to avoid the effects of the buildings. Much of what is known of the effects of buildings on plume transport and diffusion has been obtained from wind tunnel studies and field studies.

When the airflow meets a building (or other obstruction), it is forced up and over the building. On the lee side of the building, the flow separates, leaving a closed circulation containing lower wind speeds (see Figure 3). Farther downwind, the air flows downward again. In addition, there is more shear and, as a result, more turbulence. This is the turbulent wake zone.

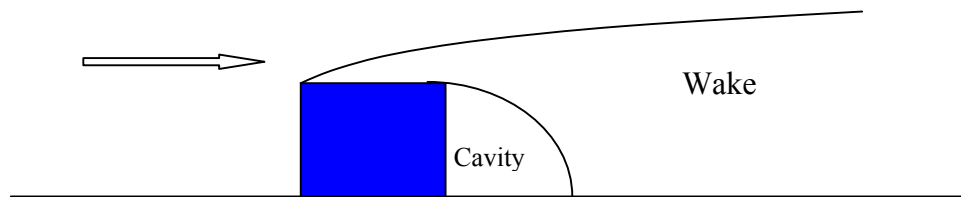


Figure 3. Formation of cavity and wake behind building.

If a plume gets caught in the cavity, concentrations next to the building can be relatively high. If the plume escapes the cavity, but remains in the turbulent wake, it may be carried downward and dispersed more rapidly by the turbulence. This can result in either higher or lower concentrations than would occur without the building, depending on whether the reduced height or increased turbulent diffusion has the greater effect. The height to which the turbulent wake has a significant effect on the plume is generally considered to be about the building height plus 1.5 times the lesser of the building height or width. This results in a height of 2.5 building heights for cubic or squat buildings, and less for tall, slender buildings. Since it is considered good engineering practice to build stacks taller than adjacent buildings by this amount, this height is called the “good engineering practice” (GEP) stack height.

Most treatments of building effects on dispersion are based on incorporating two effects: 1) the effective reduction of source height associated with the trapping of pollutants in the cavity, and 2) the increased turbulence in the building wake. If the emissions are entrained into the cavity, the source is assumed to be at ground-level, but the plume is assigned initial values to account for the fact that the emissions originate from a cavity whose size scales with the dimensions of the building. For example, the initial spreads of the plume can be taken to be

$$\begin{aligned}\sigma_{y_0} &= \alpha w \\ \sigma_{z_0} &= \beta h\end{aligned}\tag{24}$$

where w and h are the width and height of the building, and α and β are constants. Alternatively, these initial spreads can be modeled in terms of a “virtual” source at ground-level at an upwind distance that results in these spreads. For example, the upwind distance of the location of the virtual source resulting in the initial horizontal spread can be calculated from

$$\sigma_{y_0} = ax_0^b\tag{25}$$

where the coefficients, a and b , correspond to atmospheric stability of the incoming flow. This virtual distance x_0 is added to the source-receptor distance used to estimate horizontal spread.

The fraction of the emissions that is entrained into the building cavity is taken to be a function of the stack height, and the building height. The fraction that is not entrained into the cavity is treated as a conventional point source, except that plume dispersion is enhanced to account for the increased turbulence levels in the building cavity. The concentration at a downwind receptor is then a sum of the concentrations from the elevated source and the ground-level source, corresponding to the emissions from the cavity. Current models use approaches based on these ideas.

In the original version of the U.S. EPA ISC (Industrial Source Complex) Model (Bowers, et al., 1979), building downwash calculations were included for any stack within five times the lesser of the height or the width (the so-called “5L” rule) of building and less than GEP based on the same building (Huber and Snyder, 1982). Calculations were made assuming the stack was located at the highest point of the deflected flow, essentially at the lee edge of the building, and using the maximum projected width (of all wind directions). This was essentially the worst-case location of the stack, regardless of where the stack really was located in relation to the building, and the worst-case wind direction, regardless of the actual wind direction. In addition, the full effect of the building wake on plume dispersion was used, even when the plume had risen above the top of the wake region.

The ISC model was modified around 1986 to incorporate an approach developed by Schulman and Scire (1980). As implemented in the model, the Schulman-Scire downwash algorithm was used for stack heights less than 1.5 building heights, while the older Huber-Snyder approach was retained for the higher stack. The most apparent change implemented by this approach is that the amount of building downwash would change with wind direction, thus allowing for the effects of the change in building profile with different wind directions. The Schulman-Scire downwash algorithm also accounts for reduced plume rise due to

initial plume dilution that results from building downwash. Thirdly, this algorithm calculates a reduced effect of downwash on a plume that has risen higher, and is exposed to less downwash-induced turbulence.

As implemented in the ISCST3 modeling system, a determination is made as to whether building downwash due to a particular building affects the plume from a stack based on wind direction. This is calculated on an objective basis by a preprocessor program called BPIP (Building Profile Input Program), which is a part of the ISCST3 system. When more than one building, or more than one tier on a building, may affect the plume, BPIP also calculates which building or tier dominates, and provides the ISCST3 model with building height and projected width for the appropriate building or tier for each wind direction. More details on the treatment of building wake effects in ISCST3 can be found in U.S. EPA (1995a) and U.S. EPA (1995b).

The inclusion of the PRIME algorithm (Schulman, et al., 2000) to compute building downwash has produced more accurate results in air dispersion models. Unlike the earlier algorithms used in ISC3, the PRIME accounts for a) the location of the stack relative to the building, b) the deflection of streamlines up over the building and down the other side, c) the effects of the wind profile at the plume location for calculating plume rise, d) pollutants captured in the recirculation cavity to be transported to the far wake downwind (this is ignored in the earlier algorithms), and e) discontinuities in the treatment of different stack heights, which were a problem in the earlier algorithms. Details of the PRIME algorithm are given in Schulman, et al. (2000).

6 Terrain Treatment

Several complicated processes govern dispersion in complex terrain. Under unstable conditions, the plume is depressed towards the surface of the obstacle as it goes over it. The implied compression of the streamlines is associated with a speed-up of the flow and an amplification of vertical turbulence. Under stable conditions, part of the flow flowing towards an obstacle tends to remain horizontal, while the other part climbs over the hill. Experiments show (Snyder *et al.*, 1983) that this tendency for the flow to remain horizontal can be described using the concept of the dividing streamline height, denoted by H_c . Below this height, the fluid does not have enough kinetic energy to surmount the top of the hill; a plume embedded in the flow below H_c either impacts on the hill or goes around it. On the other hand, the flow and hence the plume above H_c can climb over the hill. Terrain features can rise toward the plume, deflecting its flow over or around, or allowing the plume to come in contact with the terrain. In convective (unstable) conditions, the airflow, and thus the plume, will be forced over the terrain obstacle. On the lee side of the obstacle, a wake or cavity may

occur in the flow, resulting in high concentrations on that side of the terrain feature.

The alignment of ridges and valleys can channel the flow. This can result in high concentrations appearing in areas quite different than would be expected if this effect were not accounted for. The presence of hills and valleys can also help to create local wind flows. These flows may alter the transport of low-level plumes. Modeling these flows using wind data from above or distant from the site may result in incorrect modeling results. Conversely, wind measurements that are influenced by these local flows, if used to model a tall stack source that emits above the local flow, can also result in incorrect modeling results. One example is the case of a narrow valley with a north to south orientation. In the morning, the sun will first heat the west wall of the valley. This warmer air will rise, creating a cross-valley flow from east to west (in the absence of strong winds aloft). Conversely, in the evening, the east wall will be heated more, resulting in a cross-valley flow from the west.

Accounting for these effects in air quality models presents a significant challenge. The effects cannot be ignored in regulatory modeling, since terrain effects generally contribute to higher concentrations than would be observed in flat terrain situations. On the other hand, representing terrain effects accurately may require the use of computational fluid dynamics models, or other modeling approaches that require extensive computer resources, and are difficult and time-consuming to use.

6.1 Approaches Taken in Short-Range Models

Early attempts to incorporate terrain heights into regulatory air quality models were to simply subtract the terrain elevation above the source from the calculated plume height, an approach used in the ISCST2 model (USEPA, 1992). Since, in reality, the plume will be deflected along with the wind, this modeling approach often results in severe over predictions of concentrations. In response to this problem, some fairly simple complex terrain screening models were developed, including the use of a “half-height correction,” and modified plume impact.

The “half-height” correction assumed that the plume height in terrain (usually under stable conditions, i.e., P-G stabilities E and F, although some models use it for neutral and unstable cases as well) would rise at half the rate as the terrain would rise between the source and receptor. While the theoretical basis for this approach is weak, it prevents the direct impact of plume centerline on the terrain feature, giving concentration estimates that are, at least, appear to be more reasonable.

The COMPLEX-I model (U.S. EPA, 1995) uses this same formulation for P-G stabilities E and F, at any wind speed, and a half-height terrain adjustment for P-G stabilities A through D. For regulatory applications, the EPA initially allowed the

use of COMPLEX-I in combination with ISCST2. For each hour and source-receptor combination, when the terrain was below *stack* height, called “simple terrain,” ISCST2 would be used; when the terrain was above *plume* height, called “complex terrain,” COMPLEX-I would be used; and between the two, called “intermediate terrain,” both would be used and the larger of the two calculated concentrations selected. This was a complicated approach, which was best implemented in a computer code.

The Complex Terrain Dispersion Model (CTDMPLUS, Perry, 1992) accounts for the major effects associated with the concept of the dividing streamline height described in the previous section. AERMOD incorporates a semi-empirical model (Venkatram *et al.*, 2001) that mimics the major features of CTDM. It assumes that the concentration at a receptor, located at a position (x, y, z) , is a weighted combination of two concentration estimates: one assumes that the plume is horizontal, and the other assumes that the plume climbs over the hill.

The concentration associated with the horizontal plume dominates during stable conditions, while that caused by the terrain-following plume is more important during unstable conditions. These assumptions allow us to write the concentration, $C(x, y, z)$, as

$$C(x, y, z) = fC_f(x, y, z) + (1 - f)C_f(x, y, z_e) \quad (26)$$

The first term on the right-hand side of Equation (26) represents the contribution of the horizontal plume, while the second term is the contribution of the terrain-following plume. The concentration, $C_f(x, y, z)$, is that associated with a plume unaffected by the terrain; the plume axis remains horizontal. In the first term, $C_f(x, y, z)$ is evaluated at the receptor height, z , to simulate a horizontal plume. In the second term, the concentration is evaluated at the height of the receptor above local terrain, z_e , to simulate the plume following the terrain contour.

The weighting factor, f , is a function of the fraction of the plume above the dividing streamline height. When the entire plume lies below H_c , f goes to unity, and the concentration corresponds to a plume that does not see the hill. When the dividing streamline height goes to zero under unstable conditions, f becomes $1/2$. This means, that under unstable conditions, the concentration at an elevated receptor is the average of the contributions from the horizontal plume and the terrain-following plume.

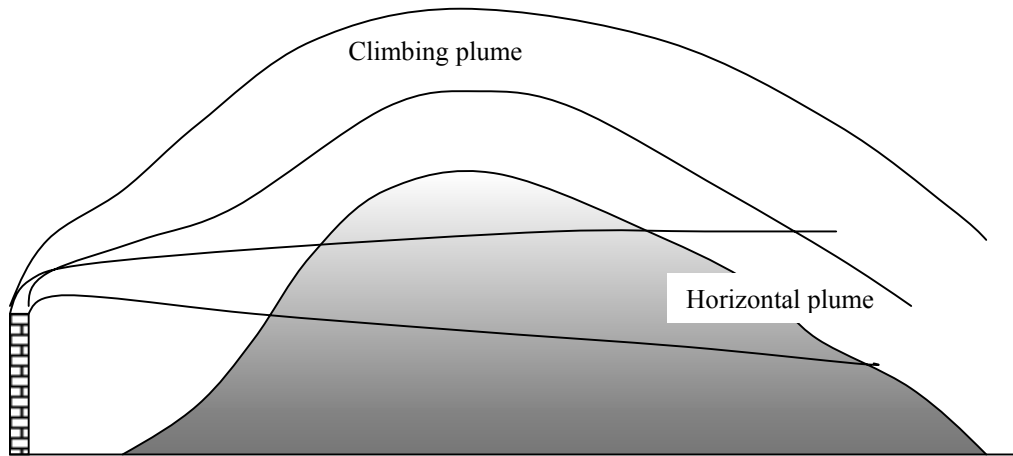


Figure 4. The two states of the plumes used to formulate the complex terrain model.

This formulation of the complex terrain model ensures that the model estimates are sensible in that they range between values corresponding to two limits of plume behavior. This simple semi-empirical model has been tested at several complex terrain sites, and it performs at least as well as CTDM in the limited task of describing concentration statistics.

7 Modifications to the Gaussian Framework

New models, such as AERMOD, incorporate physics that cannot be readily accommodated within the framework of the Gaussian distribution of the concentration. One example is dispersion in the unstable boundary layer. In the unstable boundary layer, both the mean wind and turbulence levels are relatively uniform above a height of about $1/10^{\text{th}}$ of the boundary layer height. In principle, this should allow a straightforward application of Taylor's equations for plume spread in the Gaussian expression. However, the Gaussian equation is not appropriate because the turbulent vertical velocities in the middle of the convective boundary layer do not follow a Gaussian distribution; the distribution has a negative mode, and has a long positive tail as shown in Figure 5. This implies that material released in the middle of the boundary layer has a greater probability of being caught in downdrafts than in updrafts. This leads to the descent of the plume centerline, which cannot be described with a symmetric Gaussian model. Several approaches have been used to capture this feature of dispersion of elevated releases in the convective boundary layer.

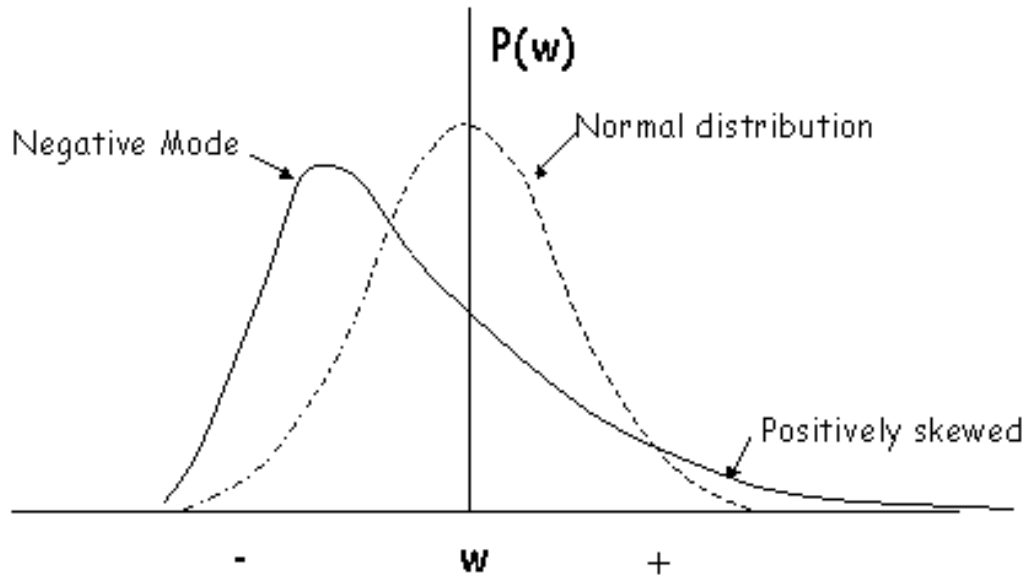


Figure 5. Vertical Velocity Distribution in the CBL.

AERMOD uses what is commonly referred to as the probability density function (pdf) approach, which assumes that a particle does not forget its velocity at release. This implies that the crosswind-integrated concentration at ground-level is determined by the probability density function of vertical velocities at the source.

$$\bar{C}_y = \frac{2Q}{U\sigma_z} \sigma_w P\left(w = -\frac{uh}{x}\right) \quad (27)$$

where $\mathbf{P}(w=-uh/x)$ is the probability density function evaluated at the vertical velocity that brings plume material from the elevated release to the receptor at \mathbf{x} in a straight line. The factor 2 accounts for reflection at the ground.

It is easy to see that the Gaussian formulation is recovered if the pdf is Gaussian. AERMOD uses a skewed pdf that allows for the plume centerline to descend towards the ground, and leads to concentrations that can be over 30% higher than that associated with a Gaussian pdf (See Venkatram, 1993). The actual formulation in AERMOD combines plume rise with dispersion, and mimics the non-Gaussian pdf in Equation (27) as a sum of two Gaussian distributions, which results in the required mode and skewness.

7.1 Other Features in Regulatory Models

Regulatory models also need to account for special features of urban areas. In ISC, dispersion in urban areas is treated using empirical dispersion curves derived from tracer experiments conducted in St. Louis (McElroy and Pooler, 1968).

These so-called McElroy Pooler curves, which are keyed to stability classes, lead to enhanced dispersion in urban areas.

AERMOD treats urban dispersion by accounting for the processes that lead to the enhancement of turbulence in urban areas. When rural air flows into a warmer urban area, the boundary layer becomes convective because of surface heating. Thus, when the rural boundary layer is stable during the night, the urban boundary layer can be convective. AERMOD accounts for this effect by formulating an upward heat flux and a boundary layer height in terms of the urban-rural temperature difference, which in turn is parameterized in terms of the population of the urban area. Then, a convective velocity scale is calculated using this heat flux, and the associated boundary layer height. This convective velocity scale is then used to calculate a turbulence profile, which is then added to that from the rural area. The increased roughness over an urban area is included in the calculation of the rural turbulence profile.

When the wind speeds become comparable to the turbulent velocities, it becomes necessary to account for dispersion along the wind direction, which is neglected in most regulatory dispersion models, including ISC. Such conditions are common in urban areas, where buildings can enhance turbulence and reduce the mean flow. Neglecting along-wind dispersion can lead to underestimation of concentrations upwind of the source.

AERMOD accounts for low wind speed conditions by assuming that the concentration is a weighted average of concentrations in two possible states: a random spread state, and plume state. In the random spread state, the release is allowed to spread equally in all directions. Then, the weighted horizontal distribution is written as:

$$H(x, y) = f_r \frac{1}{2\pi r} + (1 - f_r) \frac{1}{\sqrt{2\pi}\sigma_y} \exp\left(-\frac{y^2}{2\sigma_y^2}\right) \quad (28)$$

where the first term represents the random state, and the second term is the plume state. The plume is transported at an effective velocity given by

$$U_e = \left(2\sigma_v^2 + U_m^2\right)^{1/2} \quad (29)$$

where U_m is the velocity obtained by taking the absolute value of the average values of the U and V components of the wind measured during the averaging period. Equation (29) is derived by assuming that the mean and turbulent velocities are the result of a vector with magnitude, U_e , oscillating about the direction of U_m and that $\sigma_u = \sigma_v$. The weight for the random component in Equation (28) is taken to be

$$f_r = \frac{2\sigma_v^2}{U_e^2} \quad (30)$$

This ensures that the weight for the random component goes to unity when the mean wind approaches zero.

Modeling dispersion of plumes from stacks on the shoreline needs to account for features governed by the horizontal inhomogeneity associated with the flow of air from the water to the land surface. In an area close to water, the land surface is warmer because the water heats up less rapidly than land in response to solar heating during the day. These essentially two-dimensional effects, especially those related to the temperature differences between urban and rural areas, are not treated reliably in models such as AERMOD and ISC.

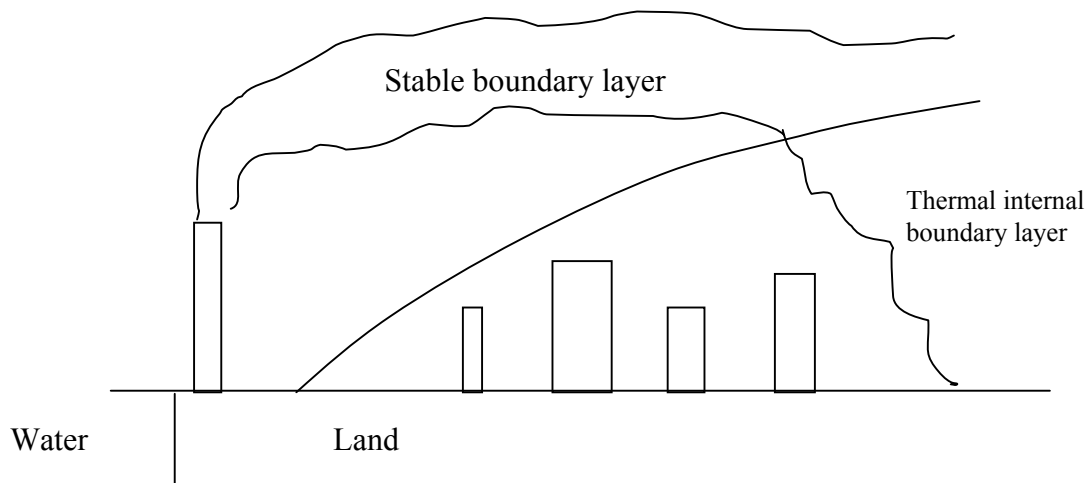


Figure 6. The growth of the urban thermal internal boundary layer (TIBL).

As the stable air from the water flows onto the warmer land, the resulting upward heat flux gives rise to an internal boundary layer that has a significant effect on the ground-level impact of elevated power plant sources. Elevated emissions, even when initially released into a stable layer, can be brought down to the ground when it intersects the growing thermal boundary layer, as shown in Figure 6. The concentration close to the point of fumigation is given by Equation (3) corresponding to the well-mixed boundary layer, where z_i is now the height of the boundary layer where the elevated plume intersects the internal boundary layer. It is clear that estimating the height of the internal boundary layer is important to calculating the ground-level concentration.

8 Concluding Remarks

The Gaussian model plays a critical role in the formulation of air quality models used in regulatory practice. It is really a framework that allows the incorporation of several processes that affect ground-level concentrations. We have demonstrated how it can accommodate building effects, terrain effects, and dispersion in shoreline and urban areas.

The Gaussian framework can be readily used to interpret data from field studies, and thus can be improved empirically to provide better descriptions of dispersion. These features, coupled with its computational simplicity, explain its popularity in applications that require realism as well as transparency. Although the model has shortcomings, it should not be discarded in favor of more complicated approaches unless there is a compelling reason to do so.

Acknowledgements

We would like to thank Dr. Jeetendra K. Upadhyay for his comments on this document, and Mr. Russell Lee for the support on the plume rise, building downwash, and terrain treatment.

References

- Barad, M. L., 1958: Project Prairie Grass. A Field Program in Diffusion. Vol. 1 Geophysics Research paper No. 59, Air Force Cambridge Research Center, Bedford, MA.
- Bowers, J.F., J.R. Bjorklund and C.S. Cheney, 1979: *Industrial Source Complex (ISC) Dispersion Model User's Guide*. Volume II, EPA-450/4-79-031, U.S. Environmental Protection Agency, Research Triangle Park, NC 27711.
- Burt, E.W., 1977: *Valley Model User's Guide*. Publication EPA-450/2-77-018, U.S. Environmental Protection Agency, Office of Air Quality Planning and Standards, Research Triangle Park, NC 27711.
- Cimorelli, A.J., S.G. Perry, A. Venkatram, J.C. Weil, R.J. Paine, R.B. Wilson, R.F. Lee, W.D. Peters, R.W. Brode, J.O. Paumier, 2002: *AERMOD: Description of Model Formulation (Version 02222)*, EPA-454/R-02-002d. U.S. Environmental Protection Agency, Research Triangle Park, NC 27711. Available from website <http://www.epa.gov/scram001> as of January 2003.
- Csanady, G. T., 1973: *Turbulent Diffusion in the Environment*. Reidel, Dordrecht, p 248.
- ERT, 1987. User's Guide to the Rough Terrain Diffusion Model (RTDM), Rev. 3.20. ERT Document No. P-D535-585. Environmental Research and Technology, Inc. (now ENSR, Inc.), Concord, MA. (NTIS No. PB 88-171467).
- Hanna, S.R., G.A. Briggs and R.P. Hosker, Jr., 1982: *Handbook on Atmospheric Dispersion*. Technical Information Center, U.S. Department of Energy. DOE/TIC-11223.
- Lavery, T. F. *et al.*, 1982: *EPA Complex Terrain Model Development: First Milestone Report-1981* EPA-600/3-82-036, Research Triangle Park, NC p 304.

McElroy, J. L., and F. Pooler, 1968: St. Louis Dispersion Study, Volume II - Analysis. Arlington, Virginia, US Dep. HEW.

Pasquill, F. 1961: The estimation of the dispersion of wind-borne material. *Meteor. Mag.* 90, 33-49.

Perry, S. G., 1992: CTDMPLUS: A dispersion model for sources in complex topography. Part I: Technical formulations. *J. Appl. Meteor.* **31**, 633-645.

Schulman, L.L., and J.S. Scire, 1980: Modeling Plume Rise from Low-level Buoyant Line and Point Sources. *Proceedings, Second Joint Conference on Applications of Air Pollution Meteorology*, 24-28 March, New Orleans, LA. pp. 133-139.

Schulman, L.L., D.G. Strimaitis and J.S. Scire, 2000: Development and evaluation of the PRIME plume rise and building downwash model. *Journal of the Air & Waste Management Association*, 50:378-390.

Sheppard, P. A., 1956: Airflow over mountains. *Quart.J.Roy.Meteor.Soc.*, 82, 528-529.

Snyder, W. H., R. S. Thompson, R. E. Eskridge, R. E. Lawson, I. P. Castro, J. T. Lee, J. C. R. Hunt, and Y. Ogawa, 1985: The structure of the strongly stratified flow over hills: Dividing streamline concept. *J.Fluid Mech.*, 152, 249-288.

Taylor, G. I., 1921: Diffusion by continuous movements. *Proc. Lond. Math. Soc.* **2**, 196-211.

Thomson, D. J. and A. J. Manning, 2001: Along-wind dispersion in light wind conditions. *Boundary-Layer Meteorology* **98**, 341-358.

U.S. EPA, 1995a: *User's Guide for the Industrial Source Complex (ISC3) Dispersion Models: Volume 2—Description of Model Algorithms*. U.S. Environmental Protection Agency, OAQPS, EMAD, Research Triangle Park, NC. EPA-454/B-95-003b.

U.S. EPA, 1995b: *User's Guide to the Building Profile Input Program*. U.S. Environmental Protection Agency, Research Triangle Park, NC 27711.

US EPA, 1992: *User's Guide for the Industrial Source Complex (ISC2) Dispersion Models: Volume II—Description of Model Algorithms*. U.S. Environmental Protection Agency, OAQPS, Research Triangle Park, NC 27711. Publication No. EPA-450/4-92-008b.

Van Ulden, A. P., 1978: Simple estimates for vertical dispersion from sources near the ground. *Atmos. Environ.* 12, 2125-2129.

Venkatram, A. 1993: Estimates of maximum ground-level concentration in the convective boundary layer—The error in using the Gaussian distribution. *Atmos. Environ.*, **27(A)**, 2187-2191.

Venkatram, A., 1992: Vertical dispersion of ground-level releases in the surface boundary layer. *Atmos. Environ.* 26A 947.

Venkatram, A., D. Strimaitis, and D. Dicristofaro. 1984. A semiempirical model to estimate vertical dispersion of elevated releases in the stable boundary layer. *Atmos. Environ.* **18**, 923-928.

Venkatram, A., R. W. Brode, A. J. Cimorelli, R. F. Lee, R. J. Paine, S. G. Perry, W. D. Peters, J.C. Weil, and R. B. Wilson, 2001: A complex terrain dispersion model for regulatory applications. *Atmos. Environ.*, in press.

Weil, J. C., 1985: Updating applied diffusion models. *J.Climate Appl.Meteor.*, 24(11), 1111-1130.

Chapter 8

Gaussian Puff Models

Gaussian puff models present substantial improvements in comparison with Gaussian plume models. Future volumes in this book series will cover this topic.

The reader can gather information on Gaussian puff models at:

- <http://www.src.com/calpuff/calpuff1.htm> (CALPUFF)
- <http://www.epa.gov/scram001/calpufflit.htm> (CALPUFF)
- http://www.weblakes.com/calpuff/calpuff_view.pdf (CALPUFF VIEW)
- <http://www.epa.gov/scram001/7thconf/calpuff/conseq.pdf> (CALPUFF vs. MESOPUFF II)

BRANK
Page

Chapter 9

Special Applications of Gaussian Models

Gaussian models have been successfully used for decades throughout the world. One of the reasons for their widespread use is the simplicity of their basic formulation. Gaussian models have also been modified and adjusted with algorithms designed to handle complex dispersion scenarios. Future volumes in this book series will present and illustrate special applications, modifications, and tests of Gaussian models.

The reader can gather preliminary information at:

- <http://www.epa.gov/scram001/userg/regmod/caline3.pdf>
CALINE3 - for predicting air pollutant levels near highways and arterial streets.
- <http://www.epa.gov/scram001/tt22.htm#ctdmplus>
CTDMPLUS – a point source Gaussian air quality model for use in all stability conditions for complex terrain.
- <http://www.epa.gov/scram001/tt22.htm#ocd>
OCD - a straight line Gaussian model developed to determine the impact of offshore emissions from point, area or line sources on the air quality of coastal regions.
- <http://www.epa.gov/scram001/userg/other/degugv1.pdf>
DEGADIS – for simulating the atmospheric dispersion of dense gas (or aerosol) clouds released with zero momentum into the atmospheric boundary layer over flat, level terrain.

BRANK
P
2000

Byun, D. et al. (2003) *Eulerian Dispersion Models*. Chapter 10 of *AIR QUALITY MODELING - Theories, Methodologies, Computational Techniques, and Available Databases and Software. Vol. I - Fundamentals* (P. Zannetti, Editor). Published by The EnviroComp Institute (<http://www.envirocomp.org/>) and the Air & Waste Management Association (<http://www.awma.org/>).

Chapter 10

Eulerian Dispersion Models

Daewon W. Byun ^{(1)*}, Avraham Lacser ^{(2)*}, Robert Yamartino ⁽³⁾, and Paolo Zannetti ⁽⁴⁾

⁽¹⁾ *Department of Geosciences, University of Houston, 4800 Calhoun, Houston, TX 77204, USA*

dwbyun@math.uh.edu

⁽²⁾ *Israel Institute for Biological Research, POB 19 Ness Ziona 74100, Israel*

lacser@iibr.gov.il

⁽³⁾ *191 East Grand Ave. #206, Old Orchard Beach, ME, USA*

rjy@maine.rr.com

⁽⁴⁾ *EnviroComp Consulting Inc., 2298 Ocaso Camino, Fremont, CA, USA*

zannetti@envirocomp.com

**Work performed while serving at the National Oceanic and Atmospheric Administration, on assignment to National Exposure Research Laboratory, EPA, Research Triangle Park, NC, USA*

Abstract: The main objectives of this chapter are to introduce the state-of-the-art numerical algorithms for the advection and diffusion used in Eulerian models and to discuss their theoretical and numerical characteristics. The Eulerian approach allows incorporation of different physical and chemical processes involved with the gaseous and particulate constituents in the atmosphere. The governing conservation equation for tracer species dispersion is derived. Approximations in the atmospheric dynamics and fundamental concepts used in the description of turbulence are explained. Some analytical solutions are provided for simplified dispersion conditions to illustrate basic processes in the atmospheric dispersion models. In the Eulerian approach, governing equations can be solved with a fractional time step or an explicit-implicit method to take advantage of numerical efficiency and knowledge of physical parameterizations of atmospheric surface flux exchange, advection, and diffusion processes. This chapter describes numerical solution methods for each physical process component in the Eulerian dispersion model. We provide fundamental steps used in the derivation of numerical advection algorithms, horizontal and vertical eddy diffusivity formulations, and local and non-local vertical diffusion methods. In the Appendix we have compiled vertical eddy diffusivity formulations in the literature, numerical

solution methods of the local and non-local vertical diffusion algorithms, and Numerical algorithms with two-level time differencing for constant grid spacing.

Key Words: Air quality modeling, advection, diffusion, numerical algorithms, Eulerian modeling, local and non-local closure, eddy diffusivity.

Air pollution diffusion can be numerically simulated by several techniques that are generally divided into two categories based on the frame of references: Eulerian models and Lagrangian models. Figure 1 shows that the Eulerian reference system is fixed with respect to earth while the Lagrangian reference system follows the atmospheric motion. Russell and Dennis (2000), in their recent critical review of photochemical models, state that Eulerian models are becoming dominant. This chapter describes the Eulerian formulations for the atmospheric advection and diffusion processes used in comprehensive air quality models. The basic governing conservation equation for tracer species is derived. To help reader's understanding of the physical processes involved, analytical solutions for simplified dispersion models are provided and discussed. For realistic atmospheric conditions where simple assumptions on the wind field or the diffusion parameters are not available, highly accurate numerical solutions are applied to solve the governing dispersion equation. The Eulerian approach allows incorporation of different physical and chemical processes involved with the atmospheric gaseous and particulate constituents. The governing equations can be solved with a fractional time step or explicit-implicit method to take advantage of numerical efficiency and knowledge of physical parameterizations of atmospheric surface flux exchange, advection, and diffusion processes. The main objectives of this chapter are to introduce the state-of-the-art numerical algorithms for the advection and diffusion used in Eulerian models and to discuss their theoretical and numerical characteristics.

1 Air Quality Modeling Methods

Many different numerical techniques can be used for studying the behavior of the atmosphere. Lewis F. Richardson around 1910 made first attempt of numerical weather prediction with mechanical calculators and complex computing forms. In the mid-1940s, John von Neumann of the Institute of Advanced Studies at Princeton began to redesign the first electronic computer ENIAC (developed by J. Mauchly and P. Eckert) primarily for the purpose of weather prediction with the stored - program technique, which is now known as the von Neumann's design. Since, the development of modern digital computers has followed closely to the von Neumann's design and new computational capabilities have been regularly tested with "grand challenge" problems of other computational science fields. Very often, weather prediction models have been among the initial testing programs for newer, faster, and larger computer architectures.

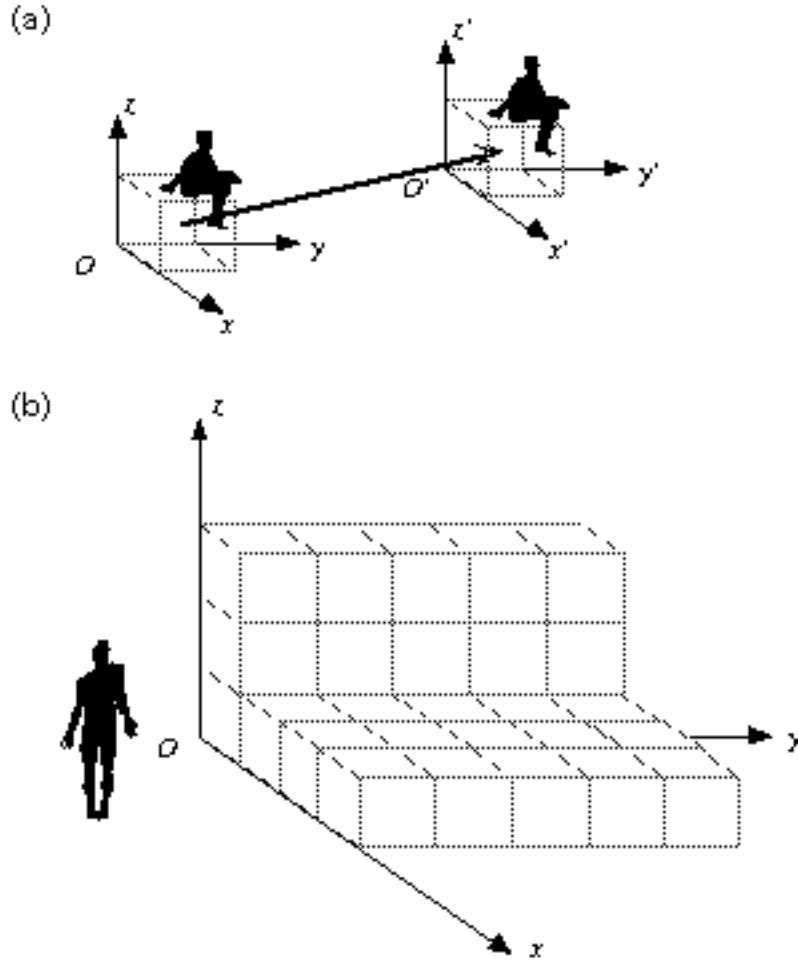


Figure 1. (a) In the Lagrangian system, the observer follows movement of air parcel, and (b) in the Eulerian system, the observer studies atmospheric motion at a fixed reference point.

As digital computer memory capacity has become larger, and CPU speed has become faster, the complexity of weather prediction models has increased tremendously. As a part of atmospheric processes, techniques used for solving atmospheric diffusion have been slowly but surely benefiting from the developments in atmospheric science and computer hardware development. For example, simple approaches such as Gaussian and box modeling techniques were popular initially and then use of Lagrangian modeling paradigm followed. Starting in the mid-1970s, the Eulerian or hybrid air quality models have been available for air pollution assessment studies and the acceptance has been strengthened by the need to include complex atmospheric processes under one system. In the following, we briefly introduce different modeling techniques.

1.1 Gaussian Models

Gaussian models have been used for last forty years as the most common air pollution models for regulatory applications as they are based on analytical solutions that require less computational power than numerical models. They employ Gaussian statistical distribution formulas to describe the three-dimensional concentration field generated by the diffusion of emissions of inert species under static meteorological and emission conditions. Because that the Gaussian formulation is based on the uniformity of the eddy diffusivity, the validity deteriorates severely in vertical wind shear, diurnal variations of wind and atmospheric stability, and topography and land use variations. Furthermore, their applicability is affected by certain temporal and spatial scale considerations for which the averaged conditions can be estimated to satisfy the limiting assumptions. Because of this, various types of special Gaussian models have been built to address specific environmental conditions. EPA distributed many of these models as a part of UNAMAP models starting in the late 1960s. EPA has advertised most UNAMAP (User's Network for Applied Modeling of Air Pollution; see Zannetti, 1990) models to be just guideline models and stressed that the models may be used only if the situations are suitable for the particular model. For the details, readers should refer to Chapter 7 for the Gaussian plume models and Chapter 8 for Gaussian puff models.

1.2 Box Models

Box models are zero-dimensional models that assume pollutants in an imaginary box or column are bounded by the ground and the potential temperature inversion base and spatially homogeneous, instantaneously well mixed. Using a continuity equation, the rates of pollutant concentration changes in the box (caused by horizontal advection, emission, entrainment of background pollutants due to mixing layer growth, and chemical reactions) can be simulated. The box model can then predict the temporal variations of the spatially averaged concentrations, and can estimate mass balances of multiple pollutants over the limited domain represented in the box. Because of the simplifications used in the development of these box models, they are incapable of predicting air quality for regions with significant spatially inhomogeneous emissions, or where the characteristic turbulent mixing time scale is larger than the chemical reaction time scales. Refer to Chapter 2 for additional description of box models.

1.3 Lagrangian Models

Lagrangian (or Trajectory) models are based on species conservation equations describing atmospheric diffusion and chemical reactions stated in terms of moving coordinates. The observer adopts moving coordinates that follow sets of hypothetical columns of air similar to the ones described in the photochemical box models. The air columns move along with the prevailing winds, so there are no advection terms in the set of governing equations. Primary pollutant emissions

are injected into the columns when they pass over source regions. Similar to box models, trajectory models simulate chemical reactions in each column. While Lagrangian models are one step beyond box models in logical development, the assumptions they carry are not appropriate when topographical features cause complex wind fields or vertical wind shear within the columns. Uncertainty in the trajectory of column of air under large wind shear, and difficulties in describing source and sink processes are almost insurmountable because of the inherent assumption that the integrity of air parcels must be maintained with the Lagrangian approach. Trajectory modeling is good when simple back-trajectory transport can be used to adequately describe the motion of pollutants. Lagrangian models require a factor of one to two orders of magnitude more computational resources than box models depending on the number of atmospheric columns followed. Lagrangian models, however, are not as computationally expensive as Eulerian models. Consult Chapter 11 for an in-depth description of the Lagrangian models.

1.4 Eulerian Models

In the Eulerian approach, the observer adopts a fixed frame of reference, usually the surface of the earth. This enables easy representation of the pollutant production and transformation processes. Most Eulerian models use a grid system defined in an orthogonal set of coordinates to describe atmospheric dynamics (advection and diffusion), emissions sources, and chemical production and destruction. Most numerical weather prediction models and comprehensive air quality models rely on this paradigm. Eulerian models generate four-dimensional (space and time) trace species concentration fields for each of the species modeled. Eulerian models generally use fewer simplifying assumptions in the simulation of atmospheric transport compared to other modeling techniques. By the nature of the grid discretization, Eulerian models cannot resolve trace species concentration features at sub-grid scales because emissions are instantly mixed into the grid. Although one can attempt to use very small grid size to resolve the detailed emissions distributions, there is a practical limit at which atmospheric turbulence statistics cannot be described with parameterizations in terms of the mean state variables (such as wind and temperature) as well as the inhibiting high computational cost. To compensate for this deficiency, some Eulerian models include either trajectory submodels or Gaussian dispersion submodels to treat initial transport and chemical transformations of pollutants coming from large point source emissions within the grid. These hybrid (e.g., "plume-in-grid") grid models attempt to minimize the effect of instantaneous dilution of pollutants over the entire grid box assumed by pure Eulerian models. Once the point source plumes reach a certain size, they are added to the existing concentrations in the appropriate grid cells, and subsequently go through transformation and transport processes within the grid model. Numerical diffusion in the advection process and difficulties in representing atmospheric mixing processes are some of the drawbacks of Eulerian models (see section 5).

2 Eulerian Formulations

Here we introduce the governing equations for Eulerian dispersion modeling. We discuss assumptions used for the description of atmospheric dynamics, turbulence, and averaging techniques that allow deterministic formulations of the stochastic atmospheric dispersion phenomena.

2.1 Conservation Equations for Air Pollutants

First, we assume that pollutant concentrations are sufficiently small, such that their presence would not affect the meteorology to any detectable extent. Hence, the species conservation equations can be solved independently of the Navier-Stokes and energy equations. In a Cartesian coordinate system, the continuity equation for air and the governing conservation equation for a pollutant are given

$$\frac{\partial \rho}{\partial t} + \frac{\partial \rho u}{\partial x} + \frac{\partial \rho v}{\partial y} + \frac{\partial \rho w}{\partial z} = 0 \quad (1)$$

$$\frac{\partial \varphi_i}{\partial t} + \frac{\partial \varphi_i u}{\partial x} + \frac{\partial \varphi_i v}{\partial y} + \frac{\partial \varphi_i w}{\partial z} = Q_{\varphi_i} \quad (2)$$

where x and y are horizontal coordinates of the reference rotated earth-tangential coordinates and z is the distance normal to the x - y surface; u , v , and w are corresponding wind components; ρ is air density, φ_i represents concentration of trace species i , and Q_{φ_i} is the source/sink of the pollutant through emissions, deposition, and reactions with other pollutants.

In this chapter, for simplicity we have adapted a Cartesian coordinate system. However, operational mesoscale meteorological models often use quasi-orthogonal terrain-following coordinates. Because the large-scale motions of the atmosphere are quasi-horizontal with respect to the earth's surface, motions in horizontal and vertical directions can be separated using the metric tensor components that define the coordinate transformation in the meteorological generalized coordinate system. Refer to Byun (1999a) for the corresponding governing set of equations.

Eqs. (1) and (2) can be combined to provide a conservation equation for the species mixing ratio, $q_i = \frac{\varphi_i}{\rho}$

$$\frac{dq_i}{dt} = \frac{\partial q_i}{\partial t} + u \frac{\partial q_i}{\partial x} + v \frac{\partial q_i}{\partial y} + w \frac{\partial q_i}{\partial z} = \frac{Q_{\varphi_i}}{\rho} \quad (3)$$

Eq. (3) is the governing equation of the Lagrangian model, which is based on the principle that mixing ratio is conserved following the air parcel when there is no source term (i.e., $Q_{\phi_i} = 0$). Eulerian models can also realize the same constraint.

However, because the information must be discretized on the Eulerian grid, a numerical advection scheme based on Eq. (3) is sometimes called a Semi-Lagrangian Transport (SLT) method.

2.2 Assumptions on Atmospheric Dynamics

The temporal and spatial scales of atmospheric motion span many orders of magnitude (see Figure 2). Therefore, it is impossible to model the motion with a straightforward explicit method. To make atmospheric simulations manageable, scientists have applied several techniques to reduce the range of scales involved by applying simplification assumptions and averaging techniques. The spectral gap (low dynamic energy region which can vary from tens of minutes to a few hour time-scale) helps to separate weather from turbulence. Because of this gap, it is possible to consider these two entities (weather and turbulence) independently and to execute proper mathematical operations to determine the statistical properties. The nonlinear Navier-Stokes equations contain information about atmospheric motion and transport over a broad range of spatial and temporal scales, ranging from global scale eddies to the smallest eddies contributing to molecular dissipation.

Several important hypotheses, basic assumptions, limits of applications in air quality modeling, and examples of usage of atmospheric turbulence and dispersion theories, are briefly discussed below. More detailed information on atmospheric turbulence and diffusion can be found in Pasquill and Smith (1983), Panofsky and Dutton (1984), Stull (1988), and Arya (1988, 999).

2.2.1 Hydrostatic and Non-Hydrostatic Assumptions

The hydrostatic equilibrium assumption states that gravity and the vertical pressure gradient force are in balance. Under hydrostatic equilibrium, the atmospheric pressure at a given height is simply related to the weight of the air above. Since the atmosphere is constantly moving, the hydrostatic assumption considers not only the static components of pressure and density but also the dynamic perturbation pressure field (which is responsible for the horizontal velocity field) to the perturbation density field. The vertical acceleration due to gravity is smaller than the horizontal acceleration driven by the horizontal pressure difference. The result is that the vertical acceleration cannot be easily determined from the vertical momentum equation for large-scale atmospheric motions.

This hydrostatic approximation is invalid for small-scale motions such as convection where the vertical acceleration has a magnitude similar to gravity. For

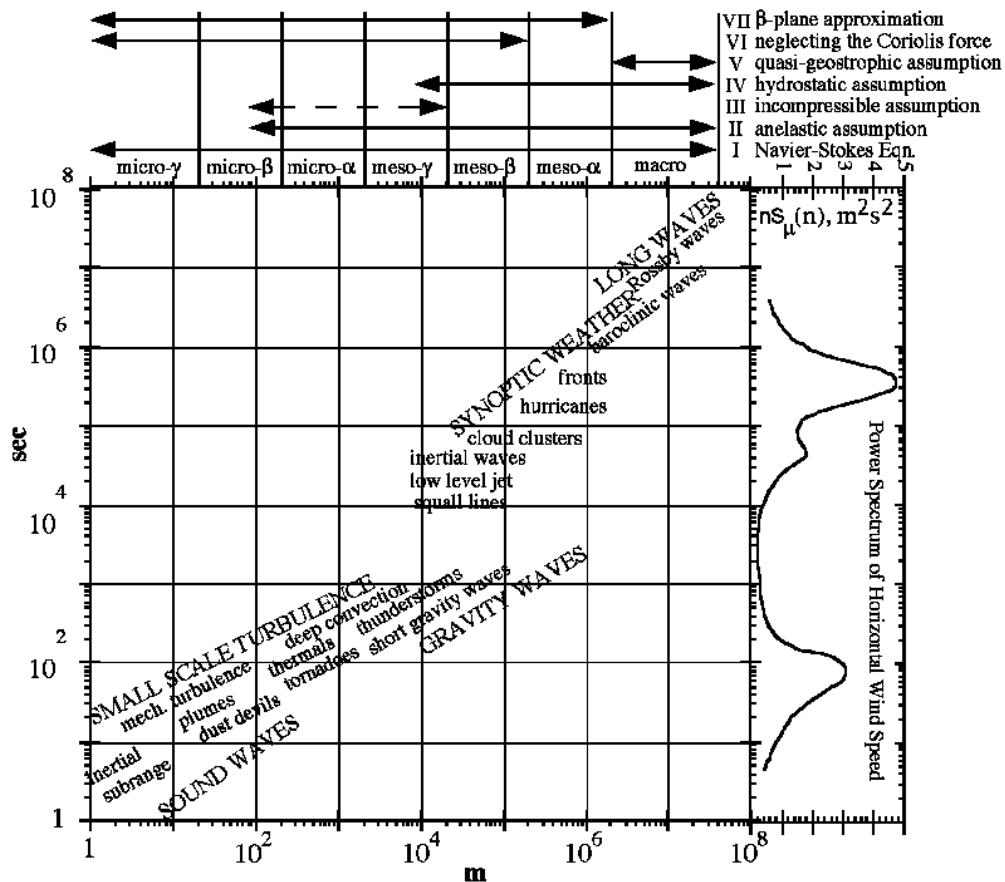


Figure 2. Temporal and spatial scales for atmospheric dynamic systems. A spectral gap is apparent around the time scale of thousand seconds. (Dennis et al., 1996).

mesoscale atmospheric models with small horizontal grid sizes (e.g., less than 2 km) where the influence of thermodynamics has direct impact on the atmospheric motions, the hydrostatic pressure calculation may result in less realistic predictions of the atmospheric flows. For this reason, the nonhydrostatic primitive set of equations has recently been applied to study small-scale atmospheric features. The primary difference between the nonhydrostatic model and its hydrostatic counterpart is that the nonhydrostatic model requires explicit integration of the vertical velocity component.

There are two methods for nonhydrostatic pressure calculation. One uses a fully compressible continuity equation. The other employs an elastic continuity equation. For the latter, a Poisson partial differential equation for pressure has to be solved at each time step. Furthermore, when terrain-following coordinate transformations are used solving the Poisson equation is very costly. Researchers

have found that the integration time step for an elastic nonhydrostatic model can be much larger than that for a hydrostatic model, especially when the acoustic waves are solved separately from other meteorological waves (e.g., Klemp and Wilhelmson, 1978).

2.2.2 Incompressible Atmosphere Assumption

The incompressible atmosphere assumption involves the thermodynamic characteristics of air. The equation of state describes how density is affected by the changes in pressure and temperature fields. The incompressibility of air can be assumed if the time rate of change of density variation is much smaller than the time scales of motion (Batchelor, 1967). This condition is satisfied mostly for the case when wind speed is substantially less than the speed of sound, and the speeds of gravity waves are much slower than the speed of sound, and limits the vertical extent of motion to be less than about one kilometer. The result is that the change of density due to pressure variation is negligible, and so the fluid behaves as if it were incompressible. Basically, the incompressible atmosphere assumption is a shallow-water approximation for an adiabatic atmosphere. With the incompressibility assumption, the distinction between the conservative form equation (Eq. 2) and its advective form (Eq. 3) becomes blurred. Consequently, concentrations in the form of either density or mixing ratio are often used indiscriminately in atmospheric diffusion equations. One might expect that as long as the wind field satisfies the nondivergent flow approximation, an air quality model would satisfy the pollutant species mass conservation. The implication of this assumption is that a nondivergent wind field does not guarantee the mass conservation of pollutant species if there is inconsistency in air density and wind fields. It is surprising that the lack of mass conservation under the nondivergent flow has not been addressed rigorously in air quality modeling studies.

2.2.3 Boussinesq Approximations

The set of Boussinesq approximations used in atmospheric boundary layer studies can be summarized as follows:

- Deviations of thermodynamic variables from reference values (denoted by subscript o) are small (hydrostatic atmosphere at rest):

$$\frac{p - p_o}{p_o} \ll 1, \quad \frac{T - T_o}{T_o} \ll 1, \quad \frac{\rho - \rho_o}{\rho_o} \ll 1 \quad (4)$$

- Molecular properties are essentially constant. Since deviation of temperature is small, most molecular properties such as viscosity (ν), molecular diffusivity (γ), and molecular heat conductivity (κ) are constant at the given temperature T_o .

- Variations in temperature and density can be ignored except when they are associated with buoyancy forces. By carefully ordering the derivation steps from the more fundamental compressible equations to the Boussinesq equations, it can be shown that the fluctuations in density become only significant when multiplied by the acceleration due to gravity.

The Boussinesq approximations are often used in air quality modeling to simplify equations of motion and trace gas conservation. However, for small horizontal scales or for deep atmospheric layers, the assumptions in the Boussinesq approximations may not hold. Using Boussinesq approximations lead to the following simplification of the equations of motions in the planetary boundary layer (PBL):

- Flows can be treated as incompressible.
- The equation of state for fluctuating components is simplified so the ratio of fluctuating density to total density can be approximated by the ratio of temperature fluctuation to the reference temperature.

Many Eulerian dispersion models use such limiting assumptions on atmospheric dynamics as described above. Often an incompressible atmosphere assumption is used with the Boussinesq approximations. These assumptions are acceptable only for certain limited situations such as studying atmospheric dispersion in the shallow boundary layer with little topographic features and nondivergent wind field. Recently, air quality models with nonhydrostatic assumptions have been developed (e.g., Chang et al., 1997; Byun and Ching, 1999), and the effects of air density variations on pollutant transport are considered in such models.

2.3 Assumptions on Atmospheric Turbulence

We cannot explicitly solve the instantaneous species conservation equation for the smallest scales due to computer limitations and uncertainties in the input data. We must then transform Eqs. (1) and (2) to form a deterministic relation. We assume that there is a natural separation of atmospheric motions between a homogeneous fine scale and the inhomogeneous mesoscale that is affected by the topography, surface conditions, and large-scale weather. Then we introduce the concept of turbulence and mean components for studying stochastic atmospheric flows. We expect that as long as the turbulent components can be parameterized we can obtain deterministic governing equations for the mean flow. Basic concepts of atmospheric turbulence are reviewed below and more detailed information can be found in Stull (1988) and Arya (1999).

2.3.1 Isotropic Turbulence

Isotropy implies that fluid motions are invariant with respect to rotation and reflection of the coordinates. True isotropy occurs only when homogeneity is present in all directions. In isotropic turbulence, the variances of the three

velocity components are the same because they are invariant with the rotation of the coordinate axis. Another consequence of isotropy is that the velocity components are not correlated with each other. However, in the PBL, the variances of the velocity components are not equal, and the horizontal and vertical velocity components are correlated near the ground. Thus the atmospheric turbulence in the PBL is not strictly isotropic. However, the smallest fluctuations imbedded in the larger scales of motions can be isotropic. The invariant characteristic of the smallest scales of turbulence is termed local isotropic turbulence. Measurements of boundary-layer turbulence show that these predictions are indeed satisfied, provided that the size of the turbulent eddies involved is small compared to the distance to the surface. Such eddies are far enough from the surface that they are independent of boundary influences. In the case of isotropy, or local isotropy, the nine components of Reynolds stress (momentum fluxes) can be reduced to just functions of the longitudinal (along the wind) and lateral (across the wind) covariances. By rotation of coordinates, any longitudinal spectrum can be transformed into any other longitudinal spectrum. However, rotation of coordinates cannot transform longitudinal functions into lateral functions. Since all longitudinal functions are the same and all lateral functions are the same under coordinate rotations, these two functions describe spectral properties of isotropic or locally isotropic turbulence.

2.3.2 Taylor's Hypothesis

When the mean velocity of a flow which carries eddies is much greater than the turbulent fluctuations, one may assume that the sequence of change in turbulent components at a fixed point is simply due to the passage of an unchanging pattern of turbulent motion over that point. The field of turbulence is translated by the mean velocity and the spatial turbulence pattern can be depicted exactly with the temporal turbulence pattern by the transformation $x = U t$, where x is the longitudinal distance, U is the transport mean wind speed, and t is the travel time. This is called the Taylor's hypothesis or the frozen-wave hypothesis. The Taylor's hypothesis is significant as it enables to infer spatial structure of turbulence from measurements at one point. For the Taylor's hypothesis to be valid, the turbulence must be temporally stationary and spatially homogeneous at least along the direction of mean wind. These conditions are often satisfied in wind tunnels, and are often approximately valid in the atmosphere provided the measurement location and period are chosen carefully. Strong wind shears in the vertical will generally distort eddies as they move (tearing them apart, in effect) so that the Taylor's frozen-wave hypothesis cannot be sustained. In spectral terms, the hypothesis fails at frequencies f smaller than vertical wind shear. Taylor's hypothesis can hardly be valid when standing waves (such as those produced by hills and mountains) cause spatial variations but have little effect on temporal measurements at one location. In atmospheric dispersion modeling, a relationship between the Lagrangian and Eulerian spectra is often derived from the Taylor's frozen-wave hypothesis.

2.3.3 Homogeneity

A turbulent flow is homogeneous if its statistics do not vary in space. The presence of the earth's surface is important in two ways with respect to homogeneity. First, statistics will vary relative to distance from the ground so that it is unlikely that homogeneity could prevail, even approximately, except in the horizontal. Second, if the terrain and land use are inhomogeneous, with hills and valleys, or with cities, fields, and forests, then the flow near the ground can hardly be expected to be horizontally homogeneous because of the effects of the surface on the flow itself. Horizontal homogeneity of small-scale motions near the ground is usually not a good approximation over most continental areas. The terrain is neither flat enough nor sufficiently homogeneous, and in general, local statistics over large areas will not be the same. Perhaps, at higher levels in the boundary layer, horizontal homogeneity is more nearly approached. The assumption of vertical homogeneity is almost never valid because of the presence of wind shear and stratification. Mean wind speed and temperature vary rapidly with height near the terrain surface, and then somewhat less rapidly aloft. In a homogeneous turbulence, the spatial correlation is not a function of the spatial coordinate but instead is only a function of the separation vector.

2.3.4 Stationarity

A random variable is said to be stationary if its one-dimensional probability functions are independent of time and its joint (multi-dimensional) probability functions are invariant with respect to a fixed translation in time (i.e., dependent only on time difference rather than time itself). In reality we do not insist that the variable be exactly stationary. Instead we accept quasi-stationarity (a series of near-equilibrium states) if there is a significant separation between the time scales of turbulence and of large-scale weather phenomena. Usually this assumption is valid for small-scale flows under steady meteorological conditions where influence of synoptic scale disturbance is not present.

2.3.5 Ergodicity

The ergodicity hypothesis states that for stationary random fields time averages converge to ensemble (probability) averages as the averaging interval becomes very long. Similarly, for homogeneous random fields, spatial averages converge to ensemble averages (discussed in Section 2.4) as the spatial interval for averaging becomes very large. When temporal and ensemble averages coincide in a suitable sense, the stochastic process is referred to as ergodic. Ergodicity is a very important concept involving volume-preserving coordinate transformations. Ergodicity requires stationarity. To ensure ergodicity, one must establish or assume certain properties for ensemble-averaged quantities such as second- or fourth-order covariances. This assumption allows linkage of theoretical turbulence description to the experiment results where time averages in statistically stationary flows are used. Mean-square ergodicity is possible even

for nonstationary processes, and therefore is often applied in the study of atmospheric turbulence. It implies that the variance of the sample averages vanishes as time goes to infinite, even though they may not converge to an ensemble average.

2.3.6 Similarity and Dimensional Analysis

Before detailed causal relations can be identified in a system, a dimensional analysis can provide a simple but powerful method to establish relationships between the various quantities in the system based on their fundamental dimensions (Arya, 1988). If conditions surrounding two experiments are identical, the result should be similar. By dimensional analysis, a similarity relationship may be found. Similarity theory predicts universal functions, which may be determined experimentally and tested for reproducibility at other locations. The surface boundary layer theory used in describing atmospheric mixing characteristics is mostly derived from the similarity theory.

2.4 Averaging Techniques

Atmospheric motions consist of a vast spectrum of temporal and spatial scales. For convenience, the scales are separated to isolate properties of atmospheric motions to a limited portion of the spectrum. The set of primitive equations that represents the stochastic atmospheric system must be averaged to a set of deterministic equations before the equations can be solved numerically. The averaging process filters the total flow into mean and turbulent components. The spectral gap discussed above (see Figure 2), is not deep enough to provide a completely satisfactory solution, but it guides us on how to separate the mean and turbulent motions. For example, to characterize turbulence and mean flow in the surface layer, one-hour averages are often used to separate large-scale from micro-scale processes. In this averaging process we limit the descriptions of the atmospheric motions to terms of statistical characterization. However, the averaging processes in atmospheric numerical models are more complex than the simple distinction between instantaneous descriptions and statistical averages. Because we rely on a grid system to represent atmospheric motions and processes over a large domain, in effect we are applying spatial averaging over the grid size to represent atmospheric phenomena in a grid cell. The governing set of equations for the atmospheric motions and reactions are obtained by applying the ensemble averaging to transform the stochastic atmospheric system (described in 3.2.1) to a deterministic system and, by applying discrete volume averaging, to convert into the numerical solution space.

Cotton and Anthes (1989) summarized expected characteristics of averaging operators for use in atmospheric modeling as follows:

- The operators should provide formal mechanisms for distinguishing between resolvable and unresolvable eddies.

- The operators should provide sets of equations that are more amenable to integration (either analytically or numerically) than unaveraged systems of equations.
- The average set of atmospheric variables should be capable of being measured by current or anticipated atmospheric sensing systems.

The following averaging techniques fit the above characteristics.

2.4.1 Ensemble Averaging

Atmospheric motions are composed of a variety of eddies whose behavior is mostly stochastic and random. This makes a deterministic approach of solving the governing Navier-Stokes equations of motion for the entire spectrum of eddies in the atmosphere impossible; instead, one has to rely on statistical methods. Ensemble averaging is an ideal concept that completely removes randomness and filters out eddies of all sizes. Therefore, the ensemble-averaged equation must contain parameterization covering the entire spectral range of eddy motions including the largest energy-containing scales. The largest eddies in any turbulent flow are very sensitive to atmospheric and surface conditions. Therefore, such a parameterization cannot be uniformly valid in a wide range of flows. Turbulent flows differ from one another principally in their large-eddy structure. Small-scale eddies in turbulent flows seem to be statistically similar. The ensemble averaging process enables us to describe the stochastic atmospheric processes in a deterministic sense. The equation for ensemble averaging is:

$$\bar{f}_e = \lim_{N \rightarrow \infty} \frac{1}{N} \sum_{k=1}^N f_k \quad (5)$$

where f_k , $k=1, N$ are different realizations of f .

However, because atmosphere is neither stationary nor homogeneous, we need to find alternative average operators that are suitable for the understanding of field measurements as well as for the implementation in computational models. The ensemble averaging is often substituted by the temporal averaging, which will be described below.

2.4.2 Reynolds Decomposition and Averaging

Although behaviors of atmospheric motions are stochastic, only average statistics are important and their detailed fluctuation of individual eddies is little or no concern. Osborne Reynolds toward the end of nineteenth century suggested decomposition of atmospheric variables into mean (denoted with over bar) and turbulent components (denoted with prime), i.e., $f = \bar{f} + f'$; $g = \bar{g} + g'$ where f and g are two dependent variables or functions of random variables. The Reynolds averaging conditions are (Arya, 1999):

$$\overline{f + g} = \overline{f} + \overline{g} \quad (6a)$$

$$\overline{cf} = c\overline{f} \quad (6b)$$

$$\overline{gf} = \overline{g}\overline{f} \quad (6c)$$

$$\frac{\partial \overline{f}}{\partial s} = \overline{\frac{\partial f}{\partial s}} \quad (6d)$$

$$\overline{\int f ds} = \int \overline{f} ds \quad (6e)$$

where c is a constant, $s = x, y, z,$ or t . The only averaging operation that satisfies the Reynolds averaging conditions is ensemble averaging, defined above.

2.4.3 Temporal Averaging

Temporal averaging is the most popular averaging technique used because many instruments are available that are capable of measuring time series of atmospheric parameters at low cost. Other techniques (such as the ensemble averaging) are extremely difficult to obtain under varying atmospheric conditions. Temporal averaging has been used as a substitute for the ensemble averaging when atmospheric turbulence is assumed to satisfy the ergodicity condition described earlier. In order for temporal averaging to characterize atmospheric turbulence, the optimal selection of an averaging period is essential. The averaging period should be sufficiently long to ensure a stable averaging of signals from the energy containing eddies but not too long to the point that diurnal variations or synoptic changes in the atmospheric conditions are masked. In most studies of PBL, the optimum averaging time ranges between 10^3 to 10^4 seconds, depending on the height of observation, the stability condition, and the moment of the parameter under study (Arya, 1988). An atmospheric model that relies on PBL parameterizations should be considered as having corresponding inherent uncertainties in its predictions due to the temporal averaging technique applied. The equation for temporal averaging is:

$$\overline{f}_t = \lim_{T \rightarrow \infty} \frac{1}{2T} \int_{-T}^T f dt \quad (7)$$

where T is one half of the period around the time at which the average is evaluated.

2.4.4 Grid-Volume Averaging

Using a grid-volume averaging method, eddies smaller than the spatial scale are removed, leaving a filtered field that is defined at every point continuously in the modeling domain. Grid-volume averaging is similar to applying a moving

average to a time series, Eq. (7). It is simply averaging over fixed volumes, so that the averaged field is defined only at the center of the (non-overlapping) averaged volumes. When the grid size is much smaller than the wavelength of the energy containing eddies of the system, the grid-volume average is a well-defined function. A volume-averaged model with a grid size much smaller than the energy containing eddies requires a very simple parameterization. This forms the basis of the large eddy simulation (LES). If the grid size is of comparable magnitude to the energy-containing scales, or greater than the turbulent integral scale, the Reynolds flux in the sub-grid scale must be parameterized. Therefore, if the same parameterization is used, the volume-averaged model with sufficiently large grid size becomes similar to the ensemble-averaged model where the turbulent transfer must always be parameterized. Because the grid-volume average is defined over a finite volume at an instant in time, it is not measurable and models based on grid-volume average cannot be conventionally tested against the measurement. A volume-averaged model cannot provide information on the variability across the model grid volume.

The running volume-averaging process results in another continuous function in space. For example, simple volume averaging over a rectangular cell is defined as:

$$\langle f(x, y, z) \rangle = \frac{1}{\Delta V} \int_{z-\Delta z/2}^{z+\Delta z/2} \int_{y-\Delta y/2}^{y+\Delta y/2} \int_{x-\Delta x/2}^{x+\Delta x/2} f(x', y', z') dx' dy' dz' \quad (8)$$

where $\Delta V = \Delta x \Delta y \Delta z$. A general volume averaging is defined with a filter function as:

$$\langle f_G(x, y, z) \rangle = \frac{1}{\Delta V} \int_{z-\Delta z/2}^{z+\Delta z/2} \int_{y-\Delta y/2}^{y+\Delta y/2} \int_{x-\Delta x/2}^{x+\Delta x/2} G(x-x', y-y', z-z') f(x', y', z') dx' dy' dz' \quad (9)$$

where G is the appropriate weighting function whose modulus is one. In the Eulerian modeling, a discrete averaging is applied to a deterministic function (an ensemble averaged quantity here) over the fixed volume of the cell (i, j, k) to provide a discrete formulation of the governing equation:

$$\langle \bar{f}_\ell(x_i, y_j, z_k) \rangle = \frac{1}{\Delta V} \int_{z-\Delta z/2}^{z+\Delta z/2} \int_{y-\Delta y/2}^{y+\Delta y/2} \int_{x-\Delta x/2}^{x+\Delta x/2} \bar{f}_e(x', y', z') dx' dy' dz' \quad (10)$$

2.5 Reynolds-Averaged Conservation Equations for Air Pollutants

To make the instantaneous species continuity equation useful for air quality simulation, we need to derive the governing diffusion equation. The first step is to decompose variables in Eq. 1 into mean and turbulent components. The velocities and concentrations of the various species in atmospheric flow are turbulent quantities and undergo turbulent diffusion. Because turbulent diffusion is much greater than molecular diffusion for most trace species, the latter can be ignored. Also we assume the ergodic hypothesis holds for the ensemble averaging process, which means the ensemble average of a property can be substituted with the time average of that property. The turbulence is assumed stationary for the averaging time period of interest (e.g., 30 minutes to one hour for atmospheric applications). The Reynolds decompositions of air density (ρ) and species concentration (φ_i) are expressed as:

$$\rho = \bar{\rho} + \rho' \quad (11)$$

$$\varphi_i = \bar{\varphi}_i + \varphi_i' \quad (12)$$

Some of the parameters in the conservation equations (1), (2) and (3) are nonlinearly related to each other and, therefore, direct application of Reynolds decomposition to these parameters will introduce covariance terms that complicates the turbulence equations. Instead, we define averaged mixing ratio and its fluctuation component based on Eqs. (11) and (12):

$$\bar{q}_i \equiv \bar{\varphi}_i / \bar{\rho} \quad (13a)$$

$$q_i' \equiv \varphi_i' / \bar{\rho} \quad (13b)$$

Similarly, the average contravariant wind components and their fluctuations are defined as

$$\bar{u} \equiv \overline{\rho u} / \bar{\rho}; \quad \bar{v} \equiv \overline{\rho v} / \bar{\rho}; \quad \bar{w} \equiv \overline{\rho w} / \bar{\rho} \quad (14a)$$

$$u' \equiv u - \bar{u}; \quad v' \equiv v - \bar{v}; \quad w' \equiv w - \bar{w} \quad (14b)$$

This definition allows the continuity equation for the Reynolds averaged variables to keep the original conservation form shown in Eq. (1) as

$$\frac{\partial \bar{\rho}}{\partial t} + \frac{\partial \bar{\rho u}}{\partial x} + \frac{\partial \bar{\rho v}}{\partial y} + \frac{\partial \bar{\rho w}}{\partial z} = 0 \quad (15)$$

Decomposing velocity components in Eq. (2) using Eqs. (14a) and (14b), the Reynolds averaged trace species conservation equation, neglecting the molecular diffusion, is:

$$\frac{\partial \bar{\varphi}_i}{\partial t} + \frac{\partial}{\partial x} (\overline{(\varphi_i + \varphi_i')(\bar{u} + u')}) + \frac{\partial}{\partial y} (\overline{(\varphi_i + \varphi_i')(\bar{v} + v')}) + \frac{\partial}{\partial z} (\overline{(\varphi_i + \varphi_i')(\bar{w} + w')}) = \bar{Q}_{\varphi_i} \quad (16)$$

The source function (i.e., emissions of pollutants) is assumed to be deterministic for all practical purposes and there is no turbulent component. The Reynolds flux terms in Eq. (16) can be approximated in terms of the mixing ratio to give:

$$\frac{\partial \bar{\varphi}_i}{\partial t} + \frac{\partial \bar{\varphi}_i \bar{u}}{\partial x} + \frac{\partial \bar{\varphi}_i \bar{v}}{\partial y} + \frac{\partial \bar{\varphi}_i \bar{w}}{\partial z} + \frac{\partial}{\partial x} (\overline{\rho q_i' u'}) + \frac{\partial}{\partial y} (\overline{\rho q_i' v'}) + \frac{\partial}{\partial z} (\overline{\rho q_i' w'}) = \bar{Q}_{\varphi_i} \quad (17)$$

Equation (17) has the "closure problem" that prevents direct solution. This problem occurs because of the nonlinearity of the conservation equations, which, upon averaging a random field, leads to unknown turbulence flux terms (Reynolds flux) involving the correlations of the random field components. Meteorological models only resolve the mean wind components (u, v, w) leaving an unresolved portion that is sometimes of the same magnitude as the mean wind. Therefore, the turbulent flux terms can be very large. Even a very fine scale meteorological model (e.g., grid resolution of 1 km) cannot provide detailed enough information about the turbulent fluctuations. The spatial and temporal scales of the smaller turbulent eddies are so small that a correct numerical integration of Eq. (17) would be practically impossible. Wyngaard (1982) suggested that it would probably require a grid size of about 1 mm in the entire computational domain, which is computationally impractical for air quality problems.

The recognition that the uncertainties brought by the turbulent component can be minimized but never eliminated is the key to understanding the significance of the ensemble averaging. This point can be clarified by noting that state variables such as wind components and concentrations are stochastic variables; i.e., there exists an infinite family of functions of these state variables that satisfy the equation of motion and atmospheric diffusion equation. The situation is described in Figure 3, where each possible member of wind of the family generates a different concentration. The average, at a certain point and time, of all possible concentrations generated by the different wind gives the theoretical ensemble mean concentration. Naturally, if we could measure wind and concentration continuously and in space and time, we could evaluate the exact member of the family that has occurred in reality. Lacking this information, we must assume that all theoretically acceptable wind fluctuations are equally possible, thus allowing, in the best of possible conditions, the computation of mean concentration ($\bar{\varphi}_i$) instead of the instantaneous (actual) φ_i . *An important conclusion that follows from the ensemble averaging process is that the concentration output provided by all Eulerian models is conceptually different from the air quality data gathered*

from monitoring activities. The monitoring data provide estimates of the actual concentration within the error limit of the monitoring technique while model outputs are estimates of the ensemble average. The monitoring data may have representativeness problem and model output has certain degree of error caused by the uncertainties in the input data and approximations in the numerical and/or analytical solutions.

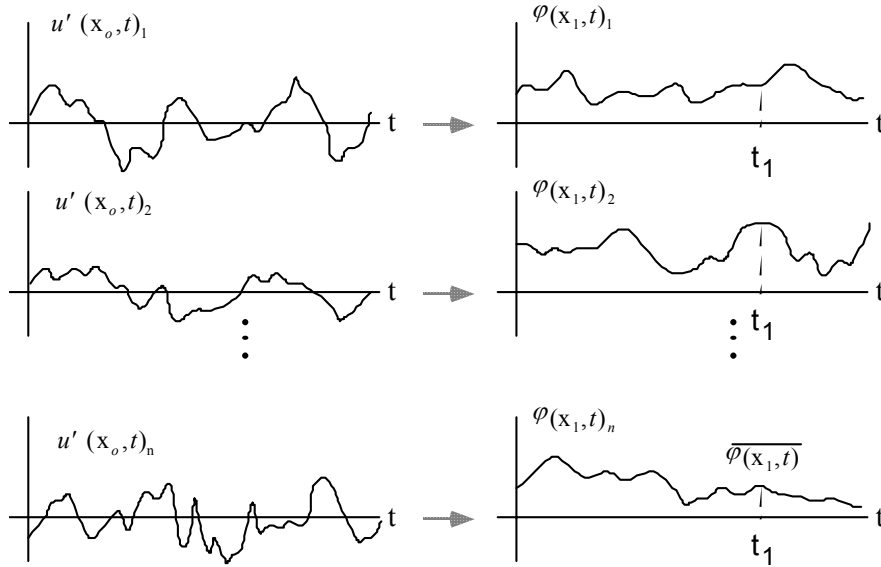


Figure 3. The infinite family or ensemble of velocity functions (turbulent component) u' and the corresponding family of concentration distributions (φ) each portrayed at fixed points x_o and x_1 as functions of time. The subscript n ($n=1,2,\dots$) denotes the member of realization of the ensemble. The ensemble mean value $\bar{\varphi}$ at a given time t_1 is formed by averaging $\varphi(x_1, t)_n$ over the infinite ensemble, as indicated by the vertical dashed line (adapted from Lamb; in Longhetto, 1980).

The turbulent flux terms can be parameterized using a simple closure scheme such as the eddy diffusion concept (K-theory):

$$\overline{q_i' u'} = -K^{1l} \frac{\partial \bar{q}_i}{\partial x^l}; \quad \overline{q_i' v'} = -K^{2l} \frac{\partial \bar{q}_i}{\partial x^l}; \quad \overline{q_i' w'} = -K^{3l} \frac{\partial \bar{q}_i}{\partial x^l} \quad (18)$$

where K^{jl} denotes the eddy diffusivity tensor over the index l ($l=1,2,$ or 3) and repeated index l in the equation represents summation over the all three components. For convenience, we postulate that the diffusivity tensor in Cartesian coordinates is diagonal, i.e., all the off-diagonal components vanish such that $K^{11} = K_{xx}$, $K^{22} = K_{yy}$, $K^{33} = K_{zz}$, and $K^{ij} = 0$ for $i \neq j$. Then the governing atmospheric diffusion equation (when the turbulent flux terms are expressed with the eddy diffusion theory) is:

$$\frac{\partial \bar{\varphi}_i}{\partial t} + \frac{\partial \bar{\varphi}_i \bar{u}}{\partial x} + \frac{\partial \bar{\varphi}_i \bar{v}}{\partial y} + \frac{\partial \bar{\varphi}_i \bar{w}}{\partial z} - \frac{\partial}{\partial x} (\bar{\rho} K_{xx} \frac{\partial \bar{q}_i}{\partial x}) - \frac{\partial}{\partial y} (\bar{\rho} K_{yy} \frac{\partial \bar{q}_i}{\partial y}) - \frac{\partial}{\partial z} (\bar{\rho} K_{zz} \frac{\partial \bar{q}_i}{\partial z}) = \bar{Q}_{\varphi_i} \quad (19)$$

(a) (b) (c) (d) (e) (f)

The terms in Equation (19) are summarized as follows:

- (a) time rate of change of pollutant concentration;
- (b) horizontal advection;
- (c) vertical advection;
- (d) horizontal eddy diffusion (diagonal term);
- (e) vertical eddy diffusion (diagonal term);
- (f) emissions, loss of pollutant at boundaries, and effects of chemical reactions.

3 Analytical Solutions for Ideal Atmospheric Conditions

The governing atmospheric diffusion equation, Eq. (19), can only be solved with a numerical technique. Analytical solutions are available under special simplifying assumptions. In the natural Cartesian coordinate where the wind is assumed to blow towards the positive x -axis (i.e., $\bar{u} = U$, $\bar{v} = 0$) and the vertical velocity is negligible ($\bar{w} = 0$), the governing equation for a trace species is simplified as:

$$\frac{\partial \bar{\varphi}}{\partial t} + U \frac{\partial \bar{\varphi}}{\partial x} = \frac{\partial}{\partial x} \left(K_{xx} \frac{\partial \bar{\varphi}}{\partial x} \right) + \frac{\partial}{\partial y} \left(K_{yy} \frac{\partial \bar{\varphi}}{\partial y} \right) + \frac{\partial}{\partial z} \left(K_{zz} \frac{\partial \bar{\varphi}}{\partial z} \right) + \bar{Q}_{\varphi} \quad (20)$$

in which Boussinesq approximation and incompressible flow assumptions were applied. Analytical solutions to Eq. (20) and its simplified form are discussed in Hanna et al (1982), Pasquill and Smith (1983), Seinfeld (1986), Tirabassi et al. (1986), and Arya (1999). One common method for obtaining an analytical solution is reducing the dimensionality of the problem. A two-dimensional solution for ground-level sources and a solution valid for linear profiles of K_{zz} can be found, for example, in Calder (1949) and Rounds (1955). Smith (1957) found a solution for elevated sources with U and K_{zz} profiles following Schmidt's conjugate power law:

$$U = U_r (z / z_r)^\alpha \quad (21)$$

$$K_{zz} = K_{zr} (z / z_r)^\beta \quad (22)$$

in which the powers of momentum profile and eddy diffusivity strictly satisfy the conjugate relationship $\alpha + \beta = 1$. U_r and K_{zr} are wind speed and eddy diffusivity, respectively, at the reference height z_r . Yeh and Huang (1975) and

Demuth (1978) obtained more general analytical solutions. They considered a steady state condition with accompanying boundary conditions

$$\bar{\varphi} = \frac{\bar{Q}_\varphi}{U(h_e)} \delta(z - h_e) \delta(y) \quad \text{at } x = 0 \quad (23a)$$

and

$$K_{zz} \frac{\partial \bar{\varphi}}{\partial z} = 0 \quad \text{at } z = 0 \text{ and } h \quad (23b)$$

where h_e is the final effective height of the emissions (i.e., height of pollutant after plume rise), and h is the depth of the PBL, and \bar{Q}_φ is the source term. We assume that atmospheric dispersion along the x -axis (stream-wise diffusion) is negligible in comparison to the transport term:

$$\left| U \frac{\partial \bar{\varphi}}{\partial x} \right| \gg \left| \frac{\partial}{\partial x} \left(K_{xx} \frac{\partial \bar{\varphi}}{\partial x} \right) \right| \quad (24)$$

This assumption has been challenged recently by a few researchers. For example, Du and Venkatram (1998) have studied the effect of stream-wise diffusion on ground-level concentration. They found that the neglected term increases the dispersion rate to produce concentration decrease with distance following -2 power law (i.e., $\sigma_y^2 \propto x^2$) instead of $-3/2$ (i.e., $\sigma_y^2 \propto x^{3/2}$), which is predicted by the one-dimensional formula for the unstable boundary layer. Results from the wind tunnel experiment by Raupach and Legg (1983) also support the -2 power law. However, for the purpose of deriving analytical solutions, the assumption in Eq. (24) is used here. For convenience, the crosswind-integrated concentration is defined as

$$\langle \bar{\varphi} \rangle_y(x, z) = \int_{-\infty}^{\infty} \bar{\varphi}(x, y, z) dy \quad (25)$$

With the power-law expressions of wind and eddy diffusivity of Eqs. (21) and (22), but without the strict conjugate assumption, Yeh and Huang (1975) obtained a ground level crosswind integrated concentration for the case $h \rightarrow \infty$:

$$\langle \bar{\varphi} \rangle_y(x, 0) = \frac{Q_\varphi}{\lambda^\nu} \frac{1}{\Gamma(\gamma)} \frac{h^\nu}{U_r^\nu (xK_{zo})^\gamma} \exp \left[-\frac{U_r z_r^\omega h_e^\lambda}{\lambda^2 K_{zr} x} \right] \quad (26)$$

where

$$\lambda = \alpha - \beta + 2 \quad (27a)$$

$$\nu = (1 - \beta) / \lambda \quad (27b)$$

$$\gamma = (\alpha + 1) / \lambda \quad (27c)$$

$$\eta = (\alpha + \beta) / \lambda \quad (27d)$$

$$\omega = \beta - \alpha \quad (27e)$$

and Γ denotes the Gamma function.

With a finite mixing height (i.e., $h < \infty$) and for a plume within the PBL (i.e., $h_e < h$), the steady state solution is (Demuth, 1978)

$$\begin{aligned} (\bar{\phi})_y(x, 0) &= \frac{Q_\phi \lambda z_r^\alpha}{U_r h^{\alpha+1}} \cdot \\ &\left\{ \gamma + R^p \sum_{i=1}^{\infty} \left[\frac{J_{\gamma-1}(\sigma_{\gamma(i)} R^{\lambda/2}) \sigma_{\gamma(i)}^{\gamma-1}}{\Gamma(\gamma) J_{\gamma-1}^2(\sigma_{\gamma(i)}) 2^{\gamma-1}} \cdot \exp\left(-\frac{\sigma_{\gamma(i)}^2 \lambda^2 K_{zr} x}{4U_r z_r^\omega h^\lambda}\right) \right] \right\} \end{aligned} \quad (28)$$

where

$$R = h_e / h \quad (29a)$$

$$p = (1 - \beta) / 2 \quad (29b)$$

In Eq.(28), J_γ represents the Bessel function of the first kind of order γ , and $\sigma_{\gamma(i)}$ ($i=1, 2, \dots$) are its roots, i.e., $J_\gamma(\sigma_{\gamma(i)}) = 0$. The solutions given by Eqs. (26) and (28) represent the ground-level concentrations (i.e., $z = 0$). The elevated crosswind integrated concentrations $\langle \bar{\phi} \rangle_y(x, z)$ for the case $h \rightarrow \infty$ is derived by Huang (1979):

$$(\bar{\phi})_y(x, z) = \frac{Q_\phi (zh_e)^p z_r^\beta}{\lambda K_{zr} x} \exp\left(-\frac{U_r z_r^\omega (z^\lambda + h_e^\lambda)}{\lambda^2 K_{zr} x}\right) I_{-p}\left(\frac{2U_r z_r^\omega (zh_e)^\lambda}{\lambda^2 K_{zr} x}\right) \quad (30)$$

where I_{-p} is the modified Bessel function of the first kind of order $-p$.

For a finite mixing height ($h < \infty$), the crosswind-integrated concentration is obtained from Demuth (1978), giving

$$(\bar{\phi})_y(x, z) = \frac{Q_\phi \lambda z_r^\alpha}{U_r h^{\alpha+1}}$$

$$\left\{ \gamma + \left(\frac{zR}{h} \right)^p \sum_{i=1}^{\infty} \left[\frac{J_{\gamma-1}(\sigma_{\gamma(i)} R^{\lambda/2}) J_{\gamma-1}(\sigma_{\gamma(i)} (z/h)^{\lambda/2})}{J_{\gamma-1}^2(\sigma_{\gamma(i)})} \cdot \exp\left(-\frac{\sigma_{\gamma(i)}^2 \lambda^2 K_{zr} x}{4U_r z_r^{\omega} h^{\lambda}} \right) \right] \right\} \quad (31)$$

Tirabassi et al. (1986) verified, analytically and numerically, that as $z \rightarrow 0$, the limit of Eq.(30) and (31) converges to Eq.(26) and (28), respectively; and that as $h \rightarrow \infty$, the limit of Eqs.(28) and (31) gives Eqs. (26) and (30), respectively.

These formulae, Eqs. (30) and (31), deal with the crosswind integrated concentration $\langle \bar{\varphi} \rangle_y$. To calculate the three-dimensional concentration, $\bar{\varphi}(x, y, z)$, horizontal diffusion needs to be included. Let's assume that the crosswind diffusivity is of the form

$$K_y = U(z)f(x) = \frac{U(z)}{2} \frac{d\sigma_y^2}{dx} \quad (32)$$

where σ_y is the standard deviation of lateral dispersion. Eq. (32) can be obtained by relating the Fickian diffusion coefficient with the Gaussian dispersion (e.g., Arya, 1999) with the help of Taylor's Hypothesis. Then the solution is

$$\bar{\varphi}(x, y, z) = \langle \bar{\varphi} \rangle_y(x, z) \frac{1}{\sqrt{2\pi}\sigma_y} \exp\left(-\frac{y^2}{2\sigma_y^2} \right) \quad (33)$$

The formulae above have been incorporated into an organized computer package KAPPA-G (Tirabassi et al., 1986), which allows computation of three-dimensional steady-state simulations as proposed by Huang (1979).

Table 1 provides a few other analytical solutions of the Eulerian dispersion equation for simplified meteorological and boundary conditions. They can be used to study characteristics of simplified advection and diffusion equations and to verify numerical implementation of Eulerian dispersion models.

Table 1. Analytical solutions of advection-diffusion equation in the incompressible atmosphere

Classification	Equations and Boundary Conditions (B/C)	Solution	References
1-D, time-dependent, constant K , no wind, instantaneous area source	$\frac{\partial \varphi}{\partial t} = K \frac{\partial^2 \varphi}{\partial x^2}, \text{ with } K = K_o \text{ (constant).}$ B/C: $\varphi \rightarrow 0$ as $t \rightarrow \infty \forall x$ $\varphi \rightarrow 0$ as $t \rightarrow 0$ all except $x=0$. $\int_{-\infty}^{\infty} \varphi dx = Q_{ia}$, instantaneous area source (over y-z plane)	$\varphi = \frac{Q_{ia}}{(4\pi K_o t)^{1/2}} \exp\left[-\frac{x^2}{4K_o t}\right]$	Hanna et al. (1982)
3-D, time-dependent, constant K , no wind, instantaneous point source	$\frac{\partial \varphi}{\partial t} = K_{x_o} \frac{\partial^2 \varphi}{\partial x^2} + K_{y_o} \frac{\partial^2 \varphi}{\partial y^2} + K_{z_o} \frac{\partial^2 \varphi}{\partial z^2}, \text{ with constant } K.$ B/C: $\varphi \rightarrow 0$ as $t \rightarrow \infty \forall (x, y, z)$ $\varphi \rightarrow 0$ as $t \rightarrow 0$ all except $(x, y, z) = (0, 0, 0)$. $\int \int \int_{-\infty-\infty-\infty}^{\infty \infty \infty} \varphi dx dy dz = Q_p$, instantaneous point source	$\varphi = \frac{Q_p}{(4\pi K_o t)^{3/2}} \exp\left[-\frac{1}{4t} \left(\frac{x^2}{K_o} + \frac{y^2}{K_o} + \frac{z^2}{K_o}\right)\right]$	Hanna et al. (1982)
2-D, time-independent, variable U and K , continuous ground-level line source	$U \frac{\partial \varphi}{\partial x} = \frac{\partial}{\partial z} \left(K_z \frac{\partial \varphi}{\partial z} \right)$ B/C: $\varphi \rightarrow 0$ as $x, z \rightarrow \infty$ and $\varphi \rightarrow \infty$ as $x, z \rightarrow 0$ $K_z \frac{\partial \varphi}{\partial z} \rightarrow 0$ as $z \rightarrow 0$ and $x > 0$ $\int_0^{\infty} U \varphi dz = Q_{cl}$, $\forall x > 0$ instantaneous line source, given $K_z = K_1(z/z_1)^n$ and $U = U_1(z/z_1)^m$	$\varphi(x, z) = \frac{(m-n+2)Q_{cl}z_1^m}{2U_1\Gamma(s)} \left[\frac{U_1}{(m-n+2)^2 z_1^{m-n} K_1 x} \right]^s$ $\times \exp\left[\frac{U_1 z^{m-n+2}}{(m-n+2)^2 z_1^{m-n} K_1 x} \right]$ where $s = (m+1)/(m-n+2)$ and Γ is the gamma function	Roberts (1923), Hanna et al. (1982)
3-D, time-independent, constant U , variable K , continuous-point source at height $z=h_e$	$U \frac{\partial \varphi}{\partial x} = \frac{\partial}{\partial x} (K_x \frac{\partial \varphi}{\partial x}) + \frac{\partial}{\partial y} (K_y \frac{\partial \varphi}{\partial y}) + \frac{\partial}{\partial z} (K_z \frac{\partial \varphi}{\partial z})$ $K_x = \alpha U x, K_y = \beta U x, \text{ and } K_z = \gamma U x$ B/C: $\varphi \rightarrow 0$ as $x, y , z \rightarrow \infty$ and $\varphi \rightarrow \infty$ as $x, y, z \rightarrow 0$ $K_z \frac{\partial \varphi}{\partial z} \rightarrow 0$ as $z \rightarrow 0$; and $U \varphi = Q_{cp} \delta(z-h_e) \delta(y)$, continuous-point source at $(x, y, z) = (0, 0, h_e)$	$\varphi(x, z) = \frac{Q_{cp}}{2\pi x^2 U \sqrt{\beta \gamma}} [F_{z+h_e} + F_{z-h_e}]$, where $F_{z+h_e} = \left[1 + \frac{\alpha}{x^2} \left(\frac{y^2}{\beta} + \frac{(z+h_e)^2}{\gamma} \right) \right]^{-(1+1/2\alpha)}$ $F_{z-h_e} = \left[1 + \frac{\alpha}{x^2} \left(\frac{y^2}{\beta} + \frac{(z-h_e)^2}{\gamma} \right) \right]^{-(1+1/2\alpha)}$	Sharan and Yadav (1998)

4 Numerical Solution Methods

Numerical methods allow the computation of approximate solutions using an integration technique such as the operator splitting (fractional time steps) or a global implicit method with a spatial approximation method such as finite difference or finite element method. Other discretization methods such as spectral methods, boundary element methods, and particle methods are occasionally applied in computational fluid dynamics, but are not frequently used in mesoscale Eulerian dispersion models and thus will not be discussed.

4.1 Grid-Volume Averaged Atmospheric Diffusion Equation

A control volume approach is commonly used in atmospheric modeling. Using a control volume approach, the physical law governing the problem (i.e., the conservation principle) is examined. This principle is, then, applied to a control volume around the node. For example, in air quality modeling, the atmospheric continuity equation is written for each control volume by establishing a mass balance. It is important to note that, in this approach, the discrete nature of the finite difference method is recognized at the outset. Finally, a mathematical statement of the physical conservation principle is obtained in a way somewhat similar to the procedures used to derive the partial differential equations. The control volume approach is relatively simple when regular grids are used. In this case, the choice for the control volume is simply the grid cell itself. However, if nodes are to be placed at the boundaries of the domain, then the boundary cells must be a certain fraction of the interior cells (e.g., 1/2 or 1/4 for an equal spacing of the nodes). In the case of unequal spacing nodes the situation is more complicated, and therefore it is customary to write special finite difference equations at the boundary of domain. However, no limit is taken for shrinking the control volume to a point.

We apply volume averaging represented in Eq. (10) to the diffusion equation for trace species, Eq. (19), to obtain

$$\begin{aligned} & \frac{\partial \langle \bar{\phi}_i \rangle}{\partial t} + \frac{\partial \langle \bar{\phi}_i \bar{u} \rangle}{\partial x} + \frac{\partial \langle \bar{\phi}_i \bar{v} \rangle}{\partial y} + \frac{\partial \langle \bar{\phi}_i \bar{w} \rangle}{\partial z} \\ & - \frac{\partial}{\partial x} \left\langle \bar{\rho} K_{xx} \frac{\partial \bar{q}_i}{\partial x} \right\rangle - \frac{\partial}{\partial y} \left\langle \bar{\rho} K_{yy} \frac{\partial \bar{q}_i}{\partial y} \right\rangle - \frac{\partial}{\partial z} \left\langle \bar{\rho} K_{zz} \frac{\partial \bar{q}_i}{\partial z} \right\rangle = \left\langle Q_{\phi_i} \right\rangle \end{aligned} \quad (34)$$

where the off-diagonal terms were neglected for simplicity. For example, a derivative of the volume average can be approximated by the finite difference scheme as

$$\frac{\partial \langle \bar{\varphi}_i \bar{u} \rangle}{\partial x} = \frac{1}{\Delta V} \frac{\partial}{\partial x} \left[\int_{z-\Delta z/2}^{z+\Delta z/2} \int_{y-\Delta y/2}^{y+\Delta y/2} \int_{x-\Delta x/2}^{x+\Delta x/2} \bar{\varphi}_i \bar{u} dx dy dz \right] \cong \frac{1}{\Delta x} \left[\langle \bar{\varphi}_i \bar{u} \rangle^{x+\Delta x/2} - \langle \bar{\varphi}_i \bar{u} \rangle^{x-\Delta x/2} \right] \quad (35)$$

The volume averaged pollutant flux is further approximated by

$$\langle \bar{\varphi}_i \bar{u} \rangle^{x+\Delta x/2} \cong \langle \bar{u} \rangle^{x+\Delta x/2} \left[\frac{\langle \bar{\varphi}_i \rangle^x + \langle \bar{\varphi}_i \rangle^{x+\Delta x}}{2} \right] \quad (36)$$

where the wind components are defined at the cell interfaces. This type of two-dimensional staggered distribution of scalar and vector components is referred to as the Arakawa-*C* grid (Mesinger and Arakawa, 1976) and is often used in Eulerian modeling for solving the flux-form transport equations like Eq. (34).

4.2 Numerical Solution Techniques

The operators in Eq. (34) resulting from the discretization of the atmospheric diffusion equation are three-dimensional. Incorporating the approximations like Eqs. (35) and (36) in the spatial derivatives and applying temporal derivative like the Crank-Nicholson method (e.g., Pielke, 1984), Eq. (34) is reduced to a nonlinear algebraic equation involving a sparse matrix as an operand. Usually it is extremely expensive to solve the nonlinear algebraic equation with very large rank (for typical atmospheric diffusion problem, when the three dimensional problem is solved simultaneously, the rank is of order of 10^6). Furthermore, the characteristic time scales associated with the chemical production and the turbulent diffusion rates in the atmosphere are very small (usually a few seconds). Thus, very small time steps are required to get accurate solutions. On the other hand, multi-day simulations are typically performed in many applications of atmospheric models. Inversion of the large matrix thousands of times, at every time step, is costly despite of the rapid development of computer capability now and in near future. The required computational resources for comprehensive air quality models that include various other atmospheric processes in addition to the transport and diffusion usually dictates the use of operator splitting techniques.

4.2.1 Operator and Time Splitting

The various physical processes in the Eulerian dispersion equation have different mathematical properties. Because they impose different restrictions in the numerical solutions, it is difficult to evaluate if a suite of numerical schemes for the physical processes is accurate and stable. When a time splitting technique is applied, the system is split into a number of simpler subsystems, which can be solved consecutively one at a time. When applying the splitting method, equal time steps are not required for each of the subsystems. A relatively long time step may be used for the subsystem governing a slow process, while many smaller

steps calculate faster processes. In Eulerian dispersion modeling, the advection and diffusion and chemistry processes, for example, are separated, and they can be further split into one-dimensional operators using local approximations. The three-dimensional problem is thus reduced to a sequence of one-dimensional problems, which Yanenko (1971) called the method of fractional steps. The time-splitting method is also often called as the operator-splitting method (Otey and Dwyer, 1978). Furthermore, each component can be solved using different numerical techniques suitable to the characteristics of the described physical problem.

Operator splitting methods have been used in most air quality models, primarily due to different time steps allowed for physical processes representing atmospheric transport and chemistry (McRae et al., 1982). However, to best maintain numerical accuracy, the time splitting method requires detailed understanding of the temporal scales of individual physical processes to determine proper sequence of operator calls.

4.2.2 Global Implicit/Explicit Method

An alternative to the splitting methods is a global implicit method. With this method, all the physical processes are parameterized and discretized over the entire three-dimensional grid simultaneously. Because all the processes are being simulated at the same time and has to meet the Courant number requirement of the fastest process, the global implicit method requires large computational resources. Also, it is difficult to know if the solution converged due to the numerical damping associated with the numerical algorithms. The method is difficult to implement because of the weak modularity. The fact that the time step splitting demands more thought and effort for arranging the computational sequence of the operators is counterbalanced by the fact that the resulting simulations are generally faster than those using global-implicit methods.

To overcome this limitation, an implicit-explicit (IMEX) method has been suggested (Ascher, et al., 1995; Knoth and Wolke, 1998a, b). In the IMEX approach the (horizontal) advection is handled explicitly with a large time step and act as an artificial source in the coupled implicit integration of all the vertical transport processes (Knoth and Wolke, 1998b). For the implicit part of solution, either semi-implicit Runge-Kutta methods or a second order explicit-implicit backward differentiation formula (BDF) can be applied. The resulting numerical scheme can be very efficient while removing the arbitrary determination of the sequence of operators associated with a time-splitting method. A thorough review on the numerical time integration methods for photochemical air quality models with a large number of chemical species in three space dimensions is provided by Verwer et al. (1998).

4.3 Spatial Approximation and Discretization Methods

The equations governing atmospheric dynamics and chemistry are nonlinear partial differential equations that must be solved numerically. On a computer with a limited amount of memory, the values of the solutions cannot be represented everywhere, but only at a limited number of sample points in the modeling domain. The collection of sample points makes up a grid, while the individual locations at which the field variables are to be determined are called grid points or nodes. The process of representing a continuum by a finite number of points in space and time is known as discretization.

In this section, two common methods for spatial discretization are discussed—the finite difference method and the Galerkin method. The way in which the discretization is done is fundamentally different in each method. These discretization methods are fundamentally different and have major differences in their formulations.

4.3.1 Finite Difference Method

The most common numerical integration procedure for atmospheric modeling has been the finite difference method. In the finite difference method, the region being modeled is divided into a finite number of grid cells. Each of these cells is assumed to have a uniform (well-mixed) value for the pertinent dependent variable. For this reason, it seems natural that the node should be associated with the centroid (geometric center) of the cell. Note that this is different than the finite element method (discussed later), where the nodes are placed at the corners of the cell. With the finite difference method, the derivatives in the governing differential equations are replaced by finite difference approximations (for example, using a Taylor series expansion) to establish algebraic equations at the discrete set of points (usually of order of hundred thousands for atmospheric simulations) in space and time. The computers today can solve such large algebraic equations in a relatively short time. Many Eulerian transport models, in particular those with regular grid system, rely on the finite difference for their basic discretization method.

4.3.2 Galerkin Method

In the Galerkin method the spatial structure of each dependent variable is represented by basis functions. Suppose that a partial differential equation with appropriate boundary conditions is to be solved in a certain domain. When the approximation to the dependent variable(s), which is a sum of the products of the time dependent coefficients with the basis functions, is substituted into the partial differential equation, it yields a residual (i.e., an error). The Galerkin method requires that the residual be orthogonal to each basis function. Since the orthogonality requirement is expressed as a weighted integral of the residual, the Galerkin method is alternately known as the *weighted residual method*. In the

classical Galerkin method, the weighting functions (i.e., the weights of the residual) are chosen from the same space as the basis functions used to approximate the dependent variable. This procedure known as the Bubnov-Galerkin method is very effective in solving elliptic partial differential equations. For hyperbolic problems, more stable solutions are obtained when the weighting functions are selected from a space different than the basis functions. Such methods are usually associated with the name of Petrov-Galerkin (Brooks and Hughes, 1982). Recently, other methods have been introduced that may be very useful in atmospheric modeling, such as the Taylor-Galerkin method (Donea, 1984) and the Characteristic Galerkin method (Childs and Morton, 1990).

The two most useful Galerkin algorithms are finite element and spectral methods. The finite element method employs simple polynomials that are local (i.e., equal to zero except in a limited region), while the spectral method utilizes global basis orthogonal functions. The spectral method is often used in meteorological and global modeling. The introduction of the finite element method into atmospheric modeling is more recent. The finite element method should not always be viewed as a weighted residual method. The latter always leads to equations of integral form, which can be obtained by summation of contributions from various subdomains. Similar integral forms can be obtained from the variational method when the problem is governed by a variational principle.

In the finite element method the region can be divided into triangular as well as rectangular elements. The nodes are placed at the corners of the elements. This is quite different from the way in which discretization is done in the finite difference method. The dependent variable (e.g., pollutant concentration in air quality models) is generally not constant over an element but varies in some prescribed manner, depending on the interpolation polynomial (i.e., the basis function) being used. There are several advantages of the finite element method. The approach is readily adapted to the boundaries, especially in the case of irregular grids. Flux type boundary conditions are automatically included in the finite element formulation. The advantage of the weighted residual approach over the mass balance approach used in finite differences becomes evident in the presence of unstructured irregular grids. In fact, one of the main advantages of the finite element method over other spatial approximation techniques is that the finite element method can handle irregular grids routinely. Often models that use Galerkin methods solve the advection-diffusion equation with a global implicit method, instead of using the time splitting, to reduce the computational burden of minimization of the residual errors repeatedly.

4.4 Grid Structure of Eulerian Models

The accuracy of numerical solution of the atmospheric diffusion equation depends heavily on the discretization method. As discussed earlier, it is customary to treat the vertical and horizontal coordinates separately in meteorological models. Almost all the atmospheric models use a structured vertical grid system

discretized along the vertical coordinate. Except for models intended to study atmospheric phenomena near surface with limited vertical extent, a non-uniform vertical grid is usually used. In general, the grid spacing increases logarithmically with height to account for the variation in the air density. The grid spacing can be further modified based on the need for accurate descriptions of important dynamics and physics, such as cloud mixing and PBL structure.

In principle, simulations with higher horizontal grid resolutions provide more accurate solutions unless there are scale dependencies among physical parameterizations used in the model. However, as will be shown later, decreasing the grid spacing increases the number of cells and requires a reduced time step size to achieve stable computational results. Practical limitations in computer size and speed prohibit the use of uniformly high spatial resolution appropriate for the smallest scales of interest. Two such methods of increasing resolution are nested approaches with a structured uniform grid and an unstructured grid. In the following, we describe issues associated with these two contrasting approaches.

4.4.1 Structured Grid and Nesting

Most atmospheric models rely on regular (structured and uniform) horizontal grid systems for simplicity. To obtain accuracy of simulations for a desired area, a grid nesting technique can be used. Grid nesting involves the sequential placement of multiple finer-scale meshes in desired regions of the domain so as to provide increased spatial resolution locally. Nesting can be divided into static and dynamic nesting. In the static nesting, the resolution and size of each grid are determined *a priori* and remain fixed throughout the model simulation. In the dynamic nesting, grids may be changed following changes in the control parameters during the simulation to obtain efficient yet accurate solutions. The static nesting approach is illustrated in Figure 4. The spatial resolution of the coarse grid is usually an integer multiple of that of the fine grid. First, the coarse grid solution is marched forward one time step. This solution provides initial and lateral boundary conditions (both concentration and flux) to the fine grid solution that is advanced at a smaller time step (usually an integer fraction of the time step of coarse grid). It is customary to set the time step ratio between the coarse and fine grids to equal the grid size ratio between the same two grids in order to retain the numerical accuracy at the same order of approximation. After multiple steps of the fine grid computations are completed to catches up with the coarse grid solution, the former may or may not be used to update the latter (i.e., two-way vs. one-way nesting). Although dynamic nesting with a structured grid is used in some atmospheric models, it may not be efficient for dynamic grid adaptation because the fine nest grid generation requires a high degree of user interaction and user expertise.

There are a few shortcomings of using grid nesting. One is the tendency for propagating dispersive waves to discontinuously change their speeds upon passing from a mesh to the next and to reflect off the boundaries of each nest due

to an impedance mismatch across the mesh boundaries. In addition, when dealing with chemical reactions, there is a problem of species mass conservation across the grid interface because the chemical production and loss of trace species are nonlinearly related with the ratios of mixtures, which in turn depend on the grid size. The mass of certain species (e.g., radicals) may no longer be conserved because, when advancing the fine grid solution, the non-linear chemical reactions happen in addition to transport. However, the mass of the basic chemical elements such as sulfur, nitrogen, and carbon must be conserved. This requirement is often handled by re-normalization of the concentration of each species based on the assumption that the ratio of the species mass to element mass will remain the same before and after the correction.

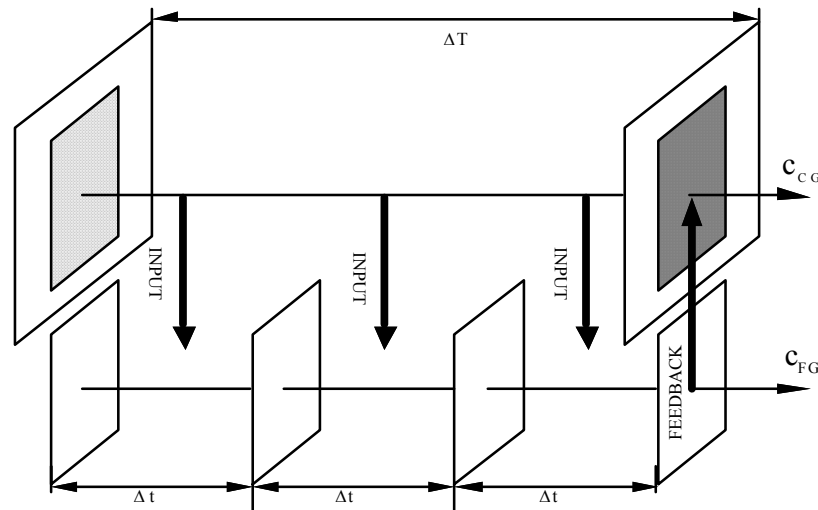


Figure 4. Static grid nesting example. Multi-level nesting is capable through a natural extension of the single static grid nesting. ΔT and Δt represent computational time steps of coarse and fine nest runs, respectively. In two-way nesting, the concentration from the fine nest grid simulation (C_{FG}) is used to update the coarse grid concentration (C_{CG}).

4.4.2 Unstructured Grid

A few atmospheric models with unstructured horizontal grids have been developed recently. For example, a dynamically adapting weather and dispersion model, the Operational Multiscale Environmental Model with Grid Adaptivity (OMEGA) (Bacon et al., 2000) utilizes an adaptive unstructured grid technique that allows continuously varying horizontal grid resolutions ranging from 100 km down to 1 km. OMEGA can adapt its grid both statically to topographical features and dynamically to different adaptivity criteria such as fronts, clouds, hurricanes, and plumes. Also, Ghorai et al. (2000) solve the three-dimensional atmospheric dispersion equation using a time dependent adaptive grid technique based on tetrahedral elements. The unstructured grid technique is rather new to the atmospheric science community. In many fields of engineering applications, the unstructured grid method has been in use for more than a decade due to its

efficiency in the modeling of irregular domains. The flexibility of unstructured grids and their ability to adapt to transient physical phenomena are the features that give unstructured grid algorithms for partial differential equations their great power.

Grid refinement techniques can be subdivided into two basic categories. The first includes methods in which grid points are added locally to the computational domain as the calculation proceeds, or finite elements are subdivided locally, to provide increased spatial resolution based on predetermined physical criteria. The second category of refinement technique involves methods that redistribute a fixed number of grid points so as to provide locally increased resolution and thus an improved solution in certain regions of the domain. The static grid adaptability of an unstructured grid allows reduction of the total number of cells necessary to correctly simulate underlying physics, such as caused by the topography and land use. Further, a dynamic grid technique allows refinement of grids to resolve important physical events and features as the simulation is in progress. Bacon et al. (2000) summarize the dynamic grid adaptation process with four major steps: 1) at a predetermined time step specific variables or their gradients are evaluated to see if they meet the adaptivity criteria, 2) the mesh is refined where these criteria are satisfied, 3) the physical variables are interpolated to new cell centers, and finally 4) the mesh is coarsened where the criteria are not met. Setting the right criteria for adaptation is very important. There is a significant cost associated with a grid adaptation; hence, the ideal criteria are those that require minimum computational effort to evaluate yet indicate key regions requiring additional resolution.

5 Numerical Algorithms for Advection

In this section, we present advection separately from diffusion processes following the fractional time splitting concept. The algorithm discussions are mostly based on finite difference schemes on a structured grid system. In general, two transport processes are considered in atmospheric models: convection (or advection) and (turbulent) diffusion. Convection can only transport a disturbance in the direction of wind velocity. Turbulent diffusion, on the other hand, can spread a disturbance in every direction. The atmospheric continuity equation that governs pollutant transport and chemistry describes these transport mechanisms mathematically. Horizontal transport in the atmosphere is advection dominated. Numerical approximations to this equation have the *transportive* property, i.e., $d\langle q \rangle / dt = 0$. In Eulerian air quality models, the volume-integrated quantities for each cell are subject to following conservation equation:

$$\frac{\partial \langle \bar{\rho} \rangle}{\partial t} + \left[\frac{\partial}{\partial x} \langle \bar{\rho} \bar{u} \rangle \right] + \left[\frac{\partial}{\partial y} \langle \bar{\rho} \bar{v} \rangle \right] + \left[\frac{\partial}{\partial z} \langle \bar{\rho} \bar{w} \rangle \right] = \langle \bar{Q}_\rho \rangle \quad (37)$$

The source term in the continuity equation $\langle \bar{Q}_\rho \rangle$ represents the error that might exist due to the mass-inconsistency in the input wind and density fields or deficiencies in the numerical scheme. Imposing the necessary condition $d(q)/dt = 0$ for the numerical transport under the possible mass consistency error, we obtain the following flux form conservation equation (Byun, 1999b).

$$\frac{\partial \langle \bar{\varphi}_i \rangle}{\partial t} + \left[\frac{\partial}{\partial x} \langle \bar{\varphi}_i \bar{u} \rangle \right] + \left[\frac{\partial}{\partial y} \langle \bar{\varphi}_i \bar{v} \rangle \right] + \left[\frac{\partial}{\partial z} \langle \bar{\varphi}_i \bar{w} \rangle \right] = \langle \bar{\varphi}_i \rangle \frac{\langle \bar{Q}_\rho \rangle}{\langle \bar{\rho} \rangle} \quad (38)$$

5.1 Numerical Advection Algorithms

There have been many studies on the numerical advection algorithms used in air quality models (e.g., Chock and Dunker, 1983; Chock, 1985, 1991; Rood, 1987) and the list is continuously growing. Numerical advection has attracted so much attention because it is the difficulty in obtaining a good numerical solution under variety of wind conditions and source distributions. Discretization of the hyperbolic equation generates only a finite number of Fourier modes that travel at different speeds and sometimes leads to destructive interference that causes interpretation of signals at different wavelengths. Various errors introduced by advection algorithms have historically been a major source of inaccuracy in air quality models. A classical problem in numerical analysis is to construct an advection scheme for a grid system that is not specially oriented to follow the characteristics of the solution. While it is essential to maintain conservative and transportive properties in the equations, the scheme must also satisfy stability and accuracy requirements. A signal being advected along the line of flow may also spread in a direction normal to the line of flow. This diffusion is referred to as artificial diffusion because it is inherent with the lack of numerical consistency in the numerical solutions.

The numerical algorithm is described with the one-dimensional version of the advection term with $\bar{u} = U$,

$$\frac{\partial \varphi}{\partial t} + \frac{\partial (U\varphi)}{\partial x} = 0 \quad (39)$$

where we replaced $\langle \bar{\varphi}_i \rangle$ with φ for the simplicity in the expression. Eq. (39) is the flux (or conservation) form and the quantity $F_x = U\varphi$ is defined as the one-dimensional constituent flux. The flux form is a natural choice here because it is based on the continuity equation without any assumptions on the atmospheric dynamics. Discretization of the flux form of Eq. (39) results in

$$\varphi_j^{n+1} = \varphi_j^n - \frac{\Delta t}{\Delta x_j} (F_{j+1/2}^n - F_{j-1/2}^n) \quad (40)$$

where $F_{j+1/2}^n$ and $F_{j-1/2}^n$ denote the advective fluxes through the interfaces of cell j , Δt is the time step, and Δx_j is the cell length in the same metric space that the velocities are defined.

While it may appear that we have lost some coordinate system generality, multiplication of Eq.(40) by the cell's volume to yield cell mass, now leads us to a geometrical picture of the advection process that transcends the preceding mathematical complexity and leaves us with the simple algebraic equation:

$$M_j^{n+1} = M_j^n + (\Delta M_{j-1/2}^n - \Delta M_{j+1/2}^n) \quad (41)$$

where $M_j^n = \Delta x_j \phi_j^n$ and $\Delta M_{j+1/2}^n = \Delta t_j F_{j+1/2}^n$. Basically, the mass in cell j at the end of the time step is the mass at the beginning of the time step plus the mass increment entering the cell from its left-hand neighbor minus the mass increment passed along to the cell's right-hand neighbor (assuming all cell-face velocities are positive). The complexity is now buried in how we define the mass transfers, ΔM , and the CFL numbers, β , at the cell faces. For a temporally-explicit (i.e., forward-in-time) scheme, and a positive value of $U_{j+1/2}$, we define the Courant-Fridlich-Lewy (CFL) as:

$$\beta_{j+1/2} = U_{j+1/2} \frac{\Delta t}{\Delta x_j} \quad (42)$$

Should $U_{j+1/2}$ be negative, the appropriate Δx to be considered would be that of the upwind cell Δx_{j+1} . Similarly, the cell to be considered for the mass transfers is always the upwind cell, so for the case of the positive value of $U_{j+1/2}$, we define the current $\Delta M_{j+1/2}^n$ as: $\Delta M_{j+1/2}^n = -\beta_{j+1/2} M_j^{*n}$, where M_j^{*n} can be a high-spatial-order definition of the mass distribution within the cell or reduces to the cell mass M_j^n itself for the case of low-order, Donor-cell treatment or when $\beta_{j+1/2} = 1$. Thus, in the simple case of Donor-cell advection, the fraction of a cell's mass that is transferred across a face is just equal to the outgoing CFL number at that face. To maintain numerical stability and to accommodate other physical changes such as emissions input in a synchronized way, the time step of 1-D advection should satisfy the CFL condition for the whole domain:

$$\beta_{\max} = \max_j \frac{|U_{j+1/2}| \Delta t}{\Delta x_j} \leq 1 \quad (43)$$

The only geometrical factor not considered in this view is the local spatial variation of the map factor within the particular cell being depleted. Though this

gradient term is present in the formulation of transport, these gradients are mostly discarded in finite difference implementations as being "higher-order" differentials. However, as they relate simply to the "shape" of the cell (i.e., to the cell being non-square), they may be easily included by a multiplicative "keystoning factor". Thus, in the two-dimensional transport example we now allow the cell to be trapezoidal in shape with differing transverse widths, $\Delta y_{j+1/2}$ and $\Delta y_{j-1/2}$, at the right and left faces and correct the CFL with the easily visualized and derived, multiplicative "keystoning factor", expressed as, for $\beta_{j+1/2} > 0$:

$$K_{j+1/2} = \beta_{j+1/2} + 2(1 - \beta_{j+1/2}) \frac{\Delta y_{j+1/2}}{\Delta y_{j+1/2} + \Delta y_{j-1/2}} \quad (44)$$

Using this corrected CFL, $K_{j+1/2} \cdot \beta_{j+1/2}$, means that advection will now transfer the correct fraction of cell area or mass destined to be transferred rather than the correct, x -directional fraction of cell length. It is interesting that by folding the length-scale parallel to the wind component into the face CFL and the aerial and vertical map factors into computation of the total cell mass, one is then able to proceed with the development of a sophisticated, mass-conservative, advection scheme for an arbitrary metric grid with simple arithmetic.

Although the Donor-cell advection scheme, which assumes a constant concentration distribution within each cell, has several necessary properties (i.e., it is mass-conservative, positive-definite, and transports material at the correct speed), it is extremely diffusive. The many dozens of pollutant advection schemes developed over the past decades attempt to minimize this numerical diffusion of material by employing a more accurate description of the concentration distribution within each cell. This is accomplished generally by describing the in-cell distribution with some higher-order polynomial and basing the coefficients of that polynomial on local or global variations of the gridded, average concentrations. For example, some schemes utilize a fairly local definition of a first-derivative, such as: $(\partial \varphi / \partial x)_j = (\varphi_{j+1} - \varphi_{j-1}) / 2\Delta x$, whereas other schemes would call upon more distant point pairs (e.g., $(j+2, j-2)$, $(j+3, j-3)$, and beyond) to compute this first derivative and/or higher derivatives, and are often referred to as higher-order-accurate or 'global' derivative definitions, those the term global is sometimes reserved for schemes where derivatives are computed based on implicit relationships rather than on an explicit, truncation-error-reducing series involving the more distant grid point information. The virtue of these higher-order polynomial schemes that involve various definitions of the spatial derivatives is that they can accurately capture realistic and dramatic spatial variations in φ_j within in the cell j ; however, such dramatic variations can also include undesired concentration overshoots and undershoots (e.g., Gibbs

ringing, negative concentrations, antidiffusive instability) that must be suitably blocked ahead of time or filtered out after the fact.

In Eulerian dispersion modeling, it is essential that an advection scheme be mass-conservative, but we have seen that this is guaranteed by the flux-formulation and not by the details of the advection scheme itself. If non-linear chemistry is to be modeled as well, then the scheme must be positive-definite (i.e., not permitting negative concentration solutions that would cause the chemical solver to add to this unphysical behavior) and should also avoid any excessive erosion of a uniform background concentration. Beyond these 'musts', the importance given to minimizing various uncertainty measures (e.g., root-mean-square error, maximum error, average error, sum of concentrations squared), or such measures applied to $\log(\phi)$ or any measure as a function of the wavelength/shape of the test distribution, still remains rather subjective and, as a result, has inhibited converging on an algorithm that could reasonably be called the 'best'. For example, were it not for an abysmal response to single point-source emissions, few would contest the superiority of spectral methods in providing very high-fidelity response to longer wavelength distributions; however, computational expense is also a factor that weighs into this subjective judging, and this factor weighs against the spectral techniques. In addition, most advection tests are performed on uniform, constant thickness grids. An advection scheme should also yield smooth, accurate non-negative solutions over differently scaled portions of irregular grid systems. Similarly, sharp concentration gradients or horizontal variations in the vertical dimensions of grid cells should not lead to accelerations or decelerations of material in the horizontal direction (see Table 4 for the algorithms of several advection schemes often used in Eulerian dispersion modeling).

Performance characteristics of these advection schemes should also be studied for realistic atmospheric conditions rather than just for over-simplified flows and idealized distributions. The traditional long-wave propagation tests, such as the cosine-hill rotation test case (Crowley, 1968) tend to show an advection scheme at its best; however, adequate short wavelength performance is also extremely important in Eulerian dispersion models. One of the most stringent tests involves the two-dimensional transport and diffusion of emissions from a single-grid source (Yamartino, 1993). This situation often arises in air quality modeling despite the fact that the maximum resolution of transport algorithms is limited to two grid cell lengths (i.e., $\lambda = 2\Delta x$ waves are very rapidly diffused). Such test problems are often neglected in evaluating advection algorithms, but later become inevitable in actual simulations. Thus, identification of suitable evaluation cases is an issue just as important as developing advection schemes with *acceptable* characteristics.

5.2 Artificial Diffusion

It is well documented that numerical advection schemes are associated with the major sources of inaccuracy, particularly from artificial numerical diffusion and dispersion. Usually, low-order schemes display considerable diffusive dissipation. The amount of artificial diffusion introduced by low-order numerical algorithms can easily outweigh physical diffusion. On the other hand, higher-order schemes are dispersive and generate spurious oscillations that can even lead to instabilities. The more popular algorithms try to find the best compromise between these two sources of inaccuracy to arrive at an *acceptable* solution. What is meant by acceptable is still a major topic of discussion among atmospheric modelers.

The numerical dispersion can be easily understood by analyzing the one-dimensional version, Eq. (39). With a central first-order finite-difference scheme and for a constant wind speed U , we obtain

$$\frac{\varphi_j^{n+1} - \varphi_j^n}{\Delta t} = -U \frac{\varphi_{j+1}^n - \varphi_{j-1}^n}{2\Delta x} \quad (45)$$

where we used a central spatial differencing. Analysis of the truncation terms shows that the error ε generated by the approximation of using Eq. (45) instead of Eq.(39) is

$$\begin{aligned} \varepsilon &= \frac{U\Delta x}{2} \left(1 - U \frac{\Delta t}{\Delta x}\right) \frac{\partial^2 \varphi}{\partial x^2} + H.O.T \\ &= D_N \frac{\partial^2 \varphi}{\partial x^2} + H.O.T \end{aligned} \quad (46)$$

which is a diffusion-type term with the associated diffusivity D_N equal to

$$D_N = \frac{U\Delta x}{2} (1 - \beta) \quad (47)$$

where $\beta = U\Delta t / \Delta x$ represents the CFL number (signed) and *H.O.T.* denotes the higher-order terms. In general, the even-ordered derivatives in terms of x represent the diffusion errors (i.e., loss of peak magnitude) while the odd-ordered derivatives represent the dispersion error (displacement of peak location in the signal, or phase-speed error). This analysis demonstrates that the numerical dispersion with the central difference scheme is proportional to the grid size Δx and is dependent on the Courant number of the flow. Different advection algorithms exhibit different numerical diffusion characteristics.

5.3 Mass Correction after Numerical Advection

A fundamental requirement for the numerical transport algorithms is the conservation of trace species in the domain. A conservative numerical advection algorithm can conserve trace mass when driven by the mass consistent wind and density fields. However, the meteorological data used in trace transport are often mass inconsistent. Simulating meteorological conditions for a limited area like urban or regional scale, the total air mass in the modeling domain is subject to the inflow, outflow, top, and bottom boundary conditions imposed by large synoptic scale weather systems and surface exchanges of heat and moisture. Furthermore, the time splitting of the original three-dimensional transport into a sequence of one-dimensional solutions introduces cross-term errors that must be corrected. To take into account the residual (error) term as part of the numerical transport process, we must solve the following correction term as a part of the numerical transport.

$$\frac{\partial \langle \bar{\varphi}_i \rangle}{\partial t} = \langle \bar{\varphi}_i \rangle \frac{\langle \bar{Q}_\rho \rangle}{\langle \bar{\rho} \rangle} \quad (48)$$

Ideally, $\langle \bar{Q}_\rho \rangle$ must vanish everywhere in the computational cells. If not, an algorithm that theoretically conserves mass may fail to conserve trace species mass in the application. Byun (1999b) and others proposed to handle the mass inconsistency by forcing conservation of mixing ratio (instead of mass) during the advection process. The undesirable effects of the mass-inconsistent error can then be corrected with:

$$(\bar{\varphi}_i)^{cor} = (\bar{\varphi}_i)^T \exp\left[\int \frac{(\bar{Q}_\rho)}{(\bar{\rho})} dt\right] \quad (49)$$

where superscripts T and cor represent values after transport (advection) and after correction, respectively. An adequate correction scheme conserves the trace mixing ratio even if wind and density fields are not mass consistent. It is given as:

$$(\bar{\varphi}_i)^{cor} = \frac{(\bar{\varphi}_i)^T}{(\bar{\rho})^T} (\bar{\rho})^{int} \quad (50)$$

where $(\bar{\rho})^{int}$ is the volume-weighted density interpolated in time at the integration time step.

For a limited-area atmospheric model where air mass in the model domain is not conserved, the mixing-ratio conservation scheme is demonstrated to be useful for photochemical air quality simulations where chemical production and loss terms

are computed using molar mixing ratio. However, one should be reminded that the above approach only fulfills a necessary condition, but not sufficient condition, for mass conservation. Therefore, before applying this final correction step, the mass inconsistency in the meteorology data must be minimized such as using a variational wind field adjustment scheme. The correction scheme fixes mixing ratio conservation errors due to the time splitting, numerical algorithms, and the mass inconsistent meteorological data input altogether. It does not, however, improve the inherent properties of a numerical advection scheme such as monotonicity, or numerical diffusivity. It must be emphasized that time splitting of advection into horizontal direction and vertical direction is for the convenience of obtaining numerical solution. The three-dimensional advection and the mass adjustment are the necessary steps to simulate inseparable atmospheric advection process.

6 Horizontal Diffusion Algorithm

For atmospheric modeling the three-dimensional diffusion is often decomposed into horizontal and vertical directions because the two are subject to different distinctly different atmospheric processes. The horizontal mixing is influenced by the heterogeneous atmospheric conditions in a grid cell and is frequently parameterized with the eddy-diffusion theory. From Eq. (34) in which the off-diagonal terms are neglected, the horizontal diffusion equation is given as:

$$\frac{\partial(\bar{\varphi}_i)}{\partial t} = \frac{\partial}{\partial x} \left(\bar{\rho} K_{xx} \frac{\partial \bar{q}_i}{\partial x} \right) + \frac{\partial}{\partial y} \left(\bar{\rho} K_{yy} \frac{\partial \bar{q}_i}{\partial y} \right) \quad (51)$$

The horizontal diffusion is often solved with an explicit finite difference method to minimize memory requirements in Eulerian transport models with a sufficiently small time step to ensure the positivity of solution. In Eulerian air quality modeling, eddy diffusivities are usually not distinguished in two different horizontal directions (i.e., $K_{xx} = K_{yy} = K_H$). Then, the problem is reduced to parameterization of the eddy diffusivity to reflect the sub-grid scale diffusion.

6.1 Horizontal Diffusivity Estimated from the Lagrangian Dispersion Theory (from Section 6.3.2 of Zannetti, 1990)

Estimation of the horizontal diffusivity presents several intriguing aspects. It is often (and perhaps, improperly) assumed that $K_H \approx K_y$, where K_y is the crosswind eddy diffusivity (i.e., with wind blowing along the positive x -axis). K_y is not necessarily equivalent to K_{yy} used for the Eulerian modeling exactly. For a plume originated at $x = 0$ and carried by the wind along the x -axis, K_y is related through Eq. (32) to the standard deviation of σ_y of the crosswind plume concentration spread. For a short travel time ($t = x/U(z) < T_L$)

$$K_y = c \left(\frac{U}{\Delta x} \right)^2 T_L \sigma_y^2 \quad (52)$$

where c is a constant that depends on the distance from the source and T_L is the Lagrangian turbulence time scale, which is the characteristic time scale determined by the auto-spectral correlation function following the movement of plume (with typical value of 100 sec for convective PBL). For a travel time much larger than the Lagrangian time scale (i.e., $t \gg T_L$), the Lagrangian dispersion theory predicts that:

$$K_y = \frac{1}{2} \left(\frac{U}{\Delta x} \right) \sigma_y^2 \quad (53)$$

To estimate the horizontal eddy diffusivity σ_y must be estimated from meteorological measurements. For example, the horizontal diffusion in a grid model is related to the long-range transport and diffusion of a plume from a point source at the ground surface (Pasquill, 1976):

$$\sigma_y = \sigma_\theta \Delta x f(\Delta x) \quad (54)$$

in which σ_θ is the standard deviation of the horizontal wind direction expressed in radians. The empirical function $f(\Delta x)$ is specified following Hanna et al. (1977); Irwin (1979); and Arya (1999):

$$f(\Delta x) = \begin{cases} [1 + 0.308 \Delta x^{0.455}]^{-1}, & \text{for } \Delta x \leq 10^4 \text{ m} \\ 33.3 \Delta x^{-1/2}, & \text{for } \Delta x > 10^4 \text{ m} \end{cases} \quad (55)$$

Eq. (55) represents a curve fit to Table 2.

Table 2. Pasquill's (1976) empirical function $f(\Delta x)$

Δx (m)	0	100	200	400	1000	2000	4000	10000	>10000
$f(\Delta x)$	1.0	0.8	0.7	0.65	0.6	0.4	0.4	0.33	$33.3(\Delta x)^{1/2}$

The horizontal eddy diffusivity is:

$$K_y = \begin{cases} c (U \sigma_\theta)^2 \frac{T_L}{[1 + 0.308 \Delta x^{0.455}]^2}, & \text{for } \Delta x \leq 10^4 \text{ m} \\ 0.5 \times 10^3 U \sigma_\theta^2, & \text{for } \Delta x > 10^4 \text{ m} \end{cases} \quad (56)$$

As expected, K_y is independent of the grid size for large downwind distance (which corresponds to the grid size in Eulerian models).

For $\Delta x > 10^4$ m, given typical values of $\sigma_\theta < 0.5$ radian and $U < 10$ ms^{-1} , Eq. (56) gives K_y values one to two orders of magnitude lower than the bottom range of $K_H = 10^4$ to 10^7 $\text{m}^2 \text{s}^{-1}$ currently used in most long-range models and considered to be the best values to fit actual measurements. This inconsistency can be traced back to the implicit assumption of the Lagrangian transport that the plume trajectory is known exactly and that σ_y and K_H characterizes only the horizontal growth of plume and not the uncertainty in the plume location. There are serious limitations estimating the Eulerian eddy diffusivity (K_H) at a certain location (x,y,z) , for example at the boundary of a grid cell, with the Lagrangian dispersion theory. Different values of K_y would be required for the pollutant plumes traveling from different sources, and therefore, having different travel times. An Eulerian model cannot handle this, because, after pollutants are injected into the grid cells, the memory of their different origins is lost. Actual modeling simulations, however, use meteorological wind fields, which contain a large degree of uncertainty when used for trajectory computations. Therefore, it is not surprising that actual model calibration tests suggest large values of K_H . This indicates that horizontal diffusion needs to be artificially enhanced for the model to incorporate the uncertainties in the wind fields.

To visualize the above considerations, consider a simple example shown in Figure 5, in which the contributions of three air pollution sources (S_1 , S_2 , and S_3) at the receptor R are evaluated through dispersion modeling with large K_H values. Although the model largely overestimates horizontal diffusion, it provides a total concentration value at R (the sum of three dashed curves) that is quite similar to the measured value (on the solid curve) due to compensation of errors in diffusion and wind fields. The model is, in a way, “validated”, but its use for evaluating emission reduction strategies will provide incorrect results; specifically in the case of emission reductions in S_1 , S_3 with insufficient control of S_2 . It is true that regular fluctuations in wind direction cause the solid plumes in Figure 5 to sweep around the azimuth in such a way that they all may envelope the receptor R . This variation of the short-term average wind can sometimes be correctly simulated, for long-term averages, by the dashed plumes, which are computed with an enhanced horizontal diffusion. However, wind direction fluctuations often do not show regular behavior and therefore, do not support the approximation. In complex terrain, especially, preferred directional patterns play important roles in determining plume trajectories, and the artificial enhancement of horizontal diffusion for long-term averages may provide incorrect results. Moreover, if nonlinear chemical reactions are used, the formation of secondary pollutants is incorrectly computed when the plume is diffused with artificially high dispersion rate, since the centerline plume concentration is consistently underestimated.

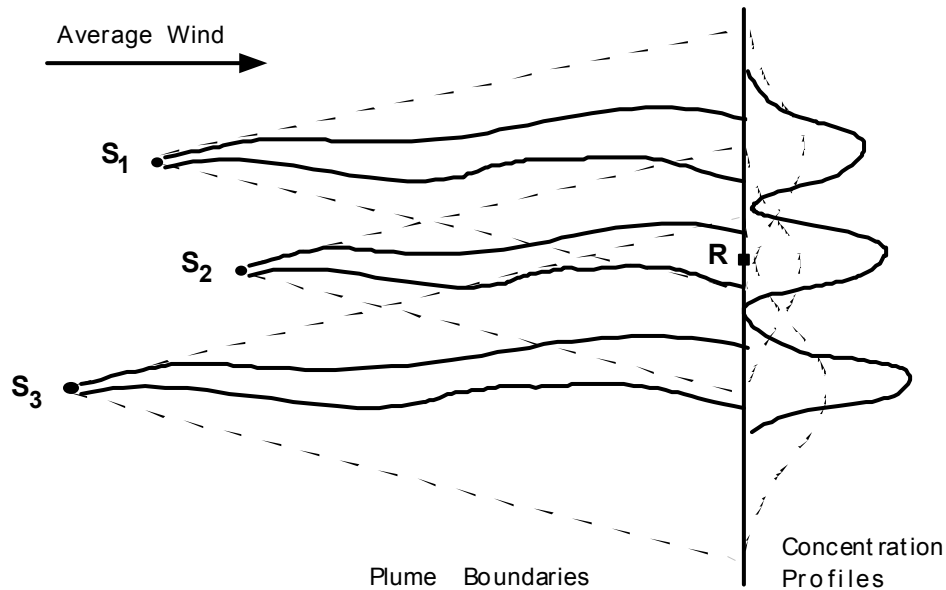


Figure 5. An example of the consequence of overestimating horizontal diffusion on the concentration at the receptor R. Solid lines show the actual average plume, while dotted lines show the plumes as simulated by the model.

6.2 Other Approaches for Estimating Horizontal Eddy Diffusivity

In an ideal case, the process must represent the effects of physical diffusion on pollutant dispersion. Although our understanding of horizontal turbulence is rather limited, appropriate accounting of physically based horizontal diffusion is necessary. We can identify certain types of nonphysical horizontal diffusion such as numerical diffusion resulting from the inconsistency (i.e., errors in higher-order expansion terms) in the advection scheme and artificial diffusion resulting from the instantaneous dilution of emissions and concentrations by the finite volume of the Eulerian grid cells. In the past, the horizontal diffusion process was often omitted because the numerical diffusion associated with the advection algorithm was large. It is also important to realize that the Eulerian simulation takes into account for the genuinely advective characteristics of pollutants.

For example, Smargorinsky's (1963) horizontal diffusivity algorithm accounts for the transport (stretching and shearing deformation) characteristics of wind flows:

$$K_{HT} = 2\alpha_o^2 (S_r^2 + S_A^2)^{1/2} (\Delta x)^2 \quad (57)$$

where $\alpha_o \cong 0.28$ and stretching strength (S_r) and shearing (S_A) strength are defined by

$$S_{\Gamma} = \frac{1}{2} \left(\frac{\partial U}{\partial x} - \frac{\partial V}{\partial y} \right) \quad (58a)$$

$$S_{\Lambda} = \frac{1}{2} \left(\frac{\partial V}{\partial x} + \frac{\partial U}{\partial y} \right) \quad (58b)$$

Because Eq. (57) relies on the grid-scale wind components, it is not suitable for estimating the sub-grid scale diffusion not resolved by the provided wind fields. Furthermore, for coarse resolution where numerical diffusion is already large, use of this formula seems inadequate. Draxler and Hess (1997) used similar formula in the HYSPLIT, a Lagrangian modeling system where numerical dispersion is not much an issue.

Yamartino and Machiraju (2000) suggest a method to determine appropriate horizontal diffusion coefficients by subtracting the numerical diffusivity already accompanying the advection scheme (see above). Artificial diffusion refers to the instantaneous dilution of emissions and concentrations by the finite volume of the grid cells. This instantaneous diffusion has traditionally been accepted as a penalty for using Eulerian grid models. If a few sources contributing to a cell are deemed important enough to avoid the instantaneous diffusion, they must be treated by either a finer nested mesh to cover the sub-domain of interest, or with a plume-in-grid module (see section 1.4) to describe the early dispersion/chemistry evolution of pollutants emitted. The specified horizontal diffusion term in Eulerian dispersion models, when combined with the effects of the input wind fields, the numerical diffusion of the advection scheme and the instantaneous dilution in the grid cell, should best simulate diffusion that is observed in the atmosphere. To achieve this goal, the artificial diffusion and numerical diffusion terms must be quantified for each of the advection algorithms. This is difficult, though not impossible, to accomplish because the numerical diffusion characteristics of a specific advection algorithm are not only dependent on the wave number of the signal but also the CFL number of the transport flow (Odman, 1998).

If numerical diffusion dominates, to compensate for the effectively larger instantaneous dilution in a larger grid size, eddy diffusivity component accounting for the grid size difference, K_{HN} , may be parameterized to counter act the numerical diffusivity D_N to give (e.g., Byun et al., 1999):

$$K_{HN}(\Delta x) = K_{Hf}(\Delta x_f) \left(\frac{\Delta x_f}{\Delta x} \right)^2 \quad (59)$$

where $K_{Hf}(\Delta x_f)$ is a uniform eddy diffusivity at a fixed resolution Δx_f . In Eulerian dispersion models, $K_{Hf}(\Delta x_f)$ of order of 50-2000 m^2s^{-1} is used,

depending on the magnitude of Δx_f . The formula, however, is inadequate for a very fine grid size where the physical dispersion dominates over the numerical diffusion. The difference between the grid size dependencies represented in Eqs. (57) and (59), respectively, is striking. A heuristic method combining the two formulae is suggested here with an analogy to the resistance law concept used for the estimation of deposition velocity:

$$\frac{1}{K_H} = \frac{1}{K_{HT}} + \frac{1}{K_{HN}} \quad (60)$$

This formula, which has yet to be evaluated with realistic Eulerian dispersion simulations, attempts to resolve the dichotomy existing between the contrasting dependencies on grid resolution in the components of horizontal diffusivity. For a large grid size, the effect of the transportive dispersion is minimized while for a small grid size the impact of the numerical diffusion term is reduced.

In the literature, there are a few horizontal-diffusivity formulations that depend on the atmospheric stability and/or height from the surface. In the Fifth-Generation Penn State/NCAR Mesoscale Model (MM5) (Grell et al., 1994), both the second-order diffusion similar to Eq. (51) and a more scale-selective fourth-order diffusion are used. The second-order diffusion is applied only for the coarsest MM5 simulation domain and the fourth-order form is used in the interior of the coarsest domain as well as in the entire domain of any refinement mesh. The horizontal diffusion coefficient K_H consists of a background value K_{H0} and a term proportional to the deformation $D = 2(S_\Gamma^2 + S_\Lambda^2)^{1/2}$:

$$K_H = K_{H0} + 0.5k^2\Delta x^2D \quad (61)$$

where $K_{H0} = 3.0 \times 10^{-3} \Delta x^2 / \Delta t$. In RAMS, the eddy mixing coefficient is a function determined by the deformation (D), Brunt-Vaisala frequency (N_B), and the Richardson number (Ri)

$$K_{hi} \sim (c_x \Delta x)(c_z \Delta z) f(D, N_B, Ri) \quad (62)$$

where c_x and c_z are dimensionless coefficients multiplying the horizontal and vertical spacings Δx and Δz to obtain characteristic horizontal and vertical mixing length scales, respectively. There are a few formulations that depend on the boundary layer height h . For example, for unstable conditions, K_H is parameterized by (Seinfeld, 1986)

$$K_H = 0.1w_*h = 0.1h^{3/4}(-k/L)^{-1/3}u_* \quad (63)$$

which was derived from the measurements of Willis and Deardorff (1976). Eppel et al. (1995) parameterized horizontal diffusivity as a simple factor of the vertical

eddy diffusivity, such as $K_H = 2.3 K_{zz}$, in which K_{zz} is in turn dependent on the mixing length scale. Considering the size of eddies grow with height, and assuming the continuity of eddy motion, the dependency of K_H on altitude is plausible. However, in Eulerian models, K_H must represent the effects of horizontal wind variability, which in fact is reduced with height as the air moves away from the surface roughness elements.

Hanna (1994) stated that the procedure for estimating horizontal diffusion at the sub-grid scale has not yet been resolved in a consistent manner in three-dimensional Eulerian models. He concluded that the Eulerian models must employ wind fields that include the full spectrum of mesoscale and regional fluctuations in space and time. Overly smooth wind fields provided by the diagnostic wind field modeling or mesoscale meteorological models cannot yield sufficient horizontal diffusion in the model. McNider et al. (1996) stated that in current meteorological models the energy spectrum corresponding to 120 km (or four times the horizontal grid spacing used) to 1 km (below which boundary layer turbulence is parameterized) is not well represented. Furthermore, the parameterizations of sub-grid scale horizontal diffusivities incorporated in commonly used regional models produce K_H values that range over several orders of magnitude.

Once the value of eddy diffusivity is defined, we can use an explicit solution method for Eq. (51):

$$\begin{aligned}
 (\rho)_{l,m}^{n+1} q_{l,m}^{n+1} = & (\rho)_{l,m}^n q_{l,m}^n + \frac{\Delta t}{(\Delta x)^2} \left[(\rho)_{l+1,m}^n \overline{K_{l+1,m}^{11}} (q_{l+1,m}^n - q_{l,m}^n) - (\rho)_{l,m}^n \overline{K_{l,m}^{11}} (q_{l,m}^n - q_{l-1,m}^n) \right] \\
 & + \frac{\Delta t}{(\Delta y)^2} \left[(\rho)_{l,m+1}^n \overline{K_{l,m+1}^{22}} (q_{l,m+1}^n - q_{l,m}^n) - (\rho)_{l,m}^n \overline{K_{l,m}^{22}} (q_{l,m}^n - q_{l,m-1}^n) \right] \quad (64)
 \end{aligned}$$

where $\overline{K_{l,m}^{11}} = (K_{l,m+1}^{11} + K_{l,m}^{11})/2$ and $\overline{K_{l,m}^{22}} = (K_{l+1,m}^{22} + K_{l,m}^{22})/2$. At the boundary cells, a zero-gradient Neumann boundary condition can be applied. The implicit scheme is not used here to minimize the computer memory requirement for handling large horizontal grid in the subroutine. Because Eq. (61) is an explicit scheme, the time-step should be chosen to prevent numerical instability and to maintain positivity. With an appropriate CFL number for horizontal diffusion β_{hdiff} , when $\Delta x = \Delta y$, the time-step can be determined with:

$$\Delta t|_{hdiff} = \beta_{hdiff} \frac{(\Delta x)^2}{\max_{\forall(l,m)} (K_{l,m}^{11}, K_{l,m}^{22})} \quad (65)$$

A range of β_{hdiff} value 0.5-0.75 is often used in air quality modeling.

As discussed above, specification of horizontal eddy diffusivity is one of critical problems associated with the K -theory grid models. In order to compensate for uncertainties in wind direction and speed information, these models always overestimate horizontal diffusion in a process that smears concentration peaks. With more or less uniformly distributed emission sources and with wind spectrum following a normal Gaussian distribution, this assumption is quite acceptable. But, in many cases, this smoothing process creates a loss of deterministic information related to the source-receptor relationship. This loss becomes particularly critical when selective emission reduction strategies are inferred from modeling outputs in order to meet air quality goals.

7 Vertical Diffusion Algorithm

Sub-grid-scale vertical diffusion of trace pollutants in the atmospheric boundary layer is an important physical process that must be addressed in Eulerian dispersion models. It needs to be modeled to allow realistic mixing under various meteorological conditions. Two different turbulence closure schemes, *local* closure and *nonlocal* closure, have been used for the parameterization of vertical diffusion. Local closure assumes that turbulence is analogous to molecular diffusion, i.e., the flux at any point in space is parameterized by known mean values at the same point (Stull, 1988). Most models use either a first order K -theory or simplified second order closure for the local approach. In a nonlocal closure the turbulent flux at one point is parameterized by mean quantities at many vertical layers thus allowing exchange of mass between nonadjacent layers. The nonlocal closure usually is intended for convectively unstable conditions, while the first and second order closures can be applied to both stable and unstable conditions.

7.1 First-Order Local Closure Techniques

First-order closure retains the prognostic equations for only the mean variables such as wind, temperature, humidity, and trace-gas concentrations while the second-order moments (Reynolds fluxes) are modeled. The Reynolds flux term is approximated with a gradient transport theory (K -theory), or mixing length theory. These methods are widely used in both meteorological and air quality modeling studies because of their simplicity. These methods frequently fail however when eddies larger than the grid size are present in the flow. For example, in the presence of convective conditions, K -theory is not recommended. With the K -theory, the vertical diffusion equation is given in the Cartesian coordinate system as

$$\left. \frac{\partial \bar{\phi}_i}{\partial t} \right|_{\text{vdiff}} = \frac{\partial}{\partial z} \left(\bar{\rho} K_{zz} \frac{\partial \bar{q}_i}{\partial z} \right) \quad (66)$$

One of the problems with first-order closure is finding a rational basis for parameterizing the eddy diffusivity. Only routinely measured or model-resolvable meteorological variables are used to explicitly specify a K -profile.

7.1.1 Vertical Eddy Diffusivity Parameterizations

While models with constant K values are easily solved analytically, they do not represent the turbulent exchange characteristics of the planetary boundary layer very well. Therefore, a more physically realistic K -profile that varies with height is often used. K_{zz} is allowed to vary depending on height, thermal stability, local gradients of potential temperature. There is a drawback in that the parameterizations sometimes cannot characterize the total turbulent flow adequately. A slightly different approach uses K_{zz} parameterization in terms of a mixing length l so that one must directly determine l instead of K_{zz} . Blackadar (1962) extended Prandtl's mixing length hypothesis to determine the length at which an eddy loses its identity and mixes completely with the environment. Lacser and Arya (1986) summarized many related works and provided a review of mixing length parameterizations in the stable stratified nocturnal boundary layer.

Hanna (1994) expressed some concerns about the proper formulation of K_{zz} in Eulerian dispersion models. In particular, the accurate specification of vertical diffusivity is highly important during stable conditions near the ground and aloft throughout a day. Observations often show layers of pollutants persisting at elevations of a few hundred meters during most of the night. If a value is specified for K_{zz} that is too large, these layers are diffused away. The problem with specifying K_{zz} is that very little is known about the stable boundary layer near the ground and aloft. Turbulence is chaotic, intermittent and unpredictable. Gravity waves are often present and the layer structure depends on factors outside the influence of local space and time constraints.

We assume that eddy diffusivity for trace species have non-dimensional profile characteristics similar to potential temperature, θ , i.e., $K_{zz} = K_h$. Numerous authors including O'Brien (1970), Businger and Arya (1974), Brost and Wyngaard (1978), and Bodin (1980) have considered this approach to study a variety of atmospheric conditions. Pielke and Mahrer (1975) combined O'Brien's (1970) formulation with Deardorff's (1974) prognostic equation for mixed layer height to better resolve boundary layer growth.

Most of modern Eulerian models employ the eddy diffusivity concepts described by Louis (1979). He proposed the use of Monin-Obukhov similarity theory to parameterize surface fluxes and vertical profiles. The Monin-Obukhov similarity is well described in references such as Businger et al. (1971), Panofsky and Dutton (1984), Pielke (1984), Stull (1988) and Arya (1988; 1999). The stability regime is defined with a nondimensional number z/L , where z is the height above

the ground and L is the Monin-Obukhov length. For the surface layer, the non-dimensional profile functions of the vertical gradient of Θ are expressed as:

$$\phi_h = \text{Pr}_o \left(1 + \beta_h \frac{z}{L}\right) \quad \text{for moderately stable conditions } (1 \geq z/L \geq 0) \quad (67)$$

$$\phi_h = \text{Pr}_o \left(1 - \gamma_h \frac{z}{L}\right)^{-1/2} \quad \text{for unstable conditions } (z/L < 0) \quad (68)$$

where Pr_o is the Prandtl number for neutral stability and β_h and γ_h are coefficients of the profile functions determined through field experiments. In addition, following Holtslag et al. (1990) we add a function for the very stable condition ($z/L \geq 1$) to extend the applicability of the surface layer similarity:

$$\phi_h = \text{Pr}_o \left(\beta_h + \frac{z}{L}\right) \quad (69)$$

Parameterizations for eddy diffusivity for the surface layer can be represented as:

$$K_h = \frac{ku_*z}{\phi_h(z/L)} \quad (70)$$

where u_* is the surface friction velocity.

Previous studies (Chang et al., 1987; Hass et al., 1991) indicated that this type of formulation can represent turbulent mixing in air quality models adequately. For the PBL (above the surface layer), eddy diffusivity is parameterized with:

$$K_h = \frac{ku_*z(1 - z/h)^{3/2}}{\phi_h(z/L)} \quad \text{for } \frac{z}{L} > 0 \text{ (stable)} \quad (71)$$

$$K_h = kw_*z(1 - z/h) \quad \text{for } \frac{z}{L} < 0 \text{ (unstable)}. \quad (72)$$

In the above expressions, h is the depth of the boundary layer, k the von Karman constant, and w_* the convective velocity.

In the free atmosphere above the mixed layer, the eddy diffusivity can be represented as a function of the bulk Richardson number and vertical wind shear:

$$K_h = K_o + S \frac{Ri_c - Ri_B}{Ri_c} l^2 \quad (73)$$

where K_o is the background value set at $1 \text{ m}^2 \text{ s}^{-1}$, S is the vertical wind shear, $S = \sqrt{(\Delta U)^2 + (\Delta V)^2} / \Delta z$, the Richardson number is defined as

$$Ri_B = \frac{g}{\Theta_o S^2} \frac{\Delta \Theta}{\Delta z} \quad (74)$$

and its critical value is assumed to be $Ri_c=0.25$, and l is the mixing length. Usually a constant value around 40 m is used for the mixing length for the free-tropospheric exchange. For different K_h formulations in the literature, refer to Appendix A.

7.1.2 Numerical Solver

When the temporal change in air density during computational time step can be ignored, Eq. (66) is given in a generic form as,

$$\frac{\partial q}{\partial t} = \frac{\partial}{\partial z} \left(K \frac{\partial q}{\partial z} \right) \quad (75)$$

To account for the loss process due to deposition in the lowest model layer, dry deposition flux is considered as the flux boundary condition at the surface, i.e.,

$$\left. \frac{\partial q_1}{\partial t} \right|_{dep} = - \frac{v_d}{h_{dep}} q_1 \quad (76)$$

where the geometric thickness of the lowest model layer is used for h_{dep} and v_d is the deposition velocity. The diffusion equation can be discretized and solved with explicit, semi-explicit or fully implicit algorithms (see Table 3 in Appendix B). The tridiagonal system can be solved with a Thomas algorithm (Gaussian elimination without pivoting) followed by back substitution.

7.2 Higher-Order Local Closure Techniques

Improvements to the simplicity of first order closure are closure schemes in which more of the physics of the atmosphere is taken into account in the formulation of the eddy diffusivity coefficient. They are the turbulent kinetic energy (TKE) closure and second-order closure schemes. Higher-order closure is accomplished by parameterizing high-order terms in terms of mean variables and lower-order terms.

7.2.1 Second-Order Closure Techniques

Several basic closure ideas such as down-gradient diffusion, return to isotropy, and turbulent dissipation in the inertial sub range are used in the

parameterizations of the third moment terms. These parameterizations must be especially applicable to the scales of the energy containing eddies which are very sensitive to atmospheric stability. Measurements of high-order moments in the real atmosphere are very difficult because there is a large amount of scattering in the direct flux measurements and a long averaging time is required to estimate higher-order moments using the eddy-correlation methods. For air quality applications, especially for a complicated reactive system, the technique requires several ad hoc assumptions that cannot be supported by observations or other theoretical reasoning.

The set of second-order turbulence equations includes the prognostic equations of the mean variables and the equations of their variances. Instead of parameterizing these fluxes, conservation equations are written for each flux term. This leads to the presence of third moment fluxes on the right side of the conservation equations for the second moment fluxes. To close the system, we must parameterize the third-moments in these equations with known parameters. Thus, second-order closure involves increased complexity and computation. In closing the set of equations, higher order terms are parameterized and these assumptions may not be valid for all types and scales of atmospheric motions. In the third-order closure scheme, conservation equations for third moments are considered and closure is achieved by parameterizing the fourth moments. This involves further increased complexity and computation. Literature indicates that only slight improvements are found over the TKE closure method (see next section) at the expense of huge computation and added complexity with the higher-order schemes. Very limited studies are available on the performance of the second-order methods applied to air quality modeling.

7.2.2 TKE Closure Technique

TKE closure is a simplification of the second-order closure technique. Instead of using the velocity component variance equations, the turbulent kinetic energy equation is used. Other equations can be used, together with the TKE, like the equations for the turbulent variances of temperature and humidity (e. g., Mellor and Yamada, 1974) or the turbulent kinetic energy dissipation rate (ε) equation (e. g., Alapaty et. al., 1996). The eddy diffusivity can be represented as,

$$K_{zz} = cTKE^2 / \varepsilon \quad (77)$$

where c is an experimental constant.

This type of closure is also more economical as compared to higher-order closure schemes. The TKE scheme requires additional equations relative to the first order closure thus providing more physically realistic solutions to the closure problem than first order. Thus, TKE closure is often termed as 1.5-order closure (Mellor and Yamada, 1974). Literature indicates that numerical simulations are far better with the TKE closure method than with the first order closure K-theory techniques without a large jump in computational expense.

7.3 Non-Local Closure Techniques

Non-local methods have been used mostly with first-order closure. Generally, the higher-order local closures and the nonlocal closures yield more accurate solutions than lower order, but they do so at added expense and complexity. Nonlocal closure recognizes that larger-size eddies can transport fluids across finite distances before the smaller eddies have a chance to cause mixing. This advective-like concept is supported by observations of thermals rising with undiluted cores, finite size swirls of leaves or snow, and the organized circulation patterns sometimes visible from cloud photographs.

Two main approaches to nonlocal closure methods are transilient turbulence theory and spectral diffusivity theory. Both allow a range of eddy sizes to contribute to the turbulent mixing process. A variety of physical processes can be modeled with a transilient scheme depending on the form of the transilient matrix. Examples include complete mixing, top-down/bottom-up mixing, asymmetric convective mixing, small-eddy mixing, cloud top entrainment, a detraining updraft core, patchy turbulence, no turbulence, or eddies triggered by the surface layer. Some closure schemes that have strong applicability to air quality modeling are described in the following subsections. Nonlocal closure schemes are the most suitable for describing the vertical turbulence mixing process, which should represent turbulent diffusion and atmospheric transport by eddies simultaneously.

In the non-local closure method, larger-size eddies can transport fluid across finite distances before the smaller eddies have a chance to cause mixing. In the literature mostly first-order nonlocal closure models can be found, except the study of Stull and Driedonks, (1987) where TKE (one-and-a-half-order closure) is used. In the nonlocal closure method mixing is done from the surface layer to the top of the convective boundary layer. The vertical diffusion of trace gases is accomplished by determining a matrix containing the fraction of mass entering or leaving each particular layer. This matrix containing information about the rate of mass fractional mixing from one level to another level is often called the

transilient matrix. There are several ways to specify this matrix (Stull and Driedonks, 1987; Chatfield and Crutzen, 1984; Fiedler and Moeng, 1985). The Blackadar scheme (Zhang and Anthes, 1982) uses the conservation of heat flux in a vertical column to determine the matrix.

Recent studies using a nonlocal closure technique (Pleim and Chang, 1992) for vertical diffusion during convective conditions indicated that it was able to simulate rapid transport upward from the surface layer to all levels in the convective boundary layer. Also, the study results indicate that air quality model simulations are better with this nonlocal closure technique compared to that with the simple *K*-theory (local closure) technique. Some of the disadvantages of this technique are that during nonconvective conditions the model has to rely on other closure methods, and that turbulence generated by vertical wind shear is neglected.

Transilient turbulence representation (Stull and Driedonks, 1987; Zhang and Stull, 1992; Stull, 1993) provides a general paradigm for the description of the nonlocal diffusion algorithms. However, it has high computational cost and there are some difficulties in determining the exchange coefficients among the model layers. Instead, there are a few simple nonlocal models that can be applied to Eulerian dispersion modeling, as described below.

7.3.1 Blackadar Convective Scheme

It is the simplest form of nonlocal scheme used in atmospheric modeling. This scheme, first introduced by Blackadar (1978), has long been used as one of the PBL schemes in MM5 and its predecessors. The concept of the Blackadar convective mixing scheme is that during conditions of free convection air in the surface layer is heated, to a superadiabatic potential temperature by the sensible heat flux from the surface. Thermal plumes rise from the surface layer due to their buoyancy until encountering air with higher potential temperature at the top of the convective boundary layer. Mixing occurs at all heights through plume detrainment while the plume core maintains the characteristics of the surface layer. Upward mixing and downward mixing are symmetric as in the case of Blackadar convection as shown in Figure 6a. Penetration into the capping inversion can be included by allowing a small amount of over-shooting into a region of negative buoyancy. This scheme is used only in the convective boundary layer and must be coupled with another scheme for non-convective conditions and above the boundary layer, such as *K*-theory. The Blackadar model does not take the effect of asymmetric vertical velocity spectra into account.

The convective mixing is assumed to be dominated by eddies of varying sizes but all having roots in the surface layer, with each eddy exchanging a certain amount of its mass with the air around it as it ascends. The rate of change of mean potential temperature caused by the mass exchange in the mixed layer can be expressed as

$$\frac{\partial \bar{\theta}}{\partial t} = M_u \omega(z) (\bar{\theta}_{sfc} - \bar{\theta}) \quad (78)$$

where $\omega(z)$ is a weight function that accounts for the variation of exchange rate with height. The mass exchange rate, M_u , can be estimated from conservation of energy, which requires the heat flux at any level to satisfy the equation

$$H = H_{sfc} - M_u \int_{z_{sfc}}^z c_p \rho (\bar{\theta}_{sfc} - \bar{\theta}) \omega(\xi) d\xi \quad (79)$$

where H_{sfc} is the sensible heat flux leaving the surface layer and c_p is the specific heat at constant pressure. When the integration limit is extended to the top of the boundary layer, where H is assumed to be zero, we can estimate M_u with

$$M_u = H_{sfc} / \int_{z_{sfc}}^{z_h} c_p \rho (\bar{\theta}_{sfc} - \bar{\theta}) \omega(\xi) d\xi \quad (80)$$

Usually the weight function w is approximated to be unity in the mixed layer. With this information, one can solve Eq. (75) with the deposition flux as the bottom boundary condition, Eq. (76). With the Blackadar scheme, the mixing algorithm is represented with,

$$\frac{\partial q_1}{\partial t} = -\frac{v_d}{h_{dep}} q_1 - \sum_{k=1}^{L_p} M_u \frac{\Delta z_k}{\Delta z_1} [q_1(t) - q_k(t)] \quad (81)$$

for the lowest model layer, where L_p is the index for the PBL top, and

$$\frac{\partial q_j}{\partial t} = -M_u \frac{\Delta z_1}{\Delta z_j} [q_j(t) - q_1(t)] \quad \text{for } 2 \leq j \leq L_p \quad (82)$$

The system can be solved with the numerical scheme described in Table 3 (Appendix B).

7.3.2 Asymmetric Convective Model (ACM)

The Asymmetric Convective Model (ACM) (Pleim and Chang, 1992) is based on Blackadar's nonlocal closure scheme (Blackadar, 1978) but has a different scheme for downward mixing in the convective boundary layer (CBL). Observational evidence and large-eddy simulation modeling studies indicate that mixing processes in a convective boundary layer are essentially asymmetric (i.e., turbulence is anisotropic; Schumann, 1989) with fast upward buoyant plumes and slow broad compensatory subsidence. Therefore the direct, non-local downward

transport of the Blackadar scheme is replaced with layer by layer subsidence which increases in mass flux as it descends, like a cascading waterfall (see Figure 6b).

Because the mass influx to the lowest model layer is from the second layer only in ACM, we can write

$$\frac{\partial q_1}{\partial t} = -\frac{v_d}{h_{dep}} q_1 - \frac{1}{\Delta z_1} [M_u(z_h - z_1)q_1(t) - M_{d2}\Delta z_2 q_2(t)] \quad (83)$$

For $2 \leq j \leq L_p$, we have

$$\frac{\partial q_j}{\partial t} = M_u q_1 - M_{dj} q_j + M_{dj+1} \frac{\Delta z_{j+1}}{\Delta z_j} q_{j+1} \quad (84)$$

where M_u represents upward mixing rate, Eq. (80), and M_{dj} represents downward mixing rate at layer j . It is determined by

$$M_{dj} = M_u \frac{z_h - z_{j-1}}{\Delta z_j} \quad (85)$$

Then the system can be solved with the algorithm described in Table 3 (Appendix B). As with the Blackadar model, the ACM can only be used during convective conditions in the PBL. For other stability regimes, one needs to rely on other schemes such as K -theory.

7.3.3 Ertel Non-Local Scheme

The local diffusion approach described earlier can be extended to include the nonlocal mixing under convective boundary layer. Ertel (1942) first proposed that the potential temperature (θ) flux could be expressed with two terms, the eddy diffusion term and the nonlocal Ertel flux (N) to account for the counter-gradient flux:

$$\overline{w'\theta'} = -K_{zz} \frac{\partial \bar{\theta}}{\partial z} + N \quad (86)$$

Similarly, Deardorff (1966) suggested the vertical turbulent mixing for the unstable boundary layer could be parameterized by

$$\frac{\partial q}{\partial t} = \frac{\partial}{\partial z} \left[K_{zz} \left(\frac{\partial q}{\partial z} - \gamma_q \right) \right] \quad (87)$$

where γ_q is a correction to the local gradient that incorporates the contribution of the large-scale eddies to the total flux. This formulation was initially introduced to handle vertical mixing of potential temperature (i.e., when $q = \theta$) under strong convective conditions where the stability $\partial\bar{\theta}/\partial z$ can change sign above the surface layer and remain slightly positive over most of the mixed layer (Wyngaard, 1982). This implies negative eddy diffusivity values.

One obvious difficulty of this method is how to determine the magnitude of γ_q , nonlocal transport correction factor. Several authors have suggested similar methods to estimate γ_q :

$$\text{Troen and Mahrt (1986):} \quad \gamma_q = C \frac{\overline{w'q'_s}}{w_* h}, \quad C \approx 10 \quad (88a)$$

$$\text{Holtslag et al. (1995):} \quad \gamma_q = a w_* \frac{\overline{w'q'_s}}{w_m^2 h}, \quad a \approx 7.2 \quad (88b)$$

$$\text{Hong and Pan (1996):} \quad \gamma_q = b \frac{\overline{w'q'_s}}{w_s h}, \quad b \approx 7.8 \quad (88c)$$

$$\text{Siebesma and Teixeira (2000):} \quad \gamma_q = a w_* \frac{\overline{w'q'_s}}{\sigma_w^2 h}, \quad a \approx 2 \quad (88d)$$

where w_* is the convective velocity scale, w_m is the velocity scale combining the influence of shear and convection (with free convection limit $w_m \sim 0.85 w_*$), w_s is the mixed-layer velocity scale represented as $w_s = u_* \phi_m^{-1}$, and σ_w is the standard deviation of vertical wind fluctuation.

For potential temperature, γ_q can be estimated by relating the counter-gradient term with the flux-profile formulation at the top of the surface layer (Troen and Mahrt, 1986; Hong and Pan, 1996) to give $\gamma_q = \gamma_\theta \sim 0.7 \times 10^{-3} \text{ m}^{-1} \text{ K}$. As shown by Stevens (2000), the Ertel nonlocal scheme approaches to the well-mixed boundary layer asymptotically. The nonlocal scheme transports scalar quantities away from the surface more rapidly than the local scheme (Holtslag and Boville, 1993; Holtslag et al., 1995). Although the Ertel nonlocal scheme is used in some meteorological models, it has not been used in Eulerian transport models because of the uncertainties in determining the nonlocal flux correction factors for different air pollutants.

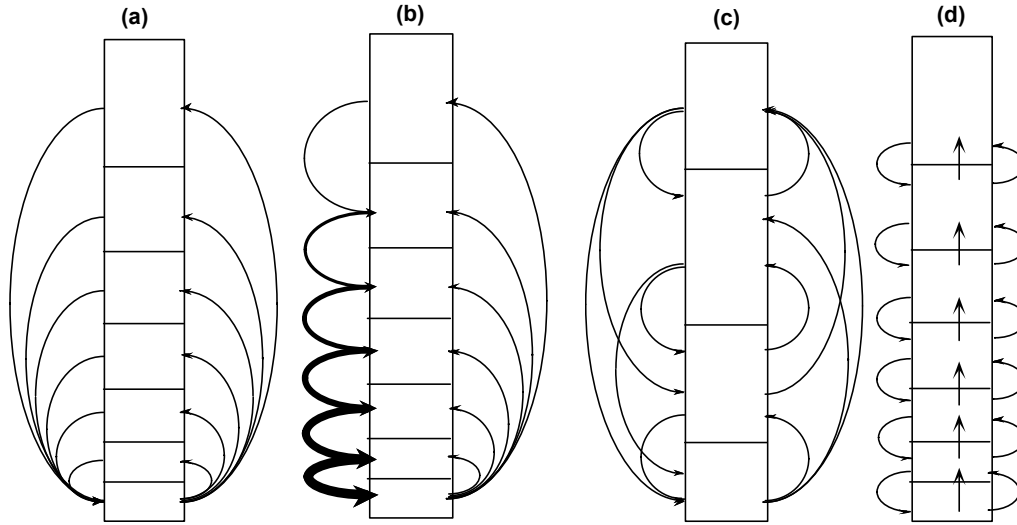


Figure 6. Schematics of nonlocal schemes: (a) the Blackadar scheme (b) the asymmetric convective model, (c) the transient turbulence model, and (d) eddy diffusion with nonlocal Ertel flux. The arrows point directions of mass fluxes, the relative sizes of boxes represent the volume of air in vertical cells and the line thickness is related with the relative magnitudes of fluxes.

8 Simplified Eulerian Models

Although most modern operational Eulerian air quality models are based on numerical methods described above, simplified models can provide useful insights of the atmospheric dispersion processes. We describe these models from a historic perspective.

8.1 Single Box Models

The single box model (Lettau, 1970) is the simplest air pollution model and is based on the mass conservation of pollutant inside a Eulerian box, which generally represents a large area such as a city. The physical concept underlying the box model approach is depicted in Figure 7. Mass conservation gives

$$\frac{\partial}{\partial t}(\bar{\varphi}h) = -\bar{\varphi}h \frac{U}{L_x} + \bar{\varphi}_b h \frac{U}{L_x} + \bar{\varphi}_a \frac{\partial h}{\partial t} + Q_a \quad (89)$$

in which $\bar{\varphi}_a$ is the (average) concentration aloft ($z > h$) over the city, for example, and $\bar{\varphi}_b$ is the background concentration at the upwind location. The term $\bar{\varphi}_a \frac{\partial h}{\partial t}$ represents entrainment effects of pollutants due to the growth of the boundary layer. For simple conditions with negligible background concentrations (i.e.,

$\bar{\varphi}_a = 0$ and $\bar{\varphi}_b = 0$) one can find the solution to Eq. (89) readily (Venkatram, 1978)

$$\bar{\varphi}(t)h(t) = \bar{\varphi}_o h_o \exp(-t/T_f) + Q_a T_f [1 - \exp(-t/T_f)] \quad (90)$$

where $\bar{\varphi}_o$ and h_o are initial concentration and boundary layer height, at $t = t_o$ respectively, and $T_f = L_x/U$ is the "flushing time" required for the air to pass completely over the urban area. If the diurnal evolution of the boundary layer are known, Eq. (90) allows the computation of pollutant concentrations at a given time t . In a theoretical stationary condition (i.e., $t = \infty$), φ tends to the limit φ_e :

$$\bar{\varphi}_e = \bar{\varphi}|_{t=\infty} = Q_a T_f / h \quad (91)$$

which is sometimes a reasonable quasi-stationary approximation in the urban areas.

The single box modeling approach, which is a simplest form of the Eulerian model, provides a basis for regional scale Lagrangian models in which a volume of air is assumed to move along with the prevailing wind without losing its integrity. The single box model has been applied for both inert and reactive pollutants. The model for the latter case is called the Photochemical Box Model (PBM) and Eq. (89) is modified to incorporate effects of photochemical reactions in the mass balance expression (Schere and Diemrjian, 1984):

$$\frac{\partial \bar{\varphi}_i}{\partial t} = -U \frac{\partial \bar{\varphi}_i}{\partial x} + \frac{\partial h}{\partial t} \frac{\partial \bar{\varphi}_i}{\partial z} + \frac{Q_a}{h} + R_i(\bar{\varphi}_1, \dots, \bar{\varphi}_n) \quad (92)$$

where $\bar{\varphi}_i$ is mean concentration of species i within the PBM, and R_i is rate of production and/or destruction of species i by chemical reactions. Refer to Figure 7 for the schematic illustration of processes simulated in PBM. Diemrjian and Schere (1979) used such a model to predict ozone concentrations over a city. The vertical entrainment is important for the ozone predictions because ozone is often trapped above the boundary layer at night and is mixed down to the surface by the convective mixing in the following morning. Meszaros et al. (1978) used a box model to compute anthropogenic emissions and dry/wet deposition processes. Jensen and Petersen (1979), who used an acoustic sounder for evaluating the boundary layer height, found a very good agreement between the single box model output and urban concentration measurements. One variant of the photochemical box model that has been widely used for estimating ozone concentration in urban areas is EKMA (empirical kinetic modeling approach) technique (Dodge, 1977).

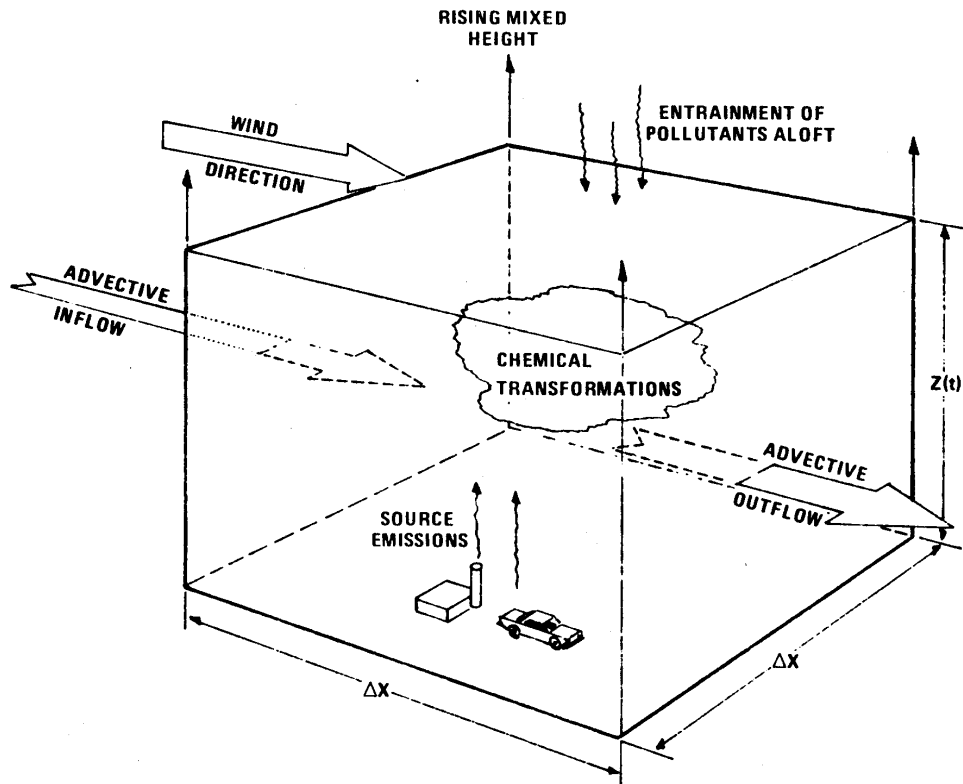


Figure 7. Schematic illustration of the photochemical box model (PBM) domain. [from Schere and Diemrjian, 1984]

8.2 The Slug Model

Venkatram (1978) showed that the box model has unrealistic inertia and cannot properly handle rapid temporal changes in either Q or U . He proposed the slug model as an improvement to the box model, especially during stagnation episodes (Figure 8). The slug model allows a concentration ϕ to vary in the along-wind direction x and in the vertical direction z , but assumes that the concentration does not vary in the crosswind direction y . This allows us to write the mass conservation equation within the single box in terms of two distances (x, z) as

$$\frac{\partial \phi}{\partial t} + U \frac{\partial \phi}{\partial x} = Q_i \quad (93)$$

where x is the downwind distance inside the box and U is assumed to be independent of height. We can avoid making assumptions about the vertical concentration distribution by integrating Eq. (93) in vertical direction:

$$\frac{\partial \Phi}{\partial t} + U \frac{\partial \Phi}{\partial x} = \int_0^{h(x)} Q_i dz \quad (94)$$

where $\Phi(x) = \int_0^{h(x)} \varphi(x,z) dz$ and h is either the mixing height or the vertical height of the box (may be dependent on the distance x) that encompasses the plume generated by the emission Q_l .

The steady state solution of Eq. (94) is

$$\Phi(x)|_{\infty} = \frac{1}{U} \int_0^x \int_0^{h(x')} Q_l dz dx' \tag{95}$$

The solution at time t after the emission is shut off (i.e., Q_l becomes zero),

$$\Phi(x,t) = \Phi(x - Ut)|_{\infty} = \frac{1}{U} \int_0^{x-Ut} \int_0^{h(x')} Q_l dz dx' ; t \leq T_f \tag{96a}$$

$$\Phi(t) = 0 ; t > T_f \tag{96b}$$

As before, $T_f = L_x / U$ is the flushing time. For a special case that the vertically integrated source strength does not change with distance x , (i.e., $\int_0^{h(x)} Q_l dz = \text{constant}$), we have

$$\Phi(t) = \frac{x - Ut}{U} \int_0^{h(x)} Q_l dz ; t \leq L_x / U \tag{97}$$

One of advantage of the slug model over the box model is that the volume is completely flushed out after the flushing time, where as the single box solution of Eq. (89) is not able to reproduce this complete flushing.

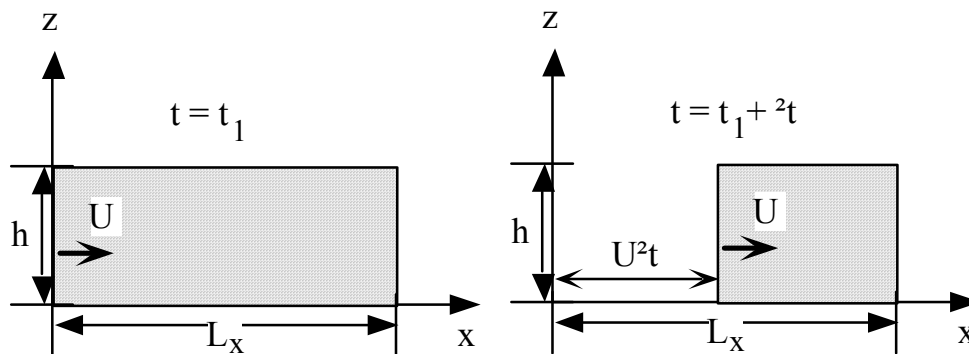


Figure 8. A schematic illustration of flushing of pollutants through a city. (After Venkatram, 1978)

Appendix A

K_{zz} Formulations in the Literature

Following Yamartino et al. (1992), Nikomo et al. (1999) divided the PBL into several atmospheric turbulence regimes (see Figure A-1) and for each regime they proposed K_{zz} parameterization:

For surface layer,	$K_{zz} = ku_*z / \phi_h(z/L)$
near neutral upper layer	$K_{zz} = ku_*z / \phi_h(z_{SL}/L)$
free convection	$K_{zz} = 1.22w_fz$, with $w_f = (zg \overline{w'\theta'}/\Theta_o)^{1/3}$
mixed layer	$K_{zz} = 0.57w_*z$, with $w_* = (hg \overline{w'\theta'_s}/\Theta_o)^{1/3}$
local scaling layer	$K_{zz} = ku_lz / \phi_h(z/\Lambda)$
z-less scaling	$K_{zz} = 0.17ku_l\Lambda$
intermittent layer	$K_{zz} = 10\%$ of the layer below,

where k is the Von Karman constant, u_* friction velocity, L is the Monin-Obukhov length, and ϕ is the similarity function for heat, h is the boundary layer height, z_{SL} is the surface layer height, approximated by $0.1h$, u_l is the local friction velocity, Λ is the local Monin-Obukhov length.

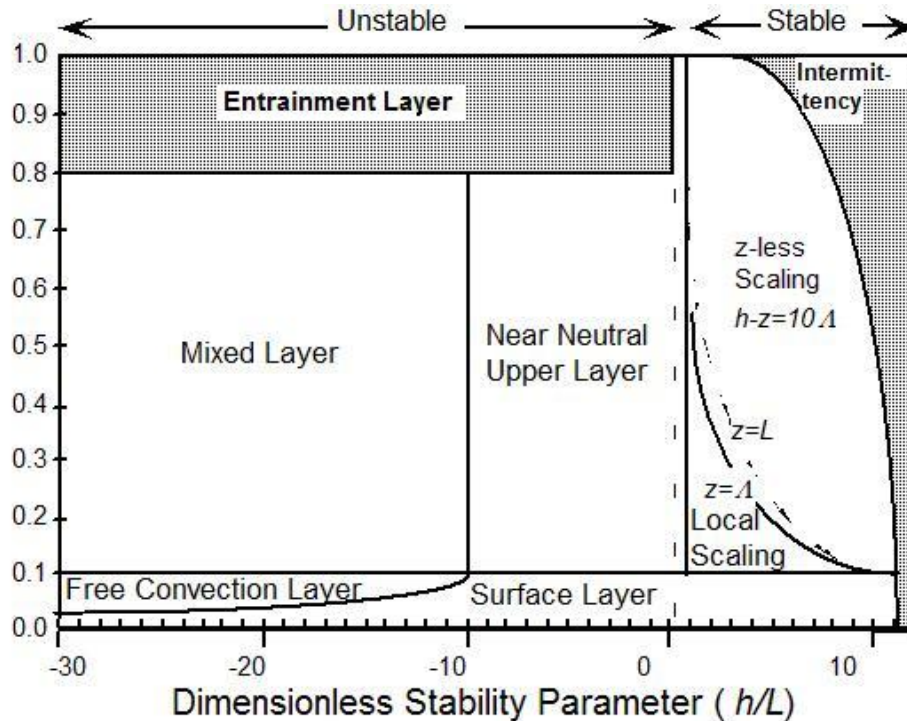


Figure A-1. Stability regimes of the atmospheric boundary layer (From Nikomo et al., 1999)

Yamartino et al. (1992) used similar approach:

For unstable case ($L < 0$)

surface layer where $z/h < 0.1$ and $-z/L < 1$

$$K_{zz} = ku_*z / \phi_h(z/L), \text{ with } \phi_h(z/L) = 0.74(1 - 9z/L)^{-1/2}$$

free convection where $z/h < 0.1$ $-z/L > 1$

$$K_{zz} = w_*z$$

near neutral upper layer where $0.1 < z/h < 1$ and $-h/L < 10$

$$K_{zz} = 0.1ku_*h / \phi_h(0.1h/L)$$

mixed layer where $0.1 < z/h < 1$ and $-h/L > 10$

$$K_{zz} = 0.1w_*h$$

and where $z/h > 1$, $K_{zz} = 10\%$ of the value below

For the stable cases ($L > 0$),

surface layer where $z/h < 0.1$, $(h-z)/\Lambda < 10$

$$K_{zz} = ku_*z / \phi_h(z/L), \text{ with } \phi_h(z/L) = 0.74(1 + 5z/L)$$

in the boundary layer where $0.1 < z/h < 1$ and $h/L < 1$

$$K_{zz} = 0.1ku_*h / \phi_h(0.1h/L)$$

where $z/h > 0.1$ and $h/L > 1$

$$K_{zz} = ku_*(1 - z/h)^{3/4} z / \phi_h(z/\Lambda)$$

where $z/h > 0.1$, $h/L > 1$, and $1 < z/\Lambda < (h/\Lambda - 10)$,

$$K_{zz} = ku_*(1 - z/h)^{3/4} \Lambda$$

outer layer where $z/h > 1$ and $z/\Lambda > (h/\Lambda - 10)$

$$K_{zz} = 10\% \text{ of the value below}$$

Some other formulations, which appear in the literature, are mentioned below:

For unstable conditions:

Yokoyama et al. (1979)

$$K_{zz} = cw_*h(z/h)^{1/3}(1 - z/h)^{1/3}, \text{ with } c = 0.06 \sim 0.13,$$

Sorbjan (1986b), above $z/h=0.77$ the flux is negative,

$$K_{zz} = 1.54w_*h(z/h)^{4/3}(1 - 1.3z/h)^{1/3}$$

Troen and Mahrt (1986), for $z/h > 0.1$,

$$K_{zz} = kh(u_*^3 + 0.7kw_*^3)^{1/3}(z/h)(1 - z/h)^2,$$

Lange (1989)

$$K_{zz} = ku_*z / \phi_h(z/L) \exp(-V_g h / u_*z), \text{ where } V_g \text{ is geostrophic wind}$$

Pleim and Chang (1992)

$$K_{zz} = ku_*z / \phi_h(z/L) \text{ for surface layer}$$

$$K_{zz} = kw_*z(1 - z/h) \text{ for mixed layer}$$

Holtslag and Boville (1993)

$$K_{zz} = l_c^2 SF_c(Ri), \text{ where } S \text{ is local vector wind shear,}$$

Ri is the Richardson number

$$F_c(Ri) = (1 - 18Ri)^{1/2}$$

$$1/l_c = 1/kz + 1/\lambda, \quad \lambda = 30 + 270 \exp(1 - z/1000)$$

Liu and Caroll (1996)

$$K_{zz} = l_c^2 S(1 - 87 Ri)^2$$

$\lambda = 80$ in the boundary layer

$\lambda = 60\%$ of grid size in the free atmosphere

Tirabassi and Rizza (1997)

$$K_{zz} = kw_*z(1 - z/h) \text{ for } h/L < -10$$

Degrazia et al. (1997)

$$K_{zz} = 0.15w_*h \left[\left(1 - \frac{z}{h}\right)^2 \left(\frac{-z}{L}\right)^{-2/3} + 0.75 \right]^{1/2} F\left(\frac{z}{h}\right)$$

or,
$$K_{zz} = 0.22 \left(\frac{z}{h}\right)^{1/3} \left(1 - \frac{z}{h}\right)^{1/3} F\left(\frac{z}{h}\right),$$

where
$$F\left(\frac{z}{h}\right) = \left[1 - \exp\left(-4\frac{z}{h}\right) - 0.0003 \exp\left(8\frac{z}{h}\right)\right]^{4/3}$$

Prabha et al. (1999)

$$K_{zz} = 2.5w_*h \left(\frac{kz}{h}\right)^{4/3} \left(1 - 15\frac{z}{L}\right)^{1/4}, \quad 0 < z/h < 0.05$$

$$K_{zz} = w_*h f\left(\frac{z}{h}\right),$$

where $f(\eta) = 0.021 + 0.408\eta + 1.351\eta^2 - 4.096\eta^3 + 2.56\eta^4$,

for $0.05 < \eta = z/h < 0.6$

$$f(\eta) = 0.2 \exp(6 - 10\eta), \text{ for } 0.6 < \eta = z/h < 1.1$$

$$f(\eta) = 0.0013, \text{ for } \eta = z/h > 1.1$$

Ulke (2000)

$$K_{zz} = ku_*h \left(\frac{z}{h}\right) \left(1 - \frac{z}{h}\right) \left[1 - 22\left(\frac{h}{L}\right)\left(\frac{z}{h}\right)\right]^{1/4}$$

Degrazia et. al. (2000)

$$K_{zz} = 0.16w_*h \left[0.01\left(-\frac{h}{L}\right)\right]^{1/2} \left[1 - \exp\left(-4\frac{z}{h}\right) - 0.003 \exp\left(8\frac{z}{h}\right)\right]^{4/3}$$

Siebesma and Teixeira (2000)

$$K_{zz} = ku_*z \left(1 - \frac{z}{h}\right)^2 \left(1 - 39\frac{z}{L}\right)^{-1/3}$$

For stable conditions, we have:

Brost and Wyngaard (1978)

$$K_{zz} = 1.25ku_*z \left(1 - \frac{z}{h}\right)^{3/2} \left(1 + 4.7\frac{z}{L}\right)$$

Yokoyama et al. (1979)

$$K_{zz} = cu_*z \left(1 - \frac{z}{h}\right) \left(1 + 6\frac{z}{L}\right), \quad c = 0.06 \sim 0.13$$

Sorbjan (1986a)

$$K_{zz} = ku_*z \left(1 - \frac{z}{h}\right) \left(0.74 + 4.7\frac{z}{L}\right)$$

Sorbjan (1986b)

$$K_{zz} = ku_*z(1 - \frac{z}{h})^{(2\alpha_1 - \alpha_2)} / (1 + 5.2 \frac{z}{L}), \alpha_1=2; \alpha_2=3$$

Lange (1989)

$$K_{zz} = \frac{ku_*z}{\phi_h(z/L)} \exp(-\frac{V_g z}{u_* h})$$

Pleim and Chang (1992)

$$K_{zz} = \frac{ku_*z}{\phi_h(z/L)}, \text{ for } z/h < 0.1,$$

where $\phi_h(z/L) = 0.74 + 4.7z/L, 0 < z/L < 1$

$$\phi_h(z/L) = 4.7 + 0.74z/L, z/L > 1$$

$$K_{zz} = \frac{ku_*z(1 - z/h)^2}{\phi_h(z/L)}, \text{ for } 1 > z/h > 0.1$$

Holtslag and Boville(1993)

$$K_{zz} = l_c^2 SF_c(Ri), \text{ where } F_c(Ri) = [1 + 10Ri(1 + 8Ri)]^{-1}$$

Liu and Carroll (1996)

$$K_{zz} = l_c^2 S(1 - Ri / Ri_c)^2$$

Degrazia et. al. (2000)

$$K_{zz} = ku_*z(1 + 3.7z/L)^{1/3} / (1 + 15f_c z / u_* + 3.7z/L)^{4/3}, \text{ in stable shear layer}$$

where $f_c \sim 10^{-4} s^{-1}$ is the Coriolis factor

$$L = L(1 - \frac{z}{h})^{(1.5\alpha_1 - \alpha_2)}, \alpha_1=1.5; \alpha_2=1$$

$$K_{zz} = \frac{ku_*z(1 - z/h)^{4/3}}{[1 + 3.7(z/L)(1 - z/h)^{5/4}]}, \text{ for highly stable case } (z/L \rightarrow \infty)$$

$$K_{zz} = 0.11u_*L(1 - z/h)^2, \text{ when eddy sizes are limited by stability}$$

Ulke (2000)

$$K_{zz} = \frac{ku_*z(1 - z/h)}{(1 + 6.9z/L)}$$

Ha and Mahrt (2000)

$$K_{zz} = l^2 \left| \frac{dV_h}{dz} \right|, \text{ where } l = l_o [\exp(-c_1 Ri) + c_2 / (Ri + c_3)],$$

$$c_1=8.5, c_2=0.15, c_3=3, l_o=8.5.$$

This is applied at all levels subject to $l_o < kz$.

Within the PBL, they use the larger value between the formula above and

$$K_{zz} = ku_*z(1 - \frac{z}{h})^2 / \text{Pr } \phi_m(\frac{z}{L}),$$

where $\text{Pr} = 1.5 + 3.08Ri$, and $\phi_m(\frac{z}{L}) = 1 + 4.7(z/L)$.

For $z/L > 1$, z/L in above formula is replaced by 1.

Table 3. Vertical diffusion algorithms (Byun and Ching, 1999)

Classification	Algorithm	Solver
Semi-implicit eddy diffusion solver	<p>For j=1 (layer 1):</p> $q_1^{n+1} = q_1^n - \Delta t \frac{v_d}{h_{dep}} [\theta q_1^{n+1} + (1-\theta)q_1^n]$ $+ \frac{\Delta t}{\Delta \xi_1} \left[\frac{K_{1+1/2}}{\Delta \xi_{1+1/2}} (\theta(q_2^{n+1} - q_1^{n+1}) + (1-\theta)(q_2^n - q_1^n)) \right]$ <p>For $2 \leq j \leq L-1$:</p> $q_j^{n+1} = q_j^n + \frac{\Delta t}{\Delta \xi_j} \bullet$ $\left[\frac{K_{j+1/2}}{\Delta \xi_{j+1/2}} (\theta(q_{j+1}^{n+1} - q_j^{n+1}) + (1-\theta)(q_{j+1}^n - q_j^n)) \right.$ $\left. - \frac{K_{j-1/2}}{\Delta \xi_{j-1/2}} (\theta(q_j^{n+1} - q_{j-1}^{n+1}) + (1-\theta)(q_j^n - q_{j-1}^n)) \right]$ <p>At the top of layer</p> $q_N^{n+1} = q_N^n - \frac{\Delta t}{\Delta \xi_N} \frac{K_{N-1/2}}{\Delta \xi_{N-1/2}} (\theta(q_N^{n+1} - q_{N-1}^{n+1}) + (1-\theta)(q_N^n - q_{N-1}^n))$	$\begin{pmatrix} d_1 & c_1 & \dots & 0 & \dots & 0 \\ a_2 & d_2 & c_2 & 0 & \dots & 0 \\ \vdots & a_3 & \ddots & \dots & \dots & 0 \\ 0 & \vdots & \vdots & d_j & \vdots & \vdots \\ \vdots & 0 & 0 & 0 & \ddots & c_{L-1} \\ 0 & \dots & 0 & 0 & a_L & d_L \end{pmatrix} \begin{pmatrix} q_1^{n+1} \\ q_2^{n+1} \\ \vdots \\ q_j^{n+1} \\ \vdots \\ q_L^{n+1} \end{pmatrix} = \begin{pmatrix} b_1 \\ b_2 \\ \vdots \\ b_j \\ \vdots \\ b_L \end{pmatrix}$ $d_1 = 1 + \frac{\theta \Delta t}{\Delta \xi_1} \frac{K_{1+1/2}}{\Delta \xi_{1+1/2}} + \theta \Delta t \frac{v_d}{h_{dep}}; c_1 = -\frac{\theta \Delta t}{\Delta \xi_1} \frac{K_{1+1/2}}{\Delta \xi_{1+1/2}}; a_N = -\frac{\theta \Delta t}{\Delta \xi_N} \frac{K_{N-1/2}}{\Delta \xi_{N-1/2}}; d_N = 1 + \frac{\theta \Delta t}{\Delta \xi_N} \frac{K_{N-1/2}}{\Delta \xi_{N-1/2}}$ $b_1 = \left(1 - \frac{(1-\theta)\Delta t}{\Delta \xi_1} \frac{K_{1+1/2}}{\Delta \xi_{1+1/2}} - (1-\theta)\Delta t \frac{v_d}{h_{dep}} \right) q_1^n + \frac{(1-\theta)\Delta t}{\Delta \xi_1} \frac{K_{1+1/2}}{\Delta \xi_{1+1/2}} q_2^n$ $b_N = \left(1 - \frac{(1-\theta)\Delta t}{\Delta \xi_N} \frac{K_{N-1/2}}{\Delta \xi_{N-1/2}} \right) q_N^n + \frac{(1-\theta)\Delta t}{\Delta \xi_N} \frac{K_{N-1/2}}{\Delta \xi_{N-1/2}} q_{N-1}^n$ <p>for $2 \leq j \leq L-1$: $a_j = -\frac{\theta \Delta t}{\Delta \xi_j} \frac{K_{j+1/2}}{\Delta \xi_{j+1/2}}; d_j = 1 + \frac{\theta \Delta t}{\Delta \xi_j} \left(\frac{K_{j+1/2}}{\Delta \xi_{j+1/2}} + \frac{K_{j-1/2}}{\Delta \xi_{j-1/2}} \right); c_j = -\frac{\theta \Delta t}{\Delta \xi_j} \frac{K_{j+1/2}}{\Delta \xi_{j+1/2}}$</p> $b_j = \left(1 - \frac{(1-\theta)\Delta t}{\Delta \xi_j} \left[\frac{K_{j+1/2}}{\Delta \xi_{j+1/2}} + \frac{K_{j-1/2}}{\Delta \xi_{j-1/2}} \right] \right) q_j^n + \frac{(1-\theta)\Delta t}{\Delta \xi_j} \frac{K_{j+1/2}}{\Delta \xi_{j+1/2}} q_{j+1}^n + \frac{(1-\theta)\Delta t}{\Delta \xi_j} \frac{K_{j-1/2}}{\Delta \xi_{j-1/2}} q_{j-1}^n$

θ =a time-step weighting factor (0.5 for Crank-Nicholson method) and $\xi_{j+1/2} = (\xi_j + \xi_{j+1})/2$; $\Delta \xi_{j+1/2} = \xi_{j+1/2} - \xi_{j-1/2}$; $\Delta \xi_{j+1} = \xi_{j+1} - \xi_j$.

Table 3. (continued)

Classification	Algorithm	Solver
Blackadar symmetric eddy; Blackadar (1978)	<p>For $j=1$ (layer 1):</p> $\frac{\hat{\alpha}q_1}{\hat{\alpha}} = -\frac{v_d}{h_{dep}} q_1 - \sum_{k=1}^{L_p} m_{1k}(t)[q_1(t) - q_k(t)]$ <p>, for $2 \leq j \leq L_p$:</p> $\frac{\hat{\alpha}q_j}{\hat{\alpha}} = -\sum_{k=1}^{L_p} m_{jk}(t)[q_j(t) - q_k(t)]$ <p>where m_{jk} = rate of mass exchange between two layers</p> $m_{1k} = M_u \frac{\Delta\xi_k}{\Delta\xi_1}; m_{j1} = M_u \frac{\Delta\xi_1}{\Delta\xi_j}$ <p>and the upward flux is obtained from</p> $M_u = H_{sfc} / \int_{\xi_{sfc}}^{\xi_h} C_{pd} \rho(\Theta_{sfc} - \Theta) w(\xi) J_\xi d\xi$	<p>Crank-Nicholson time differencing</p> $\begin{pmatrix} d_1 & f_2 & \cdots & f_j & \cdots & f_{L_p} \\ e_2 & d_2 & 0 & 0 & \cdots & 0 \\ \vdots & 0 & \ddots & \cdots & \cdots & 0 \\ e_j & \vdots & \vdots & d_j & \vdots & \vdots \\ \vdots & 0 & 0 & 0 & \ddots & 0 \\ e_{L_p} & \cdots & 0 & 0 & 0 & d_{L_p} \end{pmatrix} \begin{pmatrix} q_1^{n+1} \\ q_2^{n+1} \\ \vdots \\ q_j^{n+1} \\ \vdots \\ q_{L_p}^{n+1} \end{pmatrix} = \begin{pmatrix} b_1 \\ b_2 \\ \vdots \\ b_j \\ \vdots \\ b_{L_p} \end{pmatrix}$ $d_1 = 1 + \mathcal{G} \frac{v_d \Delta t}{h_{dep}} + \mathcal{G} \frac{\Delta t M_u}{\Delta \xi_1} (\xi_h - \Delta \xi_1)$ $b_1 = \left[1 - (1 - \mathcal{G}) \frac{v_d \Delta t}{h_{dep}} - (1 - \mathcal{G}) \frac{\Delta t M_u}{\Delta \xi_1} (\xi_h - \Delta \xi_1) \right] q_1^n + (1 - \mathcal{G}) \frac{\Delta t M_u}{\Delta \xi_1} \sum_{k=2}^{L_p} \Delta \xi_k q_k^n$ <p>for $2 \leq j \leq L_p$: $f_j = -\mathcal{G} \left(\frac{\Delta t M_u}{\Delta \xi_j} \right) \Delta \xi_1$; $e_j = -\mathcal{G} \left(\frac{\Delta t M_u}{\Delta \xi_1} \right) \Delta \xi_j$; $d_j = 1 + \mathcal{G} \left(\frac{\Delta t M_u}{\Delta \xi_j} \right) \Delta \xi_1$;</p> $b_j = \left[1 - (1 - \mathcal{G}) \left(\frac{\Delta t M_u}{\Delta \xi_j} \right) \Delta \xi_1 \right] q_j^n + (1 - \mathcal{G}) \left(\frac{\Delta t M_u}{\Delta \xi_j} \right) \Delta \xi_1 q_1^n$

Table 3. (continued)

Classification	Algorithm	Solver
Asymmetric Convective Model (Pleim and Chang, 1992)	<p>For $j=1$ (layer 1): $\frac{\partial q_1}{\partial t} = -M_u \frac{\xi_h - \xi_1}{\Delta \xi_1} (q_1 - q_2) - \frac{v_d}{h_{dep}} q_1$</p> <p>for $2 \leq j \leq L_p$:</p> $\frac{\partial q_j}{\partial t} = M_u \left[q_1 - \left(\frac{\xi_h - \xi_{j-1}}{\Delta \xi_j} \right) q_j + \left(\frac{\xi_h - \xi_j}{\Delta \xi_{j+1}} \right) q_{j+1} \right]$ <p>where M_u represents upward mixing rate. M_{dj} represents downward mixing rate at layer j and is defined as:</p> $M_{dj} = M_u \frac{\xi_h - \xi_{j-1}}{\Delta \xi_j}$ <p>and the upward flux is obtained from</p> $M_u = H_{sfc} / \left[c_p \rho (\bar{\theta}_{sfc} - \theta_2) J_\xi (\xi_1 - \xi_h) \right]$ $M_{dj-1} = M_u + M_{dj} \frac{\Delta \xi_{j+1}}{\Delta \xi_j}$	$\begin{pmatrix} d_1 & c_1 & \cdots & 0 & \cdots & 0 \\ e_2 & d_2 & c_2 & 0 & \cdots & 0 \\ \vdots & 0 & \ddots & \ddots & \cdots & 0 \\ e_j & \vdots & \vdots & d_j & c_j & \vdots \\ \vdots & 0 & 0 & 0 & \ddots & c_{L_p-1} \\ e_{L_p} & \cdots & 0 & 0 & 0 & d_{L_p} \end{pmatrix} \begin{pmatrix} q_1^{n+1} \\ q_2^{n+1} \\ \vdots \\ q_j^{n+1} \\ \vdots \\ q_{L_p}^{n+1} \end{pmatrix} = \begin{pmatrix} b_1 \\ b_2 \\ \vdots \\ b_j \\ \vdots \\ b_{L_p} \end{pmatrix}$ $d_1 = 1 + \left(\frac{v_d}{h_{dep}} + M_u \frac{\xi_h - \xi_1}{\Delta \xi_1} \right) \mathcal{G} \Delta t; \quad c_1 = -M_u \frac{\xi_h - \xi_1}{\Delta \xi_1} \mathcal{G} \Delta t$ $b_1 = \left[1 - \left(\frac{v_d}{h_{dep}} + M_u \frac{\xi_h - \xi_1}{\Delta \xi_1} \right) (1 - \mathcal{G}) \Delta t \right] q_1^n + M_u \frac{\xi_h - \xi_1}{\Delta \xi_1} (1 - \mathcal{G}) \Delta t q_2^n$ <p>for $2 \leq j \leq L_p$:</p> $e_j = -M_u \mathcal{G} \Delta t; \quad d_j = 1 + M_u \left(\frac{\xi_h - \xi_j}{\Delta \xi_{j+1}} \right) \mathcal{G} \Delta t; \quad c_j = -M_u \left(\frac{\xi_h - \xi_j}{\Delta \xi_j} \right) \mathcal{G} \Delta t;$ $b_j = \left[1 - M_u \frac{\xi_h - \xi_{j-1}}{\Delta \xi_j} \right] (1 - \mathcal{G}) \Delta t q_j^n + M_u \frac{\xi_h - \xi_j}{\Delta \xi_{j+1}} (1 - \mathcal{G}) \Delta t q_{j+1}^n + M_u (1 - \mathcal{G}) \Delta t q_1^n$

Appendix C

Table 4. Numerical algorithms with two-level time differencing for constant grid spacing (Sources: Pielke, 1984; Long and Pepper, 1981; Odman, 1998; Chock and Dunker, 1983, Chock, 1985; Chock, 1991)

Classification	Scheme	Algorithm	Characteristics	References
Flux form finite Difference	Donor Cell (upwind difference) Scheme, forward in time	$\varphi_j^{n+1} = \varphi_j^n - [F(\varphi_j^n, \varphi_{j+1}^n, u_{j+1/2}) - F(\varphi_{j-1}^n, \varphi_j^n, u_{j-1/2})],$ where $F(\varphi_j, \varphi_{j+1}, u) = [(u + u)\varphi_j + (u - u)\varphi_{j+1}] \frac{\Delta t}{2\Delta x}$	Very diffusive, Positive definite, monotonic, linear, fast	Roache (1972)
Flux form, iterative finite Difference	Smolarkiewicz Scheme	$\varphi_j^* = \varphi_j^n - [F(\varphi_j^n, \varphi_{j+1}^n, u_{j+1/2}) - F(\varphi_{j-1}^n, \varphi_j^n, u_{j-1/2})],$ $\varphi_j^{n+1} = \varphi_j^* - [F(\varphi_j^*, \varphi_{j+1}^*, \tilde{u}_{j+1/2}) - F(\varphi_{j-1}^*, \varphi_j^*, \tilde{u}_{j-1/2})],$ where $F(\varphi_j, \varphi_{j+1}, u) = [(u + u)\varphi_j + (u - u)\varphi_{j+1}] \frac{\Delta t}{2\Delta x}$ $\tilde{u}_{j+1/2} = \frac{(u_{j+1/2} \Delta x - \Delta t u_{j+1/2}^2)(\varphi_{j+1}^* - \varphi_j^*)}{(\varphi_{j+1}^* + \varphi_j^* + \varepsilon)\Delta x}, \quad \varepsilon = \text{a small value } (10^{-15})$	Moderately diffusive, Positive definite, nonlinear, relatively fast	Smolarkiewicz (1983)
Advective form, upstream interpolation	Upstream Cubic-spline Scheme, forward in time	$\varphi_j^{n+1} = \begin{cases} S(x_j - \beta_j \Delta x), & \text{for } u_j \geq 0 \\ S(x_j + \beta_j \Delta x), & \text{for } u_j < 0 \end{cases}, \text{ where}$ $S(x_j - \beta_j \Delta x) = \varphi_j^n - \beta_j ^2 [\Delta x N_j + \beta_j^2 [\Delta x N_{j-1} + 2 \Delta x N_j + 3(\varphi_{j-1}^n - \varphi_j^n)]$ $- \beta_j ^3 [\Delta x N_{j-1} + \Delta x N_j + 2(\varphi_{j-1}^n - \varphi_j^n)]$ $S(x_j + \beta_j \Delta x) = \varphi_j^n + \beta_j ^2 [\Delta x N_{j+1} + 2 \Delta x N_j + 3(\varphi_j^n - \varphi_{j+1}^n)]$ $+ \beta_j ^3 [\Delta x N_j + \Delta x N_{j+1} + 2(\varphi_j^n - \varphi_{j+1}^n)],$ and $S'(x_j) = N_j$ satisfies $3(\varphi_{j+1}^n - \varphi_{j-1}^n) / \Delta x = N_{j-1} + 4N_j + N_{j+1}$.	Diffusive, Produces negative conc.	

$\beta_j = u_j \Delta t / \Delta x$ and $\beta_{\max} = \max(|\beta_j|)$, the maximum Courant-Fridlich-Lewy (CFL) number for the grid domain.

Table 4. (continued)

Classification	Scheme	Algorithm	Characteristics	References
Flux form, Galerkin Finite element	Chapeau Function Scheme, implicit (Crank-Nicholson)	$[2 - (2\beta_{j-1} + \beta_j)]\phi_{j-1}^{n+1} + [8 + (\beta_{j+1} - \beta_{j-1})]\phi_j^{n+1} + [2 + (\beta_j + 2\beta_{j+1})]\phi_{j+1}^{n+1}$ $= [2 + (2\beta_{j-1} + \beta_j)]\phi_{j-1}^n + [8 - (\beta_{j+1} - \beta_{j-1})]\phi_j^n + [2 - (\beta_j + 2\beta_{j+1})]\phi_{j+1}^n$	Less diffusive. Spurious oscillations. Produces negative conc. Often needs a smoothing filter	McRae et al. (1982), Odman and Russell (1993)
Flux form, Pseudo-spectral technique	Accurate Space Derivative Method	<p>Expand the flux form advection as a truncated Taylor series in time.</p> $\phi^{n+1} = \phi^n + \left(\frac{\partial\phi}{\partial t}\right)^n \Delta t + \left(\frac{\partial^2\phi}{\partial t^2}\right)^n \frac{\Delta t^2}{2!} + \left(\frac{\partial^3\phi}{\partial t^3}\right)^n \frac{\Delta t^3}{3!} + \dots$ <p>Assuming the velocity is not a function of time, the spatial equivalents of time derivatives are computed in chain rule form with the fast Fourier transform:</p> $\frac{\partial\phi}{\partial t} = -\phi \frac{\partial u}{\partial x} - u \frac{\partial\phi}{\partial x},$ $\frac{\partial^2\phi}{\partial t^2} = \frac{\partial}{\partial x} \left[u \frac{\partial u \phi}{\partial x} \right] = \phi \left[u \frac{\partial^2 u}{\partial x^2} + \left(\frac{\partial u}{\partial x}\right)^2 \right] + 3u \frac{\partial\phi}{\partial x} \frac{\partial u}{\partial x} + u^2 \frac{\partial^2\phi}{\partial x^2},$ $\frac{\partial^3\phi}{\partial t^3} = -\phi \left[4u \frac{\partial u}{\partial x} \frac{\partial^2 u}{\partial x^2} + u^2 \frac{\partial^3 u}{\partial x^3} + \left(\frac{\partial u}{\partial x}\right)^3 \right]$ $- \frac{\partial\phi}{\partial x} \left[4u^2 \frac{\partial^2 u}{\partial x^2} + 7u \left(\frac{\partial u}{\partial x}\right)^2 \right] - 6u^2 \frac{\partial^2\phi}{\partial x^2} \frac{\partial u}{\partial x} - u^3 \frac{\partial^3\phi}{\partial x^3}.$ <p>Due to the dispersive quality, it produces high-frequency noise. Often used in combination with a filter (e.g., Forest filter)</p>	Very accurate, Produces negative conc. High computational cost Needs a smoothing filter	Gazdag (1973) Dabdub and Seinfeld (1994)

Table 4. (continued)

Classification	Scheme	Algorithm	Characteristics	References
Flux form, finite volume scheme	Piecewise Parabolic Method (PPM)	<p>Concentration distribution is assumed to be parabolic in any given grid cell. $\varphi_j^{n+1}(\eta) = \varphi_{L,j} + \eta \left[(\varphi_{R,j} - \varphi_{L,j}) + 6 \left(\varphi_j^n - \frac{\varphi_{L,j} + \varphi_{R,j}}{2} \right) (1 - \eta) \right]$,</p> <p>Where η is the nondimensional coordinate and left and right boundary values are defined as $\varphi_{L,j+1} = \varphi_{R,j} = \varphi_{j+1/2}^*$ with initial guess, $\varphi_{j+1/2}^* = \frac{7}{12}(\varphi_j^n + \varphi_{j+1}^n) - \frac{1}{12}(\varphi_{j+2}^n + \varphi_{j-1}^n)$.</p> <p>Edge values are modified such that the results are monotonic: (1) if φ_j is a local extremum, then the distribution is assumed to be constant, (2) when φ_j is between $\varphi_{L,j}$ and $\varphi_{R,j}$, but sufficiently close to one of the values, one of the edge values is reset so that the derivative of $\varphi(\eta)$ is zero at the opposite edge</p>	Moderately diffusive, Positive definite, monotonic	Colella and Woodward, (1984) Carpenter et al., (1990)
Flux form, finite volume scheme	Bott's Scheme	<p>The distribution of the concentration within the cell is represented by a polynomial of order l: $\varphi_j(\eta) = \sum_{k=0}^l a_{j,k} \eta^k$. The polynomial can be made to preserve area by requiring: $\varphi_{j+i} = \int_i^{i+1} \sum_{k=0}^l a_{j,k} \eta^k d\eta$, $i = 0, \pm 1, \pm 2, \dots, \pm \frac{l}{2}$ over a stencil of $l+1$ grid cells by varying the value of i. The solution to this linear system yields the coefficients $a_{j,k}$. For example, coefficients for a quadratic ($l=2$) scheme are; $a_0 = -\frac{1}{24}(\varphi_{j+1} - 26\varphi_j + \varphi_{j-1})$, $a_1 = \frac{1}{2}(\varphi_{j+1} - \varphi_{j-1})$, and $a_2 = \frac{1}{2}(\varphi_{j+1} - \varphi_j + \varphi_{j-1})$</p>	Mildly diffusive, Positive definite*, nonlinear, relatively fast, non-monotonic	Smolarkiewicz (1983)

Non-dimensional local coordinate is defined as $\eta = (x - x_{j-1/2}) / \Delta x$.

*Small negative numbers can result for a signal with large gradients due to machine precision problems

Table 4. (continued)

Classification	Scheme	Algorithm	Characteristics	References
Flux form, finite volume scheme	Yamatino-Blackman Cubic scheme	<p>Interpolating cubic spline: $\varphi_j(\eta) = a_0 + a_1\eta + a_2\eta^2 + a_3\eta^3$, with</p> $a_0 = \varphi_j, \quad a_1 = d_j \Delta x, \quad a_2 = -\frac{1}{4}(\varphi_{j+1} - 2\varphi_j + \varphi_{j-1}) + \frac{3\Delta x}{8}(d_{j+1} - d_{j-1}),$ $a_3 = (\varphi_{j+1} - \varphi_{j-1}) - \frac{\Delta x}{6}(d_{j+1} + 10d_j + d_{j-1})$ <p>The spline derivatives, d_j, are obtained from the tridiagonal system:</p> $\alpha d_{j-1} + (1 - 2\alpha) d_j + \alpha d_{j+1} = \frac{\varphi_{j+1} - \varphi_{j-1}}{2\Delta x}. \quad (\alpha=0.22826).$ <p>Positivity is maintained by (1) when φ_j is a local minimum, a donor-cell scheme is used instead of the cubic spline; (2) the spline is spectrally limited by the relation: $a_k/a_0 \leq \pi^k/k!$, $k = 1, 2, 3$. (3) a mass conservative flux renormalization is applied, and finally (4), a mildly diffusive filter is applied in an attempt to block the depletion of donor cells.</p>	A little diffusive, Positive definite, non-monotonic	Yamatino (1993)
Advective form, Semi-Lagrangian Transport (SLT) scheme	SLT with cubic spline interpolation	<p>The Lagrangian solution to this equation determines the departure point (x_D, y_D) of a particle at (x_A, y_A) as $(x_D, y_D) = (x_A - \Delta t u, y_A - \Delta t v)$.</p> <p>This scheme first determines the midpoint of the trajectory iteratively as</p> $(x_M^{k+1}, y_M^{k+1}) = (x_A - \frac{\Delta t}{2} u(x_M^k, y_M^k), y_A - \frac{\Delta t}{2} v(x_M^k, y_M^k))$ <p>Four iterations are used for the very first time step which starts with the arrival points as a first guess (for the midpoints) and one iteration thereafter where the midpoints from the previous time step are used as a first guess. The velocities at the midpoints are calculated using Lagrange cubic interpolation. Monotonicity is maintained by limiting the interpolated value.</p>	Diffusive, Positive definite Monotonic.	Williamson and Rasch (1989)

References

- Alapaty, K., R. Mathur, and D.W. Byun, 1996: A modeling study of vertical diffusion of passive and reactive tracers using local- and nonlocal-closure boundary layer schemes. *Air Pollution Modeling and Its Application XI*, ed. S.E. Gryning and F. Schiermeier. 433-442.
- Alapaty, K.A., J.E. Pleim, S. Raman, D.S. Niyogi, and D.W. Byun. 1997: Simulation of atmospheric boundary layer processes using local- and nonlocal-closure schemes. *J. Applied Meteor.* Vol. **36**. 214-233.
- Arya. S. P. , 1988. *Introduction to Micrometeorology*. Academic Press, San Diego, CA. 307 pp.
- Arya. S. P. , 1999. *Air Pollution Meteorology and Dispersion*. Oxford University Press, New York, NY. 310 pp.
- Ascher, U.M., S.J. Ruuth, and B.T.R. Wetton, 1995: Implicit-explicit methods for time-dependent PDE's, *SIAM J. Numer. Anal.*, **32**, 797-823.
- Bacon, D.P., N.N. Ahmad, Z. Boybeyi, T.J. Dunn, M.S. Hall, P.C.S. Lee, R. A. Sarma, and M.D. Turner, 2000: A dynamically adapting weather and dispersion model: The Operational Multiscale Environment Model with Grid Adaptivity (OMEGA). *Mon. Wea. Rev.* **121**. 2637-2641.
- Batchelor, G.K., 1967: *An Introduction to Fluid Mechanics*. Cambridge University Press, London.
- Blackadar, A. K., 1962: The vertical distribution of wind and turbulent exchange in neutral atmosphere. *J. of Geophys. Res.*, **67**, 3095-3103.
- Blackadar, A. K., 1978: Modeling pollutant transfer during daytime convection, *Preprints, Fourth Symposium on Atmospheric Turbulence, Diffusion, and Air Quality*, Reno, Am. Meteor. Soc., 443-447.
- Bodin, S., 1980: Applied numerical modeling of the atmospheric boundary layer, *Atmos. Plan. Bou. Lay. Phy.*, A. Longhetto, Ed., Elsevier Scientific Publ. Co., Amsterdam, 1-76.
- Bott, A., 1989: A positive definite advection scheme obtained by nonlinear renormalization of the advective fluxes. *Mon. Wea. Rev.* **117**, 1006-1015.
- Bott, A., 1992: Monotone flux limitation in the area-preserving flux-form advection algorithm. *Mon. Wea. Rev.* **120**, 2592-2602.
- Bott, A., 1993: The monotone area-preserving flux-form advection algorithm: reducing the time-splitting error in two-dimensional flow fields. *Mon. Wea. Rev.* **121**. 2637-2641.
- Briggs, G. A., 1973: Diffusion estimates for small emissions. ATDL Contribution No. 79 [Available from Atmospheric Turbulence and Diffusion Laboratory, Oak Ridge, Tenn.]
- Brooks, A. N., and T. J. R. Hughes, 1982: Streamline upwind/Petrov-Galerkin formulations for convection dominated flows with particular emphasis on the incompressible Navier-Stokes equations. *Comp. Meth. Appl. Mech. Eng.* **32**, 199-259.
- Brost R. A. and J. C. Wyngaard, 1978: A model study of the stably stratified planetary boundary layer. *J. Atmos. Sci.*, **35**, 1427-1440.
- Burk, S.D., and W.T. Thompson, 1989: A vertically nested regional numerical weather prediction model with second-order physics. *Mon. Wea. Rev.* **117**, 2305-2324.

Businger, J.A., and Arya, S.P.S., 1974: Height of the mixed layer in the stably stratified planetary boundary layer. *Advan. Geophys.*, **18A**, 73-92.

Businger J. A., J. C. Wyngaard, Y. Izumi, and E. F. Bradley, 1971: Flux profile relationships in the atmospheric surface layer, *J. Atmos. Sci.*, **28**, 181-189.

Byun, D. W., 1999a: Dynamically consistent formulations in meteorological and air quality models for multi-scale atmospheric applications: I. Governing equations in a generalized coordinate system. *J. Atmos. Sci.*, **56**, 3789-3807.

Byun, D. W., 1999b: Dynamically consistent formulations in meteorological and air quality models for multi-scale atmospheric applications: II. Mass conservation issues. *J. Atmos. Sci.*, **56**, 3808-3820.

Byun, D.W. and J.K.S. Ching, ed., 1999: *Science Algorithms of the EPA Models-3 Community Multiscale Air Quality (CMAQ) Modeling System*. EPA Report. EPA/600/R-99/030. [Available from National Exposure Research Laboratory, U.S. Environmental Protection Agency, Research Triangle Park, NC 27711]

Byun, D. W., and R. L. Dennis, 1995: Design artifacts in Eulerian air quality models: Evaluation of the effects of layer thickness and vertical profile correction on surface ozone concentrations. *Atmos. Environ.*, **29**, 105-126.

Byun, D.W., J. Young., J. Pleim, M.T. Odman, and K. Alapaty, 1999: Numerical transport algorithms for the community multiscale air quality (CMAQ) chemical transport model in generalized coordinates. pp 58, Chapter 7 in *Science Algorithms of the EPA Models-3 Community Multiscale Air Quality (CMAQ) Modeling System*. Byun, D.W. and J.K.S. Ching, ed., National Exposure Research Laboratory, U.S. Environmental Protection Agency, Research Triangle Park, NC.

Calder, K.L, 1949: Eddy diffusion and evaporation in flow over aerodynamically smooth and rough surfaces: A treatment based on laboratory laws of turbulent flow with special reference to conditions in the lower atmosphere. *Quart. J. Mech. Math.*, **2**, 153.

Carpenter, R. L., K. K. Droegemeier, P. R. Woodward, and , C. E., Hane, 1990: Application of the piecewise parabolic method (PPM) to meteorological modeling. *Mon. Wea. Rev.* **118**, 586-612.

Chang, J.S., P.B. Middleton, W.R. Stockwell, C.J. Walcek, J.E. Pleim, H.H. Lansford, S. Madronich, F.S. Binkowski, N.L. Seaman, and D.R. Stauffer, 1990: The Regional Acid Deposition Model and Engineering Model, NAPAP SOS/T Report 4, in: National Acid Precipitation Assessment Program: State of Science and Technology, Volume 1, National Acid Precipitation Assessment Program, 722 Jackson Place, N.W., Washington, D.C.

Chang, J.S., R.A. Brost, I.S.A. Isaksen, S. Madronich, P. Middleton, W.R. Stockwell, and C.J. Walcek, 1987: A three-dimensional Eulerian acid deposition model: Physical concepts and formulation, *J. of Geophys. Res.*, **92**, 14,681-700.

Chang J. S., S. Jin, Y. Li, M. Beauharnois, C.-H. Lu, H.-C. Huang, S. Tanrikulu, and J. DaMassa, 1997: *The SARMAP air quality model. Final Report*, SJVAQS/AUSPEX Regional Modeling Adaptation Project, 53 pp. [Available from California Air Resources Board, 2020 L Street, Sacramento, California 95814.]

Chatfield, R.B. and P.J. Crutzen, 1984: Sulfur dioxide in remote oceanic air: cloud transport of reactive precursors, *J. Geophys. Res.*, **89**, 7111-7132.

- Childs, P. N., and K. W. Morton, 1990: Characteristic Galerkin methods for scalar conservation laws in one dimension. *SIAM J. Numer. Anal.* **27**, 553-594.
- Chock, D. P., and A. M. Dunker, 1983: A comparison of numerical methods for solving the advection equation. *Atmos. Environ.* **17**(1), 11-24.
- Chock, D. P., 1985: A comparison of numerical methods for solving the advection equation - II. *Atmos. Environ.* **19**(4), 571-586.
- Chock, D. P., 1991: A comparison of numerical methods for solving the advection equation-III. *Atmos. Environ.* **25A**(5/6), 853-871.
- Colella, P., and P. R. Woodward, 1984: The piecewise parabolic method (PPM) for gas-dynamical simulations. *J. Comp. Phys* **54**, 174-201.
- Cotton, W.R. and R.A. Anthes, 1989: *Storm and Cloud Dynamics*, Academic Press, San Diego, CA.
- Crowley, W.P., 1968: Numerical advection experiments, *Mon. Weather Rev.*, **96**, 1-11.
- Dabdub, D., and Seinfeld, J. H., 1994: Numerical advective schemes used in air quality models - sequential and parallel implementation. *Atmos. Environ.* **28**(20), 3369-3385.
- Deardorff, J.W., 1966: The counter-gradient heat flux in the lower atmosphere and in the laboratory. *J. Atmos. Sci.*, **23**, 503-506.
- Deardorff, J.W., 1972: Theoretical expression for the counter gradient vertical heat flux. *J. Geophys. Res.*, **77**, 5900-5904.
- Deardorff, J.W., 1974: Three-dimensional numerical study of the height and mean structure of a heated planetary boundary layer. *Bound.-Layer Meteor.*, **7**, 81-106.
- Degrazia, G.A., U. Rizza, C. Mangia, and T. Tirabassi, 1997: Valication of a new turbulent parameterization for dispersion models in convective conditions. *Bound.-Layer Meteor.*, **85**, 243-254.
- Degrazia, G.A., D. Anfossi, J.C. Carvalho, C. Mangia, T. Tirabassi, and H.F. Campos Velho, 2000: Turbulence parameterizations for PBL dispersion models in all stability conditions. *Atmos. Environ.* **34**, 3575-3583.
- Demuth, C., 1978: A contribution to the analytical steady solution of the diffusion equation for line sources. *Atmos. Environ.* **12**, 1255-1258.
- Dennis, R.L., D.W. Byun, J.H. Novak, K.J. Galluppi, C.J. Coats, and M.A. Vouk, 1996: The next generation of integrated air quality modeling: EPA's Models-3. *Atmos. Environ.* **30**, 1925-1938.
- Detering, H.W., and D. Etling, 1985: Application of E- ϵ turbulence model to the atmospheric boundary layer. *Bound.-Layer Meteor.*, **33**, 113-133.
- Diemrjian, K.L. and K.L. Schere, 1979: Applications of a photochemical box model for ozone air quality in Houston, Texas. Proceedings, *Ozone/Oxidants: Interactions with the Total Environment II*, Houston, TX, 14-17 Oct. 1979, APCA, Pittsburgh, PA, 329-352.
- Dodge, M.C., 1977: Combined Use of Modeling Techniques and Smog Chamber Data to Derive Ozone Precursor Relationships, Rep. EPA-600/3-77-001a, pp 881-889.

- Donea, J., 1984: A Taylor-Galerkin method for convective transport problems. *Int. J. Num. Meth. Engng* **20**, 109-119.
- Draxler, R.R. and G.D. Hess, 1997: Description of the HYSPLIT 4 modeling system. *NOAA Technical Memo ERL, ARL-224*, Dec., 24pp.
- Du, S. and A. Venkatram, 1998: The effect of streamwise diffusion on ground-level concentrations. *Atmos. Environ.* **32**(11), 1955-1961.
- Ebert, E.E., U. Schumann, and R. B. Stull, 1989: Nonlocal turbulence mixing in the convective boundary layer evaluated from large-eddy simulation. *J. Atmos. Sci.*, **46**, 2178-2207.
- Eppel, D.P., H. Kapitza, M. Claussen, D. Jacob, W. Koch, L. Levkov, H.-T. Mengelkamp, and N. Werrmann, 1995: The nonhydrostatic mesoscale model GESIMA. Part II: Parameterizations and applications. *Beitr. Phys. Atmosph.*, **68**, 15-41.
- Ertel, H., 1942: Der vertikale Turbulenz-Wärmestrom in der Atmosphäre. *Metreor. Z.*, **59**, 250-253.
- Fiedler, B.H. and C.H. Moeng, 1985: A practical integral closure model for mean vertical transport of a scalar in a convective boundary layer, *J. Atmos. Sci.*, **42**, 359-363.
- Flatoy, F., 1993: Balanced wind in advanced advection schemes when species with long lifetimes are transported. *Atmos. Environ.* **27A**(12), 1809-1819.
- Ghorai, S., A.S. Tomlin, and M. Berzins, 2000: Resolution of pollutant concentrations in the boundary layer using a fully 3D adaptive gridding technique. *Atmos. Environ.* **34**, 2851-2863.
- Grell, G. A., J. Dudhia, and D. R. Stauffer, 1994: A description of the fifth-generation Penn State/NCAR mesoscale model (MM5). NCAR Tech. Note NCAR/TN 398+STR, 117 pp. [Available from the National Center for Atmospheric Research, P. O. Box 3000, Boulder, CO 80307.]
- Ha, K.J. and L. Mahrt, 2000: A new nocturnal boundary layer model. Proceedings. *14th Symposium on Boundary Layers and Turbulence*. Aspen, CO, AMS, pp. 581-584.
- Hanna, S.R., G.A. Briggs, J. Deardorff, B.A. Egan, F.A. Gifford, and F. Pasquill, 1977: AMS Workshop on Stability Classification Schemes and Sigma Curves—summary of recommendations. *Bull. Amer. Meteorol. Soc.*, **58**, 1305-1309.
- Hanna, S.R., G.A. Briggs, and R.P. Hosker, 1982: *Handbook on Atmospheric Diffusion*. U.S. Department of Energy, Technical Information Center, Oak Ridge, TB.
- Hanna, S.R., 1994: Random variability in mesoscale wind observations and implications for diffusion models. Preprints. *Eighth Joint Conference on Applications of Air Pollution Meteorology with A&WMA*. Nashville, Tennessee, AMS, pp. 1-5.
- Hass, H., H.J. Jacobs, M. Memmescheimer, A. Ebel, and J.S. Change, 1991: Simulation of a wet deposition case in Europe using the European Acid Deposition Model (EURAD). *Air Pollution Modelling and Its Applications*, Vol. VIII (edited by van Dop H. and D.G. Steyn), Plenum Press, 205-213.
- Holtslag, A. A. M., E. I. F. de Bruin, and H.-L. Pan, 1990: A high resolution air mass transformation model for short-range weather forecasting. *Mon. Wea. Rev.*, **118**, 1561-1575.

- Holtslag, A. A. M., and C.-H. Moeng, 1991: Eddy diffusivity and countergradient transport in the convective atmospheric boundary layer. *J. Atmos. Sci.*, **48**, 1690-1698.
- Holtslag, A. A. M., and B. A. Boville, 1993: Local versus nonlocal boundary-layer diffusion in a global climate model. *J. Climate.*, **6**, 1825-1842.
- Holtslag, A. A. M., E. van Meijgaard, and W.C. de Rooy, 1995: A comparison of boundary layer diffusion schemes in unstable conditions over land. *Bound.-Layer Meteor.*, **76**, 69-95.
- Hong, S.-Y., and H.-L. Pan, 1996: Nonlocal boundary layer vertical diffusion in a medium-range forecast model. *Mon. Wea. Rev.*, **124**, 2322-2339.
- Huang, C.H., 1979: A theory of dispersion in turbulent shear flow. *Atmos. Environ.* **13**, 453-463.
- Irwin, J.S., 1979: Estimating plume dispersion—A recommended generalized scheme. Presented at 4th Symposium on Turbulence and Diffusion, American Met. Soc., Reno, Nevada.
- Jensen, N.O., and E. L. Petersen, 1979: The box model and the acoustic sounder, a case study. *Atmos. Environ.* **13**, 717-720.
- Klemp J.B., and R. Wilhelmson, 1978: The simulation of three dimensional convective storm dynamics. *J. Atmos. Sci.*, **35**, 1070-1096.
- Knoth, O. and R. Wolke, 1998a: An explicit-implicit numerical approach for atmospheric chemistry–transport modeling. *Atmos. Environ.* **32**, 1785-1797.
- Knoth, O. and R. Wolke, 1998b: Implicit-explicit Runge-Kutta methods for computing atmospheric reactive flows. *Appl. Numer. Math.* **28**, 327-341.
- Lacser, A. and S.P.S. Arya, 1986: A comparative assessment of mixing-length parameterizations in the stably stratified nocturnal boundary layer, *Bound. Layer Meteor.*, **36**, 53-70.
- Lange, R., 1989: Transferability of a 3-D air quality model between two different sites in complex terrain. *J. Appl. Meteor.*, **28**, 665-679.
- Lettau, H. H., 1970: Physical and meteorological basis for mathematical model of urban diffusion processes. *Proceedings*, Symposium on Multiple-Source Urban Diffusion Models. U.S. EPA Publication No. AP-86.
- Liu, M and J. J. Carroll, 1996: A high resolution air pollution model suitable for dispersion studies in complex terrain. *Mon. Wea. Rev.*, **124**, 2396-2409.
- Löhner, R., K. Morgan, J. Peraire, and M. Vahdati, 1987: Finite element flux-corrected transport (FEM-FCT) for the Euler and Navier-Stokes Equations. *Finite Elements in Fluids. Vol. 7*. John Wiley & Sons. 105-121.
- Long, P.E., and D.W. Pepper, 1981: An examination of some simple numerical schemes for calculating scalar advection, *J. Appl. Meteor.*, **20**, 146-156.
- Longhetto, A., ed., 1980: *Atmospheric Planetary Boundary Layer Physics*. New York, Elsevier.
- Louis, J.F., 1979: A parametric model of vertical eddy fluxes in the atmosphere. *Bound.-Layer Meteor.*, **17**, 187-202.

McNider, R.T., M. P. Singh, and S. Gupta., 1996: Nocturnal wind structure and plume growth rates due to inertial oscillation. Preprints. *Ninth Joint Conference on Applications of Air Pollution Meteorology with A&WMA*. Atlanta, Georgia, AMS, pp. 455-458.

McRae, G.J., W.R. Goodin, and J.H. Seinfeld, 1982: Development of a second generation mathematical model for urban pollution: I. Model formulation. *Atmos. Environ.* **16**, 679-696.

Mellor, G.L. and T. Yamada, 1974: A hierarchy of turbulence closure models for planetary boundary layers, *J. Atmos. Sci.*, **31**, 1791-1806.

Mellor, G.L. and T. Yamada, 1982: Development of a turbulence closure model for geophysical fluid problems. *Reviews of Geophysical and Space Physics*, **20**, 851-875.

Mesinger, F. and A. Arakawa, 1976: *Numerical Methods Used in Atmospheric Models*. In: Global Atmospheric Research Programme (GARP), Joint Organization Committee, GARP Publication Series, No 17 [Available from WMO Secretariat, Geneva].

Meszaros, E., G. Varhelyi, and L. Haszpra, 1978: On the atmospheric sulfur budget over Europe. *Atmos. Environ.* **12**, 2273-2277.

Nikomo, J., J.P. Tuovinen, J. Kukkonen and I. Valkama, 2000: A hybrid plume model for local scale atmospheric dispersion, *Atmos. Environ.* **33**, 4389-4399.

O'Brien, J., 1970: On the vertical structure of the eddy exchange coefficient in the planetary boundary layer, *J. Atmos. Sci.*, **27**, 1213-1215.

Odman, M. T., 1998: Research on Numerical Transport Algorithms for Air Quality Simulation Models. EPA Report. EPA/660/R-97/142. [Available from National Exposure Research Laboratory, U.S. Environmental Protection Agency, Research Triangle Park, NC 27711].

Odman, M. T., and Russell, A. G., 1993: A nonlinear filtering algorithm for multi-dimensional finite element pollutant advection schemes. *Atmos. Environ.* **27A**, 793-799.

Odman, M. T., A. Xiu, and D. W. Byun, 1993: Evaluating advection schemes for use in the next generation of air quality modeling systems, Paper OT7-I.5, International Specialty Conference on Regional Photochemical Measurement and Modeling Studies, Air & Waste Management Association, Pittsburgh, PA. 1386-1401.

Oran, E., and J. Boris, 1987: *Numerical Solution of Reactive Flow*, New York, Elsevier.

Otey, G. R. and H.A. Dwyer, 1978: Numerical study of the interaction of fast chemistry and diffusion. *AIAA J.* **17**, 606-613.

Otte, M.J. and J.C. Wyngaard, 1996: A general framework for an "unmixed layer" PBL model. *J. Atmos. Sci.*, **53**, 2652-2670.

Panofsky, H. A. and J. A. Dutton, 1984: *Atmospheric Turbulence*. Wiley-Interscience, New York.

Pasquill, F., 1976: Atmospheric dispersion parameters in Gaussian plume modeling. Part II. Possible requirements for change in the Turner Workbook values. Report No. EPA-600/4-76-030b, U.S. Environmental Protection Agency, Research Triangle Park, NC.

Pasquill, F. and F. B. Smith, 1983: *Atmospheric Diffusion*, 3rd ed. Ellis Horwood Ltd., Chichester, England.

- Pielke, R.A., 1984: *Mesoscale Meteorological Modeling*, Academic Press, Orlando, FL.
- Pielke, R.A. and Y. Mahrer, 1975: Technique to represent the heated planetary boundary layer in mesoscale models with coarse vertical resolution. *J. Atmos. Sci.*, **32**, 2288-2308.
- Pleim, J.E. and J. Chang, 1992: A non-local closure model for vertical mixing in the convective boundary layer. *Atmos. Envi.*, **26A**, 965-981.
- Prabha, T.V. and E. Mursch-Radlgruber, 1999: Modeling of diffusion in a Wide Alpine Valley. *Theor. Appl. Climatol.*, **64**, 93-103.
- Raupach, M.R., and B.J. Legg, 1983: Turbulent dispersion from an elevated line source: Measurements of wind-concentration moments and budgets. *J. Fluid Mech.*, **136**, 111-137.
- Raymond, W.H. and R.B. Stull, 1990: Application of transient turbulence theory to mesoscale numerical weather forecasting. *Mon. Weather Rev.*, **118**, 2471-2499.
- Roache, P.J., 1972: *Computational Fluid Dynamics*, Hermosa Publishers, Albuquerque, New Mexico.
- Rood, R. B., 1987: Numerical advection algorithms and their role in atmospheric transport and chemistry models. *Rev. Geophysics* **25**(1), 71-100.
- Rounds, W., 1955: Solutions of the two-dimensional diffusion equation. *Trans. Am. Geophysical Union* **36**, 395.
- Russell, A, and R. Dennis, 2000: NARSTO critical review of photochemical models and modeling. *Atmos. Envi.*, **34**, 2283-2324.
- Schere, K. L. and K. L. Diemrjian, 1984: User's Guide for the Photochemical Box Model (PBM). U.S. EPA Report. EPA-600/8-84-022a, Research Triangle Park, NC.
- Schumann, U., 1989: Large-eddy simulation of turbulent diffusion with chemical reactions in the convective boundary layer. *Atmos. Envi.*, **26A**, 965-981.
- Seinfeld, J.H., 1986: *Atmospheric Chemistry and Physics of Air Pollution*. John Wiley and Sons, New York.
- Siebesma, A.P. and J. Teixeira, 2000: An advection-diffusion schema for the CBL: description and 1-D results. Proceedings. *14th Symposium on Boundary Layers and Turbulence*. Aspen, CO, AMS, pp. 133-136.
- Smagorinsky, J., 1963: General circulation experiments with the primitive equations: 1. The basic experiment. *Mon. Wea. Rev.* **91**, 99-164.
- Smith, F.B., 1957: The diffusion of smoke from a continuous elevated point source into a turbulent atmosphere. *J. Fluid Mech.*, **2**, 491-508.
- Smolarkiewicz, P.K., 1983: A simple positive definite advection transport scheme with small implicit diffusion. *Mon. Wea. Rev.* **111**, 479-486.
- Sorbjan Z., 1986a, On similarity in the atmospheric boundary layer, *Bound.-Layer Meteor* **34**, 377-397.

- Sorbjan Z., 1986b, On the vertical distribution of passive species in the atmospheric boundary layer, *Bound.-Layer Meteor.*, **35**, 73-81.
- Stevens, B., 2000: Quasi-steady analysis of a PBL model with an eddy-diffusivity profile and nonlocal fluxes. *Mon. Wea. Rev.* **128**, 824-836.
- Stull, R. B., 1988: *An Introduction to Boundary Layer Meteorology*. Kluwer Academic, 666 pp.
- Stull, R. B., 1993: Review of non-local mixing in turbulent atmosphere: Transilient turbulence theory. *Bound.-Layer Meteor.*, **62**, 21-96.
- Stull, R. B., and A.G.M. Driedonks, 1987: Applications of the transilient turbulence parameterization to atmospheric boundary layer simulations. *Bound.-Layer Meteor.*, **40**, 209-239.
- Tirabassi, T., M. Tagliazucca, and P. Zannetti, 1986: KAPPA-G, a non-Gaussian plume dispersion model: Description and evaluation against tracer measurements. *JAPCA*, **36**, 196-211.
- Tirabassi, T., and U. Rizza, 1997: Boundary layer parameterization for a non-Gaussian puff model. *J. Appl. Meteor.*, **36**, 1031-1037.
- Tremback, G. J., Powell, J., Cotton, W. R. and Pielke, R. A., 1987: The forward-in-time upstream advection scheme: extension to higher orders. *Mon. Wea. Rev.*, **115**, 540-555.
- Troen, I. B., and L. Mahrt, 1986: A simple model of the atmospheric boundary layer: Sensitivity to surface evaporation. *Bound.-Layer Meteor.*, **37**, 129-148.
- Ulke, A. G., 2000: New turbulent parameterization for a dispersion model in the atmospheric boundary layer. *Atmos. Envi.*, **34**, 1029-1042.
- Venkatram, A., 1978: An examination of box models for air quality simulation. *Atmos. Envi.*, **12**, 2243-2249.
- Verwer, J.G., W.H. Hundsdorfer, and J.G. Blom, 1998: Numerical time integration for air pollution models. *Modeling, Analysis and Simulation (MAS)*, MAS-R9825, 58pp.
- Williamson, D.L., and P.J. Rasch, 1989: Two-dimensional semi-Lagrangian transport with shape-preserving interpolation. *Mon. Wea. Rev.* **117**, 102-117.
- Willis, G.E., and J.W. Deardorff, 1976: A laboratory model of diffusion into the convective planetary boundary layer. *Quart. J. R. Met. Soc.*, **102**, 427-446.
- Wyngaard, J.C., 1982: Boundary-layer modeling. In *Atmospheric Turbulence and Air Pollution Modelling* (F.T.M. Nieustadt and H. van Dop., eds.), pp. 69-106. D. Reidel Pub. Co., Dordrecht, Holland.
- Yamartino, R. J., 1993: Nonnegative, conserved scalar transport using grid-cell-centered, spectrally constrained Blackman cubics for applications on a variable-thickness mesh. *Mon. Wea. Rev.* **121**, 753-763.
- Yamartino, R.J., J.S. Scire, G.R. Carmichael, and Y.S. Chang, 1992: The CALGRID mesoscale photochemical grid model - Part I. Model formulation, *Atmos. Environ.* **26A**, 1493-1512.
- Yamartino, R.J., 1998: Improvements to horizontal transport in grid models. *Preprints*, 23rd International Technical Meeting on Air Pollution Modelling and its Application, Varna, Bulgaria, NATO/CCMS, pp. 51-56.

Yamartino, R.J., and S. Machiraju, 2000: Determination of the Horizontal Diffusion Coefficient for Use in the SARMAP Air Quality Model. SCARB Report, State of California Air Resources Board, Sacramento, CA.

Yanenko, N.N., 1971: The method of fractional steps: The solution of problems of mathematical physics in several variables, (M. Holt, ed.) Springer-Verlog, New York.

Yeh, G.T., and C.H. Huang, 1975: Three-dimensional air pollutant modeling in the lower atmosphere. *Bound.-Layer Meteor.*, **9**, 381-390.

Yokoyama, O., Gamo M. and Yamamoto S., 1979, The vertical profiles of the turbulence quantities in the atmospheric boundary layer, *J. Met. Soc. Japan*, *57*(3), 264-272.

Zannetti, P., 1990: *Theories, Computational Methods, and Available Software*, Computational Mechanics Publications, Southhampton and Van Nostrand Reinhold, New York.

Zhang, D., and R.A. Anthes, 1982: A high-resolution model of the planetary boundary layer - Sensitivity tests and comparisons with SESAME-79 data, *J. Appl. Meteo.*, **21**, 1594-1609.

Zhang, Q., and R. B. Stull, 1992: Alternative nonlocal descriptions of boundary-layer evolution. *J. Atmos. Sci.*, **49**, 2267-2281.

BRANKIN Page

Chapter 11

Lagrangian Particle Models

Lagrangian particle models are powerful, advanced tools for simulating atmospheric dispersion and air pollution phenomena. The next volume in this book series will present a comprehensive chapter on this topic. A brief introduction to this subject is presented below, courtesy of Domenico Anfossi anfossi@to.infn.it

Basically two kinds of models are available to numerically simulate air pollution dispersion: Eulerian models and Lagrangian models. The main difference between the Eulerian and Lagrangian view is that the Eulerian reference system is fixed (with respect to the earth) while the Lagrangian reference system follows the instantaneous fluid velocity.

In a Lagrangian stochastic model (LSM), also called Lagrangian Particle or Random Walk model, the motion of air masses or particles passively following the flow is studied. To simulate the presence of turbulent eddies, particle velocities are subjected to a random forcing. Consequently, these models are of stochastic type. The fictitious particles (computer-particles), which represent pollutant gases or aerosols, are considered small enough to follow the motion of the smallest eddies and, at the same time, big enough to represent a large number of molecules. Each particle is moved, at each time step, by transport, due to the mean wind, and diffusion, related to the turbulent wind velocity fluctuations, without any grid.

In the single particle models, the trajectory of each particle represents an individual statistical realization in a turbulent flow characterized by certain initial conditions and physical constraints. Thus the motion of any particle is independent of the other particles, and consequently the concentration field must be interpreted as an ensemble average.

The Lagrangian approach is a more natural way of describing the dispersion process. It allows a high resolution, particularly in complex terrain. Moreover, due to present days computer capabilities, these models begin to be used for regulatory applications in some European Countries.

In the next volume, a review of the present state-of-the-art of Lagrangian stochastic models for the description of airborne dispersion in the Planetary Boundary Layer will be presented. It will cover various aspects of LSM derivation and applications. The theoretical bases of LSMs (Markov process, Langevin equation, Fokker-Plank equation, Well-mixed condition, Probability Density Functions (PDFs), Turbulence parameterisation) will be described and the related technical information (link with meteorological models, boundary conditions, concentration calculation) will be presented. Particular topics that can be covered within the framework of LSMs (plume rise, reactive chemistry and the prediction of higher order concentration moments) will also be included. Then, application of LSMs under various conditions, will be reviewed, and many examples of main applications presented and discussed. They will include the simulation of dispersion in the following conditions: convective conditions (including fumigation), neutral and stable conditions, urban environment and low wind speed conditions, the simulation of transport and dispersion at the mesoscale and at long range, and the footprint analysis of scalar fluxes.

The reader interested in this topic will find additional information at:

- http://www.aria-net.it/PDF/e_spray3.pdf
SPRAY model, ARIANET, Milano, Italy
- www.dar.csiro.au/ladm/
LADM model, CSIRO Australia
- http://www.frii.com/~uliasz/modeling/lpd_appl.htm
Atmospheric Modeling & Analysis by M.Uliasz (USA)
- www.frii.com/~uliasz/modeling/ref/lpd_bib.htm
A comprehensive list of literature references on Lagrangian air dispersion modeling
- <http://www.arl.noaa.gov/ss/models/hysplit.html>
HYSPLIT model
- <http://www.harmo.org/publishedSections/Pages153to158.pdf>
The new German regulatory model - a Lagrangian particle dispersion model
- <http://www.environmental-center.com/software/ysa/ysa.htm>
RAPTAD model

References

- Brusasca G., G. Tinarelli, D. Anfossi (1989). Comparison between the results of a Monte Carlo atmospheric diffusion model and tracer experiments. *Atmos. Environ.*, 23, 1263 – 1280
- Brusasca, G., G. Tinarelli, and D. Anfossi, (1992). Particle model simulation of diffusion in low wind speed stable conditions. *Atmos. Environ.*, 4, 707-723
- Ferrero E., Anfossi D. and Tinarelli G. (2001). Simulations of Atmospheric Dispersion in Urban Stable Boundary Layer, *Int. Jour. of Environment and Pollution*, in press.
- Flesch, T. K., (1996). The footprint for flux measurements, from backward Lagrangian stochastic models. *Bound-Layer Meteorol* 78, 399–404.
- Franzese P., A. Luhar and M. Borgas (1999). An efficient Lagrangian stochastic model of vertical dispersion in the convective boundary layer, *Atmos. Environ.*, 33, 2337-2345.
- Hurley P.J. and Physick W.L. (1991). A Lagrangian particle model of fumigation by breakdown of the nocturnal inversion. *Atmos. Environ.*, 25A, 1313-1325.
- Hurley P. and W. Physick (1993a). A skewed, homogeneous Lagrangian particle model for convective conditions, *Atmos. Environ.*, 27A, 619-624.
- Luhar A.K., and Britter R.E. (1989). A random walk model for dispersion in inhomogeneous turbulence in a convective boundary layer. *Atmos. Environ.*, 23, 1191-1924.
- Luhar A., M. Hibberd, and P. Hurley (1996). Comparison of Closure Schemes used to Specify the Velocity PDF in Lagrangian Stochastic Dispersion Models for Convective Conditions, *Atmos. Environ.*, 30, 1407-1418.
- Nasstrom, J.S. and D.L. Ermak (1999a). A homogeneous Langevin equation model, Part I: simulation of particle trajectories in turbulence with a skewed velocity distribution. *Boundary-Layer Meteorol.*, 92, 343-369.
- Nasstrom, J.S. and D.L. Ermak (1999b). A homogeneous Langevin equation model, Part II: simulation of dispersion in the convective boundary layer. *Boundary-Layer Meteorol.*, 92, 371-405.
- Oettl, D., R. A. Almbauer, and P. J. Sturm, (2001). A new method to estimate diffusion in stable, low wind conditions, *J. Appl. Meteorol.*, in press.
- Physick, W.L., J.A. Noonan, J.L. M^cGregor, P.J.Hurley, D.J. Abbs and P.C. Manins (1994b). LADM: A Lagrangian Atmospheric Dispersion Model. *CSIRO Division of Atmospheric Research Technical Report No. 24*, 146pp.
- Rodean H.C. (1996). Stochastic Lagrangian models of turbulent diffusion. Meteorological Monographs, 26, Amer. Met. Soc., Boston, USA.
- Rotach M., S. Gryning and C. Tassone (1996). A two-dimensional Lagrangian stochastic dispersion model for daytime conditions, *Q. J. R. Meteorol. Soc.*, 122, 367-389.
- Sawford B.L. (1993). Recent developments in the Lagrangian stochastic theory of turbulent dispersion. *Bound-Layer Meteorol.*, 62, 197-215.

- Sawford, B., A. Luhar, J. Hacker, S. Young, I.-H. Yoon, J. Noonan, J. Carras, D. Williams and K. Rayner (1998). The Kwinana coastal fumigation study: I-Program overview, experimental design and selected results, *Bound-Layer Meteorol.*, 89, 359-
- Thomson D.J., (1987). Criteria for the selection of stochastic models of particle trajectories in turbulent flows. *J. Fluid Mech.*, 180, 529-556.
- Thomson, D.J., and Montgomery, M.R., (1994). Reflection boundary conditions for random walk models of dispersion in non-Gaussian turbulence. *Atmos. Environ.*, 28:1981-1987.
- Thomson, D.J., Physick, W.L., and Maryon, R.H., (1997). Treatment of interfaces in random walk dispersion models. *J. Appl. Meteor.*, 36(9), 1284-1295.
- Tinarelli G., Anfossi D., Brusasca G., Ferrero E., Giostra U., Morselli M.G., Moussafir J., Tampieri F., Trombetti F. (1994). Lagrangian particle simulation of tracer dispersion in the lee of a schematic two-dimensional hill. *J. Appl. Meteor.*, 33, No. 6, 744-756.
- Tinarelli G., Anfossi D., Bider M., Ferrero E., Trini Castelli S. (2000). A new high performance version of the Lagrangian particle dispersion model SPRAY, some case studies. *Air Pollution Modeling and its Application XIII*, Gryning S.E. and Batchvarova E. Eds.
- Uliasz, M. (1994). Lagrangian particle dispersion modelling. In: *Environmental Modeling, Vol II*, Computational Mechanics Publications, Southampton.
- Weil J.C. (1990). A diagnosis of the asymmetry in top-down and bottom-up diffusion using a Lagrangian stochastic model, *J. Atmos. Sci.*, 47, 501-515.
- Weil, J. C., (1994). A hybrid Lagrangian dispersion model for elevated sources in the convective boundary layer. *Atmospheric Environment* 28, 3433–3448.
- Wilson J., G. Thurtell and G. Kidd (1981). Numerical simulation of particle trajectories in inhomogeneous turbulence, II: systems with variable turbulent velocity scale, *Bound-Layer Meteorol.*, 21, 423-441.
- Wilson J.D. and Flesch T.K. (1993). Flow boundaries in random-flight dispersion models: enforcing the well-mixed condition. *J. Appl. Meteor.*, 32, 1695-1707.
- Wilson J.D., Thurtell G.W. and Kidd G.E. (1981). Numerical simulation of particle trajectories in inhomogeneous turbulence Part II: Systems with variable turbulence velocity scale. *Bound-Layer Meteorol.*, 21, 423-441.
- Zannetti P. (1984). New Monte Carlo scheme for simulating Lagrangian particle diffusion with wind shear effects. *Appl. Math. Modeling*, 8, 188-192.

Chapter 12

Atmospheric Transformations

The modeling of chemical and physical transformations of pollutants in the atmosphere is an important task, in order to fully understand the ultimate fate of chemical emissions. The next volume in this book series will present a comprehensive chapter on this topic. A brief introduction to this subject is presented below, courtesy of Betty K. Pun

bpun@aer.com

A typical air quality model tracks the transport and transformation of chemicals in the atmosphere. In a general sense, the term transport refers to physical movement and includes dispersion, emissions, and deposition of pollutants. Horizontal and vertical advection and diffusion constitute the dispersion processes typically tracked in an air quality model. While emissions represent the influx of chemical or precursors into the system, wet deposition and dry deposition represent their removal. Atmospheric transformations encompass both physical and chemical changes of chemicals in the atmosphere. Without these transformation processes, some of the more pressing environmental impacts would simply cease to exist. For example, photochemical smog is created by a series of complex atmospheric reactions involving organic compounds and nitrogen oxides. The depletion of ozone in the lower stratosphere is due to a series of reactions occurring both in the gas phase and on the surface of aerosol particles. Fine particles are responsible for the haziness of many US National Parks and Class I areas and unhealthy air in many urban areas. These particles are formed in some cases from the atmospheric oxidation of sulfur dioxide, nitrogen oxides, and organic compounds and the subsequent phase transition of the products of these reactions to form fine particulate matter sulfate, nitrate, and organic compounds. Therefore, the modeling of atmospheric transformations includes complex processes that may be quite unique to each pollutant of concern.

A common theme of atmospheric transformations seems to be atmospheric chemistry for many pollutants of concern. In the next volume, we will provide a review of the fundamentals of gas phase chemical reactions, phase transitions, and aqueous phase reactions. In the course of this review and subsequent sections, we will also provide an overview of the key processes involved in the formation of ozone, particulate matter, hazardous air pollutants, and halogen chemistry. Additional information can be found in textbooks such as Finlayson-Pitts and Pitts (2000) and Seinfeld and Pandis (1998). Modeling air quality entails the mathematical representation of the atmospheric transformations and the numerical solution of the algebraic equations and ordinary differential equations, which will be developed in the chapter.

The treatment of chemical transformations in current models will also be discussed. We will start with plume models and discuss the gas-phase chemistry at different stages of the plume. We will then discuss several Eulerian models or 3-dimensional source models, including both research grade models and models used more routinely. Several atmospheric mechanisms are used in these Eulerian models. Those include the Carbon Bond Mechanism (CBM)-IV, the GATOR derivative of the extended CBM version, the Statewide Air Pollution Research Center mechanisms, the Regional Acid Deposition Model mechanism version 2, the Regional Atmospheric Chemistry mechanism, the Caltech Atmospheric chemistry mechanism, the Regional Lumped Atmospheric Chemical Scheme, and Micro-CB4. Each mechanism has also been modified or extended for additional species (e.g., isoprene addition to the original RADM2) or the modeling of condensable species, especially from organic compounds.

The modeling of particulate matter and droplets requires a mathematical description of the aqueous-phase and heterogeneous chemistry. These mechanisms range from relatively simple mechanisms with only a few reactions to highly complex ones with over 100 reactions. Modules that describe the gas/particle partitioning of inorganic species and organic species will be discussed. Note that the distribution of the semi-volatile products of gas-phase, aqueous, and heterogeneous reactions onto particles depends on the representation of the particle size distribution.

In a one-atmosphere approach, a single model would suffice if it included a comprehensive chemical mechanism containing all gas-phase, heterogeneous, and aqueous-phase reactions for all air pollutants of concern and a phase transition module describing all relevant dynamic processes for different types of particles. In practice, chemical mechanisms have been developed to describe the chemical transformation processes specific for certain air pollutants. Therefore, specific models exist for hazardous air pollutants and other models describe the stratosphere. To complete the overview of available models for chemical transformations, plume-in-grid type models that combine plume chemistry with urban/regional chemistry will be discussed last. Available resources on the

modeling of atmospheric transformations include Jacobson (1999) and the Community Modeling and Analysis System website (<http://www.cmascenter.org>).

References

Finlayson-Pitts, B.J. and J.N. Pitts, 2000. *Chemistry of the Upper and Lower Atmosphere*. Academic Press, San Diego, CA.

Jacobson, M.Z., 1999. *Fundamentals of Atmospheric Modeling*, Cambridge University Press, Cambridge, United Kingdom.

Seinfeld J.H. and S.N. Pandis, 1998. *Atmospheric chemistry and Physics*. John Wiley and Sons, New York, NY.

<http://uamv.saintl.com/> (UAM-V)

<http://www.camx.com/overview.html> (CAMx)

<http://www.arb.ca.gov/eos/soft.html> (CALGRID)

BRANK
P
2000

Chapter 13

Deposition Phenomena

Deposition phenomena are the physical and chemical processes in which the atmosphere cleans itself by depositing pollutants on the surface of the earth. There are two types of deposition mechanisms: dry deposition, i.e., the uptake at the earth's surface (e.g., soil, water, or vegetation); and wet deposition, i.e., absorption into droplets followed by droplet precipitation (e.g., rain) or impaction on the earth's surface (e.g., fog droplets).

The next volumes in this book series will present technical material on this topic and a description of the modeling algorithms and parameterizations used to simulate dry and wet deposition. Most air pollution models, in fact, include deposition modules, i.e., subprograms that calculate the deposition fluxes of chemicals at the ground.

BRANKLEY
PAGE

Chapter 14

Indoor Air Pollution Modeling

Indoor air pollution phenomena involve atmospheric transport of chemicals in confined environments (e.g., an office area or a working space). Sometimes indoor pollution is generated by intrusion of chemicals from outside. More often, however, chemicals are emitted by indoor activities and may have a potential for indoor accumulation.

The next volume in this book series will present a comprehensive chapter on this topic.

The reader will find useful information on this subject at:

- <http://www.epa.gov/iaq/> (EPA)
- <http://www.epa.gov/appcdwww/iemb/model.htm> (EPA)
- http://www.unlv.edu/Research_Centers/NCACM/HTML/research/iaq/index.html (computer simulation)

BRANK
P
2000

Chapter 15

Modeling of Adverse Effects

Air pollution causes several types of adverse effects. Special modeling calculations are often required to identify and quantify adverse effects, which include acute effects caused by short exposures (episodes) and chronic effects caused by prolonged periods of contamination (e.g., a lifetime exposure).

Adverse effects include: 1) effects on human health, animals, and plants; 2) damage to human welfare, such as atmospheric visibility impairment, odors, and undesired changes in local weather; 3) economical damages to materials, structures, real estate values, and artistic heritage; and 4) global effects, such as possible climatic changes and depletion of stratospheric ozone.

Modeling adverse effects is a very important task in air quality studies, especially in optimization studies where, for example, an optimal reduction strategy of air pollution emissions needs to be defined by minimizing costs and/or maximizing benefits (i.e., minimizing adverse effects).

The next volumes in this book series will present chapters on these topics. In particular, a chapter on modeling of health risks associated with combustion facility emissions is expected in Volume II.

The reader can find useful information on air pollution adverse effects at:

- <http://www.epa.gov/ebtpages/airairpollutioneffects.html> (EPA)
- <http://www.ces.ncsu.edu/depts/pp/notes/Ozone/ozone.html> (Ozone effects on plants)
- <http://www.aqd.nps.gov/ard/vis/visitexp.html> (Visibility)
- <http://www.doh.gov.uk/airpollution/index.htm> (U.S. Department of Health)

Blank Page

Chapter 16

Statistical Modeling

Statistical methods and modeling are often used in air quality studies. Applications include: 1) frequency distribution estimates of air quality measurements, e.g., for the purpose of identifying the probability of extreme episodes; 2) time series analysis of air quality and meteorological data, e.g., for the purpose of short-term, real-time forecasting of air pollution episodes; 3) joint application of deterministic and statistical techniques, e.g., using Kalman filters; 4) receptor modeling; 5) statistical methods for performance evaluation of dispersion models (see Chapter 17 in this Volume I); 6) optimization methods; and 7) other methods, such as pattern recognition, cluster analysis, fractal analysis.

The next volumes in this book series will present chapters on these topics.

BRANKIN
P
2000

Chapter 17

Evaluation of Air Pollution Models

The next volume will present a chapter on evaluation of air pollution models. Some preliminary information is presented below, courtesy of Elisa Canepa canepae@fisica.unige.it

Model quality assurance is a collection of activities one should perform in order to promote the development and application of good air quality simulation models. One of the elements of model quality assurance is model evaluation. The chapter will present information about model evaluation, the overall system of procedures designed to measure model performance, and in particular the process of statistical performance evaluations. Statistical performance evaluation is an assessment of model performance based on the comparison of model outputs with experimental data. Some performance measures, consisting of statistical indices and graphical methodologies currently used, will be described. Problems related to uncertainty analysis will be highlighted.

References

Standard Guide for the Statistical Evaluation of Atmospheric Dispersion Model Performance, D6589, Annual Book of Standards Volume 11.03, American Society for Testing and Materials, West Conshohocken, PA 19428 (<http://www.astm.org>).

Model Evaluation Group (1994): Model Evaluation Protocol. Can be requested from Dr. S. Cole, DG XII/D1, Rue de la Loi 200, B-1049 Belgium. Fax +32 2 296 3024.

There is an effort that has been ongoing since 1991 to harmonize the methods used to evaluate the performance of air quality models. To date the focus has been on dispersion models. It is envisioned that models for characterizing regional-scale transport and the formation of secondary species will eventually be a topic within this forum. See:

<http://www.dmu.dk/atmosphericenvironment/harmoni.htm>, and
http://www.dmu.dk/atmosphericenvironment/Harmoni/M_V_KIT.htm

There is a newsletter that tracks many of the air quality modeling initiatives and issues with a focus on Europe, which can be obtained from:

<http://www.meteo.bg/EURASAP/Newsletter.html>

The U.S. EPA publishes guidance information promoting quality assurance in all phases of air quality assessments. This material can be found at:

http://www.epa.gov/quality/qa_docs.html

Chapter 18

Regulatory Air Quality Models

Air models are often applied for regulatory purposes, i.e., to comply with laws and regulations. Typically, these applications must follow precise modeling guidelines and require the use of pre-approved modeling software. The next volume will present a chapter with a historical look at the development of regulatory air quality models for the United States Environmental Protection Agency. Some preliminary information on this topic is presented below, courtesy of John S. Irwin

irwin.john@epa.gov

Public Laws and Regulations have been primary sources for funding the development of air quality models. Certainly the Atomic Energy Act in 1954 (which ultimately founded the Nuclear Regulatory Agency) and Public Law 159 in 1955 (which ultimately founded the Environmental Protection Agency) were instrumental in stimulating research activities. There have been a number of critical science reviews on the subject of the development of air quality models. The purpose of this discussion is to review the development of regulatory air quality models within the United States as viewed from within EPA. This chapter is intended to complement these science reviews.

Describing historical development poses a dilemma. For discussion purposes it is easier if we focus on one topic; however, it creates a false sense of order, which is more related to the wisdom of hindsight. In reality, since everything is happening at once, it is difficult to determine the significance of individual developments when viewed in context. At various points, we will attempt to make some of the connections, but most of the assimilation work is left for the reader. Section 2 of this chapter will focus on the legislative events that influenced the development of air quality models. Section 3 reviews the development of the early plume models for non-reactive pollutants, their evolution and specialization for characterizing dispersion from large individual industrial sources, and the current trend towards puff models. Section 4 will summarize the development of long-term air quality

models that provide estimates of seasonal and annual average concentration for an urban area for non-reactive pollutants. In the early to mid-1970's, these long-term models proved the feasibility of designing emission control strategies for entire cities for non-reactive pollutants, and thus offered a basis for considering development of air quality regulations. During the late 1990's as computers became more powerful, the use of long-term approximate solutions and long-term models seems to have declined. Section 5 will review the development of tropospheric chemistry models, which first were designed solely for estimating ozone impact for cities. As experience and understanding was gained, it became clear that all secondary pollutants (e.g., ozone, sulfate, and nitrates) involved regional-scale formation and transport. Section 6 will attempt to summarize the issues (some resolved, many still pending) that are influencing current model development.

In developing this review, three issues seem to resurface more than once, and appear to deserve special comment, namely: 1) a trend to require a complete documentation of the assumptions made (transparency) and a formal exploration of the consequences of these assumptions in air quality assessments (U.S. Environmental Protection Agency, 1992¹ and 1998²); 2) a need for the use of standardized methods in development of emission inventories³; and 3) a need for development and use of science-based model performance standards⁴.

¹ <http://www.epa.gov/ncea/exposure.htm>

² <http://www.epa.gov/ncea/ecorsk.htm>

³ Emissions Inventory Improvement Program, (1997): EIPP Technical Report Series, Volumes I through X, available from: <http://www.epa.gov/ttn/chief/eiip/techreport/index.html>

⁴ ASTM International Standard Guide D6589 available from: <http://www.astm.org>

Moussiopoulos, N. and P. M. Turlou (2003) *Case Studies – Air Pollution Modeling at Local, Regional, Continental, and Global Scales*. Chapter 19 of *AIR QUALITY MODELING - Theories, Methodologies, Computational Techniques, and Available Databases and Software. Vol. I - Fundamentals* (P. Zannetti, Editor). Published by The EnviroComp Institute (<http://www.envirocomp.org/>) and the Air & Waste Management Association (<http://www.awma.org/>).

Note from the editor: We provide here a first, preliminary list of case studies. We encourage the readers to email new entries to the first author and the editor.

Chapter 19

Case Studies – Air Pollution Modeling at Local, Regional, Continental, and Global Scales

Nicolas Moussiopoulos⁽¹⁾ and Paraskevi-Maria Turlou⁽²⁾

⁽¹⁾ *Aristotle University Thessaloniki, Greece*
moussio@eng.auth.gr

⁽²⁾ *Aristotle University Thessaloniki, Greece*
evelina@aix.meng.auth.gr

Abstract: In this chapter various case studies are presented, which are relevant to air pollution modeling/simulation and pollution control/abatement issues. Several groups active in air pollution modeling (see also chapter 21) submitted pre-defined information on individual cases, thus providing insight to a variety of details with regard to the scientific objectives of the particular study. This includes information on the physico-chemical processes analyzed, the origin of the data used, the main results and their application potential, the collaborating groups/scientists and publications that have resulted from the study. The inclusion of several case studies had the purpose of presenting in detail the research areas and activities that were lately or are currently being elaborated by the scientific community, thus underlying various issues and outstanding problems of particular interest with regard to air pollution simulation and prevention. A thorough examination of these case studies allows for detecting those research fields that are still open for further elaboration and exploitation.

Keywords: air pollution, modeling / simulation, pollution control / abatement, ozone formation, urban plume, dispersion / transport / deposition of air pollutants, street canyon, air pollution episode, air quality forecasting.

➔ **For detailed information on case studies please examine the hyperlinks as indicated by arrows**

1 List of Case Studies

- **1998 ACP Field Campaign in Phoenix** →

Pacific Northwest National Laboratory →

Institution URL: <http://www.pnl.gov>

Provision of an improved description of the processes leading to ozone formation, transport, and removal. Determination of boundary layer processes in an arid metropolitan area and their effect on ozone.

- **Acidification of the Northern Hemisphere (1996)** →

EMEP MSC-East

Assessment of the scale of the acid pollution transport in the Northern Hemisphere and evaluation of the capabilities of different models to reproduce it. In particular, assessment of the impact of different vertical model structures to the final results.

- **Athens 2004 Air Quality Study** →

Laboratory of Heat Transfer and Environmental Engineering (LHTEE), Aristotle University Thessaloniki →

Case study URL: <http://www.envirocomp.org/html/publish/CDROM/Athens/flyer.pdf>

Institution URL: <http://www.auth.gr>

Analysis of the expected evolution of the air quality in Athens until the year 2004 (year of the XXVIII Olympic Games), in view of the ongoing public works and the major infrastructure changes in the specific area.

- **Atmospheric Cycling of Mercury and Persistent Organic Pollutants** →

Institute of Program Systems Russian Academy of Sciences →

Identification and assessment of the regional and global cycling of semi-volatile species like mercury and persistent organic pollutants.

- **Auto Oil II Programme, Generalized Empirical Approach** →

European Topic Centre on Air Quality

Case study URL: <http://www.etcaq.rivm.nl/news.htm>

Assessment of the fraction of the urban population that lives in European cities that are not in compliance with air quality objectives in future years and estimation of additional emission reductions needed to reach compliance.

- **BASYS (Baltic Sea System Study) Subproject 5 (Atmospheric Load)** ↪

Finnish Meteorological Institute, Air Quality Research ↪

Case study URL: <http://www.io-warnemunde.de/public/bio/basys/con3/con3.htm>
& <http://www.io-warnemuende.de/Projects/Basys/logistic/cruises.htm>

Institution URL: <http://www.fmi.fi/ENG>

Use of integrated measurement-model approach for producing an improved estimate of the fluxes of heavy metals and nitrogen to the Baltic Sea. Construction of a database of the modelled fluxes with high time- and space-resolution to be available for environmental researchers.

- **Bozen Air Quality Study (Determinazione dei parametric meteorologici necessari alla creazione di prognosi di inquinamento atmosferico nelle valli della Provincia Autonoma di Bolzano)** ↪

Fraunhofer-Institute for Environmental Atmospheric Research Garmisch-Partenkirchen ↪

Institution URL: <http://www.ifu.fhg.de/>

Analysis of the diurnal evolution of local winds, the boundary layer depth and the air quality in the valleys of the Province of Bozen (Italy) during smog episodes.

- **Calculation of the Frequency of Odor Perceptions in the Vicinity of the Piggery in Radefeld** ↪

Lohmeyer Consulting Engineers ↪

Case study URL: <http://www.lohmeyer.de/air-eia/casestudies/odeur/Beri-1417n.htm>

Institution URL: <http://www.Lohmeyer.de>

Analysis of dispersion of odors in a topographically structured region, accounting for valley drainage flows and flow influences by the topography.

- **Chemistry-Transport-Modeling for the Berlin Ozone Experiment**↪

EURAD, University of Cologne↪

Case study URL: <http://www.uni-koeln.de/math-nat-fak/geomet/eurad/index.html>

Numerical simulation of chemical and dynamical processes in the urban plume of Berlin during the BERLIOZ experiment. Comparison with measurement and evaluation of model results.

- **Climatological Study of the Air Pollution Potential in Buenos Aires, Argentina**↪

Department of Atmospheric Sciences, Faculty of Sciences, University of Buenos Aires↪

Analysis of the air pollution potential of Buenos Aires city atmosphere.

- **“Demokritos” Contribution to Study Air Pollution Modelling in a Street Canyon in Hannover, Germany**↪

Environmental Research Laboratory, National Centre for Scientific Research↪

Case study URL: <http://www.lohmeyer.de/modellvergleich/>

Institution URL: <http://milos.nrcps.ariadne-t.gr/>

Prediction of the air quality in a real-city street canyon under realistic situations, comparison with the results of other numerical urban air pollution models, physical modelling in the same geometry and field campaign measurements on-site.

- **Determination of Emission Rates from Diffuse Sources by Inverse Modelling**↪

Fraunhofer-Institute for Environmental Atmospheric Research Garmisch-Partenkirchen↪

Institution URL: <http://www.ifu.fhg.de/>

Development of a method, based on downwind path-integrated immission measurements and a subsequent inverse dispersion modelling, for the determination of emission rates from diffuse sources.

- **Diffusion-Deposition of Pollutants Released in the Atmospheric Boundary Layer**↪

Department of Atmospheric Sciences, Faculty of Sciences, University of Buenos Aires↪

Development, evaluation and application of an atmospheric dispersion model for releases in the atmospheric boundary layer, in different stability and roughness conditions.

- **Environmental Outlook 5. 1980-2030 Air Quality Study in the Netherlands**↪

Air Research Laboratory, National Institute for Public Health and the Environment↪

Institution URL: <http://www.rivm.nl>

Analysis of the trend in air quality and deposition in the Netherlands for the period 1980-2030.

- **Exposure to Arsenic and Cancer Risk**↪

T H Huxley School of Environment, Earth Sciences and Engineering↪

Assessment of exposure pathways for arsenic and associated risk of cancer in an East European population.

- **Global Tropospheric NO₂ Column Distributions**↪

Air Research Laboratory, National Institute of Public Health and the Environment↪

Institution URL: <http://www.rivm.nl/>

Comparison of tropospheric NO₂ columns derived from the GOME satellite instrument with model calculations from two global three-dimensional chemistry-transport models, to study the inversion techniques applied to retrieve tropospheric NO₂, our current understanding of the global sources and sinks of NO₂, and the role of NO₂ in radiative forcing.

- **Imperial College Integrated Assessment Unit**↪

T H Huxley School of Environment, Earth Sciences and Engineering↪

Development and application of methodologies for integrated assessment of costs and benefits of air pollution abatement strategies.

- **Intercomparison of Two New Generation Dispersion Models and a Wind Tunnel Study, for a Large New Cement Works in the UK** ↗

Environmental Resources Management (ERM)

Institution URL: <http://ww.erm.com>

Application of the UK ADMS and US AERMOD models for assessing the dispersion of emissions from a new cement works.

- **Intermittent Control System** ↗

EnviroComp-Air Pollution Modeling ↗

Institution URL: <http://www.envirocomp.com>

Design and implementation of a computerized system for the real-time forecasting of air pollution episodes in the city of Ilo, Peru, to allow emission control measures to be implemented.

- **Local Scale Dispersion Model Evaluation Exercise** ↗

Environmental Research Laboratory, Institute of Nuclear Technology & Radiation Protection, National Centre for Scientific Research ↗

Institution URL: <http://milos.nrcps.ariadne-t.gr/>

CFD modelling of complex effects in dense gas dispersion and validation of the ADREA-HF code against the EEC-55 field experiment, involving a two phase continuous propane jet release with and without obstruction.

- **LOOP** ↗

Laboratory of Atmospheric Chemistry (LAC) ↗

Institution URL: <http://www.psi.ch>

Investigation of the NO_x / VOC limitation of oxidant production in the Milan area for May 1998. Sensitivity to various meteorological conditions and emission levels.

- **Modeling Studies with MCCM on the Transport and Transformation of Atmospheric Trace Compounds in the Graz Area** ↗

Fraunhofer-Institute for Environmental Atmospheric Research (IFU) Garmisch - Partenkirchen ↗

Analysis of the regional- and local-scale transport and immission of SO₂, NO_x and ozone in the city of Graz and the Mur valley. Assessment of the role of local wind fields on the regional-scale pollutant distribution.

- **Modelling Activities related to BEMA (Biogenic Emissions in the Mediterranean Area)** ↗

Environmental Research Laboratory, Institute of Nuclear Technology & Radiation Protection, National Centre for Scientific Research ↗

Institution URL: <http://milos.nrcps.ariadne-t.gr/>

Study the impact of biogenic volatile organic compound emissions on ozone under specific meteorological conditions in a coastal area of eastern Spain.

- **Modelling Air Quality in Central London** ↗

Cambridge Environmental Research Consultants (CERC) ↗

Institution URL: <http://www.cerc.o.uk>

Development of an air quality model for Central London to help local government fulfil legal duties: defining air quality management areas. Assessment of current air quality and prediction of future air quality for comparison with UK and EU air quality objectives, in particular the geographical areas of exceedence.

- **Modelling Exposure to Particulate Air Pollution** ↗

T H Huxley School of Environment, Earth Sciences and Engineering ↗

Measurement of road user personal exposure to PM_{2.5} in London and assessment of the capability of ADMS-Urban to model this. Comparison of road user exposure with measurements and modelling of total exposure from the EU EXPOLIS programme.

- **Neural-Network Based SO₂ Air Pollution Forecasting Model for the Sostanj (Slovenia) Thermal Power Plant** ↗

AMES (Automatic Measuring Systems for the Environment) ↗

Institution URL: <http://amesnt.ijs.si/>

Development of an efficient forecasting model for the seriously polluted sites around TPP, where automatic measuring stations are located. Study advanced methods of construction neural network based models.

- **Ozone Episodes in the Greater Surroundings of Vienna in Summer 1995 - Significance of the Meteorological Input**↪

ZAMG - Central Institute for Meteorology and Geodynamics

Institution URL: <http://www.zamg.ac.at>

Simulation of ozone episodes in the greater surroundings of Vienna with the urban ozone airshed model CALGRID linked to a diagnostic windfield model and a new pre-processor based on on-line data from the semi-automatic network of ZAMG (TAWES).

- **Perimeter Road for Glennstadt, Germany: Air Quality Effects**↪

Lohmeyer Consulting Engineers↪

Case study URL: <http://www.lohmeyer.de/air-eia/casestudies/mlus/mlusberi.htm>

Institution URL: <http://www.Lohmeyer.de>

Study the influence of the perimeter road planned for the village Glennstadt on air quality.

- **Phoenix Air Flow Experiments**↪

Arizona State University

Study the flow and dispersion in complex terrain using the Phoenix metropolitan region as a test basin. The project activities were centered on two field experiments, known as Phoenix Air Flow Experiments conducted during the winter and summer of 1998.

- **Photochemical Modeling for the Determination of the Critical Loads**↪

Dept. of Chemical Engineering, University of Santiago de Compostela↪

Institution URL: <http://www.usc.es/enxqu>

Evaluation of past, current and future acid deposition over EMEP 17,6 cell, from 1990 to 2000 and forehead in order to estimate the effectiveness of the acid gases

emission reductions applied or previewed over that cell, in relationship with the critical loads map.

- **PM10 and PM2.5 Concentration Levels in Switzerland** →

INFRAS, METEOTEST, Fed. Office of the Environment, Forests and Landscape →

Case study URL: <http://www.infras.ch> & <http://www.meteotest.ch>

Modelisation of actual and forecast concentration levels for PM10 and PM2.5 in Switzerland.

- **POLLUMET** →

Laboratory of Atmospheric Chemistry (LAC) Paul Scherrer Institute (PSI) →

Institution URL: <http://www.psi.ch>

Simulation of the Swiss air quality for summer and winter smog conditions. Investigation of the NO_x / VOC limitation. Assessment of environmental impacts for various energy / emission scenarios.

- **Quantification of Alkaline and Acidifying Deposition Loads from Estonian Industry** →

Group of Dynamic Meteorology, Tartu Observatory (TO) →

Institution URL: <http://apollo.aai.ee>

Quantitative analysis of regional and transboundary air pollution transport and deposition from large thermal power plants in the northeast of Estonia. Model validation and understanding of physical processes behind the deposition patterns.

- **Street Canyon Geometry and Roof Shape Effects on Urban Air Quality** →

Environmental Research Laboratory, National Centre for Scientific Research →

Institution URL: <http://milos.nrcps.ariadne-t.gr/>

Modelling of the flow and pollutant dispersion in two-dimensional urban domains of identical-geometry street canyons parallel with each other.

- **Street Canyons and Street Canyon Intersections**↪

T H Huxley School of Environment, Earth Sciences and Engineering↪

Analysis of the flow and dispersion at the intersection between two city street canyons i.e. in the space between four cuboid-shaped buildings and other common elements of the urban environment.

- **Study of Air Pollution and Microscale Climate for a Region for Different Designs of the Planning of the Stuttgart Main Railway Station**↪

Lohmeyer Consulting Engineers↪

Case study URL: http://www.stadtklima.de/stuttgart/websk21/Heft8/index_h8.htm

Institution URL: <http://www.Lohmeyer.de>

Analysis of the influence on the air quality and climate in that part of Stuttgart where it is planned to put the main railway station under the ground and to construct a densely built up city quarter above it.

- **Traffic induced Air Pollution Related to the Planning of the Stuttgart Main Railway Station**↪

Lohmeyer Consulting Engineers↪

Case study URL http://www.stadtklima.de/stuttgart/websk21/Heft8/index_h8.htm

Institution URL: <http://www.Lohmeyer.de>

Analysis of the influence on the air quality in the whole city and in that part of Stuttgart where it is planned to put the main railway station under the ground and to construct a densely built up city quarter above it.

- **Urban Aerosol Microphysics Modelling**↪

T H Huxley School of Environment, Earth Sciences and Engineering↪

Development of techniques for modelling the microphysical evolution and dispersion of an urban aerosol.

- **Vertical Transports of Ozone in the Alps**↪

Fraunhofer-Institute for Environmental Atmospheric Research, Garmisch-Partenkirchen↪

Institution URL: <http://www.ifu.fhg.de/>

Analysis of synoptic-scale, regional-scale, and local-scale transport of ozone towards the Alps and in the Alps. Assessment of the role of the Alps in a regional-scale ozone budget.

2 Additional Information on Case Studies Relevant to Air Pollution Modeling/Simulation

- **MCNC**
<http://www.iceis.mcnc.org/projects/index.html>
- **Ozone Transport Assessment Group (OTAG)**
<http://capita.wustl.edu/OTAG>
- **Air Resources Laboratory (ARL)**
<http://www.arl.noaa.gov/research/programs/aqm.html>
- **Chesapeake Bay Program**
<http://www.chesapeakebay.net/pubs/subcommittee/air/min-08-24-00.pdf>
- **Gulf Coast Ozone Study**
<http://gcos.saintl.com>
- **UAM-ICF Consulting**
<http://www.icfconsulting.com>
- **California Air Resources Board Information**
<http://www.arb.ca.gov/html/soft.htm>
- **The Models Inventory**
http://www.mi.uni-hamburg.de/technische_meteorologie/cost/cost_615/models_inventory/index.html

BRANK
P
2000

Oettl, D. and R. San Jose (2003) The Future of Air Pollution Modeling. Chapter 20 of AIR QUALITY MODELING - Theories, Methodologies, Computational Techniques, and Available Databases and Software. Vol. I - Fundamentals (P. Zannetti, Editor). Published by The EnviroComp Institute (www.envirocomp.org) and the Air & Waste Management Association (www.awma.org).

Chapter 20

The Future of Air Pollution Modeling

Dietmar Oettl ⁽¹⁾ and Roberto San Jose ⁽²⁾

⁽¹⁾ *Institute for Internal Combustion Engines and Thermodynamics, Graz University of Technology, Inffeldgasse 25, 8010 Graz, Austria*
oettl@vkmb.tu-graz.ac.at

⁽²⁾ *Computer Science School - Technical University of Madrid, Campus de Montegancedo - Boadilla del Monte-28660, Madrid, Spain*
roberto@fi.upm.es

Abstract: In the following chapter a discussion is presented about some future trends and developments regarding air pollution modeling. The main emphasis of the chapter deals with the progress of Internet technologies for future air pollution modeling systems. Comprehensive modeling systems are also discussed and the basic needs and structures explained. Some future activities regarding advanced remote sensing techniques from space are also examined, together with future research needs in air pollution modeling. Model evaluation issues – an area of major concern - are also discussed.

Keywords: air pollution modeling, Internet, future modeling.

1 Processor Technology and Air Pollution Modeling

The modeling of air pollution is strongly connected with computer technology. Hence, it is reasonable to start this chapter with a brief overview about what might be expected in the near future – let's say by the year 2010 – regarding advances in computer technology. Clearly, the great strides in the area of computer technology have pushed and enabled the usage of complex dispersion models. Today the progress in pre- and post-processing techniques is probably stronger than that in the development of new models (from the physical point of view) or new theories regarding atmospheric turbulence, where many phenomena have been well described for decades. Russell and Dennis (2000) hypothesize that

the future advances in our understanding of photochemical pollutant dynamics at the regional scale will more likely come from improvements of the modeling process than from improvements in model physics and numerics. The main objectives of this chapter are to provide the reader with a preliminary understanding of Geographical Information Systems (GIS), Remote Sensing techniques, the Internet, and other computer technology issues related to air pollution modeling.

While at the beginning of the 1990s, a shift from using supercomputers and mainframe computers to Unix workstations in the scientific community could be recognized (Zannetti, 1996), and by the end of the 1990s another shift became evident - from workstations to personal computers for many tasks regarding air pollution modeling. This trend toward PCs was caused by their fast processors, the availability of inexpensive software, and their user-friendliness. In addition, PC's provided the possibility not just to perform the simulations, but also to visualize the results with powerful GIS software on the same platform, and to include figures and tables produced by such software in reports, which in turn are highly compatible and therefore, can be easily distributed electronically via e-mail or the Internet.

The enormous development of semiconductor electronics may be understood by the fact, that today there is more processing power in cars than it was in the 1969 Lunar Module, or by the fact, that in 1980 there was not a single personal computer in the world. Coming back to air pollution modeling, we ask: What implication will the improvements in microprocessor technology have in that particular working area? To be able to draw a realistic picture of the future, it is very helpful first to look back into history.

As soon as six years after the invention of the planar transistor in 1959 by Jean Hoerni, Gordon Moore made an interesting observation: The complexity for minimum component costs had increased at a rate of roughly a factor of two per year. Although this observation was only supported by three data points, it has held true ever since and became known as Moore's law. It can also be presented in the mathematical form:

$$(\text{Circuits per chip}) = 2^{(\text{year} - 1975)/1.5} \quad (1)$$

A graphical representation of Moore's law is given in Figure. 1. Industrial experts believe that the exponential growth of computer power will hold at least until the year 2017. This would mean that the number of transistors in a micro-processor would be increased by a factor of 20 in the year 2010 compared to the year 2000.

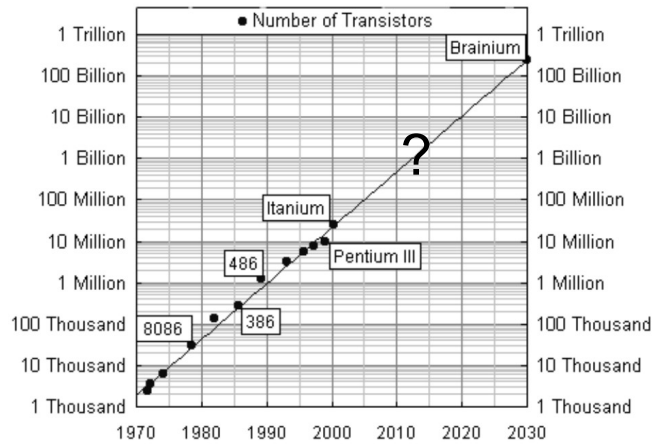


Figure 1. Graphical presentation of Moore's Law.
<http://www.chartoftheday.com/20000719b.htm>

Especially for engineering applications, it is important to assess which types of numerical models can be applied for particular technical problems in the future. As soon as one is capable to use an advanced model for a certain task, the usage may still be hindered by the input requirements of that model, which are not always available or adequate. For instance, it may not be difficult to run mesoscale- γ models on a conventional PC to predict annual mean values for an urban environment in the near future. But will the various input parameters be available to set up the boundary conditions in a reasonable manner? If not, the complex model could even give worse results than those obtained with a simpler model, as pointed out by Hanna (1989). Hence, the usage of complex models depends not only upon the computer power but also on the data quality of meteorological and air quality instrumentations.

In the following discussion, we anticipate the progress regarding the applicability of existing air quality models to technical problems. For that purpose, two different applications were defined and modelers were asked to give an estimate about the CPU requirements of their models when solving those applications. After taking an average over certain groups of models, the present stage of CPU time is obtained from which the future stage can be estimated trusting in Moore's law.

Two factors determine mainly the computational time needed for a certain task: (i) The spatial extensions of the domain of interest (i.e. local-, regional-, or global-scale), and (ii) the number of cases to be considered. Clearly, other parameters do also affect the CPU-time depending on the type of model used. For a Gaussian dispersion model, the number of receptor points and sources is also a key factor, while for Lagrangian models the number of particles, which are traced, and the temporal scale is of importance regarding the computational time. The spatial resolution of models is determined by the considered task and does, of course, also influence the CPU-time of all models, except for Lagrangian models.

For the latter models, the horizontal resolution is only limited by the number of particles released to get statistically stable results. In other words, the higher the number of particles, the higher the possible resolution. Hence, there are several ways for each type of model to eat up the increasing computer power.

The most widespread application of numerical models for a certain task is weather forecasting. A discussion of possible future trends in that area was presented by Schär (2001). Here, the rapid progress in semiconductor technology will lead to a better (mostly horizontal) resolution of the models. This can be seen nicely from the development of the ECMWF (European Center for Medium Weather Forecast) deterministic forecast model's resolution between the years 1979 – 2001. The corresponding grid spacing had been reduced from 200 km to 26 km, a refinement by almost a factor of 8 (Schär, 2001). Following basic numerical scaling considerations, the number of grid points of a three-dimensional model should increase with $P^{3/4}$, where P denotes the computing power (measured in floating point operations per second), while the grid spacing should decrease with $P^{-1/4}$. Assuming that Moore's law will be valid in the future, the resolution of the ECMWF model should be approximately 12 km by the year 2010. The horizontal spacing may even be lower on cost of the vertical grid sizes (Figure 2).

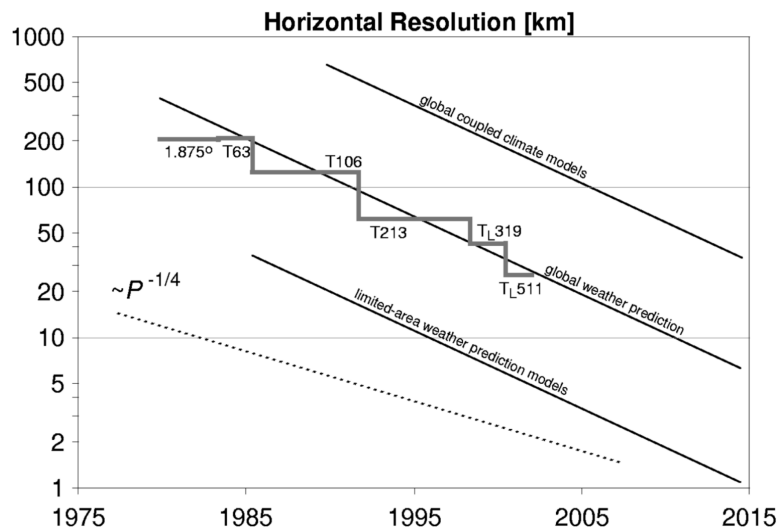


Figure 2. Approximate equivalent horizontal resolution of the ECMWF deterministic forecasting model 1979-2001 (bold line). The thin lines are trend estimates of the expected development, appropriate for global coupled climate models, global weather prediction models, and limited-area weather prediction models, respectively. The dashed line provides an estimate of the development based on simple numerical scaling arguments and the observed increase in computational power P (an increase by a factor 104 in 30 years). Note, how the ECMWF model developed at a faster pace than anticipated from such considerations. (Reprinted with permission from C. Schär, ETH-Zurich, Switzerland).

When a study aims at the computation, for example, of annual mean concentrations, then the number of calculations can be reduced by applying

meteorological statistics based on wind speed, wind direction and some kind of stability class (e.g., Pasquill-Gifford-Turner). This procedure may be well suited for constant emitting sources, but it is not clear if it yields good results for time-dependent emissions too (e.g. road traffic). At this stage, it would be good to know, for instance, when it might be possible to calculate a whole time-series of at least one year with a certain kind of air quality model. For such purposes, the average CPU-requirements of different model groups for two distinct applications are given in Table 1, based on the computing power, as it was available in the year 2000.

Table 1. Approximate CPU requirements of different types of models for two distinct cases based on processor technology (PC) of the year 2000.

Scale	Resolution in space	Time range	Chemical transformations	Model type	Comp. Time
Local (here: 1x1x0.3 km)	10x10x1 ¹ m ³	1 hour, stationary wind field	No	Gaussian	<2 min.
				Lagrangian	2-30 min.
				RANS ²	3-9 h
Regional (here: 250x250x10 km)	1000x1000x20 ¹ m ³	1 day, non-stationary wind field	Yes, for O ₃ forecasts	Lagrangian ³	30-60 min.
				RANS	12-36 h

By far, the fastest models are Gaussian models at the local scale (Note that Gaussian models are not applied at the regional scale), making them the most wide spread models in that field. It will also be possible with Lagrangian models to calculate a time-series of one year by 2010 on a PC, while the calculation of a high-resolution wind field with RANS models will not be possible in the future. Hence, the usage of meteorological statistics will still be necessary, if an annual mean concentration has to be calculated, for example in urban area or very complex terrain, where the wind fields are not horizontally homogenous.

On the regional scale, the computation of a time-series of one year will also only be accomplished with Lagrangian dispersion models. It has to be mentioned that current Lagrangian models are not designed to account for complex chemical reactions of various species, which are necessary for example to forecast O₃ concentrations. RANS models require again very much CPU time and will not be applicable for the calculation of a time-series of one year by 2010. What can be

¹ The vertical spacing may be stretched with increasing height.

² Reynolds averaged Navier-Stokes equations.

³ No chemical transformations included.

done to overcome that problem at the regional scale is that computed time-series of wind fields with RANS models such as MM5 are provided for certain areas, pre-calculated on supercomputers. Those wind fields are then input to dispersion models requiring much less CPU time (e.g. Morris et al. 2001).

Dabbert and Miller (2000) anticipate the following air quality issues to be high-priority in the near-to-intermediate future: (1) routine operational forecasting of adverse air quality episodes; (2) real-time high-level support to emergency response activities; and (3) quantification of model uncertainty. Issue (1) requires a CPU time for the computation of a 24-hour forecast less than about 6 hours – a task that can be accomplished by the years 2005-2007 (for coarser grids as in Table 1 it should be already possible). The second issue however demands for a computational time of the order of minutes. Apart from Gaussian models, Lagrangian dispersion models will be applicable in that field soon, while it will take at least 10-15 years until RANS-type models will be used for emergency response activities. The last topic concerns model uncertainty. Dabbert and Miller (2000) used ensemble modeling to assess probabilistic concentrations. This resulted in 162 air quality simulations, where uncertainties both in measured variables (wind speed, wind direction, stability, plume rise, source strength, and mixing height) and model parameterizations were reflected. Besides the huge number of simulations needed to assess uncertainties anyway, the usage of such an approach with more complex models is almost impossible, because the more complex a model gets, the more model parameterizations and model input data need to vary, resulting in even a higher numbers of simulations necessary to obtain a probabilistic distribution of concentration. Hence, ensemble modeling will only be possible with Gaussian and Lagrangian models in the near future.

2 Comprehensive Modeling Systems (CMS)

For many air pollution problems it is highly desirable to cover many different temporal and spatial scales with one single model to account properly for physical and chemical interactions. For instance, the dispersion and transformation of chemical species like NO (and NO₂) emitted from a motorway in a valley may be influenced by different local winds covering different scales, e.g. slope winds, gravity waves, or valley winds, while the chemical transformation of primary emitted NO into NO₂ takes place at a different scale, which needs to be accounted for in the simulations. Such considerations led to the development of Comprehensive Modeling Systems (CMS), which aim at the simulation of various scales, from the local to the global scale. A CMS consists of many different GIS-based (Geographic Information System) models and pre-/post-processing tools, such as:

- Terrain- and land use pre-processors
- Meteorological pre-processors
- Emission models
- Traffic flow models

- Meteorological models
- Dispersion models
- Chemistry transport models
- Model interfaces
- GIS based visualization and data analysis software
- Exposure models

As to the CPU-times needed by a CMS: In 1996 Dennis et al. (1996) estimated an increase of a factor of 1000 to possibly 100,000 of computer processing capabilities will be necessary to run future CMS. As can be seen from Figure 1, this will not be accomplished by the conventional advances in computer technology, and therefore new approaches, such as the use of scalable or massively parallel computers operating in concert with conventional computers in heterogeneous systems, are necessary (e.g. Hillis and Boghosian, 1993).

Besides its huge computational demands, a CMS, also requires a good user-knowledge in different fields, such as meteorology, climatology, numerics, engineering, computer technology. To keep a CMS also accessible to the non-scientific community, it is imperative to design it as user-friendly as possible. A CMS can be defined as a problem-solving environment (PSE), which allows for a simpler and faster way to handle complex air pollution problems at different scales and for various pollutant sources. It should be mentioned that PSEs are not only used for air quality issues but are also utilized for other engineering purposes, such as car manufacturing. A definition of a PSE can be as follows (Houstis and Rice, 2000): “A PSE is a computer system that provides all the computational facilities necessary to solve a target class of problems.” These facilities include advanced solution methods, automatic or semiautomatic selection of solution methods and ways to easily incorporate novel solution methods. Furthermore, PSEs allow users to solve problems without specialized knowledge of the underlying computer hardware or software.

In the future, a CMS will take full advantage of the Internet in contacting suitable hosts to retrieve terrain or land use data, or to get an up-to-date initialization of the meteorological model by on-line observations or the output of a larger scale model run by the various weather services (client-server technology). Given a particular problem, a CMS will suggest, which type of models and input parameters will be the best choice. The advantage will be a decrease of errors from to the wrong usage of the various tools (especially by non-scientific personnel). Besides, there are several other advantages and some disadvantages of a strong coupling of the various tools in a CMS, compared to a system where those tools are not (or only loosely) coupled (Table 2).

Table 2. Advantages and disadvantages of non- and tight-coupling of air quality modeling tools according to Brandmeyer and Karimi (2000).

	Advantages	Disadvantages
Non-coupling	Programming changes to the models unnecessary. Source code not required; suitable for proprietary models. Faster implementation with lower initial costs. Suitable for converting data between model versions.	Data conversion required between spatial and temporal scales, data file formats. Manual data editing. Quality assurance required for data conversions. New conversion procedures required when update model or system. User responsible for documenting all data transfer and conversion steps. Increased modeler, simulation time.
Tight-coupling	Supports community model development. Supports both legacy and new models. Supports version control for data and code. Supports distributed computing. Supports automated data backup. Supports DBMS with data dictionary.	Higher initial cost due to framework design and development. Relies on network and server speed. Model applications and user needs must be anticipated. Requirement for rich data language.

Figures 3 and 4 show several schemes for off-line and on-line air quality modeling systems, respectively, commonly used at the present time. (Off-line models refer to those in which the meteorological module runs independently from the air quality transport and transformation module. On-line mode refers to those models, where meteorology and air quality transport and transformation are coupled and run in a coupled and dependent way). Table 3 shows some aspects related to dynamical consistency, process interactions, system and application characteristics of both methods (Byun and Ching, 1999). The next generation of air quality modeling systems should include a complete development of the fully coupled chemistry-transport model to a meteorological model. This concept requires a fundamental rethinking of the atmospheric modeling approach in general. Some of the suggested requirements for the next generation of mesoscale meteorological model can be used as a host of the on-line/off-line modeling paradigms such as:

- Scaleable dynamics and thermodynamics: use fully compressible form of governing set equations and a flexible coordinate system that can deal with multi-scale dynamics.
- Unified governing set of equations: not only the weather forecasting, dynamics and thermodynamics research but also the air quality studies should rely on the same general governing set of equations describing the atmosphere.
- Cell-based mass conservation: as opposed to the simple conservation of domain total mass, cell-based conservation of the scalar (conserving) quantities is needed. The use of density and entropy, as proper state variables instead of pressure and temperature, is also needed. It is also recommended to represent the governing equations in the conservation form instead of the advective form.
- State-of-the-art data assimilation method: new satellite and remote sensing data should be included in the data set to be used by the assimilation adjoint model together with the already used surface measurements from air quality and meteorological networks and upper air soundings.
- Multi-scale physics descriptions: improvement on the parameterization schemes focusing on a more general approach is needed, since certain parameterizations of physical processes, including clouds, used in the present weather forecasting models are scale dependent.

Figure 5 shows the expected future air quality modeling systems, which will integrate most of the actual recommendations from experts in that field. An important element is the unified governing set of equations plus consistency with the numerics. Another essential element is to build flexible and user friendly API's (Application Program Interfaces) to analyze the complexity of the results and to integrate different algorithms in the code without re-coding the central module of the subroutines. The unified governing set of equations - represented by a consistent set of modules simulating meteorology, emission processes and chemical transformations – plus consistent numerics (which is easily obtained by integrating the meteorological equations and chemical transformations) and the possibility to incorporate real-time I/O API feedback (on-line future air quality models concept) present the framework of the goals in operational and scientific air quality modeling. The progress on developing the next generation of weather forecasting models such as the Weather Research & Forecasting System (Dudhia et al., 1998) is expected to meet most of the above requirements. Figure 6 shows the expected time schedule for developing the next generation of meteorological modeling systems.

Table 3. Some aspects of modeling paradigms when building the systems as on-line/off-line approaches

	Off-line modeling	On-line modeling
Dynamic Consistency	<ul style="list-style-type: none"> • Need sophisticated interface processors • Need careful treatment of meteorology data in AQM 	<ul style="list-style-type: none"> • Easier to accomplish but must have proper governing equations. • Meteorology data available as computed
Process Interactions	<ul style="list-style-type: none"> • No two-way interactions between meteorology and air quality 	<ul style="list-style-type: none"> • Two-way interaction • Small error in meteorological data will cause large problem in air quality simulation (positive feedback problem)
System Characteristics	<ul style="list-style-type: none"> • Systems maintained at different institutions • Modular at system level. Different algorithms can be mixed and tested. • Large and diverse user base • Community involvement 	<ul style="list-style-type: none"> • Proprietary ownership • Expensive in terms of computer resource need (memory and CPU). • Unnecessary repeat of computations for control strategy study • Low flexibility • Limited user base • Legacy complex code, which hinders new developments
Application Characteristics	<ul style="list-style-type: none"> • Easy to test new science concept. • Efficient for emission control study • Good for independent air quality process study 	<ul style="list-style-type: none"> • Difficult to insolate individual effects • Excellent for studying feedback of meteorology and air quality.

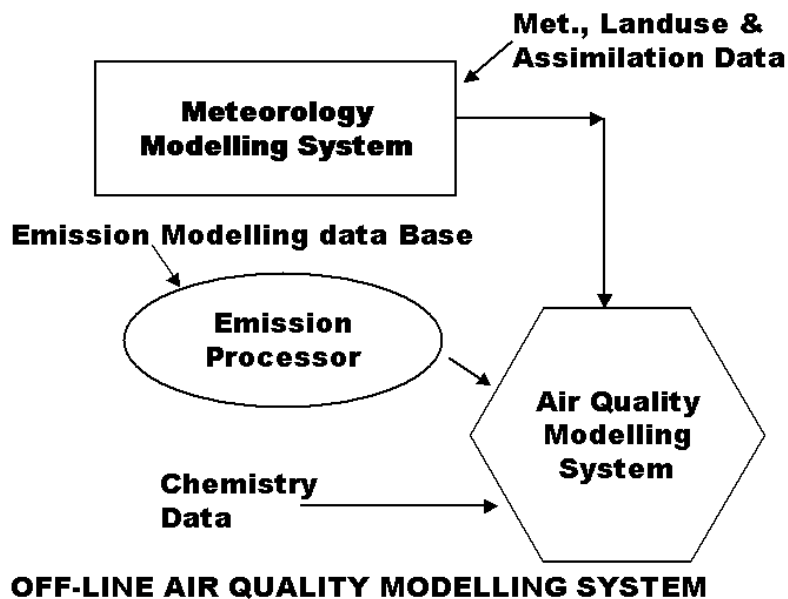


Figure 3. Schematic representation of the Off-line Air Quality Modeling System.

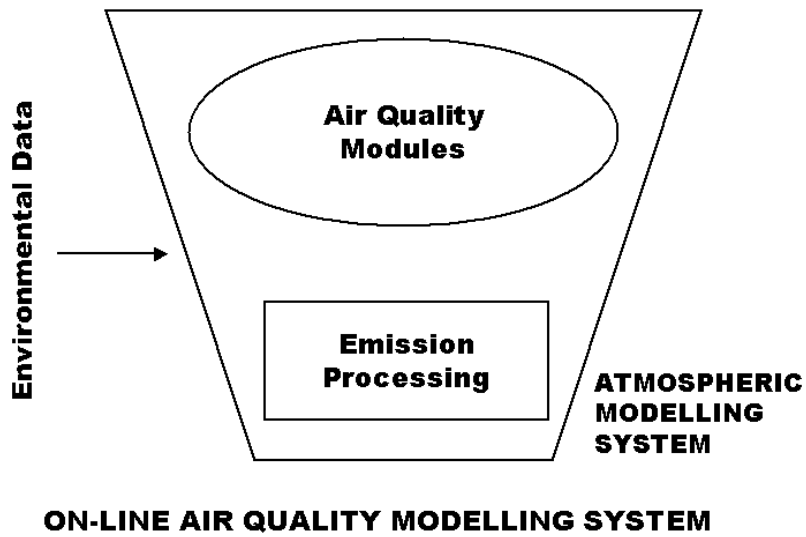


Figure 4. Schematic representation of the On-line Air Quality Modeling System.

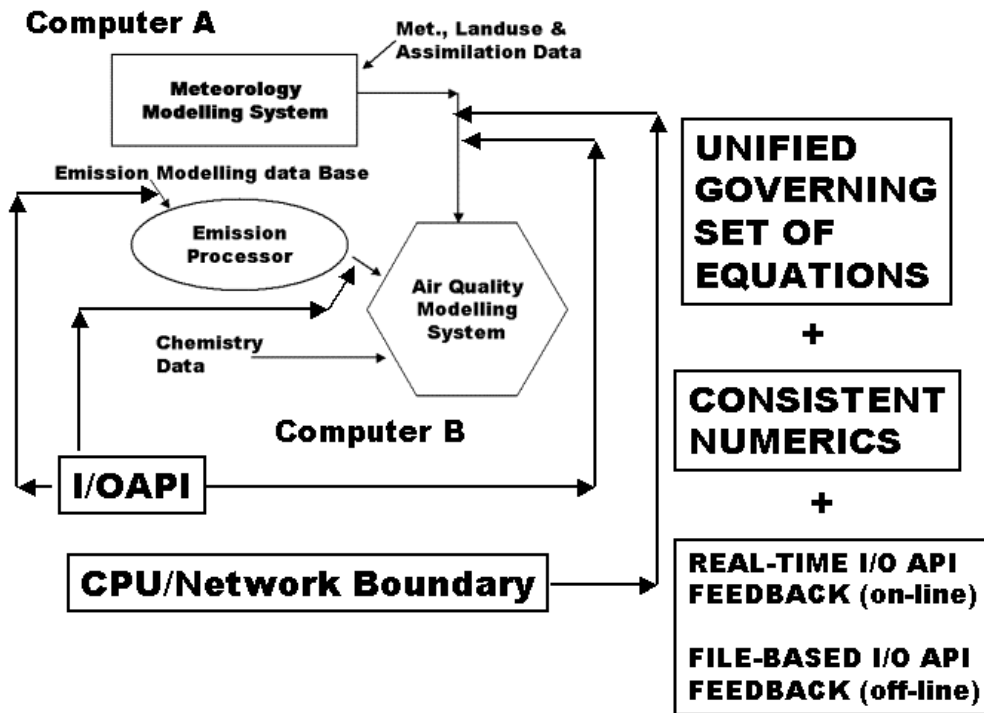


Figure 5. Future Air Quality Modeling System Architecture.

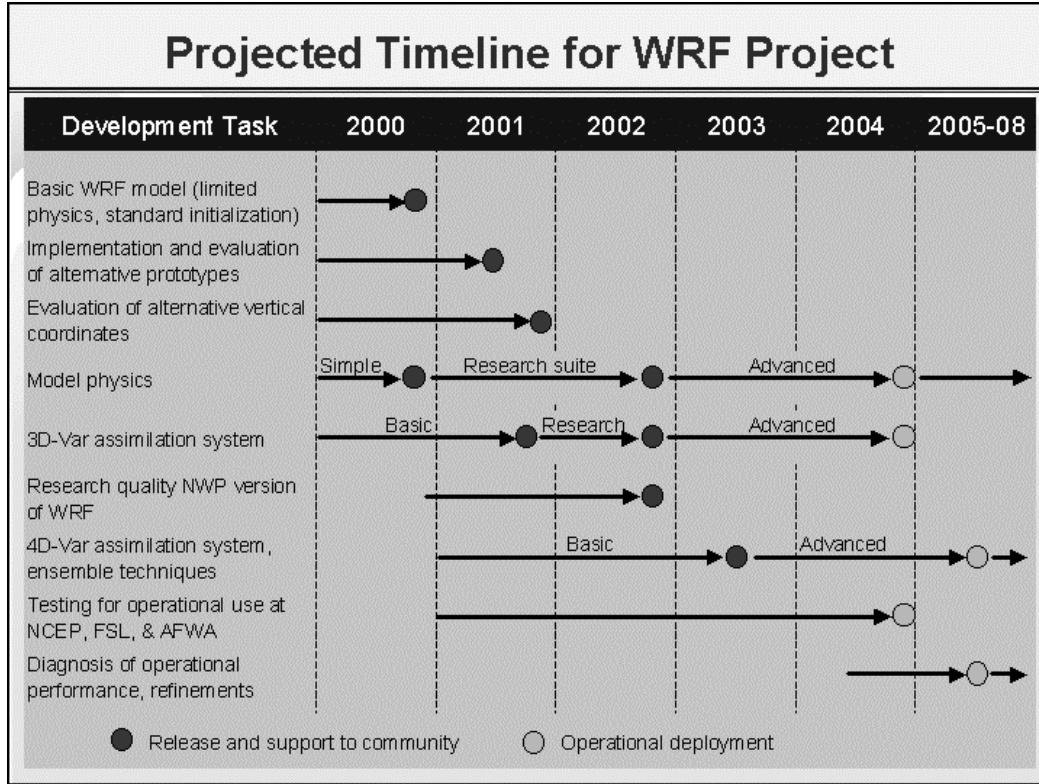


Figure 6. WRF project time schedule and principal work packages.⁴

The Weather Research and Forecasting Model is set up as the next generation of meteorological forecasting models developed in a fully modular way. The operational use of the model is expected to start in 2002 at different laboratories (NCEP, FSL & AFWA).

The next step forward will be multimedia modeling, because many complex environmental problems involve processes that occur both within and between environmental media (e.g. air, surface water, groundwater, soil, and biota). Brandmeyer and Karimi (2000) identified four multimedia modeling requirements:

(i) Locking of Data Files

The data management subsystem (DMS) manages the level of access available to each process. Typically, two different kinds of data locking are utilized: file locking or record locking. Access levels could be exclusive, share, and no lock. For a specific datum, only one process may have an exclusive lock, while

⁴ http://wrf-model.org/PRESENTATIONS/2001_02_NCEP_Presentations/intro/Slide2.GIF

processes that either update a datum or need to have the most current copy specify share lock access. No lock access permits processes to read a datum without waiting for another process to finish.

Locking of environmental data files, which may consume hundreds of megabytes of storage, need to be handled at the data element/geographic level (defined as spatial locking). Spatial locking permits more than one process to update a data element, provided that each process is updating a different geographic area.

Another important feature will be referential integrity, because a data element may be composed of multiple pieces of information residing in more than one file. Referential integrity ensures that each datum is associated with a valid identifier, and transaction processing assures that, if a datum is deleted, either all of its associated data are deleted or the delete process is reversed if a portion of the delete process fails.

(ii) Metadata (i.e. data describing data)

Metadata is usually provided as a text file describing the content of a data file. In the Models-3 framework, a user can register data files and their associated metadata for access through the DMS (Novak and Leduc, 1999).

Metadata will also be important for components in a code library. Here, the history of a component may be supplied by the metadata. Further, it will be very useful to automatically generate metadata within the CMS for documentation purposes of a simulation process, which supports also quality assurance activities.

(iii) Simulation Verification

Several levels of simulation verification exist, depending on the complexity of the modeling task. The simulation verification is performed within the so-called model builder subsystem (MBS). In a framework without dynamic feedback, it is sufficient to check if all necessary tools were selected by the user to run a simulation. When dynamic feedback exists, the MBS has to verify that the selected model components are logically consistent. This will be enabled by the metadata in the code library, where all information about each tool is stored (e.g., tool type, required and optional data and parameters, output information, pre- and post-conditions, required machine configuration). For multimedia simulations, differences in spatial and temporal resolution have to be examined by the MBS. If so, appropriate interpolation or aggregation procedures must be selected.

(iv) Simulation Auto-Recovery

For computations distributed over a network of computers, the model execution subsystem (MES) has to assure that, if one computer becomes unavailable, either an image of the simulation is saved immediately for restart or the computation is

shifted automatically to another computer. Such processes are imperative for multimedia simulations, because of the long computer times required.

Multimedia models can be seen as the fourth generation of air quality models, which extend linkages and process feedback to include air, water, land, and biota to simulate the transport and fate of chemical and nutrients throughout an ecosystem. One may not expect such models to come up before 2003-2005, because of their enormous complexity.

2.1 GIS in CMS

Many scientific tools for environmental models can explicitly represent spatial variables in one, two or three dimensions, usually with dynamic, time-varying simulations. Geographic information systems (GIS), on the other hand, are designed to efficiently capture, store, update, manipulate, analyze, and display all forms of geographically referenced information. Thus, the integration of GIS and environmental models is an obvious approach.

While a GIS is a type of database application, all data in a GIS are linked to a spatial reference on the surface of the earth. The ability to integrate information and support decision-making is the true power of a GIS. Common capabilities of a GIS include⁵ cartography, spatial statistics, and data integration by means of “layers” laid one on top of the other.

Figure 7 shows an example of the integration of GIS in a modeling system to predict air pollution from urban traffic for the city of Florence (Italy) according to Gualtieri and Tartaglia (1998). The example displays a three-level structure, including the whole database, various mathematical models, and the results in terms of thematic mappings. The GIS model section consists of three different sub-models (traffic, emission, and dispersion) aimed at simulating each sub-process required for the simulation. The database within the GIS was designed according to the following attributes:

- Topographic: nodes, UTM co-ordinates, street axis direction, total length.
- Toponomastic: street names, physical attributes (driving directions, number of lanes)
- Morphological: street canyons, inter-section links, open areas.
- Transport: road typology by means of flow-speed curves.
- Geometrical: canyon width, building mean height.

⁵ See: <http://home.earthlink.net/~rpmfonet/whatsgis.html>

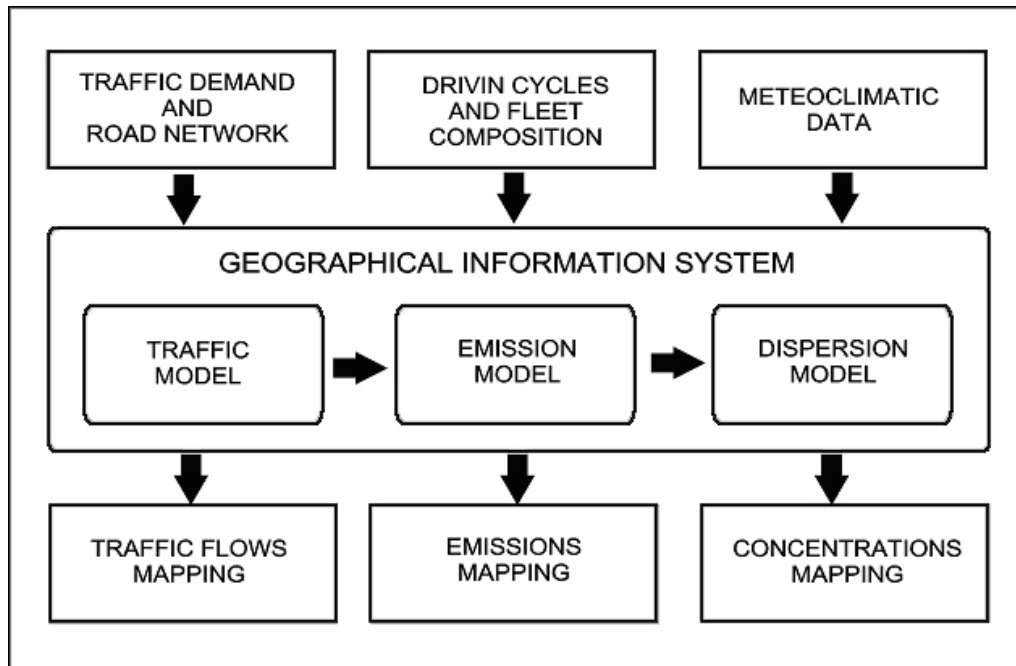


Figure 7. GIS structure for a modeling system to predict air pollution from road traffic (Gualtieri and Tartaglia, 1998).

Traffic demand characteristics were expressed in terms of the origin-destination matrix of road vehicles, requiring a definition of a proper zoning of the entire urban context, and an investigation of the corresponding traffic demand. Subsequent to the provision of the traffic demand data, the traffic behavior within each link of the network can be reproduced. The traffic model then assigns a certain traffic flow over each link and, by means of flow-speed curves, it is possible to calculate pollutant emissions over the entire road network. These emissions are a critical input for the dispersion model.

Another section of the GIS database was designed to manage meteorological variables, which are needed as input to the emission and dispersion model. The variables needed for the dispersion model are: wind speed and direction, solar radiation, air temperature, and atmospheric stability class. Meteorological parameters were arranged in arrays that represent typical meteorological scenarios, which can be defined by the user.

Finally, an integration of population maps makes it possible to access other key parameters, such as population exposure levels, which are very important for health-related studies and other investigations. Other examples of GIS-based urban air quality modeling systems are described by Reynolds and Broderick (1999), for Dublin (Ireland), and Karppinen et al. (2000) for Helsinki (Finland).

2.2 Examples of CMS

2.2.1 The EUMAC Zooming Model (EZM)

The EUMAC (European Modeling of Atmospheric Constituents) Zooming Model (EZM) is a CMS to simulate wind flows, pollutant transport and transformation in the atmosphere in the sub-regions of the EUMAC domain. It has been developed very early in the beginning of the 1990s and is the most widely tested and verified European air pollution model at urban scale and hence, especially suited for urban air quality studies. Areas where the modeling system was tested successfully were the Greater Athens area, Barcelona, Lisbon, Bulgaria, Greece, Thessaloniki, Graz, Basel, Upper Rhine valley region, Madrid, Norway, and others (Moussiopoulos, 1994).

Initially the modeling system was designed to be used in conjunction with the EURAD model, but is now a stand-alone tool. An overview of the EUMAC Zooming Model is given in Figure 8.

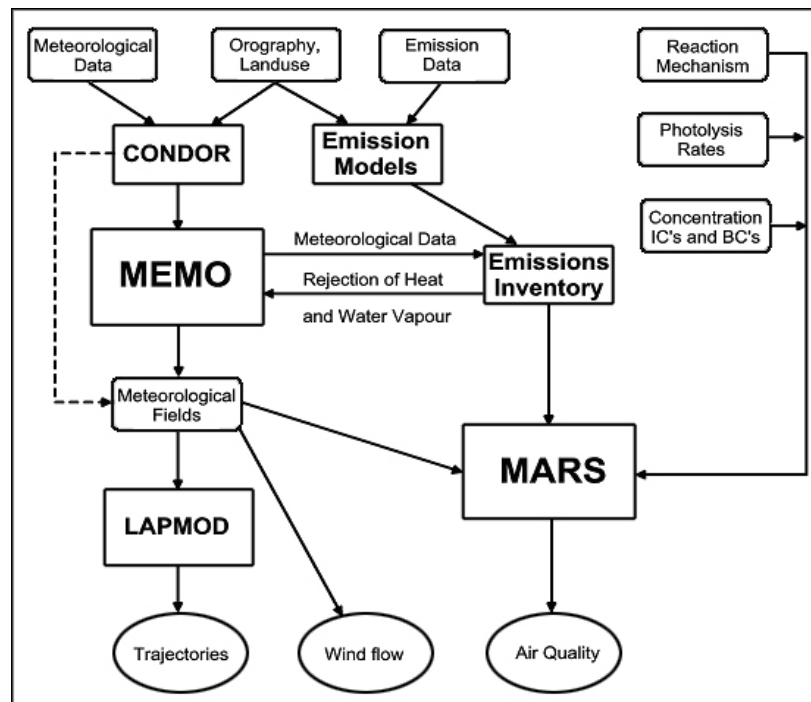


Figure 8. The structure of the EUMAC Zooming Model (EZM).

Core models of the EZM are the non-hydrostatic prognostic mesoscale model MEMO and the photochemical dispersion model MARS. Moreover, it is possible to use the diagnostic wind field model CONDOR instead of MEMO, or to initialize MEMO with a diagnostic wind field from observational data computed with CONDOR. The dispersion phenomena can then be calculated for non-reactive pollutants with the Lagrangian particle model LAPMOD, or alternatively for chemical reactive species with MARS. All these models were developed at the

Institute for Technical Thermodynamics University of Karlsruhe (Germany) in the period 1983-1989.

The development of the modeling system at one unique institute not only has logistic advantages, but also makes it easier to create all modules in a uniform manner – especially as numerical grid, data structure and algorithm characteristics are concerned. The EZM, however, does not provide yet a particular tool for the emissions inventory, or pre-processors for orography, land-use and meteorology, nor does it automatically or semi-automatically provide links to on-line databases for the model initialization via the Internet (server-client technology).

2.2.2 EPA's Model-3

The U.S. EPA began in the early 1990s to develop the Models-3 framework designed to be used by both scientists and decision makers. Models-3 has two main goals:

1. To provide an effective decision support system.
2. To provide a framework to support the evolution of models and modeling systems.

There are various features of Models-3 (i.e., the so-called third generation air pollution models) that make this system unique and different from the first and second generations of air quality models (Table 4).

Models-3 consists of three modeling tools, which are illustrated in Figure 9:

- **Meteorology:** The MM5 model with utilities and processors for: the definition of the simulation domain (TERRAIN), background fields (DATAGRID), for objective analysis of the meteorological input (RAWINS), for setting up the initial and boundary conditions (INTERP), and for the calculation of the time-dependent meteorological fields (MM5v2).
- **Emissions:** Emission rates are calculated as a function of socio-economic activities (e.g., industrial processes) and meteorology. Emissions include: point sources (e.g. stacks), line sources (e.g. roads), and area sources (e.g. biogenic and off-road emissions). Emissions are computed with the Models-3 Emission Projection and Processing System (MEPPS), which contains the Inventory Data Analyzer (IDA), the Input Emission Processor (INPRO), the Emission Processor (EMPRO), the Output Processor (OUTPRO), and the Models-3 Emission Projections processor (MEPPRO).
- **Chemistry:** The chemical transport modeling system contains the land-use processor (LUPROC), the meteorology-chemistry interface processor (MCIP), the emissions-chemistry interface processor (ECIP), the photolysis rate processor (JPROC), the initial conditions processor (ICON), the boundary conditions processor (BCON), the main chemical-

transport model processor (CCTM), and the process analysis processor (PROCAN).

Table 4. Differences in Models-3 to former air quality models (Dennis et al., 1996).

	First and second generation air quality models	Models-3 (CMS)
Users	High educated experts.	High educated experts and average users.
User-Machine	Hand-off of model predictions for analysis. ASCII. User-specified I/O.	Embedded decision support. GUIs System-specified, transparent I/O.
Machine	Sequential. Single machine.	Parallel. Distributed; clusters of workstations.
Machine-Science	Algorithms limited by speed and memory.	New, flexible chemical solvers; implicit advection solvers; multigrid algorithms.
Science	Ad hoc modular codes. Predefined coordinate system. 5-20 km scale phenomena ; gas-phase chemistry, and advection. Separate meteorology	Plug and play. Generic coordinate system. Subgrid-scale behavior; clouds and precipitations, and cloud venting. Coupled meteorology and chemistry.
Framework	Obsolescence requires recoding a new system. Home grown and likely proprietary. Hardwired links among system components. Manual execution. Ad hoc decentralized data management. Add-on visualization.	Object oriented design for flexibility and reuse. Community system with open data/module sharing. Isolation layering for system components. Automated execution. Systematic, distributed data management. Integrated visualization.

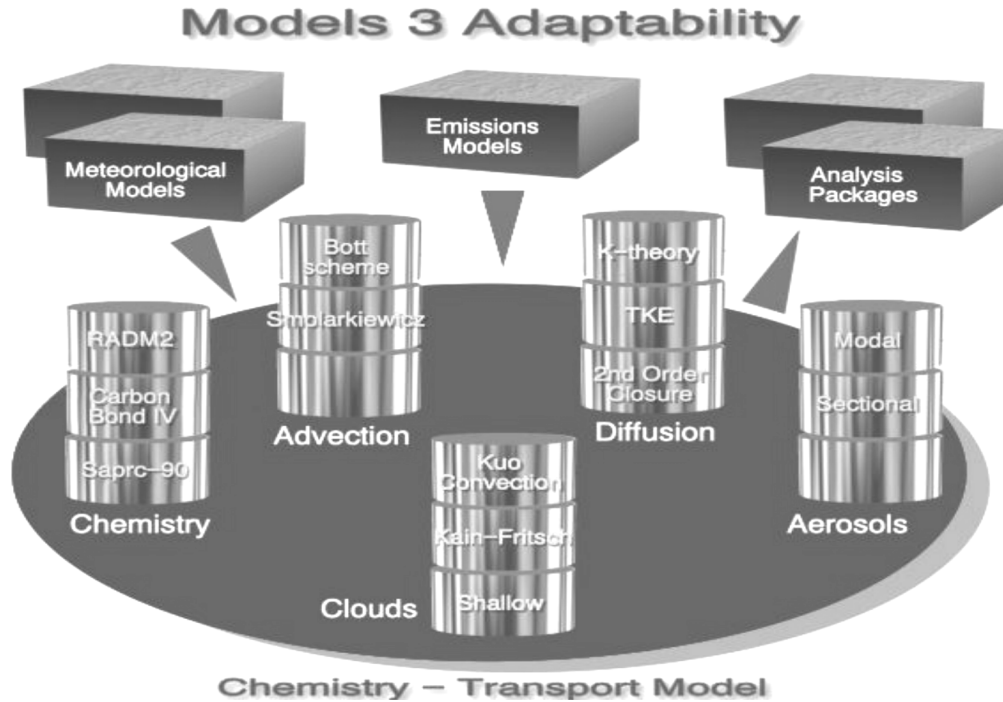


Figure 9. Models-3 modeling and analysis systems (source: <http://www.epa.gov/asmdner/models3/doc/overview3.html>).

Models-3 has also an integrated visualization and analysis package to plot, graph, and animate data created by the modeling system, or imported into Models-3. It consists of two non-proprietary tools (PAVE, VIS5D), and three commercial software products.

Various framework components guide the user through the modeling and analysis system:

- **Program Manager:** The Program Manager allows the user to register, update, and search for executable programs and/or scripts to make them available for use in defining studies within the Study Planner component. Metadata about the executables is provided. In addition, recommended model configurations for standard domains will be pre-registered in the system, eliminating the need for the average user to deal with the details of program registration.
- **Source Code Manager:** The Source Code Manager allows the user to store or retrieve the source codes of the mathematical models. In this way source codes can be changed and updated by scientists. The source code manager provides also historical information about the source codes.
- **Science Manager:** The Science Manager provides global sharing of model information such as grid coordinates, map projections, chemical

mechanisms. It can also be used to edit existing information, such as chemical mechanisms. Those changes are accounted for in all other modeling tools (e.g., the emission model) where a certain species is generated consistently with a new chemical reaction mechanism.

- **Model Builder:** The Model Builder assists the user in changing grid resolutions of a model, specifying particular features of the model (e.g., a chemical mechanism needed or not needed), interchanging science components within a model, modifying details within an existing chemistry mechanism, and other purposes.
- **File Converter:** The File Converter processes raw input data from ASCII or SAS files and converts them into formats used in the Models-3 framework (I/O API and SAS). The File Converter can also be used to convert meteorological data into a proper format within the Models-3 framework.
- **Dataset Manager:** The Dataset Manager helps the registration of datasets to be used for modeling analysis purposes within Models-3. The Federal Geospatial Metadata Standard is used for metadata storage. The dataset may be located on any network-connected computer system. Data is automatically moved to the host where it is needed for a model run.
- **Strategy Manager:** The Strategy Manager provides future year estimates of emissions to determine the relative effectiveness of specified control scenarios.
- **Tools Manager:** The Tools Manager provides access to a variety of visualization, statistical analysis, and emission processing tools that are registered within the Models-3 framework.
- **Study Planner:** The Study Planner assists in defining a simulation and controlling the execution of its associated models and processors. The interdependencies between the models and processors can be user-defined through the process of constructing and annotating a graphical diagram. Studies can be stored and re-used, or adopted by subsequent users.
- **Framework Administrator:** The Framework Administration allows the registration, update, and removal of users, hosts, devices, compilers, operating systems, and other entities by the administrator.

2.3 Remote Sensing, Advanced Air Quality, and Meteorological Measurement Techniques

As it can be seen from the advances in computer technology, more complex dispersion models can be used for certain tasks in the future, compared to rather simple modeling techniques used nowadays. Nevertheless, the successful application of improved dispersion models can only be accomplished when there is also a progress in air monitoring techniques, especially meteorological monitoring. For instance, the standard meteorological monitoring stations currently in use for air quality purposes measure: wind speed, wind direction, temperature, pressure, net radiation, and humidity. The parameters wind speed, wind direction and net radiation (instead of cloud cover) are necessary to run a simple Gaussian model, but are insufficient for more advanced models, such as Lagrangian or RANS models. To run Lagrangian or other advanced models, it is necessary to calculate additional parameters with a suitable meteorological pre-processor – a calculation that introduces errors. But the same parameters (e.g., Monin-Obukhov length, friction velocity, standard deviation of wind component fluctuations) can instead be measured with sonic anemometers. Such devices are becoming more and more applicable for air quality purposes, because of their decreasing costs (today: ~4,000 U.S.\$), their robustness compared to cup anemometers, and finally their ability to measure very low wind speeds (<0.5 m/s) with sufficient accuracy. In addition, SODAR devices could be used to provide inputs for Lagrangian and RANS models with vertical profiles of wind data. Clearly, SODARs can not be installed in populated area, due to the noise they produce, but only at critical sites, such as close to pollutant sources. SODARs can be very helpful, especially in locations where hazardous releases are possible.

On larger scales, satellite observations of tropospheric chemistry will probably become more and more available. To date, information on tropospheric composition above the surface is scarce, because aircraft observations are very limited. In contrast, the stratosphere has been investigated successfully by means of satellites and detailed chemical data on the global distribution of key trace gases has been provided. Tropospheric composition is much more difficult to observe with satellites, because of complexities arising by interactions with clouds, aerosols, water vapor, and the stratospheric ozone layer (Singh and Jacob, 2000).

Current observations from space cover: a few weeks of CO measurements from the MAPS (Measurement of Atmospheric Pollution from Satellites) instrument aboard the NASA space shuttle; indirect inferences of tropical ozone from satellite measurements of the total ozone column; and preliminary data sets from the column content of a few species (O₃, NO₂, HCHO, SO₂, BrO) from the GOME (Global Ozone Monitoring Experiment) solar backscatter instrument launched in 1995. Until now, no vertical structure of the tropospheric chemical composition could be measured from space.

There are several projects, which have already started or will be launched in the near future. A good overview on this topic is given in Singh and Jacob (2000). In December 1999 a satellite was launched carrying MOPITT (Measurement of Pollution in the Troposphere), a gas correlation spectrometer, to provide vertically resolved CO concentrations, and MODIS (Moderate Resolution Imaging Spectroradiometer), a device to measure column concentrations of aerosols.

Two major satellite launches, ENVISAT (<http://envisat.esa.int/>) by the ESA (European Space Agency), and AURA (<http://eos-chem.gsfc.nasa.gov/>) by the NASA (National Aeronautics and Space Administration) will take place in the next few years. The ENVISAT satellite will carry the following instruments: MIPAS (Michelson Interferometer for Passive Atmospheric Sounding), a high-resolution FTIR (Fourier Transform Infrared Spectroscopy) spectrometer observing in the limb, and SCIAMACHY (Scanning Imaging Absorption Spectrometer for Atmospheric Chartography), a solar backscatter device with both nadir and limb viewing capabilities. The AURA satellite, on the other hand, will carry a limb-scanning IR radiometer with a high vertical resolution (HIRDLS-High Resolution Dynamic Limb Sounder), a solar backscatter device observing in the visible and UV range (OMI-Ozone Monitoring Instrument), and TES (Tropospheric Emission Spectrometer), a high-resolution FTIR spectrometer observing in both the limb and nadir. With both these satellites it will be possible to observe vertical distributions of ozone and its key precursors in the troposphere. In addition TES has the potential to measure chemical species such as H₂O₂, acetone, methanol, HCN, HNO₄, SO₂, and PAN.

In the next 3-5 years there will be further launches, such as GOME-2, IASI (Infrared Atmospheric Sounding Interferometer), and PICASSO (Pathfinder Instruments for Cloud and Aerosol Spaceborne Observation). So far only polar orbiting satellites are available. An FTIR spectrometer named GIFTS (Geostationary Imaging Fourier Transform Spectrometer) will be the first geostationary instrument launched in 2003. It will be capable of detecting CO and possibly ozone. As pointed out by Singh and Jacob (2000), such devices not only will allow for controlling the transport of environmentally important gases from geopolitical entities, but also allow for a critical testing of global models of tropospheric chemistry. Nevertheless, it should be mentioned that there exist limitations of satellite observations regarding vertical resolution, precision, and the suite of observable species.

The R&D program of the European Union created the Center for Earth Observation and several projects are related to the integration of satellite products into Air Quality Modeling Systems. One of these projects is called DECAIR (Development of an Air Observation Data Converter with Application to Air Quality Forecast) and is currently underway. Figure 10 shows general information and architecture of the project.

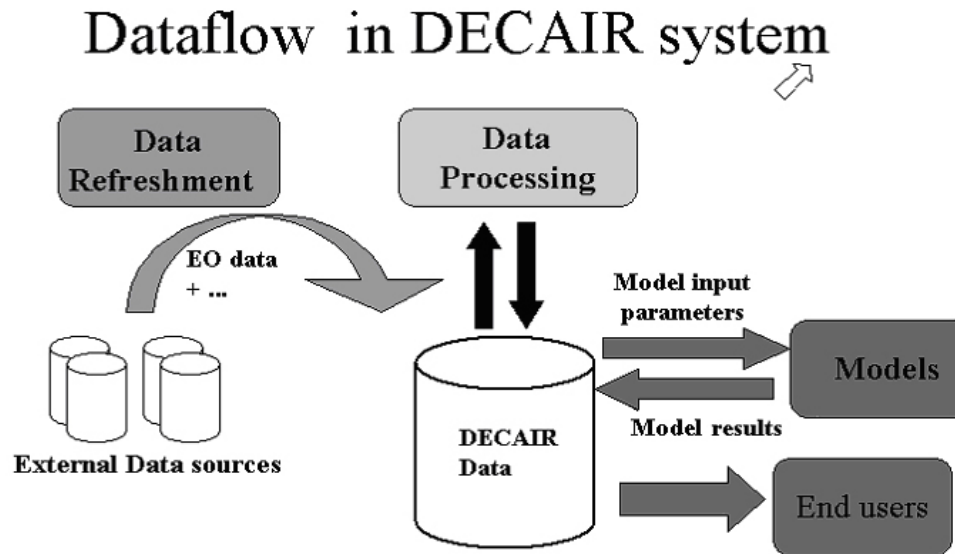


Figure 10. DECAIR Architecture and objectives.

DECAIR focuses on the creation of an API, which allows the AQM user to update the land-use information and several initial soil and thermodynamic parameters for running the current AQM models. This updating process can be done because of the large improvement in the speed of data transfer by using state-of-the-art telecommunication networks and the Internet. The quality of input information is improved and the accuracy of the forecast is expected to benefit from this improvement. Future developments of these concepts will include the use of GPS for improving the inputs for emission modules (which will be connected in on-line mode to meteorological and chemical modules as discussed above). Microwave satellite generation will allow the program to provide initial vertical concentrations for initialization of the model from many different types of pollutant species with a high vertical resolution – this will improve the boundary concentrations in the AQM models for pollutant species and it will benefit the quality of the forecasts, particularly on the aqueous phase and particulate areas.

2.4 Internet and Air Pollution Modeling

The use of the Internet in air pollution modeling has contributed significantly to the development of operational versions of complex research mesoscale air quality models, which before 1995 were only used at research laboratories. Between 1970 to 1995, operational air quality models were based on Gaussian approaches. At the end of the 1980's, Lagrangian approaches started to be implemented on PC and as a consequence, these models started to be used in

operational mode. The Eulerian approach was very expensive and it was difficult to implement because of the large CPU requirements. At the beginning of the 1990's, Eulerian models started to be used in operational mode. One of these models was OPANA, which means Operational version of ANA model. ANA stands for Atmospheric numerical pollution model for urban and regional areas and is the so-called «research version» (see Figure 11). This model was developed by San José et al. (1997), although previous versions are reported in the literature (San José et al., 1994). The most important features of this model are the inclusion of Internet-based applications to get real-time boundary conditions and initial conditions provided by models running over larger domains (but with coarser grid resolutions) to assure a good quality (limited by the Internet connection speed and the CPU performance) in the air quality forecasts. This is possible because of the extraordinary contribution of the Internet. Operational versions of these models are usually required by regional or city environmental offices, who also require a high spatial and temporal resolution. All these requirements cannot be fulfilled unless we use high-speed communications and the Internet.

Limited area models require meteorological variables and pollutant concentrations for filling up the boundary files. This information can only be provided in forecasting mode by outputs of operational models over larger areas and lower spatial resolution. This scheme is known as nesting approach. Operational simulations require about 96-120 hours, due to the time consumed when running the model and also the need to use surface observational data. Outputs of large domain operational meteorological models such as MM5, ETA, or ECMWF models can be transferred by the Internet to be used as boundary conditions for high resolution air quality models over regional or urban domains. In the middle of the 1990's the OPANA model started to use vertical meteorological forecasting soundings provided by AVN/MRF (Medium/Large range weather forecast model) in operational mode in the ARL web site (<http://www.arl.noaa.gov/ready.html>). These vertical meteorological soundings were downloaded automatically by using daily a JAVA application to launch the OPANA application. Today this situation continues but because of the increase of the computer capability, MM5 outputs are used to incorporate more initial datasets to OPANA (forecasted cloud cover) and land use data from results of operating with DECAIR API. Figure 12 shows this structure.

2.5 Future Research Needs

Air pollution modeling is an interdisciplinary science that covers many different working areas, such as meteorology, mathematics, physics, chemistry, geosciences, computer sciences, and others. Although the basic equations – the Navier-Stokes equations – describing fluid flows are known since the 19th century (Claude Louis Marie Navier, 1785-1836; Sir George Gabriel Stokes, 1819-1903) there is still a lot of research to do in different disciplines and the linking of the various findings. Today the research is strongly coupled with computer technology as outlined in the first section. There are a tremendous number of published papers, 15 – 20 per week on the average, dedicated only to the Navier-Stokes equations (<http://www.lma.univ-bpclermont.fr/NSenet/>). Since it is impossible to be well informed on all sciences connected with air pollution modeling, we refrain from giving a detailed analysis of future research in the various working fields in this chapter but we will focus on a more basic need in air pollution modeling.

As evidenced by the ongoing conference series on “Harmonisation within Atmospheric Dispersion Modelling for Regulatory Purposes”, model harmonization and evaluation is of great concern among policy makers and scientists. Some researchers even give model evaluation the highest priority when speaking about future research needs (e.g. Kukkonen, 1998).

The chaotic behavior of turbulent flows and the uncertainties in the boundary conditions result in unavoidable uncertainties in model predictions. Additional uncertainties arise from the model simplifications compared to real processes, programming errors, use of incorrect measurements and other problems. Hence, decision-making based on model predictions should always be done very carefully. The most complex models do not necessarily give the best results, as previously discussed by Hanna (1989), since such models not only are difficult to run but also need detailed information for initialization and for the boundary conditions. Sometimes, it may be better to use simple models adapted to a specific problem and applied with the use of affordable field observations. For instance, the Environmental Protection Agency in the United States recommends models mostly based on the Gaussian approach (e.g. CALINE3, CTDMPLUS, ISC3) that are easy to use compared with other more complex models. The goal should be to use models that provide similar results, independently from the user's skills. Consequently, the modeling application procedures should be similar in different regions. However, if the model simplifies reality too much (e.g., a simple Gaussian model used in a very complex terrain region), the modeling errors in predicting air quality may become very high. These errors may affect the credibility of the model and its acceptability. Also, the approval of a model by a governmental authority may reduce the incentive for researchers to develop new, more complex and comprehensive approaches.

In contrast with the U.S., in Europe we find more choices for regulatory air pollution models. Although there are regulations for specific models in some countries, there seems to be more latitude for using alternative models for particular problems. For instance, Lagrangian dispersion models are quite commonly used in Germany (e.g. Janicke, 2000), Austria (e.g. Oettl et al., 2001), and Italy (e.g. Brusasca et al., 1992). Instead of settling on specific models it may be more appealing to establish guidelines for model evaluation. Such guidelines would not hinder the progress in model development but would set up minimum performance requirements for dispersion models. Standardized protocols on model validation would indeed be a valuable and helpful tool for air pollution experts to compare different models for specific applications.

Some efforts are already on the way to set up such guidelines and the databases needed for model validation. Among the most popular databases, one finds the so-called “Model validation kit” (Olesen, 1995), including experimental data from point source releases (Kincaid, Indianapolis, Lillestrøm, Copenhagen). There is also a comprehensive overview of databases for validation purposes (Galmarini et al., 2001) accessible through the Internet run by the Joint Research Center in Ispra, Italy (<http://rtmod.ei.jrc.it/dam>). One actual guideline for model validation is the ASTM Guide D6589-00 (Standard Guide for Statistical Evaluation of Atmospheric Dispersion Model Performance), which can be downloaded⁶. An evaluation guideline for prognostic microscale wind field models is currently being prepared in Germany (VDI 3783, 2001). The idea is to set up test cases and criteria for models, which have to be fulfilled. The test cases are mostly derived from wind tunnel data (<http://www.mi.uni-hamburg.de/cedval/>) or field experiments (e.g., street canyons).

Unfortunately, high-quality databases for model evaluation are very scarce, and existing data sets have different data formats. It would indeed be quite valuable to agree on certain data formats to make experimental data sets easier to use by the modeling community. A useful data format could be the netCDF-Format (<http://www.unidata.ucar.edu/packages/netcdf/>), associated with large amounts of free software for visualization and analysis from the Internet (e.g. FERRET, <http://ferret.wrc.noaa.gov/Ferret/>).

Another important issue is model evaluation and which group should perform it. To guarantee an objective evaluation of a model, it would be necessary to send the model to be tested by an independent institution (e.g. the US EPA). It would also be useful, for model developers, to follow an official evaluation protocol, where the performance and the applicability of their model to specific problems are described. Then, industrial clients would have better criteria to decide which model to select for their environmental assessment studies.

⁶ <http://www.astm.org/cgi-bin/SoftCart.exe/DATABASE.CART/PAGES/D6589.htm?L+mystore+rkuq6443>

2.6 Conclusions

The future of air quality modeling is very promising since the parallel development of communication technologies, such as mobile communications (WAP 2.0, GPRS and UMTS) all based on the INTERNET development, the advances in physical and natural sciences (improvements of the knowledge of parameterization processes), the advances in remote sensing techniques (accuracy of land-use and topographical datasets with higher spatial and temporal resolution; improvements in air pollution vertical and horizontal concentrations from satellite based instruments) and the advances of CPU power, all together will provide new horizons for air quality models. The capability of analyzing the environmental impact of point sources using Eulerian models will also be improved. This will provide tools for industrial partners to use in operational mode, in order to simulate the impact of industrial emissions and take appropriate actions.

These technologies will also be capable of informing the user in real-time mode, suggesting specific emergency actions to be adopted, and recommending emission reduction strategies based on the air quality modeling forecasts.

Acknowledgements

First of all we wish to thank Jaakko Kukkonen for the careful reading of the manuscript and his numerous and valuable comments on it. The provision of CPU requirements of particular dispersion models is greatly acknowledged to Domenico Anfossi, Elisa Canepa, Ari Karppinen, Koen De Ridder, Guy Schayes, and Paolo Zannetti.

References

- Anfossi, D., E. Ferrero, G. Brusasca, A. Marzorati, G. Tinarelli (1993): A simple way of computing buoyant plume rise in a Lagrangian stochastic dispersion model for airborne dispersion. *Atmospheric Environment*, **27 A**, 1443-1451.
- Brandmeyer, J.E., and H.A. Karimi (2000): Coupling methodologies for environmental models. *Environmental Modelling & Software*, **15**, 479-488.
- Brusasca, G., G. Tinarelli, and D. Anfossi (1992): Particle model simulation of diffusion in low wind speed stable conditions. *Atmos. Environ.*, **4**, 707-723.
- Byun, D.W., and J.K.S. Ching (1999): Science Algorithms of the EPA Models-3 Community Multiscale Air Quality (CMAQ) Modelling System. EPA/600/R/99/030.
- Canepa, E., F. Modesti, and C.F. Ratto (2000): Evaluation of the SAFE_AIR code against air pollution field and laboratory experiments. *Atmospheric Environment*, **34**, 4805-4818.
- Carvalho, J., G. Degrazia, D. Anfossi, S. Trini Castelli (2001): Study of the transport and diffusion process in the PBL using the RAMS and SPRAY models: application to the TRACT experiment. Air Pollution Modelling and its Applications XIV, S.E. Gryning and F.A. Schiermeier eds., Kluwer Academic / Plenum Press, New York, in press.

Dabbert, W.F., and E. Miller (2000): Uncertainty, ensembles and air quality dispersion modelling: application and challenges. *Atmospheric Environment*, **34**, 4667-4673.

Dennis, R.L., D.W. Byun, J.H. Novak, K.J. Galluppi, C.J. Coats, and M.A. Vouk (1996): The next generation of integrated air quality modelling: EPA's models-3. *Atmos. Environ.*, **30**, 1925-1938.

Dudhia, J., D. Gill, J. Klemm and W. Skamarock (1998) : Current status of model developments and plans for the future. Preprints of the PSU/NCAR Mesoscale Model User's Workshop. Boulder, Colorado, 15-16 June.

Ferrero, E., D. Anfossi, G. Brusasca, G. Tinarelli (1995): Lagrangian particle model LAMBDA: evaluation against tracer data. *Int. J. Environment and Pollution*, **5**, 360-374.

Galmarini, S., G. Graziani, R. Bellasio, and R. Bianconi (2001): DAM: Datasets for atmospheric modeling. Proceedings of the 7th Int. Conf. On Harmonisation within Atmospheric Dispersion Modelling for Regulatory Purposes. Belgirate, Italy 28-31.5.2001, pp. 30-32.

Gualtieri, G., and M. Tartaglia (1998): Predicting urban traffic air pollution: A GIS framework. *Transpn Res.-D.*, **3**, 329-336.

Hanna, S.R. (1989): Plume dispersion and concentration fluctuations in the atmosphere. *Encyclopedia of Environmental Control Technology: Volume 2, Air Pollution Control*. P.N. Cheremisinoff, Editor. Houston, Texas: Gulf Publishing Co.

Härkönen, J., Lahtinen, K., Valkonen, E. and Kukkonen, J. (1997): An operational model for vehicular pollution from a road network. *International Journal of Environment and Pollution*, **8**, Nos. 3-6, pp. 436-437.

Hillis, W.D., and B.M. Boghosian (1993): Parallel scientific computation. *Science*, **261**, 856-863.

Houstis, E.N., and J.R. Rice (2000): Future problem solving environments for computational science. *Mathematics and Computers in Simulation*, **54**, 243-257.

Janicke, L. (2000): A random walk model for turbulent diffusion. Reports on Environmental Physics. ISSN 1439-8222 (Internet: ISSN 1439-8303), p.10.

Karppinen, A., J. Kukkonen, T. Elolähde, M. Kontinen, T. Koskentalo, and E. Rantakrans (2000): A modelling system for predicting urban air pollution: model description and applications in the Helsinki metropolitan area. *Atmospheric Environment*, **34**, 3723-3733.

Kukkonen, J. (1998): Research needs and problems in modeling urban air quality. COST CITAIR Newsletter 1/98. p. 9-11.

Moore, G. (1965) : Cramming more components onto integrated circuits. *Electronics*, **38**, 114-117.

Morris, R.E., Ch. Emery, and E. Tai (2001): Application of CALPUFF model to address visibility issues in the western U.S. *Proceedings of the conference on guideline on air quality models: A new beginning 4-6.4.2001, Newport RI*.

Moussiopoulos, N. (Ed., 1994): The EUMAC Zooming Model: Model structure and applications. p. 266. (Available from: Laboratory of heat Transfer and Environmental Engineering, Box 483, Aristotle University Thessaloniki, GR-54006 Thessaloniki, Greece).

Novak, J., and S. Leduc (1999): Models-3 architecture: a unifying framework for environmental modeling and assessment. In: Byun, D., Ching, J.S. (Eds.), Science Algorithms of the Models-3/Community Multiscale Air Quality (CMAQ), chapter 2, EPA 600/R-99/030. Model National Exposure Research Laboratory, RTP (NC), pp.00-00.

Oettl, D., R.A. Almbauer, and P.J. Sturm (2001): A new method to estimate diffusion in stable, low wind conditions. *J. of Appl. Meteor.*, **40**, 259-268.

Olesen, H.R. (1995): Datasets and protocol for model validation. *International Journal of Environmental and Pollution*, **5**, 4-6, pp. 693-701.

Reynolds, A.W., and B.M. Broderick (1999): Development of a GIS based urban air quality modelling system for transport related pollution. *Proceedings of the 6th conference on harmonisation of atmospheric dispersion models in Rouen*, 1-10.

Russell, A. and R. Dennis (2000): NARSTO critical review of photochemical models and modelling. *Atmos. Environ.*, **34**, 2283-2324.

San José, R., J.F. Prieto, N. Castellano, and J.M. Arranz (1997): Sensitivity study of dry deposition fluxes in ANA air quality model over Madrid mesoscale area. *Measurements and Modelling in Environmental Pollution*, Ed: R. San José and C. Brebbia. WIT (ISBN: 1-85312-461-3), pp. 119-130.

San José, R., L. Rodríguez, J. Moreno, M.A. Sanz, and M. Delgado (1994): Photochemical Air Pollution Model over Madrid Area. Envirosoft'94, Computational Mech. Publ. Clave: CL (ISBN: 1-56252-295-7), pp. 79-88.

Schaller, B. (1996): The origin, nature and implications of "Moore's Law". The benchmark of progress in semiconductor electronics. *Internet Publication* http://research.microsoft.com/~gray/Moore_Law.html, p 34.

Schär, C. (2001): Alpine numerical weather prediction 2000-2020: A look back to the future. *The Mesoscale Alpine Programme Newsletter*, **14**, 6-13. (Available from: c/o MeteoSwiss, Krähbühlstrasse 58, CH-8044-Zürich, Switzerland).

Schayes, G., P. Thunis, and R. Bornstein (1996): Topographic Vorticity-Mode Mesoscale- β (TVM) Model. Part I: Formulation. *J. Appl. Meteor.*, **35**, 1815-1823.

Singh, H.B., and D.J. Jacob (2000): Future directions: Satellite observations of tropospheric chemistry. *Atmospheric Environment*, **34**, 4399-4401.

Thunis, P., and A. Clappier (2000): Formulation and Evaluation of a nonhydrostatic Mesoscale Vorticity Model (TVM). *Mon. Wea. Rev.*, **128**, 3236-3251.

Tinarelli, G., D.Anfossi, M. Bider, E. Ferrero, S. Trini Castelli (2000): A new high performance version of the Lagrangian particle dispersion model SPRAY, some case studies. *Air Pollution Modelling and its Applications XIII*, S.E. Gryning and E. Batchvarova eds., Kluwer Academic / Plenum Press, New York, 499-507.

VDI 3783 (2001): Umweltmeteorologie – Prognostische mikroskalige Windfeldmodelle: Evaluierung für Gebäude- und Hindernisumströmung. Blatt 9 (Vorentwurf).

Zannetti, P. (1996): Environmental Modeling – Today and Tomorrow. *Environmental Modeling Volume III* (Ed. P. Zannetti), Computational Mechanics Publications and Elsevier Applied Science.

Moussiopoulos, N. and P.M. Turlou (2003) *Active Groups in Air Pollution Modeling*. Chapter 21 of *AIR QUALITY MODELING - Theories, Methodologies, Computational Techniques, and Available Databases and Software. Vol. I - Fundamentals* (P. Zannetti, Editor). Published by The EnviroComp Institute (<http://www.envirocomp.org/>) and the Air & Waste Management Association (<http://www.awma.org/>).

Note from the editor: We provide here a first, preliminary list of active groups. We encourage the readers to email new entries to the first author and the editor.

Chapter 21

Active Groups in Air Pollution Modeling

Nicolas Moussiopoulos⁽¹⁾ and Paraskevi-Maria Turlou⁽²⁾

⁽¹⁾ *Aristotle University Thessaloniki, Greece*
moussio@eng.auth.gr

⁽²⁾ *Aristotle University Thessaloniki, Greece*
evelina@aix.meng.auth.gr

Abstract: The air pollution modeling group database/guide was built with the aim to summarize theory, computational methods and software available for the description of transport and transformation of air pollutants in the atmosphere. This database provides specific information on the groups' main objectives regarding air pollution modeling issues, the model tools either developed or used, the major research projects carried out during the past five years and other services provided by each modeling team listed. Inclusion of a group in the database is by no means associated with any form of endorsement for selecting/promoting the particular group or one of its models; the modeling group database allows the dissemination of the information collected to all researchers, scientists and modelers who are either interested or involved in relevant issues. In this sense, it provides insight to the activities, competence and skills of each group, thus aiming in facilitating the collaboration, strengthening the bonds between different air pollution modeling teams and guiding third parties to select the most appropriate group/model in accordance to the specifications submitted by each study or project undertaken. In addition, it pictures the state-of-the-art with regard to the air pollution modeling groups and tools in different parts of the world.

Keywords: air pollution, modeling / simulation, pollution control / abatement, ozone formation, urban plume, dispersion / transport / deposition of air pollutants, street canyon, air pollution episode, air quality forecasting.

➡ **For detailed information on active groups please examine the hyperlinks as indicated by arrows**

1 List of Active Groups

- **3D Model Group for Baltic Sea Studies at the Finnish Meteorological Institute** ↗

Finnish Meteorological Institute (FMI), Air Quality Research, Finland

Group URL: <http://www.fmi.fi/IL/ILAA/itamry.html>

Institution URL: <http://www.fmi.fi/ENG>

- **AMES (Automatic Measuring Systems for the Environment)** ↗

Slovenia

Group URL: <http://amesnt.ijs.si/>

- **Air Research Laboratory (LLO)** ↗

National Institute of Public Health and the Environment (RIVM), Netherlands

Group URL: <http://www.lml.rivm.nl>

Institution URL: <http://www.rivm.nl>

- **Atmospheric Physics Group** ↗

Defense Research Establishment, Division of NBC Defense

- **Atmospheric Sciences Technical Group** ↗

Pacific Northwest National Laboratory, USA

Group URL: http://www.pnl.gov/atmos_sciences/

Institution URL: <http://www.pnl.gov>

- **Atmospheric Dispersion Modelling** ↗

Finnish Meteorological Institute (FMI), Finland

Group URL: http://www.fmi.fi/ENG/ILA/dispersion_model.html

Institution URL: <http://www.fmi.fi/ENG/index.html>

- **Atmospheric Modelling Group in the Research Centre of the System Analysis** ↗

Institute of Program Systems, Russian Academy of Sciences, Russia

- **Cambridge Environmental Research Consultants (CERC)** ↗

UK

Group URL: <http://www.cerc.co.uk>

- **EnviroComp-Air Pollution Modeling** ↗

The EnviroComp Institute, USA

Group URL: <http://www.envirocomp.org>

Institution URL: <http://www.envirocomp.org>

- **Environmental Measurement, Monitoring and Assessment (EMMA)** ↗

Imperial College of Science, Technology and Medicine, London University, UK

Group URL: <http://www.huxley.ic.ac.uk/research/AIRPOLL>

Institution URL: <http://www.ic.ac.uk>

- **Environmental Modeling** ↗

University of Santiago de Compostela (USC), Spain

Group URL: <http://www.usc.es/enxqu>

Institution URL: <http://www.usc.es>

- **Environmental Physical Chemistry** ↗

Center for Research on Parallel Computing and Supercomputers, Italy

Institution URL: <http://www.dichi.unina.it> and <http://pixel.dma.unina.it>

- **Environmental Research Laboratory (EREL)** ↗

National Centre for Scientific Research, Greece

Group URL: <http://milos.ipta.demokritos.gr/>

Institution URL: <http://www.demokritos.gr/>

- **EURAD, Institute for Meteorology and Geophysics** →

University of Cologne, Germany

Group URL: <http://www.uni-koeln.de/math-nat-fak/geomet/eurad/index.html>

Institution URL: <http://www.uni-koeln.de>

- **Group of Dynamic Meteorology** →

Tartu Observatory (TO), Estonia

Group URL: <http://www.apollo.aai.ee>

Institution URL: <http://www.aai.ee>

- **IFU: Fraunhofer Institute for Atmospheric Environmental Research** →

Fraunhofer Society, Germany

Group URL: <http://www.ifu.fhg.de>

Institution URL: <http://www.fhg.de>

- **INFRAS/METEOTEST** →

INFRAS, METEOTEST: Private Consultant Institutions Mandated by the Federal Office of the Environment, Forests and Landscape, Switzerland

Group URL: <http://www.infras.ch> & <http://www.meteotest.ch>

Institution URL: <http://www.infras.ch>, <http://www.meteotest.ch> & <http://www.buwal.ch/>

- **Laboratory of Air Pollution Meteorology and Dispersion** →

Ciudad Universitaria, Pab. University of Buenos Aires (UBA), Argentina

Institution URL: <http://www.uba.ar/>

- **Laboratory of Atmospheric Chemistry (LAC)** ↗

Paul Scherrer Institute (PSI), Switzerland

Group URL: <http://www.psi.ch>

- **Laboratory of Heat Transfer and Environmental Engineering (LHTEE)** ↗

Aristotle University Thessaloniki (AUT), Greece

Group URL: <http://aix.meng.auth.gr>

Institution URL: <http://www.auth.gr>

- **Lohmeyer Consulting Engineers** ↗

Lohmeyer Consulting Engineers, Germany

Group URL: <http://www.Lohmeyer.de>

Institution URL: <http://www.Lohmeyer.de>

- **Meteorology and Climate Group** ↗

Electricite de France

Institution URL: <http://www.edf.fr>

- **Modelling and Expertise Pool Section** ↗

Czech Hydrometeorological Institute, Czech Republic

Group URL: http://www.chmi.cz/uoco/odd/ome_idxe.html

Institution URL: <http://www.chmi.cz>

- **NARAC Modeling** ↗

Lawrence Livermore National Laboratory, USA

Group URL: <http://www.llnl.gov/ees/NARAC>

Institution URL: <http://www.llnl.gov>

- **NERI (Denmark): Department of Atmospheric Environment (ATMI)** ↗

National Environmental Research Institute, Denmark

Group URL: <http://www.dmu.dk/AtmosphericEnvironment/>

Institution URL: <http://www.dmu.dk>

- **TSA-4 Air Quality Modeling Team** ↗

Los Alamos National Laboratory, USA

Group URL: <http://www.lanl.gov/orgs/d/d4/aquality/airquality.html>

Institution URL: <http://www.lanl.gov>

- **Troposphärische Umweltforschung (TrUmF, Tropospheric Environmental Research)** ↗

Institut fuer Meteorologie, Freie Universität Berlin, Germany

Group URL: <http://trumf.fu-berlin.de>

Institution URL: <http://www.met.fu-berlin.de>

- **UK Pollution Climate Mapping** ↗

AEA Technology Environment, UK

Group URL: <http://www.aeat.co.uk/netcen/airqual>

Institution URL: <http://www.aeat.co.uk>

2 Additional Information on Groups Working on Air Pollution Modeling Issues

- **EPA ORD**
<http://www.epa.gov/asmdnerl/index.html>

- **EPA HPCC**
<http://www.epa.gov/HPCC/homep.html>

- **EPA NERL**
<http://www.epa.gov/nerl>

- **EPA Visualization**
<http://www.epa.gov/vislab/index.html>
- **EPA (other groups)**
<http://www.epa.gov/oar/oaqps/modeling.html>
- **Texas Natural Resource Conservation Commission (TNRCC)**
<http://www.tnrcc.state.tx.us/air/aqp/airmodeling.html>
- **Earth Tech Atmospheric Studies Group (ASG)**
<http://www.src.com/index.htm>
<http://www.src.com/calpuff/calpuff1.htm>
- **ENVIRON**
<http://www.environcorp.com/PRACTICES/PAIRpage.html>
<http://www.camx.com>
- **University of Leeds, School of Chemistry**
<http://www.chem.leeds.ac.uk/Atmospheric/MCM/main.html>
- **MCNC**
<http://www.iceis.mcnc.org>
<http://www.iceis.mcnc.org/staff/index.html>
- **UCLA**
http://www.atmos.ucla.edu/research/mod_earth.html
- **HARVARD UNIVERSITY**
<http://www-as.harvard.edu/chemistry/trop>
- **CGRER**
<http://www.cgrer.uiowa.edu>
<http://www.cgrer.uiowa.edu/people/carmichael/Carmichael.html>
- **AEES**
<http://environmental.gatech.edu>
<http://environmental.gatech.edu/~trussell/page.html>
- **CHRONOS**
http://www.cmc.ec.gc.ca/~arqidor/chronos_description/chronos_description.html
- **NYSDEC**
<http://www.dec.state.ny.us/website/dar/index.html>
<http://www.dec.state.ny.us>

- **CE-CERT**
<http://www.cert.ucr.edu/research>
- **Atmospheric Turbulence Lab, UC Irvine**
<http://wave.eng.uci.edu/ATRL.html>
- **Chemical Engineering CMU**
<http://www.cheme.cmu.edu/who/faculty>
<http://www.cheme.cmu.edu/who/faculty/pandis.html>
- **Dept. Environmental Science and Engineering (UNC)**
<http://www.northcarolina.edu>
- **California Institute of Technology**
<http://www.caltech.edu>
<http://www.its.caltech.edu/~seinfeld/bio.html>
- **University of Texas**
<http://www.utexas.edu>

Thé, J. and R. Lee (2003) *Available Software*. Chapter 22 of *AIR QUALITY MODELING - Theories, Methodologies, Computational Techniques, and Available Databases and Software. Vol. I - Fundamentals* (P. Zannetti, Editor). Published by The EnviroComp Institute (<http://www.envirocomp.org/>) and the Air & Waste Management Association (<http://www.awma.org/>).

Chapter 22

Available Software

Jesse Thé ⁽¹⁾ and Russell Lee ⁽²⁾

⁽¹⁾ *Lakes Environmental Software Inc., 306 Milla Court, Waterloo - Ontario - N2L 6N4, CANADA*

jesse@lakes-environmental.com

⁽²⁾ *Private Consulting Meteorologist, 5806 Prosperity Church Road, Suite A2-128, Charlotte, NC 28269-1138, USA*

Russell.Lee@RFLee.com

Abstract: This chapter identifies a variety of air quality models and model-related products and services that have been developed by government environmental and meteorological agencies, universities, non-profit groups and for-profit companies. Many of the models are available free of charge. Others are available for a fee. Model-related products and services include preprocessors, visualization software, emission factor methodologies, meteorological data, terrain data and training programs. These models, products and services are available from a variety of sources including the World Wide Web.

Key Words: air quality models, air dispersion models, meteorological data, terrain data, short-range models, Gaussian models, plume models, puff models, Lagrangian models, particle models, photochemical models, urban models, regional models, long-range transport, acid deposition, visibility, complex terrain, emergency releases, dense gas models, diagnostic models, prognostic models, four-dimensional data assimilation.

A variety of air quality models and model-related products and services have been developed in recent years by government environmental agencies, universities, non-profit groups and for-profit companies. Model-related products and services include preprocessors and postprocessors, visualization software, emission factor methodologies, meteorological data, terrain data and training programs. With the advent of the Internet World Wide Web, many of these products are now more readily available. This chapter will discuss several classes of models that are available, along with a variety of model-related products and services that can be obtained from various sources, including the World Wide Web.

One of the most useful sites in this regard is the U.S. Environmental Protection Agency's Technology Transfer Network (TTN) (<http://www.epa.gov/ttn/>). The TTN is a function of the USEPA Office of Air Quality Planning and Standards (OAQPS). The TTN is a collection of technical websites containing information about many areas of air pollution science, technology, regulation, measurement, and prevention. In addition, the TTN serves as a public forum for the exchange of technical information and ideas among participants and USEPA staff.

The most well known part of the TTN is the Support Center for Regulatory Air Models (SCRAM) website (<http://www.epa.gov/scram001/>). This site contains most of the USEPA regulatory air quality models available for download without charge. In addition, it contains meteorological data, and modeling guidance documents published by the USEPA. Links to state and regional websites can also be found on this website.

Less well known are the other sites that make up the TTN. The following descriptions are extracted and summarized from the respective websites.

- AIRS, the Aerometric Information and Retrieval System, contain information on concentrations and emissions of various pollutants throughout the United States.
- AMTIC, the Ambient Monitoring Technology Information Center, contains information on ambient air quality monitoring programs, details on monitoring methods, relevant documents and articles, information on air quality trends and non-attainment areas, and federal regulations related to ambient air quality monitoring.
- ATW, the Air Toxics website, is a website for Federal, State, tribal, and local air toxics programs. This is the US EPA and central repository for air toxics information. (<http://www.epa.gov/ttn/atw/>)
- CATC, the Clean Air Technology Center, serves as a resource for all areas of emerging and existing air pollution prevention and control technologies, and provides public access to data and information on their use, effectiveness, and cost. (<http://www.epa.gov/ttn/catc/>)
- CHIEF, the Clearing House for Inventories and Emission Factors, contains the latest information on emission inventories and emission factors. It provides access to the latest information and tools for estimating emissions of air pollutants and developing air emission inventories. (<http://www.epa.gov/ttn/chief/>)
- CICA, Centro de Información sobre Contaminación de Aire, is the U.S. - Mexico Information Center on Air Pollution. This site provides technical support and assistance in evaluating air pollution problems along the U.S.-

Mexico border. The EPA's Clean Air Technology Center (CATC) sponsors the CICA web site. (<http://www.epa.gov/ttn/catc/cica/>)

- ECAS, the Economics and Cost Analysis and Support website is a function of the Innovative Strategies and Economics Group. This group conducts analyses of costs, benefits, and economic and regulatory impacts of air quality management strategies, programs, and regulations developed throughout the Office of Air Quality Planning and Standards (OAQPS). Publications from this group are available on this website. (<http://www.epa.gov/ttn/ecas/>)
- EMC, the Emission Measurement Center, provides access to emission test methods and testing information for the development and enforcement of national, state, and local emission prevention and control programs.
- FACA contains information related to the EPA advisory committee, and its subcommittees, formed under the provisions of the Federal Advisory Committee Act. (<http://www.epa.gov/ttn/faca/>)
- GEI, the Geographic/Ecosystems Initiatives, are geographically focused environmental activities, which leverage the resources of states, local governments, regulated communities, tribal programs, environmental groups, and citizens. (<http://www.epa.gov/ttn/gei/>)
- NELAC, the National Environmental Laboratory Accreditation Conference, promotes acceptable performance standards for the operation of environmental laboratories. (<http://www.epa.gov/ttn/nelac/>)
- NSR, The New Source Review website, is designed to provide material and information pertaining to NSR permitting. (<http://www.epa.gov/ttn/nsr/>)
- OARP&G, the OAR Policy and Guidance website, is designed to provide access to rules, policy, and guidance documents produced by the US EPA Office of Air and Radiation (OAR). (<http://www.epa.gov/ttn/oarpg/>)
- RTO, the Regional Transport of Ozone group, focuses on matters dealing with ground-level ozone (smog) and its precursors (including nitrogen oxides or NO_x). (<http://www.epa.gov/ttn/rto/>)
- SBAP, the Small Business Assistance Program, has been developed to help state and EPA small business assistance programs share information about their materials and activities. (<http://www.epa.gov/ttn/sbap/>)

Another very useful website is the Model Documentation System of the European Topic Centre on Air Quality, sponsored by the European Environment Agency (<http://www.etcaq.rivm.nl/databases/mds.html>). Over 100 models are listed on this site, a number of which are summarized in this chapter. This site provides details on the models organized under a series of standard descriptive headings, as provided by the respective developers.

There are various research centers and free private websites that contain model descriptions, emissions inventory calculators (<http://www.webthermal.com>), historical meteorological data (<http://www.webmet.com>), digital elevation and other GIS maps (<http://www.webgis.com>) and repositories for air quality models (<http://www.epamodels.com>). Another useful air dispersion model repository is the GAIA Model Database: Air quality simulation models website (<http://www.ess.co.at/GAIA/>). This database lists over 25 air quality models. Each entry contains a brief description of the model, its availability, authors, and technical references.

The Office of the Federal Coordinator for Meteorological Services and Supporting Research (OFCM), U.S. Department of Commerce, has published a “Directory of Atmospheric Transport and Diffusion Consequence Assessment Models,” (Document FCM-I3-1999, published in 1999). A copy of this document is available on-line at the OFCM website (<http://www.ofcm.gov>, under “Publications”). This site also provides details on the models organized under standard descriptive headings. A useful additional feature is a series of “extract tables” which provide model-to-model comparisons of features important for various categories of applications for over 60 models.

The remainder of this chapter will focus primarily on sources of air quality models, associated software, input data required to run the models, and support for running the models. A substantial amount of software, information and support is available on the Web, or from sources identified on various websites. This chapter is intended to put you in touch with the air quality models or modeling information you need to carry out your projects. The information contained here was obtained from a variety of sources, including the four websites described above and, in some cases, the authors themselves. The descriptions are necessarily brief. The reader is advised to use the following information only as a guide to identify potential models for a given use, then to get additional information from the author or supplier of the model, published model validation documents, and from the above websites before making any decisions as to their intended use.

1 Short-Range Models

This category includes the traditional Gaussian plume models based on the methods developed by Frank Pasquill in the 1950’s. In these models, plume

transport is represented as a straight-line plume. Pollutant concentrations are assumed to follow a Gaussian distribution through the plume in both the vertical and horizontal directions. In Pasquill's method, meteorological conditions are categorized into *stability classes*. For each stability class, the plume is assumed to have specific vertical and horizontal dimensions that are a function only of downwind distance. More modern plume models allow the distribution of pollutants through the plume to differ from the Gaussian form. Further, they allow the plume size to be a continuous function of stability and height, as well as distance. Calculations are generally made for each hour. Using the meteorological conditions for that hour, the plume is assumed to extend steadily in a straight line for the entire hour, for as far as the plume can travel. Since meteorological conditions change from hour to hour, the real plume may be traveling through a range of wind directions, wind speeds and stabilities before it gets to its destination. For this reason, accuracy deteriorates at larger downwind distances. Generally, such models are accepted for regulatory use for source to receptor distances of up to 50km, although in many conditions and locations, the accuracy may deteriorate beyond 20km. Some of these models can treat effects of complex terrain, such as mountains and shorelines. Most, however, are useful only over simple, relatively flat terrain.

1.1 Sources of Short-Range Regulatory Models

Many of the short-range regulatory models can be obtained without charge from governmental websites. Most of these models can be run on a personal computer. Meteorological data, terrain data (for the models that require it), and emission factor information can often be obtained from free sources as well (e.g., the U.S. EPA TTN). Table 1 lists some free sources of short-range regulatory models while Table 2 lists some additional sources of models for a fee. Descriptions of the models are provided in Tables 3 and 4.

Table 1. Sources of free (or low cost) short-range models.

Source (website or company)	Available models and data
ENEA—C.R.E. Casaccia in Rome, Italy. Contact M.C. Cirillo, ENEA—C.R.E. Casaccia, C.P. 2400, 00100 Roma, Italy.	DIMULA
FAA website: http://www.aee.faa.gov/aee-100/aee-120/edms/banner.htm	EDMS (Emissions and Dispersion Modeling System) for air quality modeling of airports.
NTIS (National Technical Information Service, U.S. Dept. of Commerce) website: http://www.ntis.gov	PAL-DS, PTPLU, TUPOS and all models available from the EPA websites.

Nuclear Regulatory Commission. Contact Ms. Leta A. Brown, US Nuclear Regulatory Commission, Mail Stop O-10 D4, Washington, DC 20555. Email LAB2@nrc.gov .	ARCON96
Power Plant Siting Program, Department of Natural Resources, Tawes State Office Building, Annapolis, MD 21401, Attn: Dr. Michael Hirschfield	PPSP
SCRAM website (alternative models): http://www.epa.gov/scram001	LONGZ, SDM, SHORTZ.
SCRAM website (preferred regulatory models): http://www.epa.gov/scram001	AERMOD, BLP, CALINE3, CDM2, CTDMPLUS, ISCST3, ISC-PRIME, OCD, RAM
SCRAM website (screening models): http://www.epa.gov/scram001	CAL3QHC/CAL3QHCR, COMPLEX1, CTSCREEN, LONGZ, RTDM3.2, SCREEN3, SHORTZ, VALLEY.
Science Applications International Corporation. Contact Dr. David P. Bacon, Science Applications International Corporation, 1710 Goodridge Dr., McLean, VA 22102. Email: bacon@apo.saic.com	OMEGA/ADM
Istituto FISBAT del C.N.R., Via de' Castagnoli 1, 40126 Bologna, Italy	KAPPA-G

Table 2. Sources of short-range models that can be purchased for a fee.

Source (website or company)	Available models and data
ARGUSOFT - Umweltmeteorologie Software (Germany) http://www.argusoft.de/	AUSTAL2000 (free) and AUSTAL View (free in selected circumstances). German version http://www.austalview.com , and English version available at http://www.weblakes.com
Cambridge Environmental Research Centre (UK) http://www.cerc.co.uk/	ADMS-3 (link to private source at CERC site, free in selected circumstances), ADMS-Roads, ADMS-Screen, ADMS-Urban
Czech Hydrometeorological Institute, Dpt. of Air Quality Protection, Na Sabatce 17, CZ-146 03 Prague 4, Czech Republic	SYMOS97

Exponent, Inc. Contact Dr. Paolo Zannetti, QEP-EnviroComp Consulting, Inc., 2298 Ocaso Camino, Fremont, CA 94539	AVACTA II
General Motors. Contact Dr. D.P. Chock, Environmental Science Department, General Motors Research Laboratories, General Motors Technical Center, Warren, MI 48090	Simple Line Source Model
Institut für Technische Thermodynamik, Fakultät für Maschinenbau, Universität Karlsruhe, Kaiserstr.12, D-76128 Karlsruhe, Germany	MIMO
Lakes Environmental Software Inc. www.weblakes.com	ISC-AERMOD View, CALPUFF View, AUSTAL View, CALROADS View, SCREEN View
National Environmental Research Institute, P.O. Box 358, DK-4000 Roskilde, Denmark, Att. H.R. Olesen	OML
Swedish Meteorological and Hydrological Institute (SMHI), S-601 76 Norrköping, Sweden	DISPERSION
Tartu Observatory, 61602 Toravere, Tartumaa, Estonia. Contact Marko Kaasik.	AEROPOL
Trinity Consultants Inc. http://www.breeze-software.com/	Breeze-AERMOD, Breeze-ISC, Breeze-Screen3, Breeze-Roads
VITO, Boeretang 200, B2400 Mol, Belgium	IFDM
WYNDsoft, Inc., 6333 77 th Avenue, SE, Mercer Island, WA 98040	WYNDVALLEY

1.2 Descriptions of Models

Tables 3 and 4 provided brief descriptions of the individual models.

Table 3. Short-range models available free (or at low cost).

Model	Description and sources
AERMOD	AERMOD is an advanced for assessment of pollutant concentrations from a variety of sources. Type: Non-Gaussian plume model. Source types: Multiple point, area and volume sources. Features: Planetary boundary layer similarity profiling;

	<p>rural and urban areas; simple and complex terrain; building downwash; averaging times 1-hour to annual.</p> <p>Availability: SCRAM website at http://www.epa.gov/scram001.</p>
ARCON96	<p>ARCON96 is a model for calculating concentrations in the vicinity of buildings and used to assess control room habitability under accident conditions.</p> <p>Type: Gaussian plume.</p> <p>Source types: Point sources.</p> <p>Features: Relative concentrations are calculated for averaging periods ranging from 1 hour to 30 days duration.</p> <p>Notes: Intake height limited to < 100m; downwind distance limited to < 10km.</p> <p>Availability: ARCON96 is available from the Nuclear Regulatory Commission. Contact Ms. Leta A. Brown, US Nuclear Regulatory Commission, Mail Stop O-10 D4, Washington, DC 20555. Email LAB2@nrc.gov.</p>
AUSTAL2000	<p>AUSTAL2000 is a Lagrangian particle model designed to handle dispersion cases in flat and complex terrain as well as respecting flow around buildings. This is the regulatory model in Germany (TA Luft).</p> <p>Type: Lagrangian particle tracking.</p> <p>Source types: Point, area, line, and volume sources.</p> <p>Features: This particle model computes concentration, deposition, accounts for building downwash, flat and complex terrain, and varying wind fields. Averaging time from 1-hour to annual.</p> <p>Availability: The German Federal Environmental Agency http://www.austal2000.de/ and also from Argusoft: http://www.argusoft.de.</p>
BLP	<p>BLP (Buoyant Line Plume) is designed to handle unique modeling problems associated with aluminum reduction plants, and other industrial sources where plume rise and downwash effects from stationary line sources are important.</p> <p>Type: Gaussian plume.</p> <p>Source types: Buoyant line sources, in addition to point, area, line and volume sources.</p> <p>Features: In addition to buoyant line source treatment, features are similar to those of ISCST.</p> <p>Availability: SCRAM website at http://www.epa.gov/scram001.</p>

CAL3QHC/ CAL3QHCR	<p>CAL3QHC is an episodic model based on CALINE3 that predicts concentrations of CO or other inert pollutants from traffic at roadway intersections.</p> <p>Type: Gaussian plume.</p> <p>Source types: Roadways and intersections.</p> <p>Features: CAL3QHC calculates emissions for roads and signalized intersections based on traffic; 1-hour averaging time. CAL3QHCR allows averaging times from 1-hour to annual.</p> <p>Notes: The model includes a traffic algorithm for estimating vehicular queue lengths at signalized intersections.</p> <p>Availability: SCRAM website at http://www.epa.gov/scram001.</p>
CALINE3	<p>CALINE3 is designed to determine air pollution concentrations near roadways.</p> <p>Type: Gaussian plume model.</p> <p>Source types: Highways, including at-grade, fill, bridges, and cut sections.</p> <p>Features: 1-hour concentrations; relatively uncomplicated terrain.</p> <p>Availability: SCRAM website at http://www.epa.gov/scram001.</p>
CDM2	<p>CDM2 is a model for calculating long-term (e.g., seasonal or annual) average ground-level concentrations of an inert pollutant.</p> <p>Type: Gaussian plume model.</p> <p>Source types: Point and area sources.</p> <p>Features: Monthly to annual averaging times; flat terrain; inert pollutants only.</p> <p>Availability: SCRAM website at http://www.epa.gov/scram001.</p>
COMPLEX1	<p>COMPLEX1 is a multiple source screening model for complex terrain.</p> <p>Type: Gaussian plume in the vertical; sector in horizontal</p> <p>Source types: Point sources.</p> <p>Features: Complex terrain screening using the plume impaction algorithm of the VALLEY model.</p> <p>Availability: SCRAM website at http://www.epa.gov/scram001.</p>
CTDMPLUS	<p>CTDMPLUS (Complex Terrain Dispersion Model Plus Algorithms for Unstable Situations) is a refined point source Gaussian air quality model for use in all stability conditions for complex terrain.</p> <p>Type: Gaussian plume model with boundary layer scaling.</p> <p>Source types: Point sources.</p>

	<p>Features: Complex terrain model making use of dividing streamline concepts. The model contains, in its entirety, the technology of CTDM for stable and neutral conditions.</p> <p>Notes: Requires detailed terrain input as well as hourly meteorology and source information.</p> <p>Availability: SCRAM website at http://www.epa.gov/scram001.</p>
CTSCREEN	<p>CTSCREEN (Complex Terrain Screening Model) is a screening version of the CTDMPLUS complex terrain model.</p> <p>Type: Gaussian plume screening model.</p> <p>Source types: Point sources.</p> <p>Features: Screening version for CTDMPLUS.</p> <p>Notes: Meteorology is built in. All other inputs applicable to CTDMPLUS must be supplied, including terrain.</p> <p>Availability: CTSCREEN is available from the SCRAM website at http://www.epa.gov/scram001.</p>
DIMULA	<p>DIMULA is a multiple source air pollution dispersion model based on the Gaussian plume approximation, with a special correction to deal with calm conditions (where the classical analytical formula is not applicable).</p> <p>Type: Gaussian plume model.</p> <p>Source types: Point, area and line sources.</p> <p>Features: 1-hour to annual averaging times; flat terrain; non-reactive (inert) pollutant.</p> <p>Availability: DIMULA is available from ENEA—C.R.E. Casaccia in Rome, Italy. Contact M.C. Cirillo, ENEA—C.R.E. Casaccia, C.P. 2400, 00100 Roma, Italy.</p>
EDMS	<p>EDMS (Emissions and Dispersion Modeling System) is designed to assess the air quality impacts of airport emission sources, particularly aviation sources.</p> <p>Type: Non-Gaussian plume—uses AERMOD as the dispersion component. (Earlier versions used the Gaussian plume model ISCST.)</p> <p>Source types: All airport emission sources, including aircraft, auxiliary power units and ground support equipment</p> <p>Features: EDMS is one of the few air quality assessment tools specifically engineered for the aviation community. It includes emissions and dispersion calculations, the latest aircraft engine emission factors from the International Civil Aviation Organization (ICAO) Engine Exhaust Emissions Data Bank, vehicle emission factors from the Environmental Protection Agency's (EPA) MOBILE5a, and EPA-validated dispersion algorithms.</p> <p>Availability: EDMS is available from the FAA website at http://www.aee.faa.gov/aee-100/aee-120/edms/banner.htm</p>

ISCST3	<p>Industrial Source Complex Short-Term, ISCST3, model is a Gaussian plume designed to assess concentrations due to a variety of sources such as is found in industrial source complexes.</p> <p>Type: Gaussian plume model.</p> <p>Source types: Point, area, line and volume sources, at multiple locations.</p> <p>Features: Building downwash, and settling and deposition</p> <p>Notes: A long-term version, ISCLT3, is also available.</p> <p>Availability: SCRAM website at http://www.epa.gov/scram001.</p>
ISC-PRIME	<p>PRIME (Plume RIse Model Enhancements) is an improved building downwash treatment that has been incorporated into ISCST3</p> <p>Type: Gaussian plume model.</p> <p>Source types: Point, area, line and volume sources, at multiple locations.</p> <p>Features: Same as ISCST except with addition of an improved building downwash treatment.</p> <p>Availability: SCRAM website at http://www.epa.gov/scram001.</p>
KAPPA-G	<p>KAPPA-G model simulates air pollution from a point source using a Gaussian approximation for the horizontal diffusion, but a Demuth solution of the vertical diffusion.</p> <p>Type: Non-Gaussian plume.</p> <p>Source types: Multiple point sources.</p> <p>Features: Non-reactive pollutant over flat terrain. Non-Gaussian plume in the vertical (using Demuth solution of vertical diffusion).</p> <p>Availability: Istituto FISBAT del C.N.R., Via de' Castagnoli 1, 40126 Bologna, Italy.</p>
LONGZ	<p>LONGZ is a long-term model for urban and rural areas, and flat and complex terrain.</p> <p>Type: Gaussian plume model.</p> <p>Source types: Multiple point and area sources.</p> <p>Features: Non-reactive pollutant; includes sedimentation and dry deposition of particulates; flat or complex terrain; seasonal and annual averaging times.</p> <p>Availability: SCRAM website at http://www.epa.gov/scram001.</p>
OCD	<p>OCD (Offshore and Coastal Dispersion Model) is a Gaussian model developed to determine the impact of offshore emissions on the air quality of coastal regions.</p> <p>Type: Gaussian plume model.</p> <p>Source types: Point, area and line sources over water.</p> <p>Features: OCD incorporates over water plume transport</p>

	<p>and dispersion as well as changes that occur as the plume crosses the shoreline.</p> <p>Notes: Hourly meteorological data are needed from both offshore and onshore locations.</p> <p>Availability: SCRAM website at http://www.epa.gov/scram001.</p>
OMEGA/ ADM	<p>OMEGA is a fully functional numerical weather prediction model with an embedded Atmospheric Dispersion Model (ADM). This system can be used to monitor the dispersion of hazardous aerosols and gases, including chemical, biological, and nuclear hazards.</p> <p>Type: Eulerian, Lagrangian particle or Gaussian puff mode may be selected. Transport model is Eulerian grid.</p> <p>Source types: Single source, including evaporation of liquid pools, sublimating solids, explosions, and fires.</p> <p>Features: Complex terrain; regions that are data-sparse; true forecast mode, or in analysis mode to aid in the reconstruction of past events. Databases are available for required input of land/water fraction, vegetation, soil type, land use, soil temperature, sea surface temperature, and soil moisture.</p> <p>Notes: Intended for use with X-Windows/Motif operating system, on a Cray or similar computer. Runtime comparisons available for Cray Y-MP, IBM R/S 6000, SGI Origen 2000 and SUN SPARC-20.</p> <p>Availability: Contact Dr. David P. Bacon, Science Applications International Corporation, 1710 Goodridge Dr., McLean, VA 22102. Email: bacon@apo.saic.com</p>
PAL-DS	<p>PAL-DS is an episodic Gaussian plume model.</p> <p>Type: Gaussian plume model.</p> <p>Source types: Multiple point, area and line sources</p> <p>Features: Dry deposition and sedimentation.</p> <p>Availability: NTIS (National Technical Information Service, U.S. Dept. of Commerce) website: http://www.ntis.gov.</p>
PPSP	<p>PPSP is a Gaussian dispersion model for tall stack sources in either urban or rural areas and essentially flat terrain.</p> <p>Type: Gaussian plume model with boundary layer scaling.</p> <p>Source types: Collocated point sources.</p> <p>Features: Urban or rural; flat terrain; 1-hour to annual averaging times—functionally similar to CRSTER. Differences include daytime stability class based on u/w^*, and use of Briggs dispersion functions.</p> <p>Availability: Power Plant Siting Program, Department of Natural Resources, Tawes State Office Building, Annapolis, MD 21401, Attn: Dr. Michael Hirschfield.</p>

PTPLU	<p>PTPLU is typically used for evaluating the position of the peak ground level concentration that may be computed by automatically testing several tens of combinations of meteorological factors.</p> <p>Type: Gaussian plume model.</p> <p>Source types: Single point source.</p> <p>Features: Flat terrain; non-reactive pollutant. Built in meteorology that it searches to obtain the highest 1-hour concentration.</p> <p>Notes: Use has been largely supplanted by SCREEN3.</p> <p>Availability: NTIS (National Technical Information Service, U.S. Dept. of Commerce) website: http://www.ntis.gov.</p>
RAM	<p>RAM is designed to estimate concentrations due to multiple sources in urban and rural areas.</p> <p>Type: Gaussian plume model.</p> <p>Source types: Point and area sources.</p> <p>Features: Similar to ISCST but lacking some features such as building downwash.</p> <p>Notes: Use has been largely supplanted by ISCST3</p> <p>Availability: SCRAM website at http://www.epa.gov/scram001.</p>
RTDM3.2	<p>RTDM is designed to estimate ground-level concentrations from a single source or multiple co-located sources in rough (complex) terrain.</p> <p>Type: Gaussian plume model.</p> <p>Source types: Single or multiple collocated point sources.</p> <p>Features: Complex terrain.</p> <p>Availability: SCRAM website at http://www.epa.gov/scram001.</p>
SCREEN3	<p>SCREEN3 is a screening version of the ISCST3 model. It calculates maximum concentrations due to a single source.</p> <p>Type: Gaussian plume model.</p> <p>Source types: Single point, area, flare or volume source.</p> <p>Features: Same as ISCST3, except uses built-in array of meteorological conditions and calculates worst case 1-hour average concentrations. Also treats inversion breakup fumigation and shoreline fumigation.</p> <p>Availability: SCRAM website at http://www.epa.gov/scram001.</p>
SDM	<p>SDM (Shoreline Dispersion Model) is designed to calculate the ground-level concentrations from tall stack sources near a shoreline.</p> <p>Type: Gaussian plume model.</p> <p>Source types: Multiple point (tall stack) sources.</p> <p>Features: Treats shoreline fumigation.</p>

	<p>Availability: SCRAM website at http://www.epa.gov/scram001.</p>
SHORTZ	<p>SHORTZ is a short-term steady model for urban and rural areas, and flat and complex terrain.</p> <p>Type: Gaussian plume model.</p> <p>Source types: Multiple point and area sources.</p> <p>Features: Non-reactive pollutant; sedimentation and dry deposition of particulates; 1-hour through 24-hour averaging times;</p> <p>Notes:</p> <p>Availability: SCRAM website at http://www.epa.gov/scram001.</p>
TUPOS	<p>TUPOS is a multiple source Gaussian dispersion algorithm that can use on-site turbulence data.</p> <p>Type: Gaussian plume model.</p> <p>Source types: Point and area sources.</p> <p>Features: TUPOS can accommodate on-site turbulence data; develops vertical wind profile; flat terrain; no deposition.</p> <p>Notes: TUPOS is a refinement of the MPTER model, a predecessor to the ISCST model.</p> <p>Availability: NTIS (National Technical Information Service, U.S. Dept. of Commerce) website: http://www.ntis.gov</p>
VALLEY	<p>VALLEY is a complex terrain screening model.</p> <p>Type: Gaussian (in vertical), sector in horizontal.</p> <p>Source types: Point and area.</p> <p>Features: 24-hour and annual average concentrations; complex terrain.</p> <p>Notes: Model assumes direct plume impact on a hillside is the worst case scenario.</p> <p>Availability: SCRAM website at http://www.epa.gov/scram001.</p>

Table 4. Short-range models that can be purchased for a fee.

Model	Description and sources
ADMS-3	<p>ADMS is an advanced model for calculating concentration and deposition from a variety of source types over a variety of terrain types.</p> <p>Type: Non-Gaussian plume model with boundary layer scaling.</p> <p>Source types: Continuous emissions from point, area, line and volume sources; instantaneous emissions from point sources.</p> <p>Features: Building downwash; complex terrain; wet</p>

	<p>deposition, gravitational settling and dry deposition; chemical reactions; radioactive decay; jets and directional releases; averaging times ranging from seconds to years; plume visibility impact.</p> <p>Notes: ADMS is free in selected circumstances; otherwise there is a cost.</p> <p>Availability: Cambridge Environmental Research Centre (CERC) at http://www.cerc.co.uk/</p>
ADMS-Roads	<p>ADMS-Roads models the air pollution impact of street traffic.</p> <p>Type: Non-Gaussian plume model with boundary layer scaling.</p> <p>Source types: Up to 150 road sources and 7 industrial (point, line, area, volume) sources.</p> <p>Features: Includes street canyon and basic plume chemistry; 1-hour to annual averages.</p> <p>Notes: Charge is made for an annual license.</p> <p>Availability: Cambridge Environmental Research Centre (CERC) at http://www.cerc.co.uk/.</p>
ADMS-Screen	<p>ADMS-Screen is a screening model based on the ADMS-3 dispersion model.</p> <p>Type: Non-Gaussian plume.</p> <p>Source types: Single point (stack) source.</p> <p>Features: Short-term average concentrations for a range of meteorological conditions; long-term average concentrations and two percentiles of a user-specified pollutant.</p> <p>Availability: Cambridge Environmental Research Centre (CERC) at http://www.cerc.co.uk/.</p>
ADMS-Urban	<p>ADMS-Urban is a significant enhancement to ADMS-3, with features of particular value for modeling urban areas, such as calculating emissions from traffic data, accounting for the effects of street canyons on dispersion.</p> <p>Type: Non-Gaussian plume model with boundary layer scaling.</p> <p>Source types: Point, line, area, volume and road sources.</p> <p>Features: Street canyons; complex terrain; building effects; basic NO, NO₂ and ozone chemistry; averaging times from seconds to years.</p> <p>Availability: Cambridge Environmental Research Centre (CERC) at http://www.cerc.co.uk/.</p>
AEROPOL	<p>AEROPOL is a steady-state Gaussian dispersion model, including wet and dry deposition.</p> <p>Type: Gaussian plume model.</p> <p>Source types: Point, line and area sources.</p> <p>Features: Settling, deposition and depletion; building</p>

	<p>effects.</p> <p>Availability: Tartu Observatory, 61602 Toravere, Tartumaa, Estonia. Contact Marko Kaasik.</p>
AVACTA II	<p>AVACTA II is a Gaussian model in which atmospheric dispersion phenomena are described by the evolution of plume elements, either segments or puffs.</p> <p>Type: Gaussian puff; Gaussian plume segment.</p> <p>Source types: Point, area and volume sources.</p> <p>Features: Flat or complex terrain; 1-hour to 24-hour averaging times; intended to run for up to a day's data; first order chemical reactions (primary-to-secondary pollutants); computes 3-D wind fields; first order dry and wet deposition computations; can handle calm conditions.</p> <p>Availability: Dr. Paolo Zannetti, QEP-EnviroComp Consulting, Inc., 2298 Ocaso Camino, Fremont, CA 94539</p>
DISPERSION	<p>The DISPERSION model is an air quality model intended to be used for prediction of air pollutants from industrial and urban sources.</p> <p>Type: Gaussian plume model with boundary layer scaling.</p> <p>Source types: Point, area, line and road traffic.</p> <p>Features: Based on boundary layer scaling; local to urban scale; nested street canyon model; inert pollutants; building effects; NO_x chemistry; includes topography;</p> <p>Availability: Swedish Meteorological and Hydrological Institute (SMHI), S-601 76 Norrkoping, Sweden</p>
IFDM	<p>IFDM (Immission Frequency Distribution Model) is intended for a range of modeling applications including regulatory modeling and environmental impact assessment.</p> <p>Type: Gaussian plume model.</p> <p>Source types: Point and area sources.</p> <p>Features: Dispersion based on a Richardson number approach; inert pollutants; 1-hour and 24-hour average over a year of data; includes dry and wet deposition; flat and gently rolling terrain.</p> <p>Availability: VITO, Boeretang 200, B2400 Mol, Belgium. Contact Guido Cosemans.</p>
MIMO	<p>MIMO (Microscale MOdel) simulates microscale flow and pollutant dispersion in the vicinity of complex building structures.</p> <p>Type: 3-Dimensional prognostic microscale (Eulerian grid) model.</p> <p>Source types: Emissions described for each grid cell.</p> <p>Features: Horizontal resolution is 1m to 10m with domain size from 100m to 5000m; requires profiles of temperature and wind for initialization; building data.</p> <p>Availability: Institut für Technische Thermodynamik,</p>

	Fakultät für Maschinenbau, Universität Karlsruhe, Kaiserstr.12, D-76128 Karlsruhe, Germany.
OML	OML is a modern Gaussian plume model, based on boundary layer scaling instead of relying on Pasquill stability classification. Type: Gaussian plume model with boundary layer scaling. Source types: Point and area sources. Features: Planetary boundary layer scaling; 1-hour average concentrations; essentially flat terrain. Availability: National Environmental Research Institute, P.O. Box 358, DK-4000 Roskilde, Denmark, Att. H.R. Olesen. It belongs to the same class of models as UK-ADMS and HPDM.
OND-86	OND-86 is intended for regulatory use and calculates the 98 th percentile concentration at local and local to regional scales. Type: Non-Gaussian plume model. Source types: Point and area sources. Features: Complex terrain; building downwash; sedimentation of heavy particles; requires special parameters derived from climatological data, which currently exist over the territory of the former USSR. Notes: Consists of analytical formulae for the calculation of 3D concentration fields. Formulae are analytical approximations of the numerical solution of the advection-diffusion equation. Availability: The mathematical model was developed at the Main Geophysical Observatory (MGO) in St. Petersburg, Russia. Computer codes have been developed by several developers, and are available from these developers. The list of the developers of these codes can be obtained from Eugene Genikhovich, Main Geophysical Observatory, 7 Karbysheva Street, 194021, St. Petersburg, Russia.
Simple Line Source	The "Simple Line Source" model is designed to determine concentrations of exhaust gases within 100m of a roadway on relatively flat terrain. Type: Gaussian plume model. Source types: Line (roadway) source. Features: 1-hour (or half-hour) averaging time; uses three stability classes; accounts for traffic-generated turbulence. Availability: Dr. D.P. Chock, Environmental Science Department, General Motors Research Laboratories, General Motors Technical Center, Warren, MI 48090
SYMOS97	SYMOS97 is intended for regulatory modeling of industrial sources.

	<p>Type: Gaussian plume model.</p> <p>Source types: Point, area and line sources.</p> <p>Features: 1-hour concentration to annual average; complex terrain and valley inversions; dispersion from cooling towers;</p> <p>Notes: Uses Bubnik Koldovsky stability classes.</p> <p>Availability: Czech Hydrometeorological Institute, Dpt. of Air Quality Protection, Na Sabatce 17, CZ-146 03 Prague 4, Czech Republic.</p>
WYND-VALLEY	<p>WYNDVALLEY is an Eulerian grid dispersion model useful for modeling valley stagnation episodes.</p> <p>Type: 3-D Eulerian grid model.</p> <p>Source types: Point and area sources.</p> <p>Features: 24-hour averages; includes wet and dry deposition; inert pollutants; uses Monin-Obukhov similarity.</p> <p>Availability: WYNDsoft, Inc., 6333 77th Avenue, SE, Mercer Island, WA 98040.</p>

2 Urban and Regional Photochemical Models

Photochemical models are generally required to model ozone concentrations. These models range from models that account in detail for the complex chemical reactions that account for the creation of ozone from sulfur oxide and nitrogen oxide emissions, to screening models that approximate ozone concentrations very simplistically. The models described in this section are valid from up to a few tens of kilometers downwind, to a few hundreds of kilometers, depending on the model. Most photochemical models are Eulerian grid models or Lagrangian models, although some are puff models. Eulerian grid models are based on a fixed three-dimensional ground-based grid. Pollutant transport and diffusion are calculated by computing how much of the pollutant is transferred to the next grid cell. Lagrangian particle models follow the center of mass of each emission of a given mass of pollutant. These computations can also account for changes in wind and stability as they occur. Puff models treat the plume as a series of overlapping puffs. Each puff is followed mathematically, and can change direction and growth rate as the wind and stability change. These models may be used in combination, where an Eulerian grid model is used to “predict” (between observations) a wind and stability parameters as functions of space and time, which is then provided as input to a puff model, which can predict concentrations in a more computationally-efficient manner.

2.1 Sources of Urban and Regional Photochemical Models

Photochemical models are available, some for free, from both governmental and private sites. Some are available from the EPA SCRAM website. This site also

links to other sites for models that the U.S. EPA accepts on a case-by-case basis as a substitute for a recommended model (see the SCRAM website for details). Models, which are identified as “recommended models” (sometimes called “Appendix A models,” because they were identified Appendix A of earlier editions of the Modeling Guidelines) are available for free, or for a small nominal fee. The “Alternative Models” (sometimes called “Appendix B models,” because they were identified in Appendix B of earlier editions of the Guideline on Air Quality Models) are available, often for a charge.

Table 5. Sources of free (or low cost) urban and regional photochemical models.

Source (website or company)	Available models and data
CAMx website at ENVIRON: http://www.camx.com	CAMx
EPA MODELS-3 website: http://www.epa.gov/asmdnerl/models3	CMAQ
EPA SCRAM website: http://www.epa.gov/scram001	EKMA, OZIPR, RPM-IV, UAM-IV
NTIS (National Technical Information Service, U.S. Dept. of Commerce) website: http://www.ntis.gov	PBM, PEM and all models available from the EPA websites.
UAMV websites http://uamv.saintl.com/	UAM-V

Table 6. Sources of urban and regional photochemical models that can be purchased for a fee

Source (website or company)	Available models and data
Aristotle University Thessaloniki, Laboratory of Heat Transfer and Environmental Engineering, Box 483, 54006 Thessaloniki, GREECE	MARS
Cambridge Environmental Research Centre (UK) http://www.cerc.co.uk/	ADMS-Urban
Earth Tech at the Atmospheric Studies Group, Earth Tech, Concord, MA 01742 (http://www.src.com/)	CALGRID
Finnish Meteorological Institute at Air Quality Research, Sahaajankatu 20 E, FIN-00810 Helsinki, Finland	CAR-FMI
Norwegian Institute for Air Research (NILU), P.O. Box 100, N-2007 Kjeller, Norway	EPISODE
TNO Institute of Environmental Sciences, P.O. Box 3427300 AH Apeldoorn, The Netherlands	CAR-International

Aristotle University Thessaloniki, Laboratory of Heat Transfer and Environmental Engineering, Box 483, 54006 Thessaloniki, GREECE	MUSE
--	------

2.2 Descriptions of Models

Tables 7 and 8 provide descriptions of several urban and regional Photochemical Models. For urban area models not involving photochemistry, see the section on “Short-range Models.”

Table 7. Urban and regional photochemical models available free (or at low cost).

Model	Description and sources
CAMx	<p>CAMx (Comprehensive Air quality Model with extensions) is a publicly available computer modeling system for the integrated assessment of photochemical and particulate air pollution.</p> <p>Type: Multi-scale 3-D Eulerian grid model with plume-in-grid.</p> <p>Source types: Point and area sources.</p> <p>Features: CB-IV and SAPRC97 photochemistry mechanisms available; O₃, NO_x, VOC, CO, primary and secondary PM, SO_x, NH₃; non-reactive mode for inert species; outputs concentrations and dry and wet deposition fluxes; urban to regional scale.</p> <p>Notes: Built on today’s understanding that air quality issues reach beyond the urban scale, CAMx is designed to 1) evaluate the impacts of air pollution over all geographic scales, 2) be computationally efficient and 3) be easy to use.</p> <p>Availability: CAMx website at http://www.camx.com</p>
CMAQ	<p>CMAQ (Community Modeling Air Quality) is a multiscale, one atmosphere model. It is designed to assist the environmental management community's ability to evaluate the impact of air quality management practices for multiple pollutants at multiple scales and equip the scientist's ability to better understand, and simulate chemical and physical interactions in the atmosphere.</p> <p>Type: Eulerian grid model.</p> <p>Source types: Point, line and area sources.</p> <p>Features: Part of the Models-3 system, although it can also be run as a stand-alone model; urban scale to regional scale and larger; O₃, acid deposition, visibility, PM; uses MM5 meteorological model; MEPS emissions processing system;</p> <p>Notes: CMAQ is designed as an open system to allow the use of alternative models (e.g., for emissions, and transport.</p>

	<p>Availability: EPA MODELS-3 website: http://www.epa.gov/asmdnerl/models3</p>
EKMA	<p>EKMA is an empirical, city-specific model that is used to fill the gap between more sophisticated photochemical dispersion models and proportional (rollback) modeling techniques. Type: Semi-empirical. Source types: Gridded emissions. Features: Empirical photochemical model Availability: SCRAM website at http://www.epa.gov/scram001</p>
OZIPR	<p>OZIPR (A one-dimensional photochemical box model) is an alternative version of the OZIP model (see EKMA) that deals with air toxic pollutants. Type: Semi-empirical. Source types: Gridded emissions. Features: Empirical photochemical model. Availability: SCRAM website at http://www.epa.gov/scram001.</p>
PBM	<p>PBM (Photochemical Box Model) is a simple numerical air quality model that simulates photochemical smog at an urban scale. Type: Numerical photochemical box model. Source types: Point, line and area sources. Features: Best suited to treating low wind, sunny conditions; treats NO_x, O₃, hydrocarbons. Notes: The urban area under study is subdivided into cells, within which chemical reactions are computed in particular to evaluate the concentrations of hydrocarbons and ozone. Availability: NTIS (National Technical Information Service, U.S. Dept. of Commerce) website: http://www.ntis.gov.</p>
PEM	<p>PEM (Pollution Episodic Model) has been developed to study urban air pollution problems. Type: Gaussian plume model. Source types: Point and area sources. Features: Deposition; dense gas. Availability: NTIS (National Technical Information Service, U.S. Dept. of Commerce) website: http://www.ntis.gov. PEM can take into account up to 300 point sources and 50 area sources. It simulates the concentrations of two pollutants together both if they are chemically non-reactive and if they are heavy and have a certain deposition.</p>

RPM-IV	<p>RPM-IV (Reactive Plume Model) is a model used for estimating short-term concentrations of primary and secondary pollutants resulting from point or area source emissions.</p> <p>Type: Photochemical model.</p> <p>Source types: Point and area sources.</p> <p>Features: Photochemistry.</p> <p>Availability: SCRAM website at http://www.epa.gov/scram001.</p>
UAM-IV	<p>Urban Airshed Model IV (UAM-IV) is a three-dimensional urban scale, grid simulation model that is designed to compute ozone concentrations for short term episodes of one or two days due to emissions of nitrogen oxides (NO_x), volatile organic compounds (VOCs) and carbon monoxide (CO).</p> <p>Type: 3D Eulerian grid model.</p> <p>Source types: Point and area sources.</p> <p>Features: Urban scale; calculates O₃ from emissions of NO_x, VOCs, CO; designed for short term (1- or 2-day) episode modeling;</p> <p>Availability: SCRAM website at http://www.epa.gov/scram001.</p>
UAM-V	<p>The UAM-V Model is a significant upgrade of the UAM-IV model. UAM-V is a three-dimensional, multi-scale photochemical grid model that calculates concentrations of ozone and its precursors for episodes of up to three days in urban applications and up to two weeks for some regional scale applications.</p> <p>Type: 3-D Eulerian grid photochemical model.</p> <p>Source types: Point and area sources.</p> <p>Features: Multi-scale (urban to regional); calculates concentrations of O₃ and its precursors for episodes of up to 3 days (urban scale applications) or two weeks (some regional scale applications)</p> <p>Notes: An upgrade of UAM-IV; improvements include a variable vertical grid, updated chemical reaction mechanisms and a prognostic meteorological model utilizing four-dimensional data assimilation (which allows use over larger regions), et al.</p> <p>Availability: UAM-V website at http://uamv.saintl.com/.</p>

Table 8. Urban and regional photochemical models that can be purchased for a fee (or if the cost is unknown)

Model	Description and sources
ADMS-Urban	<p>ADMS-Urban is a significant enhancement to ADMS-3, with features of particular value for modeling urban areas, such as calculating emissions from traffic data, accounting for the effects of street canyons on dispersion.</p> <p>Type: Non-Gaussian plume model with boundary layer scaling.</p> <p>Source types: Point, line, area, volume and road sources.</p> <p>Features: Street canyons; complex terrain; building effects; basic NO, NO₂ and ozone chemistry; averaging times from seconds to years.</p> <p>Availability: Cambridge Environmental Research Centre (CERC) at http://www.cerc.co.uk/.</p>
CALGRID	<p>CALGRID (California Grid Model) is a three-dimensional Eulerian photochemical model. Simulation of reactive pollutants dispersion and transformation on mesoscale and on regional scale.</p> <p>Type: 3-D Eulerian grid photochemical model.</p> <p>Source types: Point and area sources.</p> <p>Features: Horizontal advection and diffusion is a finite difference scheme based on cubic spline. Vertical dispersion is based on planetary boundary layer similarity theory. Dry deposition is accounted for.</p> <p>Availability: Earth Tech at the Atmospheric Studies Group, Earth Tech, Concord, MA 01742 (http://www.src.com/) or the California Air Resources Board website at http://www.arb.ca.gov/eos/soft.html.</p>
CAR-FMI	<p>CAR-FMI is a local scale Gaussian model, which evaluates atmospheric dispersion and chemical transformation from a network of line sources.</p> <p>Type: Gaussian plume model.</p> <p>Source types: Line (roadway) sources.</p> <p>Features: Includes chemical transformations for NO, NO₃ and O₃;</p> <p>Notes: The modeling system includes an emission model, a dispersion model, statistical analysis of the computed time series of concentrations and a graphical Windows-based user interface.</p> <p>Availability: Finnish Meteorological Institute at Air Quality Research, Sahaajankatu 20 E, FIN-00810 Helsinki, Finland.</p>

CAR-International	<p>CAR-International, Calculation of Air pollution from Road traffic, International (English language) version, calculates emissions and resulting concentrations due to road traffic.</p> <p>Type: Roadway model.</p> <p>Source types: Line sources (roads).</p> <p>Features: Calculates emissions.</p> <p>Availability: TNO Institute of Environmental Sciences, P.O. Box 3427300 AH Apeldoorn, The Netherlands.</p>
EPISODE	<p>EPISODE is a three-dimensional, combined Eulerian/Lagrangian air quality model that accounts for inert and photochemical pollutant dispersion and dry deposition at local-to-regional scale.</p> <p>Type: Combined Eulerian and Lagrangian photochemical model.</p> <p>Source types: Point, line and area sources.</p> <p>Features: Local to regional scales; handles inert and photochemical pollutants; includes dry and wet deposition; complex terrain.</p> <p>Availability: Norwegian Institute for Air Research (NILU), P.O. Box 100, N-2007 Kjeller, Norway.</p>
MARS	<p>MARS (Model for the Atmospheric Dispersion of Reactive Species) is a 3-D Eulerian model designed to predict photochemical smog formation in urban areas.</p> <p>Type: 3-D Eulerian model.</p> <p>Source types: Gridded emissions.</p> <p>Features: Photochemistry.</p> <p>Availability: Aristotle University Thessaloniki, Laboratory of Heat Transfer and Environmental Engineering, Box 483, 54006 Thessaloniki, GREECE</p>
MUSE	<p>MUSE (Multilayer dispersion model) for photochemical smog formation in urban areas.</p> <p>Type: Photochemical model.</p> <p>Source types: Gridded emissions.</p> <p>Features: Urban scale; includes dry deposition; photochemistry.</p> <p>Availability: Aristotle University Thessaloniki, Laboratory of Heat Transfer and Environmental Engineering, Box 483, 54006 Thessaloniki, GREECE</p>

3 Long-Range Transport Models for Acid Deposition, Visibility Impairment and Complex Terrain

This section includes models that are appropriate for calculating the effects of plume transport over distances from a few kilometers to potentially several hundred kilometers, depending on the model. Many of these models also include the formulation to calculate photochemistry and deposition effects to permit estimates of acid deposition (acid rain) and visibility impairment from fine particulates. These fine particulates are often sulfates and nitrates that result from chemical reactions of the sulfur and nitrogen oxides emitted from combustion sources. Three kinds of models are most commonly included in this category. Puff models treat the plume as a series of overlapping puffs. Each puff is followed mathematically, and can change direction and growth rate as the wind and stability change. Eulerian grid models are based on a fixed three-dimensional ground-based grid. Pollutant transport and diffusion are calculated by computing how much of the pollutant is transferred to the next grid cell. Lagrangian particle models follow the center of mass of each emission of a given mass of pollutant. These computations can also account for changes in wind and stability as they occur. These models may be used in combination, where an Eulerian grid model is used to “predict” (between observations) a wind and stability parameters as functions of space and time, which is then provided as input to a puff model, which can predict concentrations in a more computationally-efficient manner. Depending on the detail included in these models, they may be appropriate not only for long-range transport situations, but also for calculating flow and dispersion in mountains and near shorelines.

3.1 Sources of Long-Range Transport Models

Many long-range transport models are available, some for free, from both governmental and private sites. Some are available from the USEPA SCRAM website. This site also links to other sites for models that the USEPA accepts on a case-by-case basis as a substitute for a recommended model (see the SCRAM website for details). Models, which are identified as “recommended models” (sometimes called “Appendix A models,” because they were identified Appendix A of earlier editions of the Modeling Guidelines) are available for free, or for a small nominal fee. The “Alternative Models” (sometimes called “Appendix B models,” because they were identified in Appendix B of earlier editions of the Guideline on Air Quality Models) are available, often for a fee.

Table 9. Sources of free (or low cost) long-range transport models.

Source (website or company)	Available models and data
EPA SCRAM website: http://www.epa.gov/scram001	MESOPUFF, MTDDIS, PLUVUE-II, REMSAD, VISCREEN
EPA MODELS-3 website: http://www.epa.gov/asmdnerl/models3	CMAQ

NOAA/ARL READY website http://www.arl.noaa.gov/ready/hysplit4.html	HYSPLIT
NTIS (National Technical Information Service, U.S. Dept. of Commerce) website: http://www.ntis.gov	ERT and all models available from the EPA websites.
Earth Tech, CALPUFF site http://www.src.com/calpuff/calpuff1.htm	CALPUFF and associated pre- and post-processors
TITAN Research and Technology http://www.titan.com/appliedtech/Pages/TRT/pages/scipuff/scipuff.htm	SCIPUFF

Table 10. Sources of long-range transport models that can be purchased for a fee.

Source (website or company)	Available models and data
CSIRO Division of Atmospheric Research, PB 1, Aspendale, Victoria 3195, Australia	LADM
Earth Tech at the Atmospheric Studies Group, Earth Tech, Concord, MA 01742 (http://www.src.com/)	CALGRID
Environmental Research Laboratory, Institute of Nuclear Technology and Radiation Protection, National Centre for Scientific Research DEMOKRITOS, 15310 Aghia Paraskevi, Athens Greece http://milos.nrcps.ariadne-t.gr	ADREA, ADREA-HF
Lakes Environmental Software Inc. Ontario, CA, http://www.weblakes.com	CALPUFF View
National Institute of Meteorology and Hydrology, 66 Tzarigradsko chaussee, 1784 Sofia, Bulgaria	EMAP, LED
University of Hamburg, Meteorological Institute at Meteorological Institute, Bundesstr. 55, 20146 Hamburg, Germany	METRAS
YSA Corporation (information on SCRAM website at http://www.epa.gov/scram001)	HOTMAC/RAPTAD,
Transoft US, Inc. (information on SCRAM website at http://www.epa.gov/scram001)	Panache

3.2 Descriptions of Models

Tables 11 and 12 provide descriptions of several available regional and long-range transport models.

Table 11. Long-range transport models available free (or at low cost).

Model	Description and sources
CALPUFF	<p>CALPUFF is a multi-layer, multi-species non-steady-state puff dispersion model that simulates the effects of time- and space-varying meteorological conditions on pollutant transport, transformation and removal.</p> <p>Type: 3-D Lagrangian puff model.</p> <p>Source types: Point and area.</p> <p>Features: Scales from 10s of meters to 100s of kilometers; complex terrain; subgrid scale effects (e.g., terrain impingement); wet and dry deposition; chemical transformation; visibility effects due to fine particulates.</p> <p>Availability: CALPUFF is available from the Earth Tech CALPUFF website at http://www.src.com/calpuff/calpuff1.htm</p>
CMAQ	<p>CMAQ (Community Modeling Air Quality) is a multiscale, one atmosphere model. It is designed to assist the environmental management community's ability to evaluate the impact of air quality management practices for multiple pollutants at multiple scales and equip the scientist's ability to better understand, and simulate chemical and physical interactions in the atmosphere.</p> <p>Type: Eulerian grid model.</p> <p>Source types: Point, line and area sources.</p> <p>Features: Part of the Models-3 system, although it can also be run as a stand-alone model; urban scale to regional scale and larger; O₃, acid deposition, visibility, PM; uses MM5 meteorological model; MEPS emissions processing system;</p> <p>Notes: CMAQ is designed as an open system to allow the use of alternative models (e.g., for emissions, transport, etc.).</p> <p>Availability: EPA MODELS-3 website: http://www.epa.gov/asmdnerl/models3</p>
ERT	<p>ERT (Visibility Model) is a Gaussian dispersion model designed to estimate visibility impairment for arbitrary lines of sight due to isolated point source.</p> <p>Type: Gaussian plume model.</p> <p>Source types: Isolated point source.</p> <p>Features: Visibility impairment calculations for arbitrary lines of sight; includes gas to particle chemical conversion,</p>

	<p>dry deposition, NO to NO₂ conversion, and linear radiative transfer in its computations.</p> <p>Availability: NTIS (http://www.ntis.gov).</p>
HYSPLIT	<p>The HYSPLIT (HYbrid Single-Particle Lagrangian Integrated Trajectory) model is a complete system for simulating long-range transport, dispersion and deposition of pollutants.</p> <p>Type: Hybrid single particle Lagrangian integrated trajectory model.</p> <p>Source types: Point, vertical line and gridded emission sources.</p> <p>Features: The model supports a wide range of modeling applications including accidental radiological releases, volcanic ash eruptions as well as routine air quality assessments.</p> <p>Notes: The model can be run interactively on the Web on the READY website or the code executable and meteorological data can be downloaded to a Win95/98/NT PC.</p> <p>Availability: NOAA READY website at http://www.arl.noaa.gov/ready/hysplit4.html.</p>
MESOPUFF-II	<p>MESOPUFF II is a short term, regional scale puff model designed to calculate concentrations of up to 5 pollutant species (SO₂, SO₄, NO_x, HNO₃, NO₃).</p> <p>Type: Puff model.</p> <p>Source types: Point and area sources.</p> <p>Features: Regional scale; calculates concentrations for one or more of: SO₂, SO₄, NO_x, HNO₃, NO₃; chemical transformation, and wet and dry deposition are accounted for;</p> <p>Availability: SCRAM website at http://www.epa.gov/scram001.</p>
MTDDIS	<p>MTDDIS (<u>M</u>esoscale <u>T</u>ransport <u>D</u>iffusion and <u>D</u>eposition <u>M</u>odel for <u>I</u>ndustrial <u>S</u>ources) is a variable-trajectory Gaussian puff model applicable to long-range transport at point source emissions over level or rolling terrain.</p> <p>Type: Gaussian puff model.</p> <p>Source types: Point sources.</p> <p>Features: Long-range transport; variable trajectory; 3-hour and 24-hour averaging times; inert pollutants; level or rolling terrain.</p> <p>Availability: Environmental Modeling & Analysis. See the SCRAM website at http://www.epa.gov/scram001 for details.</p>

PLUVUE-II	<p>PLUVUE-II is a model used for estimating visual range reduction and atmospheric discoloration caused by plumes resulting from the emissions of particles, nitrogen oxides, and sulfur oxides from a single source.</p> <p>Type: Gaussian plume model.</p> <p>Source types: Point and area sources.</p> <p>Features: Includes chemical reactions; optical effects; surface deposition.</p> <p>Availability: SCRAM website at http://www.epa.gov/scram001.</p>
REMSAD	<p>REMSAD (Regional Modeling System for Aerosols and Deposition) is a three dimensional grid model designed to calculate concentrations of both inert and chemically reactive pollutants by simulating the physical and chemical processes in the atmosphere that affect pollutant concentrations.</p> <p>Type: 3-D Eulerian grid model.</p> <p>Source types: Elevated stack sources and gridded (all low level sources are gridded).</p> <p>Features: Urban to continental scales; inert and chemically reactive pollutants; wet and dry deposition; mercury chemistry; secondary organic aerosols.</p> <p>Availability: SCRAM website at http://www.epa.gov/scram001.</p>
SCIPUFF	<p>SCIPUFF is a Lagrangian puff dispersion model that uses a collection of Gaussian puffs to represent an arbitrary, three-dimensional, time-dependent concentration field.</p> <p>Type: Lagrangian puff model.</p> <p>Source types: Continuous, instantaneous, moving and stack sources.</p> <p>Features: Flat and complex terrain; dry and wet deposition; gravitational settling of particles; linear decay; short and long range transport; estimates of uncertainty.</p> <p>Availability: Titan Research and Technology SCIPUFF website at http://www.titan.com/appliedtech/Pages/TRT/pages/scipuff/scipuff.htm</p>
VISCREEN	<p>VISCREEN is a visibility screening model that calculates the potential impact of a plume of specified emissions for specific transport and dispersion conditions.</p> <p>Type: Gaussian plume model.</p> <p>Source types: Single point source.</p> <p>Features: Visibility impairment.</p> <p>Availability: SCRAM website at http://www.epa.gov/scram001.</p>

Table 12. Long-range transport models that can be purchased for a fee.

Model	Description and sources
ADREA-D	<p>ADREA-D is an Eulerian dispersion model for describing the dispersion of inert and radioactive pollutants over complex topography.</p> <p>Type: Eulerian grid model.</p> <p>Source types: Point and area sources.</p> <p>Features: Inert and radioactive pollutants; scavenging and wet deposition; multiple pollutants.</p> <p>Availability: NCSR "Demokritos" Institute of Nuclear Technology and Radiation Protection, Attiki, Greece.</p>
ADREA-HF	<p>ADREA-HF is a three-dimensional time dependent model applicable to complex terrain.</p> <p>Type: Eulerian grid model.</p> <p>Source types: Point and area sources.</p> <p>Features: Complex terrain; liquid-gas phase transitions;</p> <p>Availability: Information available at http://milos.nrcps.ariadne-t.gr. ADREA-HF is available from NCSR "Demokritos" Institute of Nuclear Technology and Radiation Protection, Attiki, Greece.</p>
CALGRID	<p>CALGRID (California Grid Model) is a three-dimensional Eulerian photochemical model.</p> <p>Type: 3-D Eulerian grid model.</p> <p>Source types: Point and area sources.</p> <p>Features: Reactive pollutant dispersion and transformation; mesoscale and regional scale; Vertical dispersion is based on planetary boundary layer similarity theory. Dry deposition is accounted for.</p> <p>Availability: Earth Tech at the Atmospheric Studies Group, Earth Tech, Concord, MA 01742 (http://www.src.com/) or the California Air Resources Board website at http://www.arb.ca.gov/eos/soft.html.</p>
CALPUFF View	<p>CALPUFF View is a GIS-based front and back end interface to CALMET, CALPUFF, CALPOST, and supporting pre-processors. CALPUFF is a multi-layer, multi-species non-steady-state puff dispersion model that simulates the effects of time- and space-varying meteorological conditions on visibility, pollutant transport, transformation and removal.</p> <p>Type: 3-D Lagrangian puff model.</p> <p>Source types: Point and area.</p> <p>Features: Scales from 10s of meters to 100s of kilometers; complex terrain; subgrid scale effects (e.g., terrain impingement); wet and dry deposition; chemical transformation; visibility effects due to fine particulates.</p>

	<p>Availability: CALPUFF View is available from the Lakes Environmental Software website at http://www.weblakes.com</p>
EMAP	<p>EMAP (Eulerian Model for Air Pollution) is a three-dimensional, Eulerian model that can model multiple pollutants.</p> <p>Type: 3-D Eulerian grid model.</p> <p>Source types: Point sources.</p> <p>Features: Includes wet and dry deposition; gravitational settling; simple chemical transformation.</p> <p>Availability: National Institute of Meteorology and Hydrology, 66 Tzarigradsko chaussee, 1784 Sofia, Bulgaria.</p>
HOTMAC/ RAPTAD	<p>HOTMAC is a 3-dimensional Eulerian model for weather forecasting; RAPTAD is a 3-dimensional Lagrangian random puff model for pollutant transport and diffusion. These models are used for prediction of transport and diffusion processes over complex terrain where conventional models fail.</p> <p>Type: HOTMAC: 3-D Eulerian model (meteorology); RAPTAD: 3-D Lagrangian random walk puff model (transport and diffusion).</p> <p>Source types: Point sources.</p> <p>Features: Complex terrain.</p> <p>Availability: YSA Corporation. See SCRAM website at http://www.epa.gov/scram001/ for details.</p>
LADM	<p>LADM (Lagrangian Atmospheric Dispersion Model) is applicable to air quality studies that involve simple to very rugged terrain, time-varying conditions such as the diurnal cycle, and the interaction of complex wind flows such as sea breezes and drainage winds.</p> <p>Type: 3-D prognostic (Eulerian) meteorological model coupled with a Lagrangian random walk particle dispersion model.</p> <p>Source types: Point and area sources.</p> <p>Features: Scale from hundreds of meters to a few hundred kilometers; complex terrain; non-steady state conditions; complex wind flows such as sea breezes and drainage winds;</p> <p>Availability: CSIRO Division of Atmospheric Research, PB 1, Aspendale, Victoria 3195, Australia.</p>
LED	<p>LED (Lagrangian-Eulerian Diffusion) model is a Lagrangian puff model with Eulerian dispersion of puffs.</p> <p>Type: Lagrangian puff model with Eulerian dispersion of puffs.</p> <p>Source types: Point sources.</p>

	<p>Features: Local-to-regional and regional-to-continental scale The model accounts for chemical (radioactive) transformations, dry and wet deposition, and acid rain.</p> <p>Availability: National Institute of Meteorology and Hydrology, 66 Tzarigradsko chaussee, 1784 Sofia, Bulgaria.</p>
METRAS	<p>METRAS is a 2D and 3D nonhydrostatic Eulerian mesoscale transport, chemistry and fluid model that models Atmospheric flows in mesoscale gamma and beta range, wind, temperature and humidity fields over complex terrain, studies on mesoscale effects, transport of air pollutants, chemical reactions, deposition of species, atmospheric inputs to coastal waters, tidal effects on atmospheric phenomena.</p> <p>Type: 2-D and 3-D nonhydrostatic Eulerian grid model.</p> <p>Source types: Point sources.</p> <p>Features: Mesoscale range; treats complex terrain; chemical reactions; deposition.</p> <p>Availability: University of Hamburg, Meteorological Institute at Meteorological Institute, Bundesstr. 55, 20146 Hamburg, Germany.</p>
Panache	<p>Panache is an Eulerian (and Lagrangian for particulate matter), 3-dimensionl finite volume fluid mechanics code designed to simulate continuous and short-term pollutant dispersion in the atmosphere, in simple or complex terrain.</p> <p>Type: 3-D Eulerian grid model (Lagrangian model for particulate matter).</p> <p>Source types: Point sources.</p> <p>Features: Simulates continuous and short-term emissions; simple or complex terrain.</p> <p>Availability: Transoft, US, Inc. See the SCRAM website http://www.epa.gov/scram001/ for details.</p>

4 Emergency Release and Dense Gas Models

This category includes both emergency release models and dense gas models. Dense gas releases are generally emergency releases (e.g., tank truck accident or railroad accident), so it is reasonable to group these models together. In addition to transportation accidents, emergency releases also include rupture of storage tanks, pipelines or valves, evaporation from a toxic liquid spill, or a fire in a building containing toxic substances.

4.1 Sources of Emergency Release and Dense Gas Models

Many emergency release models and dense gas models are available without charge from government sources. In addition, some are available from commercial sources. Virtually all such models can be run on either a PC or a Macintosh, or both. In many cases, these models are specifically designed to be used in the field near the site of the release. Table 13 lists models available free or at minimal cost, while Table 14 lists models for which a fee is charged. Brief descriptions of the models are provided in Tables 15 and 16, respectively.

Table 13. Sources of free (or low cost) emergency release and dense gas models.

Source (website or company)	Available models and data
Alpha-TRAC, Incorporated. Contact C. Reed Hodgin, President, Alpha-TRAC, Incorporated, Sheridan Park 8, Suite 120, 8670 Wolff Court, Westminster, Colorado, 80030-3692. e-mail: Alphatrac@eazy.net	TRAC
Atmospheric Environment Service, Canada. Contact Dr. Sam M. Daggupaty, Atmospheric Environmental Service, 4905 Dufferin Street, Downsview, Ontario, Canada M3H 5T4. Email sam.daggupaty@tor.ec.gc.ca	PC-AQPAC
CAMEO website at http://www.epa.gov/swercepp/cameo/ .	ALOHA
Defense Special Weapons Agency. Contact David B. Myers DSWA/WEL 6801 Telegraph Road Alexandria, VA 22310. Email: myersd@hq.dswa.mil	HPAC
Lawrence Livermore National Laboratory. Livermore, CA 94551.	ARAC (MATHEW/ADPIC) (Contact: Hoyt Walker, Mail Code L-103, email walker7@llnl.gov), FEM3C (Contact: Diana L. West, Mail Code L-795, Phone (510) 423-8030), HOTSPOT (Contact: Steven G. Homann, Mail Code L-380, Email shomann@llnl.gov .)
Ministry of the Environment, Ontario, Canada. Contact Dr. Robert Bloxam, Science & Technology Branch, 2 St. Clair Ave. W. Floor 12A, Toronto, Ontario M4V 1L5. Telephone (416) 323-5073.	EMGRES

NTIS (National Technical Information Service, U.S. Dept. of Commerce) website: http://www.ntis.gov	HGSYSTEM and all models available from the EPA websites.
NOAA Air Resources Laboratory. Contact Will R. Pendergrass, NOAA ARL/ATDD, P.O. Box 2456, 456 South Illinois Avenue, Oak Ridge, TN 37831. Phone (423) 576-6234	HARM-II
NOAA Atmospheric Turbulence and Diffusion Division. Contact K. Shankar Rao, NOAA/ATDD, P.O. Box 2456, Oak Ridge, TN 37831. Email: eao@atdd.noaa.gov	TRIAD 2-1
Sandia National Laboratory. Contact Bruce Boughton, Sandia National Laboratory, Albuquerque, New Mexico 87185. Phone (505) 844-8545	ERAD
Savannah River Technology Center. Contact Robert J. Kurzeja, Savannah River Technology Center, P.O. Box 616, Aiken, SC 29808. E-mail: Robert.Kurzeja@SRS.gov	PUFF-PLUME
SCRAM website: http://www.epa.gov/scram001	ADAM, AFTOX, DEGADIS, OBODM, SLAB, TSCREEN
Universität Hamburg. Contact Dr. Michael Schatzmann, Meteorologisches Institut, Universität Hamburg, Bundesstrasse 55, D-20146 Hamburg, Germany. Phone 49-40-41235090; 49-40-41173350 (Fax)	VDI

Table 14. Sources of emergency release and dense gas models that can be purchased for a fee.

Source (website or company)	Available models and data
ATM-PRO – Atmospheric Transport Models for Professional Applications http://www.atmpro.be and Lakes Environmental Software Inc. http://www.weblakes.com	SEVEX View
Cambridge Environmental Research Centre (UK) http://www.cerc.co.uk/	GASTAR
Electricite de France, Direction des Etudes et Recherches, 6 Quai Watier, 78401 Chatou Cedex, France	MERCURE

Finnish Meteorological Institute, Air Quality Research, Sahaajankatu 20 E, FIN-00810 Helsinki, Finland	BUO-FMI
Geophysical Institute of the Slovak Academy of Sciences, Dubravska cesta 9, 842 28 Bratislava, Slovakia	AUTOMOD
Istituto di Cosmogeofisica, Consiglio Nazionale delle Ricerche, Corso Fiume, 4, I-10133 Torino, Italy	MILFORD
National Institute of Meteorology and Hydrology. Contact Dr. Ion Sandu, Laboratory of Atmospheric Physics, National Institute of Meteorology and Hydrology, Sos Bucuresti-Ploiesti 97, 71552 Bucharest, Romania	INPUFF-U
National Centre for Scientific Research DEMOKRITOS. Contact Alexander G. Venetsanos, Environmental Research Laboratory, Institute of Nuclear Technology and Radiation Protection, National Centre for Scientific Research DEMOKRITOS, 15310 Aghia Paraskevi, Athens Greece	DISPLAY-2

4.2 Descriptions of Models

Tables 15 and 16 provide descriptions of several available emergency release models and dense gas models.

Table 15. Emergency release and dense gas models available free (or at low cost).

Model	Description and sources
ADAM	<p>ADAM (Air Force Dispersion Assessment Model) is designed to calculate concentrations due to accidental releases of Chlorine, Fluorine, nitrogen tetroxide, hydrogen sulfide, hydrogen fluoride, sulfur dioxide, phosgene and ammonia.</p> <p>Type: Modified box & Gaussian plume model.</p> <p>Source types: Area and point; continuous and instantaneous; pressurized and unpressurized; gas and liquid phases.</p> <p>Features: Includes thermodynamics, chemistry, heat transfer, aerosol loading and dense gas effects; gas/liquid phase changes and chemical reactions for the eight specified pollutants.</p>

	<p>Notes: Passive dispersion treatment is equivalent of the AFTOX model.</p> <p>Availability: SCRAM website at http://www.epa.gov/scram001.</p>
AFTOX	<p>AFTOX (Air Force Toxics Model) is intended to model accidental releases of gases or evaporating liquids.</p> <p>Type: Gaussian plume model.</p> <p>Source types: Point and area sources.</p> <p>Features: Continuous or instantaneous emissions; elevated or surface releases; calculates evaporation rate from liquid spills;</p> <p>Availability: SCRAM website at http://www.epa.gov/scram001.</p>
ALOHA	<p>ALOHA (Areal Locations of Hazardous Atmospheres) is used for evaluating the release of hazardous chemical vapors. It is intended for rapid deployment by responders as well as for use in emergency preplanning.</p> <p>Type: Gaussian puff and plume model, and dense gas dispersion.</p> <p>Source types: Evaporation from puddles, release of liquid or pressurized or non-pressurized gas from a storage vessel, release of pressurized gas from a pipeline.</p> <p>Features: Includes chemical properties of over 700 chemicals. Models non-reactive pollutants only. Can produce a “foot-print” plot showing where concentrations are calculated to exceed a threshold set by the user.</p> <p>Notes: ALOHA is the atmospheric dispersion model module of the CAMEO system (Computer-Aided Management of Emergency Operations). ALOHA accesses an extensive chemical property library contained in the CAMEO system.</p> <p>Availability: ALOHA (or the entire CAMEO system) is available from the CAMEO website at http://www.epa.gov/swercepp/cameo/.</p>
ARAC	<p>The ARAC models can be used to make both real-time responses as well as assessments of radiological or chemical releases using sequential time-varying meteorological and source term inputs.</p> <p>Type: Particle-in-Cell dispersion.</p> <p>Source types: Point, area, line and volume sources.</p> <p>Features: The diagnostic models are applicable to all mesoscale meteorological and topographic settings (domain of a few km to thousands of km). The ARAC Model Set consists of six codes which are 1) topographic grid generation code, 2) meteorological data interpolation code, 3) conjugate-gradient mass-adjusted three-dimensional wind field, 4) atmospheric dispersion by particle-in-cell, a</p>

	<p>graphical contour plot generator, and 5) a time history statistical analysis of output values at individual receptors with optional comparison with measurement data.</p> <p>Notes: MATHEW/ADPIC are the core codes for the DOE Atmospheric Release Advisory Capability (ARAC) program at Lawrence Livermore National Laboratory.</p> <p>Availability: Lawrence Livermore National Laboratory. Contact Hoyt Walker, LLNL Mail Code L-103, P.O. Box 808, Livermore, CA 94551-0808. Email walker7@llnl.gov.</p>
DEGADIS	<p>DEGADIS (Dense Gas Dispersion Model) is designed to simulate dispersion of dense gases over flat, level terrain. simulates the atmospheric dispersion at ground-level, area source dense gas (or aerosol) clouds released with zero momentum into the atmospheric boundary layer over flat, level terrain.</p> <p>Type: Dense gas model.</p> <p>Source types: Area source of dense gas.</p> <p>Features: Flat level terrain; accounts for gravity-driven flow and entrainment of the gas into the boundary layer.</p> <p>Availability: SCRAM website at http://www.epa.gov/scram001.</p>
EMGRES	<p>EMGRES is a PC-based emergency response tool in the event of a release of a hazardous chemical.</p> <p>Type: For continuous release, Gaussian plume model; for instantaneous non-dense gas, instantaneous puff model; for dense gas, dense gas box model.</p> <p>Source types: Point and area source (gas release from reservoir, liquid release from a vessel, liquid pool evaporation).</p> <p>Features: The program provides hazardous contaminant information, calculates toxic concentrations at various distances downwind of a release, and displays the information on the screen compared to threshold exposure levels such as the Threshold Limit Values (TLV), Short Term Exposure Limits (STEL), and Immediately Dangerous to Life and Health (IDLH). Finally, in the event the release possesses combustible properties, the code gives an estimate of the mass of vapor within the flammable limits.</p> <p>Notes: source term and dispersion screening tool designed for obtaining downwind distances to select levels of concern with a minimum of user input and computational expense.</p> <p>Availability: EMGRES is available from the Canadian Ministry of the Environment. Contact Dr. Robert Bloxam, Science & Technology Branch, 2 St. Clair Ave. W. Floor 12A, Toronto, Ontario M4V 1L5. Telephone (416) 323-5073.</p>

ERAD	<p>The Explosive Release Atmospheric Dispersion (ERAD) was developed to provide</p> <p>Type: 3-D simulation of particle dispersion.</p> <p>Source types: Explosive release.</p> <p>Features: real-time predictions of the near-field concentrations resulting from an explosive release of hazardous material.</p> <p>Availability: Sandia National Laboratory. Contact Bruce Boughton, Sandia National Laboratory, Albuquerque, New Mexico 87185. Phone (505)844-8545.</p>
FEM3C	<p>FEM3C is a three-dimensional finite element model designed to simulate the atmospheric dispersion of heavier-than-air gas (dense gas) release. The code may be applied to the release of an inert gas or an atmospheric pollutant in the form of vapor/droplets.</p> <p>Type: 3-D finite element model.</p> <p>Source types: Dense gas release.</p> <p>Features: Simulates dense gas release; can be applied to release of inert gas or a pollutant in the form of vapor or droplets.</p> <p>Availability: Lawrence Livermore National Laboratory. Contact Diana L. West, L-795, Technology Transfer Initiative Program, Lawrence Livermore National Laboratory, Livermore, CA 94551. Phone (510) 423-8030.</p>
HARM-II	<p>HARM-II is an interactive dose assessment model designed to predict consequences of accidental releases of hazardous materials, either chemical or radioactive.</p> <p>Type: Dense gas and standard diffusion model.</p> <p>Source types: Accidental release.</p> <p>Features: The model combines both passive and heavy gas codes for chemical spills, as well as standard transport and diffusion codes for radionuclide releases. Reactive chemistry is considered for those chemicals with exothermic reaction characteristics. The calculations are performed on a scale of 10 meters to 30 kilometers.</p> <p>Availability: NOAA Air Resources Laboratory. Contact Will R. Pendergrass, NOAA ARL/ATDD, P.O. Box 2456, 456 South Illinois Avenue, Oak Ridge, TN 37831. Phone (423) 576-6234.</p>
HGSYSTEM	<p>HGSYSTEM is a collection of computer programs designed to predict the source-term and subsequent dispersion of accidental chemical releases with an emphasis on denser-than-air (dense gas) behavior.</p> <p>Type: Contains various model types.</p> <p>Source types: A wide range of accidental release scenarios.</p> <p>Features: Includes treatment of complex thermodynamic</p>

	<p>behavior for some chemical species; time averaging and dosage calculations; dense gas; terrain with varying surface roughness; aerosol effects on cloud density.</p> <p>Availability: Contact Shell Research and Technology Centre ORNL, Doug Lombardi Thornton, P.O. Box 1 Bethel Valley Rd., Chester, CH1 3SH Oak Ridge, TN 37831-6200. Also order from NTIS, Order Number PB96-501960.</p>
HOTSPOT	<p>HOTSPOT provides a fast, field-portable calculation tool for evaluating accidents involving radioactive materials.</p> <p>Type: Contains four models for treating plume/puff dispersion, explosion, fuel fire and resuspension of radionuclides from a contaminated area.</p> <p>Source types: Continuous or instantaneous release, explosion, fuel fire and area resuspension of radionuclides.</p> <p>Features: Includes capability to assess effects of releases of radionuclides, including expected dosage due to inhalation.</p> <p>Availability: Lawrence Livermore National Laboratory. Contact Steven G. Homann, Lawrence Livermore National Laboratory, 7000 East Avenue L-380, Livermore, CA 94551. Email: shomann@llnl.gov.</p>
HPAC	<p>HPAC is intended to assess nuclear, chemical and biological hazards from facilities, weapons, accidents, et al. atmospheric dispersion of vapors, particles, or liquid droplets from multiple sources, using arbitrary meteorological input ranging from a single surface wind speed and direction up to 4-dimensional gridded wind and temperature field input.</p> <p>Type: Second order closure Lagrangian puff model (SCIPUFF is the dispersion component)</p> <p>Source types: Multiple sources of hazardous releases of hazardous materials.</p> <p>Features: Plume rise and dense gas effects; time- and space varying boundary layers; complex terrain; includes 3-D concentration field, integrated inhalation dosage and surface deposition; droplet evaporation.</p> <p>Notes: The dispersion model component of HPAC is SCIPUFF, which is described in Table 11.</p> <p>Availability: Defense Special Weapons Agency. Contact David B. Myers, DSWA/WEL, 6801 Telegraph Road, Alexandria, VA 22310. Email: myersd@hq.dswa.mil</p>
OBODM	<p>OBODM (Open Burn/Open Detonation Model) is intended for use in evaluating the potential air quality impacts of the open burning and detonation (OB/OD) of obsolete munitions and solid propellants.</p> <p>Type: Open burning, detonation.</p> <p>Source types: Instantaneous (detonation) or quasi-</p>

	<p>continuous (open burning) releases from multiple point, volume and line sources.</p> <p>Features: High and high-second high output for range of averaging times; cloud/plume rise dispersion, and deposition algorithms taken from existing models to predict the downwind transport and dispersion of pollutants.</p> <p>Availability: SCRAM website at http://www.epa.gov/scram001.</p>
PC-AQPAC	<p>PC-AQPAC is a personal computer version of the Air Quality PACKage. This model is designed for field use in emergency responses to accidental releases of hazardous substances into the atmosphere.</p> <p>Type: Gaussian puff, Gaussian plume and dense gas models.</p> <p>Source types: Emergency releases and spills.</p> <p>Features: The system predicts the following four hazard zones for potential evacuation: LFL (Lower Flammability Limit), IDHL (Immediately Dangerous to Life or Health), STEL (Short Term Exposure Limit) and TLV (Threshold Limit Value).</p> <p>Availability: Dr. Sam M. Daggupaty, Atmospheric Environmental Service, 4905 Dufferin Street, Downsview, Ontario, Canada M3H 5T4. Email sam.daggupaty@tor.ec.gc.ca</p>
PUFF-PLUME	<p>PUFF-PLUME is one of a suite of codes for atmospheric releases and is used primarily for preliminary estimates in emergency situations.</p> <p>Type: Gaussian plume and plume model.</p> <p>Source types: Emergency releases.</p> <p>Features: Chemical and radonuclide diffusion; wet and dry deposition; dose estimates from inhalation and gamma shine</p> <p>Notes: It is the primary model for emergency response use for atmospheric releases at the Savannah River Site.</p> <p>Availability: Savannah River Technology Center. Contact Robert J. Kurzeja, Savannah River Technology Center, P.O. Box 616, Aiken, SC 29808. E-mail: Robert.Kurzeja@SRS.gov</p>
SLAB	<p>SLAB is a dense gas model.</p> <p>Type: Dense gas model.</p> <p>Source types: Ground level and elevated jets, liquid pool evaporation, instantaneous volume source.</p> <p>Features: The SLAB model treats denser-than-air releases by solving the one-dimensional equations of momentum, conservation of mass, species, and energy, and the equation of state.</p> <p>Availability: SCRAM website at http://www.epa.gov/scram001.</p>

TRAC	<p>TRAC (Terrain Responsive Atmospheric Code) addresses risk assessments and hazard assessments in complex terrain.</p> <p>Type: 3-D Lagrangian complex terrain dispersion model</p> <p>Source types: Releases of radiological particles and gases.</p> <p>Features: Treats plume transport and diffusion in complex terrain fields; develops 3-D time-and-space-varying meteorological fields, including winds, releases simulated puffs of material into the flow.</p> <p>Availability: Contact C. Reed Hodgkin, President, Alpha-TRAC, Incorporated, Sheridan Park 8, Suite 120, 8670 Wolff Court, Westminster, Colorado, 80030-3692. e-mail: Alphatrac@eazy.net</p>
TRIAD 2-1	<p>TRIAD is a multiple-source, Gaussian-puff dispersion model capable of modeling the accidental release of instantaneously reactive gas to the atmosphere.</p> <p>Type: Gaussian puff model.</p> <p>Source types: Multiple source accidental release, including multiple moving sources.</p> <p>Features: Release of reactive gas (currently only uranium hexafluoride is included); dry deposition; wind field interpolation from multiple towers;</p> <p>Availability: NOAA Atmospheric Turbulence and Diffusion Division. Contact K. Shankar Rao, NOAA/ATDD, P.O. Box 2456, Oak Ridge, TN 37831. Email: eao@atdd.noaa.gov</p>
TSCREEN	<p>TSCREEN (Toxics Screening) a Gaussian screening model that implements the procedures to correctly analyze toxic emissions and their subsequent dispersion from one of many different types of possible releases for superfund sites.</p> <p>Type: Gaussian plume model.</p> <p>Source types: Several, including point, volume and area.</p> <p>Features: Contains three models: SCREEN3, PUFF, and RVD (Relief Valve Discharge).</p> <p>Availability: SCRAM website at http://www.epa.gov/scram001.</p>
VDI	<p>VDI Parts 1 and 2 are individual computer programs designed to model the dispersion of vapor plumes (positively and neutrally buoyant), and denser-than-air vapor releases, respectively.</p> <p>Type: Gaussian plume model and an empirically-derived dense gas model.</p> <p>Source types: Point, line, area and volume sources.</p> <p>Features: Part 1—vapor plumes (buoyant and neutral), concentration and dose exposure. Part 2—dense gas release, calculates distance to LFL (lower flammability limit), distance to where it behaves as a neutrally buoyant plume.</p>

	<p>The dense gas model can account for obstacles to flow.</p> <p>Notes: Parts may be run separately or in combination.</p> <p>Availability: Universität Hamburg. Contact Dr. Michael Schatzmann, Meteorologisches Institut, Universität Hamburg, Bundesstrasse 55, D-20146 Hamburg, Germany. Phone 49-40-41235090; 49-40-41173350 (Fax)</p>
--	---

Table 16. Emergency release and dense gas models that can be purchased for a fee.

Model	Description and sources
AUTOMOD	<p>AUTOMOD calculates concentrations due to pollutants emitted from automobile traffic in an urban area.</p> <p>Type: Roadway model.</p> <p>Source types: Automobile traffic.</p> <p>Features: Accounts for street canyons.</p> <p>Availability: Contact Ferdinand Heseck at the Geophysical Institute of the Slovak Academy of Sciences, Dubravska cesta 9, 842 28 Bratislava, Slovakia, regarding availability.</p>
BUO-FMI	<p>BUO-FMI treats fires of warehouses and chemical storage.</p> <p>Type: Combination of Gaussian plume and gradient transfer (K-theory).</p> <p>Source types: Warehouse and chemical storage fires.</p> <p>Features: Uses planetary boundary layer scaling; includes dry deposition; assumes passive plume.</p> <p>Availability: Finnish Meteorological Institute, Air Quality Research, Sahaajankatu 20 E, FIN-00810 Helsinki, Finland.</p>
DISPLAY-2	<p>DISPLAY-2 calculates vapour cloud dispersion in complex terrain, including two-phase releases.</p> <p>Type: 2-D shallow layer numerical model based on ADREA-HF.</p> <p>Source types: Jet releases, instantaneous releases.</p> <p>Features: Complex terrain, with obstacles as needed; two-phase releases.</p> <p>Availability: Alexander G. Venetsanos, Environmental Research Laboratory, Institute of Nuclear Technology and Radiation Protection, National Centre for Scientific Research DEMOKRITOS, 15310 Aghia Paraskevi, Athens Greece; or Jorgen Wurtz, Institute for Systems Informatics and Safety, Joint Research Centre ISPRA, I-21020 Ispra (VA) Italy.</p>
GASTAR	<p>GASTAR is a dense gas model that models the pollutant cloud from its initial state as a dense gas to the passive state.</p> <p>Type: Dense gas model.</p> <p>Source types: Puffs; plumes; transient releases, including two-phase jet source and pools.</p>

	<p>Features: Two-phase release; effects of slopes and obstacles downwind.</p> <p>Availability: Cambridge Environmental Research Centre (UK) http://www.cerc.co.uk/.</p>
INPUFF-U	<p>INPUFF-U is a Lagrangian puff dispersion model of local to urban scale, capable of simulating accidental or continuous release for both stationary and moving point sources over a spatially and temporally variable wind field.</p> <p>Type: Lagrangian puff.</p> <p>Source types: Stationary or moving point source, instantaneous or continuous release.</p> <p>Features: Includes for different puff dispersion—Pasquill-Gifford, “on-line,” OML and “long travel time.” Includes dry and wet deposition, gravitational settling and radioactive decay. Assumes vertically uniform wind field.</p> <p>Availability: Dr. Ion Sandu, Laboratory of Atmospheric Physics, National Institute of Meteorology and Hydrology, Sos Bucuresti-Ploiesti 97, 71552 Bucharest, Romania</p>
MERCURE	<p>MERCURE is an atmospheric version of a general purpose CFD core code, named ESTET, developed by the Laboratoire National d'Hydraulique in France.</p> <p>Type: 3-D CFD (computational fluid dynamics) model.</p> <p>Source types: Individual sources and gridded emissions.</p> <p>Features: Instantaneous and continuous releases of heavy gases; mountain waves in stable atmosphere; land-sea breeze; local to urban scales.</p> <p>Availability: Electricite de France, Direction des Etudes et Recherches, 6 Quai Watier, 78401 Chatou Cedex, France.</p>
MILFORD	<p>MILORD is a long-range Lagrangian particle model that simulates transport, dispersion and deposition (radioactive decay or first order chemical reactions are included) of tracers or accidental releases.</p> <p>Type: Lagrangian particle model.</p> <p>Source types: Tracers and accidental releases.</p> <p>Features: Includes deposition, radioactive decay (i.e., first order reactions).</p> <p>Availability: Istituto di Cosmogeofisica, Consiglio Nazionale delle Ricerche, Corso Fiume, 4, I-10133 Torino, Italy.</p>
SEVEX View	<p>SEVEX View is an accident release model that uses a complete prognostic meteorological processor. Therefore, this unique model can simulate dense gas and other accidental releases in complex situations, such as non-flat terrain and large water bodies from hundreds of meters to over 50km. Additionally, it does not require a local multi-</p>

	<p>level meteorological tower. SEVEX View was developed as a joint efforts by ATM-PRO, Lakes Environmental Software Inc., and three Belgium universities.</p> <p>Type: CFD, Particle, and plume model..</p> <p>Source types: Dense gas, BLEVE, explosions, fire, and other accidental release source types.</p> <p>Features: Instantaneous and continuous releases of heavy gases; explosion, hydrocarbon fires, non-flat terrain under all atmospheric stabilities, land-sea breeze; and short- to mid-range scales.</p> <p>Availability: Atmospheric Transport Models for Professional Applications – ATM-PRO http://www.atmpro.be and Lakes Environmental Software Inc. http://www.weblakes.com</p>
--	--

5 Meteorological Models

Meteorological Models compute important atmospheric behavior and processes that affects weather and pollutant transport. Relevant results from meteorological models include:

- Three-dimensional spatially-varying wind field
- Atmospheric turbulence structure
- Relative humidity
- Three-dimensional temperature field
- Convective and mechanical mixing heights

Meteorological models are classified according to the methods used to determine the wind field and other atmospheric variables. According to Seaman (Seaman 2000) these models can be classified in three categories:

- Diagnostic or kinematic
- Dynamical
- Four-dimensional data assimilation (FDDA)

5.1 Diagnostic Models

Diagnostic models are those that analyze observations taken at discrete points in space and time. Meteorological models that solve the coupled conservation equations of mass, momentum, and energy are classified as dynamic models. Four-dimensional data assimilation models include the features of the diagnostic and dynamical models.

Table 20. Meteorological Models.

Source (website or company)	Available models and data
Earth Tech, CALPUFF download site http://www.src.com/calpuff/calpuff1.htm	CALMET
J.T. Lee, Los Alamos National Laboratory Phone: (505) 667-8352	ATMOS1

5.2 Dynamic Models

Dynamic models, known as prognostic models, are more complex than diagnostic models in the sense that they integrate the non-linear hydrodynamic equations of motion in a numerical framework. These equations are the conservation of mass, conservation of momentum, and conservation of energy. Dynamic models are classified in two ways, hydrostatic, and non-hydrostatic models.

Table 21. Dynamic Hydrostatic Meteorological Models.

Source (website or author)	Available models and data
Pennsylvania State University / National Center for Atmospheric Research	Pennsylvania State University PSU/NCAR - MM4
Prof. Roger Pielke, Sr. - Department of Atmospheric Science, Colorado State University - pielke@atmos.colostate.edu	Colorado State University Mesoscale Model – CSU-MM

Table 22. Dynamic Non-Hydrostatic Meteorological Models.

Source (website or company)	Available models and data
Pennsylvania State University / National Center for Atmospheric Research http://www.mmm.ucar.edu/mm5/mm5.html	Pennsylvania State University PSU/NCAR – MM5
Canadian Centre for Climate Modelling and Analysis http://www.cccma.bc.ec.gc.ca/eng_index.html	Environment Canada – Mesoscale Compressible Community Model – MC2
Department of Atmospheric Science, Colorado State University http://rams.atmos.colostate.edu/	Colorado State University – Regional Atmospheric Modeling System - CSU-RAMS
Center for Analysis and Prediction of Storm, University of Oklahoma http://www.caps.ou.edu/ARPS/index_flash.html	University of Oklahoma – Atmospheric Regional Prediction System – ARPS

Marine Meteorology Division (MMD) of the Naval Research Laboratory (NRL), U.S. Navy http://www.nrlmry.navy.mil/projects/coamps/	U.S. Navy – Coupled Ocean- Atmospheric Mesoscale Prediction System – COAMPS
--	---

5.3 Four-dimensional Data Assimilation Models (FDDA)

Four-dimensional data assimilation models are a variation of the dynamical model. These models numerically integrate the equations of motion, while including data throughout the integration period. FDDA models incorporate meteorological observations distributed in space and time to correct for unavoidable deviations of model solution. These deviations can be significant for meteorological forecast longer than 48 hours (Seaman, 2000). The Pennsylvania State University PSU/NCAR – MM5 model is an example of a dynamical model that can operate, optionally, with data assimilation

References

- American Petroleum Institute (API), 1997, “Review of Air Quality Models for Particulate Matter”
- Seaman, N. L., 2000, “Meteorological Modeling for Air-Quality Assessment” *Atmospheric Environment*, 34, P2231-2259.

Lyons, W. et al. (2003) *Available Databases*. Chapter 23 of *AIR QUALITY MODELING - Theories, Methodologies, Computational Techniques, and Available Databases and Software. Vol. I - Fundamentals* (P. Zannetti, Editor). Published by The EnviroComp Institute (<http://www.envirocomp.org/>) and the Air & Waste Management Association (<http://www.awma.org/>).

Chapter 23

Available Databases

Walter A. Lyons⁽¹⁾, Joseph L. Eastman⁽¹⁾, Thomas E. Nelson⁽¹⁾, Dennis A. Moon⁽²⁾ and Cecil S. Keen⁽³⁾

⁽¹⁾ *FMA Research, Inc., 46050 Weld County Rd. 13, Ft. Collins, CO 80524, USA*
walyons@frie.com ; eastman@hsb.gsfc.nasa.gov ; tnelson@frie.com

⁽²⁾ *SSESCO Inc., 1217 Bandana Boulevard North, St. Paul, MN 55108, USA*
dam@ssesco.com

⁽³⁾ *Atmospheric Sciences Program, Minnesota State University, Mankato, MN 56002, USA*
cecil.keen@mnsu.edu

Abstract: There have been significant enhancements in the sophistication of regulatory dispersion models being developed for use in the United States, including those for local impacts from point sources (AERMOD) and multiple source impacts at ranges of 50 km and beyond (CALPUFF). Less well known, however, are the implications for modelers of the \$5 billion investment by the National Weather Service over the last decade in the national meteorological infrastructure. There have been dramatic enhancements in the quantity and quality of meteorological data and analyses, such as those generated by the National Centers for Environmental Prediction (NCEP). As an example, the Rapid Update Cycle (RUC2) generates nationwide, hourly, physically consistent mesoscale analyses on a 20 km mesh with 50 vertical layers. RUC2 produces gridded meteorological fields suitable as direct input into CALMET for simulations using a relatively coarse horizontal mesh. Alternately, RUC2 would serve as ideal initializing fields for finer mesh prognostic model runs to be used as CALPUFF input. The options now becoming available to the air quality community to employ greatly enhanced meteorological inputs to regulatory models are presented.

Key Words: Air pollution models, meteorological data, AERMOD, RUC2, CALMET, CALPUFF

1 Overview

Over the past decade, the U.S. National Weather Service (NWS) modernization program invested several billion dollars to upgrade the nation's weather

observation, telecommunication and numerical prediction infrastructure. This has resulted in many additional sources of meteorological data. Weather data resources now extend far beyond twice daily radiosondes ascents and widely separated airport surface weather observations. New data resources include an expanded network of automated weather stations, boundary layer and tropospheric wind profilers, NEXRAD (Next Generation Radar) Doppler radar precipitation and wind measurements, GOES (Geostationary Operational Environmental Satellite) satellite cloud mapping, buoys, and data collection platforms on hundreds of commercial airliners.

Access to government weather data, especially in real time, has also been dramatically improved. Today, a significant fraction of all raw data and gridded analyses and prognostic model output are broadcast via satellite on NOAAPort. For those not investing in the receivers required to intercept this public domain data stream, the Internet provides access to a large fraction of these resources. One impact of the explosion in meteorological data and analysis products made available in real-time by the federal weather service is that not all can be archived by the National Climatic Data Center (NCDC), the primary weather data resources used by the air quality modeling community. This is particularly true of the gridded analysis fields that will be discussed below. Thus capturing these data in real time as they are disseminated becomes an imperative for those organizations wishing to avail themselves of these products. An approach for doing this is described below.

Concurrent with the above developments, there have been dramatic advances in high performance desktop computing. This now allows many organizations to run advanced meteorological and dispersion models, both of which are highly sensitive to the quality of their meteorological inputs. These newer models, typified by CALPUFF and point source dispersion codes such as AERMOD, have the capability of utilizing more detailed meteorological information. Currently, running point-source codes usually involves applying limited on-site measurements. Absent those, the modeler must rely upon government surface and upper air observations, often not collocated, from distances of 100 km or more. Regional models might be exercised using a small subset of existing NWS data resources (surface and upper air soundings) or pre-packaged low resolution (as coarse as 80 km mesh) prognostic model output.

In light of recent advances, there are several approaches emerging, which may improve the meteorological inputs to air quality codes. The first would be to apply data extracted from NWS gridded meteorological fields routinely produced in the conduct of its daily operations. The NWS continuously assimilates all available meteorological observations into national 3-D analyses on scales of 20 km or less. These analyses can yield pseudo-soundings capable of driving most new regulatory dispersion models. Second, the NWS gridded fields can themselves serve as the bases for reanalyses onto much finer grids (sub-20 km), which can also incorporate additional local data (aerometric networks, sodar and profiler winds) Third, these gridded fields can serve as initializing fields for prognostic

models such as MM5, which are well-suited as drivers for CALMET, the front end for CALPUFF. This chapter describes the several approaches the authors' organizations have adopted to archive relevant NWS data products and to apply them to the new generation of air quality models that are being deployed in the United States. [For information on similar efforts within the European modeling community, we refer readers to <http://www.dmu.dk/Atmosphericenvironment/cost715.htm>]

2 The Challenges

There is an ever increasing reliance on the use of dispersion models in the regulation of air pollutants in the United States and, indeed, worldwide. While there is a plethora of existing models, given the desire to improve their utility and reliability, new approaches are continually being introduced. Among the codes now coming to the forefront are AERMOD¹, for local, point-source emissions, CALPUFF² for local and regional scale problems, and Models 3³, to address regional photochemical and visibility issues. Of these CALPUFF appears likely to be the most widely employed. The CALPUFF modeling system makes possible the use of detailed three-dimensional wind, temperature, turbulence and moisture fields. Spatially and temporally varying meteorology on a variety of scales permits CALPUFF to apply more sophisticated treatments of previously challenging regimes such as calms, sea and lake breezes, fumigation and transport in complex terrain. Therein lies the challenge. CALPUFF's ability to define meteorological conditions at not just one, but literally thousands of points within the domain, greatly magnifies the need to properly characterize the meteorology. Errors influencing transport and diffusion can now be introduced not only near the source but throughout the model domain.

These newer air quality codes are capable of utilizing improved characterizations of the atmosphere to drive their diffusion, transport and deposition routines. There are still, however, many other avenues, some not yet well explored, by which meteorological data may be acquired and incorporated into these models. The recent upgrades in weather observation systems and analysis techniques in the U.S. should be more closely scrutinized. These represent an opportunity for the newer dispersion codes to approach their full potential.

The recently completed US\$5 billion NWS modernization effort resulted in a greatly expanded observation program. Over 1000 automated surface weather stations (ASOS, AWOS) have been installed. Tropospheric wind profilers are operating within the central United States providing hourly wind profiles to altitudes of 15 km or more. Instrumented commercial aircraft now provide thousands of take-off and landing soundings and in-route weather reports each day. High resolution cloud mapping is provided every 30 minutes by the visible and infrared sensors on the advanced GOES geostationary weather satellites. Buoys and ship reports help fill the data voids over the Great Lakes and coastal waters. The WSR-88D radar network provides national mapping of radar

reflectivity (convertible to precipitation rates) as well as tropospheric wind soundings (VAD winds).

The data are continuously assembled at the National Centers for Environmental Prediction (NCEP) where new and powerful data fusion systems create nationwide, gridded 3-D meteorological analyses on an hourly basis. These analyses provide physically consistent descriptions of atmospheric wind, turbulence, humidity, and cloud microphysical properties that are much more advanced than have been heretofore available to the air quality modeling community. While the purpose of NCEP is to initialize prognostic modeling systems for operational forecasting, these analyses themselves may have great value in and of themselves. Conducted on mesh sizes of 20 km or less, they in effect can be considered as a “network” of surface and upper air reports of very high spatial and temporal resolution. And they represent more than mere interpolations of data since at their core they are prognostic models. This in turn partially accounts for smaller scale processes not necessarily resolved by the raw observations themselves, especially in coastal and complex terrain.

Most regulatory air quality models consist of several key components, including (1) a representation of the physics of the transport, dispersion, transformation and deposition of chemical species released from a variety of source configurations, (2) specifications of the physical and chemical characteristics of the emissions, and (3) an adequate representation of the meteorological factors, which influence these processes. In the past, the majority of regulatory models attempted to describe the atmosphere using data from selected subsets of NWS surface and upper air observations, possibly augmented by on-site measurements. Today a much greater menu of weather data resources are available. All modeling components must perform to an acceptable level or the end result will be a level of uncertainty unsatisfactory for the intended use of the modeling system⁴. These applications could range from new source permitting, prevention of significant deterioration (PSD) reviews or regional photochemical oxidant reduction. This chapter will focus on one component of the modeling process, the meteorological input to the primary atmospheric dispersion models.

When dispersion models first began to play a key role in source permitting, they were often simple, point source Gaussian plume models, which could only use relatively basic meteorological information. Typically, the preferred source of the meteorological data was on-site instruments. In lieu of their availability, modelers could use ostensibly nearby surface and upper air observational data collected and archived by the National Weather Service. As regional models arose to meet requirements for assessing long-range transport, acid deposition, visibility and photochemical oxidant problems, it became more common to consider the output of mesoscale prognostic models as the meteorological driver for the transport and chemistry modules. Today there exist several current and potential methodologies for providing meteorological input to regulatory dispersion models for use in the United States, including:

- use of on-site observations
- use of data from “nearby” observation stations (typically NWS data)
- use of pseudo-surface and upper air observations extracted from hourly gridded national meteorological analyses provided by NCEP
- reformatting of the output of mesoscale prognostics models (MM5, ARPS, RAMS, WRF) for direct coupling to a given target air quality model
- use of reanalyses, which produce hybrid data sets, again reformatted to meet the input requirements of the target air quality model

Some of the factors involved in the application of each of these options are discussed below.

3 Characteristics of Weather Data Sets

While it would seem preferable to rely on actual measurements of atmospheric parameters as inputs to local dispersion models, closer examination reveals that these are at times inaccurate, unrepresentative and even misleading. Thus, in considering other alternatives, there may not be such a drastic “flight from quality” as some would suspect.

In traditional point-source modeling, typically involving steady-state Gaussian plume models, the most desirable option would be to utilize on-site meteorological data collected over an extended period (1 to 5 years). While ideal, this is also expensive. And moreover, in many cases, on-site surface layer point measurements cannot fully resolve atmospheric factors influencing short-range plume dispersion. Even for low-plume rise, low emission sources not affecting receptors beyond the fence line parameters such as mixing depth and its diurnal fluctuation have to be inferred indirectly. For larger sources with greater effective stack heights, towers might have to be supplemented by Doppler sodars or boundary layer profiler/RASS systems, at far greater cost. And since the models employed often utilize the “searchlight” plume of the steady-state model, a realistic assessment of dispersion except in the simplest of cases could suggest that measurements made at the base of the source may not be representative of those at the impact receptors, often several tens of kilometers downwind. Wind shear and especially mesoscale vertical motion fields can play a crucial role in even relative short-range (sub-10 km) dispersion, as repeatedly shown in tests^{5,6,7}. Studies suggest that one may not be able to consistently measure winds that are representative of immediately adjacent areas even under the ideal conditions to much better than 1 m/sec⁸. Furthermore even the most complete on-site monitoring system is subject to instrument sensor failures, incorrect or drifting calibrations, data logger outages and other failure modes, some of which may be obvious, and others very subtle and not always detected even with rigorous QA procedures.

Frequently on-site data are not available. The usual option is to acquire long term summaries of NWS station data. Such observations (designed for aviation meteorology, often with wind speed threshold values >1.0 m/sec) are often not located within 10 km or even 100 km of the source. Mixing heights may be extracted from NWS twice-daily upper air soundings by algorithms of questionable generality and accuracy. Naturally these soundings are rarely collocated with the surface data source, and are often two or even three times further away, and take no account of critical parameters such as soil moisture. Given the extreme heterogeneity of the boundary layer in coastal regions, complex terrain and in regions frequented by mesoscale weather features (convective storms, low level jets), it is a wonder that data from such remote sources can shed any light at all on local plume behavior. Recent practice often found modelers accessing historical NWS databases from the archives of the National Climatic Data Center (NCDC). Yet we can note that the surface stations available at NCDC represent just a small fraction of the presently available surface observations (only 8 of the 71 stations in Minnesota and Iowa, for instance). Also, significant changes in local land use within the last 10-20 years have occurred. These can influence local dispersion in ways, which are only now becoming appreciated⁹.

While the modernization of the NWS surface observation system did increase the number of surface observation stations, it was not designed with the needs of the air quality community in mind. While some air quality models require input as to the percent cloud cover, that parameter is no longer consistently available from current NWS observations. By automating the cloud cover measurements (and removing the human observer from the loop), current observations only report clouds below 12,000 feet. Thus dense layers of altocumulus, altostratus or cirriform clouds, totally obscuring the sun, are not indicated. Other problems, notably in detecting hydrometeors, have plagued the new and “improved” surface observation systems. Wind averaging techniques have also changed from older systems in which speed and direction averages were often little more than “guesstimates” eyeballed from wind dials taken over a few seconds once per hour. Thus questions in data consistency within long periods of record spanning the technological upgrade discontinuities cannot be ignored.

4 NCEP Gridded Data Products

Every hour, NCEP receives, processes, error checks and assimilates a vast quantity of meteorological data. As mentioned, these data sets are far more comprehensive than those typically utilized by the air quality modeling community. Each hour the state of atmosphere over the nation and beyond is analyzed and represented as 3-D gridded fields. The primary NCEP analysis tool is the RUC2 (Rapid Update Cycle, version 2)¹⁰. (A similar analysis is prepared every three hours for runs of the Eta forecasting model.) The RUC2 is a state-of-the art data assimilation and forecasting system. At NCEP, the hourly analyses are

used as initial fields to run a detailed prognostic model for the next 12 hours. This model uses a hybrid isentropic-sigma coordinate system, which enhances the definition of both boundary layer features and synoptic discontinuities such as fronts. The 301 by 225 horizontal grid has a 20 km average mesh size. There are 50 layers in the vertical. Figure 1 shows a cross section of the grid through the central U.S. The RUC2 employs the MM5 cloud microphysics and radiation parameterizations, the Burk-Thompson technique (a level 3.0 scheme explicitly forecasting turbulent kinetic energy, replacing the earlier Mellor-Yamada level 2.0 scheme used in earlier implementations). A detailed soil model enhances the surface energy budget calculations, as does a snow cover module (which appears to be more accurate than the U.S. Air Force daily snow cover analyses). It is anticipated that in upcoming years the mesh size employed by NCEP will continue to decrease and the number of vertical levels will increase, thus further enhancing the value of this resource to air quality professionals.

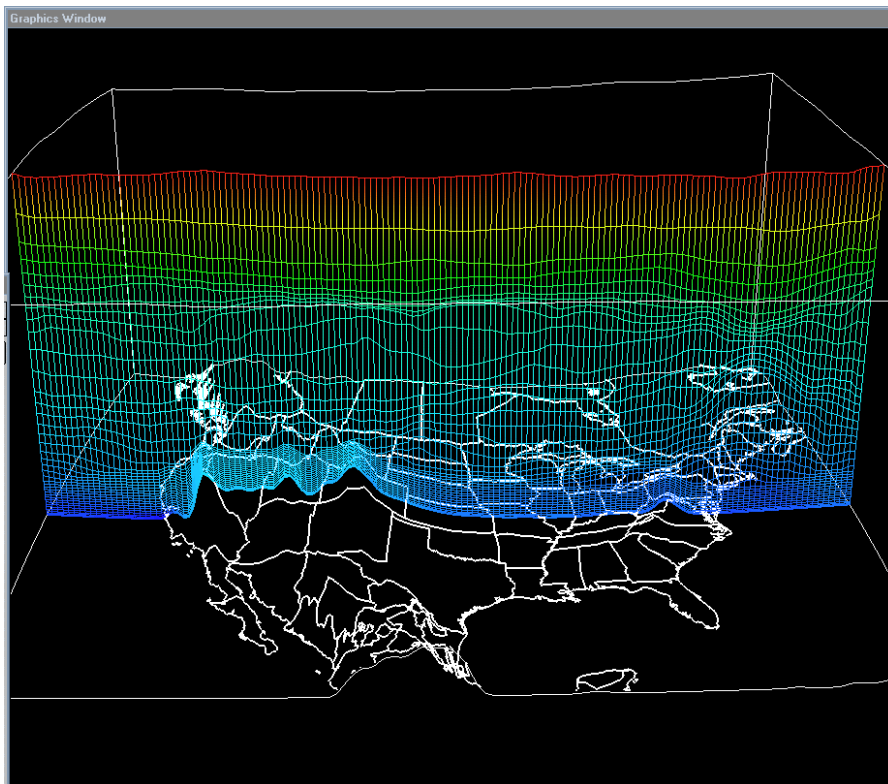


Figure 1. The RUC2 analysis grid illustrated using a vertical east-west cross section through the central US. The grid is similar in the north-south direction.

Since the hourly RUC2 analyses use the previous run of the prognostic model as initial conditions, it provides for enhanced consistency in data void regions containing circulations induced by terrain or inhomogenities in surface heat and moisture fluxes. The effects of surface snow cover, soil moisture, land use, roughness and vegetative cover are included. The RUC2 analysis fields, since

they are available in a gridded format (WMO GRIB), are relatively easy to archive, manipulate and display, using various software packages¹¹. Selected RUC2 output parameters include:

U, V Wind Components	Evapotranspiration Rate
Vertical Motion	Snow Depth
Pressure, Height	Soil Moisture
Temperature, Potential Temperature	Soil Temperature
Relative Humidity, Mixing Ratio	Soil Sensible Heat Flux
Turbulent Kinetic Energy (TKE)	Soil Moisture Flux
Cloud Water Mixing Ratios	Net Shortwave Radiation at Surface
Ice, Snow, Graupel Mixing Ratios	Net Longwave Radiation at Surface
Precipitation Rate and Character	MSL Pressure

The RUC2 analyses could be employed in several ways. For use with AERMOD, the most direct would be to extract single point pseudo-soundings at the location of the source to be modeled. These analyses can also be reconfigured as input to both meteorological diagnostic codes such as CALMET, and prognostic meteorological codes such as MM5 and ARPS¹². In order to do this, the fields must be transformed to match the domain, coordinate systems and file structures of the target air quality or prognostic models.

While the RUC2 analyses are extremely comprehensive, using most weather data observations acquired by the federal government, we note that the RUC2 process does not include local data sources such as those from aerometric networks, Sodars, profilers, agricultural and road weather observation systems and other sensors employed in air quality monitoring.

5 Data Archival

While NCDC archives a substantial amount of the raw observations used to create the NCEP gridded analyses, as of this writing there is no formal government archive of RUC2 products. To meet the expanding data requirements of its air quality modeling activities, the authors' organizations began an ongoing automated archival program of the various relevant data sets in 1998. Using both NOAAPort transmissions, as well as polling NWS Internet sites, the desired data files were obtained in real time and archived onto CD-ROM and DVD-RAM media. (For additional information, see <http://www.enviromod.com/>.)

The current archival processes includes:

- NCEP Hourly National Gridded Analyses (RUC2)
- Eta Model Analyses
- METARs (surface observations)
- Upper Air and Profiler Soundings
- GOES Digital IR and Visible Satellite Data

- Processed GOES Satellite Images
- NEXRAD Radar Reflectivity Data
- Soil Moisture, Snow Cover, SST Data
- Land Use, Topography, Vegetative Cover

EDIS is part of a larger system which can provide (1) raw observations, (2) NCEP gridded analyses, (3) re-analyzed gridded fields incorporating NWS observations and local air quality network data, and (4) gridded output from mesoscale and regional prognostic models¹² (Figure 2). Data sets are formatted for specific time periods, spatial domains, horizontal and vertical grid structures, map projections, and data formats. The files are designed to be directly importable into target air pollution models such as CALMET /CALPUFF. Moreover, EDIS will supply meteorological and supporting files suitable for immediate use by those practitioners wishing to run their own mesoscale meteorological models (MM5, ARPS). Alternately, the user can request detailed prognostic model output suitable to drive Models3 and similar codes.

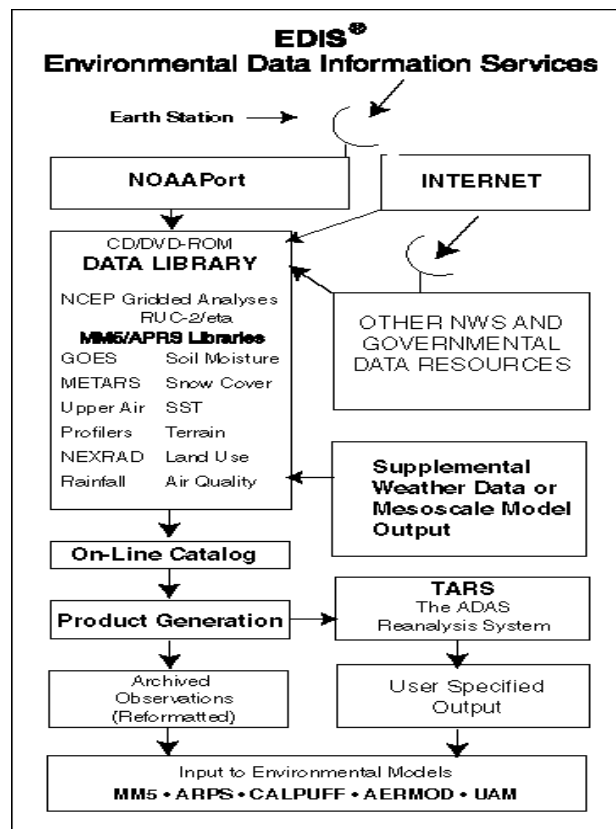


Figure 2. The data archival processes at SESCO and FMA.

6 Reanalysis Techniques

The native NCEP gridded analyses may, without alteration, suffice for certain applications, but it is likely that in most cases, the air quality specialist will require further refinements. Once a domain is selected, a different horizontal and vertical mesh may be required in order to resolve topographic and geographic-induced features. Thus the need arises to reanalyze available NCEP data onto a finer grid. This process then creates the opportunity of introducing new, non-standard weather data sets available for a given locale (surface wind networks, tall towers, Doppler sodars, and wind profilers) These reanalyzed fields can be configured to serve as input to diagnostic (CALMET) or prognostic meteorological models (MM5, ARPS, and WRF) or directly into dispersion models (CALPUFF, CAMx, MAQSIP, Models 3). It may often be necessary to compute additional derived variables (mixing depth and Monin-Obukhov length) and transform the grids into the appropriate formats suitable for ingest into their target codes.

The approach adopted by the authors to accomplish these tasks is called TARS - The ADAS Reanalysis System. The TARS methodology provides gridded, integrated meteorological data sets formatted for use in a specific modeling system (Figure 3). At the core of TARS is ADAS - the ARPS Data Analysis System^{13, 14} - developed by the Center for the Analysis and Prediction of Storms

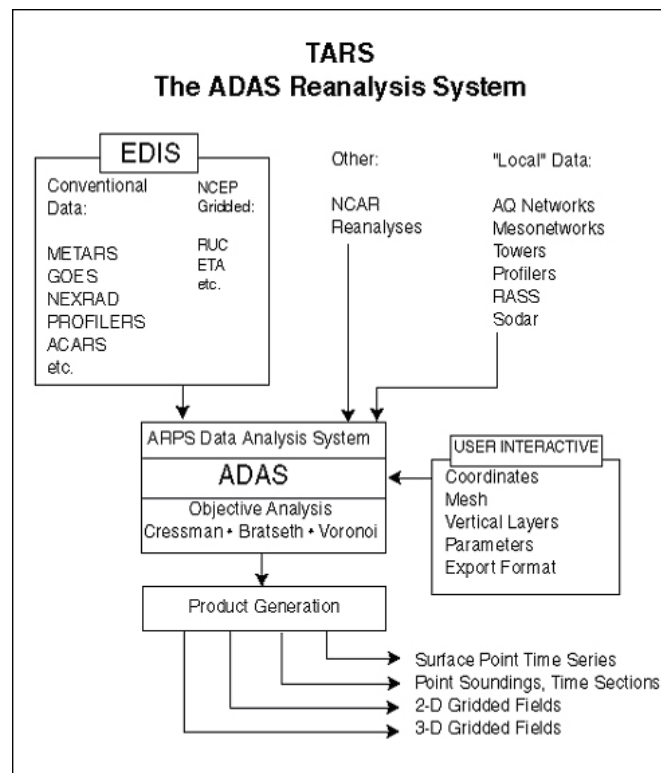


Figure 3. Schematic of TARS- The ADAS Reanalysis System.

(CAPS) at the University of Oklahoma. ADAS is essentially the initialization package for the ARPS (the Advanced Regional Prediction System) prognostic modeling system. ADAS is a descendant of the Local Analysis and Prediction System (LAPS) developed by NOAA's Forecast Systems Lab. Among its many features is a terrain-following sigma-z coordinate system. ADAS allows great flexibility in specifying the domain, mesh sizes and the number of vertical levels. ADAS employs advanced objective analysis schemes such as the Bratseth technique. TARS has been further enhanced by the Natural Neighbor objective analysis technique using the Voronoi tessellation, ideal for highly spatially inhomogeneous data sources. In most applications, ADAS would typically use the RUC2 (or Eta) gridded fields as a "first guess". Depending upon the problem, both standard and special weather observations, GOES visible and infrared radiance data, and NEXRAD base reflectivity data (or more complete Level II reflectivity and wind data) could be introduced. A strength of ADAS is the ability to employ any available data type to generate meteorologically consistent 3-D fields of state and derived variables, including cloud and precipitation quantities. The derived fields which can be generated include mixing depth, percent cloud cover, cloud thickness, precipitation rate and type, solar insolation, lapse rates, shear, Richardson number, heat and moisture fluxes, and micrometeorological parameters (Monin-Obukhov length, L , U^* , W^* , θ^*). Output can be configured for a given geographical coordinate system, horizontal mesh, number of vertical layers, and the required grid structure of the target model. The results can be formatted as surface station time series, vertical soundings, time-height series, 2-D and, most commonly, 3-D gridded fields (Figures 3 and 4).

RUC2, TARS and prognostic model data sets are extremely large and complex. For an end user to evaluate their quality and extract the inherent information content, it is essential that an interactive visualization system be available. Several public domain and commercial visualization systems are suitable for this task. An example using an interactive 3-D visualization and animation system, which will run on a standard PC (under NT or Windows), called the Environmental Work Bench [EWB] has been developed for this purpose^{11,15}. It displays and manipulates raw observations, gridded fields or prognostic model results (such as ARPS, MM5) as well as output from air quality models and observations.

TARS has been employed on a national scale, creating transport wind and turbulence fields as part of a long term study of long range transport of mercury in the environment¹⁶. On a very local level, TARS was used to demonstrate the creation of a 3-D time dependent wind field in the airspace above the Kennedy Space Center¹⁷. Using RUC gridded fields, additional data included an array of instrumented towers, a surface mesonet, boundary layer and tropospheric profilers, rawinsonde and jimsphere soundings, and aircraft reports.

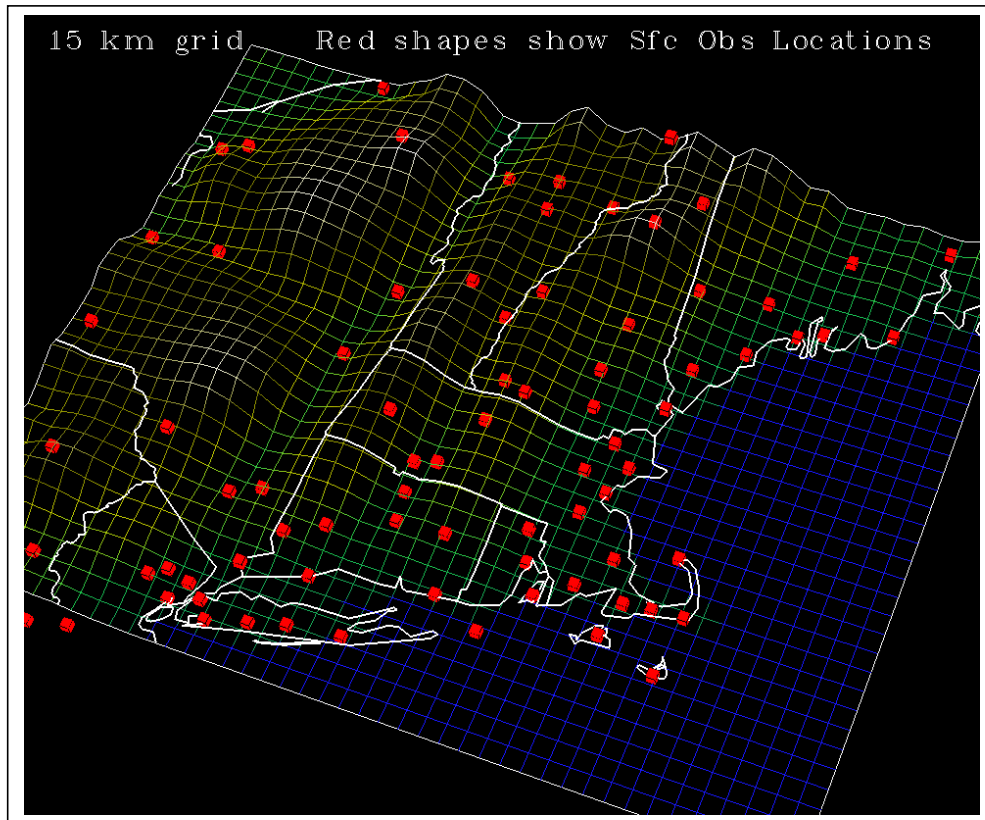


Figure 4. The TARS reanalysis domain used to incorporate RUC2 data for 1999 reanalyzed to 15 km mesh in preparation to drive the CALPUFF system. The region shown is New England and parts of New York and New Jersey.

In a current project, RUC2 gridded fields are being reanalyzed for the entire 1999 year to serve as input into CALMET. The target model domain is New England with a grid of 15 km (Figure 4). The reanalysis onto finer grids, especially using the advanced natural neighbor objective analysis scheme, often materially improves the quality of the model input. In typical cases, the RMS differences between the initial RUC2 10 meter wind speed analysis and available point wind observations are on the order of 3.0 m/sec. The RMS surface temperature differences can reach 3.0 C¹². Upon reanalysis, the RMS wind difference was reduced to the 0.5 to 1.0 m/s range while the RMS temperature differences also improved to about 0.5 C. A visualization of typical TARS reanalysis product as prepared to drive the CALMET system is shown in Figure 5.

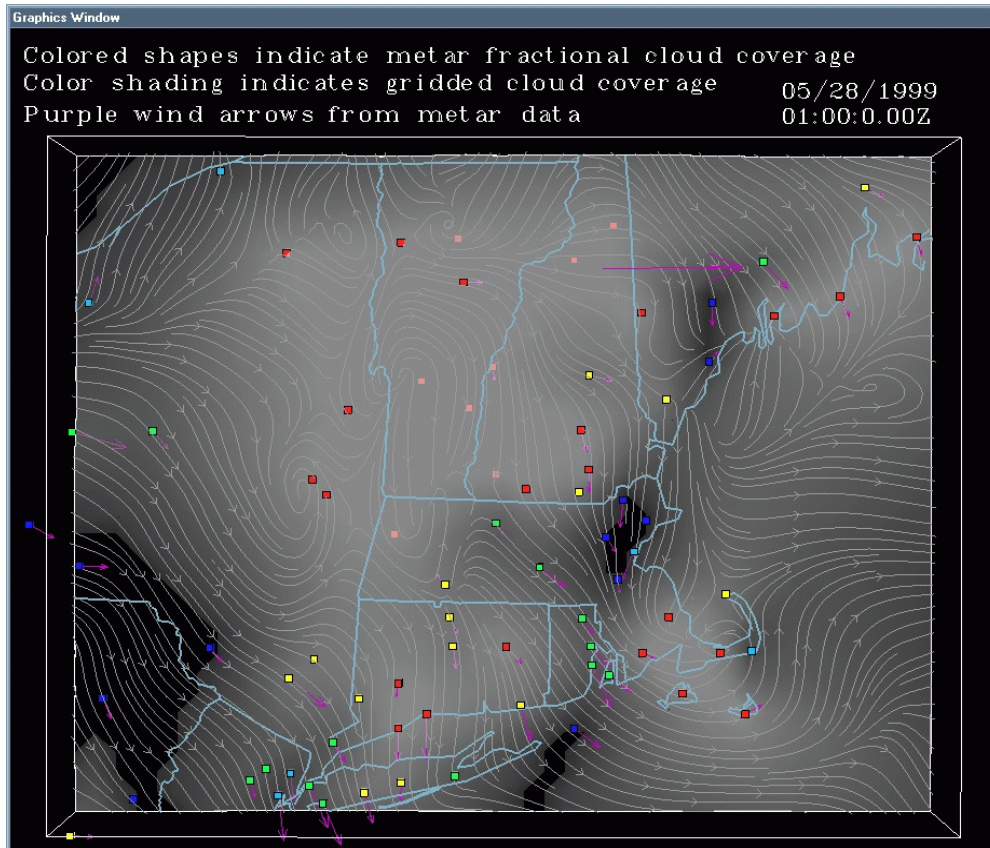


Figure 5. Typical TARS reanalysis, using RUC2 gridded fields and METARs, to provide a 15 km mesh file suitable for direct import into CALMET. The EWB display shows 10 m wind streamlines, diagnosed cloud cover, and observed surface wind and sky cover.

7 Mesoscale Prognostic Models

Techniques such as the TARS reanalysis technique have many potential benefits for enhancing the quality of meteorological fields being prepared for use in air quality models. Such approaches also have one fundamental limitation. As analysis mesh size decreases without a corresponding increase in the density of meteorological observations, TARS cannot create formerly sub-grid scale circulations (such as lake breezes) that were not inherently represented by the data. While some features such as slope flows may be parameterized when operating within systems such as CALMET, only a properly configured prognostic model can reveal the true complexity of small scale circulations that can affect plume dispersion. Prognostic codes such as MM5¹⁸ and RAMS¹⁹ have been used in air quality analyses for over a decade, typically in conjunction with regional photochemical grid models and emergency response assessment^{6,19}.

These were often large scale projects with considerable budgets due to the considerable costs involved in applying prognostic meteorological codes.

Recently, a convergence of events has made it increasingly practical to consider employing prognostic meteorological models in more routine model applications, such as with CALPUFF. Several modeling systems are available in the public domain that have achieved considerable maturity and acceptance due to widespread use, MM5 and ARPS being prime examples. Such would not have occurred without the recent extraordinary advances in affordable desktop high performance computing. The multi-processor PCs of today have considerably greater computational throughput than the supercomputer of a not much more than a decade ago. Numerous non-federal organizations such as airlines, media operations and utilities, are now running mesoscale models operationally^{20,21}. Assuming access to the required meteorological data files, running simulations of past weather scenarios using a code such as MM5 is becoming relatively straightforward²¹. This process is being assisted by the availability of experienced consultants as well as trained university graduates familiar with the complexities of such modeling projects. Access to geophysical data sets such as topography and land use is becoming increasingly facilitated by the efforts of agencies such as the U.S. Geological Survey. Visualization and model evaluation tools are now both affordable and widely used^{15,19}. The required meteorological data files can be retrieved through several organizations, including the EDIS system. Increasingly outputs from codes such as MM5 are being linked more directly with systems such as CALPUFF. Regulatory acceptance of the use of such models is longstanding in matters dealing with state implementation plans for ozone. The trend now extends to include MM5/CALPUFF simulations support of PSD assessments, especially in complex terrain and coastal zones²³.

Several key points must be remembered when designing such prognostic model runs for use in air quality models. The task of properly specifying surface boundary conditions is not to be underestimated. In particular, the characterization of the initial of soil moisture patterns is of paramount importance as it substantially modulates the development of mesoscale circulations, surface heat and moisture fluxes and mixing depths^{19,24}. Perhaps most essential is the requirement to have a sufficiently fine horizontal mesh plus an adequate number of vertical layers defining the boundary layer. It is axiomatic that to define a circulation induced by a topographic feature, it must be covered by *at least* four grid points²⁶. The true resolution of a prognostic code is not the model's "delta x" but four times that distance (or more). Since the run time for most codes varies roughly with the cube of the inverse of the grid size, this criterion can quickly impose considerable computational constraints, especially in highly complex terrain. Prognostic model output from operational forecasting runs can be archived and, over the course of time, extended digital climatologies can be created. A second approach is to run the model in near-real time that is taking 22 hours to create a 24-hour simulation. This allows the use of finer grids than if production forecasts were the purpose of the runs. It also allows for running the

model in a continuous data assimilation mode, thus permitting the nudging of the model towards observations rather than allowing for the accumulation of error in the 12 or 24-hour periods before reinitialization. Figure 6 shows a visualization of MM5 runs performed for the U.S. High Plains in which wind fields associated with large convective storm systems were modeled. These MM5 runs were completed on a conventional desktop PC initialized with EDIS-provided RUC2 and GOES satellite data. Visualization employed the EWB software. Regional simulations with mesh sizes as small as 3 km are now eminently feasible using affordable multi-processor desktop systems when running in an essentially 1:1 run time retrospective mode. Done continuously, over one year a one-year digital climatology can be assembled.

8 Future Developments

In the United States, new data resources developed by the NWS have created exciting opportunities to improve the performance of various types of air quality models^{12,13,25}. The NCEP gridded analyses, especially when reanalyzed onto appropriate grids and formats by techniques such as TARS, can be considered an important new source of “data.” For instance a “sounding” can be extracted from these hourly reanalyses which should be more representative of conditions at a given point source than an actual upper air observation that was taken a hundred kilometers away and several hours earlier/later. Especially in complex terrain and coastal zones, mesoscale prognostic model output can provide improved inputs to a wide variety of air quality models. The use of mesoscale prognostic model output as air quality model drivers is also greatly facilitated by employing these rich initializing data sets, which contain more information than traditionally used for meteorological model inputs. State, regional and local air agencies as well as environmental consultants need easier and more reliable access to the ever-growing stream of meteorological data and derived analyses. In particular, the fields created by data assimilation systems and prognostic models are expected to play a steadily increasing role in air quality decision making, especially for regional ozone, PM_{2.5} and visibility.

While new resources such as RUC2 files, reanalyzed gridded data sets, and prognostic model output would appear to have many advantages over some past sources of meteorological data, their utility in air quality modeling must be further demonstrated. This must be done in full cooperation with regulatory agencies so that the end users of the models will have a clear understanding of what is expected of them when they apply these newer meteorological methodologies.

We should also note that outside the United States, access to government-produced meteorological data can often be quite restricted. This would complicate the tasks of potential air quality model users of advanced weather data products. It is hoped that as more and more nations understand the benefits of free

and open access to resources funded by their own taxpayers, these impediments will begin to disappear.

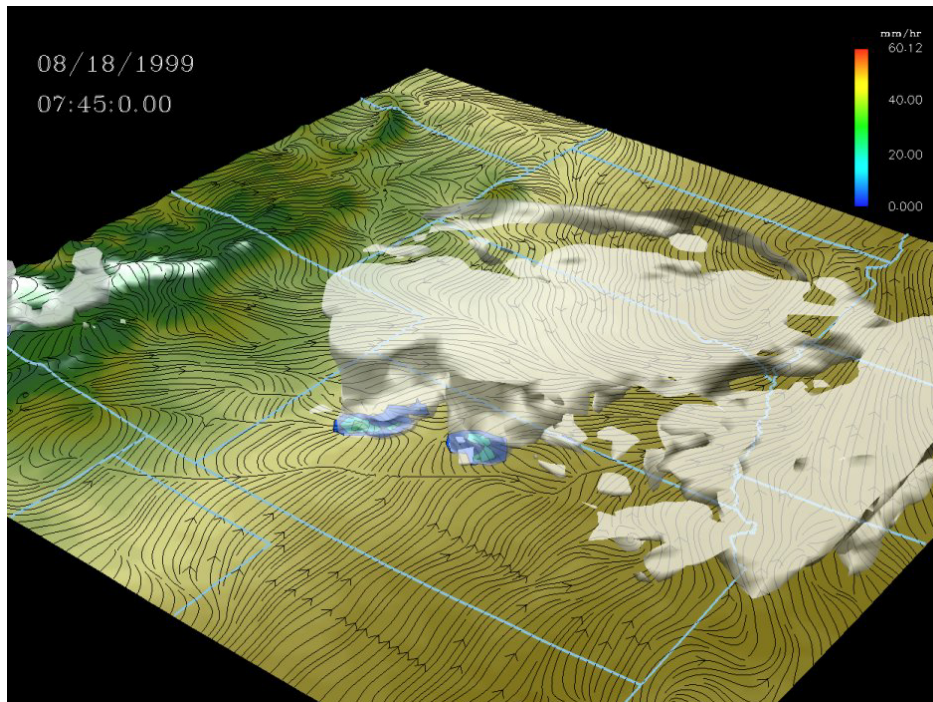


Figure 6. EWB visualization of MM5 output showing deep convection, cloud isosurfaces, surface rainfall and surface wind streamlines. These fields can be reformatted for use within codes such as CALMET/CALPUFF and Models3.

Acknowledgments

The genesis of this project was an SBIR project from NASA, Kennedy Space Center, under Contract NAS10-97026. We also acknowledge the contributions of Gene Bassett and Richard Carpenter, Center for Computational Geosciences, and Prof. Kelvin Droegemeier, of the University of Oklahoma. We appreciate the many helpful discussions on mesoscale models and air pollution modeling with Prof. Roger A. Pielke (Colorado State University) and John Irwin (US EPA).

References

1. EPA's AERMOD model: <http://www.epa.gov/scram001/tt26.htm>
2. Scire, J.S.; Strimaitis, D.G.; Yamartino, R.J. *A User's Guide to the CALPUFF Dispersion Model (Version 5.0)* EarthTec, Inc., Concord, MA, 1999, <http://www.epa.gov/scram001/tt22.htm#calpuff>
3. EPA's Models 3: <http://www.epa.gov/asmdnerl/models3/announce.html>
4. Pielke, R.A.; M Uliasz. *Atmospheric Environment* **1998**, 32, 1455-1466.

5. Lyons, W.A., Eastman, J.L. Pielke, R.A.; Wilkerson, G.W. *The use of a mesoscale prognostic model to design a field tracer experiment for the Lake Michigan Ozone Study*. Preprints, Paper 92-87.10, 85th Annual Meeting, AWMA, 1992, 16 pp.
6. Lyons, W.A., Pielke, R.A.; Walko, R.L.; D.A. Moon; Keen, C.S. *Atmospheric Environment* **1995** 29, 283-301.
7. Eastman, J.L.; Pielke, R.A.; Lyons, W.A. *J. Appl. Meteor.* **1995**, 34, 1398-1418.
8. Hanna, S.R. Proceedings, *Objectives for next Generation of Practical Short-Range Atmospheric Dispersion Models*. Riso, Denmark, 1992, 77-85.
9. Pielke, R.A.; Uliasz M., 1993: *J. Air & Waste Management* **1993**, 43, 989-994.
10. NOAA's RUC2 Information. <http://maps.fsl.noaa.gov/>
11. Moon, D.A.; Lyons, W.A. *The Environmental Workbench- An interactive 3D analysis and visualization tool for meteorology and environmental applications*. Preprints, 16th IIPS Conf., AMS, Long Beach, 2000, 4 pp.
12. Lyons, W.A.; Nelson, T.E.; Moon, D.A.; Schwamb P.; Keen, C.S. *Applications of the Environmental Data Information System (EDIS) to Air Pollution Meteorology*. Paper 99-246, AWMA Annual Meeting, St. Louis, 1999, 16 pp.
13. Lyons, W.A.; Nelson, T.E.; Eastman, J.L.; Moon, D.A.; Keen, C.S. *New meteorological data resources suitable for the next generation of air quality models*. Preprints, 11th Joint Conf. on Applications of Air Pollution Meteorology, AMS/AWMA, 2000, Long Beach, CA, 2000, 4 pp.
14. Brewster, K. *3-D Analysis with ARPS Data Assimilation System: ADAS. Supplemental S-1, ARPS User's Guide*, CAPS, University of Oklahoma URL: <http://www.caps.ou.edu/ARPS>, 1998.
15. Further Information. <http://www.EnviroMod.com>
16. Moon, D.A.; Pai, P. *An application of a meteorological data assimilation system to drive regional air quality models*. Preprints, 92nd Annual AWMA Meeting. St. Louis, 1999, 16 pp.
17. Lyons, W.A.; Moon, D.A. *A Four-Dimensional Wind Analysis System for the Kennedy Space Center*; Preprints, 14th IIPS Conference, American Meteorological Society, Phoenix, 1998, 4 pp.
18. Grell, G.A., Dudhia, J., Stauffer, D.R. *A Description of the Fifth-Generation Penn State/NCAR Mesoscale Model (MM5)*. National Center for Atmospheric Research, Boulder, CO, NCAR Technical Note: NCAR/TN-398+STR, June 1995.
19. Lyons, W.A.; Tremback, C.; Pielke, R.A. *J. Applied Meteor.* **1995**, 34, 1762-1786
20. Cotton, W.R.; Thompson, G.; Mielke, P.W. Jr. *Bull. Amer. Meteor. Soc.* **1994**, 75, 349-362
21. Mass C.F.; Kuo, Y.H. *Bull. Amer. Meteor. Soc.* **1998**, 79, 253-263.

22. Moon, D.A.; Lyons, W.A.; Eastman, J.L.; Nelson, T.E.: *A common system to initialize multiple prognostic codes for air quality modeling*. Millennium NATO/CMA Intl. Technical Meeting on Air Pollution Modeling and Its Application. 2000, Boulder.
23. Richmond, K. *Application of MM5 and the CALPUFF Modeling System for Class 1 Area Assessments*. AWMA paper. Session AB-3e, 2000, Salt Lake City, 20 pp
24. Lyons, W.A. *Soil moisture influences on the performance of mesoscale and cloud-scale prognostic models*. In, *Environmental Modeling*, Vol. 3, P. Zannetti, Editor, Computational Mechanics Publications, London, 1996, 183-215.
25. Schulze, R.H.; Turner, D.B. *Environmental Manager* **1998**, March, 12-21.
26. Pielke, R.A., Sr., *Further comments on "The differentiation between grid spacing and resolution and their application to numerical modeling."* Bull. Amer. Meteor. Soc., 82, 699.

Authors' Index

Anfossi, Domenico	I – p 103
Builtjes, Peter	I – p 1
Byun, Daewon W.	I – p 213
Canepa, Elisa	I – p 103
Eastman, Joseph L.....	I – p 409
Keen, Cecil S.	I – p 409
Lacser, Avraham	I – p 213
Lee, Russell	I – p 363
Lyons, Walter A.	I – p 409
Moon, Dennis A.	I – p 409
Moussiopoulos, Nicolas	I – p 313 , 355
Nelson, Thomas E.	I – p 409
Oettl, Dietmar	I – p 325
Reynolds, Steven D.	I – p 13
Roth, Philip M.	I – p 13
San Jose, Roberto	I – p 325
Sorbjan, Zbigniew	I – p 37
Thé, Jesse	I – p 185 , 363
Tourlou, Paraskevi-Maria.....	I – p 313 , 355
van Dop, Han.....	I – p 103
Venkatram, Akula	I – p 185
Yamartino, Robert.....	I – p 213
Zannetti, Paolo	I – p 213

Blank Page

Subject Index

Abatement	I – p	313 , 355
Acid deposition	I – p	363
Advection	I – p	213
AERMOD.....	I – p	185 , 409
Air dispersion models.....	I – p	363
Air pollution	I – p	1 , 185 , 313 , 355
Air pollution episode.....	I – p	313 , 355
Air pollution model(s).....	I – p	185 , 409
Air pollution modeling	I – p	1 , 325
Air pollution regulations	I – p	1
Air quality	I – p	185
Air quality forecasting.....	I – p	313 , 355
Air quality modeling	I – p	13 , 213
Air quality models.....	I – p	363
Ambient turbulence.....	I – p	103
Atmospheric boundary layer	I – p	37 , 185
Atmospheric motions	I – p	37
Building effects	I – p	185
Buoyant plumes.....	I – p	103
CALMET	I – p	409
CALPUFF	I – p	409
Chemical transformation	I – p	13
Complex terrain.....	I – p	363
Complex terrain dispersion	I – p	185
Convection	I – p	37
Convective boundary layer.....	I – p	185
Data needs	I – p	13
Dense gas models	I – p	363
Deposition of air pollutants	I – p	313 , 355
Diagnostic models	I – p	363
Diffusion.....	I – p	37 , 213
Dispersion.....	I – p	185 , 313 , 355
Dispersion modeling.....	I – p	13 , 103
Eddy diffusivity.....	I – p	213
Effective plume heights.....	I – p	103
Emergency releases	I – p	363
Emissions modeling	I – p	13
Eulerian modeling	I – p	213
Four-dimensional data assimilation.....	I – p	363
Future modeling	I – p	325
Gaussian dispersion model.....	I – p	185
Gaussian model(s)	I – p	13 , 363
Grid-based models.....	I – p	13
Internet	I – p	325
ISC.....	I – p	185
Jet plumes	I – p	103
Lagrangian models	I – p	363
Local and non-local closure	I – p	213
Long-range transport	I – p	363
Meteorological data	I – p	363 , 409
Mixed layers.....	I – p	37
Mixing	I – p	37

Model performance evaluation.....	I – p 13
Modeling	I – p 313 , 355
Numerical algorithms	I – p 213
Ozone formation.....	I – p 313 , 355
Particle models	I – p 363
Photochemical models.....	I – p 13 , 363
Plume models	I – p 363
Pollution control.....	I – p 313 , 355
Prognostic models	I – p 363
Puff models	I – p 363
Regional models.....	I – p 363
Regulatory application	I – p 13
Regulatory model	I – p 185
Resolution.....	I – p 13
RUC2.....	I – p 409
Self-induced turbulence.....	I – p 103
Short-range models.....	I – p 363
Similarity theories	I – p 37
Simulation	I – p 313 , 355
Simulation models.....	I – p 13
Stability conditions.....	I – p 103
Stable boundary layer.....	I – p 185
Street canyon	I – p 313 , 355
Terrain data	I – p 363
Transport	I – p 313 , 355
Turbulence.....	I – p 37
Uncertainty.....	I – p 13
Urban models	I – p 363
Urban plume.....	I – p 313 , 355
Visibility.....	I – p 363
Weather systems.....	I – p 37

Additional Information About the Chapter Authors

Anfossi, Domenico

-  [CV](#)
-  [Picture](#)

Builtjes, Peter

-  [Picture](#)

Byun, Daewon W.

-  [Bio](#)
-  [Picture](#)

Canepa, Elisa

-  [CV](#)
-  [Picture](#)

Lacser, Avraham

-  [CV](#)

Lee, Russell

-  [CV](#)

Lyons, Walter A.

-  [CV](#)
-  [Bio](#)
-  [Picture](#)

Moussiopoulos, Nicolas

-  [Picture](#)

Öetl, Dietmar

-  [CV](#)
-  [Picture](#)

Roth, Philip M.

-  [CV](#)

San Jose, Roberto

-  [CV](#)
-  [Picture](#)

Sorbjan, Zbigniew

-  [CV](#)
-  [Picture](#)

van Dop, Han

-  [CV](#)
-  [Picture](#)

Venkatram, Akula

-  [Picture](#)

Yamartino, Robert

-  [CV](#)
-  [Picture](#)

Zannetti, Paolo

-  [CV](#)
-  [Picture](#)